



Short-Period Building Collapse Performance and Recommendations for Improving Seismic Design

Volume 2 – Study of One-to-Four Story Wood Light-Frame
Buildings

FEMA P-2139-2 / October 2020



FEMA



Short-Period Building Collapse Performance and Recommendations for Improving Seismic Design

Volume 2 – Study of One-to-Four Story Wood Light-Frame Buildings

Prepared by

APPLIED TECHNOLOGY COUNCIL
201 Redwood Shores Parkway, Suite 240
Redwood City, California 94065
www.ATCouncil.org

Prepared for

FEDERAL EMERGENCY MANAGEMENT AGENCY
Mai (Mike) Tong, Project Officer
Robert D. Hanson, Technical Advisor
Washington, D.C.

APPLIED TECHNOLOGY COUNCIL
Jon A. Heintz, Project Executive
Justin Moresco, Project Manager
Scott D. Schiff, Associate Project Manager

PROJECT TECHNICAL COMMITTEE
Charles A. Kircher (Project Tech. Director)
Jeffrey W. Berman
Kelly Cobeen
J. Daniel Dolan
Andre Filiatrault
James R. Harris
Gregory Kingsley
Dawn Lehman
Weichiang Pang
P. Benson Shing

SOIL-STRUCTURE INTERACTION
WORKING GROUP
Lisa Star
Jonathan P. Stewart

PROJECT REVIEW PANEL
Anthony Court*
William T. Holmes
Onder Kustu
Phil Line
James O. Malley
Steve Pryor

WOOD WORKING GROUP
D. Jared DeBock
Maria Kolou
Ershad Ziae

*ATC Board Representative



FEMA



Notice

Any opinions, findings, conclusions, or recommendations expressed in this publication do not necessarily reflect the views of the Applied Technology Council (ATC), the Department of Homeland Security (DHS), or the Federal Emergency Management Agency (FEMA). Additionally, neither ATC, DHS, FEMA, nor any of their employees, makes any warranty, expressed or implied, nor assumes any legal liability or responsibility for the accuracy, completeness, or usefulness of any information, product, or process included in this publication. Users of information from this publication assume all liability arising from such use.

Cover photograph – One-story wood light-frame building (photo credit: Degenkolb Engineers).

Foreword

Most buildings in the United States are less than five stories tall. These low-rise buildings typically possess fundamental periods less than one-half second and thus are referred to as short-period buildings. Many commonly used analytical models have predicted that short-period buildings designed to current building codes are likely to suffer severe damage or collapse during design-level earthquakes. However, post-earthquake field investigations have not confirmed these predictions. Since this uncertainty is found across all types of building structures and construction materials permitted by current building codes and standards, it decreases confidence in the earthquake resilience of such code-compliant buildings. This technical resource series provides the findings and conclusions related to this issue and recommendations for improving seismic design of short-period buildings.

The National Earthquake Hazards Reduction Program (NEHRP) at the Federal Emergency Management Agency (FEMA) has a responsibility to help translate and implement new knowledge and research results to increase earthquake resilience nationwide. This FEMA-supported multi-year project series has successfully applied new analytical modeling techniques to investigate the long-standing problem of short-period building seismic collapse performance. This report is the second volume of the series, and it summarizes a study on one-to-four story wood light-frame buildings designed in accordance with the ASCE/SEI 7-10 standard for high-seismic regions. The study has examined various contributing factors to the uncertainty. Through advanced modeling and parametric evaluation, the study has shown that the uncertainty can be resolved and further improvements to seismic design of wood light-frame buildings can be achieved.

FEMA is grateful to the Applied Technology Council (ATC) for managing this sophisticated multi-year project series to a successful completion, to the Project Technical Committee and the Project Review Panel for their dedicated effort leading to invaluable technical findings and recommendations. FEMA is also thankful to the project workshop participants for their scrutiny and valuable comments. Resolving the uncertainty in short-period building seismic collapse performance will strengthen confidence in seismic building codes. This project series will also contribute to improving seismic design and predicting collapse potential of short-period buildings in high-seismic communities in the nation.

Federal Emergency Management Agency

Preface

Recent analytical studies investigating a wide range of modern seismic-force-resisting systems have predicted collapse rates for short-period buildings that are significantly larger than those observed in earthquakes during the past 50 years. This gap between analytically predicted and historically observed collapse rates is known as the *short-period building seismic performance paradox*. Analytically predicted collapse rates for short-period buildings are also generally larger than maximum collapse rates used in national model building codes and standards to establish seismic design requirements. If these analytical predictions are accurate, it means that the goal of acceptable collapse performance for all seismic-force-resisting systems at all building periods is not being achieved.

In 2013, the Applied Technology Council (ATC) was awarded the first in a series of task orders under contracts HSFE60-12-D-0242 and HSFE60-17-D-0002 with the Federal Emergency Management Agency (FEMA) to investigate “Solutions to the Issue of Short Period Building Performance,” designated the ATC-116 Project series. The purpose of this series of projects was to investigate the response behavior and collapse performance of different structural systems, and to identify causes and develop solutions for the short-period building seismic performance paradox. Studies investigated three structural systems: wood light-frame, special reinforced masonry shear wall, and steel special concentrically braced frame (SCBF) systems.

This report, which focuses on the investigation of wood light-frame systems, is one of four principal products of the ATC-116 series of projects:

- FEMA P-2139-1, *Short-Period Building Collapse Performance and Recommendations for Improving Seismic Design, Volume 1 – Overarching Findings, Conclusions, and Recommendations*
- FEMA P-2139-2, *Short-Period Building Collapse Performance and Recommendations for Improving Seismic Design, Volume 2 – Study of One-to-Four Story Wood Light-Frame Buildings*
- FEMA P-2139-3, *Short-Period Building Collapse Performance and Recommendations for Improving Seismic Design, Volume 3 – Study of One-to-Four Story Special Reinforced Masonry Shear Wall Buildings*

- FEMA P-2139-4, *Short-Period Building Collapse Performance and Recommendations for Improving Seismic Design, Volume 4 – Study of One-to-Four Story Steel Special Concentrically Braced Frame Buildings*

These reports are the result of a collaborative effort of more than 30 individuals tasked with the design of archetypes, development of numerical models, and interpretation of results across all three structural systems, in addition to the many others who participated in review workshops where draft versions of the reports were presented and discussed. ATC is indebted to the leadership of Charlie Kircher, Project Technical Director, and to the other members of the ATC-116 project team for their efforts in developing these reports. The Project Technical Committee, consisting of Jeff Berman, Kelly Cobeen, Dan Dolan, Andre Filiatral, Jim Harris, Greg Kingsley, Dawn Lehman, Weichiang Pang, and Benson Shing, managed and performed the technical development effort.

Jared DeBock assisted in the design of wood light frame archetypes, and Maria Koliou and Ershad Ziaeи assisted in the wood numerical modeling. Jon Stewart and Lisa Star provided technical guidance on the development of the soil-structure interaction and foundation flexibility parametric study. The Project Review Panel, consisting of Tony Court, Bill Holmes, Onder Kustu, Phil Line, Jim Malley, and Steve Pryor, provided technical review and advice at key stages of the work.

ATC also gratefully acknowledges Mike Tong (FEMA Project Officer) and Bob Hanson (FEMA Technical Advisor) for their input and guidance in the preparation of this report, Scott Schiff who assisted in ATC project management, and Carrie J. Perna who provided ATC report production services. The names and affiliations of all who contributed to this report, including those who participated in the review workshop focused on wood light frame systems, are provided in the list of Project Participants at the end of this report.

Justin Moresco
ATC Director of Projects

Jon A. Heintz
ATC Executive Director

Table of Contents

Foreword.....	iii
Preface.....	v
List of Figures.....	xi
List of Tables	xxv
1. Introduction	1-1
1.1 Background and Purpose.....	1-2
1.2 Approach and Scope.....	1-6
1.3 Organization and Content.....	1-11
2. Observed Response and Performance Benchmarks	2-1
2.1 Introduction	2-1
2.2 Significant Earthquakes and Sources of Data	2-2
2.2.1 U.S. Earthquakes (1964 - 2014)	2-2
2.2.2 World-Wide Earthquakes (1980 - 2014)	2-7
2.2.3 Building Records of Earthquake Response	2-7
2.3 Overview of Methods Used to Establish Benchmark Properties of Short-Period Wood Light-Frame Buildings.....	2-11
2.3.1 Benchmark Response Properties	2-11
2.3.2 Benchmark Performance Properties	2-11
2.3.3 Definitions and Relationship of Complete Structural Damage, Collapse, and Post-Earthquake Safety Evaluation Criteria	2-13
2.4 Measured Periods of Wood Light-Frame Buildings.....	2-21
2.5 Observed Damage and Collapse of Wood Light-Frame Buildings in the 1994 Northridge Earthquake.....	2-25
2.6 Observed Collapse Performance of Buildings in the 1995 Kobe Earthquake	2-36
2.7 Observed Performance of Full-Scale Wood Light-Frame Buildings in Shake Table Tests	2-46
2.7.1 Shake Table Tests of a Two-Story Japanese Home at the E-Defense Facility, Miki, Japan	2-46
2.7.2 Shake Table Tests of a Two-Story Townhouse at the Structural Engineering and Seismic Simulation Laboratory, University at Buffalo	2-51
2.8 Summary of Key Findings and Benchmark Properties of Short-Period Wood Light-Frame Buildings	2-55
2.8.1 Key Findings	2-55
2.8.2 Response Behavior	2-56
2.8.3 Collapse Performance.....	2-57

3.	Development of Building Archetype Configurations and Designs.....	3-1
3.1	Introduction.....	3-1
3.2	Factors Influencing Building Response and Performance.....	3-1
3.2.1	Seismic Design Level	3-2
3.2.2	Building Age and Configuration	3-2
3.2.3	Structural Component Properties.....	3-3
3.2.4	Architectural and Nonstructural Components and Finishes.....	3-4
3.2.5	Site Class and Foundation	3-5
3.2.6	Design and Construction Practice.....	3-5
3.3	Building Types and Occupancies for Development of Archetypes	3-6
3.3.1	FEMA Model Building Types	3-6
3.3.2	Commercial Buildings	3-7
3.3.3	Multi-Family Dwellings	3-7
3.3.4	Single-Family Dwellings	3-8
3.4	Archetype Design Criteria and Representative Configurations	3-8
3.4.1	Gravity Loads	3-8
3.4.2	Seismic Loads.....	3-9
3.4.3	Foundation Design Criteria.....	3-10
3.4.4	Design Approach	3-10
3.4.5	Representative Archetype Configurations	3-11
3.5	Commercial Buildings	3-13
3.6	Multi-Family Dwelling Buildings	3-16
3.7	Single-Family Dwelling Buildings	3-22
4.	Numerical Modeling for Parametric Studies	4-1
4.1	Modeling Methods.....	4-1
4.1.1	Overview of <i>Timber3D</i>	4-1
4.1.2	Typical <i>Timber3D</i> Models.....	4-2
4.1.3	Nonlinear Wall Building Blocks	4-3
4.1.4	Building Block Nonlinear Component Properties	4-6
4.2	Overview of Parametric Studies and Variations in Archetypes	4-18
4.3	Baseline Configuration Parametric Study.....	4-22
4.4	Collapse Displacement Capacity Parametric Study.....	4-23
4.5	Nonstructural Interior and Exterior Wall Finishes Parametric Study.....	4-24
4.6	Soil-Structure Interaction and Foundation Flexibility Parametric Study.....	4-24
4.6.1	Details of Modeling for SSI and Foundation Flexibility.....	4-24
4.7	Backbone Curve Shape Parametric Study	4-29
4.7.1	Details of Modeling Backbone Curve Shape.....	4-29
4.8	Analysis Methods	4-32
4.8.1	Overview	4-32
4.8.2	Free Vibration Analyses	4-32
4.8.3	Nonlinear Static Pushover Analyses.....	4-32
4.8.4	Incremental Dynamic Analyses and Collapse Evaluation.....	4-33
4.8.5	Peak Response Calculations	4-38

5.	Numerical Results of Parametric Studies	5-1
5.1	Overview	5-1
5.2	Baseline Configuration Parametric Study	5-3
5.2.1	Baseline Configuration Archetypes and Variants	5-4
5.2.2	Numerical Results	5-4
5.2.3	Interpretation of Results	5-15
5.3	Collapse Displacement Capacity Parametric Study	5-19
5.3.1	Collapse Displacement Capacity Archetypes and Variants	5-19
5.3.2	Numerical Results	5-22
5.3.3	Interpretation of Results	5-38
5.4	Nonstructural Interior and Exterior Wall Finishes Parametric Study	5-41
5.4.1	Nonstructural Interior and Exterior Wall Finish Archetypes and Variants	5-42
5.4.2	Numerical Results	5-43
5.4.3	Interpretation of Results	5-51
5.5	Soil-Structure Interaction and Foundation Flexibility Parametric Study	5-52
5.5.1	Soil-Structure Interaction and Foundation Flexibility Archetypes and Variants	5-53
5.5.2	Numerical Results	5-54
5.5.3	Interpretation of Results	5-61
5.6	Backbone Curve Shape Parametric Study	5-65
5.6.1	Backbone Curve Shape Archetypes and Variants	5-65
5.6.2	Numerical Results	5-66
5.6.3	Interpretation of Results	5-74
5.7	Overarching Findings on Parametric Studies	5-75
6.	Findings, Conclusions, and Recommendations	6-1
6.1	Introduction	6-1
6.2	Key Findings of the Parametric Studies	6-1
6.2.1	Baseline Configuration Study	6-2
6.2.2	Collapse Displacement Capacity Parametric Study	6-10
6.2.3	Nonstructural Interior and Exterior Wall Finishes Parametric Study	6-14
6.2.4	Soil-Structure Interaction and Foundation Flexibility Parametric Study	6-16
6.2.5	Backbone Curve Shape Parametric Study	6-18
6.3	Conclusions and Recommendations	6-21
6.3.1	Comparison with Prior FEMA P-695 Collapse Studies	6-22
6.3.2	Recommendations for Improved Seismic Design Codes and Standards	6-25
6.3.3	Recommendations for Advanced Seismic Design and Analysis Practices	6-29
6.3.4	Recommendations for Enhanced Modeling and Testing	6-31
Appendix A:	Archetype Design Criteria and Details.....	A-1
A.1	Introduction	A-1
A.2	Design of Wood Light-Frame Archetypes	A-1

A.2.1	Structural Properties for Engineered Designs.....	A-2
A.2.2	Wall Locations and Configurations	A-4
A.3	Commercial Building Shear Wall Designs.....	A-5
A.4	Multi-Family Dwelling Shear Wall Designs	A-9
A.4.1	One-Story Multi-Family Dwelling Shear Walls.....	A-10
A.4.2	Two-Story Multi-Family Dwelling Shear Walls	A-13
A.4.3	Four-Story Multi-Family Dwelling Shear Walls	A-17
A.5	Single-Family Dwelling Engineered Shear Wall Designs....	A-25
A.6	Single-Family Dwelling Conventional Construction Shear Wall Designs.....	A-33
A.7	Foundation Designs for Wood Light-Frame Building Archetypes	A-35
Appendix B: Archive of Peak Response Calculations.....		B-1
B.1	Peak Response Calculations from Parametric Studies.....	B-1
B.2	Peak Response Calculations from the Study on Effect of Viscous Damping.....	B-1
B.3	Response Parameters Archived for Each Model	B-1
Appendix C: Effect of Viscous Damping on Collapse Performance of Wood Light-Frame Archetypes		C-1
C.1	Introduction.....	C-1
C.2	Equation of Motion and Damping Model.....	C-1
C.2.1	Rayleigh Damping Model.....	C-2
C.2.2	Variation of Damping Ratios with Natural Periods	C-3
C.3	Sensitivity Study on Addition of Viscous Damping.....	C-4
C.3.1	Modal and Pushover Analyses.....	C-4
C.3.2	Incremental Dynamic Analyses	C-5
C.4	Discussion.....	C-6
Appendix D: Validation Study		D-1
D.1	Introduction.....	D-1
D.2	Measured Response Behavior in the 2003 San Simeon Earthquake	D-1
D.3	Validation of Numerical Modeling.....	D-7
D.3.1	Modeling and Scope	D-7
D.3.2	Main Findings – Model 1	D-8
D.3.3	Main Findings – Model 2	D-10
D.3.4	Summary of Findings	D-13
References		E-1
Project Participants.....		F-1

List of Figures

Figure 1-1	Trends in the probability of collapse of selected systems as a function of design period	1-4
Figure 2-1	Collapse of URM buildings in the 1983 Coalinga earthquake (top left), the 1987 Whittier earthquake (top right), and the 1987 Loma Prieta earthquake (bottom).....	2-5
Figure 2-2	Collapse of non-ductile concrete frame buildings at the Veterans Administration (VA) complex in the 1971 San Fernando earthquake.....	2-5
Figure 2-3	Collapse of the first floor of the two-story Community Mental Health Building (upper right) and severe damage to the five-story main building at the Olive View Hospital in the 1971 San Fernando earthquake	2-6
Figure 2-4	Collapse of soft-story wood light-frame multi-family dwellings in the 1987 Loma Prieta earthquake (left) and 1994 Northridge earthquake (right)	2-6
Figure 2-5	Average building period as a function of building height, obtained from CSMIP earthquake data, forced vibration tests, or full-scale shake table tests.....	2-25
Figure 2-6	Red-tag percentages of Table 2-12, plotted as function of 0.3-second spectral acceleration along with two notional collapse fragility curves assumed to be lognormally distributed with plausible values of median collapse and lognormal standard deviation (β)	2-27
Figure 2-7	Individual values of 0.3-second spectral accelerations for each of the 308 census tracts in the MMI 8 region of the 1994 Northridge earthquake based on: (1) Shake Map data, maximum direction; (2) Shake Map data, mean direction (taken as 0.75 of maximum); and (3) Somerville map data.....	2-28
Figure 2-8	Red-tag percentages as a function of 0.3-second spectral acceleration developed from post-earthquake safety inspections of 24,710 post-1960 wood light-frame buildings following the 1994 Northridge earthquake, along with a lognormal best fit collapse fragility curve based on census-tract group red-tag percentages, and a theoretical collapse curve for newer W1 buildings developed by the ATC-71-6 Project	2-32

Figure 2-9	View of Kobe City looking northwest from Osaka Bay	2-37
Figure 2-10	Southern portion of Hyogo Prefecture and neighboring areas of the Osaka Prefecture, showing Kobe City and other nearby cities of the region affected by the 1995 Kobe earthquake.....	2-37
Figure 2-11	Typical street scene in Kobe City immediately after the earthquake; damage at a ferry terminal due to ground failure (liquefaction); and a neighborhood destroyed by fire	2-38
Figure 2-12	Partial first-story collapse of a two-story house with a heavy tile roof in Nishinomiya after the 1995 Kobe earthquake	2-40
Figure 2-13	Severe leaning and incipient collapse of a two-story mixed-use building in Kobe City	2-41
Figure 2-14	First-story and second-story plan views of the E-Defense test building.....	2-47
Figure 2-15	Test building on the E-Defense shake table prior to testing, showing views of the front (left) and back (right) of the test building.....	2-47
Figure 2-16	Observed story drift in the three sequential collapse tests using the JR Takatori shake	2-49
Figure 2-17	Severe first-story damage and leaning of the test building after the second JR Takatori shake	2-50
Figure 2-18	Collapsed test building after the third JR Takatori shake.....	2-50
Figure 2-19	Plan views of the upper-level and lower-level floors of the CUREE-Caltech Woodframe Project test building, and summary of structural details	2-52
Figure 2-20	CUREE-Caltech Woodframe Project test building on the SEESL shake tables: Test Phase 1 (SFRS only) configuration (top); and Test Phase 5 (SFRS with interior gypsum board and exterior stucco finishes) configuration (bottom)	2-53
Figure 3-1	Isometric rendering of a one-story commercial building archetype	3-14
Figure 3-2	Typical floor and roof framing plan for a two-story commercial building archetype, showing diaphragm sheathing and locations of perimeter shear walls.....	3-15

Figure 3-3	Typical longitudinal wall elevation for one-story commercial building archetypes	3-15
Figure 3-4	Typical longitudinal wall elevation for two-story commercial building archetypes (four-story similar).....	3-15
Figure 3-5	Typical interior partition plan for two-story and four-story commercial building archetypes	3-16
Figure 3-6	Isometric rendering of a two-story multi-family dwelling archetype.....	3-17
Figure 3-7	Typical floor and roof framing plan for a two-story multi-family dwelling archetype, showing diaphragm sheathing and locations of perimeter and interior shear walls.....	3-17
Figure 3-8	Typical floor and roof framing plan for a four-story multi-family dwelling archetype, showing diaphragm sheathing and locations of perimeter and interior shear walls (one-story similar)	3-18
Figure 3-9	Typical transverse section of a four-story multi-family dwelling archetype showing double-loaded corridor walls.....	3-19
Figure 3-10	Typical longitudinal wall elevation for two-story multi-family dwelling archetypes	3-20
Figure 3-11	Typical longitudinal wall elevation for four-story multi-family dwelling archetypes	3-20
Figure 3-12	Typical interior partition plan for two-story multi-family dwelling archetypes	3-21
Figure 3-13	Typical interior partition plan for one-story multi-family dwelling archetypes, or the fourth floor (top story) of four-story multi-family dwelling archetypes	3-21
Figure 3-14	Typical interior partition plan for the first, second, and third floors of four-story multi-family dwelling archetypes	3-22
Figure 3-15	Isometric rendering of a two-story single-family dwelling archetype.....	3-22
Figure 3-16	Typical floor framing plan for two-story single-family dwelling archetypes, showing diaphragm sheathing and locations of perimeter and interior shear walls	3-23
Figure 3-17	Typical roof framing plan for two-story single-family dwelling archetypes, showing diaphragm sheathing and locations of perimeter and interior shear walls	3-23

Figure 3-18	Typical longitudinal wall elevation for two-story single-family dwelling archetypes (one-story similar).....	3-24
Figure 3-19	Typical transverse wall elevation for two-story single-family dwelling archetypes (one-story similar).....	3-24
Figure 3-20	Typical interior partition plan for one-story multi-family dwelling archetypes, or the second floor (top story) of two-story multi-family dwelling archetypes	3-25
Figure 3-21	Typical interior partition plan for the first floor of two-story single-family dwelling archetypes	3-25
Figure 4-1	Schematic illustration of a three-dimensional, one-story <i>Timber3D</i> model	4-3
Figure 4-2	CUREE hysteretic rule for modeling force-displacement response of wood light-frame shear walls under cyclic loading.....	4-4
Figure 4-3	Modification of the CUREE hysteretic rule for modeling residual strength	4-5
Figure 4-4	Schematic illustration of a wall building block.....	4-6
Figure 4-5	Simplified backbone curve data for gypsum wallboard with superimposed building block curve for minimum gypsum wallboard and nonstructural gypsum wallboard (red line).....	4-10
Figure 4-6	Simplified backbone curve data for stucco with superimposed building block curve for stucco (red line).....	4-11
Figure 4-7	Backbone curves for 8-foot wide by 10-foot high wall building blocks.....	4-12
Figure 4-8	Backbone curves for 4-foot wide by 10-foot high wall building blocks.....	4-13
Figure 4-9	Backbone curves for 8-foot wide by 10-foot high wall building block combinations	4-15
Figure 4-10	Backbone curves for 4-foot wide by 10-foot high wall building block combinations	4-15
Figure 4-11	Schematic illustration of nonlinear soil spring modeling.....	4-25
Figure 4-12	SSI and foundation flexibility model for the four-story multi-family dwelling archetype model, showing locations of soil springs.....	4-28

Figure 4-13	Force-displacement properties for soil spring models: horizontal direction (left); and vertical direction (right)	4-28
Figure 4-14	Backbone curve models for 8-foot wide by 10-foot high OSB-High building blocks with 30-percent residual strength.....	4-30
Figure 4-15	Acceleration response spectra for the FEMA P-695 far field ground motions scaled to the MCE _R hazard level for regions of high seismicity	4-33
Figure 4-16	IDA curves and probability density functions (PDFs) of peak roof drift and S_{MT} at incipient collapse for the baseline one-story commercial building archetype model (COM1B)	4-36
Figure 4-17	Illustration of IDA results (collapse fractions) and FEMA P-695 collapse fragility, based on median collapse $\hat{S}_{CT} = 3.1g$, derived from the IDA results and an assumed lognormal standard deviation of $\beta_{TOT} = 0.5$, for the baseline one-story commercial archetype model (COM1B).....	4-37
Figure 5-1	Undeformed shape and three mode shapes for the baseline four-story commercial building archetype model (COM3B).....	5-5
Figure 5-2	Pushover curves for baseline commercial building archetype models (top), and pushover curves normalized by total building seismic weight and roof height (bottom)	5-6
Figure 5-3	Pushover curves for baseline multi-family dwelling archetype models (top), and pushover curves normalized by total building seismic weight and roof height (bottom)	5-7
Figure 5-4	Pushover curves for baseline single-family dwelling archetype models (top), and pushover curves normalized by total building seismic weight and roof height (bottom)	5-8
Figure 5-5	Collapse rates from IDA and FEMA P-695 collapse fragility curves for baseline commercial building archetype models	5-10
Figure 5-6	Collapse rates from IDA and FEMA P-695 collapse fragility curves for baseline multi-family dwelling archetype models	5-11

Figure 5-7	Collapse rates from IDA and FEMA P-695 collapse fragility curves for baseline single-family dwelling archetype models.....	5-11
Figure 5-8	MCE_R collapse probability versus peak strength ratio (V_{max} / W) for baseline archetype models	5-16
Figure 5-9	MCE_R collapse probabilities for baseline archetype models located in high seismic (HS) and very high seismic (VHS) regions	5-16
Figure 5-10	Relative strength contributions of structural and nonstructural wall finishes for baseline archetype models located in high seismic (HS) and very high seismic (VHS) regions	5-17
Figure 5-11	MCE_R collapse probability versus fundamental period (T_I) for baseline archetype models.....	5-18
Figure 5-12	Pushover curves for one-story commercial building archetype models in collapse displacement capacity studies (top), and pushover curves normalized by total building seismic weight and roof height (bottom)	5-23
Figure 5-13	Pushover curves for two-story commercial building archetype models in collapse displacement capacity studies (top), and pushover curves normalized by total building seismic weight and roof height (bottom)	5-24
Figure 5-14	Pushover curves for one-story multi-family dwelling archetype models in collapse displacement capacity studies (top), and pushover curves normalized by total building seismic weight and roof height (bottom)	5-25
Figure 5-15	Pushover curves for two-story multi-family dwelling archetype models in collapse displacement capacity studies (top), and pushover curves normalized by total building seismic weight and roof height (bottom)	5-26
Figure 5-16	Pushover curves for one-story single-family dwelling archetype models in collapse displacement capacity studies (top), and pushover curves normalized by total building seismic weight and roof height (bottom)	5-27
Figure 5-17	Pushover curves for two-story single-family dwelling archetype models in collapse displacement capacity studies (top), and pushover curves normalized by total building seismic weight and roof height (bottom)	5-28
Figure 5-18	Collapse rates from IDA and FEMA P-695 collapse fragility curves for one-story commercial building	

archetype models in collapse displacement capacity studies	5-31
Figure 5-19 Collapse rates from IDA and FEMA P-695 collapse fragility curves for two-story commercial building archetype models in collapse displacement capacity studies	5-32
Figure 5-20 Collapse rates from IDA and FEMA P-695 collapse fragility curves for one-story multi-family dwelling archetype models in collapse displacement capacity studies	5-32
Figure 5-21 Collapse rates from IDA and FEMA P-695 collapse fragility curves for two-story multi-family dwelling archetype models in collapse displacement capacity studies	5-33
Figure 5-22 Collapse rates from IDA and FEMA P-695 collapse fragility curves for one-story single-family dwelling archetype models in collapse displacement capacity studies	5-33
Figure 5-23 Collapse rates from IDA and FEMA P-695 collapse fragility curves for two-story single-family dwelling archetype models in collapse displacement capacity studies	5-34
Figure 5-24 IDA curves and incipient collapse points for two-story single-family wood light-frame building archetype models: 30 percent residual strength (top); and 0 percent residual strength (bottom)	5-39
Figure 5-25 Median first-story drift at incipient collapse versus residual strength ratio for archetype models used in collapse displacement capacity studies.....	5-40
Figure 5-26 MCE _R collapse probability versus residual strength ratio for archetype models used in collapse displacement capacity studies	5-40
Figure 5-27 MCE _R collapse probability versus median first-story drift at incipient collapse for archetype models used in collapse displacement capacity studies.....	5-41
Figure 5-28 Pushover curves for two-story commercial building archetype models in nonstructural interior and exterior wall finish studies (top), and pushover curves normalized by total building seismic weight and roof height (bottom)	5-44

Figure 5-29	Pushover curves for two-story multi-family dwelling archetype models in nonstructural interior and exterior wall finish studies (top), and pushover curves normalized by total building seismic weight and roof height (bottom).....	5-45
Figure 5-30	Collapse rates from IDA and FEMA P-695 collapse fragility curves for two-story commercial building archetype models in nonstructural interior and exterior wall finish studies.....	5-47
Figure 5-31	Collapse rates from IDA and FEMA P-695 collapse fragility curves for two-story multi-family dwelling archetype models in nonstructural interior and exterior wall finish studies.....	5-47
Figure 5-32	Collapse rates from IDA and FEMA P-695 collapse fragility curves for engineered one-story single-family dwelling archetype models in nonstructural interior and exterior wall finish studies	5-48
Figure 5-33	Collapse rates from IDA and FEMA P-695 collapse fragility curves for conventional construction one-story single-family dwelling archetype models in nonstructural interior and exterior wall finish studies.....	5-48
Figure 5-34	MCE_R collapse probability versus peak strength ratio (V_{max} / W) for archetype models used in nonstructural interior and exterior wall finish studies.....	5-52
Figure 5-35	Pushover curves for commercial building archetypes in SSI and foundation flexibility studies (top), and pushover curves normalized by total building seismic weight and roof height (bottom).....	5-55
Figure 5-36	Pushover curves for multi-family dwelling archetypes in SSI and foundation flexibility studies (top), and pushover curves normalized by total building seismic weight and roof height (bottom).....	5-56
Figure 5-37	Collapse rates from IDA and FEMA P-695 collapse fragility curves for commercial building archetypes in SSI and foundation flexibility studies	5-58
Figure 5-38	Collapse rates from IDA and FEMA P-695 collapse fragility curves for multi-family dwelling archetypes in SSI and foundation flexibility studies	5-58
Figure 5-39	Maximum foundation stresses in the COM1B-F-DE archetype model subjected to the Northridge Beverly Hills ground motion scaled to $S_T = 1.9g$	5-63

Figure 5-40	Distribution of soil spring vertical forces in the MFD3B-F-DE archetype model under gravity load (top); and at peak strength in the X-direction pushover (middle); and deformed shaped of model in the X-direction pushover (bottom)	5-64
Figure 5-41	Pushover curves for commercial building archetypes with 30-percent residual strength in backbone curve shape studies (top), and pushover curves normalized by total building seismic weight and roof height (bottom)	5-67
Figure 5-42	Pushover curves for commercial building archetypes with 0-percent residual strength in backbone curve shape studies (top), and pushover curves normalized by total building seismic weight and roof height (bottom)	5-68
Figure 5-43	Pushover curves for commercial building archetypes with 60-percent residual strength in backbone curve shape studies (top), and pushover curves normalized by total building seismic weight and roof height (bottom)	5-69
Figure 5-44	Collapse rates from IDA and FEMA P-695 collapse fragility curves for commercial building archetype models with R1 backbone parameters used in backbone curve shape studies	5-71
Figure 5-45	Collapse rates from IDA and FEMA P-695 collapse fragility curves for commercial building archetype models with R2 backbone parameters used in backbone curve shape studies	5-71
Figure 5-46	MCE_R collapse probability versus peak strength ratio (V_{max} / W) for commercial building archetype models used in backbone curve shape studies.....	5-75
Figure 5-47	MCE_R collapse probability versus peak strength ratio (V_{max} / W) for all wood light-frame building archetype models used in parametric studies	5-76
Figure 5-48	Three-dimensional plot of MCE_R collapse probability versus peak strength ratio (V_{max} / W) and residual strength ratio, for selected wood light-frame building archetype models used in parametric studies.....	5-76
Figure 6-1	Fundamental-mode periods (T_1) of baseline archetype models, measured periods of wood light-frame buildings obtained from earthquake records, forced-vibration testing, and shake table tests, and the approximate fundamental-period ($T = C_u T_a$) from ASCE/SEI 7-10	6-4

Figure 6-2	MCE _R collapse probability versus average model period (T_1), including benchmark (BM) collapse probabilities from historical earthquake data (Chapter 2) and ASCE/SEI 7-10, for high seismic baseline archetype models	6-5
Figure 6-3	MCE _R collapse probability versus archetype model overstrength (Ω), including benchmark (BM) collapse probabilities from historical earthquake data (Chapter 2) and ASCE/SEI 7-10, for high seismic baseline archetype models	6-6
Figure 6-4	MCE _R collapse probability versus average model period (T_1), including the benchmark collapse probability from ASCE/SEI 7-10, for very high seismic baseline archetype models.....	6-7
Figure 6-5	MCE _R collapse probability versus archetype model overstrength (Ω), including the benchmark collapse probability from ASCE/SEI 7-10, for very high seismic baseline archetype models.....	6-7
Figure 6-6	MCE _R collapse probability versus first story median drift ratio at incipient collapse, including benchmark (BM) collapse probabilities from historical earthquake data (Chapter 2) and ASCE/SEI 7-10, for two-story archetype models used in the displacement capacity parametric study	6-12
Figure 6-7	MCE _R collapse probability versus first story median drift ratio at incipient collapse, including benchmark (BM) collapse probabilities from historical earthquake data (Chapter 2) and ASCE/SEI 7-10, for one-story archetype models used in the displacement capacity parametric study	6-13
Figure 6-8	MCE _R collapse probability versus archetype model overstrength (Ω), including benchmark (BM) collapse probabilities from historical earthquake data (Chapter 2) and ASCE/SEI 7-10, for archetype models used in the nonstructural wall finishes parametric study.....	6-16
Figure 6-9	MCE _R collapse probability versus archetype model overstrength (Ω), including benchmark (BM) collapse probabilities from historical earthquake data (Chapter 2) and ASCE/SEI 7-10, for commercial building archetype models, with and without nonstructural wall finishes, used in the backbone curve shape parametric study.....	6-20

Figure 6-10	MCE _R collapse probability versus first story median drift ratio at incipient collapse, including benchmark (BM) collapse probabilities from historical earthquake data (Chapter 2) and ASCE/SEI 7-10, for commercial building archetype models, with and without nonstructural wall finishes, used in the backbone curve shape parametric study.....	6-20
Figure 6-11	Comparison of MCE _R collapse probabilities for six COM, MFD and SFD archetypes without nonstructural wall finishes (WFs) from this study with eight PG-1 and PG-9 archetypes from a prior FEMA P-695 study, including adjusted collapse probabilities for PG-9 archetypes assuming a lognormal standard deviation of $\beta_{TOT} = 0.5$	6-24
Figure 6-12	Three-dimensional plot of collapse probability as a function of normalized peak strength ratio (V_{max} / W) and displacement capacity in terms of median first-floor drift ratio at incipient collapse, for high seismic wood light frame building archetypes	6-30
Figure A-1	Typical plan showing perimeter shear wall locations in commercial building archetypes	A-5
Figure A-2	Typical plan showing perimeter and interior shear wall locations in one-story multi-family dwelling archetypes	A-10
Figure A-3	Typical plan showing perimeter and interior shear wall locations in two-story multi-family dwelling archetypes	A-14
Figure A-4	Typical plan showing perimeter and interior shear wall locations in four-story multi-family dwelling archetypes	A-18
Figure A-5	Typical plan showing perimeter and interior shear wall locations in one-story and two-story single-family dwelling archetypes	A-25
Figure A-6	Foundation plan for commercial building archetypes....	A-36
Figure A-7	Foundation plan for one-story and four-story multi-family dwelling archetypes	A-36
Figure A-8	Foundation plan for two-story multi-family dwelling archetypes	A-37
Figure A-9	Foundation plan for one-story and two-story single-family dwelling archetypes	A-37

Figure A-10	Section through a typical edge footing (thickened slab).....	A-38
Figure A-11	Section through a typical interior footing (thickened slab).....	A-38
Figure C-1	Variation of modal damping ratios with natural period for COM1B baseline model with 1-percent viscous damping assigned to both mode 1 and mode 2	C-3
Figure C-2	Collapse rates from IDA and FEMA P-695 collapse fragility curves for COM1B archetype models used to investigate the effects of viscous damping.....	C-6
Figure C-3	Variation of MCE _R collapse probability with equivalent viscous damping for COM1B archetype models used to investigate the effects of viscous damping.....	C-7
Figure D-1	Templeton Hospital before the 2003 San Simeon earthquake; view looking southwest with north wing shown on the right.....	D-2
Figure D-2	Vertical elements of the SFRS of the north wing of the Templeton Hospital.....	D-2
Figure D-3	Location of nine channels of strong motion instrumentation in the Templeton Hospital.....	D-3
Figure D-4	East-west response of the north wing of the Templeton Hospital	D-4
Figure D-5	Roof response spectra of the north wing of the Templeton Hospital in the east-west direction.....	D-4
Figure D-6	Measured periods of the Templeton Hospital	D-6
Figure D-7	Measured viscous damping of the Templeton Hospital	D-6
Figure D-8	Pushover curves predicted by Model 1	D-8
Figure D-9	Natural periods and mode shapes predicted by Model 1	D-9
Figure D-10	Measured and predicted east-west response, Model 1, 2003 San Simeon earthquake ground motion.....	D-9
Figure D-11	Measured and predicted north-south response, Model 1, 2003 San Simeon earthquake ground motion.....	D-10
Figure D-12	Pushover curves predicted by Model 2	D-10
Figure D-13	Natural periods and mode shapes predicted by Model 2	D-11

- Figure D-14 Measured and predicted east-west response, Model 2,
2003 San Simeon earthquake ground motion D-12
- Figure D-15 Measured and predicted north-south response, Model 2,
2003 San Simeon earthquake ground motion D-12
- Figure D-16 Bi-directional IDA curves and collapse fragility of
the north wing of the Templeton Hospital predicted by
Model 2 D-13

List of Tables

Table 1-1	Key Configuration and Seismic-Design Criteria for Wood Light-Frame Archetypes	1-8
Table 2-1	Date, Magnitude, and Region Affected for Selected Large-Magnitude U.S. Earthquakes, 1964 - 2014	2-3
Table 2-2	Fatalities and Economic Losses for Selected Large-Magnitude U.S. Earthquakes, 1964 - 2014	2-4
Table 2-3	Economic Losses and Fatalities in the 10 Costliest Earthquakes and Tsunamis, 1980 - 2014	2-7
Table 2-4	CSMIP Record Sets of Short-Period Building Response, One-Story Buildings, in 86 Earthquakes	2-8
Table 2-5	CSMIP Record Sets of Short-Period Building Response, Two-Story Buildings, in 65 Earthquakes.....	2-9
Table 2-6	CSMIP Record Sets of Short-Period Building Response, Three-Story Buildings, in 91 Earthquakes.....	2-10
Table 2-7	Notional Relationship between Complete Structural Damage and Collapse for a Hypothetical Three-Story Wood Light-Frame Building.....	2-18
Table 2-8	Probability of Complete Structural Damage Required to Meet the 10-Percent Collapse Safety Goal of ASCE/SEI 7-10 for MCE _R Ground Motions Using the Hypothetical Three-Story Wood Light-Frame Building Example of Table 2-7	2-19
Table 2-9	Probability of Complete Structural Damage Required to Meet the Approximate One-Percent Collapse Safety Goal of the 2007 CBC OSHPD Regulations for DE Ground Motions Using the Hypothetical Three-Story Wood Light-Frame Building Example of Table 2-7.....	2-20
Table 2-10	Parameters of 12 Short-Period Wood Light-Frame Buildings with Measured Values of Building Period, Obtained from CSMIP Earthquake Data, Forced Vibration Tests, or Full-Scale Shake Table Tests.....	2-22

Table 2-11	Measured Values of Peak Response and Building Period for 12 Short-Period Wood Light-Frame Buildings, Obtained from CSMIP Earthquake Data, Forced Vibration Tests, or Full-Scale Shake Table Tests	2-24
Table 2-12	Safety Assessment Tagging Data and Damage Statistics by MMI Region for Wood Buildings Inspected after the 1994 Northridge Earthquake	2-27
Table 2-13	Census Tracts with Building Safety Inspections after the 1994 Northridge Earthquake, the Total Number of Wood Light-Frame Buildings Inspected, the Number of Wood Light-Frame Buildings Assigned Red Tags, and the Inventory of All Wood Light-Frame Buildings (W1 and W2) in these Census Tracts.....	2-29
Table 2-14	Total Number (Count) of Wood Light-Frame Buildings Inspected, Number of Wood Light-Frame Buildings Assigned Red Tags, Red-Tag Percentage, and Mean Value of 0.3-Second Spectral Acceleration for Each of 22 Census-Tract Groups of Approximately Equal Building Count from the 1994 Northridge Earthquake....	2-31
Table 2-15	One-Story and Two-Story (or More) Post-1960 Wood Light-Frame Buildings with Red, Yellow, or Green Tags, and Corresponding Fractions of One-Story and Two-Story (or More) Buildings with Red, Yellow, or Green Tags from the 1994 Northridge Earthquake.....	2-33
Table 2-16	Approximate Populations and Estimated Number of Buildings in Areas Affected by the 1995 Kobe Earthquake.....	2-38
Table 2-17	Collapse Damage, Severe Damage, or Fire Damage of Buildings Affected by the 1995 Kobe Earthquake.....	2-39
Table 2-18	Buildings with Collapse Damage or Severe Damage in All Areas Affected by the 1995 Kobe Earthquake, and the Number of Buildings with Collapse or Severe Damage Located in Areas within 5 km of Fault Rupture	2-39
Table 2-19	Building Population and Damage Data Due to the 1995 Kobe Earthquake, in the Nada Ward of Kobe City and Nishinomiya City, and Related Values of Median and Lognormal Standard Deviation Parameters of Empirical Vulnerability (Fragility) Functions for Heavy Damage to Wood-Frame Buildings, and Example Values of the Probability of Heavy Damage to Wood-Frame Buildings, Given Values of Short-Period Spectral Acceleration for Hypothetical Values of the Lognormal Standard Deviation Parameter	2-43

Table 2-20	Construction Details for the E-Defense Test Building	2-48
Table 2-21	Schedule of Shake Table Tests	2-49
Table 2-22	Test Phases, Building Configurations, and Seismic Testing Levels.....	2-54
Table 2-23	Ground Motions and Approximate Hazard Levels Used for Seismic Testing	2-54
Table 3-1	FEMA Model Building Types	3-6
Table 3-2	Gravity Loads Used for Design of Wood Light-Frame Commercial Building (COM), Multi-Family Dwelling (MFD) and Single-Family Dwelling (SFD) Archetypes	3-9
Table 3-3	Seismic Design Criteria Used for Design of Commercial Building (COM), Multi-Family Dwelling (MFD) and Single-Family Dwelling (SFD) Archetypes.....	3-9
Table 3-4	Wall Sheathing Used in Wood Light-Frame Building Archetypes	3-11
Table 3-5	Short-Period Wood Light-Frame Building Archetype Configurations and Seismic Design Criteria.....	3-12
Table 3-6	Nonstructural Interior Wall Types and Labels.....	3-16
Table 4-1	Parameters of the CUREE Hysteretic Rule	4-4
Table 4-2	Individual Wall Building Blocks	4-7
Table 4-3	Best Estimate Properties of Simplified Backbone Curves Shown in Figure 4-5	4-8
Table 4-4	Best Estimate Properties of Backbone Curves and Values of These Parameters Based on Test Data Published in FEMA P-795	4-9
Table 4-5	CUREE Hysteretic Parameters for 8-foot Wide by 10-foot High Wall Building Blocks.....	4-11
Table 4-6	CUREE Hysteretic Parameters for 4-foot Wide by 10-foot High Wall Building Blocks	4-12
Table 4-7	Wall Building Block Combinations.....	4-14
Table 4-8	Characteristic Response Parameters for Wall Building Blocks	4-16
Table 4-9	FEMA P-795 Characteristic Response Parameters for Wall Building Block Combinations.....	4-17

Table 4-10	Baseline and Variant Numerical Models for Commercial Building Archetypes in Five Parametric Studies	4-19
Table 4-11	Baseline and Variant Numerical Models for Multi-Family Dwelling Archetypes in Five Parametric Studies.....	4-19
Table 4-12	Baseline and Variant Numerical Models for Single-Family Dwelling Archetypes in Five Parametric Studies.....	4-20
Table 4-13	Baseline Commercial Building Archetypes, Key Configuration and Seismic Design Criteria	4-21
Table 4-14	Baseline Multi-Family Dwelling Archetypes, Key Configuration and Seismic Design Criteria	4-21
Table 4-15	Baseline Single-Family Dwelling Archetypes, Key Configuration and Seismic Design Criteria	4-22
Table 4-16	Physical Properties of Nonlinear Soil Springs	4-27
Table 4-17	Hysteresis Parameters for Wood Structural Panel Shear Wall Building Blocks Used to Investigate Backbone Curve Shape	4-31
Table 4-18	Description of Response Parameters Archived for Each Orthogonal Direction (EW and NS) for Numerical Models of Wood Light-Frame Archetypes	4-38
Table 5-1	Modal and Pushover Analysis Results for Baseline Archetype Models in the North-South and East-West Directions of Response.....	5-9
Table 5-2	Pushover and Collapse Analysis Results for Baseline Archetype Models	5-12
Table 5-3	Median and Lognormal Standard Deviation Values of Peak Drift Ratio and Response Spectral Acceleration at Incipient Collapse for Baseline Archetype Models.....	5-13
Table 5-4	Collapse Rates and Mean Peak First-Story Drift Ratios for Baseline Archetype Models at MCE _R and 50-Percent of MCE _R Ground Motion Intensities.....	5-14
Table 5-5	Commercial Building Archetype Models Used to Investigate Collapse Displacement Capacity	5-20
Table 5-6	Multi-Family Dwelling Archetype Models Used to Investigate Collapse Displacement Capacity	5-21
Table 5-7	Single-Family Dwelling Archetype Models Used to Investigate Collapse Displacement Capacity	5-22

Table 5-8	Modal and Pushover Analysis Results for Commercial Building Archetype Models Used to Investigate Collapse Displacement Capacity	5-29
Table 5-9	Modal and Pushover Analysis Results for Multi-Family Dwelling Archetype Models Used to Investigate Collapse Displacement Capacity	5-30
Table 5-10	Modal and Pushover Analysis Results for Single-Family Dwelling Archetype Models Used to Investigate Collapse Displacement Capacity	5-30
Table 5-11	Pushover and Collapse Analysis Results for Archetype Models Used to Investigate Collapse Displacement Capacity	5-35
Table 5-12	Median and Lognormal Standard Deviation Values of Peak Drift Ratio and Response Spectral Acceleration at Incipient Collapse for Archetype Models Used to Investigate Collapse Displacement Capacity	5-36
Table 5-13	Collapse Rates and Mean Peak First-Story Drift Ratios at MCE _R and 50-Percent of MCE _R Ground Motion Intensities for Archetype Models Used to Investigate Collapse Displacement Capacity	5-37
Table 5-14	Commercial Building, Multi-Family Dwelling, and Single-Family Dwelling Archetype Models Used to Investigate Nonstructural Interior and Exterior Wall Finishes	5-42
Table 5-15	Modal and Pushover Analysis Results for Archetype Models Used to Investigate Nonstructural Interior and Exterior Wall Finishes	5-46
Table 5-16	Pushover and Collapse Analysis Results for Archetype Models Used to Investigate Nonstructural Interior and Exterior Wall Finishes	5-49
Table 5-17	Median and Lognormal Standard Deviation Values of Peak Drift Ratio and Response Spectral Acceleration at Incipient Collapse for Archetype Models Used to Investigate Nonstructural Interior and Exterior Wall Finishes	5-50
Table 5-18	Collapse Rates and Mean Peak First-Story Drift Ratios at MCE _R and 50-Percent of MCE _R Ground Motion Intensities for Archetype Models Used to Investigate Nonstructural Interior and Exterior Wall Finishes.....	5-51

Table 5-19	Commercial Building and Multi-Family Dwelling Archetype Models Used to Investigate SSI and Foundation Flexibility.....	5-53
Table 5-20	Modal and Pushover Analysis Results for Archetype Models Used to Investigate SSI and Foundation Flexibility	5-57
Table 5-21	Pushover and Collapse Analysis Results for Archetype Models Used to Investigate SSI and Foundation Flexibility	5-59
Table 5-22	Median and Lognormal Standard Deviation Values of Peak Drift Ratio and Response Spectral Acceleration at Incipient Collapse for Archetype Models Used to Investigate SSI and Foundation Flexibility	5-60
Table 5-23	Collapse Rates and Mean Peak First-Story Drift Ratios at MCE _R and 50-Percent of MCE _R Ground Motion Intensities for Archetype Models Used to Investigate SSI and Foundation Flexibility	5-61
Table 5-24	Commercial Building Archetype Models Used to Investigate Backbone Curve Shape.....	5-65
Table 5-25	Modal Pushover Analysis Results for Commercial Building Archetype Models Used to Investigate Backbone Curve Shape	5-70
Table 5-26	Pushover and Collapse Analysis Results for Commercial Building Archetype Models Used to Investigate Backbone Curve Shape.....	5-72
Table 5-27	Median and Lognormal Standard Deviation Values of Peak Drift Ratio and Response Spectral Acceleration at Incipient Collapse for Commercial Building Archetype Models Used to Investigate Backbone Curve Shape.....	5-73
Table 5-28	Collapse Rates and Mean Peak First-Story Drift Ratios at MCE _R and 50-Percent of MCE _R Ground Motion Intensities for Commercial Building Archetype Models Used to Investigate Backbone Curve Shape.....	5-74
Table 6-1	Summary of Key Properties and Collapse Results for High-Seismic and Very High-Seismic Baseline Archetype Models	6-3
Table 6-2	Summary of Key Properties and Collapse Results for Archetype Models used in the Displacement Capacity Parametric Study	6-11

Table 6-3	Summary of Key Properties and Collapse Results for Archetype Models used in the Nonstructural Wall Finishes Parametric Study.....	6-15
Table 6-4	Summary of Key Properties and Collapse Results for Archetype Models used in the Soil-Structure Interaction and Foundation Flexibility Parametric Study	6-17
Table 6-5	Summary of Key Properties and Collapse Results for Archetype Models used in the Backbone Curve Shape Parametric Study.....	6-19
Table 6-6	Summary of Key Properties and Collapse Results for High Seismic Archetype Models from Prior FEMA P-695 Studies on Wood Light-Frame Buildings.....	6-23
Table 6-7	Recommended Design Strength for Wood Light-Frame Buildings Designed for High Seismic or Very High Seismic Loads to Meet Specific MCE _R Collapse Objectives	6-31
Table A-1	Basic Design Criteria for Wood Light-Frame Archetypes	A-1
Table A-2	Description of Wall Types for Wood Light-Frame Archetypes	A-2
Table A-3	Wall Framing Properties for Wood Light-Frame Archetypes	A-3
Table A-4	Bottom Plate Fastening Schedule for Wood Light-Frame Archetypes	A-3
Table A-5	Hold-Downs and Straps for Two-Story and Four-Story for Wood Light-Frame Archetypes.....	A-4
Table A-6	General Design Information for Commercial Building Archetypes	A-6
Table A-7	Shear Wall Schedule for Commercial Building Archetypes	A-7
Table A-8	Hold-Down Schedule for One-Story and Two-Story Commercial Building Archetypes.....	A-8
Table A-9	Anchor Rod Tie-Down Schedule for Four-Story Commercial Building Archetypes.....	A-8
Table A-10	General Design Information for Multi-Family Dwelling Archetypes	A-9

Table A-11	Shear Wall and Hold-Down Schedule for the One-Story, Multi-Family Dwelling, High Seismic Archetype	A-11
Table A-12	Shear Wall and Hold-Down Schedule for the One-Story, Multi-Family Dwelling, Very High Seismic Archetype	A-12
Table A-13	Shear Wall and Hold-Down Schedule for the One-Story, Multi-Family Dwelling, Moderate Seismic Archetype	A-13
Table A-14	General Wall Properties for Two-Story Multi-Family Dwelling Archetypes.....	A-14
Table A-15	Shear Wall and Hold-Down Schedule for the Two-Story, Multi-Family Dwelling, High Seismic Archetype	A-15
Table A-16	Shear Wall and Hold-Down Schedule for the Two-Story, Multi-Family Dwelling, Very High Seismic Archetype	A-16
Table A-17	Shear Wall and Hold-Down Schedule for the Two-Story, Multi-Family Dwelling, Moderate Seismic Archetype	A-17
Table A-18	General Wall Properties for Four-Story Multi-Family Dwelling Archetypes.....	A-18
Table A-19	Shear Wall Schedule for the Four-Story, Multi-Family Dwelling, High Seismic Archetype.....	A-19
Table A-20	Shear Wall Schedule for the Four-Story, Multi-Family Dwelling, Very High Seismic Archetype.....	A-20
Table A-21	Shear Wall Schedule for the Four-Story, Multi-Family Dwelling, Moderate Seismic Archetype	A-21
Table A-22	Tie-Down Schedule for the Four-Story, Multi-Family Dwelling, High Seismic Archetype.....	A-22
Table A-23	Tie-Down Schedule for the Four-Story, Multi-Family Dwelling, Very High Seismic Archetype.....	A-23
Table A-24	Tie-Down Schedule for the Four-Story, Multi-Family Dwelling, Moderate Seismic Archetype	A-24
Table A-25	General Design Information for Engineered Single-Family Dwelling Archetypes	A-26

Table A-26	Shear Wall and Hold-Down Schedule for the Engineered, One-Story, Single-Family Dwelling, High Seismic Archetype	A-27
Table A-27	Shear Wall and Hold-Down Schedule for the Engineered, One-Story, Single-Family Dwelling, Very High Seismic Archetype	A-28
Table A-28	Shear Wall and Hold-Down Schedule for the Engineered, One-Story, Single-Family Dwelling, Moderate Seismic Archetype.....	A-29
Table A-29	Shear Wall and Hold-Down Schedule for the Engineered, Two-Story, Single-Family Dwelling, High Seismic Archetype	A-30
Table A-30	Shear Wall and Hold-Down Schedule for the Engineered, Two-Story, Single-Family Dwelling, Very High Seismic Archetype	A-31
Table A-31	Shear Wall and Hold-Down Schedule for the Engineered, Two-Story, Single-Family Dwelling, Moderate Seismic Archetype.....	A-32
Table A-32	General Design Information for Conventional Construction Single-Family Dwelling Archetypes	A-33
Table A-33	Wall Types for Conventional Construction Single-Family Dwelling Archetypes	A-33
Table A-34	Shear Wall Schedule for Conventional Construction, One-Story, Single-Family Dwelling, High and Very High Seismic Archetypes.....	A-34
Table A-35	Shear Wall Schedule for the Conventional Construction, Two-Story, Single-Family Dwelling, High Seismic Archetype	A-34
Table A-36	Foundation Schedule for Commercial Building Archetypes	A-38
Table A-37	Foundation Schedule for Multi-Family Dwelling High Seismic Archetypes.....	A-39
Table A-38	Foundation Schedule for Multi-Family Dwelling Very High Seismic Archetypes.....	A-39
Table A-39	Foundation Schedule for Multi-Family Dwelling Moderate Seismic Archetypes	A-40
Table A-40	Foundation Schedule for Single-Family Dwelling Archetypes	A-40

Table B-1	Parametric Studies and Peak Response Archiving Files for Numerical Models of Commercial Building Archetypes.....	B-2
Table B-2	Parametric Studies and Peak Response Archiving Files for Numerical Models of Multi-Family Dwelling Archetypes.....	B-3
Table B-3	Parametric Studies and Peak Response Archiving Files for Numerical Models of Single-Family Dwelling Archetypes.....	B-4
Table B-4	Properties and Peak Response Archiving Files for Equivalent Viscous Damping Study on Wood Light- Frame Archetypes	B-4
Table B-5	Description of Response Parameters Archived for Each Orthogonal Direction (EW and NS) for Numerical Models of Wood Light-Frame Archetypes	B-5
Table C-1	Design Criteria for the COM1B Wood Light-Frame Building Archetype Used to Investigate the Effects of Viscous Damping	C-5
Table C-2	Modal and FEMA P-795 Pushover Results for COM1B Archetype Models Used to Investigate the Effects of Viscous Damping	C-5
Table C-3	FEMA P-695 Pushover and Collapse Analysis Results for COM1B Archetype Models Used to Investigate the Effects of Viscous Damping	C-6

Chapter 1

Introduction

This report describes the approach, analyses, findings, conclusions, and recommendation for one in a series of studies on the gap between analytically predicted and historically observed earthquake-induced collapse rates of short-period buildings. It presents work focused on wood light-frame buildings with structural panel sheathing (herein referred to as “wood light-frame” systems). The Applied Technology Council (ATC) was commissioned by the Federal Emergency Management Agency (FEMA) to conduct these studies as part of the ATC-116 Project series, “Solutions to the Issue of Short Period Building Performance.”

Short-period buildings, such as low-rise residential and commercial buildings, comprise a major portion of the building stock in U.S. communities with high-seismic hazard. The gap between analytically predicted and historically observed collapse rates for short-period buildings exists across many seismic-force-resisting systems and construction materials. As a result, it is believed that the seismic collapse performance for short-period buildings is not accurately predicted by current analytical models. Based on a review of previous studies and available research and data, three seismic-force-resisting systems were selected for detailed investigation in the ATC-116 Project series: wood light-frame, special reinforced masonry shear wall, and steel special concentrically braced frame (SCBF) systems.

The subject of this report is commercial buildings, multi-family dwellings, and single-family dwellings constructed using wood light-frame walls with structural panel sheathing, which accounts for the majority of short-period building construction in the United States. Studies on buildings constructed using special reinforced masonry shear walls and steel special concentrically braced frames are described in separate reports. An additional report compares results from all three studies to identify commonalities for possible extension of the findings, conclusions, and recommendations to other seismic-force-resisting systems and construction materials. The FEMA P-2139 series of reports include the following:

- FEMA P-2139-1, *Short-Period Building Collapse Performance and Recommendations for Improving Seismic Design, Volume 1 – Overarching Findings, Conclusions, and Recommendations*

- FEMA P-2139-2, *Short-Period Building Collapse Performance and Recommendations for Improving Seismic Design, Volume 2 – Study of One-to-Four Story Wood Light-Frame Buildings*
- FEMA P-2139-3, *Short-Period Building Collapse Performance and Recommendations for Improving Seismic Design, Volume 3 – Study of One-to-Four Story Special Reinforced Masonry Shear Wall Buildings*
- FEMA P-2139-4, *Short-Period Building Collapse Performance and Recommendations for Improving Seismic Design, Volume 4 – Study of One-to-Four Story Steel Special Concentrically Braced Frame Buildings*

1.1 Background and Purpose

At the time this study began, commercial buildings and multi-family dwellings were designed in accordance with ASCE/SEI 7-10, *Minimum Design Loads for Buildings and Other Structures* (ASCE, 2010), which was adopted by reference in the 2012 and 2015 editions of the *International Building Code* (IBC) (ICC, 2012a; ICC, 2015a). Residential one-family and two-family dwellings could be constructed in accordance with the 2012 and 2015 editions of the IBC or the *International Residential Code* (IRC) (ICC, 2012b; ICC, 2015b). In these codes and standards, seismic design loads are based on risk-targeted maximum considered earthquake (MCE_R) ground motions, which were introduced in FEMA P-750, *NEHRP Recommended Seismic Provisions for New Buildings and Other Structures* (FEMA, 2009a).

Buildings designed and constructed in accordance with national model codes and seismic design standards (e.g., ASCE/SEI 7-10) are expected to meet general seismic performance targets, which are described in terms of not exceeding a specified probability of collapse given MCE_R ground motions. For reference, a collapse probability of no more than 10 percent, given MCE_R ground motions, is the anticipated “reliability” in ASCE/SEI 7-10 (Table C1.3.1b) for Risk Category II buildings, which constitute the vast majority of all buildings. Further, the use of MCE_R ground motions in building design is intended to provide a reasonable assurance of seismic performance for all buildings—regardless of building period, seismic-force-resisting system, or other characteristic—designed in accordance with the governing building code.

Both the IBC and the IRC permit construction of wood light-frame buildings to be based on prescriptive requirements, often referred to as conventional construction provisions, based on the inherent assumption that methods using prescriptive provisions without detailed engineering calculations can provide comparable earthquake performance. Low-rise and short-period buildings designed and constructed in accordance with conventional construction

provisions are expected to meet the general seismic performance expectation for code-compliant buildings.

Studies conducted prior to the ATC-116 Project series have used the methodology described in FEMA P-695, *Quantification of Building Seismic Performance Factors* (FEMA, 2009b), to evaluate the collapse performance of common code-permitted seismic-force-resisting systems, such as NIST GCR 10-917-8, *Evaluation of the FEMA P-695 Methodology for Quantification of Building Seismic Performance Factors* (NIST, 2010).

Another widely cited collapse performance study is described in NIST GCR 12-917-20, *Tentative Framework for Development of Advanced Seismic Design Criteria for New Buildings* (NIST, 2012a). These and other similar studies have shown that many seismic-force-resisting systems achieve the collapse performance target (i.e., less than a 10 percent probability of collapse given MCE_R ground motions). However, these studies also found that shorter period buildings have calculated probabilities of collapse that exceed those of longer period buildings, and generally exceed the 10 percent target for acceptable collapse performance.

This can be observed in Figure 1-1, taken from NIST GCR 12-917-20. The figure shows the calculated collapse probabilities for groups of structural systems, as identified in Table 12.2-1 of ASCE/SEI 7-10, plotted over a range of periods. Bearing wall systems (diamonds) include special reinforced masonry shear walls (A.7), ordinary reinforced masonry shear walls (A.9), and light-frame (wood) walls with wood structural panel sheathing (A.15). Building frame systems (squares) include steel special concentrically braced frames (B.2), special reinforced concrete shear walls (B.4), ordinary reinforced concrete shear walls (B.5), and steel buckling-restrained braced frames (B.25). Moment frame systems (triangles) include steel special moment frames (C.1), special reinforced concrete moment frames (C.5), and ordinary reinforced concrete moment frames (C.7)

In the figure, FEMA P-695 collapse performance studies on a variety of structural systems over a range of periods suggest that, for systems with design periods less than about 0.5 seconds, the probability of collapse given MCE_R ground motions increases significantly as the design period decreases. If analytical predictions are accurate, then the goal of acceptable collapse performance for all seismic-force-resisting systems at all building periods is not being achieved, and short-period buildings are exceeding the 10 percent collapse performance target of ASCE/SEI 7.

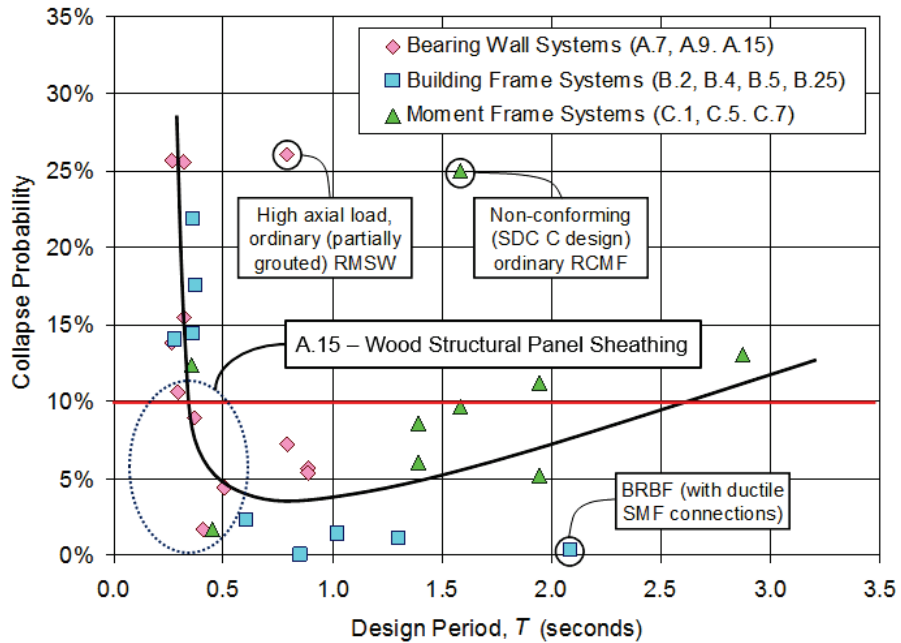


Figure 1-1 Trends in the probability of collapse of selected systems as a function of design period (adapted from NIST, 2012a).

The four diamond symbols contained in the dashed oval of Figure 1-1 are data points related to wood light-frame systems. Although these points show predicted collapse probabilities around (or below) the 10 percent target, they are part of the short-period data set exhibiting a trend of increasing probability of collapse with decreasing design period.

The importance of building period on the calculation of peak response of inelastic systems dates back to studies of response and design spectra in the 1960s and 1970s by Veletsos, Newmark, and others (e.g., Veletsos and Newmark, 1960; Veletsos et al., 1965). These studies found that the ratio of inelastic displacement to elastic displacement for simple single-degree-of-freedom numerical models was period-dependent, and increased as the periods of the numerical model decreased, implying worse collapse performance for shorter period buildings.

Findings from other numerical studies of earthquake response and collapse performance are consistent, and suggest that seismic design coefficients (e.g., R) could be period-dependent or more stringent for shorter period buildings (e.g., Miranda and Bertero, 1994). Although ASCE/SEI 7 does not include period-dependent seismic modification factors, the underlying concepts can be found in other seismic codes. For example, Section 5.2.3 of Eurocode 8 (CEN, 2004) increases inelastic seismic demands as a function of period for detailing of reinforced-concrete elements in areas of plastic hinging when the building period is relatively short (i.e., T less than T_s , where T_s is the code-

defined transition period between spectral response domains of constant acceleration and constant velocity). Explicit incorporation of period-dependent properties can also be found in the “coefficient method” of ASCE/SEI 41-17, *Seismic Evaluation and Retrofit of Existing Buildings* (ASCE, 2017).

Trends in observed earthquake damage for short-period buildings, however, do not support the high collapse probabilities shown in Figure 1-1. Analysis of available historical data on short-period building performance is described in Chapter 2. For example, based on data in OES (1995) from the 1994 Northridge earthquake, the fraction of all inspected wood frame buildings that were posted with an ATC-20 Restricted Use (yellow) placard, or an Unsafe (red) placard (ATC, 1989; 2005), suggests that collapse risk for this class of short-period buildings is not elevated, which is contrary to the results of analytical studies used to predict collapse probabilities. Because observed damage in short-period buildings is less than what is implied by the body of analytical results available in the literature, the opinion of many structural engineers suggests that numerical models overestimate the actual collapse risk of short-period buildings.

The apparent discrepancy between analytical prediction of collapse performance and the opinions and observations of structural engineers has been designated the *short-period building seismic performance paradox*. With the standardized collapse evaluation methodology of FEMA P-695, additional testing of structural elements and assemblies, and the evolution of high-speed computer processing, we now have the capability to effectively investigate and resolve this paradox.

Given this context, the purpose of the ATC-116 Project series was to investigate the response behavior and collapse performance of different short-period structural systems. The results of this work are intended to:

- Identify the causes of the short-period building seismic performance paradox, quantify factors contributing to short-period building performance, and develop solution concepts.
- Improve and validate numerical modeling methods for short-period buildings to more accurately capture response behavior and collapse performance characteristics.
- Improve code seismic design methods and engineering practices for short-period buildings so that seismic performance targets are achieved across all seismic-force-resisting systems and all design periods.

- Inform future research so that better data and improved numerical modeling can be used in the development of more efficient and effective structural systems, seismic assessment methodologies, and engineering design procedures.

1.2 Approach and Scope

A phased approach for investigation was developed and presented in the ATC-116 report, *Roadmap for Solutions to the Issue of Short Period Building Performance* (ATC, 2015). Many factors are thought to contribute to the apparent discrepancy between analyzed and observed seismic performance of short-period buildings. Reasons for the paradox could include an underestimation of the peak strength and post-peak capacity of short-period buildings, an overestimation of the demands on short-period buildings, or a combination of both. Possible causes include building configuration issues (e.g., incorporation of all structural and nonstructural components, including interior and exterior wall finishes, that contribute to building strength and stiffness), hysteretic response backbone curve issues (e.g., realistic characterization of peak strength and collapse displacement capacity), and other factors (e.g., soil-structure interaction and foundation flexibility) that affect building response behavior and collapse performance.

Overall, the approach for investigation was to: (1) establish benchmarks for the historically observed performance of short-period buildings; (2) conduct parametric analytical studies on archetypical short-period buildings using advanced numerical models and the latest available research and test data; and (3) identify modeling parameters or building characteristics that provide the best match between the simulated and benchmark performance.

Although there are a number of parameters by which seismic performance can be measured, these studies were primarily interested in collapse performance as measured by the conditional probability of collapse given a ground motion intensity (e.g., MCE_R ground motions), based on observations from historic earthquakes, as described in Chapter 2, or collapse statistics obtained from Incremental Dynamic Analysis (IDA), as described in Chapter 5.

For the purpose of these studies, short-period buildings were defined as buildings with first-mode periods less than about 0.5 seconds. Studies investigated different systems, configurations, and materials commonly used in the United States for design and construction of modern short-period buildings in regions of moderate, high, and very high seismicity.

To study wood light-frame systems, a suite of archetypes, with variations in occupancy, height, and seismic-design level, were selected. Archetypes were intended to represent code-compliant modern buildings for common occupancies classified under Risk Category II that would routinely utilize wood light-frame construction. Key configuration and seismic-design criteria for wood light-frame archetypes are provided in Table 1-1, where the design period ($T = C_u T_a$) and the seismic response coefficient (C_s) were calculated in accordance with Section 12.8.2 and Section 12.8.1.1 of ASCE/SEI 7-10, respectively. The development of wood light-frame archetypes is described in detail in Chapter 3 and summarized below.

Three occupancies were selected for study: (1) single-family dwellings (SFD); (2) multi-family dwellings (MFD); and (3) commercial (COM) buildings. The seismic-force-resisting system for all archetypes was load-bearing, light-frame (wood) walls with wood structural panel and gypsum wallboard sheathing. Archetypes included one-story, two-story, and four-story buildings, all with fundamental periods below 0.5-seconds. Wood light-frame shear wall configurations included both low aspect ratio and high aspect ratio walls.

Archetype design methods and details represent typical modern practice exercised in areas of significant seismicity based on the usual and customary standard of care. In contrast with prior FEMA P-695 collapse studies, archetype configurations for each occupancy were selected to be realistic and representative of actual buildings in terms of size and proportion. They were designed to meet code minimum base shear strength requirements, but were not biased with overstrength through deliberate conservatism in the design, or understrength caused by the use of wall configurations that would be considered unrealistic based on gravity load or architectural considerations.

Archetypes were designed for a range of seismic ground-motion levels. Moderate-seismic archetypes were designed for a value of short-period MCE_R spectral response acceleration adjusted for site class effects (S_{MS}) of 0.75g. High-seismic archetypes were designed for S_{MS} of 1.5g, and very high-seismic archetypes were designed for an S_{MS} of 2.25g. This highest value of S_{MS} is not required by FEMA P-695 (e.g., for evaluation of a new seismic-force-resisting system proposed for ASCE/SEI 7) but was used in this study to investigate the collapse performance of short-period buildings for MCE_R ground motions that are unlikely, but could occur in regions of very high seismicity (e.g., at sites located relatively close to fault rupture).

Table 1-1 Key Configuration and Seismic-Design Criteria for Wood Light-Frame Archetypes

Archetype ID	Configuration		Seismic Design Criteria					
	No. of Stories	Wall Aspect Ratio	Seismic Code	Design Period ⁽¹⁾ $T = C_u T_a$ (sec)	Seismic Design Category (SDC)	MCE _R Design Parameter, S_{MS} (g)	Response Modification Coefficient (R)	Seismic Response Coefficient, C_s (g)
Commercial Buildings: High Seismic								
COM1	1	Low	ASCE 7	0.25	D	1.5	6.5	0.154
COM2	2	Low	ASCE 7	0.26	D	1.5	6.5	0.154
COM3	4	Low	ASCE 7	0.45	D	1.5	6.5	0.154
Commercial Buildings: Very High Seismic								
COM4	1	Low	ASCE 7	0.25	E	2.25	6.5	0.231
COM5	2	Low	ASCE 7	0.26	E	2.25	6.5	0.231
COM6	4	Low	ASCE 7	0.45	E	2.25	6.5	0.231
Commercial Buildings: Moderate Seismic								
COM7	1	Low	ASCE 7	0.25	C	0.75	6.5	0.077
COM8	2	Low	ASCE 7	0.26	C	0.75	6.5	0.077
COM9	4	Low	ASCE 7	0.45	C	0.75	6.5	0.077
Multi-Family Dwellings: High Seismic								
MFD1	1	High	ASCE 7	0.25	D	1.5	6.5	0.154
MFD2	2	High	ASCE 7	0.26	D	1.5	6.5	0.154
MFD3	4	High	ASCE 7	0.45	D	1.5	6.5	0.154
Multi-Family Dwellings: Very High Seismic								
MFD4	1	High	ASCE 7	0.25	E	2.25	6.5	0.231
MFD5	2	High	ASCE 7	0.26	E	2.25	6.5	0.231
MFD6	4	High	ASCE 7	0.45	E	2.25	6.5	0.231
Multi-Family Dwellings: Moderate Seismic								
MFD7	1	High	ASCE 7	0.25	C	0.75	6.5	0.077
MFD8	2	High	ASCE 7	0.26	C	0.75	2, 6.5 ⁽²⁾	0.25, 0.077
MFD9	4	High	ASCE 7	0.45	C	0.75	6.5	0.077
Single-Family Dwellings: High Seismic								
SFD1	1	High	ASCE 7	0.25	D	1.5	6.5	0.154
SFD1C	1	High	IRC	NA	D ₂	1.5	NA	NA
SFD2	2	High	ASCE 7	0.25	D	1.5	6.5	0.154
SFD2C	2	High	IRC	NA	D ₂	1.5	NA	NA
Single-Family Dwellings: Very High Seismic								
SFD3	1	High	ASCE 7	0.25	E	2.25	6.5	0.231
SFD3C	1	High	IRC	NA	E	2.25	NA	NA
SFD4	2	High	ASCE 7	0.25	E	2.25	6.5	0.231
Single-Family Dwellings: Moderate Seismic Areas								
SFD5	1	High	ASCE 7	0.25	C	0.75	6.5	0.077
SFD5C	1	High	IRC	NA	C	0.75	NA	NA
SFD6	2	High	ASCE 7	0.25	C	0.75	6.5	0.077

⁽¹⁾ The design period is defined as $T = C_u T_a \geq 0.25$ seconds, in accordance with the analysis requirements of FEMA P-695, where the values of the parameters C_u and T_a are specified by ASCE/SEI 7-10.

⁽²⁾ R=2 in the transverse direction and R=6.5 in the longitudinal direction.

Archetype designs provided the basis for advanced numerical models. Using FEMA P-695 procedures, IDA results provided collapse performance metrics in terms of the conditional probability of collapse given MCE_R ground-motion levels. To investigate the apparent discrepancy between analyzed and observed seismic performance of wood light frame systems, five parametric studies were performed. These included: (1) baseline configuration; (2) collapse displacement capacity; (3) nonstructural interior and exterior wall finishes; (4) soil-structure interaction and foundation flexibility; and (5) backbone curve shape. Parametric studies are described in detail in Chapter 4, and summarized below:

- **Baseline Configuration Parametric Study:** investigated variation in the response behavior and collapse performance of short-period wood light-frame “baseline” archetypes representing selected combinations of building type (i.e., COM, MFD, SFD), archetype height (e.g., one-story, two-story, and four-story for COM and MFD building types) and seismic design level (high seismic and very high seismic). This study considered differences in archetype configurations compared to those of previous FEMA P-695 collapse evaluations, and compared modeled baseline collapse performance to observed earthquake data. In addition, baseline models considered the results of other parametric studies, and incorporated a best estimate for each parameter to provide an overall best estimate of the simulated response of short-period wood light-frame buildings.
- **Collapse Displacement Capacity Parametric Study:** investigated the effects of increased collapse displacement capacity on the response behavior and collapse performance of short-period wood light-frame buildings. Based on test data available at the time, prior FEMA P-695 studies limited displacement capacities to the displacement corresponding to a post-peak strength of $0.8V_{max}$, and collapse was assumed to occur at overly conservative limits on story drift. Comparison of response and collapse results of analyses with varying assumptions of component residual strength plateaus extending to large lateral displacements provided the basis for evaluating the effects of collapse displacement capacity.
- **Nonstructural Interior and Exterior Wall Finishes Parametric Study:** investigated the effects of nonstructural interior and exterior wall finishes on the response behavior and collapse performance of short-period wood light-frame buildings. Interior and exterior wall finishes (e.g., gypsum wallboard, stucco, and horizontal wood siding) are considered to be nonstructural, and are typically not considered in the

design of the seismic force-resisting system. Comparison of response and collapse results of analyses without nonstructural interior and exterior wall finishes to the results of corresponding baseline archetype models (with wall finishes) provided the basis for evaluating the effects of nonstructural interior and exterior wall finishes.

- **Soil-Structure Interaction and Foundation Flexibility Parametric Study:** investigated the effects of soil-structure interaction (SSI) and foundation flexibility on the response behavior and collapse performance of short-period wood light-frame buildings using a distributed set of discrete nonlinear soil springs (representing two soil classes) below flexible foundation elements. Comparison of response and collapse results of analyses with soil springs and flexible foundations to the results of corresponding baseline archetype models (with rigid foundations) provided the basis for evaluating the effects of SSI and foundation flexibility.
- **Backbone Curve Shape Parametric Study:** investigated the effects of backbone curve shape on the response behavior and collapse performance of short-period wood light-frame buildings by varying assumptions used to define the peak strength and post-capping strength and stiffness of shear wall components. This study focused on wood structural panel systems and used the design values published in AWC (2008) as anchors for defining peak strengths. Comparison of response and collapse results of analyses with alternative backbone curve parameters to the results of corresponding baseline archetype models (with best estimate values of key backbone parameters) provided the basis for evaluating the effects of backbone curve shape.

Although many short-period wood light-frame archetype designs were developed, because of budget and time constraints, not all archetypes were modeled and analyzed, and only selected baseline configurations were evaluated in each parametric study. A total of 90 models were developed for the five parametric studies. The number of archetypes and corresponding configurations that were considered in each parametric study are identified in Chapter 4. In general, the high-seismic ground-motion level was prioritized over moderate and very high-seismic ground-motion levels because prior FEMA P-695 studies have demonstrated that high-seismic collapse probabilities tended to control over results for moderate levels of ground motion, and because high-seismic ground motions best represent strong ground motions in major earthquakes at sites that are not close to fault rupture.

1.3 Organization and Content

This report describes an investigation of the response behavior and collapse performance of short-period wood light-frame buildings. It presents historical data on earthquake performance, typical configurations of wood light-frame construction, development of archetype designs and numerical models, results from parametric analytical studies, solutions to the short-period building seismic performance paradox, and recommendations for seismic design, engineering practice, and future research.

Chapter 2 identifies potential sources of earthquake data, describes methods for evaluation of response behavior and collapse performance using these data, presents observations of short-period wood light-frame building performance in past earthquakes, and establishes benchmarks of collapse performance for comparison with parametric study results.

Chapter 3 discusses factors influencing the performance of short-period wood light-frame buildings, identifies common building types in terms of use (occupancy) and structural configuration, defines sets of representative commercial building, multi-family dwelling, and single-family dwelling archetypes and their associated design criteria, and describes the design of these archetypes.

Chapter 4 describes the methods used to develop numerical models of short-period wood light-frame archetypes, including calibration and validation with experimental data, and provides a detailed description of the five parametric studies.

Chapter 5 summarizes the analytical results for each of the five parametric studies on short-period wood light-frame buildings.

Chapter 6 presents key findings, conclusions, and recommendations related to short-period wood light-frame buildings.

Appendix A provides additional archetype design details not included in Chapter 3.

Appendix B describes the organization and content of peak response quantities for each archetype, which have been archived for further study and future use.

Appendix C presents the results of a study on the effects of viscous damping to investigate impacts on collapse performance, and to determine the viscous damping ratio to be used in soil-structure interaction and foundation flexibility studies.

Appendix D presents the results of a study validating the numerical modeling approach on a wood light-frame building with measured response behavior and known seismic performance.

References and a list of project participants are provided at the end of this report.

Chapter 2

Observed Response and Performance Benchmarks

This chapter identifies sources of short-period building earthquake response behavior and collapse performance data, describes methods used to establish benchmark properties from these data, and develops benchmark metrics from selected sources of earthquake data and full-scale shake table tests.

Benchmark metrics are used for validation of numerical models of wood light-frame buildings (Chapter 4) and for comparison with collapse results of parametric studies (Chapter 5). Benchmark metrics include dynamic response parameters (e.g., building period), damage measures (e.g., post-earthquake safety evaluation data) and collapse performance (probability of collapse as a function of ground motion intensity). Alternative definitions of collapse are discussed and related to structural damage and post-earthquake safety evaluation criteria. Sources include post-earthquake safety evaluations of damage to wood light-frame buildings in the 1994 Northridge earthquake and surveys of damage and collapse of buildings in the 1995 Kobe earthquake.

2.1 Introduction

Available earthquake data include instrumented recordings of building response and observations of building damage and collapse performance in past earthquakes. Qualitatively, damage and collapse performance data are used to corroborate (or refute) the notion that short-period buildings built to modern seismic standards are generally no more susceptible to collapse than other (i.e., longer period) buildings, or, conversely, to corroborate (or refute) the trends of analytical studies that have consistently found short-period buildings to be more susceptible to collapse than other buildings.

Instrumented recordings of building response are used to validate dynamic properties of numerical models of short-period buildings (e.g., periods and modes of vibration). Observations of building damage and collapse performance are used to develop benchmark properties for validation of the collapse performance of numerical models of short-period buildings (i.e., probability of collapse as a function of ground motion intensity).

Although shake table tests of full-scale short-period buildings are quite limited, the few tests that have been conducted provide valuable information on nonlinear response behavior, damage, and collapse failure modes for test structures that have been subjected to simulated earthquake ground motions. In particular, observations from high-amplitude shake table tests can be used to establish qualitative targets for the behavior and performance predicted in numerical models of comparable construction and configuration.

2.2 Significant Earthquakes and Sources of Data

The most significant earthquakes in the United States in the 50-year period from 1964 to 2014, the most significant world-wide events from 1980 to 2014, and the fatalities and economic losses for each of these events are summarized in the sections that follow.

2.2.1 U.S. Earthquakes (1964 - 2014)

Table 2-1 lists 26 significant U.S. earthquakes (i.e., events with magnitudes greater than M5.5) that have occurred in the 50-year period from 1964 through 2014. These events include the 1971 San Fernando earthquake, the 1989 Loma Prieta earthquake, and the 1994 Northridge earthquake which account for 85 of the 109 building-related fatalities. Table 2-2 provides a breakdown of earthquake fatalities and the approximate amount of building economic loss for each of the 26 events. It should be noted that most of the 128 fatalities in the 1964 Anchorage earthquake were due to tsunami inundation in coastal areas.

In general, fatalities due to ground motion or ground failure are primarily due to injuries sustained as a result of building collapse, but also include fatalities due to bridge collapse (e.g., 42 fatalities in the 1989 Loma Prieta earthquake due to collapse of the Cypress viaduct) and medical-related fatalities such as heart failure brought on by the earthquake. The relatively low number of building-related earthquake fatalities in recent U.S. earthquakes reflects both good fortune (i.e., earthquakes occurring during off hours or away from areas of densest population), and the earthquake resistance of modern U.S. construction. Larger magnitude events closer to the center of dense urban areas would be expected to result in many more fatalities due to collapse of vulnerable existing buildings, such as those with older or archaic construction or significant structural irregularities.

Figures 2-1 through 2-4 are a collection of photographs showing examples of collapse of the most vulnerable types of U.S. construction in past earthquakes. Vulnerable construction includes unreinforced-masonry (URM) buildings (see Figure 2-1), non-ductile reinforced concrete buildings (see

Table 2-1 Date, Magnitude, and Region Affected for Selected Large-Magnitude U.S. Earthquakes, 1964 - 2014

Earthquake Event			
Name	Date	M	Region Affected
1964 Anchorage	3/28/1964	9.2	Prince William Sound, AK
1965 Olympia	3/28/1965	6.7	Seattle-Tacoma, WA
1969 Santa Rosa	10/2/1969	5.7	Santa Rosa, CA
1971 San Fernando	2/9/1971	6.6	San Fernando, CA
1975 Kalapana	11/29/1975	7.2	Kalapana, HI
1978 Santa Barbara	08/13/1978	5.7	Santa Barbara, CA
1979 Imperial Valley	10/15/1979	6.4	El Centro, CA
1980 Greenville	1/24/1980	6.4	Livermore, CA
1980 Livermore	1/26/1980	5.6	Livermore, CA
1983 Coalinga	5/2/1983	6.5	Coalinga, CA
1983 Borah Peak	10/28/1983	6.9	Borah Peak, ID
1984 Morgan Hill	4/24/1984	6.2	Morgan Hill, CA
1987 Whittier	10/1/1987	5.9	Los Angeles-Whittier, CA
1987 Superstition Hills	11/24/1987	6.7	Westmoreland, CA
1989 Loma Prieta	10/17/1989	6.9	Santa Cruz County, CA
1991 Sierra Madre	6/28/1991	5.8	San Gabriel Valley, CA
1992 Petrolia	4/25/1992	7.2	Cape Mendocino, CA
1992 Landers	6/28/1992	7.3	Landers, CA
1992 Big Bear	6/28/1992	6.7	Big Bear, CA
1993 Klamath Falls	9/20/1993	6.0	Klamath Falls, OR
1994 Northridge	1/17/1994	6.7	Northridge, CA
2001 Nisqually	2/28/2001	6.8	Seattle-Tacoma, WA
2003 San Simeon	12/22/2003	6.5	San Simeon, CA
2006 Hawaii	10/15/2006	6.7	Kiholo Bay, HI
2011 Mineral	8/23/2011	5.8	Mineral, VA
2014 American Canyon	8/23/2014	6.1	Napa, CA

Figure 2-2 and Figure 2-3) and soft/weak story wood light-frame buildings (see Figure 2-4). Collapse of these building types, which are typically low-rise (short-period) buildings, caused over 70 of the approximate 109 building-related earthquake fatalities listed in Table 2-2.

Table 2-2 Fatalities and Economic Losses for Selected Large-Magnitude U.S. Earthquakes, 1964 - 2014

Earthquake Event	Fatalities		Building Loss (\$ millions)	
	Total	Building	At Time of Earthquake	2014 (Estimated)
1964 Anchorage	128	10	300	5,000
1965 Olympia	7	3	13	200
1969 Santa Rosa	1	1	8	100
1971 San Fernando	65	53	1,500	20,000
1975 Kalapana	2	0	4	25
1978 Santa Barbara	0	0	14	70
1979 Imperial Valley	0	0	51	250
1980 Greenville	0	0	12	50
1980 Livermore	1	0	18	80
1983 Coalinga	0	0	42	150
1983 Borah Peak	2	2	13	50
1984 Morgan Hill	0	0	13	45
1987 Whittier	8	1	430	1,300
1987 Superstition Hills	2	0	3	10
1989 Loma Prieta	63	12	6,500	17,500
1991 Sierra Madre	2	1	36	90
1992 Petrolia	0	0	52	130
1992 Landers	2	1	50	125
1992 Big Bear	1	0	39	100
1993 Klamath Falls	2	2	10	25
1994 Northridge	57	20	25,000	55,000
2001 Nisqually	1	1	2,000	3,500
2003 San Simeon	2	2	150	250
2006 Hawaii	0	0	120	160
2011 Mineral	0	0	300	380
2014 American Canyon	0	0	300	300
Total All	346	109	36,978	104,900

In the 1987 Loma Prieta earthquake, five fatalities occurred in San Francisco (lower left of Figure 2-1) and three fatalities in Santa Cruz (lower right of Figure 2-1) due to out-of-plane failure of URM walls. In the 1971 San Fernando earthquake (Figure 2-2), 47 of the 58 fatalities occurred at the Veterans Administration (VA) complex. In the 1994 Northridge earthquake, 16 of the 20 building collapse-related fatalities occurred in the Northridge

Meadows apartment complex (upper right photo in Figure 2-4). In this case, a portion of the apartment complex collapsed at the soft (weak) first story caused by tuck-under parking. Similar first-story collapses occurred in other apartment buildings in the 1989 Loma Prieta and 1994 Northridge earthquakes.

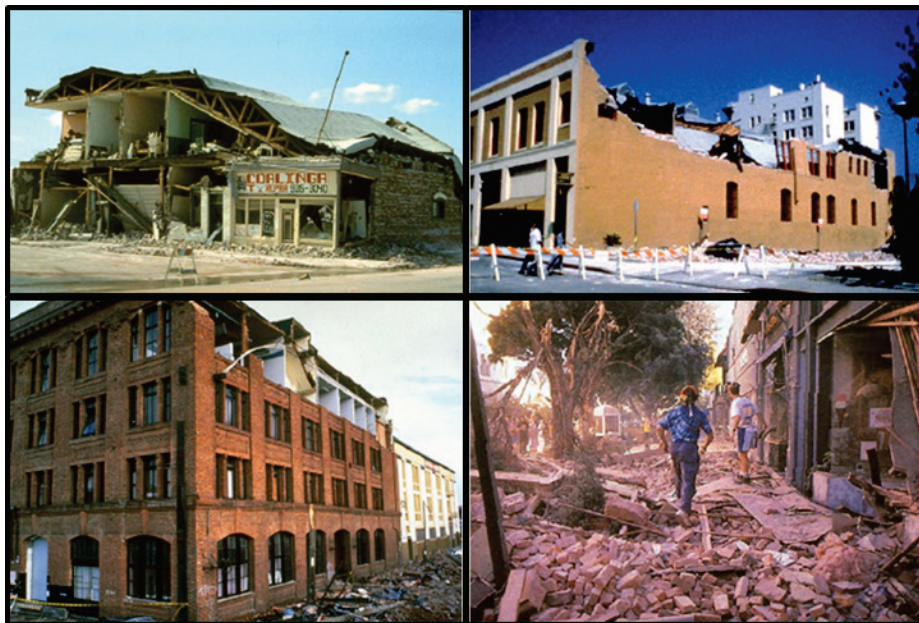


Figure 2-1 Collapse of URM buildings in the 1983 Coalinga earthquake (top left), the 1987 Whittier earthquake (top right), and the 1987 Loma Prieta earthquake (bottom).



Figure 2-2 Collapse of non-ductile concrete frame buildings at the Veterans Administration (VA) complex in the 1971 San Fernando earthquake.



Figure 2-3 Collapse of the first floor of the two-story Community Mental Health Building (upper right) and severe damage to the five-story main building at the Olive View Hospital in the 1971 San Fernando earthquake.



Figure 2-4 Collapse of soft-story wood light-frame multi-family dwellings in the 1987 Loma Prieta earthquake (left) and 1994 Northridge earthquake (right).

In URM buildings (Figure 2-1), collapse was typically associated with out-of-plane failure of bearing walls due to inadequate wall anchorage or diaphragm capacity. In non-ductile concrete buildings, structural irregularity contributed to at least some of the collapse damage at the VA complex (Figure 2-2) and to collapse of the Olive View Hospital Community Mental Health Building (Figure 2-3). In multi-story wood light-frame buildings

(Figure 2-4), collapse was directly related to their soft/weak story configuration. It should be noted that each of these vulnerable building types are either no longer permitted in regions of moderate to high seismicity (e.g., URM buildings) or more stringent code provisions are now required for seismic design (e.g., reinforced concrete buildings).

2.2.2 World-Wide Earthquakes (1980 - 2014)

Table 2-3 summarizes economic losses and fatalities in the 10 costliest world-wide earthquakes (and tsunamis) from 1980 to 2014 based on data provided by Munich RE (2015). Ignoring the 2011 Tohoku event dominated by tsunami-related losses, the costliest earthquakes are the 1995 Kobe earthquake (\$100 billion), the 2008 Sichuan earthquake (\$85 billion), and the 1994 Northridge earthquake (\$44 billion). In each of these earthquakes, losses are primarily due to building damage. It should be noted that while dollar losses in the 1994 Northridge earthquake are about half that of the 1995 Kobe or 2008 Sichuan earthquakes, fatalities are 100 to 1,000 times less.

Table 2-3 Economic Losses and Fatalities in the 10 Costliest Earthquakes and Tsunamis, 1980 - 2014 (Munich RE, 2015)

Earthquakes and Tsunamis (T)			Loss (\$ billions)		Fatalities
Date	Magnitude	Location	Total	Insured	
3/11/2011	M9.0	Tohoku, Japan (T)	210	40.0	15,880
1/17/1995	M6.9	Kobe, Japan	100	3.0	6,430
12/5/2008	M7.9	Sichuan, China	85	0.3	84,000
1/17/1994	M6.7	Northridge, CA	44	15.3	61
2/27/2010	M8.8	Maule, Chile (T)	30	8.0	520
10/23/2004	M6.6	Niigata, Japan	28	0.8	33
2/22/2011	M6.3	Christchurch, New Zealand	24	16.5	185
5/5/2012	M6.0	Emilia, Italy	16	1.6	18
9/20/1999	M7.6	Central Taiwan	14	0.8	2,400
12/7/1988	M6.8	Spitak, Armenia	14	-	25,000

2.2.3 Building Records of Earthquake Response

Benchmark response properties are typically obtained from strong-motion instrument recordings of building response during an earthquake. Notable, but rare exceptions include building recordings from in-situ, forced-vibration tests (e.g., Camelo et al., 2002) and shake table testing of full-scale test buildings (Isoda et al., 2008; Filiatrault et al., 2010).

The California Strong Motion Instrumentation Program (CSMIP) maintains record sets of recorded building response from main shocks or aftershocks in California earthquakes. These data are available online from the Center for Engineering Strong Motion Data (CESMD) database (CSMIP, 2015). There are also a number significant building records from non-U.S. earthquakes, such as the 2011 Tohoku earthquake in Japan, that could provide valuable information on short-period building response, although these data are, in general, not as readily available as those in the CESMD database.

A summary of 242 CSMIP record sets of 58 low-rise buildings recorded in a total of 106 different earthquakes is provided in Tables 2-4 through 2-6 for one-story, two-story, and three-story buildings.

Table 2-4 CSMIP Record Sets of Short-Period Building Response, One-Story Buildings, in 86 Earthquakes

Station No.	Recording Station Name	No. of EQs per Station	Structure Peak Acceleration	
			Min (g)	Max (g)
36695	Templeton - Hospital	5	0.017	1.280
58235	Saratoga – School Gymnasium	3	0.172	0.870
89473	Fortuna - Supermarket	11	0.038	0.769
23495	Redlands - Warehouse	12	0.030	0.750
12759	Indio - Hospital	5	0.030	0.571
54331	Mammoth Lakes - Hospital	4	0.049	0.495
57187	San Ramon - Warehouse	2	0.240	0.475
36531	Parkfield - School	5	0.023	0.340
12266	Hemet - Library	15	0.022	0.320
47391	Hollister - Warehouse	4	0.031	0.300
1699	El Centro - Hospital	11	0.032	0.278
23540	Colton - School Gymnasium	1	0.230	0.230
23622	San Bernardino - Commercial Building	1	0.220	0.220
34189	Tehachapi / Bear Valley - Police Station	2	0.043	0.044
36534	Parkfield - Fire Station	2	0.014	0.036
99261	Crescent City - Hospital	3	0.019	0.035
Total Number of One-Story Buildings: 16			Record Sets: 86	

Typically, each building has records from multiple events. CSMIP record sets were identified by a search of the CESMD database for “low-rise” buildings and events with a PGA greater than 0.01g at the site of interest. These tables exclude records for buildings over three stories, that are base-isolated, or were listed as “unavailable.” It is likely that a few low-rise buildings listed in these tables have periods greater than 0.5 seconds (e.g.,

steel moment frames), while certain mid-rise buildings not included in these tables (e.g., reinforced concrete shear wall buildings) have periods less than 0.5 seconds.

Table 2-5 CSMIP Record Sets of Short-Period Building Response, Two-Story Buildings, in 65 Earthquakes

Station No.	Recording Station Name	No. of EQs per Station	Structure Peak Acceleration	
			Min (g)	Max (g)
57476	Gilroy - Commercial Building	1	0.990	0.990
58224	Oakland - Office Building	7	0.029	0.690
57502	Milpitas - Industrial Building	3	0.107	0.580
58264	Palo Alto - Office Building	3	0.059	0.550
89687	Eureka - Office Building	7	0.020	0.511
24104	Simi Valley - Hospital	6	0.014	0.397
23511	Pomona - Commercial Building	8	0.033	0.303
58496	Berkeley - Hospital	5	0.033	0.300
58262	Belmont - Office Building	1	0.200	0.200
47231	King City - Hospital	2	0.110	0.151
3233	La Jolla - University Hospital	4	0.046	0.137
57301	Fremont - Hospital	1	0.110	0.110
57784	Fremont - City Library	3	0.032	0.105
57614	Morgan Hill – Hospital (former)	2	0.092	0.104
24198	Chatsworth - Commercial Building	3	0.040	0.102
58740	San Francisco - Commercial Building	5	0.034	0.072
58588	Stanford - School Admin Building	2	0.055	0.058
57200	Gilroy - Hospital	2	0.047	0.052
Total Number of Two-Story Buildings: 18		Record Sets: 65		

The CSMIP record sets include multi-channel data for a variety of different types, heights, and plan configurations of short-period buildings that have experienced one or more earthquakes. Although the amplitude of building response is typically low, these records provide a basis to investigate trends in dynamic properties (e.g., influence of diaphragm flexibility on building period). Section 2.4 includes period data obtained from CSMIP record sets for six short-period wood light-frame buildings. Appendix D utilizes CSMIP record sets from the north wing of the Templeton Hospital building during the 2003 San Simeon earthquake to conduct a pilot study validating the numerical modeling approach for wood light-frame buildings.

Table 2-6 CSMIP Record Sets of Short-Period Building Response, Three-Story Buildings, in 91 Earthquakes

Station No.	Recording Station Name	No. of EQs per Station	Structure Peak Acceleration	
			Min (g)	Max (g)
25213	Santa Barbara - Office Building	2	0.096	0.993
24332	Los Angeles - Commercial Building	3	0.18	0.97
57562	San Jose - Office Building	2	0.072	0.67
58506	Richmond - Office Building	2	0.046	0.32
23516	San Bernardino - Office Building	8	0.029	0.28
25777	Santa Barbara - Hospital	1	0.255	0.255
24517	Lancaster - Office Building	3	0.15	0.25
58503	Richmond - Government Office Building	2	0.15	0.24
58334	Piedmont - School Admin Building	6	0.027	0.232
58348	Pleasant Hill - Commercial Building	6	0.015	0.23
58263	Redwood City - School Admin Building	1	0.19	0.19
58199	Walnut Creek - Hospital	7	0.032	0.165
23701	San Bernardino Motel	7	0.036	0.157
58396	Alameda - Hospital	2	0.067	0.154
57783	Fremont - Police Station	3	0.043	0.148
13213	Moreno Valley - County Hospital	10	0.016	0.132
47796	Salinas - County Hospital	8	0.035	0.121
24454	Pasadena - University Building	1	0.114	0.114
58661	Castro Valley - Hospital	4	0.025	0.107
68032	Fairfield - Hospital	1	0.087	0.087
57251	Santa Clara - Hospital	1	0.084	0.084
58225	Oakland - Commercial Building	7	0.029	0.076
58593	Stanford - School	3	0.022	0.039
33372	Ridgecrest - College Building	1	0.031	0.031
Total Number of Three-Story Buildings: 24			Record Sets: 91	

The range (i.e., minimum and maximum values) of peak in-structure accelerations from different earthquakes is shown in Tables 2-4 through 2-6 for each of the 58 buildings. In general, peak accelerations are low, and response is only suitable for evaluating “elastic” dynamic properties of the buildings (e.g., building period). In a few cases, however, peak accelerations are large, and could be useful for benchmarking nonlinear dynamic response behavior. For example, peak acceleration in the one-story, Templeton Hospital building is 1.28g, recorded during the 2003 San Simeon earthquake.

2.3 Overview of Methods Used to Establish Benchmark Properties of Short-Period Wood Light-Frame Buildings

Benchmark properties for short-period wood light-frame buildings are developed from records of earthquake performance (and response data when available), and are used to validate the dynamic properties and response behavior of numerical models incorporating enhanced modeling methods (e.g., inclusion of nonstructural wall finishes or degradation of seismic force-resisting components) to provide a more realistic assessment of performance.

2.3.1 Benchmark Response Properties

Benchmark response properties include the measured dynamic characteristics (e.g., building periods, damping, and mode shapes) of short-period buildings. As noted above, the amplitude of building response recordings is typically low, and the dynamic properties obtained from these records are, in general, suitable only for benchmarking the elastic, or essentially elastic, properties of numerical models.

Measured values of building period are used to establish benchmark values of building period as a function of the height of generic building types (e.g., typical fundamental-mode periods of one-story wood light-frame residential buildings). In such cases, benchmark values of building period are obtained from processing of earthquake response recordings from representative buildings (see Section 2.4).

2.3.2 Benchmark Performance Properties

Benchmark performance properties relate the likelihood of damage or collapse to ground motion intensity (e.g., 0.3-second spectral acceleration). Damage functions can be thought of as empirical fragility curves for which the probability of damage at a given ground motion intensity is the ratio of the number of damaged buildings divided by the total number of buildings in the region affected by that ground motion intensity. The calculation of building damage or collapse functions requires three basic types of data: (1) ground motion data; (2) inventory data; and (3) performance data, as described below:

- 1. Ground Motion Data.** Ground motion data include maps of ground motion parameters from an earthquake, characterized by the ground motion parameter of interest (e.g., 0.3-second spectral acceleration for short-period buildings).

For U.S. earthquakes, Shake Maps developed by the U.S. Geological Survey (USGS) provide a convenient source of ground motion data that

is available on the internet (Wald et al., 1999; Wald et al., 2005). These maps characterize ground motions in terms of instrumental MMI, as well as 0.3-second and 1.0-second spectral accelerations. They are produced in different GIS formats, including a HAZUS-compatible version.

2. **Inventory Data.** Inventory data describe the short-period buildings of interest of the region affected by the earthquake (i.e., building exposure). These data include, for example, the geographical location of the buildings, the number of buildings by type or occupancy (e.g., number of wood light-frame buildings) and the replacement value of building types and occupancies (e.g., value of residential buildings).

At the finest level of geographical resolution, the specific building location (latitude/longitude) would be used to locate each building. This is generally not feasible for large regions. Inventory data is typically based on building exposure aggregated by census tract or ZIP code, for which existing databases provide requisite inventory data (e.g., the total number and total value of the building type of interest in each census tract). Inventory data may also be aggregated by other geographical units, such as larger areas of common MMI. The level of geographical resolution used for inventory data must also be used for the damage and loss data, and ground motion data.

For U.S. earthquakes, the HAZUS loss estimation technology (FEMA, 2003; Kircher et al., 2006b) provides a large number of useful building databases that are convenient for developing inventory data for a region of interest. HAZUS building inventory data include the total number, total square footage, and total replacement value of each of 15 model building types (e.g., wood light-frame) and each of 28 occupancy classes (e.g., single-family dwelling, multi-family dwelling) for each of the approximate 80,000 census tracts in the United States. HAZUS inventory data do not include building height, so other methods are required to determine height, and other properties, specific to the buildings of interest.

3. **Performance Data.** Performance data describe observed damage and loss due to an earthquake, for each inventory set of interest (e.g., number of wood light-frame buildings, posted with an Unsafe (red) Placard, in the 1994 Northridge earthquake, located in each census tract of Los Angeles County). Of the three data elements (ground motion, inventory, and performance), performance (damage and loss) data are most difficult to identify and collect.

Typically, earthquake damage and loss data have not been collected in a systematic, geographical basis. For example, after the 1971 San Fernando earthquake, a wealth of damage and loss information was compiled in a three-volume report by the National Oceanic and Atmospheric Administration (NOAA, 1973), but was not systematically related to building inventory and ground motion data. After the 1994 Northridge earthquake, however, geographic information system (GIS) technology was used to collect and process earthquake data in a more systematic manner. For example, earthquake data, including building safety evaluation data, were compiled in a geographical database by the Governor's Office of Emergency Services (OES, 1995; OES, 1997).

Perhaps the most valuable source of earthquake performance data are the building damage and loss data compiled by the insurance industry (e.g., based on claims made following an earthquake), but these data are proprietary and generally not publicly available.

2.3.3 Definitions and Relationship of Complete Structural Damage, Collapse, and Post-Earthquake Safety Evaluation Criteria

The nonlinear analysis methods of FEMA P-695 are used to calculate peak and residual displacements and to evaluate the collapse performance of nonlinear models of short-period wood light-frame building archetypes. Analytical results provide estimates of two building performance metrics: (1) complete building damage based on models exhibiting excessive residual displacement (or collapse); and (2) collapse based on models exhibiting sidesway collapse. Ideally, analytical estimates of complete building damage and collapse would be benchmarked directly with observations of excessive residual displacement or collapse of short-period buildings due to earthquake shaking. However, as noted in the previous section, such data are generally not available and must be inferred from other metrics, such as data from ATC-20 *Procedures for Postearthquake Safety Evaluation of Buildings* (ATC, 1989; 2005). These data must then be related to complete building damage and collapse as estimated by FEMA P-695 analyses, and, more broadly, to performance expectations in U.S. model building codes and standards.

U.S. building codes, such as the 2015 IBC, refer to standards, such as ASCE/SEI 7-10, for seismic design criteria that are based largely on FEMA P-1050, *NEHRP Recommended Seismic Provisions for New Buildings and Other Structures* (FEMA, 2015a). Section 1.1 of FEMA P-1050 summarizes seismic code performance objectives as follows:

“...the objectives of the provisions are to provide reasonable assurance of seismic performance that will:

1. Avoid serious injury and life loss due to
 - a. Structure collapse
 - b. Failure of nonstructural components or systems
 - c. Release of hazardous materials
2. Preserve means of egress
3. Avoid loss of function in critical facilities, and
4. Reduce structural and nonstructural repair costs where practicable.”

Section 1.1 of FEMA P-1050 further explains that target performance to meet the primary objective of avoiding serious injury and life loss is based on limiting the probability of collapse to 10 percent for a significant portion, or all, of an ordinary use (Risk Category II) building given the occurrence of relatively rare, MCE_R, ground motions. Quantitative performance criteria are not defined for other performance objectives. Section 12.2.1.1 of ASCE/SEI 7-10 (and FEMA P-1050) permits alternative seismic force-resisting systems, provided that the design demonstrates compliance with the target 10-percent objective for probability of collapse given MCE_R ground motions. The commentary to these requirements identifies FEMA P-695 as an acceptable method for demonstrating such compliance.

Thus, the seismic provisions of ASCE/SEI 7-10 and FEMA P-695 share the same common definition of collapse (i.e., partial as well as full collapse) and have the same target 10 percent probability of collapse conditioned on MCE_R ground motions, but both are silent with respect to other damage states, including complete damage. Traditionally, complete building damage is associated with 100 percent economic loss (i.e., the building is destroyed or so severely damaged such that it must be replaced), and stem from the insurance industry, which is primarily concerned with financial loss, rather than casualty losses. It should be noted that the insurance industry defines building damage in terms of the full cost of building repair or replacement, and building loss as the net cost of insured losses after policy deductibles are subtracted. Other relevant definitions of damage and collapse are provided in earthquake loss estimation technologies such as ATC-13, *Earthquake Damage Evaluation Data for California* (ATC, 1985), HAZUS (FEMA, 2003; Kircher et al., 2006a), and Appendix H of Chapter 6 of the 2007 *California Building Standards Code* (CBSC, 2007).

The seminal earthquake loss estimation technology of ATC-13 developed damage probability matrices (DPMs) from earthquake data and expert opinion. The DPMs define the probability of being in one of seven damage states as a function of Modified Mercalli Intensity (MMI). ATC-13 damage

states are defined by a damage factor (DF) range, where the DF is defined as dollar loss divided by replacement value. ATC-13 damage states include *Major* damage defined as “major widespread damage that may result in the facility being razed, demolished, or repaired” and *Destroyed* defined as “total destruction of the majority of the facility.” The DF range of the Major damage state is 60 percent to 100 percent reflecting the possibility of complete financial loss even if the damage is technically repairable. Table 9.3 of ATC-13 defines injury and fatality rates for each damage state. For example, fatality rates are 2 persons for every 100 occupying steel light-frame (S3) and wood light-frame (W1) buildings that are Destroyed (DF = 100 percent), and 20 persons for every 100 occupying all other building types with this level of damage. The low fatality rate of 2 persons for every 100 reflects observations of relatively few fatalities in destroyed wood light-frame buildings, even when such buildings are a total financial loss.

The HAZUS earthquake loss estimation technology utilizes building damage functions (i.e., lognormally-distributed fragility curves) to define the probability of being in one of five discrete structural damage states as a function of peak earthquake displacement of the building. The five HAZUS damage states: None, Slight, Moderate, Extensive, or Complete, adapted from the *Expected Seismic Performance of Buildings* (EERI, 1994), are defined in terms of the physical damage that would be observed after an earthquake. For example, HAZUS technology defines the complete structural damage state of the wood light-frame (W1) building type as:

“Structure may have large permanent lateral displacement, may collapse, or be in imminent danger of collapse due to cripple wall failure or the failure of the lateral load resisting system; some structures may slip and fall off the foundations; large foundation cracks. Approximately 3 percent of the total area of W1 buildings with complete structural damage is expected to be collapsed.”

The HAZUS technology distinguishes between collapse and complete structural damage by defining collapse as a subset of complete structural damage based on the estimated fraction of the total area of buildings with complete structural damage expected to be collapsed. For wood light-frame (W1) buildings, this fraction is small (e.g., 3 percent for new buildings) recognizing that most W1 buildings with complete damage will be leaning but not collapsed, that collapse of W1 buildings of two or more stories would likely only occur at the first-floor level, and that total collapse of W1 buildings is very unlikely. Although structural, nonstructural, and contents damage states all contribute significantly to economic losses, building collapse dominates earthquake fatalities and serious injuries that are

presumed to occur primarily in the collapsed portions of buildings (with complete structural damage).

In 2005, the California Office of Statewide Health Planning and Development (OSHPD) adopted a collapse risk-based seismic evaluation program based on the HAZUS Advanced Engineering Building Module (AEBM) methodology (FEMA, 2002). The OSHPD program evaluates and re-prioritizes older (pre-1973) hospital buildings identified as having one or more structural deficiencies (referred to as SPC-1 hospital buildings). The OSHPD Program ranks SPC-1 buildings based on their relative collapse risk, thereby enabling the policy makers to implement “worst first” compliance with the hospital seismic safety requirements (Tokas and Lobo, 2012). The HAZUS AEBM methodology of the OSHPD program was adopted as part of the administrative regulations of the 2007 *California Building Standards Code* (CBSC, 2007) including the following definitions:

“Complete Structural Damage means a significant portion of the structural elements have exceeded their ultimate capacities or some critical structural elements or connections have failed resulting in dangerous permanent lateral displacement, partial collapse or collapse of the entire building. A Complete Structural Damage would be a loss of 100 percent of the building’s replacement cost.”

“Probability of Collapse means the fraction of building that is expected to collapse given that the ground motions defined in Section 1.4.5.1.2.1.4 occur at the building site.”

“Section 1.4.5.1.2.1.4. Site seismicity parameters adjusted for soil type, as determined by the Office, shall be the lesser of:

- Deterministic ground motion due to the maximum magnitude earthquake event on the controlling fault system.
- Probabilistic ground motion having 10 percent probability of being exceeded in 50 years.”

“Probability of Collapse. The Probability of Collapse, $P[COL]$, is calculated by Equation (A6-1):

$$P[COL] = P[COL|STR_5] \times P[STR_5] \quad (A6-1)$$

Where: $P[COL|STR_5]$ = collapse factor of the HAZUS AEBM, as modified herein, and

$P[STR_5]$ = probability of Complete Structural Damage, based on HAZUS AEBM methods and parameters, as modified herein.”

In summary, the 2007 CBSC OSHPD regulations for collapse risk evaluation of SPC-1 hospital buildings define collapse as a fraction of complete structural damage (i.e., although the collapse factor specified by the 2007 CBSC is 5 percent, 10 percent, or 20 percent for wood light-frame buildings, rather than the HAZUS default value of 3 percent, depending on the type and number of significant structural deficiencies) and define ground motions that are effectively one-half to two-thirds of MCE_R ground motions (i.e., ground motion intensity approximately equal to that of design earthquake (DE) ground motions). The 2007 CBSC OSHPD regulations initially defined the less risky SPC-1 hospital buildings as those having a collapse probability, P[COL], less than or equal to 0.75 percent, although this criterion was subsequently relaxed to a P[COL] value less than or equal to 1.25 percent. Thus, the 2007 CBSC OSHPD criteria essentially define the acceptable collapse probability as about 1 percent, conditioned on DE ground motions when collapse is defined in terms of the fraction of the building area expected to be collapsed.

Hypothetically, if the 2007 CBSC OSHPD regulations had defined collapse consistent with ASCE/SEI 7-10 and FEMA P-695 (i.e., without consideration of the extent of the building area affected by collapse), then the 2007 CBSC OSHPD criteria would essentially define the acceptable probability of collapse conditioned on DE ground motions as ranging from 5 percent for wood light-frame buildings with significant structural deficiencies, to 20 percent for wood light-frame buildings without significant structural deficiencies. An acceptable collapse probability of 5 percent conditioned on DE ground motions is roughly comparable to an acceptable collapse probability of 10 percent conditioned on MCE_R ground motions.

Table 2-7 illustrates the notional relationship between complete structural damage and collapse for a hypothetical three-story wood light-frame building. In this example, it is assumed that if the building has complete structural damage, then it is equally likely to be leaning (but not collapsed) as it is to have some degree of collapse. If collapsed, it is much more likely that only the first floor has collapsed, rather than the entire building experiencing a total (pancake) collapse. The table includes the probabilities of collapse given complete structural damage for both the ASCE/SEI 7-10 (FEMA P-695) definition of collapse (i.e., without consideration of the extent of the building area affected by collapse) and the 2007 CBSC OSHPD definition of collapse, which reduces the conditional probability based on the fraction of the building area assumed to be collapsed.

Table 2-7 Notional Relationship between Complete Structural Damage and Collapse for a Hypothetical Three-Story Wood Light-Frame Building

Complete Structural Damage		P[Collapse]	Complete Structural Damage	
Type of Damage or Collapse	Likelihood of Damage or Collapse (%)	ASCE/SEI 7 (FEMA P-695) (%)	Percentage of Building Area Collapsed (%)	2007 CBSC OSHPD (HAZUS) (%)
Leaning (Not Collapsed)	50	0	0.0	0
First-Floor Collapse	45	45	33.3	15
Total (Pancake) Collapse	5	5	100.0	5
All	100	50	-	20

It should be noted, that the probability of collapse given complete structural damage is 50 percent for the ASCE/SEI 7-10 (FEMA P-695) definition of collapse, consistent with the assumption that the hypothetical building would be equally likely to be leaning (but not collapsed), as it would to be collapsed, if the structure has complete damage. The probability of collapse given complete structural damage is 20 percent for the 2007 CBSC OSHPD definition of collapse, consistent with the reduced area for a first-floor collapse. In this example, the 2007 CBSC OSHPD conditional collapse probability of 20 percent represents a SPC-1 hospital building with multiple significant structural deficiencies. The 2007 CBSC OSHPD conditional collapse probability is 5 percent for wood light-frame buildings with no significant structural deficiencies.

Many post-earthquake safety assessments use the guidelines provided in ATC-20, *Procedures for Postearthquake Safety Evaluation of Buildings* (ATC, 1989; 2005). The ATC-20 safety assessment procedure is a rapid evaluation tool that focuses on the integrity of the structural system. Inspectors are instructed to affix a placard (colored tag) on an inspected structure, according to the following guidelines:

- **Inspected Placard (green tag).** No apparent hazard found, although repairs may be required. Original lateral load capacity not significantly decreased. No restriction on use or occupancy.
- **Restricted Use Placard (yellow tag).** Dangerous condition believed to be present. Entry by owner permitted only for emergency purposes and only at own risk. No usage on a continuous basis. Entry by public not permitted. Possible major aftershock hazard.
- **Unsafe Placard (red tag).** Extreme hazard, may collapse. Imminent danger of collapse from aftershock. Unsafe for occupancy or entry, except by authorities.

Tagging data (i.e., the number of colored tags issued for damage to individual structures following a post-earthquake assessment), although imperfect, provide a measure of significant structural damage (and in some cases, significant nonstructural damage). In general, building inspectors tend to err on the conservative side, such that the initial posting of a yellow or red tag, in some cases, is removed or modified after a more thorough investigation by a structural engineer. Although a conservative measure of collapse, red-tag data provide a reasonable basis for benchmarking collapse performance. In concept, post-earthquake safety evaluations would assign a red tag to buildings that are leaning (but not collapsed) as well, and, therefore, best describe buildings with complete structural damage (e.g., as defined by the 2007 CBSC regulations for evaluation of SPC-1 hospital buildings).

The relationship between collapse and complete structural damage illustrated in the example of Table 2-7 can be used to estimate the probability that three-story wood light-frame buildings would be assigned a red tag (i.e., have complete structural damage) for an assumed fraction of all such buildings with collapse damage. For example, Table 2-8 shows example values of the probability of complete structural damage required to meet the 10-percent collapse safety goal of ASCE/SEI 7-10 for MCE_R ground motions. This example suggests that as many as 1 in every 5 (i.e., 20 percent) of all new three-story wood light-frame buildings designed to ASCE/SEI 7-10 criteria could be assigned a red tag after an earthquake in those areas shaken with MCE_R ground motions if their collapse capacity was consistent with the ASCE/SEI 7-10 collapse safety goal of 10 percent.

Table 2-8 Probability of Complete Structural Damage Required to Meet the 10-Percent Collapse Safety Goal of ASCE/SEI 7-10 for MCE_R Ground Motions Using the Hypothetical Three-Story Wood Light-Frame Building Example of Table 2-7

Complete Structural Damage		P[Complete MCE _R] = ASCE/SEI 7-10 Safety Goal		
Type of Damage or Collapse	Probability Required to Meet Safety Goal (%)	ASCE/SEI 7-10 (FEMA P-695) (%)	Percentage of Building Area Collapsed (%)	2007 CBSC OSHPD (HAZUS) (%)
Leaning (Not Collapsed)	10	0	0.0	0
First-Story Collapse	9	9	33.3	3
Total (Pancake) Collapse	1	1	100.0	1
All	20	10	-	4

In a manner similar to Table 2-8, Table 2-9 shows example values of the probability of complete structural damage required to meet the approximate one percent collapse safety goal of the 2007 CBSC OSHPD regulations for DE ground motions. The Table 2-9 example suggests that as many as one in every twenty (i.e., five percent) of all older three-story wood light-frame buildings with multiple significant structural deficiencies could be assigned a red tag after an earthquake in those areas shaken with DE ground motions if their collapse capacity was consistent with the 2007 CBSC OSHPD one-percent collapse safety goal. As described in Section 2.5, actual red-tag rates of wood light-frame buildings in the 1994 Northridge earthquake were much less than the complete structural damage probabilities in these examples, suggesting that real buildings perform much better than the collapse safety goals of ASCE/SEI 7-10 and the 2007 CBSC OSHPD regulations.

Conclusions drawn from post-earthquake safety assessment tagging data also need to consider the complexity of the existing building stock including: (1) irregular configurations present in the inventory that would result in higher damage than typical (i.e., regular) buildings; and (2) variation in the design of the building stock, including buildings that were not engineered, buildings with partially engineered design, and buildings designed in excess of current code minimums. This complexity, however, does not change the overall conclusion that red-tag data provide a conservative estimate of the percentage of the building stock that might experience collapse.

Table 2-9 Probability of Complete Structural Damage Required to Meet the Approximate One-Percent Collapse Safety Goal of the 2007 CBSC OSHPD Regulations for DE Ground Motions Using the Hypothetical Three-Story Wood Light-Frame Building Example of Table 2-7

Complete Structural Damage		$P[\text{Complete} \text{DE}] = 2007 \text{ CBSC OSHPD Safety Goal}$		
Type of Damage or Collapse	Probability Required to Meet Safety Goal (%)	ASCE/SEI 7-10 (FEMA P-695) (%)	Percentage of Building Area Collapsed (%)	2007 CBSC OSHPD (HAZUS) (%)
Leaning (Not Collapsed)	2.50	0.00	0.0	0.00
First-Floor Collapse	2.25	2.25	33.3	0.75
Total (Pancake) Collapse	0.25	0.25	100.0	0.25
All	5.0	2.5	-	1.0

2.4 Measured Periods of Wood Light-Frame Buildings

Measured values of building period were obtained from prior studies of CSMIP earthquake data, in-situ forced vibration tests, and full-scale shake table tests of wood light-frame buildings or test structures.

The CUREE-Caltech Woodframe Project (CUREE, 2010) evaluated the dynamic properties of wood light-frame buildings, including determination of the fundamental-mode building period from CSMIP earthquake records of three single-story buildings (i.e., an elementary school, a fire station and a hospital building), a two-story office building, a three-story motel, and from forced vibration tests of a two-story house and a three-story apartment building (Camelo et al., 2002). In all cases, peak building response amplitudes are at very small drift ratios (less than 0.1 percent).

CSMIP earthquake records were also used to evaluate dynamic properties of two buildings which experienced stronger earthquake shaking, a one-story elementary school in Parkfield and the north wing of the Templeton Hospital building, allowing evaluation of the change in building period with response amplitude (Sutoyo and Hall, 2006).

Additional building period data were obtained from full-scale shake table tests of a two-story Japanese house at the E-Defense facility in Miki, Japan (Isoda et al., 2008) and a two-story townhouse at the Structural Engineering and Earthquake Simulation Laboratory (SEESL), University at Buffalo (Filiatrault et al., 2010). In both cases, measured response from a sequence of earthquake shakes provides building period data for the test structures in undamaged and damaged conditions.

Table 2-10 summarizes the occupancy, number of stories, height, plan dimensions, building condition, and the source or type of shaking for the 12 short-period wood light-frame buildings or test structure configurations described above. Table 2-11 summarizes measured values of peak response and building period for each these buildings.

Figure 2-5 is a plot of the measured values of average building period as a function of building height obtained from Table 2-11 for low-amplitude measurements of response (drift ratios less than or equal to 0.5 percent) from 12 short-period buildings. Average building period is based on measured longitudinal and transverse directions (when periods are available for both directions). In the figure, vertical lines connect period data for the same building or test structure obtained from different earthquake records (CSMIP data) or from different runs of shake table tests. This illustrates the increase in building period with damage sustained in prior shake table tests (e.g.,

Japanese house periods, ID No. 9a, 9b, and 9c in Table 2-11) or the increase in period with the amplitude of earthquake response (e.g., Templeton Hospital periods, ID No. 8a, 8b, 8c, 8d, and 8e in Table 2-11), which is observed to occur even for relatively low amplitudes of response (i.e., peak roof drift ratios less than or equal to 0.5 percent).

Table 2-10 Parameters of 12 Short-Period Wood Light-Frame Buildings with Measured Values of Building Period, Obtained from CSMIP Earthquake Data, Forced Vibration Tests, or Full-Scale Shake Table Tests

ID No.	Occupancy (Location)	No. of Stories	Height (feet)	Plan Dimensions		Building Condition	Source or Type of Shaking
				Length (feet)	Width (feet)		
CSMIP Earthquake Data and Forced-Vibration Tests - CUREE Wood (Camelo et al., 2002)							
1a	Motel (San Bernardino)	3	29.9	180.5	132	In Situ	M4.2 Earthquake
1b							M3.7 Earthquake
1c							M4.5 Earthquake
2a	Elementary School (Parkfield)	1	13.2	48	30	In Situ	M4.2 Earthquake
2b							M4.7 Earthquake
3	Fire Station (Bishop)	1	17.0	62	50	In Situ	M6.0 Earthquake
4	Hospital (Indio)	1	13.7	298	148	In Situ	M4.9 Earthquake
5	Office (Eureka)	2	26.0	80	54	In Situ	M3.9 Earthquake
6	House (Pasadena)	2	20	NA	NA	In Situ	Forced Vibration
7	Apartment (Pasadena)	3	30	NA	NA	In Situ	Forced Vibration
CSMIP Earthquake Data (Sutoyo and Hall, 2006)							
2a	Elementary School (Parkfield)	1	13.2	48	30	In Situ	M4.2 Earthquake
2b							M4.7 Earthquake
2c							M6.0 Earthquake
8a	Templeton Hospital (north wing)	1	14.0	110	51	In Situ	M6.5 (Main Shock)
8b							M6.5 (After Shock)
8c							M6.5 (After Shock)
8d							M6.5 (After Shock)
8e							M4.4 Earthquake

Table 2-10 Parameters of 12 Short-Period Wood Light-Frame Buildings with Measured Values of Building Period, Obtained from CSMIP Earthquake Data, Forced Vibration Tests, or Full-Scale Shake Table Tests (continued)

ID No.	Occupancy (Location)	No. of Stories	Height (feet)	Plan Dimensions		Building Condition	Source or Type of Shaking
				Length (feet)	Width (feet)		
Full-Scale Shake Table Test Data - E-Defense Facility, Miki Japan (Isoda et al., 2008)							
9a	Japanese House (with timber bracing, interior gypsum board and ceramic siding)	2	20.0	33	27	Undamaged	White Noise (1)
9b						Post-JMA (100%)	White Noise (5)
9c						Post-JMA (110%)	White Noise (7)
9d						Undamaged	Takatori (100%)
9e						Post-Takatori	Takatori (repeat)
9f						Post-Takatori (2)	Takatori (repeat)
Full-Scale Shake Table Test Data - SEESL Facility, SUNY Buffalo (Filiatrault et al., 2010)							
10	Townhouse (California-style index building—CUREE-Caltech Woodframe Project)	2	17.4	59.5	23	SFRS* only	White Noise
11						SFRS with gyp board	White Noise
12a							White Noise
12b							Canoga (99% / 50 yr.)
12c							Canoga (50% / 50 yr.)
12d							Canoga (20% / 50 yr.)
12e							Canoga (10% / 50 yr.)
12f							Rinaldi (2% / 50 yr.)

* Seismic Force-Resisting System.

Table 2-11 Measured Values of Peak Response and Building Period for 12 Short-Period Wood Light-Frame Buildings, Obtained from CSMIP Earthquake Data, Forced Vibration Tests, or Full-Scale Shake Table Tests

ID No.	Occupancy (Location)	Height (feet)	Peak Roof Drift (%)	Building Period (seconds)		
				Longitudinal	Transverse	Average
CSMIP Earthquake Data and Forced-Vibration Tests - CUREE Wood (Camelo et al., 2002)						
1a	Motel (San Bernardino)	29.9	< 0.1	0.22	0.19	0.21
1b			< 0.1	0.20	0.21	0.21
1c			< 0.1	0.23	0.18	0.21
2a	Elementary School (Parkfield)	13.2	< 0.1	0.14	0.12	0.13
2b			< 0.1	0.15	0.12	0.14
3	Fire Station (Bishop)	17.0	< 0.1	0.11	0.18	0.15
4	Hospital (Indio)	13.7	< 0.1	0.13	0.14	0.14
5	Office (Eureka)	26.0	< 0.1	0.20	0.20	0.20
6	House (Pasadena)	20.5	< 0.1	0.180	0.204	0.19
7	Apartment (Pasadena)	30.0	< 0.1	0.196	0.238	0.22
CSMIP Earthquake Data (Sutoyo and Hall, 2006)						
2a	Elementary School (Parkfield)	13.2	< 0.1	0.14	0.12	0.13
2b			< 0.1	0.15	0.12	0.14
2c			< 0.1	0.20	0.18	0.19
8a	Templeton Hospital (north wing)	14.0	≈ 0.5	NA	0.20	0.20
8b			< 0.1	NA	0.14	0.14
8c			< 0.1	NA	0.15	0.15
8d			≈ 0.1	NA	0.17	0.17
8e			< 0.1	NA	0.14	0.14
Full-Scale Shake Table Test Data - E-Defense Facility, Miki Japan (Isoda et al., 2008)						
9a	Japanese House (with timber bracing, interior gypsum board and ceramic siding)	20.0	< 0.1	0.16	0.21	0.19
9b			< 0.1	0.30	0.26	0.28
9c			< 0.1	0.38	0.44	0.41
9d			≈ 10 (first floor)	≈ 1.2	≈ 1.2	≈ 1.2
9e			≈ 18 (first floor)	≈ 2	≈ 2	≈ 2
9f			Collapse	> 2	> 2	> 2

Table 2-11 Measured Values of Peak Response and Building Period for 12 Short-Period Wood Light-Frame Buildings, Obtained from CSMIP Earthquake Data, Forced Vibration Tests, or Full-Scale Shake Table Tests (continued)

ID No.	Occupancy (Location)	Height (feet)	Peak Roof Drift (%)	Building Period (seconds)		
				Longitudinal	Transverse	Average
Full-Scale Shake Table Test Data - SEESL Facility, SUNY Buffalo (Filiatrault et al., 2010)						
10	Townhouse (California-style index building— CUREE-Caltech Woodframe Project)	17.4	< 0.1	0.23	0.33	0.28
11			< 0.1	0.22	0.30	0.26
12a			< 0.1	0.20	0.29	0.25
12b			≈ 0.1	NA	NA	NA
12c			≈ 0.5	NA	≈ 0.5	≈ 0.5
12d			≈ 0.8	NA	NA	NA
12e			1.2	NA	≈ 0.59	≈ 0.59
12f			3.1	NA	≈ 0.77	≈ 0.77

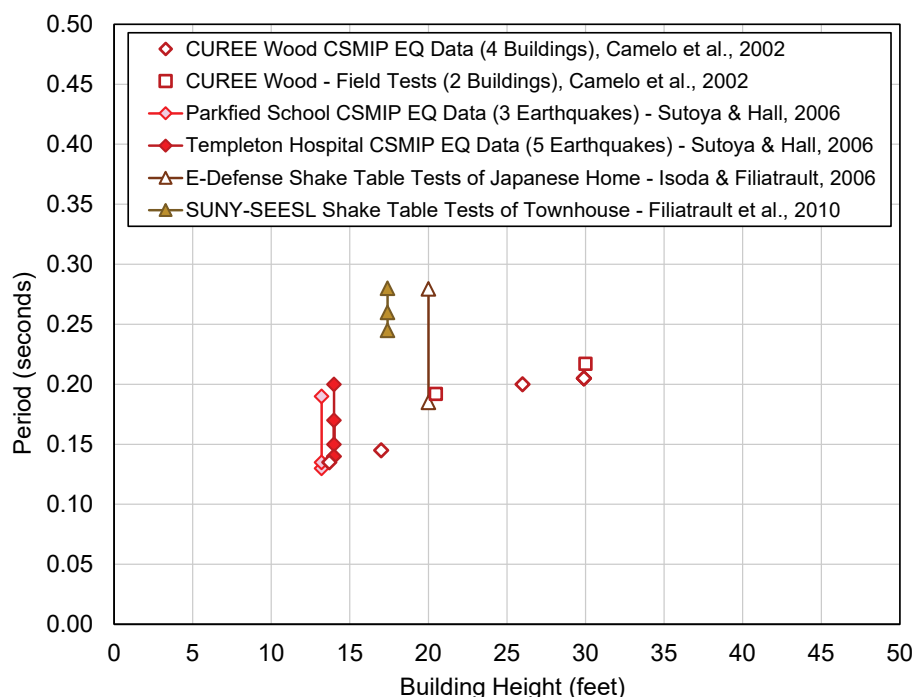


Figure 2-5 Average building period as a function of building height, obtained from CSMIP earthquake data, forced vibration tests, or full-scale shake table tests.

2.5 Observed Damage and Collapse of Wood Light-Frame Buildings in the 1994 Northridge Earthquake

This section develops benchmark collapse performance of wood light-frame buildings based on post-earthquake safety evaluations of over 100,000

buildings inspected after the 1994 Northridge earthquake. Post-earthquake safety evaluation data include ATC-20 tagging data (i.e., green tags, yellow tags and red tags) compiled by the California Governor's Office of Emergency Services (OES) (OES, 1995; 1997). Red-tag data are used to benchmark collapse performance. As discussed in Section 2.3.3, red-tag data provide a conservative (high) estimate of collapsed buildings since, by definition, they include all severely damaged buildings considered a threat to life-safety, even if not collapsed (e.g., buildings that are leaning). Initially, red-tag data geospatially grouped by MMI region were used to develop preliminary benchmark estimates of collapse behavior. Subsequently, red-tag data geospatially grouped by census tract were used to refine these estimates. Although the trends were found to be similar, red-tag statistics geospatially grouped by census tract also provide a sense of the scatter in the data, and, presumably, the collapse uncertainty.

The FEMA P-695 methodology assumes that collapse is lognormally distributed. For direct comparison with FEMA P-695 evaluations of the archetype of interest, benchmark collapse functions would ideally also be characterized by a lognormal distribution with properties based on red-tag statistics. However, red-tag data are not necessarily lognormally distributed and a lognormal distribution was found to be a difficult fit for red-tag data from the 1994 Northridge earthquake.

Techniques for fitting lognormal curves to statistical data include the maximum likelihood method of Appendix C of NIST GCR 11-917-15, *Selecting and Scaling Earthquake Ground Motions for Performing Response-History* (NIST, 2011), and fragility development methods of Appendix H of FEMA P-58-1, *Seismic Performance Assessment of Buildings, Volume 1 – Methodology* (FEMA, 2012a). These techniques are challenged by very low values of red-tag statistics which represent the extreme (very low probability) tail of the lognormal collapse curve.

Table 2-12 summarizes wood light-frame building inventory (based on Table 6 in Kircher, 2006b) and red-tag data from safety evaluations of wood buildings (OES, 1995), and develops the corresponding red-tag statistics (i.e., percentage of all wood buildings with a red tag) for each of five MMI regions in the 1994 Northridge earthquake: MMI V or smaller, MMI VI, MMI VII, MMI VIII, and MMI IX. Figure 2-6 shows a plot of the red-tag percentages of Table 2-12 as a function of the average value of 0.3-second spectral acceleration for the five MMI regions (from Table 6 in Kircher, 2006b) along with two “notional” collapse fragility curves that are assumed to be lognormally distributed with plausible values of median collapse and lognormal standard deviation. These two collapse fragility curves have

lognormal standard deviation values of $\beta_{TOT} = 0.5$ (and a median of 3g) and $\beta_{TOT} = 0.75$ (and a median of 5g), respectively, representing the range of possible values of the lognormal standard deviation parameter of FEMA P-695. As illustrated in Figure 2-6, it is difficult for a collapse fragility curve characterized by a lognormal distribution to match red-tag data over all ground motion levels of interest (e.g., 0g to 1.5g) unless the median collapse is unrealistically large (i.e., much greater than 5g).

Table 2-12 Safety Assessment Tagging Data and Damage Statistics by MMI Region for Wood Buildings Inspected after the 1994 Northridge Earthquake

Safety Tagging	MMI Region					
	< V	VI	VII	VIII	IX	All
Number of Wood Buildings with a Green, Yellow or Red Tag (OES, 1995)						
Green	260	3,068	19,429	40,367	4,494	67,618
Yellow	26	542	2,095	4,375	612	7,650
Red	4	32	325	1,023	230	1,614
Population of Wood Buildings (based on Table 6, Kircher, 2006b)						
Population	668,357	1,215,471	514,967	379,330	26,000	2,804,125
Percentage of Wood Buildings with a Yellow or Red Tag						
Yellow	0.00%	0.04%	0.41%	1.15%	2.35%	0.27%
Red	0.00%	0.00%	0.06%	0.27%	0.88%	0.06%

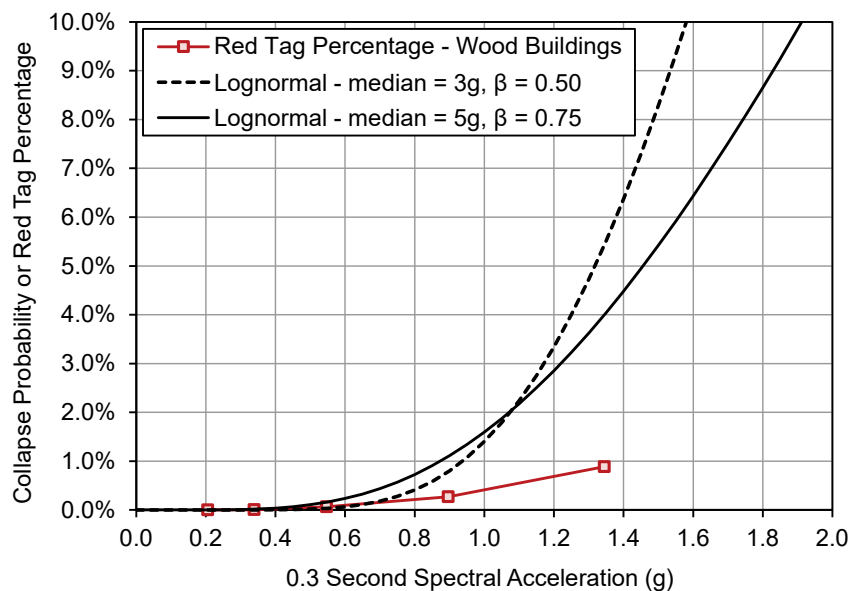


Figure 2-6 Red-tag percentages of Table 2-12, plotted as function of 0.3-second spectral acceleration along with two notional collapse fragility curves assumed to be lognormally distributed with plausible values of median collapse and lognormal standard deviation (β).

In Figure 2-6, the 0.3-second spectral acceleration value in the MMI 8 region is approximately 0.9g, which is the average value of Shake Map ground motions of 308 census tracts with individual values ranging from 0.32g to 1.48g. For each of the 308 census tracts in the MMI 8 region, Figure 2-7 shows mean and maximum values of Shake Map 0.3-second spectral acceleration ground motions plotted as function of 0.3-second spectral acceleration ground motions developed by Somerville for the SAC Steel project (SAC, 1995). While the trend in mean Shake Map data (red curve) is similar to that of the Somerville (geomean) data, there is a large amount of scatter in the individual values of recorded ground motions. If there was no difference between the two data sets, then all points would lie on a straight line (i.e., the black line). Comparison of the Shake Map and Somerville ground motion data sets illustrates the uncertainty in recorded ground motions and the large variability of individual (census tract) values of 0.3-second spectral acceleration for the same MMI region.

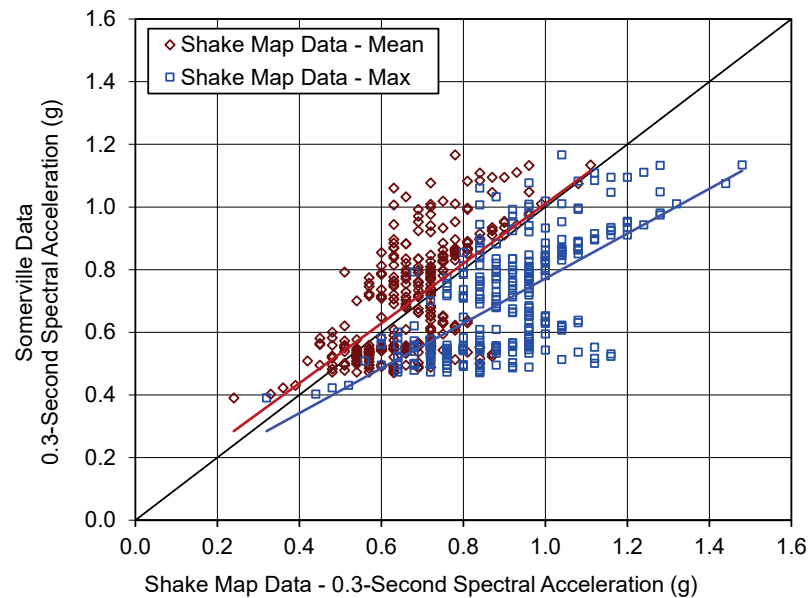


Figure 2-7 Individual values of 0.3-second spectral accelerations for each of the 308 census tracts in the MMI 8 region of the 1994 Northridge earthquake based on: (1) Shake Map data, maximum direction (Wald et al., 1999); (2) Shake Map data, mean direction (taken as 0.75 of maximum); and (3) Somerville map data (SAC, 1995).

The tagging rates summarized in Table 2-12 were grouped by MMI region, because the underlying data were reported by OES in terms of MMI. Recognizing the potentially large range of 0.3-second spectral acceleration values for each MMI region illustrated in Figure 2-7, a more refined set of post-earthquake building safety evaluation tagging data were developed on a census-tract basis. Tagging data were extracted from the original OES

database, which was the basis for aggregated results reported in OES (1995). Initial review of the OES database (now 20 years old) found the number of buildings and the tagging data in the OES database to be somewhat different from those reported in OES (1995). These relatively minor discrepancies were most likely due to updates to the OES database after data were aggregated for the OES report, and did not have a significant effect on tagging statistics.

Table 2-13 summarizes the number (count) of census tracts with building safety inspections after the 1994 Northridge earthquake, the total number of wood light-frame buildings inspected, and the number of wood light-frame buildings assigned red tags (from the OES database). Table 2-13 also summarizes the number of all wood light-frame (W1 and W2) buildings in these census tracts from the HAZUS99 building inventory and from an improved inventory of buildings developed as part of the Southern California ShakeOut Scenario (Porter et al., 2011). HAZUS99 refers to a prior release of HAZUS (FEMA, 2003) with 1990 census tract and building inventory data deemed more suitable for evaluating 1994 Northridge earthquake damage. Data groups in Table 2-13 refer to subsets of building inventories used to compare various sources of these data. For example, Data Group 1 shows good agreement between HAZUS99 and ShakeOut building inventories in terms of the total number of W1 and W2 buildings used to develop tagging statistics.

Table 2-13 Census Tracts with Building Safety Inspections after the 1994 Northridge Earthquake, the Total Number of Wood Light-Frame Buildings Inspected, the Number of Wood Light-Frame Buildings Assigned Red Tags, and the Inventory of All Wood Light-Frame Buildings (W1 and W2) in these Census Tracts

Data Group	OES Database			HAZUS99 Inventory			ShakeOut Inventory		
	Census Tract Count	Wood Bldg. Count	Red-Tag Bldg. Count	W1 Bldg. Count	W2 Bldg. Count	Wood Bldg. Count	W1 Bldg. Count	W2 Bldg. Count	Wood Bldg. Count
1	613	51,714	1,021	542,945	4,784	547,729	505,031	57,092	562,123
2	9	995	18	7,355	38	7,393	-	-	-
3	339	27,859	579	397,419	3,264	400,683	-	-	-
4	6	40	1	-	-	-	-	-	-
Total	967	80,608	1,619	947,719	8,086	955,805	505,031	57,092	562,123
Post-1960	186	24,710	435	-	-	219,301	-	-	-

Table 2-13 shows a total of 967 census tracts with inspected buildings, although only 80,608 of the 955,805 wood light-frame buildings, based on HAZUS99, have reliable tagging data. Of the 80,608 inspected buildings, 1,619 buildings were assigned a red tag. A post-1960 subset of buildings

was developed to focus on red-tag statistics for newer buildings, which consisted of a total of 219,301 wood light-frame buildings in 186 census tracts, of which 24,710 buildings were inspected and 435 buildings were assigned red tags. Little difference was found in the trends of red-tag statistics for the full set and the post-1960 subset of wood light-frame buildings. For each census tract of interest, values of 1994 Northridge earthquake 0.3-second spectral accelerations were obtained from the Somerville (geomean) data (SAC, 1995) and factored by 1.2 to represent shaking in the maximum horizontal direction of response consistent with ASCE/SEI 7-10 (and FEMA P-695).

Table 2-14 summarizes the total number of buildings, number of buildings with red tags, red-tag percentages, and mean values of 0.3-second spectral acceleration for each of 22 census-tract groups of roughly equal building count (i.e., about 10,000 buildings each) and increasing ground motion intensity. Very small red-tag percentages (rates) are shown in Table 2-14, even for census-tract groups with significant values of 0.3-second spectral acceleration. There are no red-tag rates greater than 1 percent for any census-tract group, although the 0.3-second spectral acceleration reaches or exceeds 1.5g for census-tract groups in the areas of strongest shaking. For reference, a short-period MCE_R response spectral acceleration of 1.5g is typical of ASCE/SEI 7-10 requirements for sites in areas of strongest shaking in the 1994 Northridge earthquake. There are a few individual census tracts with red-tag rates over 1 percent, but none over 2.6 percent.

Figure 2-8 shows red-tag percentages for each of the 184 individual census tracts as well as the 22 groups of aggregated data plotted as function of 0.3-second spectral acceleration. The aggregated data show the general trend of increasing red-tag rate with ground motion intensity. This trend is shown in Figure 2-8 with a best-fit lognormal fragility curve fit to the first 21 data points of the 22 building groups using the Maximum Likelihood Estimation calculation tool of Baker (2015). For comparison, Figure 2-8 also shows a theoretical collapse curve of newer W1 buildings developed on the ATC-71-6 Project and reported in FEMA P-155, *Rapid Visual Screening of Buildings for Potential Seismic Hazards: Supporting Documentation, Third Edition* (FEMA, 2015b).

Although the best fit and theoretical collapse curves of Figure 2-8 are both reasonable representations of the trend in red-tag percentages (up to values of 0.3-second spectral acceleration of about 2g), they are conceptually very different. The best-fit collapse curve of post-1960 wood light-frame buildings has a median value of 0.3-second spectral acceleration of 15g (which does not make physical sense) and a lognormal standard deviation of

0.93. The best fit curve illustrates the inherent difficulty in characterizing collapse damage by a lognormal distribution fit to very small collapse (red-tag) percentages (i.e., an unrealistically large median is required to fit observed collapse (red-tag) percentages). Conversely, a more reasonable value of the median (e.g., 5g) would over-predict the observed trend in collapse (red-tag) percentages.

Table 2-14 Total Number (Count) of Wood Light-Frame Buildings Inspected, Number of Wood Light-Frame Buildings Assigned Red Tags, Red-Tag Percentage, and Mean Value of 0.3-Second Spectral Acceleration for Each of 22 Census-Tract Groups of Approximately Equal Building Count from the 1994 Northridge Earthquake

Group No.	Building Count	Number of Red Tags	Red-Tag Percentage (%)	Mean 0.3-second RSA (g)
1	10,467	0	0.00	0.31
2	9,689	0	0.00	0.36
3	10,918	0	0.00	0.38
4	9,739	0	0.00	0.42
5	10,084	0	0.00	0.50
6	8,959	2	0.02	0.59
7	7,834	8	0.10	0.63
8	11,160	5	0.04	0.70
9	9,763	7	0.07	0.76
10	9,116	19	0.21	0.85
11	10,290	15	0.15	0.90
12	9,901	10	0.10	0.94
13	10,135	17	0.17	0.97
14	9,927	19	0.19	1.03
15	10,092	14	0.14	1.10
16	10,534	7	0.07	1.18
17	10,365	36	0.35	1.24
18	10,444	58	0.56	1.30
19	10,266	73	0.71	1.36
20	10,078	55	0.55	1.41
21	10,028	64	0.64	1.53
22	9,512	26	0.27	1.67
All	219,301	435	-	-

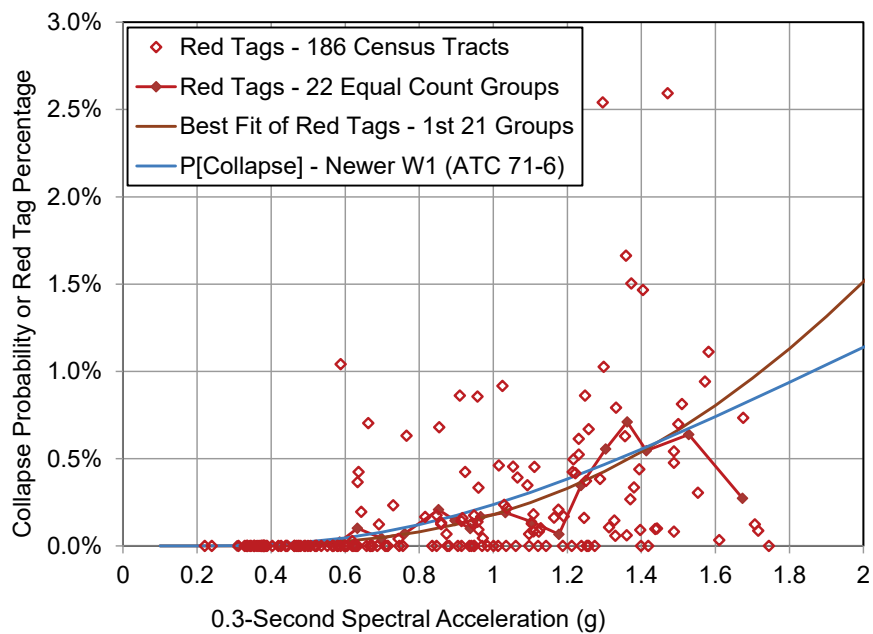


Figure 2-8

Red-tag percentages as a function of 0.3-second spectral acceleration developed from post-earthquake safety inspections of 24,710 post-1960 wood light-frame buildings following the 1994 Northridge earthquake, along with a lognormal best fit fragility curve based on census-tract group red-tag percentages, and a theoretical collapse curve for newer W1 buildings developed by the ATC-71-6 Project.

The theoretical collapse curve of newer wood light-frame (W1) buildings of FEMA 155 (ATC 71-6 Project) is based on the HAZUS AEBM methods of the 2007 CBSC OSHPD regulations for collapse evaluation of SPC-1 hospital buildings (see Section 2.3). In this case, the theoretical collapse curve is described by a lognormally-distributed complete structural damage function factored by 0.05, which is the conditional collapse rate given complete structural damage for newer wood light-frame (W1) buildings. The lognormally-distributed complete structural damage function has a median of 3.5g (which is physically possible) and a lognormal standard deviation of 0.75. The theoretical collapse curve of FEMA 155 provides a plausible alternative to the best fit assumption of a lognormal distribution of collapse damage.

The building inventory and red-tag data summarized in Table 2-12 effectively lump one-story wood light-frame buildings with buildings of two or more stories. Observations of earthquake damage, collapse, and shake table tests of full-scale test structures (see Section 2.7) suggest that multi-story wood light-frame buildings have a greater likelihood of collapse than one-story wood light-frame buildings, all else equal. This observation was investigated by parsing the 24,710 post-1960 wood light-frame buildings

with tagging data into three groups: (1) buildings of one story in height; (2) abuildings greater than one story in height; and (3) buildings of unknown height (i.e., the OES database does not always provide building height data). Green-tag, yellow-tag, and red-tag percentages were then developed separately for one-story buildings and for buildings of more than one story in height.

Table 2-15 summarizes the tagging data and the calculation of tagging percentages. In these calculations, tagging percentages are based on the number of buildings of a given tag (e.g., red tags) divided by the number of buildings inspected, rather than dividing by the total inventory of all post-1960 wood light-frame buildings. Hence, tagging rates shown in Table 2-15 are much greater than those of Table 2-13 which are based on the full inventory of post-1960 wood light-frame buildings.

Table 2-15 One-Story and Two-Story (or More) Post-1960 Wood Light-Frame Buildings with Red, Yellow, or Green Tags, and Corresponding Fractions of One-Story and Two-Story (or More) Buildings with Red, Yellow, or Green Tags from the 1994 Northridge Earthquake

Building	Number of Post-1960 Wood Light-Frame Buildings by Safety Inspections				
	All Tags	Red Tags	Yellow Tags	Green Tags	Unknown
All	24,710	435	2,342	21,533	400
Unknown	9,382	71	389	8,616	306
Known	15,328	364	1,953	12,917	94
One-Story	8,402	116	812	7,423	51
Two-Story (or More)	6,926	248	1,141	5,494	43
	Percentage of Post-1960 Wood Light-Frame Buildings of Known Height by Safety Inspections				
Fraction of One-Story (%)	99.4	1.38	9.7	88	0.6
Fraction of Two-Story (or More) (%)	99.4	3.6	16.5	79	0.6
	Comparison of Post-1960 Wood Light-Frame Buildings by Safety Inspections				
Ratio of Two-Story (or More) to One-Story Buildings	1.0	2.6	1.7	0.9	1.0

The tagging ratios (fractions) shown in Table 2-15 suggest two important trends in wood light-frame building damage. First, wood light-frame buildings of two or more stories in height are roughly 2½ times more likely to collapse or have severe structural damage (requiring a red tag) than one-

story wood light-frame buildings, all else equal. Second, the importance of height diminishes with the degree of damage. For example, there is essentially no height bias for buildings with minimal damage, as characterized by a green tag (i.e., buildings assigned a green tag are almost equally likely to be one story as two or more stories in height).

The calculation of the tagging ratios (fractions) in Table 2-15 implicitly assumes that there is no bias in the data due to potential differences in the spatial mix of building heights with respect to ground motion intensity (i.e., the fraction of all multi-story wood light-frame buildings is approximately the same for census tracts in areas of weaker and stronger shaking). The implicit assumption of unbiased tagging data is not unreasonable given that these data are based on a large number of inspected buildings (i.e., approximately 25,000 buildings) spatially distributed over many census tracts in cities and suburban areas affected by the 1994 Northridge earthquake.

The results of comprehensive statistical analyses of safety tagging data is supported by other sources of observed damage to short-period wood light-frame buildings in the 1994 Northridge earthquake. These sources include field surveys reported in ATC-38, *Database on the Performance of Structures near Strong-Motion Recordings: 1994 Northridge, California, Earthquake* (ATC, 2000), CUREE Publication No. W-09, *Northridge Earthquake Field Investigations: Statistical Analysis of Woodframe Damage* (Schierle, 2003), and in *Assessment of Damage to Residential Buildings Caused by the Northridge Earthquake* (HUD, 1994). The HUD study surveyed and assessed damage to a random sample of residential buildings located in the San Fernando Valley and nearby hills, generally within a 10-mile radius of the epicenter. Although ground motions were not determined at each sample building site, the sample area represents the region of strongest ground motions in the earthquake.

Two groups of building types were surveyed: single-family detached (SFD) properties, and single-family attached and multi-family low-rise (SFA/MFLR) properties of two stories and less. Construction characteristics and damage to 341 SFD homes and 30 SFA/MFLR buildings were recorded. Although the size of the samples of SFD and SFA/MFLR buildings are too small to accurately determine statistics of relatively rare observations of severe building damage, and damage was not correlated with ground motion intensity at sample building sites, the observations of the type and relative frequency of building damage still provide valuable insight into the likely cause of a yellow tag or red tag assigned to wood light-frame buildings in the San Fernando Valley. Further, the HUD study describes the construction characteristics of the SFD and SFA/MFLR buildings affected by the 1994

Northridge earthquake. Summaries of construction characteristics and observations of damage from the Executive Summary of the HUD study for SFD and SFA/MFLR buildings are provided below (excerpted from HUD, 1994):

Single-Family Detached Homes (SFD)

“About 90 percent of the homes in the sample were built prior to the 1971 San Fernando Valley Earthquake.”

“All homes surveyed had wood exterior wall framing. SFD homes were typically one story and nearly two-thirds had an attached garage. Homes on crawlspace foundations outnumbered those on concrete slabs by almost two-to-one, despite a notable increase in the use of slab-on-grade foundations since the 1960s. Cripple-wall foundations were infrequent. Plywood was rarely used for exterior wall sheathing. A stucco exterior finish was typically applied over wire mesh and building paper or felt applied to the studs per the LA City “Type V” prescriptive requirements. A widespread use of wood roof rafters and plaster interior finish also reflected the age of the homes.”

“SFD homes suffered minimal structural damage to elements that are critical to the safety of occupants. Structural damage was most common in the foundation system. The small percentage of surveyed homes (approximately two percent) that experienced significant foundation damage were located in areas that endured localized ground effects or problems associated with hillside sites.”

“Interior and exterior finishes fared much worse than foundations and framing with nearly 50 percent of the homes experiencing at least some damage. However, the great majority of damage was limited to the lowest level of the building. Stucco was observed on nearly all home exteriors. Damage to stucco usually appeared as hairline cracks radiating from the corners of openings, particularly larger openings such as garage doors, or along the top of the foundation. Interior finish damage paralleled the occurrence (sic) of exterior finish (stucco) damage. Resilient finishes, such as wood panel or lap board siding, fared well and often showed no evidence of damage even when stucco on other areas of the same building was modestly damaged.”

Single-Family Attached and Multifamily Low-Rise Dwellings

“The sampling method used for the multifamily low-rise (MFLR) and single-family attached (SFA) survey resulted in a very diverse sample.

Of the 30 residential sites visited, 13 were single-family attached (e.g., duplexes and townhomes) and 17 were multifamily (e.g., condominiums and garden apartments) structures.”

“Smaller SFA homes in the survey (primarily duplexes) were typically of the same construction as SFD homes. The larger SFA units were similar to MFLR construction.”

“Prior to the 1970s many MFLR buildings were built on “soft stories” comprised of open-garage parking underneath of multi-story dwelling units. The garage areas or foundations on these older buildings were typically constructed of steel pipe columns, wood-frame shear walls with stucco finish, or a combination of both. The wood-frame garage ceiling or first floor was supported by either steel or engineered wood (e.g., glulam) girders.”

“Damage to SFA construction appeared to reflect a level of performance similar to that reported for the SFD homes. However, structural damage to MFLR construction was notably more dramatic and costly to lives, especially for certain construction types located in the San Fernando Valley. The more remarkable structural failures were associated with the older MFLR buildings situated on soft-story garage foundations. In agreement with observations and expectations, the performance of stucco finishes, particularly as lateral support to walls on these larger MFLR and SFA buildings, performed noticeably worse than on the “Type V” single-family detached homes.”

2.6 Observed Collapse Performance of Buildings in the 1995 Kobe Earthquake

The M6.8 Kobe earthquake of January 17, 1995, is one of the most significant events of the twentieth century to affect an urban region of modern construction and, other than the 2012 Tohoku tsunami, the most devastating earthquake to hit Japan since 1923 when the Great Kanto earthquake destroyed Tokyo and Yokohama. Severe ground shaking was felt throughout Kobe and other nearby cities of the Hyogo Prefecture that were located close to fault rupture. Figure 2-9 is a photograph of Kobe City (view looking northwest) and Figure 2-10 is a map of the southern portion of the Hyogo Prefecture and neighboring areas of the Osaka Prefecture, showing Kobe City and other nearby cities within 5 km of fault rupture.



Figure 2-9 View of Kobe City looking northwest from Osaka Bay.

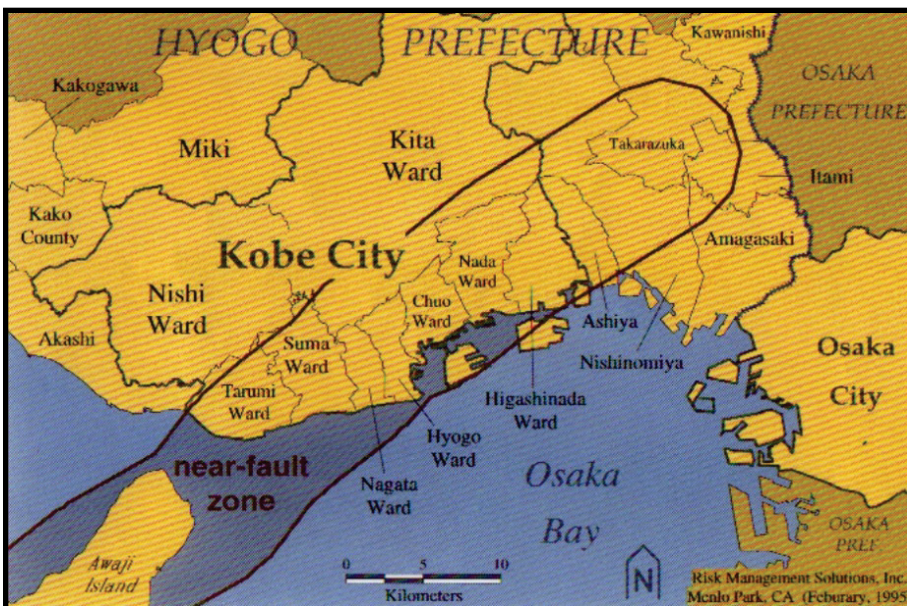


Figure 2-10 Southern portion of Hyogo Prefecture and neighboring areas of the Osaka Prefecture, showing Kobe City and other nearby cities of the region affected by the 1995 Kobe earthquake (figure by Risk Management Solution, Inc.).

The 1995 Kobe earthquake caused 6,434 fatalities (approximately 4,600 of which were from Kobe), serious injury to more than 25,000 people, and forced as many as 300,000 people to seek temporary shelter. Lifeline systems were severely damaged, in particular, highway and railway lifelines and port facilities. The Port of Kobe, which was the third largest container cargo port in Japan before the earthquake, was completely closed. Structures near the shoreline and on man-made Port and Rocco Islands were severely damaged by soil liquefaction, unless supported on deep foundations.

The earthquake caused approximately \$100 billion in damage (2.5 percent of the GDP of Japan at the time of the earthquake), of which an estimated \$80 billion was due to building damage. Of the \$80 billion in direct losses to buildings, about 10 percent was due to fire. Building damage due to ground

shaking was the primary cause of fatalities and serious injury, as well as, direct and indirect economic losses. Figure 2-11 shows a typical street scene in downtown Kobe City immediately after the earthquake, damage at a ferry terminal due to soil liquefaction, and a neighborhood destroyed by fire.

The region affected by the 1995 Kobe earthquake includes Kobe City and other nearby cities with a total population of about 4 million people (based on Japanese census data), and an estimated 800,000 buildings (assuming 5 people per building, on average), as summarized in Table 2-16.



Figure 2-11 Typical street scene in Kobe City immediately after the earthquake; damage at a ferry terminal due to ground failure (liquefaction); and a neighborhood destroyed by fire.

Table 2-16 Approximate Populations and Estimated Number of Buildings in Areas Affected by the 1995 Kobe Earthquake

Area Affected by Earthquake	Population ($\times 1$ Million)	Number of Buildings
Hyogo Prefecture:		
Kobe	1.5	300,000
Other Cities	2.0	400,000
Total	3.5	700,000
Other Prefectures	0.5	100,000
Total (All Areas)	4.0	800,000

Based on preliminary post-earthquake damage surveys by the Architectural Institute of Japan (AIJ) through April of 1995 (AIJ, 1995), over 150,000 of the estimated 800,000 buildings in the affected region had either severe structural damage, or had collapsed, as summarized in Table 2-17.

Table 2-17 Collapse Damage, Severe Damage, or Fire Damage of Buildings Affected by the 1995 Kobe Earthquake (AIJ, 1995)

Area Affected by Earthquake	Collapse Damage	Severe Damage	Fire Damage
Hyogo Prefecture			
Kobe	54,949	31,783	7,733
Other Cities	26,257	31,043	79
Total	81,206	62,826	7,456
Other Prefectures	885	5,217	0
Total (All Areas)	82,091	68,043	7,456

Building damage varied greatly from one neighborhood to another, influenced by local site conditions and other factors. In general, however, buildings in areas close to fault rupture were much more likely to have sustained collapse or severe structural damage. This is illustrated in Table 2-18, which shows the number of buildings with severe or collapse damage (referred to as complete damage in the table) for all areas of Hyogo Prefecture affected by the earthquake (144,032 buildings) and the number of buildings with severe or collapse damage for those areas within 5 km of fault rupture (131,355). Over 90 percent (i.e., 131,355/ 144,032) of the buildings with severe or collapse damage were located within 5 km of fault rupture.

Table 2-18 Buildings with Collapse Damage or Severe Damage in All Areas Affected by the 1995 Kobe Earthquake, and the Number of Buildings with Collapse or Severe Damage Located in Areas within 5 km of Fault Rupture

Area Affected by Earthquake	Number of Buildings	Collapse Damage	Severe Damage
All Wards/Cities	700,000	81,206	62,826
Within 5 km of Fault	375,000	77,259	54,096
Complete Damage (All Areas)	144,032 (~20%)		
Complete Damage (within 5 km of Fault)	131,355 (~35%)		

Table 2-18 also shows the approximate number of buildings located within 5 km of fault rupture (375,000, or about one-half of all Hyogo Prefecture buildings in the affected region). Approximately 21 percent (i.e., 77,259 / 375,000) of the buildings located within 5 km of fault rupture had collapse damage whereas only about 1.2 percent (i.e., $(81,206 - 77,259) / (700,000 - 375,000)$) of the buildings located farther than 5 km from fault rupture had such damage. Roughly one-half of all buildings with complete damage also had collapse damage. If ATC-20 would have been used for postearthquake safety evaluations, then buildings with complete damage would most likely have been assigned a red tag, implying that about one-half of the buildings that would have been assigned a red tag also collapsed.

Building damage summarized in Table 2-18 includes all building types (structural system), occupancies (building use), and design vintages. In Kobe City, building use may be crudely divided into: (1) low-rise residential buildings; (2) smaller commercial and mix-use buildings; (3) mid-rise residential and commercial buildings; and (4) high-rise (> 60 m) buildings. Low-rise residential and smaller commercial and mixed-use buildings are, by far, the most common types of buildings (roughly 90 percent of all buildings) and were also the most likely building types to be damaged in the 1995 Kobe earthquake.

Low-rise residential buildings include one-story and two-story houses of traditional Japanese Shinkabe and Okabe construction. The roof of a traditional Japanese house is typically made of heavy clay tile, often over another heavy material, rendering the house vulnerable to earthquake shaking. Figure 2-12 shows partial collapse of a two-story Japanese house in Nishinomiya.



Figure 2-12 Partial first-story collapse of a two-story house with a heavy tile roof in Nishinomiya after the 1995 Kobe earthquake.

Newer (post-1971) housing consists of pre-fabricated units and frame wall construction using 2×4 studs similar to U.S. wood light-frame construction. Unlike U.S. construction, however, the walls of traditional Japanese houses are made of tied bamboo and covered with plaster. Modern versions of this type of construction may use loose lathe in place of the tied bamboo, but in either case, the walls are inherently weaker than walls made of wood sheathing, gypsum wallboard, or stucco, typical of U.S. construction. In

contrast to Shinkabe and Okabe construction, post-1971 frame wall residential buildings were observed to have performed well in the 1995 Kobe earthquake (AIJ, 1995).

Smaller commercial and mixed-use buildings are two-story and three-story structures common to denser urban areas. The first story is often used for the family business, with the family living upstairs. Typically, several businesses (families) occupy different units of the same building. These buildings are typically made of wood, similar to low-rise residential construction, or light-gage steel buildings in the United States. It is common for these buildings to have a soft/weak first story because the first story will typically have large openings (and no walls) on the street-side of the building. Figure 2-13 shows severe leaning and incipient collapse of a mixed-use building in Kobe City typical of damage to these types of buildings.



Figure 2-13 Severe leaning and incipient collapse of a two-story mixed-use building in Kobe City.

The very high rate of collapse of short-period, low-rise, residential and smaller commercial and mixed-use buildings (i.e., greater than 20 percent in areas within 5 km of fault rupture) in the 1995 Kobe earthquake is largely due to the vulnerability of older construction built prior to current Japanese Building Standard Law (i.e., prior to 1981), but also due to the intensity of the ground motions, particularly at sites near fault rupture. It should be noted that although the buildings are essentially of the same construction, the collapse rate is only about 1 percent in areas farther than 5 km from fault rupture.

The preliminary earthquake reconnaissance report of the Architectural Institute of Japan (AIJ, 1995a) provides the basis for overall damage data reported in Table 2-17, but does not provide the requisite inventory information (e.g., type of structure, age of construction) required to quantify, for example, damage to newer wood-frame buildings. Subsequent improved studies of the 1995 Kobe earthquake compiled geospatial databases of building inventory, building damage, and ground motion parameters that permitted the development of empirical building vulnerability functions (e.g., Yamaguchi and Yamazaki, 2000; Yamazaki and Murao, 2000).

Yamaguchi and Yamazaki (2000) developed building damage functions for Nishinomiya City, and, using the same methods, Yamazaki and Murao (2000) developed building damage functions for the Nada Ward of Kobe City for various building types, including wood-frame, reinforced concrete and steel buildings. The map of the southern portion of the Hyogo Prefecture in Figure 2-10 shows the locations of Nishinomiya City and the Nada Ward of Kobe City and their respective proximities to fault rupture.

In the case of wood-frame buildings, vulnerability functions were developed for each of five construction periods: pre-1952, 1952-1962, 1962-1971, 1972-1981, and 1982-1994. At the time of the 1995 Kobe earthquake, the population of Nishinomiya City was about 412,000, of which 1,114 people were killed in the earthquake. There were a total of 96,261 buildings, of which 24,807 were heavily damaged, and most of which (about 22,500) were wood-frame buildings. Figure 2-12 depicts a typical (pre-1982) wood-frame residence in Nishinomiya City that sustained heavy damage.

At the time of the 1995 Kobe earthquake, the population of Nada Ward of Kobe City was about 125,000, of which 924 people were killed in the earthquake. There were a total of 30,544 buildings, of which 13,198 were heavily damaged, and most of which (11,907) were wood-frame buildings.

Table 2-19 summarizes population data and building damage data for the Nada Ward of Kobe City and Nishinomiya City, and related values of median and lognormal standard deviation (β) parameters of empirical vulnerability (fragility) functions for heavy damage to wood-frame buildings (Yamaguchi and Yamazaki, 2000, Yamazaki and Murao, 2000). Also included in Table 2-19, are example values of the probability of heavy damage to wood-frame buildings given estimated values of short-period spectral acceleration of either $S_T = 1.5g$ or $S_T = 2.25g$ for hypothetical values of the lognormal standard deviation parameter of either $\beta = 0.50$ or $\beta = 0.70$. The value of $S_T = 1.5g$ corresponds to high seismic ground motions, and the value of $S_T = 2.25g$ corresponds to very high seismic ground motions used in FEMA P-695

collapse evaluations. The value of $\beta = 0.50$ is the value of the lognormal standard deviation parameter used in FEMA P-695 collapse evaluations. A value of $\beta = 0.70$ represents an upper bound on the empirical values of the lognormal standard deviation parameter of the vulnerability functions of Yamaguchi and Yamazaki (2000) and Yamazaki and Murao (2000).

Table 2-19 Building Population and Damage Data Due to the 1995 Kobe Earthquake, in the Nada Ward of Kobe City and Nishinomiya City, and Related Values of Median and Lognormal Standard Deviation Parameters of Empirical Vulnerability (Fragility) Functions for Heavy Damage to Wood-Frame Buildings, and Example Values of the Probability of Heavy Damage to Wood-Frame Buildings, Given Values of Short-Period Spectral Acceleration for Hypothetical Values of the Lognormal Standard Deviation Parameter

Building Inventory	Nada Ward of Kobe City (Yamazaki and Murao, 2000)				Nishinomiya City (Yamaguchi and Yamazaki, 2000)			
	Building Population and Damage Data							
	All	Buildings with Heavy Damage			All	Buildings with Heavy Damage		
	Number	Number	Percent		Number	Number	Percent	
All Buildings	30,554	13,198	43%		96,261	24,807	26%	
All Wood	22,710	11,907	52%		67,992	22,500	33%	
Newer Wood	2,449	384	15.7%		12,072	850	7.0%	
Heavy Damage Vulnerability Parameters – All Wood-Frame Buildings								
Parameter	Median	β	P[Heavy Damage S_T]		Median	β	P[Heavy Damage S_T]	
			$S_T = 1.5$ g	$S_T = 2.25$ g			$S_T = 1.5$ g	$S_T = 2.25$ g
PGV (cm/s)	91	0.41			100	0.54		
PGA (g)	N/A	N/A			0.88	0.61		
S_T [T=0.3s] (g)	1.92	0.50	31%	62%	2.10	0.50	25%	55%
S_T [T=0.3s] (g)	1.92	0.70	36%	59%	2.10	0.70	32%	54%
Heavy Damage Vulnerability Parameters – Newer (1982-1994) Wood-Frame Buildings								
Parameter	Median	β	P[Heavy Damage S_T]		Median	β	P[Heavy Damage S_T]	
			$S_T = 1.5$ g	$S_T = 2.25$ g			$S_T = 1.5$ g	$S_T = 2.25$ g
PGV (cm/s)	167	0.50			204	0.54		
PGA (g)	N/A	N/A			2.00	0.68		
S_T [T=0.3s] (g)	3.54	0.50	4.3%	18%	4.32	0.50	1.7%	10%
S_T [T=0.3s] (g)	3.54	0.70	11.0%	26%	4.32	0.70	6.5%	18%

The vulnerability curves of Yamaguchi and Yamazaki (2000) and Yamazaki and Murao (2000) are defined in terms of peak ground velocity (PGV), and, in the case of Nishinomiya City, also in terms of peak ground acceleration (PGA), but not in terms of response spectral acceleration at the elastic period of structure, S_T , which is the ground motion parameter of the FEMA P-695 methodology. Median values of S_T at a period of 0.3 seconds (i.e.,

approximate period of peak acceleration response) were estimated from median values of PGV using the equation, S_T (g) = 3.3 × PGV (cm/s) × (2π/980 cm/s). In this equation, the 3.3 factor is the product of 2.0 times 1.65, where 2.0 is the approximate ratio of 0.3-second to 1-second response spectral acceleration, typical of ground motions at soil sites due to M6.5 to M7.0 earthquakes, and where 1.65 is the approximate ratio of 5-percent damped, 1-second response spectral velocity to PGV (e.g., Table 1, Newmark and Hall, 1982). The equation tacitly assumes that peak spectral response velocity occurs at (or near) a period of 1 second. This equation is considered reasonable because it yields median values of S_T that are 2.16 (4.32g/2.00g) and 2.39 (2.10g/0.88g) times the median values of PGA of Yamaguchi and Yamazaki (2000), typical of the spectral content of ground motions at soil sites due to M6.5 to M7.0 earthquakes.

“Heavy” damage is not defined in Yamaguchi and Yamazaki (2000) and Yamazaki and Murao (2000), but appears to correspond to complete damage (i.e., collapse plus severe damage) in Table 2-18. Compare, for example, the 26 percent (Nishinomiya City) and 43 percent (Nada Ward) of all buildings with heavy damage in Table 2-19, with the 35 percent of all buildings (within 5 km of fault rupture) with complete damage in Table 2-18. Heavy damage would also seem to be consistent with the amount and degree of building damage that would effect a red tag (Unsafe placard) rating in accordance with the post-earthquake safety assessment procedure of ATC-20 (see also Section 2.3.3).

There are a number of important observations of wood-frame building damage in the 1995 Kobe earthquake and the related probabilities of heavy building damage reported in Table 2-19, particularly for comparison with damage to wood light-frame buildings in the 1994 Northridge earthquake, discussed below:

1. **Wood-Frame Building Inventory.** Unlike older Japanese wood-frame buildings (i.e., Shinkabe and Okabe construction), newer wood-frame buildings constructed between 1982 and 1994 are more similar to U.S. wood light-frame buildings (e.g., stud-wall framing was used for many newer wood-frame buildings in Japan). Traditional use of relatively heavy clay tile roofing material, however, likely contributed to newer Japanese wood-frame buildings being more vulnerable than U.S. wood light-frame buildings, all else equal. It should also be noted that the typical wood-frame building in Japan is a two-story residence, whereas the vast majority of wood light-frame buildings in the United States are one-story residences that are inherently less vulnerable than two-story residences, all else equal (see red-tag data in Table 2-15).

2. **Very Strong Ground Motions.** Comparison of the 52 percent of all wood-frame buildings with heavy damage in the Nada Ward of Kobe City (where all areas of Nada Ward were located within 5 km of fault rupture) with the probabilities of heavy damage given $S_T = 1.5\text{g}$ (i.e., 31 percent and 36 percent) and the probabilities of heavy damage given $S_T = 2.25\text{g}$ (i.e., 59 percent and 62 percent) suggest that average, short-period ground motions in the Nada Ward of Kobe City were approximately equal to $S_T = 2.0\text{g}$. Similar comparisons, suggest that average, short-period ground motions in Nishinomiya City were slightly greater than $S_T = 1.5\text{g}$ (where most, but not all, areas of this city were located within 5 km of fault rupture). In contrast, ground motions seldom exceeded $S_T = 1.5\text{g}$ in the region most affected by the 1994 Northridge earthquake (see census-tract ground motion data of Table 2-14).
3. **Heavy Damage – All Wood-Frame Buildings.** The large number of wood-frame buildings with heavy damage (52 percent in Nada Ward and 33 percent in Nishinomiya City) reflect the relatively poor collapse performance of older Japanese wood-frame buildings (which comprise the majority of all wood-frame buildings in Nada Ward and Nishinomiya City) in very strong ground motions. Interestingly, wood-frame buildings of all vintages had more heavy damage than other building types (i.e., reinforced concrete and steel buildings were observed to have less heavy damage, on average, than wood-frame buildings).
4. **Heavy Damage – Newer Wood-Frame Buildings.** The modest number of newer wood-frame buildings with heavy damage (15.7 percent in Nada Ward and 7.0 percent in Nishinomiya City) from very strong ground motions reflect the relatively good collapse performance of newer Japanese wood-frame buildings built after 1984. Fragility functions of heavy damage as a function of short-period (0.3-second) response spectral acceleration, S_T (derived from the PGV-based vulnerability functions of Yamaguchi and Yamazaki, 2000 and Yamazaki and Murao, 2000) suggest roughly a 5 percent probability of heavy damage given $S_T = 1.5\text{g}$, and roughly a 15 to 20 percent probability of heavy damage given $S_T = 2.25\text{g}$. Given the inherent differences in construction, the 5 percent probability of heavy damage (given $S_T = 1.5\text{g}$) of newer Japanese wood-frame buildings is consistent with the similarly low percentage of 2-story (or greater) wood light-frame buildings assigned a red tag due to the 1994 Northridge earthquake (see Section 2.5).

2.7 Observed Performance of Full-Scale Wood Light-Frame Buildings in Shake Table Tests

Although limited in number, full-scale shake table tests have provided valuable insight into the seismic response behavior and collapse performance of wood light-frame buildings. This section summarizes two such test programs, one in 2006 at the E-Defense facility in Miki, Japan, and another in 2006 at the Structural Engineering and Earthquake Simulation Laboratory (SEESL) at the University at Buffalo. In both test programs, extensive instrumentation was implemented to measure overall seismic response and various parameters of interest, including the use of video recordings to visually document the behavior and collapse performance that is described in the sections that follow.

2.7.1 Shake Table Tests of a Two-Story Japanese Home at the E-Defense Facility, Miki, Japan

Full-scale, two-story, Japanese wood light-frame homes were tested on the shake table at the E-Defense facility, Miki, Japan (Isoda et al., 2008). These tests were performed as part of a Special Research Project of Earthquake Disaster Mitigation for Metropolis funded by the Japanese Ministry of Education, Culture, Sports, Science and Technology (MEXT). The main objective of the shake table tests was to evaluate the seismic capacity of homes built prior to the 1995 Kobe earthquake and the seismic safety of newer residential construction designed according to the seismic provisions of current Japanese Building Standard Law. This section summarizes the shake table tests of one of the Japanese homes of newer construction that included a seismic collapse test.

Figure 2-14 shows plan views of the configuration and seismic bracing of the first and second stories of the test building. Figure 2-15 shows photographs of the front and the back of the untested building on the shake table. The test building was designed to meet the minimum requirements of the seismic provisions of Japanese Building Standard law using allowable stress design methods and a seismic lateral force of 20 percent of the seismic weight of the test building.

Table 2-20 summarizes the dimensions, weight, and construction details. Let-in diagonal timber braces are used instead of structural panel shear walls. Although the response behavior of diagonal let-in braces differs from that of structural panel shear walls, the sequence of collapse tests and the observed collapse performance of the test building is still considered relevant. Nonstructural walls and finishes include interior gypsum board and exterior ceramic siding.

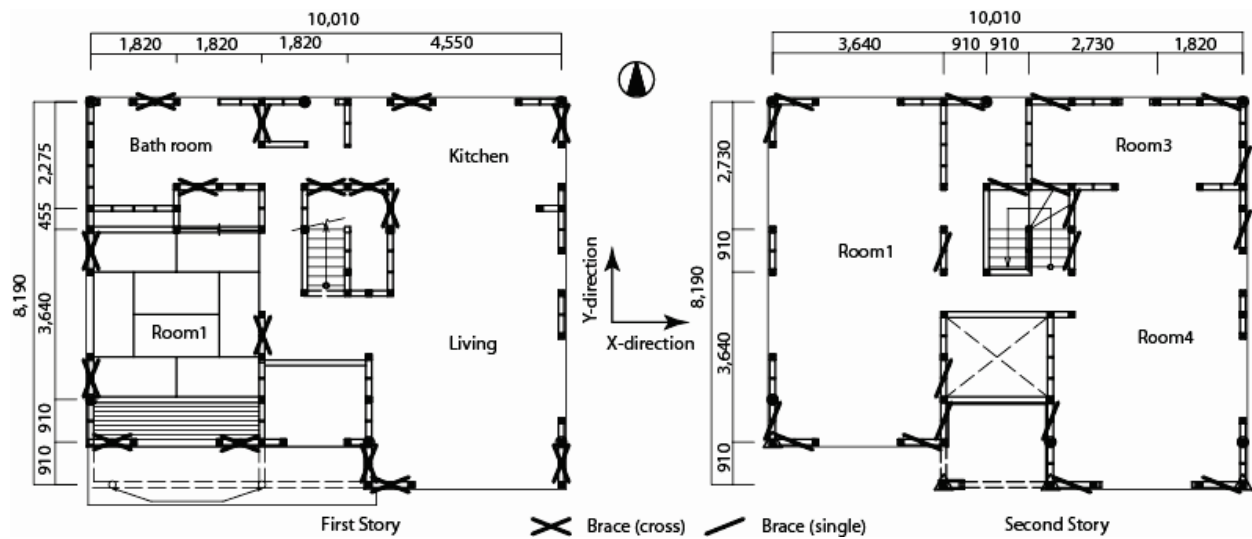


Figure 2-14 First-story and second-story plan views of the E-Defense test building (Isoda et al., 2008).



Figure 2-15 Test building on the E-Defense shake table prior to testing, showing views of the front (left) and back (right) of the test building (Isoda et al., 2008).

Table 2-21 summarizes the schedule of 3D shake table test series, which began with a sequence of damage tests, followed by repair of damage and additional tests of the repaired building, and finally a sequence of collapse tests (after repair and a base isolation test). White noise tests were used before and after strong shaking tests to measure changes in dynamic properties due to damage. Building periods from white noise Test No. 1, Test No. 5, and Test No. 7 are reported in Table 2-11.

The sequence of collapse tests is of particular interest to investigations of response behavior and collapse performance of short-period wood light-frame buildings. The measured story drift response of the test building to a

sequence of three JR (Japan Rail) Takatori motions (i.e., Test No. 13, Test No. 14, and Test No. 15) is shown in Figure 2-16.

Table 2-20 Construction Details for the E-Defense Test Building (Isoda et al., 2008)

Configuration	First Floor	Second Floor
Area (m ²)	64.5	62.9
Height (m)	3.12	2.97
Seismic Weight (kN)	181.5	86.2
Component	Description of Materials	
SFRS	30 mm by 90 mm timber let-in diagonal bracing	
Nonstructural Wall	Gypsum board (interior base wall) $t=9\text{mm}$ Ceramic siding (exterior wall)	
Roof	Tiled Roof	
Structural Floor	Second Floor: plywood ($t = 32\text{ mm}$), cement board ($t = 18\text{ mm}$), finishing wood floor ($t = 12\text{ mm}$) First Floor: plywood ($t = 9\text{ mm}$), finishing wood floor ($t = 12\text{ mm}$) Balcony: plywood ($t = 24\text{ mm}$), porcelain tile	
Ceiling	Gypsum board	
Main Fasteners	Hold-down-tie connector, NBC connector (as shown later), nails for plywood, and screws for gypsum	

The peak-story drift during the first shake was about 10 percent and the effective period during peak response was about 1.2 seconds. Residual story drift after the first JR Takatori shake was small (less than 1 percent).

Damage, primarily to structural elements and nonstructural finishes in the first story, was substantial, but likely repairable.

Peak-story drift recorded during the second JR Takatori shake was about 18 percent, and the effective period during peak response was about 2 seconds. Residual story drift after the second JR Takatori shake was large (over 10 percent). Damage, primarily to structural elements and nonstructural finishes in the first story, was severe, and most likely would not be repaired (i.e., complete damage). Figure 2-17 shows the test building leaning, with extreme damage to the first story, after the second JR Takatori shake. During the third JR Takatori shake, the test building collapsed in the first story, as shown in Figure 2-18.

The shake table tests of the Japanese home demonstrated a first-story collapse mechanism due to P-Δ effects, which is a common collapse mechanism in two (or more) story, wood light-frame buildings. The shake table tests also showed a very large displacement capacity (i.e., drift ratio well beyond 10 percent) in this relatively light-weight building, along with

Table 2-21 Schedule of Shake Table Tests (Isoda et al., 2008)

Test Type	No.	Input Motion	Max Acceleration (gal)	Notes
Damage Tests	1	White Noise	30	
	2	JMA Kobe	204	25% of record
	3	JMA Kobe	204	25% of record
	4	JMA Kobe	818	100% of record
	5	White Noise	30	
	6	JMA Kobe	900	Only 110% of N-S
	7	White Noise	30	
Repair				
Post-Repair Damage Tests	8	White Noise	60	
	9	JMA Kobe	204	25% of record
	10	JMA Kobe	818	100% of record
	11	White Noise	60	
Base Isolation Test				
Collapse Tests	12	JMA Kobe	818	100% of record No collapse
	13	JR Takatori	666	100% of record No collapse
	14	JR Takatori	666	100% of record No collapse
	15	JR Takatori	666	100% of record Collapse

a significant lengthening of the effective period during peak response (i.e., effective periods greater than 1 second). Prior to P-Δ collapse, the short-period Japanese home essentially responded as a long-period isolated structure (with isolation provided by the softened first story).

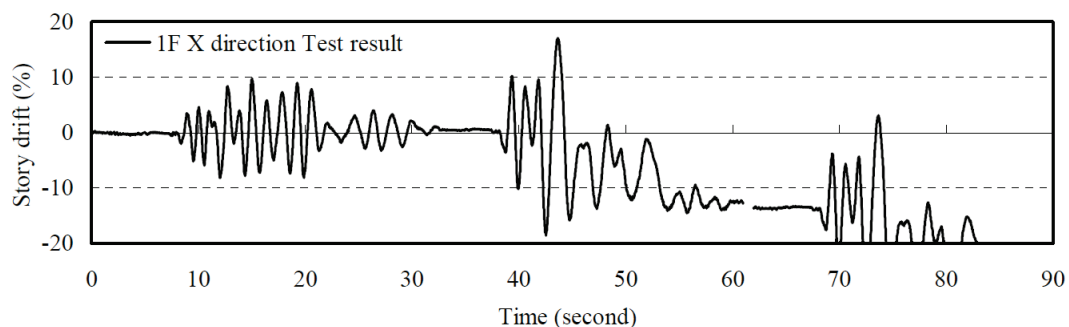


Figure 2-16 Observed story drift in the three sequential collapse tests using the JR Takatori shake (Isoda et al., 2008).



Figure 2-17 Severe first-story damage and leaning of the test building after the second JR Takatori shake (Isoda et al., 2008).



Figure 2-18 Collapsed test building after the third JR Takatori shake (Isoda et al., 2008).

Hence, collapse was a function of the displacement capacity of the test building relative to the displacement demand of the shake table (at longer periods of response). The very high rates of collapse in the 1995 Kobe earthquake for buildings in the near fault region where displacement demands were large (e.g., due to near-source velocity pulses) supports this concept of collapse failure.

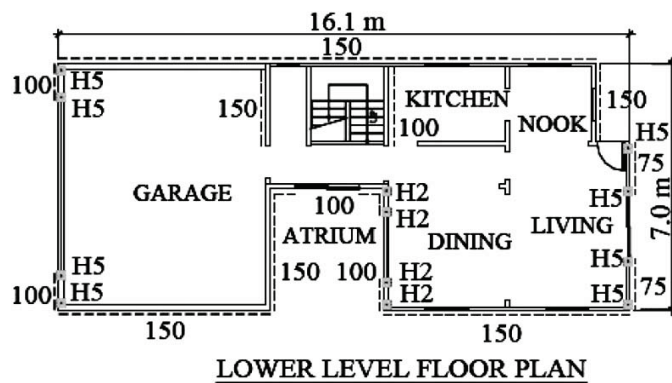
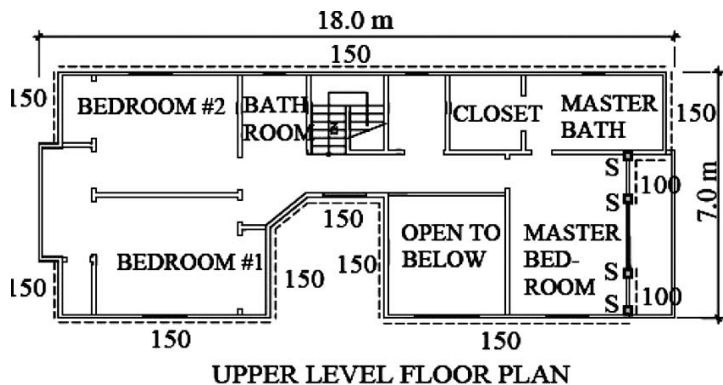
2.7.2 Shake Table Tests of a Two-Story Townhouse at the Structural Engineering and Seismic Simulation Laboratory, University at Buffalo

A full-scale, two-story, wood light-frame townhouse building, designed in accordance with modern U.S. engineered seismic design requirements, was tested on two tri-axial shake tables operating in unison at the Structural Engineering and Earthquake Simulation Laboratory (SEESL), University at Buffalo (Filiatrault et al., 2010; Christovasilis et al., 2007). The main objective of this experimental study was to determine the dynamic characteristics and the seismic performance of the test building under various base input intensities, representative of both ordinary and near-field ground motions in Southern California. The building was tested both with and without interior (gypsum wallboard) and exterior (stucco) wall finishes. The test results revealed that the installation of gypsum wallboard on the interior surfaces of walls with wood structural panel sheathing substantially improved the seismic response of the test building. The application of exterior stucco further improved seismic response, particularly in the longitudinal direction, where the shear response of low aspect ratio wall piers was dominant. These shake table test results provide evidence of the significant influence that wall finish materials have on the behavior of seismic force-resisting systems in wood light-frame construction.

The test building is one of four California-style index buildings designed within the CUREE-Caltech Woodframe Project, including an earlier test of a two-story, wood light-frame house at the University of California, San Diego, which found that wall finishes dramatically improved the seismic performance of the test structure (Fischer et al., 2001). It represents one unit of a two-story townhouse containing three units, having approximately 1,800 square feet of living space with an attached two-car garage. Figure 2-19 shows plan views of the first and second floor of the test building identifying major structural elements, and Figure 2-20 shows two configurations of the test building on the SEESL shake table prior to testing.

The footprint of the test building is 7 m by 18 m (23 feet by 59 feet). The height of the test building from the first floor slab to the roof eaves is 5.3 m (17.4 feet) and its total weight is 320 kN (72 kips). The design of the test building is based on engineered construction in accordance with the seismic provisions of the 1988 *Uniform Building Code* (UBC) (ICBO, 1988), for Seismic Zone 4 and common design practices in California. The design base shear in each orthogonal direction of the building is 18 percent of the seismic weight of the test building. The ultimate base shear capacity of the test building, considering the contributions of gypsum and stucco wall finishes,

was estimated from pushover analyses to be 220 kN (49.5 kips) in the longitudinal (East-West) direction, and 185 kN (41.6 kips) in the transverse (North-South) direction. Based on a design base shear of 13.0 kips (i.e., 0.18 × 72 kips), the pushover strengths of the test building with finishes correspond to an overstrength factor of $\Omega = 3.8$ (i.e., 49.5 kips / 13 kips) in the longitudinal (East-West) direction and $\Omega = 3.2$ (i.e., 41.6 kips / 13 kips) in the transverse (North-South) direction.



	: Indicates OSB sheathing with 75/100/150 edge nail spacing in mm
	: Indicates PHD2 and PHD5 holdown locations
	: Indicates ST6236 strap locations

Figure 2-19 Plan views of the upper-level and lower-level floors of the CUREE-Caltech Woodframe Project test building, and summary of structural details (Filiatrault et al., 2010).

Seismic tests were conducted for various configurations of the building. Table 2-22 summarizes the five seismic test phases included in the test program, and the corresponding configurations of the test building and seismic test levels. Table 2-23 summarizes the ground motions used for five seismic test levels. Before and after each test, the dynamic properties of the



Figure 2-20 CUREE-Caltech Woodframe Project test building on the SEESL shake tables: Test Phase 1 (SFRS only) configuration (top); and Test Phase 5 (SFRS with interior gypsum board and exterior stucco finishes) configuration (bottom) (Filiatral et al., 2010).

test building were estimated by simulated ambient vibration (white noise) tests. The natural periods, mode shapes, and associated modal damping ratios were determined through transfer functions of the story acceleration response of the structure and base motion. Selected ambient-level period

data were previously reported in Table 2-11 for three test configurations: Test Phase 1 (SFRS only), Test Phase 4 (SFRS with interior gypsum board finishes) and Test Phase 5 (SFRS with interior gypsum board and exterior stucco finishes).

Table 2-22 Test Phases, Building Configurations, and Seismic Testing Levels (from Table 1, Filiatroult et al., 2010)

Test Phase	Test Building Configuration	Seismic Test Levels
1	SFRS (wood structural elements only)	1 and 2
2	SFRS with passive fluid dampers incorporated into selected wood sheathed walls	1 and 2
3	SFRS with gypsum wallboard installed on structural wood sheathed walls (only)	1 and 2
4	SFRS with gypsum wallboard installed on all walls and ceilings	1 and 2
5	SFRS with gypsum wallboard installed on all walls and ceilings and stucco installed on all exterior walls	1 through 5

Table 2-23 Ground Motions and Approximate Hazard Levels Used for Seismic Testing (from Table 2, Filiatroult et al., 2010)

Seismic Test Level	1994 Northridge Ground Motion Earthquake Record	Seismic Hazard Level	Scaled PGA (g)		
			E-W	N-S	Vert.
1	Canoga Park	99.99% (in 50 years)	0.04	0.05	0.06
2	Canoga Park	50% (in 50 years)	0.19	0.22	0.26
3	Canoga Park	20% (in 50 years)	0.31	0.36	0.42
4	Canoga Park	10% (DE)	0.43	0.50	0.59
5	Rinaldi	2% (MCE)	0.47	0.84	0.85

After the completion of each seismic test, a detailed damage survey was conducted on the test building to document the evolution of damage with test phases and test levels. Seismic Test Level 5 (MCE) damage to the Test Phase 5 configuration (SFRS with interior gypsum board and exterior stucco finishes) is of particular interest to investigation of the response behavior and collapse performance of short-period wood light-frame buildings.

In this case, observations of damage included cracking of gypsum wallboard at corners of openings and at connections of partitions to ceilings, spalling and cracking of damage to stucco, and splitting of sill plates around the entire perimeter of the building. Sill plate damage was likely the result of

combined in-plane and out of plane deformations of the wall panels. In the in-plane direction, sliding of the sill plate relative to the hold-down devices induced longitudinal splitting of the sill plate. In the out-of-plane direction, eccentric vertical loading from the sheathing nails caused tension splitting perpendicular to grain in the sill plate.

As shown in test videos, the failure of the connections at the base of walls induced almost rigid-body rocking response of the test building in the transverse (North-South) direction at a period of about 0.75 seconds and a peak MCE roof displacement of about 100 mm (4 inches), which precluded the potential for shear failure of first-story walls. These shake table tests showed that installation of gypsum wallboard to the interior surfaces and application of stucco to exterior surfaces substantially stiffened and strengthened the test building, influenced response behavior (i.e., rocking) and related failure modes (i.e., connection failure at sill plates), and likely improved collapse performance (i.e., the test building did not collapse).

2.8 Summary of Key Findings and Benchmark Properties of Short-Period Wood Light-Frame Buildings

This section summarizes key findings from observations of response behavior and collapse performance of wood light-frame buildings in past earthquakes and full-scale shake table tests, and establishes (when possible) benchmark properties for validation of the response characteristics and collapse performance of numerical models of wood light-frame archetypes.

2.8.1 Key Findings

Key findings related to the behavior of short-period wood light-frame buildings are summarized as follows:

- **Collapse Failure Mode.** Collapse of wood light-frame buildings in an earthquake is typically the result of P-Δ failure in the first-story (excluding collapse damage due to foundation failure). Full-scale shake table tests confirm this mode of failure.
- **Large Lateral Displacement at Incipient Collapse.** Observations of wood light-frame buildings severely damaged in earthquakes, or strongly shaken in shake table tests, indicate large lateral displacement at the point of incipient collapse (e.g., mean story drift ratio of 10 percent or greater).
- **Low Probability of Collapse for MCE_R Ground Motions.** Based on observed damage in the 1994 Northridge earthquake, wood light-frame buildings have very low probabilities of collapse for MCE_R ground

motions (i.e., 0.3-second spectral acceleration of 1.5g) suggesting target collapse ranges of not more than 0 percent to 2 percent for one-story, and 0 percent to 5 percent for two-story (or taller) buildings for benchmarking of analytical results.

2.8.2 Response Behavior

Key findings related to the observed response behavior of short-period wood light-frame buildings are summarized as follows:

- **Building Period (Elastic).** Figure 2-5 provides measured (observed) values of building period obtained from records of low-amplitude shaking, which represent the elastic periods of wood light-frame buildings. As shown in Figure 2-5, the elastic period of wood light-frame buildings is difficult to determine uniquely because measured values of building period can vary significantly with the amplitude of response, even at relatively low amplitudes. Nonetheless, observed values of building period show a general trend of an increase in the elastic period of wood light-frame buildings with building height.
- **Building Period (Post-Yield Response).** There are no earthquake records of post-yield response of wood light-frame buildings. However, full-scale shake table tests of wood light-frame buildings to failure show significant lengthening of the building period due to softening of the structure and nonstructural components (e.g., the effective period of a two-story Japanese home lengthened to about 2 seconds before collapse). Period elongation, from the domain of constant acceleration at short periods to the domain of constant velocity at periods beyond 0.5 seconds, is an important collapse survival mechanism for short-period buildings.
- **Nonstructural Finishes (and Features).** Full-scale shake table tests of wood light-frame test buildings, both with and without nonstructural finishes, show that finishes (and other nonstructural features such as stairs) added significant strength and stiffness to the test building, which affected test building response characteristics and failure modes.
- **Flexible Connections (Failure Mechanism).** Full-scale shake table tests of a two-story wood light-frame test building with relatively strong walls, rocked with uplift failure of base connections, rather than shear failure of walls. In this case, the mode of failure was influenced by the flexibility and strength of base connections relative to the shear strength of walls above.

2.8.3 Collapse Performance

Key findings related to the observed collapse performance of short-period wood light-frame buildings are summarized as follows:

- **Collapse Displacement Capacity.** Relatively rare observations of collapse of wood light-frame buildings in an earthquake typically show very large displacement due to sidesway collapse in the first story, and observations of severely damaged wood light-frame buildings that are near the point of incipient collapse are typically leaning with at large residual displacements (e.g., residual drift ratios of 10 percent, or greater, at the first story). Similarly, shake table tests of full-scale structures show wood light-frame buildings have large displacement capacity prior to sides-way collapse. For example, the shake table test of a two-story Japanese home reached a peak drift ratio of 18 percent, and sustained a residual drift ratio of over 10 percent n the first story, prior to sidesway collapse (see Figure 2-17).

The displacement capacity (drift ratio) of archetype models of wood light-frame buildings should be at least 5 percent to 10 percent in the critical story prior to sidesway collapse.

- **Collapse Probability (from 1994 Northridge Earthquake Red-Tag Data).** Based on plots of red-tag percentages shown in Figure 2-8, and the relative fractions of one-story and two (or more) story wood light-frame buildings with red tags summarized in Table 2-14, target values (and associated ranges) of collapse probabilities are defined for MCE_R ground motions corresponding to the high seismic ground motions (i.e., MCE_R ground motions with a 0.3-second spectral acceleration of 1.5g), as follows:
 - **One-Story Buildings.** 1 percent (0 percent to 2 percent) probability of collapse given MCE_R ground motions; and
 - **Two (or More) Story Buildings.** 2.5 percent (0 percent to 5 percent) probability of collapse given MCE_R ground motions.

Target MCE_R collapse probabilities, listed above, represent partial collapse as well as full collapse of the building structure, consistent with the ASCE/SEI 7-10 (and FEMA P-695) definition of collapse.

The target MCE_R collapse probabilities assume that collapse is reasonably well characterized by red-tag data. Thus, this assumption may overstate collapse risk because red-tag data also includes, to some degree, buildings with significant structural (or non-structural) damage deemed to be life-threatening (even if there is not a collapse). As such,

red-tag data may better represent the likelihood of complete structural damage as characterized, for example, by a significant amount of residual post-earthquake drift displacement (e.g., a story drift ratio of 2 percent, or greater) as well as by partial or full collapse of the building structure.

Chapter 3

Development of Building Archetype Configurations and Designs

This chapter describes factors influencing wood light-frame system performance, types of wood light-frame construction, configurations representative of typical wood light-frame buildings, selection of design criteria, and development of wood light-frame archetype designs. The information presented in this chapter, in conjunction with additional design details provided in Appendix A, provides the basis for the numerical models described in Chapter 4.

3.1 Introduction

Wood light-frame building archetypes are intended to represent code-compliant modern construction for common occupancies that routinely utilize wood light-frame shear walls with wood structural panel sheathing and gypsum wallboard sheathing as the seismic-force-resisting system. Engineered wood light-frame building archetypes were designed in accordance with the 2015 IBC. Selected archetypes were also proportioned in accordance with the conventional construction provisions of the 2015 IRC.

The remainder of this chapter summarizes the architectural features and basic design criteria for the wood light-frame building archetypes considered in this study, along with the rationale for decisions made. Additional details on the design of structural shear walls, interior partition walls, and foundations are provided in Appendix A.

3.2 Factors Influencing Building Response and Performance

This section describes factors expected to influence the seismic response and performance of wood light-frame buildings, which were, therefore, considered in the design of wood light-frame building archetypes, numerical modeling, and parametric studies.

3.2.1 Seismic Design Level

Response behavior and collapse performance depends on the strength of the building provided at the time of design and construction. In general, weaker buildings will experience more yielding, and stronger buildings will be able to resist larger events with less inelastic activity and lower likelihood of collapse.

Three levels of seismic demand were considered in this study: moderate, high, and very high. High seismic demand is defined as a site where the MCE_R ground motion is characterized by a mapped short-period spectral response acceleration (S_s) of 1.5g. For an ordinary soil profile, this corresponds to a short-period design acceleration (S_{DS}) of 1.0g. Based on requirements in the 2015 IBC (or ASCE/SEI 7-10), normal occupancy buildings would be assigned to Seismic Design Category (SDC) D. This strength requirement is equivalent to Seismic Zone 4 in the Uniform Building Code before the introduction of near fault factors in 1997.

Moderate and very high seismic demands are taken as 50 percent and 150 percent of the high seismic demand value, respectively. S_{DS} equal to 0.5g is the threshold between SDC C and SDC D, and the design requirements for SDC C were applied at this level of seismic design. S_{DS} equal to 1.5g is high enough that the one-second ground motion will often place a building into SDC E, and design requirements for SDC E were applied at this level of seismic design.

3.2.2 Building Age and Configuration

The characteristics of wood light-frame construction have evolved over time. Solid sawn lumber joists, rafters, and beams have been replaced by I-shaped joists, metal-connected wood trusses, and various forms of engineered lumber. Structural sheathing for shear walls, floors, and roof diaphragms transitioned from lumber boards to plywood panels more than a half-century ago. A recent transition from plywood to oriented strand board (OSB), however, has not resulted in a significant change from the performance of plywood shear panels. Nonstructural wall and ceiling finishes have changed from plaster to gypsum wallboard, which occurred about the same time that plywood was introduced.

Since the 1994 Northridge earthquake, design and detailing of wood light-frame seismic-force-resisting systems has changed. New detailing requirements include steel plate washers for anchor bolts connecting sill plates to concrete or masonry foundations. Code-approved design strengths have changed over time, especially for gypsum wallboard used as a structural

shear wall. Higher design forces in regions of high seismicity, along with architectural trends towards open floor plans, have led to the use of more densely nailed shear walls, and, consequently, increased demands on hold-down devices to prevent rocking. This has led to a proliferation of manufactured devices with rated design capacities to address the challenges encountered in engineered designs.

Wood light-frame buildings are utilized in different occupancies with a wide variety of configurations. Key aspects of configuration that influence seismic response and performance include building size and shape, the distribution of seismic-force-resisting elements, and the presence of irregularities.

In this study, the most important measure of size is building height, in terms of number of stories. Few wood structures are taller than four stories, and those that are would likely not meet the definition of short period used herein. The distribution of walls and the extent of seismic-force-resisting elements provided in wood light-frame construction is often determined by architectural configuration. Residential occupancies are characterized by a relatively large number of closely spaced interior walls and partitions. In contrast, commercial occupancies have comparatively fewer interior walls and partitions, and the exterior walls are relied upon for seismic resistance. A common condition in older wood light-frame construction includes a soft or weak story irregularity, which has performed poorly in past earthquakes. Structural irregularities can negatively impact building performance, however, investigation of building irregularities is a complex topic that has been studied separately (e.g., FEMA P-2012, *Assessing Seismic Performance of Buildings with Configuration Irregularities* (FEMA, 2018a)) so consideration of irregularities was excluded from the scope of this study.

As a result, the age and configuration of wood light-frame buildings considered in this study include one-story, two-story, and four-story buildings of modern wood light-frame construction consistent with the introduction of plywood and gypsum wallboard, with interior walls and partitions of varying densities, and with symmetric and regular structural configurations.

3.2.3 Structural Component Properties

Wood light-frame seismic-force-resisting systems consist of walls, floors, and roof diaphragms acting as shear elements. Response behavior and collapse performance of wood light-frame systems depends heavily on the sheathing material and attachments to the framing. Diaphragm response can be influential, but this is primarily determined by the span of the diaphragm between vertical wall elements.

A range of wall construction was considered in this study: structural wood panel shear walls with three levels of nailing (i.e., low, medium, and high capacity patterns), three types of gypsum wallboard sheathings (i.e., two levels of sheathing designed as seismic-force-resisting, along with one “nonstructural” level), and two types of exterior sheathing (stucco and horizontal wood siding). All diaphragms were taken as nailed OSB. Some commercial configurations had diaphragms that required additional nailing, but all other configurations had diaphragm spans that were too short to require more than minimum nailing.

Beyond the selection of wall and diaphragm sheathing components, the structural properties associated with these components (e.g., peak strength, nonlinear degradation, and residual strength) are also significant. A range of properties for structural sheathing components were investigated as part of the parametric studies.

3.2.4 Architectural and Nonstructural Components and Finishes

Architectural and nonstructural components and finishes, although brittle, are relatively strong in comparison with the strength of structural wood light-frame seismic-force-resisting elements. The significant impact of nonstructural walls and sheathing materials on the response and behavior of wood light-frame systems is generally recognized, although current design procedures do not account for their effects. FEMA P-807, *Seismic Evaluation and Retrofit of Multi-Unit Wood-Frame Buildings with Weak First Stories* (FEMA, 2012b), recognizes the contribution of nonstructural sheathing, and provides a method for combining the capacities of different sheathing materials attached to the same wall framing.

In most residential construction, the ceilings are gypsum wallboard and densely spaced interior partitions extend to the underside of the framing. These characteristics do not apply in most commercial construction, where suspended ceilings are common, and the spacing of interior partitions can be much larger. In all cases, interior partitions are generally not connected to the diaphragms as well as structural walls.

The interior face of all walls and partitions is assumed to be covered with $\frac{1}{2}$ -inch gypsum wallboard. Except where gypsum wallboard is specifically designed to be part of the seismic-force-resisting system, the attachment to the framing is taken as the industry standard minimum (i.e., screws or nails spaced at 12 inches on-center to the framing, with unblocked joints).

Exterior wall finishes can vary more widely than interior finishes, and can include veneers with only limited connectivity to the structure. Exterior

faces of exterior walls in this study are covered with stucco that is applied over exterior sheathing. Where exterior sheathing is not specifically included as part of the seismic-force-resisting system, it consists of $\frac{7}{16}$ -inch OSB with minimum required nailing and unblocked joints. A second exterior wall finish, consisting of wood composite horizontal siding boards nailed to the framing, was investigated as part of the parametric studies.

3.2.5 Site Class and Foundation

The foundation system, and its connectivity and interaction with the soil underlying the site, has long been identified as a possible source for the apparent disconnect between analytically predicted and observed performance. At firm soil sites, shallow spread footings are typically used. At soft soil sites, deeper foundations (e.g., piles or caissons) are often substituted. Exceptions include “poor” sites that include soils with increased potential for liquefaction, or expansive properties.

Selection of foundation type, however, also depends on the weight of the building, and low-rise wood light-frame buildings are more likely to be placed on shallow foundations. In this study, shallow foundations placed integrally with a slab-on-grade were selected as the most representative foundation configuration. Foundation response and behavior was investigated both with and without soil springs as part of the parametric studies.

3.2.6 Design and Construction Practice

Wood light-frame buildings can be engineered in accordance with the IBC and ASCE/SEI 7, or proportioned in accordance with the conventional construction provisions of the IRC. Conventional construction provisions are deemed to comply with the requirements for engineered construction and are intended to result in comparable earthquake performance. Typically, smaller wood light-frame buildings (e.g., most single-family dwellings) are not engineered, and are constructed in accordance conventional construction requirements.

Commercial buildings and multi-family dwellings considered in this study were engineered. In the case of single-family dwellings, both engineered and conventional constructions designs were considered as part of the parametric studies.

3.3 Building Types and Occupancies for Development of Archetypes

The vast majority of short-period buildings in the United States, by number, are wood light-frame buildings for single-family dwelling occupancies. In larger urban areas, multi-family dwellings are a leading occupancy category, and nearly all low-rise, multi-family dwellings consist of wood light-frame construction. An increasing fraction of such buildings are being constructed with cold-formed steel (CFS) framing, but this increase is mainly in taller buildings. Although not as dominant in construction statistics, wood light-frame commercial buildings are still common, and this construction type provides a means to investigate variations in parameters expected to influence the performance of wood light-frame systems.

3.3.1 FEMA Model Building Types

FEMA Model Building Types (MBTs) define different types of structural systems, in terms of material and seismic-force-resisting system characteristics, believed to be useful in characterizing potential seismic performance. These designations are provided in Table 3-1, and have been used in a number of FEMA publications. The most complete discussion of FEMA MBTs is contained in Chapter 4 of the FEMA 547, *Techniques for the Seismic Rehabilitation of Existing Buildings* (FEMA, 2006).

Table 3-1 FEMA Model Building Types

Designation	Description
W1	One- and two-family detached wood light-frame dwelling < 5000 ft ²
W1A	Wood light-frame residential >5000 ft ²
W2	Wood light-frame commercial and industrial
S1	Steel moment frame
S2	Steel braced frame
S3	Light pre-manufactured steel
S4	Steel frame with concrete shear walls
S5	Steel frame with infill masonry walls
C1	Concrete moment frame
C2	Concrete shear wall
C3	Concrete frame with infill masonry walls
PC1	Tilt-up concrete shear walls
PC2	Precast concrete frame or walled building
RM1	Reinforced masonry bearing walls with flexible diaphragm
RM2	Reinforced masonry bearing walls with stiff diaphragm
URM	Unreinforced masonry bearing walls

Within the list of FEMA MBTs, wood light-frame buildings include:

- W1 (one- and two-family detached dwellings less than 5,000 ft²);
- W1A (residential over 5,000 ft²); and
- W2 (commercial and industrial).

All three FEMA MBTs related to wood light-frame buildings are considered in this study. However, although useful for classifying structural systems in a general way, FEMA MBT descriptions are not sufficient for investigating parameters expected to influence response behavior and collapse performance of wood light-frame buildings, specifically.

Instead, archetype configurations were developed for three common occupancies: (1) commercial buildings (COM); (2) multi-family dwellings (MFD); and (3) single-family dwellings (SFD). These three occupancies are each commonly found in different FEMA MBTs (e.g., single-family dwellings are typically of W1 construction, multi-family dwellings are typically of W1A construction, and commercial buildings are typically of W2 construction). Typical configurations of each of these three building occupancies are described in the sections that follow.

3.3.2 Commercial Buildings

Commercial buildings (COM) include a variety of forms. Many one-story wood light-frame commercial buildings are retail stores, repair shops, and other similar businesses, with open floor plans and few interior partitions. They are almost always engineered designs, and shear walls are usually concentrated at the perimeter (exterior) of the building. Large single-story buildings for warehouses and “big box” retailers often have wood roofs, but the walls are often concrete or masonry, so they are not included in this study. Multi-story, wood light-frame commercial buildings are more likely to consist of offices or other similar occupancies, with interior spaces divided by nonstructural partitions. Wood light-frame buildings over four stories in height are unlikely to have a period under 0.5 seconds, and thus have been excluded from consideration in this study.

3.3.3 Multi-Family Dwellings

Multi-family dwellings (MFD) share many features with single-family dwellings. The overall building footprint is much larger, with, perhaps, an even greater density of interior partitions. Modern trends are reaching five and six stories in height, whereas in the past, few wood light-frame buildings exceeded three stories. As noted in the case of commercial buildings, wood light-frame buildings over four stories in height are unlikely to have a period

under 0.5 seconds, and thus have been excluded from consideration in this study.

3.3.4 Single-Family Dwellings

Single-family dwellings (SFD) are usually one-story or two-story structures. The first floor level can be a slab-on-grade or wood light-frame construction over a basement or crawlspace. Basements are more common in the Midwest and Eastern United States, while crawl spaces are more common in the Western United States. Slab-on-grade construction in single-family dwellings is now very prevalent, and is considered in this study. Conventional construction is frequently used for single-family dwellings, and has been included in the design of selected archetypes as a variant to engineered design.

3.4 Archetype Design Criteria and Representative Configurations

Strength and other design properties for “engineered” wood light-frame building archetypes are based on the design requirements of the 2015 IBC and ASCE/SEI 7-10, and, by reference, additional requirements for the design of wood light-frame buildings, including the 2012 edition of the ANSI/AWC NDS-2012, *National Design Specification for Wood Construction* (AWC, 2012), and the 2008 edition of the ANSI/AF&PA SDPWS-2008, *Special Design Provisions for Wind and Seismic* (AWC, 2008). Strength and other properties of wood light-frame building archetypes of conventional construction (e.g., SFD buildings) are based on provisions of the 2015 IRC.

3.4.1 Gravity Loads

Archetypes are designed for dead and live loads summarized in Table 3-2. For seismic design, the weight of all walls and partitions (except exterior walls) are averaged across the floor plate and included in the tabulated floor dead loads. As a result, the interior partitions produce a uniform dead load allowance of 15 psf, regardless of the actual assumed location and distribution. Half the weight of the top-story partitions is assigned to the roof level. Exterior wall dead loads are provided in terms of pounds per square foot of wall surface, and include the weight of stucco. Half the weight of the top-story exterior walls is assigned to the roof level.

Table 3-2 Gravity Loads Used for Design of Wood Light-Frame Commercial Building (COM), Multi-Family Dwelling (MFD) and Single-Family Dwelling (SFD) Archetypes

Building Type	Floor Live Load (psf)	Floor Dead Load (psf)	Roof Dead Load (psf)	Exterior Wall Dead Load (psf)
COM	50	45	27	16
MFD	40	41	27	16
SFD	40	29	26	16

3.4.2 Seismic Loads

Archetypes were designed for three different levels of seismic demand (moderate, high, and very high) corresponding to the seismic design criteria summarized in Table 3-3. These criteria follow the seismic design loading requirements in Section 5.2.2 of FEMA P-695, considering typical intensities of MCE_R ground motions in regions of moderate and high seismicity.

Parameters for engineered designs are provided in the upper half of Table 3-3. The base shear coefficient, C_s , uses a response modification factor, $R = 6.5$, which is specified in ASCE/SEI 7-10 for wood structural panel sheathing. Archetypes for which gypsum wallboard sheathing was sufficient for providing seismic force resistance utilized a response modification factor of $R = 2$, which is not reflected in this table. Parameters for designs following IRC conventional construction provisions are provided in the lower half of Table 3-3. The IRC includes a map of seismic zones by seismic design category, and SDC D is subdivided. Because SDC can be determined from the map, numerical parameters are not necessary, but have been provided here for comparison.

Table 3-3 Seismic Design Criteria Used for Design of Commercial Building (COM), Multi-Family Dwelling (MFD) and Single-Family Dwelling (SFD) Archetypes

Building Type	Seismic Design Level	Seismic Design Category (SDC)	MCE _R Ground Motions				Design Criteria	
			S_I (g)	S_S (g)	F_a	S_{MS} (g)	S_{DS} (g)	C_s
Engineered COM, MFD, and SFD (ASCE/SEI 7-10)	Very High	E	0.9	2.25	1.0	2.25	1.5	0.231
	High	D	0.6	1.5	1.0	1.5	1.0	0.154
	Moderate	C	0.132	0.55	1.36	0.75	0.5	0.077
Conventional Construction SFD (2015 IRC)	Very High	E	0.9	2.25	1.0	2.25	1.5	NA
	High	D ₂	0.6	1.5	1.0	1.5	1.0	NA
	Moderate	C	0.132	0.55	1.36	0.75	0.5	NA

3.4.3 Foundation Design Criteria

Foundations for all archetypes were designed for typical Site Class D soil conditions. Footing widths were proportioned for an allowable bearing pressure of 2000 psf for allowable stress design (ASD) gravity load combinations, and 3000 psf for load and resistance factor design (LRFD) load combinations including seismic load. The minimum depth of exterior footings was 12 inches. Most footing widths were governed by either the gravity load combination or by minimum widths commonly adopted for constructability. Strip footings with intermittent shear walls were proportioned using a beam on compression spring model.

3.4.4 Design Approach

Archetype design methods and details represent typical practice based on the standard of care exercised in regions of significant seismicity. Archetype configurations for each occupancy were selected to be realistic in terms of size and proportion and were designed to meet minimum strength requirements. Each archetype was designed to be consistent with what a reasonable engineer might specify, given the architectural constraints of the buildings.

Minimal total lengths of shear walls were used, while also avoiding, where possible, shear walls with tight nail spacing (i.e., 2 inches o.c.). The length of a given shear wall did not change from story to story, as is common practice, although some shear wall lines were terminated below the top story. Commercial building archetypes used shear wall lengths in increments of eight feet, while all other archetypes used shear wall lengths in increments of four feet. Nonstructural sheathing on exterior and bearing walls, and the density of nonstructural partitions, were targeted to be representative of typical wood light-frame construction in each occupancy. Designs were not deliberately biased with overstrength caused by conservatism, or understrength caused by the use of wall configurations that would be considered unrealistic based on gravity load or architectural considerations.

The various options available for designing, proportioning, and constructing wood light-frame buildings were restricted for simplicity in design and convenience in numerical modeling. For example, Douglas Fir was used for all wall framing, and wall sheathing was limited to three categories of OSB and two categories of gypsum wallboard, as shown in Table 3-4. In one-story and two-story building archetypes, where overturning resistance in excess of dead load is required, conventional hold-down devices were used. In four-story building archetypes, full-height steel anchorage systems were used.

Table 3-4 Wall Sheathing Used in Wood Light-Frame Building Archetypes

Wall Type	Description	Nominal Strength (plf)
OSB-Low	7/16-inch structural panels with 8d common nails at 6 inches o.c. on edges into Douglas Fir framing	520
OSB-Med	7/16-inch structural panels with 8d common nails at 3 inches o.c. on edges into Douglas Fir framing	980
OSB-High	19/32-inch (5/8-inch) structural panels with 10d common nails at 2 inches o.c. on edges into Douglas Fir framing	1740
Min-Gyp	1/2-inch gypsum board with 5d cooler nails at 7 inches o.c. on edges, no blocked joints, studs at 16 inches o.c.	200
Max-Gyp	5/8-inch gypsum board with 6d cooler nails at 4 inches o.c. on edges, blocked joints, studs at 16 inches o.c.	350
Nonstructural	7/16-inch OSB, unblocked, with 8d nails at 6 inches o.c., on edges; 1/2-inch GWB, drywall screws at 12 inches o.c.; exterior stucco	Not used in design

The seismic force resisting system in each archetype was proportioned using the following procedure:

1. Gypsum wallboard shear walls were checked for sufficient capacity to meet the seismic demand.
2. If not, OSB shear walls were provided at selected locations distributed throughout the floor plan. Minimal total lengths of shear walls were provided, avoiding shear walls with tight nail spacing, where possible.
3. Commercial building shear walls were specified in eight-foot increments, and residential building shear walls were specified in four-foot increments. The length of a given shear wall was not changed from one story to the next, as is common in practice, although some shear wall lines were terminated below the top story of some archetypes.
4. Compression posts and tension hold-downs were then designed for seismic overturning demands based on the placement of the shear walls.
5. Foundations were proportioned for both gravity and seismic demands.

Additional details on shear wall sheathing, nailing, framing, hold-downs, and foundations for each archetype design are provided in Appendix A. The resulting set of representative wood light-frame archetypes is described below.

3.4.5 Representative Archetype Configurations

Key configuration and seismic-design criteria for wood light-frame archetypes are provided in Table 3-5, where the design period ($T = C_u T_a$) and the seismic response coefficient (C_s) were calculated in accordance with Section 12.8.2 and Section 12.8.1.1 of ASCE/SEI 7-10, respectively.

Table 3-5 Short-Period Wood Light-Frame Building Archetype Configurations and Seismic Design Criteria

Archetype ID	Configuration		Seismic Design Criteria					
	No. of Stories	Wall Aspect Ratio	Seismic Code	Design Period ⁽¹⁾ $T = C_u T_a$ (sec)	Seismic Design Category (SDC)	MCE _R Design Parameter, S_{MS} (g)	Response Modification Coefficient (R)	Seismic Response Coefficient, C_s (g)
Commercial Buildings: High Seismic								
COM1	1	Low	ASCE 7	0.25	D	1.5	6.5	0.154
COM2	2	Low	ASCE 7	0.26	D	1.5	6.5	0.154
COM3	4	Low	ASCE 7	0.45	D	1.5	6.5	0.154
Commercial Buildings: Very High Seismic								
COM4	1	Low	ASCE 7	0.25	E	2.25	6.5	0.231
COM5	2	Low	ASCE 7	0.26	E	2.25	6.5	0.231
COM6	4	Low	ASCE 7	0.45	E	2.25	6.5	0.231
Commercial Buildings: Moderate Seismic								
COM7	1	Low	ASCE 7	0.25	C	0.75	6.5	0.077
COM8	2	Low	ASCE 7	0.26	C	0.75	6.5	0.077
COM9	4	Low	ASCE 7	0.45	C	0.75	6.5	0.077
Multi-Family Dwellings: High Seismic								
MFD1	1	High	ASCE 7	0.25	D	1.5	6.5	0.154
MFD2	2	High	ASCE 7	0.26	D	1.5	6.5	0.154
MFD3	4	High	ASCE 7	0.45	D	1.5	6.5	0.154
Multi-Family Dwellings: Very High Seismic								
MFD4	1	High	ASCE 7	0.25	E	2.25	6.5	0.231
MFD5	2	High	ASCE 7	0.26	E	2.25	6.5	0.231
MFD6	4	High	ASCE 7	0.45	E	2.25	6.5	0.231
Multi-Family Dwellings: Moderate Seismic								
MFD7	1	High	ASCE 7	0.25	C	0.75	6.5	0.077
MFD8	2	High	ASCE 7	0.26	C	0.75	2, 6.5 ⁽²⁾	0.25, 0.077
MFD9	4	High	ASCE 7	0.45	C	0.75	6.5	0.077
Single-Family Dwellings: High Seismic								
SFD1	1	High	ASCE 7	0.25	D	1.5	6.5	0.154
SFD1C	1	High	IRC	NA	D ₂	1.5	NA	NA
SFD2	2	High	ASCE 7	0.25	D	1.5	6.5	0.154
SFD2C	2	High	IRC	NA	D ₂	1.5	NA	NA
Single-Family Dwellings: Very High Seismic								
SFD3	1	High	ASCE 7	0.25	E	2.25	6.5	0.231
SFD3C	1	High	IRC	NA	E	2.25	NA	NA
SFD4	2	High	ASCE 7	0.25	E	2.25	6.5	0.231
Single-Family Dwellings: Moderate Seismic Areas								
SFD5	1	High	ASCE 7	0.25	C	0.75	6.5	0.077
SFD5C	1	High	IRC	NA	C	0.75	NA	NA
SFD6	2	High	ASCE 7	0.25	C	0.75	6.5	0.077

⁽¹⁾ The design period is defined as $T = C_u T_a \geq 0.25$ seconds, in accordance with the analysis requirements of FEMA P-695, where the values of the parameters C_u and T_a are specified by ASCE/SEI 7-10.

⁽²⁾ R=2 in the transverse direction and R=6.5 in the longitudinal direction.

A suite of archetypes, with variations in occupancy, height, and seismic-design level, were selected. Occupancies included commercial buildings (COM), multi-family dwellings (MFD), and single-family dwellings (SFD).

Height variants included one-story, two-story, and four-story archetypes, all with fundamental periods below 0.5-seconds. One-story and two-story versions of the single-family dwelling archetypes were created, and one-story, two-story, and four-story versions of the multi-family dwelling and commercial building archetypes were created. Wood light-frame shear wall configurations included both low aspect ratio and high aspect ratio walls.

Engineered designs were prepared for each occupancy considering three levels of seismic hazard: moderate, high, and very high. Designs for single-family dwellings were also prepared using conventional construction provisions. All archetypes are rectangular in plan, with a symmetric and regular structural configuration, a consistent floor plate over the height of the building, and the absence of horizontal or vertical structural irregularities.

Location, length, and type of shear walls for each class of archetype are depicted in a framing plan showing all potential shear wall locations. Shear wall designs are specified in tables provided in Appendix A, listing shear wall properties for each wall, including hold-down devices and the number of studs at each end of each wall. Typical wall elevations are provided for each class of archetype to illustrate the portions of walls considered to be part of the seismic-force-resisting system.

In addition to framing plans showing shear wall locations, a second set of plans showing typical interior partition layouts are provided for each class of archetype. Nonstructural interior partitions were not considered in the design of the seismic-force-resisting system, but they were considered in numerical models for the purpose of evaluating their impact on response and performance. These plans are not considered to be representative of any particular architectural layout. However, they show the number and total length of interior partitions assumed to be present in each building type, based on a review of architectural plans for actual buildings constructed in the last fifteen years.

The basic configurations for each class of archetype are summarized in the sections that follow.

3.5 Commercial Buildings

Commercial building archetypes are rectangular in plan, measuring 48 feet by 96 feet. Two plan configurations were considered within this footprint:

one without interior partitions, representing a retail or repair shop occupancy (one-story archetypes), and one with interior partitions, representing an office occupancy (two-story and four-story archetypes). A three-dimensional, isometric rendering of a one-story commercial building archetype is shown in Figure 3-1.

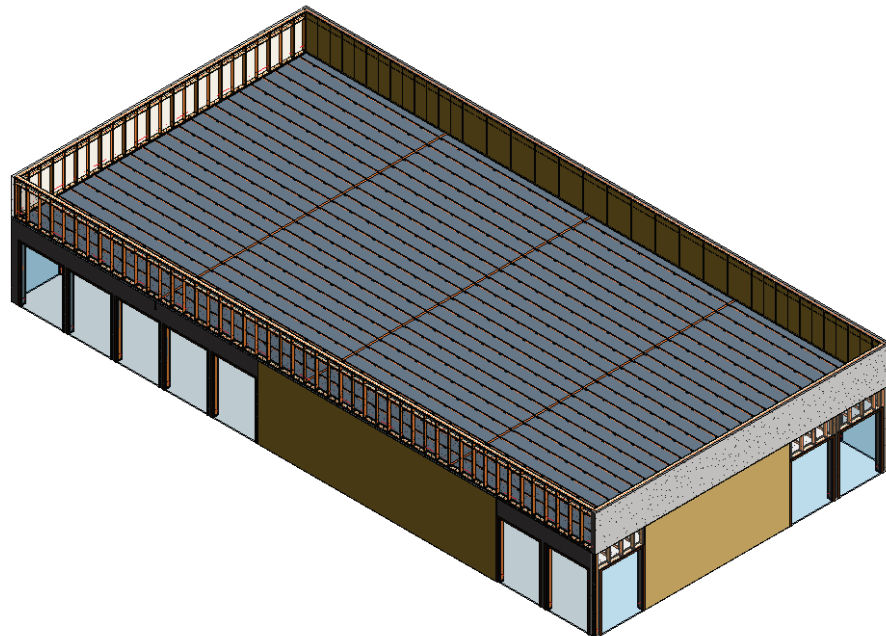


Figure 3-1 Isometric rendering of a one-story commercial building archetype.

Shear walls are provided around the perimeter of commercial building archetypes. Floor and roof diaphragms span horizontally between transverse and longitudinal exterior walls. Floor and roof structures consist of parallel chord trusses spanning in the longitudinal direction, supported on transverse post and girder lines. A typical framing plan is provided in Figure 3-2, showing floor and roof framing, diaphragm sheathing, and the locations of perimeter shear walls (shaded in black).

Typical longitudinal wall elevations are provided for a one-story commercial archetype in Figure 3-3, and for a two-story archetype in Figure 3-4. In these elevations, a portion of the exterior walls is considered part of the seismic-force-resisting system (shaded in gray), and the remainder is considered nonstructural, or open. Typical elevations for a four-story archetype would be similar to what is shown for a two-story archetype.

A typical interior partition plan for the two-story and four-story commercial archetypes is shown in Figure 3-5. Interior partitions in commercial occupancies are nonstructural walls. The labeling of interior partition walls is explained in Table 3-6.

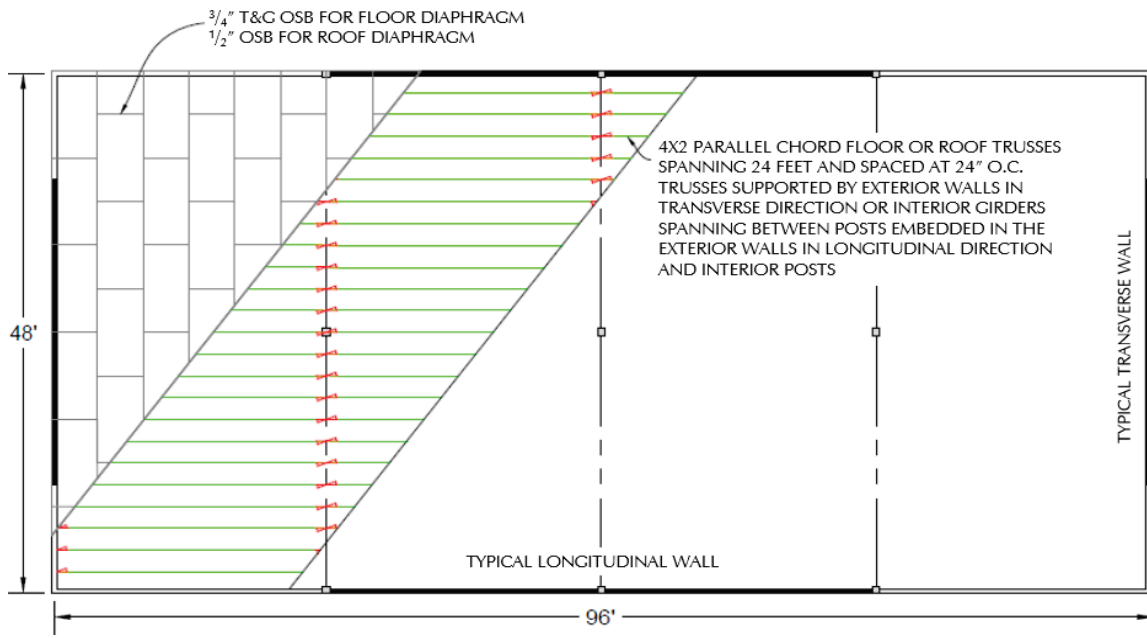


Figure 3-2 Typical floor and roof framing plan for a two-story commercial building archetype, showing diaphragm sheathing and locations of perimeter shear walls.

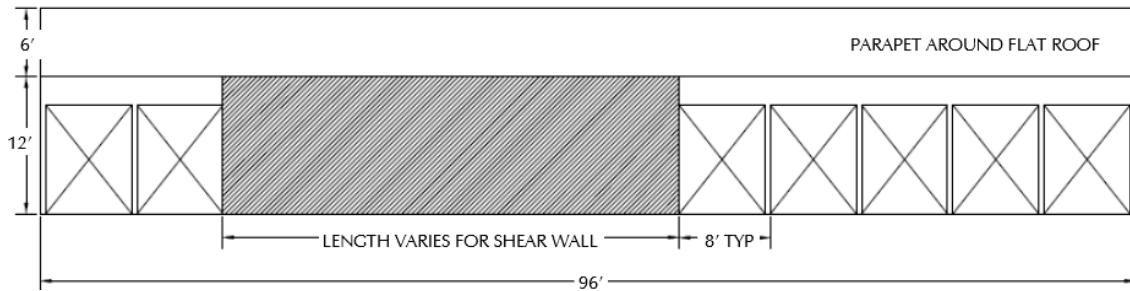


Figure 3-3 Typical longitudinal wall elevation for one-story commercial building archetypes.

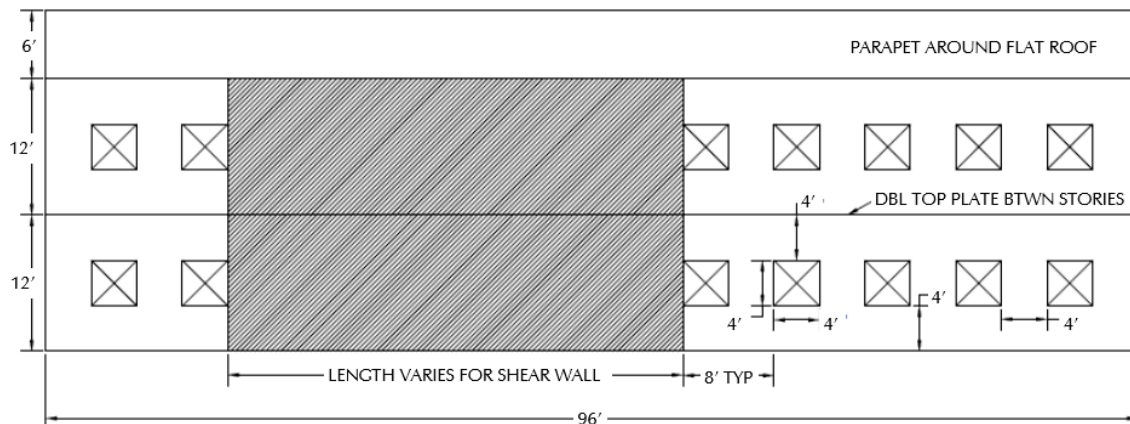


Figure 3-4 Typical longitudinal wall elevation for two-story commercial building archetypes (four-story similar).

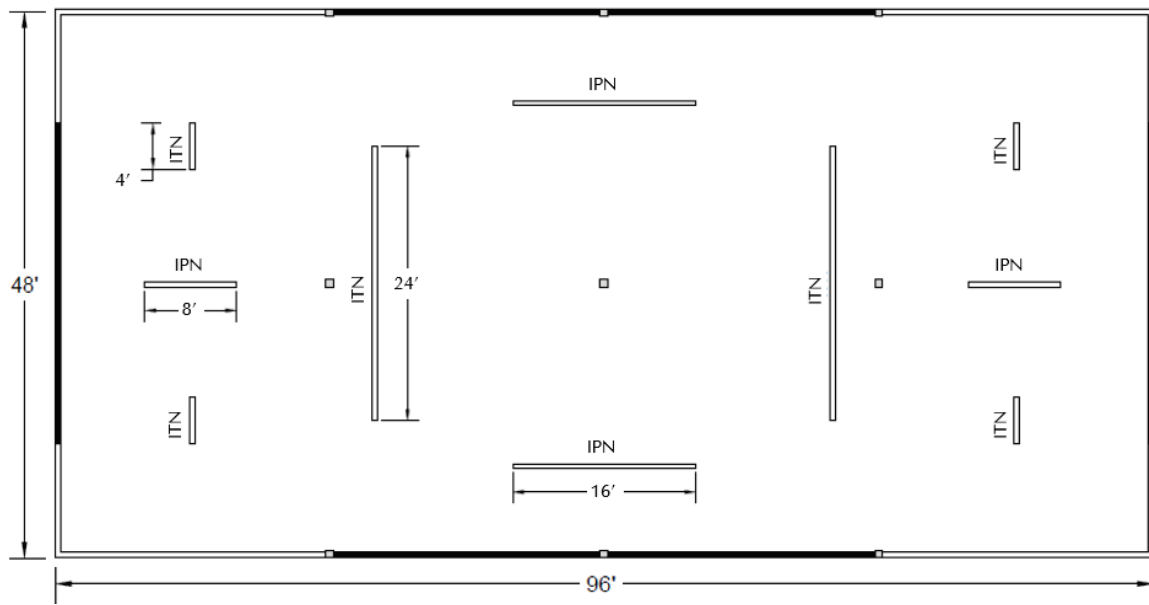


Figure 3-5 Typical interior partition plan for two-story and four-story commercial building archetypes.

Table 3-6 Nonstructural Interior Wall Types and Labels

Code	Type of Wall
CBS	Corridor bearing wall, nonstructural sheathing nailed to sill
PBS	Party bearing wall, nonstructural sheathing nailed to sill
IBS	Interior bearing wall, nonstructural sheathing nailed to sill
ITN	Interior nonstructural wall, transverse to framing above, nonstructural sheathing not nailed to sill
IPN	Interior nonstructural parallel to framing above, nonstructural sheathing not nailed to sill

3.6 Multi-Family Dwellings

Multi-family dwelling archetypes are rectangular in plan, measuring 48 feet by 96 feet. Two plan configurations were considered within this footprint: one with fewer interior shear walls and partitions (two-story archetypes), and one with more densely populated interior shear walls and partitions (one-story and four-story archetypes). A three-dimensional, isometric rendering of a two-story multi-family dwelling archetype is shown in Figure 3-6.

The two-story multi-family dwelling configuration represents a four-unit row house with a party wall between units. This configuration is often referred to as “single-family attached,” but for the purposes of this study, this configuration is grouped with multi-family dwellings because the structural features are similar. Each two-story unit is envisioned to have an interior

staircase to serve the second level of each unit. The one-story and four-story multi-family dwelling configuration represents an apartment building with 6 units per floor.

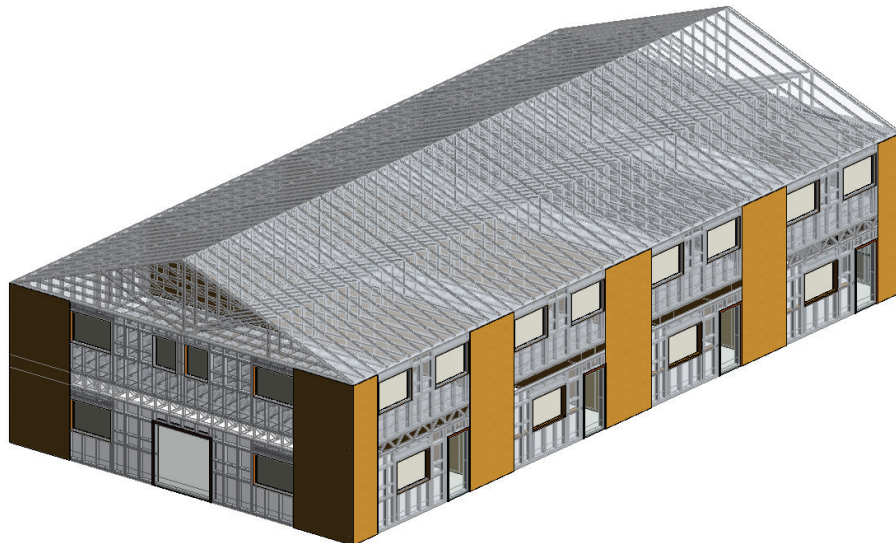


Figure 3-6 Isometric rendering of a two-story multi-family dwelling archetype.

A typical framing plan for a two-story multi-family dwelling archetype is provided in Figure 3-7, showing floor and roof framing, floor and roof diaphragm sheathing, and the locations of perimeter and interior shear walls (shaded in black).

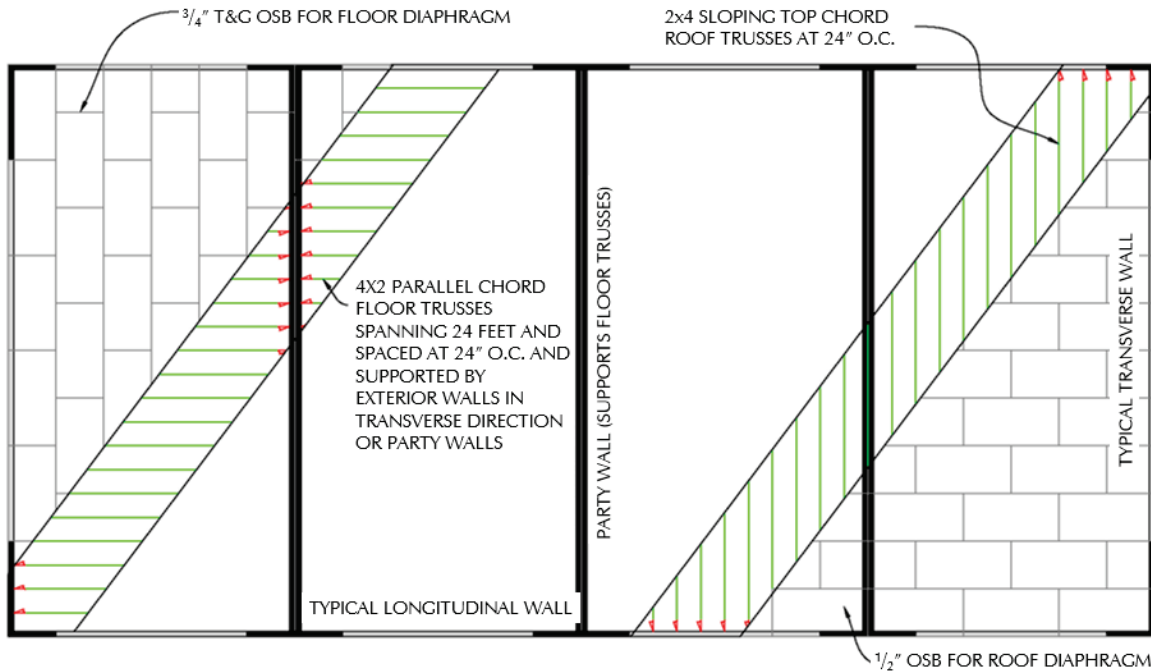


Figure 3-7 Typical floor and roof framing plan for a two-story multi-family dwelling archetype, showing diaphragm sheathing and locations of perimeter and interior shear walls.

A typical framing plan for a four-story multi-family dwelling archetype is provided in Figure 3-8, showing floor and roof framing, floor and roof diaphragm sheathing, and the locations of perimeter and interior shear walls (shaded in black). A typical framing plan for a one-story archetype would be similar to what is shown for the four-story archetype.

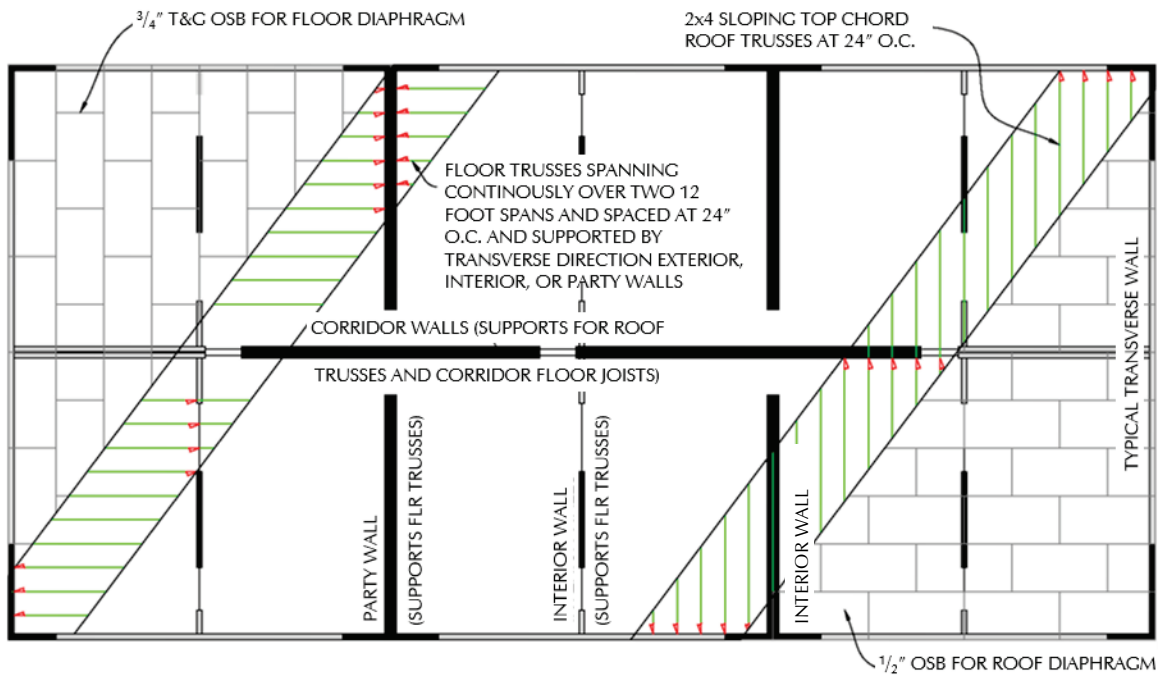


Figure 3-8 Typical floor and roof framing plan for a four-story multi-family dwelling archetype, showing diaphragm sheathing and locations of perimeter and interior shear walls (one-story similar).

Shear walls in all in multi-family dwelling archetypes are provided around the perimeter and at selected interior wall lines. Floor and roof diaphragms span horizontally between shear wall lines. Floor framing is supported on interior and exterior transverse walls, while roof framing (trusses) span between the exterior longitudinal walls (two-story archetypes), and between exterior and corridor walls (one-story and four-story archetypes).

For acoustic control, party walls are constructed as two walls with a gap between, and gypsum concrete is placed on elevated floors. Floor trusses span continuously over interior bearing walls, but do not extend across the cavity in the party walls. Floor and roof sheathing, however, is continuous across the cavity in the party walls so the buildings will behave as one structure.

A double loaded corridor extends longitudinally down the center of one-story and four-story multi-family dwelling archetypes. Isolated stairwells (not shown) are envisioned to occur at each end of the double-loaded corridor.

Walls on each side of the corridor support the floor framing for the double-loaded corridor. For acoustic control, corridor walls have gypsum wallboard on the corridor face, attached to resilient clips and not directly to the wall studs. Gypsum wallboard attached in this manner is not considered to provide any lateral strength or stiffness contribution. When OSB is added to corridor walls to make a shear wall, it is placed on the living unit face of the wall studs (and covered with gypsum wallboard). For convenience in numerical modeling, interior double-loaded corridor walls are modeled as a single wall line along the centerline of the corridor. A typical transverse section for a four-story multi-family dwelling archetype is shown in Figure 3-9, showing the actual configuration of the corridor walls on either side of the double-loaded corridor.

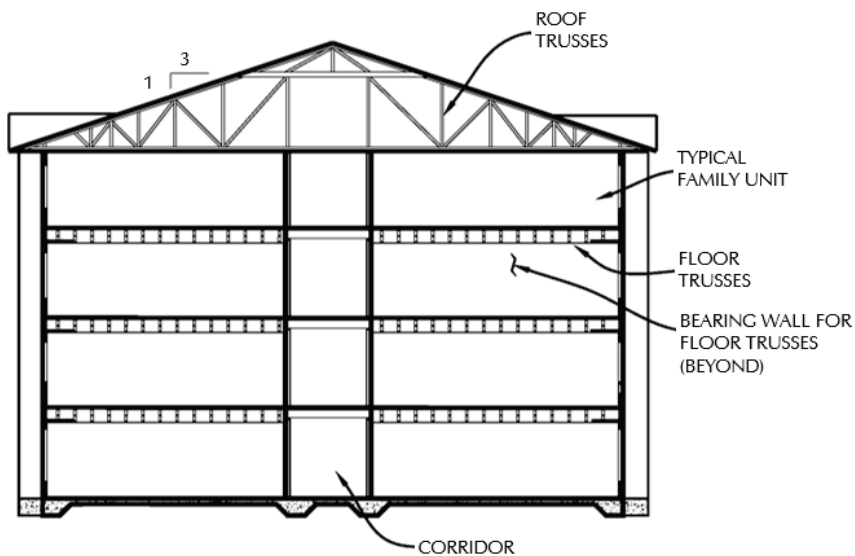


Figure 3-9 Typical transverse section of a four-story multi-family dwelling archetype showing double-loaded corridor walls.

Typical longitudinal wall elevations are provided for a two-story multi-family dwelling archetype in Figure 3-10, and for a four-story archetype in Figure 3-11. In these elevations, a portion of the exterior walls is considered part of the seismic-force-resisting system (shaded in gray), and the remainder is considered nonstructural, or open.

Interior partitions in multi-family dwelling occupancies include both structural and nonstructural walls. A typical interior partition plan for two-story multi-family dwelling archetypes is shown in Figure 3-12. A typical interior partition plan for one-story archetypes, and the fourth floor (top story) in four-story archetypes is shown in Figure 3-13. A typical interior partition plan for first, second, and third floors of four-story archetypes is shown in Figure 3-14. The labeling of interior partition walls is explained in Table 3-6.

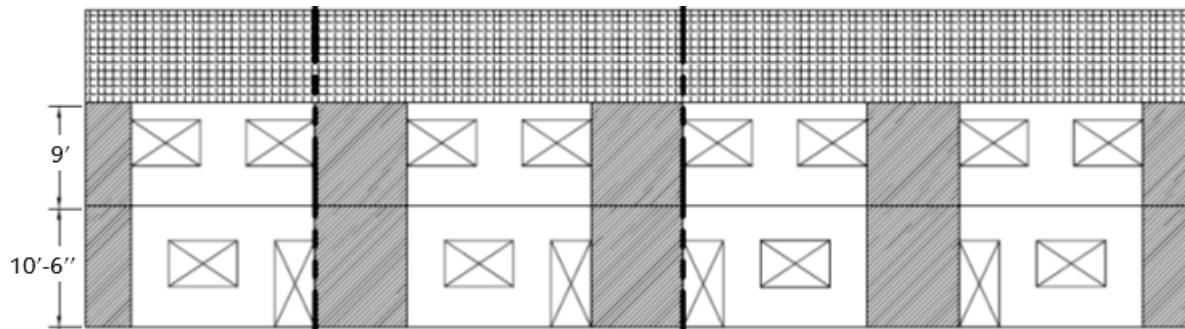


Figure 3-10 Typical longitudinal wall elevation for two-story multi-family dwelling archetypes.

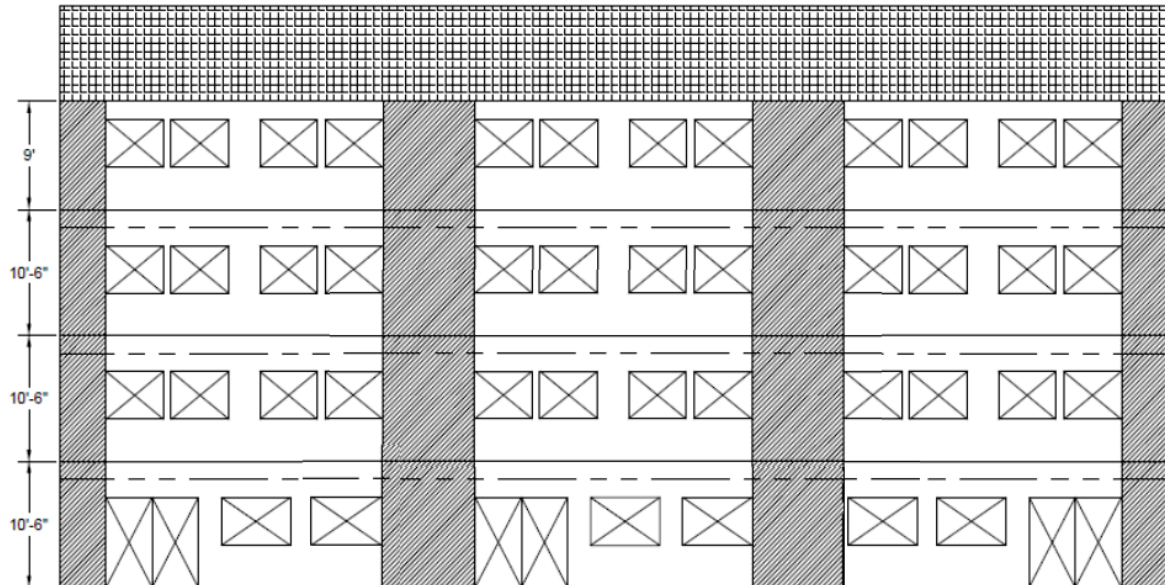


Figure 3-11 Typical longitudinal wall elevation for four-story multi-family dwelling archetypes.

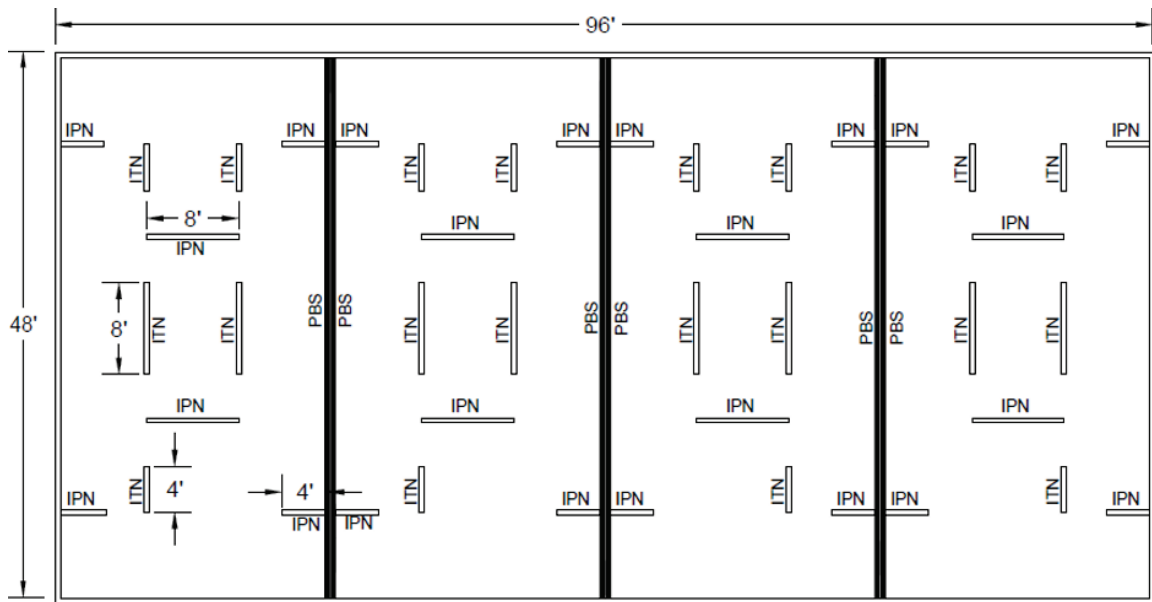


Figure 3-12 Typical interior partition plan for two-story multi-family dwelling archetypes.

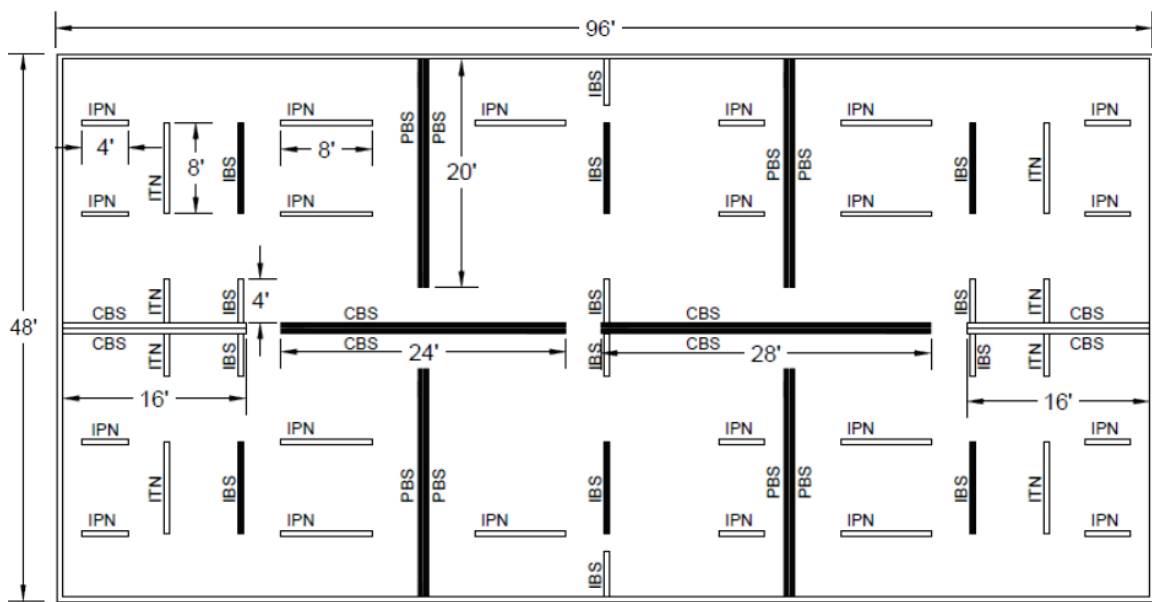


Figure 3-13 Typical interior partition plan for one-story multi-family dwelling archetypes, or the fourth floor (top story) of four-story multi-family dwelling archetypes.

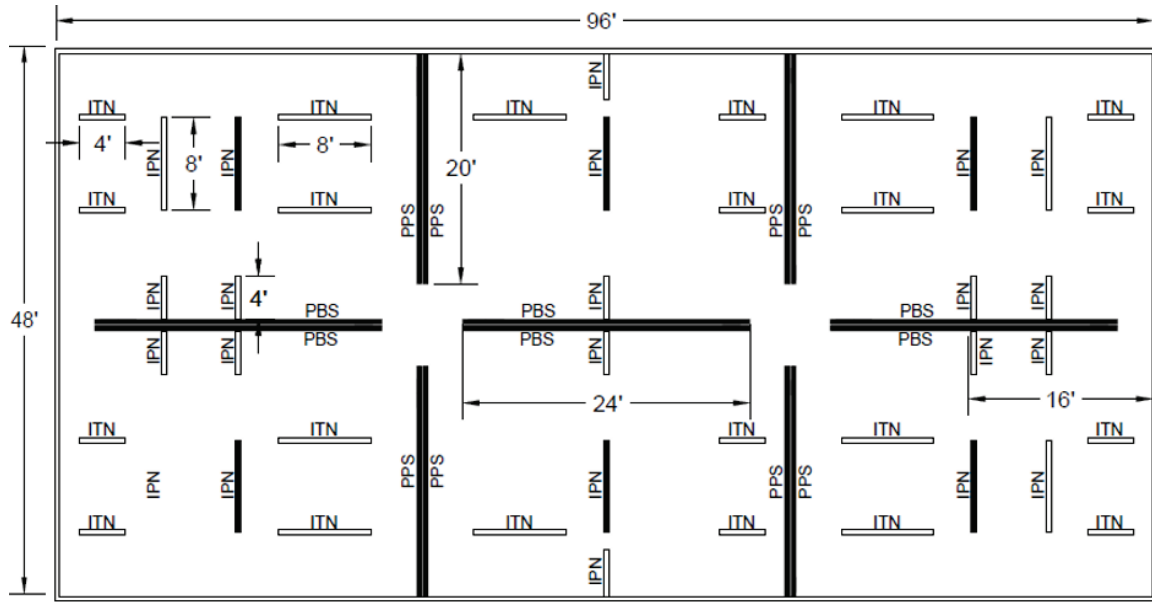


Figure 3-14 Typical interior partition plan for the first, second, and third floors of four-story multi-family dwelling archetypes.

3.7 Single-Family Dwellings

Single-family dwelling archetypes are rectangular in plan, measuring 32 feet by 48 feet. Single-family dwellings are the most prevalent type of wood-light frame building construction and many configurations exist. A three-dimensional, isometric rendering of a two-story single-family dwelling archetype is shown in Figure 3-6.

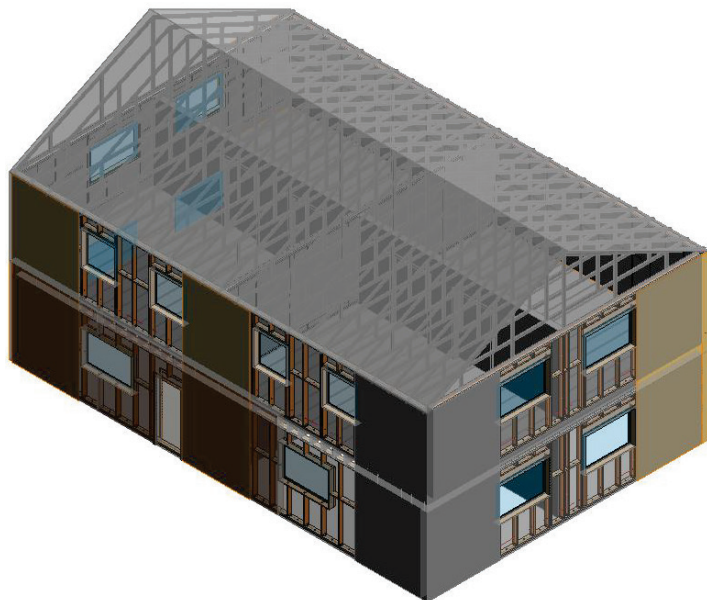


Figure 3-15 Isometric rendering of a two-story single-family dwelling archetype.

Typical framing plans for one-story and two-story single-family dwelling archetypes are provided in Figure 3-16 (floor) and Figure 3-17 (roof), showing floor and roof framing, floor and roof diaphragm sheathing, and the locations of perimeter and interior shear walls (shaded in black).

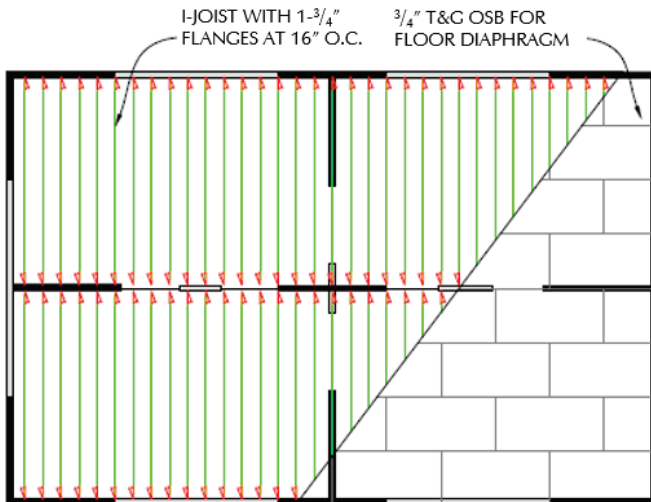


Figure 3-16 Typical floor framing plan for two-story single-family dwelling archetypes, showing diaphragm sheathing and locations of perimeter and interior shear walls.

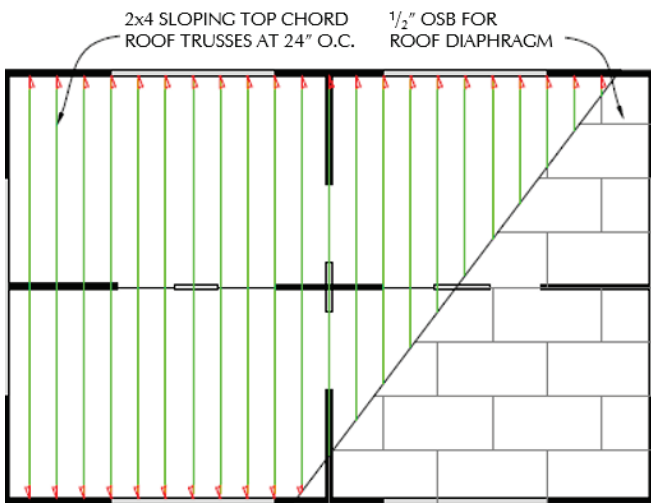


Figure 3-17 Typical roof framing plan for two-story single-family dwelling archetypes, showing diaphragm sheathing and locations of perimeter and interior shear walls.

Shear walls in both engineered and conventional construction single-family dwelling archetypes are provided around the perimeter and at selected interior wall lines. Floor and roof diaphragms span horizontally between shear wall lines. Floor framing consists of manufactured wood I-joists which are supported on interior and exterior bearing walls. Gabled roof framing

spans between exterior longitudinal walls. The first floor is a concrete slab-on-grade, with thickened portions as footings around the perimeter and under interior bearing walls. All interior and exterior walls include nonstructural sheathing and wall finishes.

Longitudinal and transverse wall elevations for two-story single-family dwelling archetypes are shown in Figure 3-18 and Figure 3-19, respectively. In these elevations, a portion of the exterior walls is considered part of the seismic-force-resisting system (shaded in gray), and the remainder is considered nonstructural, or open. Although not shown, one-story single-family dwelling archetypes would have similar shear wall configurations.

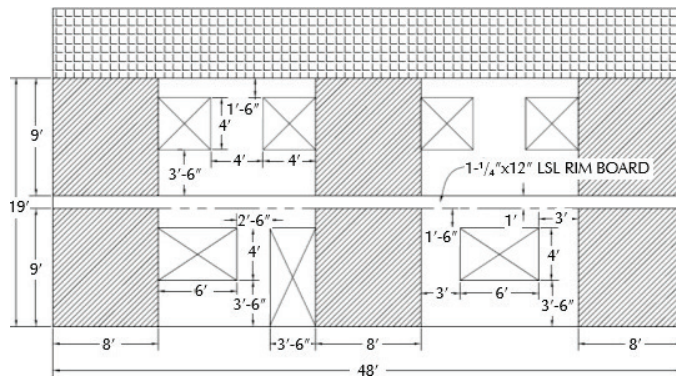


Figure 3-18 Typical longitudinal wall elevation for two-story single-family dwelling archetypes (one-story similar).

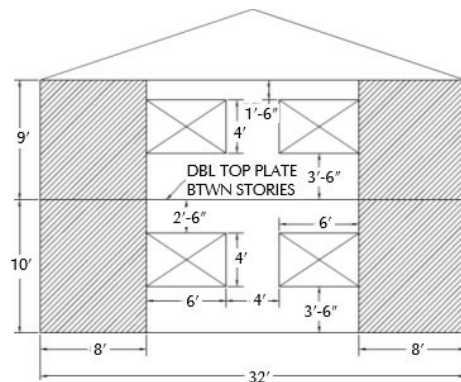


Figure 3-19 Typical transverse wall elevation for two-story single-family dwelling archetypes (one-story similar).

Interior partitions in single-family dwelling occupancies include both structural and nonstructural walls. A typical interior partition plan for one-story archetypes, and the second floor (top story) in two-story archetypes, is shown in Figure 3-20. A typical interior partition plan for first floor of two-story archetypes is shown in Figure 3-21. The labeling of interior partition walls is explained in Table 3-6.

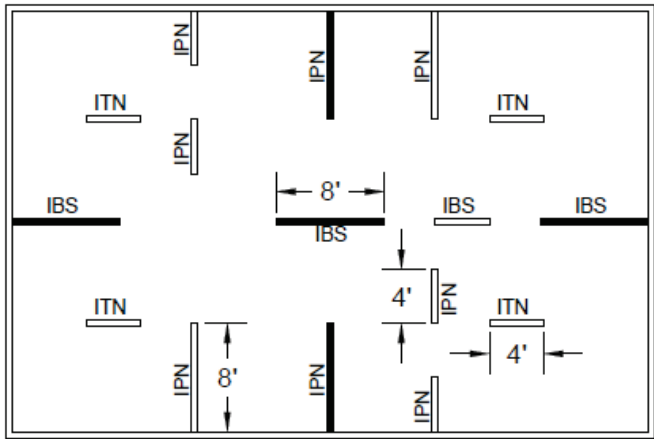


Figure 3-20 Typical interior partition plan for one-story multi-family dwelling archetypes, or the second floor (top story) of two-story multi-family dwelling archetypes.

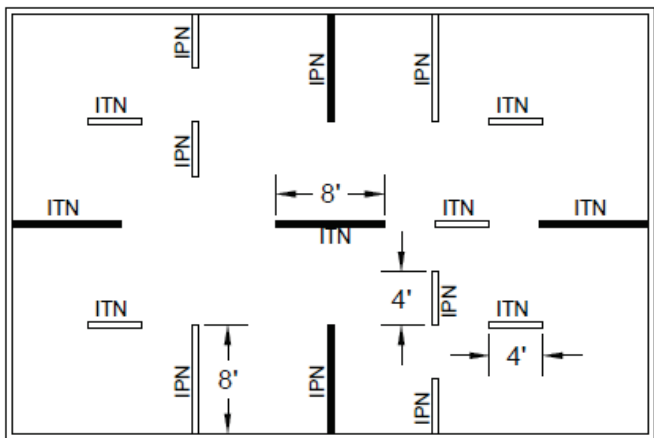


Figure 3-21 Typical interior partition plan for the first floor of two-story single-family dwelling archetypes.

Chapter 4

Numerical Modeling for Parametric Studies

This chapter describes the methods used to develop nonlinear numerical models of short-period wood light-frame buildings based on the archetype designs of Chapter 3. It also discusses analysis methods used to calculate response behavior and evaluate collapse performance. Each parametric study is described, and the model variants developed for each study are identified. Numerical results from the parametric studies are summarized in Chapter 5.

4.1 Modeling Methods

For modeling inelastic dynamic response and seismic collapse mechanisms of wood light-frame archetypes, the *Timber3D* analysis program (Pang et al., 2012), developed at Clemson University, was used. This section describes the basic modeling features of the *Timber3D* program. More advanced modeling features, where used in parametric studies, are described in Sections 4.4 to 4.8.

4.1.1 Overview of *Timber3D*

The *Timber3D* analysis program, coded using MATLAB and developed as part of the NEES-Soft project (van de Lindt et al., 2012), provides analysis capabilities for capturing the nonlinear dynamic response and seismic collapse mechanisms of three-dimensional wood light-frame buildings. The ability to analyze three-dimensional wood light-frame building models represents a significant advancement from the two-dimensional models developed and used in earlier studies of collapse performance of wood light-frame shear wall systems (Shirazi and Pang, 2012; Christovasilis and Filiatrault, 2010; Christovasilis and Filiatrault, 2013).

Timber3D uses a co-rotational formulation and large displacement theory. The horizontal (floor and roof) diaphragms and vertical wall studs are modeled using co-rotational, three-dimensional, two-node, 12-degree-of-freedom (DOF) elastic frame elements, which account for geometric nonlinearity (P-Delta effects). For each load step in a nonlinear static pushover analysis, and for each time-step in a nonlinear dynamic analysis, *Timber3D* tracks the variation of axial loads in all frame elements during the

analysis, and the geometric stiffness matrix is updated at each load/time step to account for geometric nonlinearity due to large deformations (P-Delta effects). The explicit inclusion of P-Delta effects in this study was a major difference from prior numerical studies on wood light-frame systems conducted as part of the FEMA P-695 methodology development, which neglected P-Delta effects (FEMA, 2009b).

Using a co-rotational formulation allows proper consideration of the in-plane and out-of-plane motions of the diaphragms under large deformations.

Explicit consideration of in-plane and out-of-plane deformations of horizontal diaphragms in this study was another difference from prior FEMA P-695 numerical studies on wood light-frame systems, which have implicitly assumed rigid horizontal diaphragms through the use of two-dimensional models.

The elastic flexural and axial stiffness of wall studs were modeled using three-dimensional, two-node, 12-DOF elastic frame elements. The wall panel-to-framing assemblies were modeled using 6-DOF, frame-to-frame (F2F) link elements. In this study, only one DOF of the F2F link element was activated to model lateral nonlinear cyclic response of walls sheathed with wood structural panels and other nonstructural materials.

4.1.2 Typical Timber3D Models

Figure 4-1 illustrates a one-story wood light-frame building modeled using the *Timber3D* analysis program. The horizontal roof diaphragm is modeled using co-rotational, three-dimensional, two-node, 12-DOF elastic frame elements. The flexural and shear stiffness values of the frame elements were calibrated based on a target elastic in-plane stiffness of the diaphragm. This calibration process involves the detailed modeling of the diaphragm of the building under consideration in which all joists, panels, and connectors are included. An elastic, static analysis of the detailed diaphragm model under a uniformly applied horizontal load was used to obtain the ratio of the total applied load to the peak horizontal displacement of the diaphragm (i.e., global horizontal stiffness). In the final building model, the detailed diaphragm model is then replaced by a small number of frame elements for which their flexural stiffness was adjusted to match horizontal stiffness of the detailed diaphragm model. Note that, in contrast with the validation study of the Templeton Hospital building discussed in Appendix D, the effects of diaphragm displacements are expected to be less significant for the archetype designs of Chapter 3 because of smaller plan dimensions and lower lateral strengths relative to the Templeton Hospital building structural configuration.

The model includes wall elements composed of a limited number of standard nonlinear wall building blocks. The sill plate and concrete foundation attached to the bottom nodes of the building blocks can be modeled with elastic frame elements when consideration of the flexibility of these elements is desired. Anchor bolts and hold-down devices (although not considered in this study) can be modeled with F2F link elements. F2F link elements were also used to model nonlinear soil springs, as described in Section 4.6.

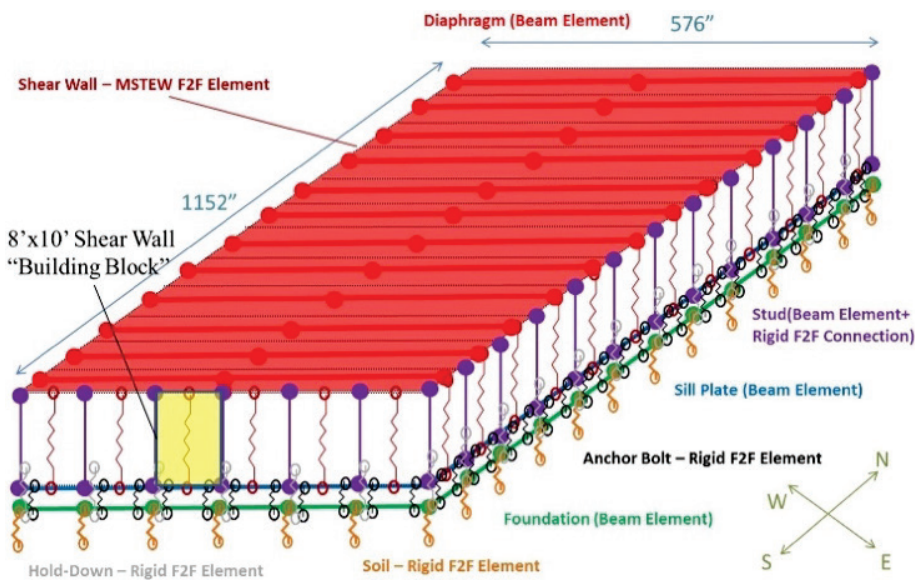


Figure 4-1 Schematic illustration of a three-dimensional, one-story *Timber3D* model.

Baseline building configurations were developed to provide a benchmark to which the other parametric studies could be compared. In the baseline configurations, only the roof and floor diaphragms and shear wall building blocks were activated, while all the other elements were assumed to be rigid. For the parametric investigations on soil-structure interaction (SSI) and foundation flexibility, additional F2F elements were activated, as necessary.

4.1.3 Nonlinear Wall Building Blocks

The nonlinear lateral cyclic response of walls was captured by the CUREE hysteretic rule (Folz and Filiatrault, 2001), as illustrated in Figure 4-2. The loading force-deformation paths OA and CD follow a nonlinear exponential monotonic envelope curve, while all other unloading and re-loading paths exhibit a linear relationship between force and deformation. This hysteretic rule allows for stiffness and strength degradation as well as post-capping strength degradation. The CUREE hysteretic rule is completely determined by ten physically identifiable parameters defined in Table 4-1.

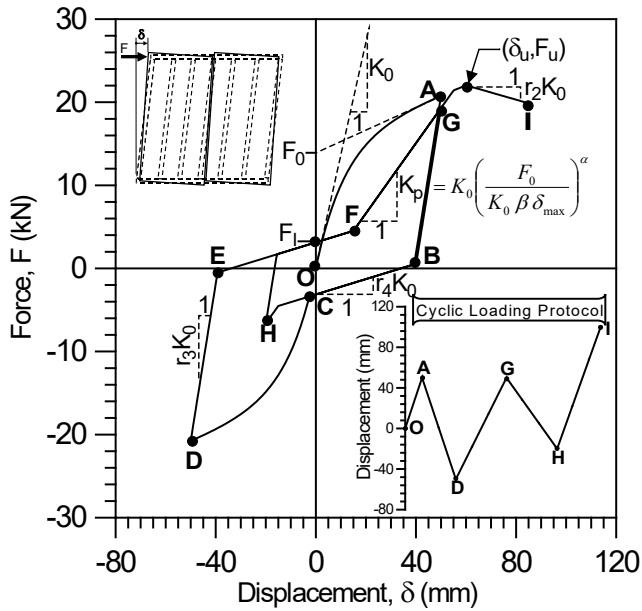


Figure 4-2 CUREE hysteretic rule for modeling force-displacement response of wood light-frame shear walls under cyclic loading (Folz and Filiatruau, 2001).

Table 4-1 Parameters of the CUREE Hysteretic Rule

Parameters Used in Figure 4-2	Definition
K_0	Initial stiffness
F_0	Force intercept of the asymptotic stiffness at ultimate strength
F_I	Zero-displacement load intercept
δ_u	Displacement at ultimate load
r_1	Asymptotic stiffness ratio under monotonic load
r_2	Post-capping strength stiffness ratio under monotonic load
r_3	Unloading stiffness ratio
r_4	Re-loading pinched stiffness ratio
α	Hysteretic parameter for stiffness degradation
β	Hysteretic parameter for stiffness degradation

The CUREE hysteretic rule was modified for this study to introduce a user-defined post-capping residual strength of walls. The reason for this modification was to provide more realistic lateral displacement capacities of building archetypes. The original CUREE hysteretic rule uses very small drift ratios at collapse of wood sheathed walls (approximately 4 percent), corresponding to a post-capping strength at 80 percent of the peak strength. This, coupled with the inclusion of P-Delta effects, would have led to overly conservative (and unrealistic) collapse displacement capacities.

(Christovasilis et al., 2009). Therefore, for this study, the post-capping strength and stiffness (r_2K_o) were replaced by an S-shaped curve anchored at a displacement D_x and converging to pre-determined post-capping residual strength level at large displacements, as shown in Figure 4-3.

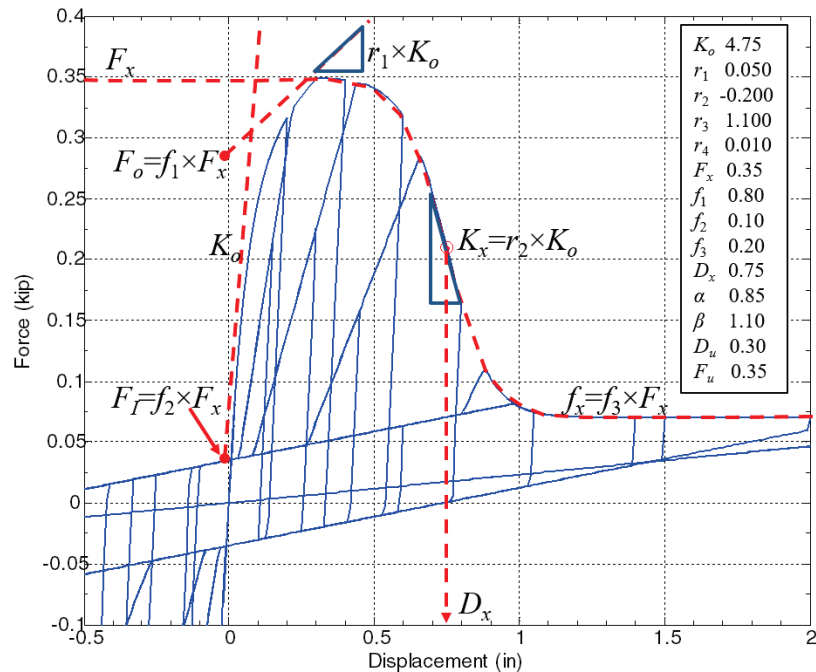


Figure 4-3 Modification of the CUREE hysteretic rule for modeling residual strength.

To avoid unnecessary detailed modeling of unique wall properties, all walls (structural and nonstructural) were based on 4-foot wide by 10-foot high and 8-foot wide by 10-foot high nonlinear wall building blocks made of various common sheathing panels and framing materials. The number and distribution of these panels were selected to be consistent with the archetype designs of Chapter 3.

A typical wall building block is illustrated in Figure 4-4. Each wall building block is composed of four nodes with two end studs and two horizontal plates modeled by elastic frame elements. In addition, each wall building block incorporates an F2F link element representing the nonlinear, lateral, in-plane cyclic response of walls using the CUREE hysteretic rule, as described above. The axial and in-plane flexural deformations of the end studs and top and bottom plates were assumed rigid, and each building block was meant to model the nonlinear lateral cyclic response of the sheathing-to-framing assembly. For this study, top plates, studs, and sill plates were modeled as rigid, so that the wall hysteretic spring was the only contributor to wall displacement.

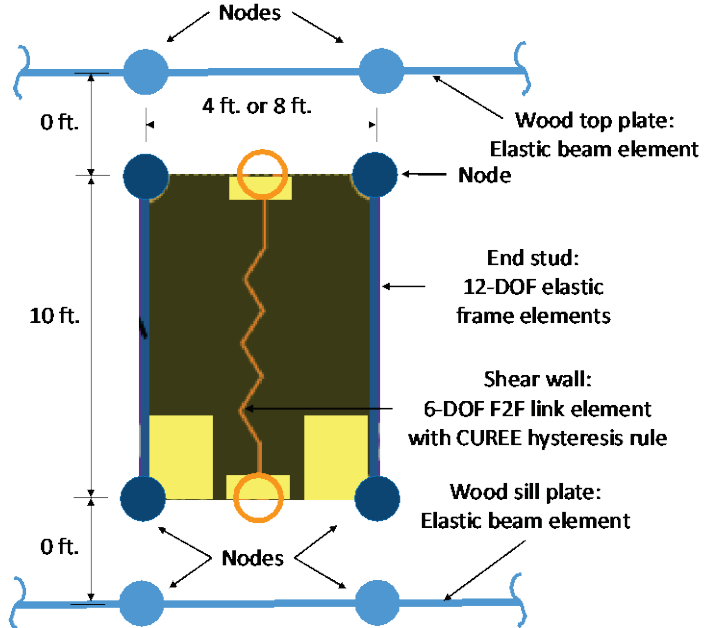


Figure 4-4 Schematic illustration of a wall building block.

4.1.4 Building Block Nonlinear Component Properties

Wall building blocks used in this study had the ability to represent walls with various sheathing materials. Each sheathing material was assigned its individual CUREE hysteretic rule parameters. Tests have shown, however, that when wood structural panels are combined with other sheathing materials in a wall assembly, the total strength is less than the sum of the strengths of the individual layers. Wood structural panels can withstand high drift ratios before losing strength. Nonstructural wall finish materials (i.e., gypsum wallboard and stucco) lose strength at much smaller drift ratios (2 percent or less). To reflect this experimental observation, the following combination rules from FEMA P-807, *Seismic Evaluation and Retrofit of Multi-Unit Wood-Frame Buildings with Weak First Stories* (FEMA, 2012b), were applied for determining how different sheathing types interact on the same wall segment.

1. Walls with similar sheathing materials on both sides were added directly in a linear manner. These included: (a) walls sheathed on two sides with wood structural panels; and (b) walls sheathed with any type of gypsum wallboard on both sides.
2. Walls with dissimilar sheathing materials were combined using 100 percent of the strength of the strongest sheathing type and 50 percent of the strength for the other sheathing types. The initial stiffness of all sheathing materials remained at 100 percent of their individual properties.

Table 4-2 defines nine different individual wall building blocks (single sheathing materials) included in the archetype designs of Chapter 3. Each of these building blocks represents a wall sheathing or finish material that is commonly specified in construction documents for new wood light-frame buildings. The occurrence of high, medium, low or nonstructural OSB is a function of the nailing schedule specified in the archetype designs of Chapter 3. The same is true for walls sheathed with maximum, minimum, and nonstructural gypsum wallboard. Description of the load-deflection properties for each of these building blocks is discussed below.

Table 4-2 Individual Wall Building Blocks

Building Block ID	Definition
OSB-Low	$\frac{7}{16}$ -inch OSB sheathing on Douglas-Fir framing, single row of 8d common nails at 6 inches on-center along all panel edges.
OSB-Medium	$\frac{7}{16}$ -inch OSB sheathing on Douglas-Fir framing, single row of 8d common nails at 3 inches on-center along all panel edges.
OSB-High	$\frac{19}{32}$ -inch OSB sheathing on Douglas-Fir framing, single row (staggered) of 10d common nails at 2 inches on-center along all panel edges.
OSB-Nonstruc	Same as OSB-Low but with minimum nailing.
Min-Gyp	$\frac{1}{2}$ -inch gypsum wallboard on unblocked studs at 16 inches on-center, 5d cooler nails at 7 inches on-center along all panel edges.
Max-Gyp	$\frac{5}{8}$ -inch gypsum wallboard on unblocked studs at 16 inches on-center, 6d cooler nails at 4 inches on-center along all panel edges.
Nonstruc-Gyp	Same as Min-Gyp, but with floating corner construction.
Stucco	New stucco construction.
Siding	Horizontal wood siding.

A set of ten CUREE hysteretic parameters was defined for each of the individual 4-foot by 10-foot and 8-foot by 10-foot building block configurations shown in Table 4-2. The definition of these hysteretic parameters was based on a combination of numerical procedures using sheathing-to-framing connection test data (Folz and Filiatrault, 2001), review of available test data, and expert judgement to model the “best estimate” of wall building block properties.

In order to arrive at best estimate properties, a limited study was made of available component tests describing the range of behavior for each building block of interest. This was made difficult by limitations in available test data and significant variation in load-deflection properties in the data that were available. Variation was due to a number of known causes, such as the boundary conditions and loading protocols used in testing. These circumstances resulted in some information being considered as better (i.e.,

more representative) than other information. The expertise of the project team was used to select best estimate properties considered to be reasonably representative and appropriate for the shear wall building blocks used in this study. The following describes information collected and the properties assigned based on that information.

Each backbone curve was described by best estimate properties of: (1) peak strength and drift ratio at peak strength; (2) drift ratio at 80-percent post-capping peak strength; and (3) residual strength and drift ratio at the initiation of the residual strength plateau. Best estimate properties are summarized in Table 4-3 for each of the backbone curves developed in this study. The curves for Min-Gyp and Nonstruc-Gyp are nearly identical except at the initial loading. This information can be used for comparison with data considered for the development of these curves. The following sections look at each group of materials.

Table 4-3 Best Estimate Properties of Simplified Backbone Curves Shown in Figure 4-5

Building Block 8' by 10'	Peak Strength, V_M (kips)	Drift Ratio @ V_M (%)	Drift Ratio @ 80% Post-Peak Strength (%)	Drift Ratio @ Residual Strength Plateau Start (%)	Residual Strength (% of V_M)
OSB-Low	6.0	2	4	10	30
OSB-Medium	10.0	2	4	10	30
OSB-High	16.0	2	4	10	30
OSB-Nonstruc	4.8	2	4	10	30
Min-Gyp	2.0	1	2	5	30
Max-Gyp	3.2	1	2	5	30
Nonstruc-Gyp	2.0	1	2	5	30
Stucco	8.0	1	3	8	30
Siding	1.5	4	10	No Plateau	No Plateau

The oriented strand board (OSB) curves were developed taking into consideration a number of sources. The curves were initially developed based on analysis results using the CASHEW program (Folz and Filiatralt, 2001) with individual nail hysteretic data. The peak capacity and deflection at peak capacity were also reviewed relative to published test data compilations (Line et al., 2008) as a check of peak capacity and displacement at peak capacity. Best estimate properties for peak strength and drift ratio at 80 percent post-peak strength were selected considering mean values of these parameters obtained from cyclic-load test data in FEMA P-795 (FEMA, 2011). Individual test results varied and were highly dependent on the cyclic-load testing protocol. For example, Table 4-4 compares best estimate

values of peak strength (V_M) and drift ratio at 80 percent post-peak strength ($\delta_{u,80}$) with mean values of these parameters from applicable test data of cyclic-load tests using the CUREE test protocol (Line et al, 2008) and applicable test data of cyclic-load tests using the SPD test protocol (CoLA, 2001). Best estimate values of peak strength (e.g., 16 kips for OSB-High) and the drift ratio at 80 percent post-peak strength (i.e., 4 percent for OSB-High) compare well with mean values of peak strength (e.g., 16.9 kips for OSB-High) and the drift ratio at 80 percent post-peak strength (e.g., 3.6 percent for OSB-High) from CUREE tests, but are often significantly greater than the corresponding values of these parameters from SPD tests.

Differences in measured values of peak strength and post-peak strength displacement capacity are attributed to differences in the number of required cycles of load to failure. The SPD test protocol requires more cycles than the CUREE test protocol, the latter of which is considered more representative of building response due to shallow crustal earthquake ground motions.

Table 4-4 Best Estimate Properties of Backbone Curves and Values of These Parameters Based on Test Data Published in FEMA P-795 (FEMA, 2011)

Building Block 8' by 10'	Peak Strength, V_M (kips)	FEMA P-795 Test Data (8' by 8' Wall)		Drift Ratio @ 80% Post-Peak Strength (%)	FEMA P-795 Test Data (8' by 8' Wall)	
		Table 4-2 ⁽¹⁾ Peak Strength, V_M (kips)	Table D-3 ⁽²⁾ Peak Strength, V_M (kips)		Table 4-2 ⁽¹⁾ Drift Ratio, $\Delta_{u,80}$ (%)	Table D-3 ⁽²⁾ Drift Ratio, $\Delta_{u,80}$ (%)
OSB-Low	6.0	6.01	4.46	4	3.0	1.6
OSB-Medium	10.0	10.84	6.08	4	3.6	1.5
OSB-High	16.0	16.91	14.84	4	3.6	2.5

⁽¹⁾ Average values of test data taken from FEMA P-795 Table 4-2 for Test Index Nos. 42 and 43 (OSB-Low), Test Index Nos. 16 through 33 (OSB-Medium), and Test Index Nos. 54 and 55 (OSB-High) using CUREE Test Protocol (Line et al., 2008).

⁽²⁾ Average values of test data taken from FEMA P-795 Table D-3 for Test Index Nos. 22 through 24 (OSB-Low), Test Index Nos. 19 through 21 (OSB-Medium), and Test Index Nos. 28 through 30 (OSB-High) using SPD Test Protocol (CoLA, 2001).

Nonstructural OSB was included in numerical modeling in locations likely to be sheathed, even though not formally designated as a structural shear wall. The fastening for this sheathing was thought likely to be close to that for the OSB low building block, but was weakened, based on judgement, to a slightly lower peak capacity.

The gypsum wallboard simplified curves were derived starting from the available test data used for FEMA P-807. The compiled simplified backbone curves for this data are shown in Figure 4-5, with the minimum gypsum wallboard and nonstructural gypsum wallboard curve superimposed for comparison (red line). No test data were available for the maximum gypsum wallboard building block with nailing at four inches on center. For this

building block, the minimum gypsum building block was scaled up based on judgement.

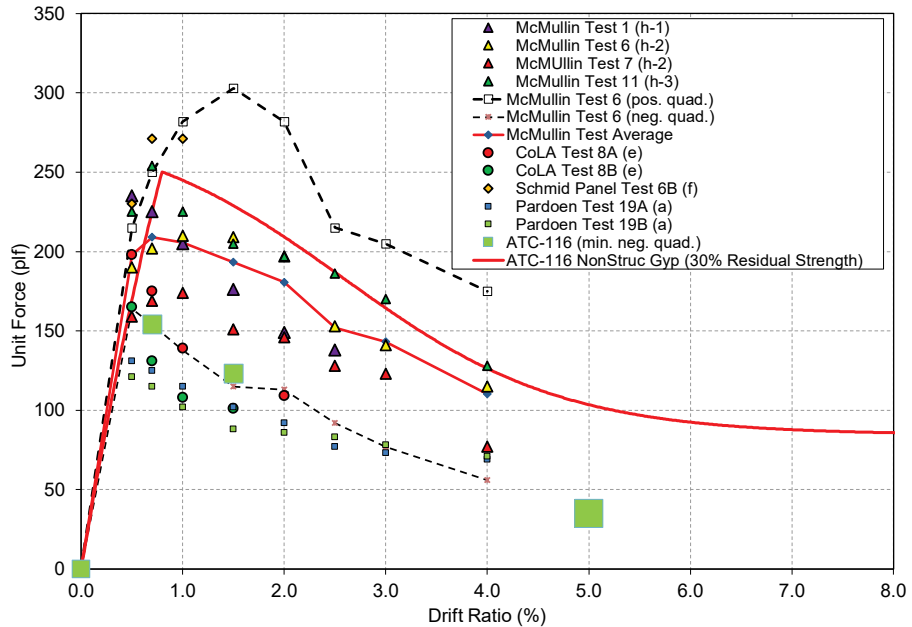


Figure 4-5 Simplified backbone curve data for gypsum wallboard with superimposed building block curve for minimum gypsum wallboard and nonstructural gypsum wallboard (red line).

The stucco building block was derived based on test data from FEMA P-807 and supplemented with test data available in CUREE Publication No. EDA-02, *General Guidelines for the Assessment and Repair of Earthquake Damage in Residential Woodframe Buildings*, (CUREE, 2010). The compiled test data is shown in Figure 4-6, along with the superimposed simplified building block curve used in this study. Note that the choice was made to fall between the P-807 and CUREE backbone curves.

The simplified backbone curve for horizontal wood siding was based on the curve used in FEMA P-807. It should be noted that for all of the simplified backbone curves in this study, the focus was on best estimate (i.e., representative) properties, without intent to capture the variability illustrated in the plotted data.

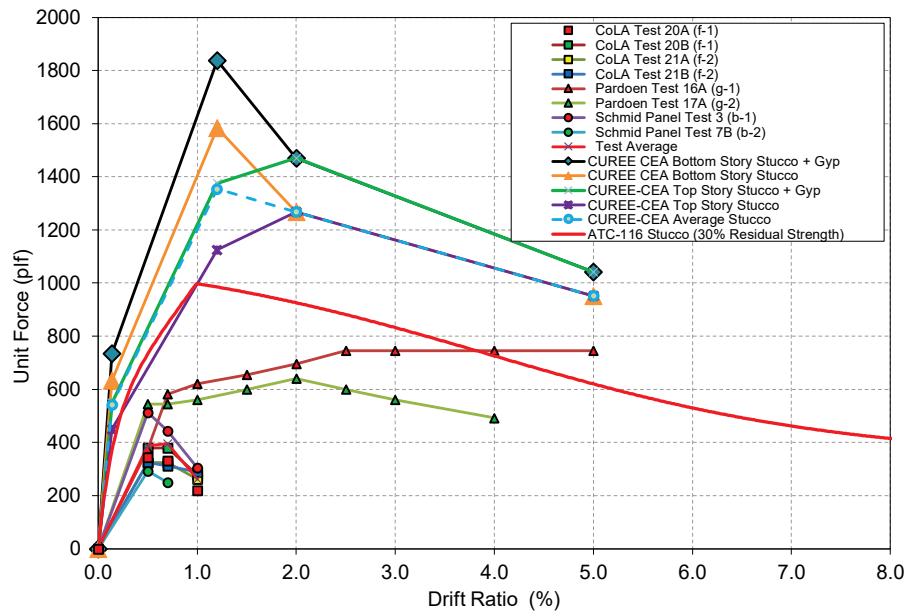


Figure 4-6 Simplified backbone curve data for stucco with superimposed building block curve for stucco (red line).

Table 4-5 and Table 4-6 list the resulting CUREE hysteretic parameters for the individual 8-foot wide by 10-foot high and 4-foot wide by 10-foot high wall building block configurations, respectively, while Figure 4-7 and Figure 4-8 compare the backbone force-displacement relationships for these same building block configurations.

Note that the initial stiffness of the 4-foot long building blocks was reduced by a factor of three compared to the initial stiffness of the 8-foot long building blocks. This reduction was not proportional to the length because of the anticipated increased bending flexibility of shorter building blocks.

Table 4-5 CUREE Hysteretic Parameters for 8-foot Wide by 10-foot High Wall Building Blocks

Building Block ID	K_0 (kip/in)	F_0 (kip)	F_I (kip)	δ_u (in)	r_1	r_2	r_3	r_4	α	β
OSB-Low	15.00	3.830	2.1600	1.91	0.0760	-0.0278	1.01	0.005	0.75	1.05
OSB-Medium	15.00	8.120	2.5000	1.92	0.0760	-0.0463	1.06	0.005	0.75	1.04
OSB-High	24.00	13.00	4.8000	1.92	0.0760	-0.0463	1.02	0.005	0.77	1.15
OSB-Nonstruc	12.00	3.064	1.7280	1.91	0.0760	-0.0278	1.01	0.005	0.75	1.05
Min-Gyp	5.20	1.190	0.3352	0.96	0.1700	-0.0534	1.45	0.017	0.38	1.09
Max-Gyp	9.10	1.940	0.5363	0.96	0.1500	-0.0488	1.45	0.017	0.38	1.09
Nonstruc-Gyp	2.50	1.260	0.3352	0.96	0.4600	-0.1111	1.45	0.017	0.38	1.09
Stucco	25.00	4.000	1.3471	1.20	0.1335	-0.0266	1.45	0.005	0.38	1.09
Siding	1.13	0.600	0.0200	4.80	0.1700	-0.0373	1.45	0.005	0.38	1.09

Table 4-6 CUREE Hysteretic Parameters for 4-foot Wide by 10-foot High Wall Building Blocks

Building Block ID	K_o (kip/in)	F_o (kip)	F_t (kip)	δ_u (in)	r_1	r_2	r_3	r_4	α	β
OSB-Low	5.0000	2.32	2.1600	1.91	0.076	-0.0417	1.01	0.005	0.75	1.05
OSB-Medium	5.0000	4.99	2.5000	1.92	0.092	-0.0695	1.06	0.005	0.75	1.04
OSB-High	8.0000	7.98	4.8000	1.92	0.092	-0.0695	1.02	0.005	0.77	1.15
OSB-Nonstruc	4.0000	1.86	1.7280	1.91	0.076	-0.0417	1.01	0.005	0.75	1.05
Min-Gyp	1.7333	1.19	0.3352	0.96	0.090	-0.0801	1.45	0.017	0.38	1.09
Max-Gyp	3.0333	1.70	0.5363	0.96	0.090	-0.0732	1.45	0.017	0.38	1.09
Nonstruc-Gyp	1.2500	0.63	0.1676	0.96	0.460	-0.1111	1.45	0.005	0.38	1.09
Stucco	8.3333	2.53	1.3471	1.20	0.155	-0.0400	1.45	0.005	0.38	1.09
Siding	0.3767	0.41	0.0200	4.80	0.200	-0.0560	1.45	0.005	0.38	1.09

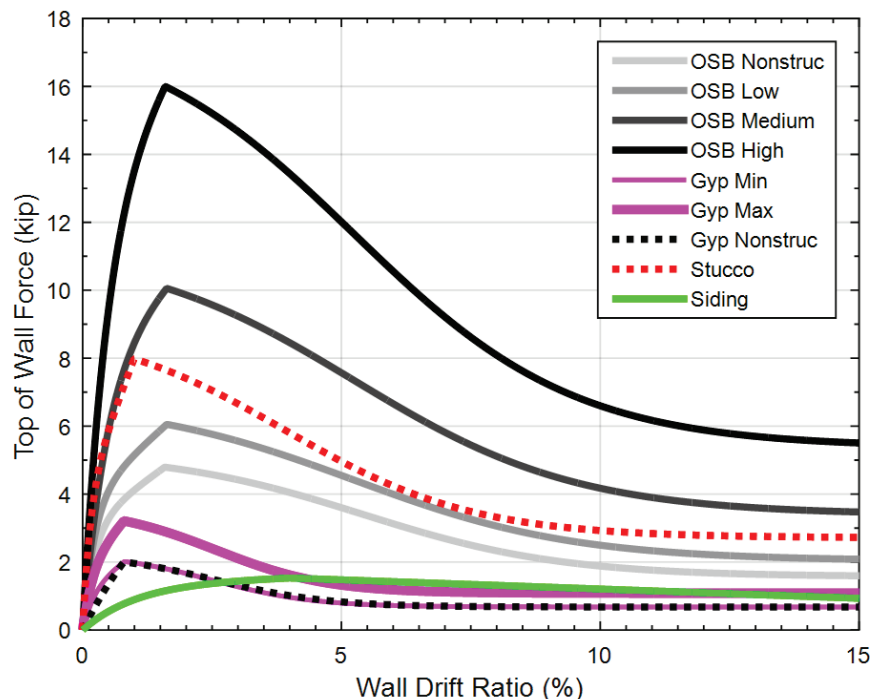


Figure 4-7 Backbone curves for 8-foot wide by 10-foot high wall building blocks.

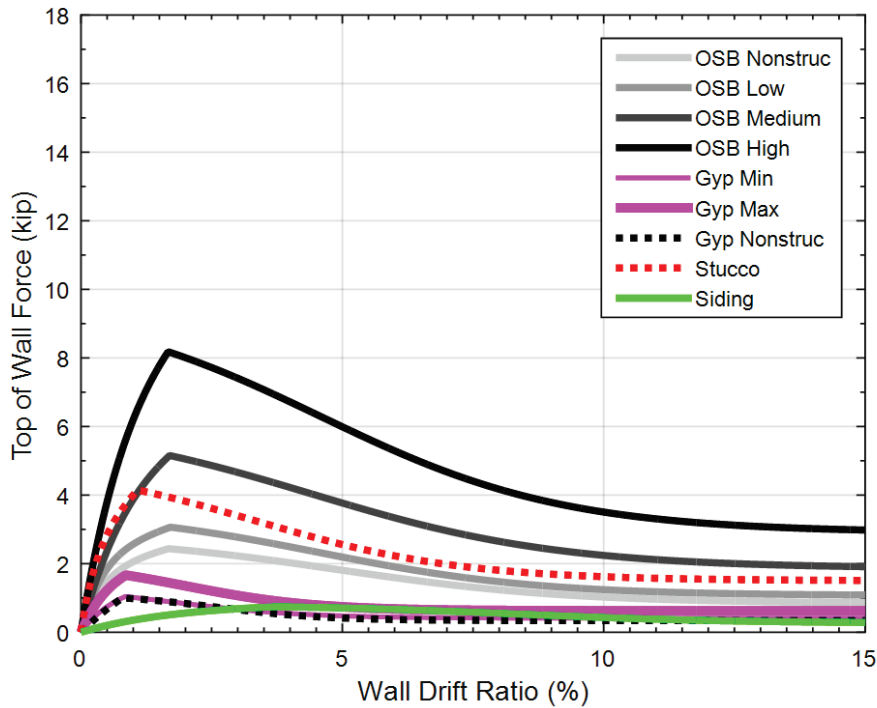


Figure 4-8 Backbone curves for 4-foot wide by 10-foot high wall building blocks.

The modified hysteretic rule in Figure 4-3, includes a residual post-capping strength to provide realistic lateral displacement capacities. A residual post-capping strength of 30 percent of peak strength was chosen for development of baseline configuration building blocks. It should be noted that individual components were assumed to have infinite displacement capacity ($\delta_u = \infty$). This infinite displacement capacity, however, was never realized because the inclusion of P-Delta effects within the numerical models leads to collapse at some finite displacement for any system experiencing significant lateral displacement.

Residual post-capping strength was used as a modeling expediency to develop more realistic lateral displacement capacities in building archetypes. In physical terms, one source of residual strength is present in the wall elements themselves as they experience inelastic demands. A second source of residual strength can be attributed to system factors that are unrelated to the wall elements, such as the strength provided by stairwells, binding effect of non-bearing partition walls, box effect of small room configurations, and out-of-plane wall effects at large displacements. Ideally, these two sources of residual strength would be modeled explicitly, but secondary sources of strength were not included in the models, so residual post-capping strength, expressed as a percentage of peak strength, was included in the wall building blocks to capture all sources of residual strength.

Table 4-7 lists the 32 building block combinations (combining multiple sheathing materials) contained in the archetype designs of Chapter 3. Figure 4-9 and Figure 4-10 compare the backbone force-displacement relationships for the 8-foot wide by 10-foot high and 4-foot wide by 10-foot high building block combinations, respectively, based on FEMA P-807 combination rules described earlier.

Table 4-7 Wall Building Block Combinations

Combo ID	Wall Type	Description
Exterior-1	Exterior	OSB-Low with stucco over it, Nonstruc-Gyp on inside.
Exterior-2	Exterior	OSB-Med with stucco over it, Nonstruc-Gyp on inside.
Exterior-3	Exterior	OSB-High with stucco over it, Nonstruc-Gyp on inside.
Exterior-4	Exterior	OSB-Nonstruc with stucco over it, Nonstruc-Gyp on inside.
Exterior-5	Exterior	OSB-Low with siding over it, Nonstruc-Gyp on inside.
Exterior-6	Exterior	OSB-Med with siding over it, Nonstruc-Gyp on inside.
Exterior-7	Exterior	OSB-High with siding over it, Nonstruc-Gyp on inside.
Exterior-8	Exterior	OSB-Nonstruc with siding over it, Nonstruc-Gyp on inside.
Exterior-9	Exterior	OSB-Low both sides with stucco over it, Nonstruc-Gyp on inside.
Exterior-10	Exterior	OSB-Med both sides with stucco over it, Nonstruc-Gyp on inside.
Exterior-11	Exterior	OSB-High both sides with stucco over it, Nonstruc-Gyp on inside.
Exterior-12	Exterior	OSB-Low both sides with siding over it, Nonstruc-Gyp on inside.
Exterior-13	Exterior	OSB-Med both sides with siding over it, Nonstruc-Gyp on inside.
Exterior-14	Exterior	OSB-High both sides with siding over it, Nonstruc-Gyp on inside.
Interior-1	Interior	Min-Gyp on both sides.
Interior-2	Interior	Max-Gyp on both sides.
Interior-3	Interior	Nonstruc-Gyp on both sides.
Interior-4	Interior	OSB-Low on one side, Nonstruc-Gyp on both sides.
Interior-5	Interior	OSB-Med on one side, Nonstruc-Gyp on both sides.
Interior-6	Interior	OSB-High on one side, Nonstruc-Gyp on both sides.
Interior-7	Interior	OSB-Low on one side, Min-Gyp on both sides.
Interior-8	Interior	OSB-Med on one side, Min-Gyp on both sides.
Interior-9	Interior	OSB-High on one side, Min-Gyp on both sides.
PartyCor-1	Party/corridor	Min-Gyp on both sides.
PartyCor-2	Party/corridor	Max-Gyp on both sides.
PartyCor-3	Party/corridor	Nonstruc-Gyp on both sides.
PartyCor-4	Party/corridor	OSB-Low with Nonstruc-Gyp on same side.
PartyCor-5	Party/corridor	OSB-Med with Nonstruc-Gyp on same side.
PartyCor-6	Party/corridor	OSB-High with Nonstruc-Gyp on same side.
PartyCor-7	Party/corridor	OSB-Low with Min-Gyp on same side.
PartyCor-8	Party/corridor	OSB-Med with Min-Gyp on same side.
PartyCor-9	Party/corridor	OSB-High with Min-Gyp on same side.

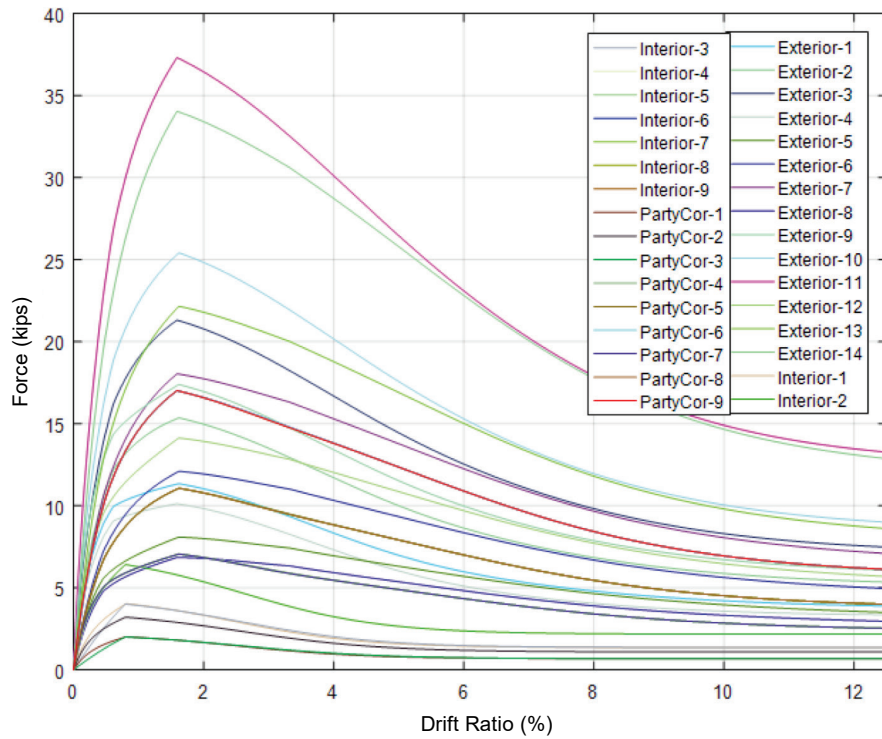


Figure 4-9 Backbone curves for 8-foot wide by 10-foot high wall building block combinations.

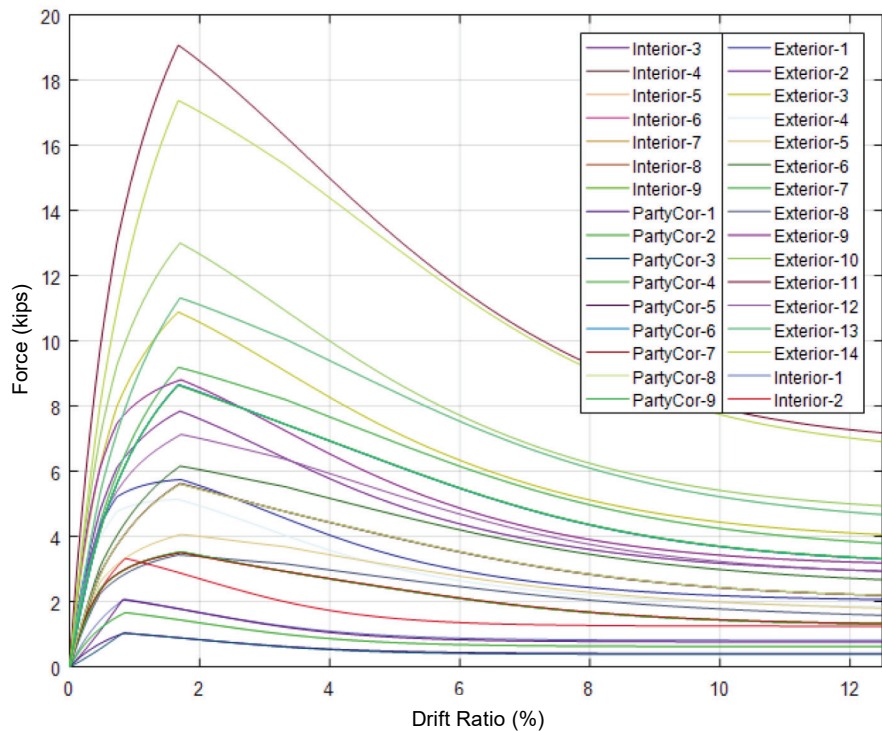


Figure 4-10 Backbone curves for 4-foot wide by 10-foot high wall building block combinations.

For the purpose of comparison and validation of analysis results, the characteristic response parameters described in Section 4.1.4 and consistent with the definitions in FEMA P-795 were calculated for the individual and combined wall building block backbone curves. Although FEMA P-795 requires calculating these parameters using cyclic test results, testing has shown that the monotonic and cyclic backbone curves under seismic input are similar for wall assemblies sheathed with OSB and gypsum (Gatto and Uang, 2001). The characteristic response parameters calculated from the monotonic backbone curves were:

- Secant stiffness at 40 percent of the peak strength, K_{40} , in loading portion of the force-displacement response.
- Drift ratio at 80 percent of the peak strength, $\Delta_{u,80}$, in post-capping portion of the force-displacement response.
- Drift ratio, $\Delta_{u,\max}$, in the post-capping portion of force displacement response. For individual and combinations of wall building block backbone curves, $\Delta_{u,\max}$, was taken as the drift ratio corresponding to the start of the residual strength plateau. This response parameter is not included in FEMA P-795, but was introduced in this study because of the consideration of residual strengths in the archetype models.

Table 4-8 and Table 4-9 present the characteristic response parameters for individual wall building blocks and for wall building block combinations, respectively. The displacements in these tables have been converted into drift ratios and are expressed as a percentage of wall height.

Table 4-8 Characteristic Response Parameters for Wall Building Blocks

Combo ID	4-foot by 10-foot Building Block			8-foot by 10-foot Building Block		
	K_{40} (kip/in)	$\Delta_{u,80}$ (%)	$\Delta_{u,\max}$ (%)	K_{40} (kip/in)	$\Delta_{u,80}$ (%)	$\Delta_{u,\max}$ (%)
OSB-Low	3.17	4.00	10.00	10.71	4.00	10.00
OSB-Medium	3.44	4.00	10.00	11.67	4.00	10.00
OSB-High	5.50	4.00	10.00	18.67	4.00	10.00
OSB-Nonstruc	2.56	4.00	10.00	8.57	4.00	10.00
Min-Gyp	1.23	2.00	5.00	3.98	2.00	5.00
Max-Gyp	2.13	2.00	5.00	6.92	2.00	5.00
Nonstruc-Gyp	0.79	2.00	5.00	2.39	2.00	5.00
Stucco	5.33	3.00	8.00	16.95	3.00	8.00
Siding	0.24	10.00	NA*	0.72	10.00	NA*

* The CUREE hysteresis model for horizontal wood siding does not have a residual strength plateau.

Table 4-9 FEMA P-795 Characteristic Response Parameters for Wall Building Block Combinations

Building Block ID	4-foot by 10-foot Building Block			8-foot by 10-foot Building Block		
	K_{40} (kip/in)	$\Delta_{u,80}$ (%)	$\Delta_{u,max}$ (%)	K_{40} (kip/in)	$\Delta_{u,80}$ (%)	$\Delta_{u,max}$ (%)
Exterior-1	7.50	3.58	10.00	20.57	3.58	10.00
Exterior-2	7.62	3.69	10.00	20.66	3.69	10.00
Exterior-3	10.05	3.77	10.00	27.46	3.77	10.00
Exterior-4	6.71	3.54	10.00	18.36	3.54	10.00
Exterior-5	4.41	4.22	NA*	12.12	4.22	NA*
Exterior-6	4.81	4.15	NA*	13.32	4.15	NA*
Exterior-7	7.31	4.10	NA*	20.33	4.10	NA*
Exterior-8	3.66	4.26	NA*	10.04	4.26	NA*
Exterior-9	11.33	3.72	10.00	31.13	3.72	10.00
Exterior-10	11.70	3.81	10.00	32.26	3.81	10.00
Exterior-11	16.64	3.87	10.00	46.29	3.87	10.00
Exterior-12	8.24	4.12	NA*	22.83	4.12	NA*
Exterior-13	8.97	4.08	NA*	24.99	4.08	NA*
Exterior-14	13.96	4.05	NA*	39.00	4.05	NA*
Interior-1	2.97	2.01	5.00	7.96	2.01	5.00
Interior-2	5.13	2.01	5.00	13.85	2.01	5.00
Interior-3	1.90	2.01	5.00	4.77	2.01	5.00
Interior-4	4.27	3.66	10.00	11.78	3.66	10.00
Interior-5	4.66	3.78	10.00	12.94	3.78	10.00
Interior-6	7.14	3.86	10.00	20.00	3.86	10.00
Interior-7	4.63	3.66	10.00	12.83	3.66	10.00
Interior-8	4.88	3.78	10.00	13.57	3.78	10.00
Interior-9	7.38	3.86	10.00	20.67	3.86	10.00
PartyCor-1	1.49	2.01	5.00	3.98	2.01	5.00
PartyCor-2	2.56	2.01	5.00	6.92	2.01	5.00
PartyCor-3	0.95	2.01	5.00	2.39	2.01	5.00
PartyCor-4	4.27	3.66	10.00	11.78	3.66	10.00
PartyCor-5	4.66	3.78	10.00	12.94	3.78	10.00
PartyCor-6	7.14	3.86	10.00	20.00	3.86	10.00
PartyCor-7	4.63	3.66	10.00	12.83	3.66	10.00
PartyCor-8	4.88	3.78	10.00	13.57	3.78	10.00
PartyCor-9	7.38	3.86	10.00	20.67	3.86	10.00

* The CUREE hysteresis model for horizontal wood siding does not have a residual strength plateau.

4.2 Overview of Parametric Studies and Variations in Archetypes

To investigate potential causes for the apparent discrepancy between analyzed and observed seismic performance of wood light frame systems, five parametric studies were performed. These included:

- baseline configuration;
- collapse displacement capacity;
- nonstructural interior and exterior wall finishes;
- soil-structure interaction (SSI) and foundation flexibility; and
- backbone curve shape.

Each parametric study evaluated the response behavior and collapse performance characteristics of a set of numerical models of representative archetypes with variations in selected parameters of interest specific to each study.

As shown in Table 4-10 for commercial (COM) building archetypes, Table 4-11 for multi-family dwelling (MFD) archetypes, and Table 4-12 for single-family dwelling (SFD) archetypes, a total of 90 short-period wood light-frame numerical models were developed for the five different parametric studies as follows:

- 28 baseline archetypes for the baseline configuration parametric study;
- 27 variants for the collapse displacement capacity parametric study;
- 11 variants for the nonstructural interior and exterior wall finishes parametric study;
- 12 variants for the soil-structure interaction (SSI) and foundation flexibility parametric study; and
- 12 variants for the backbone curve shape parametric study.

Table 4-10 Baseline and Variant Numerical Models for Commercial Building Archetypes in Five Parametric Studies

Parametric Study Archetype ID					
No. of Archetypes	(1) Baseline Configuration	(2) Collapse Displacement Capacity	(3) Interior and Exterior Wall Finishes	(4) SSI and Foundation Flexibility	(5) Backbone Curve Shape
Commercial Buildings - High Seismic					
6	COM1B	COM1B-C (3)	-	COM1B-F (2)	-
10	COM2B	COM2B-C (6)	COM2B-NS	COM2B-F (2)	-
16	COM3B	-	COM3B-NS	COM3B-F (2)	COM3B-BS (12)
Commercial Buildings - Very High Seismic					
1	COM4B	-	-	-	-
1	COM5B	-	-	-	-
1	COM6B	-	-	-	-
Commercial Buildings - Moderate Seismic					
(1)	COM7B	-	-	-	-
(1)	COM8B	-	-	-	-
(1)	COM9B	-	-	-	-

Table 4-11 Baseline and Variant Numerical Models for Multi-Family Dwelling Archetypes in Five Parametric Studies

Parametric Study Archetype ID					
No. of Archetypes	(1) Baseline Configuration	(2) Collapse Displacement Capacity	(3) Interior and Exterior Wall Finishes	(4) SSI and Foundation Flexibility	(5) Backbone Curve Shape
Multi-Family Dwelling Buildings - High Seismic					
6	MFD1B	MFD1B-C (3)	-	MFD1B-F (2)	-
10	MFD2B	MFD2B-C (6)	MFD2B-NS	MFD2B-F (2)	-
3	MFD3B	-	-	MFD3B-F (2)	-
Multi-Family Dwelling Buildings - Very High Seismic					
1	MFD4B	-	-	-	-
1	MFD5B	-	-	-	-
1	MFD6B	-	-	-	-
Multi-Family Dwelling Buildings - Moderate Seismic					
(1)	MFD7B	-	-	-	-
(1)	MFD8B	-	-	-	-
(1)	MFD9B	-	-	-	-

Table 4-12 Baseline and Variant Numerical Models for Single-Family Dwelling Archetypes in Five Parametric Studies

Parametric Study Archetype ID					
No. of Archetypes	(1) Baseline Configuration	(2) Collapse Displacement Capacity	(3) Interior and Exterior Wall Finishes	(4) SSI and Foundation Flexibility	(5) Backbone Curve Shape
Single-Family Dwelling Buildings - High Seismic					
6	SFD1B	SFD1B-C (3)	SFD1B-NS (2)	-	-
3	SFD1BC	-	SFD1BC-NS (2)	-	-
9	SFD2B	SFD2B-C (6)	SFD2B-NS (2)	-	-
3	SFD2BC	-	SFD2BC-NS (2)	-	-
Single-Family Dwelling Buildings - Very High Seismic					
1	SFD3B	-	-	-	-
1	SFD3BC	-	-	-	-
1	SFD4B	-	-	-	-
Single-Family Dwelling Buildings - Moderate Seismic					
(1)	SFD5B	-	-	-	-
(1)	SFD5BC	-	-	-	-
(1)	SFD6B	-	-	-	-

In the above tables, an archetype designation in a cell under a parametric study represents a variant of the baseline model developed for that study. Numbers in parentheses next to an archetype designation indicate the number of variants investigated in that study. Although moderate seismic numerical models were developed, they were considered lower priority than high seismic and very high seismic, and were not analyzed.

Key properties and seismic design criteria for each of the baseline wood light-frame building archetypes described in Chapter 3 are summarized in Table 4-13 for commercial building archetypes, Table 4-14 for multi-family dwelling archetypes, and Table 4-15 for single-family dwelling archetypes. In Table 4-15, the values of the design period (T) and design base shear normalized by seismic weight (V/W) for conventional construction single-family dwelling archetypes are assumed to be the same as those of the corresponding engineered archetypes.

It should be noted that the variants of a baseline model use the same seismic-force-resisting system as the baseline model. Differences in response behavior, if any, were a direct result of the changes in the numerical models to account for the parameter of interest being investigated.

Table 4-13 Baseline Commercial Building Archetypes, Key Configuration and Seismic Design Criteria

Archetype ID	Configuration			Seismic Design Criteria		
	No. of Stories	h_r (ft)	W (kips)	S_{MS} (g)	T^* (sec)	$V/W = C_s$
Commercial Buildings - High Seismic						
COM1B	1	10	180	1.5	0.25	0.154
COM2B	2	20	488	1.5	0.26	0.154
COM3B	4	40	1,106	1.5	0.45	0.154
Commercial Buildings - Very High Seismic						
COM4B	1	10	180	2.25	0.25	0.231
COM5B	2	20	488	2.25	0.26	0.231
COM6B	4	40	1,106	2.25	0.45	0.231
Commercial Buildings - Moderate Seismic						
COM7B	1	10	180	0.75	0.25	0.077
COM8B	2	20	488	0.75	0.26	0.077
COM9B	4	40	1,106	0.75	0.45	0.077

* The design period is defined as $T = C_u T_a \geq 0.25$ seconds, in accordance with the analysis requirements of FEMA P-695, where the values of the parameters C_u and T_a are specified by ASCE/SEI 7-10.

Table 4-14 Baseline Multi-Family Dwelling Archetypes, Key Configuration and Seismic Design Criteria

Archetype ID	Configuration			Seismic Design Criteria		
	No. of Stories	h_r (ft)	W (kips)	S_{MS} (g)	T^* (sec)	$V/W = C_s$
Multi-Family Dwelling Buildings - High Seismic						
MFD1B	1	10	141	1.5	0.25	0.154
MFD2B	2	20	363	1.5	0.26	0.154
MFD3B	4	40	971	1.5	0.45	0.154
Multi-Family Dwelling Buildings - Very High Seismic						
MFD4B	1	10	141	2.25	0.25	0.231
MFD5B	2	20	363	2.25	0.26	0.231
MFD6B	4	40	971	2.25	0.45	0.231
Multi-Family Dwelling Buildings - Moderate Seismic						
MFD7B	1	10	141	0.75	0.25	0.077
MFD8B	2	20	363	0.75	0.26	0.077
MFD9B	4	40	971	0.75	0.45	0.077

* The design period is defined as $T = C_u T_a \geq 0.25$ seconds, in accordance with the analysis requirements of FEMA P-695, where the values of the parameters C_u and T_a are specified by ASCE/SEI 7-10.

Table 4-15 Baseline Single-Family Dwelling Archetypes, Key Configuration and Seismic Design Criteria

Archetype ID	Configuration			Seismic Design Criteria		
	No. of Stories	h_r (feet)	W (kips)	S_{MS} (g)	T^* (sec)	V/W (C_s)
Single-Family Dwelling Buildings - High Seismic						
SFD1B	1	9	52	1.5	0.25	0.154
SFD1BC	1	9	52	1.5	0.25	0.154
SFD2B	2	19	135	1.5	0.25	0.154
SFD2BC	2	19	135	1.5	0.25	0.154
Single-Family Dwelling Buildings - Very High Seismic						
SFD3B	1	9	52	2.25	0.25	0.231
SFD3BC	1	9	52	2.25	0.25	0.231
SFD4B	2	19	135	2.25	0.25	0.231
Single-Family Dwelling Buildings - Moderate Seismic						
SFD5B	1	9	52	0.75	0.25	0.077
SFD5BC	2	19	52	0.75	0.25	0.077
SFD6B	2	19	135	0.75	0.25	0.077

* The design period is defined as $T = C_u T_a \geq 0.25$ seconds, in accordance with the analysis requirements of FEMA P-695, where the values of the parameters C_u and T_a are specified by ASCE/SEI 7-10.

4.3 Baseline Configuration Parametric Study

Representative wood light-frame building archetypes included typical configurations of commercial (COM) buildings, multi-family dwellings (MFD), and single-family dwellings (SFD) of heights up to four stories, each designed for three seismic design levels corresponding to buildings located in regions of moderate seismicity ($S_{MS} = 0.75$ g), high seismicity ($S_{MS} = 1.5$ g), and very high seismicity ($S_{MS} = 2.25$ g). Based on prior FEMA P-695 studies, archetypes located in regions high or very high seismicity, have been shown to have higher rates of collapse than archetypes located in regions of moderate seismicity.

To evaluate the effects of each parametric variation, baseline archetypes were modeled with best estimate properties for wall building blocks, including a best estimate residual post-capping strength of 30 percent of the peak strength. Baseline archetypes also incorporated typical types and configurations of nonstructural wall components and sheathing, but did not include soil structure interaction or foundation flexibility. A total of 28 baseline archetype models were developed for different combinations of

occupancy (COM, MFD, and SFD), height (one, two, and four stories), and seismic design level (moderate, high, and very high seismicity).

4.4 Collapse Displacement Capacity Parametric Study

Three high seismic, two-story baseline archetypes (i.e., COM2B, MFD2B, and SFD2B) were modified to include six variants of residual post-capping strength (i.e., 0 percent, 10 percent, 20 percent, 40 percent, 50 percent, and 60 percent) from the baseline archetype residual post-capping strength of 30 percent of peak strength. Two-story COM, MFD, and SFD archetypes were selected for this parametric study because residual post-capping strength would not be expected to have as much effect on single-story archetypes, and because a comparison of results between COM, MFD, and SFD archetypes of comparable height was desired.

Three high seismic, one-story baseline archetypes (i.e., COM1B, MFD1B, and SFD1B) were also modified to include three variants of residual post-capping strength (i.e., 0 percent, 10 percent, and 20 percent) from the baseline archetype residual post-capping strength of 30 percent of peak strength. One-story COM, MFD, and SFD archetypes were investigated to evaluate the effect of lower post-capping residual strength on the collapse capacity of one-story baseline models. A total of 27 modified archetype models were developed.

In physical terms, residual strength is a component property, but it can also exist at the system level through the presence of secondary elements, such as stairs, that provide additional resistance against collapse. Because secondary elements were not explicitly included in the models, component residual post-capping strength was used as a modeling convenience to capture all sources of residual strength. It should also be noted that individual components were assumed to have infinite displacement capacity ($\delta_u = \infty$). This infinite displacement capacity, however, was never realized because the inclusion of P-Delta effects within the numerical models leads to collapse at some finite displacement for any system experiencing significant lateral displacement.

Comparison of response and collapse results from analyses of archetypes with varying assumptions of residual post-capping strength to the results of corresponding baseline archetype models (with 30 percent residual post-capping strength) provided the basis for evaluating the effects of collapse displacement capacity.

4.5 Nonstructural Interior and Exterior Wall Finishes Parametric Study

Seven high seismic, baseline archetypes (i.e., COM2B, COM3B, MFD2B, SFD1B, SFD1BC, SFD2B, and SFD2BC) were modified by removing nonstructural wall components (interior and exterior wall finishes). Also, for the four SFD archetypes, exterior stucco finishes were replaced with horizontal wood siding. A total of 11 modified archetype models were developed.

Comparison of response and collapse results from analyses of archetype variants without wall finishes to the results of corresponding baseline archetype models (with wall finishes) provided the basis for evaluating the effects of nonstructural interior and exterior wall finishes.

4.6 Soil-Structure Interaction and Foundation Flexibility Parametric Study

Six high seismic, baseline archetypes (i.e., COM1B, COM2B, COM3B, MFD1B, MFD2B, and MFD3B) were each modified to include two variants of soil-structure interaction (SSI) and foundation flexibility through the addition of nonlinear soil springs representing two site conditions. A total of 12 modified archetype models were developed.

In general, the effects of SSI and foundation flexibility are expected to be more significant in larger (heavier) structures located on softer soil sites. SSI effects on wood light-frame archetypes in this study were expected to be minimal. Two-story COM and MFD archetypes were selected for this parametric study as a compromise between weight and period. One-story COM archetypes were also included because their periods were shorter than the one-story MFD archetypes, which have shorter shear wall segments. SFD archetypes were not included in this study because of their relatively small footprint.

Comparison of response and collapse results from analyses of archetype variants with soil springs and flexible foundations to the results of corresponding baseline archetype models (with rigid foundations) provided the basis for evaluating the effects of SSI and foundation flexibility.

4.6.1 Details of Modeling for SSI and Foundation Flexibility

This parametric study included the effect of nonlinear soil springs. For the purpose of this study, inertial soil-structure interaction effects were modeled approximately by introducing nonlinear soil springs between the concrete foundation and fixed base nodes, as illustrated in Figure 4-11. *Timber 3D*

F2F link elements were used to model the soil springs. Three degrees of freedom in the F2F link elements were released to model soil springs in the vertical and two horizontal directions. The concrete foundation was modeled as an elastic beam element with Young's modulus equal to 3.4 ksi and a flexural stiffness corresponding to the gross moment of inertia of the foundation cross-section.

Two sites were selected with different target values of time-averaged shear-wave velocity to a depth of 30 m (v_{S30}), with the intent of capturing potentially variable levels of SSI effects (with the softer sites expected to produce stronger effects). The sites were targeted to be near the boundary of the D and E site classes ($v_{S30} \approx 180$ m/s, or 600 fps) and the C and D site classes ($v_{S30} \approx 360$ m/s, or 1,200 fps).

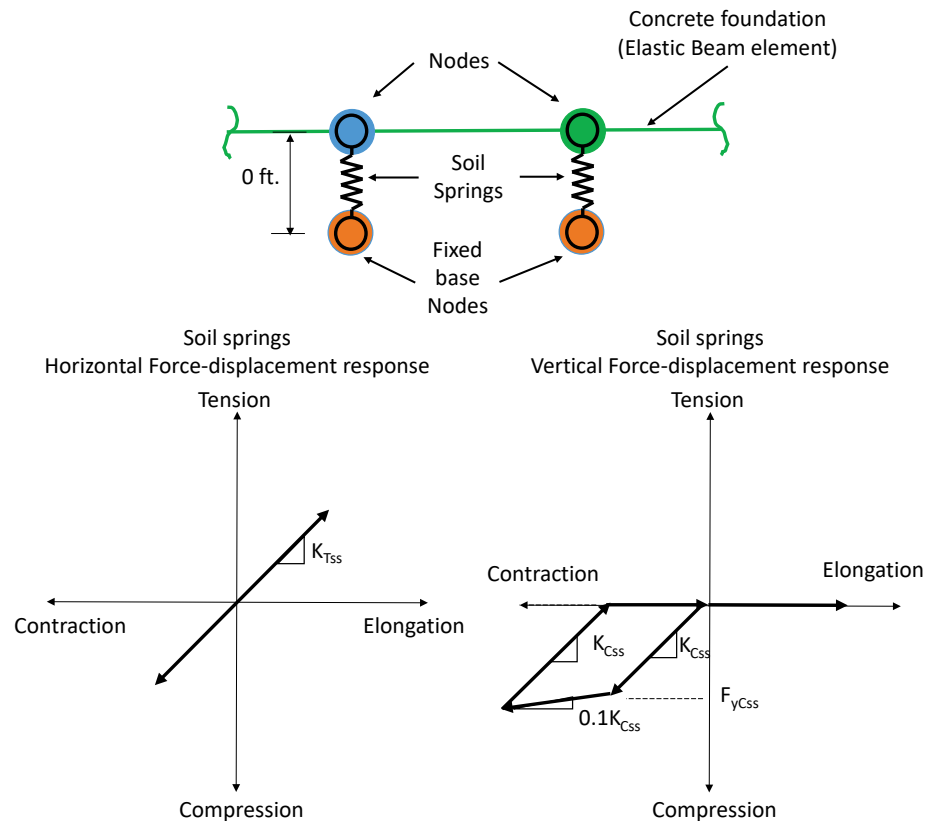


Figure 4-11 Schematic illustration of nonlinear soil spring modeling.

The soft site was taken as the Imperial Valley Wildlife Liquefaction site (PEER NGA-West2 SSN = 233) (Seyhan et al., 2014). The shear-wave velocity profile compiled from multiple sources by Star et al. (2015), which has $v_{S30} = 183$ m/s (590 fps), was used. The relatively stiff site was taken as Cholame Parkfield 12W site (PEER NGA-West2 SSN = 132). The shear-wave velocity profile from Thompson et al. (2010), which has $v_{S30} = 355$ m/s (1,180 fps), was used. It should be noted that the present application requires

information on the complete soil profile in addition to v_{S30} values because the process of evaluating soil properties for the analysis of foundation impedance depends on the details of the profile. Moreover, soil shear strength was required for limiting spring capacities, which again requires attributes of a specific site to be evaluated in a meaningful way.

In the horizontal direction, linear soil springs with stiffness K_{Tss} were developed. For the archetype designs of Chapter 3, the connectivity of footings to interior slabs provides a large area, which yields a large capacity in the horizontal direction. Horizontal foundation stiffness values were derived using two-dimensional (plane strain) models for strip foundations by Gazetas and Roessel (1976). These models were independent of foundation width. The spring stiffness values were computed using representative small-strain shear wave velocities of 330 fps or 100 m/s (soft site) and 970 fps or 295 m/s (stiff site) in the depth range of influence of the strip foundations. The modulus reduction values applied for spring computations were 0.6 (soft site) and 0.8 (stiff site), which were much less than those provided in NIST GCR 12-917-21, *Soil-Structure Interaction for Building Structures* (NIST, 2012b). The rationale is that the narrow foundation widths produce depths of influence that are shallow (about 3 feet to 10 feet, depending on vibration mode). At shallow depths, shear strains from site response are small (the ground surface is a zero-strain boundary condition), so the values in NIST GCR 12-917-21, which are intended for larger foundations and larger depths of influence, are expected to be too low. The adopted modulus reduction values consider these considerations and were based on engineering judgement.

In the vertical direction, bilinear compression-only soil springs were developed. The initial compression stiffness values of the vertical soil springs, K_{Css} , were developed using two-dimensional plane strain relations by Gazetas and Roessel (1979), which scale with the square of foundation width. The same representative small-strain shear wave velocities and modulus reduction values adopted for the horizontal direction were used here. The yield strengths of the vertical soil springs, $F_{yC_{ss}}$, were based on the bearing capacity of the strip foundation computed using standard procedures (Das, 2005). The very near-surface soils were unsaturated and were assumed to be sheared under drained conditions. Accordingly, the soil shear strength was represented with drained friction angles of 30 degrees (soft site) and 40 degrees (stiff site). Vertical effective stresses were taken as equal to total for the stiff site (with sands) but were doubled for the soft site (silt, clay) to allow for matric suction effects. No load inclination factors were applied in

the bearing capacity analysis, based on the assumption that peak vertical demands may not be aligned perfectly in time with horizontal demands.

A post-yield stiffness of 10 percent of the pre-yield stiffness was selected based on judgement and observations of typical shapes of lab stress-strain curves for soft to medium dense soil materials. No viscous damping was provided with the soils springs because of inability of the *Timber3D* software to accommodate discrete viscous dashpot elements. Hysteretic soil behavior was introduced when the vertical nonlinear soils springs yielded.

Table 4-16 lists the physical properties assigned to the various soil springs used for the SSI and foundation flexibility parametric study. The horizontal and vertical stiffness values are provided in units of stiffness per unit length. These values can be multiplied by a tributary length for a given spring to compute the stiffness for that spring. The bearing capacity values for the vertical springs are provided in units of force per area. These can be converted to a force capacity by multiplying by the footing width and tributary length.

Table 4-16 Physical Properties of Nonlinear Soil Springs

Archetype ID	Building Block Wall Configuration	Soft Site ⁽¹⁾ Vertical Spring		Stiff Site ⁽²⁾ Vertical Spring	
		K_{CSS} (kip/in/ft)	F_{yCSS} (kip/ft ²)	K_{CSS} (kip/in/ft)	F_{yCSS} (kip/ft ²)
COM1B-F	All	40.4	4.5	462.7	23.5
COM2B-F	8-foot long	41.5	6.7	475.6	50.0
	4-foot long	40.4	4.5	462.8	23.5
COM3B-F	All	43.2	10.1	503.8	86.4
MFD1B-F	All	40.4	4.5	470.8	23.8
MFD2B-F	8-foot long Min- or Max-Gyp	42.0	8.4	483.9	71.4
	4-foot long Min-, Max- or Nonstruc-Gyp, 8-foot long OSB (any)	40.3	4.5	462.7	23.5
	4-foot long OSB (High, Medium, or Low)	40.9	5.6	470.4	33.3
MFD3B-F	4-foot long along exterior perimeter	41.0	5.6	477.4	33.3
	8-foot long along exterior perimeter	40.3	4.5	470.8	23.5
	Corridor	43.8	11.2	510.3	103.6
	Party wall	43.2	10.1	503.8	86.3
	Interior wall	42.4	8.4	493.9	63.6

⁽¹⁾ Soft site horizontal springs have a stiffness (K_{TSS}) of 27.7 kips/inch/foot.

⁽²⁾ Stiff site horizontal springs have a stiffness (K_{TSS}) of 358.7 kips/inch/foot.

Figure 4-12 shows one of the baseline models, the four-story multi-family dwelling building, used for the SSI and foundation flexibility parametric study. The soil springs were placed at 2 feet on-center along the base of the

concrete foundation beams (right side of Figure 4-12). Each soil spring contains three degrees of freedom. An asymmetrical bilinear hysteresis spring was utilized to model the vertical response of the soil-to-foundation interface (right side of Figure 4-13). Linear springs were used to model the horizontal responses at the foundation.

Note that the asymmetrical bilinear spring for modeling the vertical responses of the foundation has zero tension stiffness. In other words, the building models were not restrained vertically against uplift. Any transient vertical displacement or uplift occurred in the soil spring during the iterative process of numerical integration used for time history analysis has the potential to cause numerical instability.

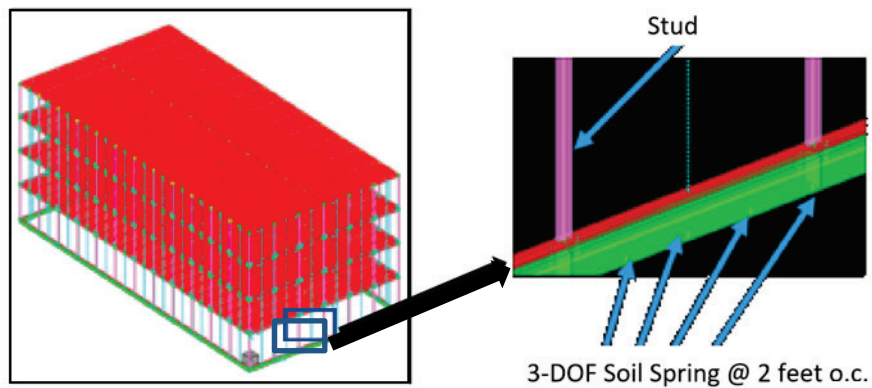


Figure 4-12 SSI and foundation flexibility model for the four-story multi-family dwelling archetype model, showing locations of soil springs.

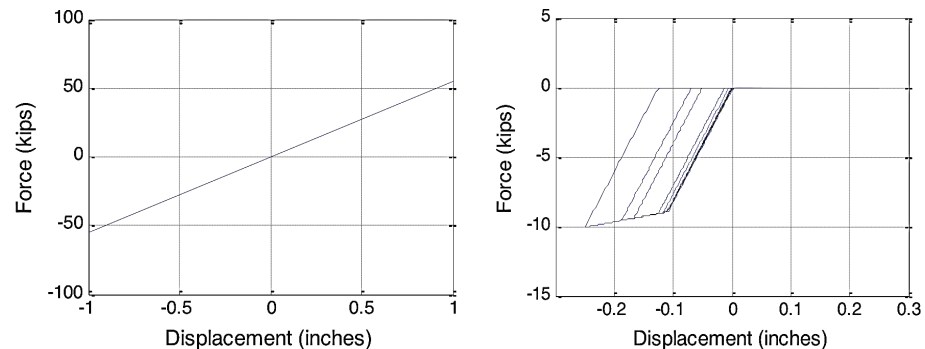


Figure 4-13 Force-displacement properties for soil spring models: horizontal direction (left); and vertical direction (right).

In order to achieve convergence and numerical stability in nonlinear time history analyses, a very small amount of viscous damping (0.1 percent of critical damping) was assigned to all models used in SSI and foundation flexibility studies, whereas models used in other parametric studies were assigned zero damping. A sensitivity study was carried out to investigate the

effect of damping on MCE collapse probability (see Appendix C). Using a damping ratio between 0 percent and 0.5 percent was found to have negligible impact on the estimated MCE collapse probability.

4.7 Backbone Curve Shape Parametric Study

Variability in the force-displacement responses of nominally identical wood structural panels is relatively high, due, in part, to the inherent randomness of the capacities of sheathing nails, construction quality, and boundary conditions. Twelve variants of the four-story commercial building archetype (COM3B), including two additional sets of wood structural panel backbone parameters, were developed to investigate the influence of backbone curve shape on response behavior and collapse performance. The COM3B archetype was selected because, in comparison with other archetype models (SFD and MFD), this model has a relatively low shear strength to weight ratio (V_{max} / W) and was expected to be more sensitive to changes in parameters defining backbone curve shape, such as peak strength, displacement at peak strength, residual strength, and drift ratio at the initiation of the residual strength plateau.

Variants included consideration of backbone shape in combination with the effects of nonstructural wall finishes (i.e., both with and without nonstructural finishes) and varying assumptions on residual post-capping strength ratios (i.e., 0, 30, and 60 percent). Comparison of response and collapse results from analyses using alternate backbone parameters to corresponding variants using baseline best estimate backbone parameters provided the basis for evaluating the effects of nonstructural interior and exterior wall finishes.

4.7.1 Details of Modeling Backbone Curve Shape

To account for variation in backbone curve shape and peak capacity, the original wood structural panel hysteresis parameters, described in Section 4.1.4, were revised into two variant models, referred to as the R1 model and the R2 model:

- **Baseline Model.** Baseline backbone parameters were developed using best estimate values of the key backbone parameters listed in Table 4-2 and Table D-3 in FEMA P-795, which included the peak strength, initial stiffness, post-yield stiffness, ductility, and ultimate deformation capacity.
- **R1 Model.** Instead of using best estimate backbone parameters, the R1 backbone parameters were fitted using the hysteresis loops of an actual shear wall test that matches the configuration of the wood structural

panel building block of interest. For example, the backbone parameters for the R1 model for OSB-High were fitted using the shear wall test data for Test Group K ($\frac{19}{32}$ " sheathing, 10d common nails, and 2-inch o.c. spacing along the perimeter and a 12-inch o.c. spacing in the field of a wood structural panel) from Line et al. (2008).

- **R2 Model.** The R2 hysteresis parameters were developed by scaling the peak strength of the R1 backbone model to 3.0 times the allowable stress design (ASD) value (i.e., 870 plf for $\frac{19}{32}$ " sheathing, 10d common nails with 2-inch o.c. spacing along the perimeter and 12-inch o.c. spacing in the field of a wood structural panel) published in the ANSI/AF&PA SDPWS-2008, *Special Provisions for Wind and Seismic Design* (AWC, 2008). The overstrength ratio of 3.0 was based on the average value from test data on 80 shear walls of different configurations (Line et al., 2008).

Figure 4-14 compares the backbone curves of the original (baseline), R1 model, and R2 model for the OSB-High building block. Table 4-17 shows hysteresis parameters for wood structural panel building blocks and their variant models used in the backbone curve shape parametric study.

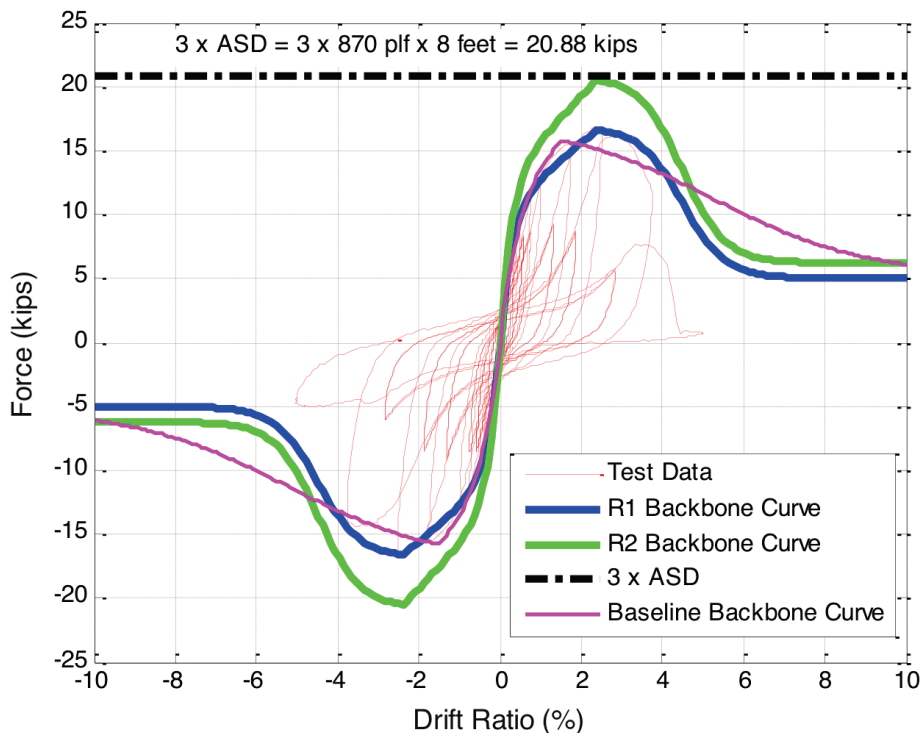


Figure 4-14 Backbone curve models for 8-foot wide by 10-foot high OSB-High building blocks with 30-percent residual strength.

Table 4-17 Hysteresis Parameters for Wood Structural Panel Shear Wall Building Blocks Used to Investigate Backbone Curve Shape

Model Type	OSB Building Block	Hysteresis Parameters											
		K_0 (kip/in)	r_1	r_2	r_3	r_4	F_x (kip)	f_1	f_2	f_3	D_x (in)	α	β
Baseline (0%)	Low	15.00	0.076	-0.031	1.010	0.005	6.79	0.565	0.127	0.0	6.30	0.75	1.05
	Medium	15.00	0.076	-0.051	1.060	0.005	11.29	0.719	0.089	0.0	6.30	0.75	1.04
	High	24.00	0.076	-0.051	1.020	0.005	17.92	0.725	0.134	0.0	6.30	0.77	1.15
Baseline (30%)	Low	15.00	0.076	-0.031	1.010	0.005	6.79	0.565	0.127	0.3	6.30	0.75	1.05
	Medium	15.00	0.076	-0.051	1.060	0.005	11.29	0.719	0.089	0.3	6.30	0.75	1.04
	High	24.00	0.076	-0.051	1.020	0.005	17.92	0.725	0.134	0.3	6.30	0.77	1.15
Baseline (60%)	Low	15.00	0.076	-0.031	1.010	0.005	6.79	0.565	0.127	0.6	6.30	0.75	1.05
	Medium	15.00	0.076	-0.051	1.060	0.005	11.29	0.719	0.089	0.6	6.30	0.75	1.04
	High	24.00	0.076	-0.051	1.020	0.005	17.92	0.725	0.134	0.6	6.30	0.77	1.15
R1 (0%)	Low	16.69	0.020	-0.070	1.010	0.016	7.21	0.700	0.065	0.0	5.13	0.73	1.13
	Medium	18.60	0.047	-0.200	1.010	0.016	11.29	0.767	0.079	0.0	5.76	0.70	1.12
	High	34.34	0.065	-0.100	1.010	0.016	17.61	0.582	0.079	0.0	6.36	0.59	1.15
R1 (30%)	Low	16.69	0.020	-0.070	1.010	0.016	7.28	0.693	0.081	0.3	4.17	0.73	1.13
	Medium	18.60	0.047	-0.080	1.010	0.016	12.04	0.720	0.090	0.3	5.55	0.70	1.12
	High	34.34	0.065	-0.137	1.010	0.016	16.79	0.610	0.106	0.3	5.40	0.59	1.15
R1 (60%)	Low	16.69	0.020	-0.062	1.010	0.016	6.18	0.817	0.089	0.6	3.94	0.73	1.13
	Medium	18.60	0.047	-0.066	1.010	0.016	11.62	0.746	0.089	0.6	4.53	0.70	1.12
	High	34.34	0.065	-0.075	1.010	0.016	16.87	0.607	0.111	0.6	4.86	0.59	1.15
R2 (0%)	Low	16.87	0.020	-0.070	1.010	0.016	7.29	0.700	0.065	0.0	5.13	0.73	1.13
	Medium	19.29	0.047	-0.200	1.010	0.016	11.70	0.767	0.079	0.0	5.76	0.70	1.12
	High	42.41	0.065	-0.100	1.010	0.016	21.75	0.582	0.079	0.0	6.36	0.59	1.15
R2 (30%)	Low	16.87	0.020	-0.070	1.010	0.016	7.36	0.693	0.081	0.3	4.17	0.73	1.13
	Medium	19.29	0.047	-0.080	1.010	0.016	12.48	0.720	0.090	0.3	5.55	0.70	1.12
	High	42.41	0.065	-0.137	1.010	0.016	20.73	0.610	0.106	0.3	5.40	0.59	1.15
R2 (60%)	Low	16.87	0.020	-0.062	1.010	0.016	6.25	0.817	0.089	0.6	3.94	0.73	1.13
	Medium	19.29	0.047	-0.066	1.010	0.016	12.04	0.746	0.089	0.6	4.53	0.70	1.12
	High	42.41	0.065	-0.075	1.010	0.016	20.83	0.607	0.111	0.6	4.86	0.59	1.15

Although the shape of the R1 backbone curve is different from the baseline curve, key control points on the backbone curve shape (i.e., the peak strength and drift ratio at 80 percent post-capping strength) were kept essentially the same in the R1 model. In the case of the R2 backbone curve, actual component overstrength in an as-built wood shear wall panel can vary (Line et al., 2019) depending on the boundary conditions and actual details of

construction (e.g., eccentrically versus concentrically placed hold-downs). The R2 model, however, is considered more representative of the details found in modern wood light-frame construction with a concentrically placed, through-floor, continuous anchor rod tie-down system.

4.8 Analysis Methods

This section describes the methods used to analyze wood light-frame archetypes and the significant response parameters that were calculated and archived. Numerical results from all analyses are summarized in Chapter 5.

4.8.1 Overview

The following analysis methods (detailed in the following sections) were conducted on each archetype configuration:

- Free vibration analyses to evaluate elastic natural periods and mode shapes
- Nonlinear static pushover analyses
- Nonlinear incremental dynamic analyses (IDAs) in accordance with the FEMA P-695 methodology (FEMA, 2009b) for a defined set of MCE_R ground motion intensities

4.8.2 Free Vibration Analyses

Eigenvalue and eigenvector analyses were conducted using elastic properties to determine the initial natural periods, T_1 , and mode shapes in each orthogonal direction of each archetype. Period calculations were particularly important to ensure that archetype designs were in the short-period ($T_1 < 0.5$ seconds) range of response.

4.8.3 Nonlinear Static Pushover Analyses

Nonlinear static pushover analyses were conducted along each direction of each archetype to extract the overall backbone base shear versus roof displacement response, and to extract the characteristic parameters defined in Section 4.1.4. The monotonic push was based on a first-mode distribution of lateral forces. P-Delta effects were included.

Consistent with the FEMA P-695 methodology, V_{max} is the maximum base shear obtained for an archetype model; Ω is the overstrength factor, which is V_{max} divided by the design base shear (V_{design}) for an archetype model; and μ_T is the period-based ductility, which is defined as the ratio of the ultimate roof displacement, δ_u , to the effective yield displacement, $\delta_{y,eff}$, where the ultimate

displacement δ_u is defined as the displacement at which the post-peak base shear drops to 80% of the peak value.

4.8.4 Incremental Dynamic Analyses and Collapse Evaluation

Nonlinear incremental dynamic analyses (IDAs) in accordance with the FEMA P-695 methodology were conducted on each archetype for specific levels of ground motion intensity (intensity stripes). The *Timber3D* analysis program was used for this purpose. P-Delta effects were included.

The FEMA P-695 far-field record set, with two horizontal components for each of 22 ground motions, was used in all IDAs. The record set was scaled based on the median spectra intensity (S_T) at a short period of 0.25 seconds for all archetypes to avoid having to use different scaled ground motions due to local variation of the S_a values on the plateau region of the median response spectrum (from approximately 0.2 to 0.4 seconds). Figure 4-15 shows the FEMA P-695 far field ground motion response spectra scaled to the MCE_R level for high seismic region. Also shown in Figure 4-15 is the median of the scaled response spectra for regions of high seismicity, which are scaled such that the median spectrum equals 1.5g at 0.25 seconds.

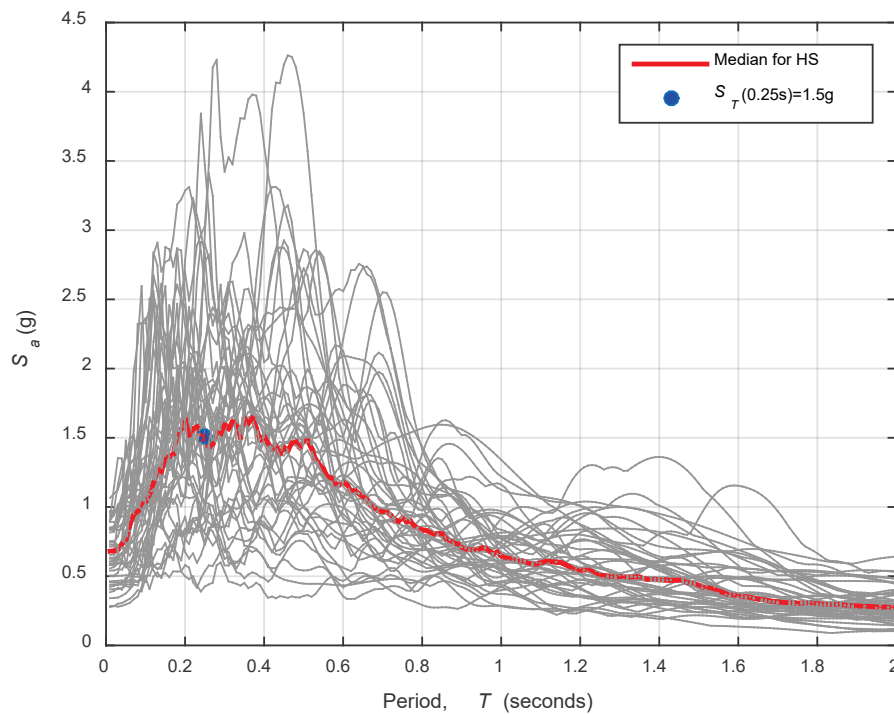


Figure 4-15 Acceleration response spectra for the FEMA P-695 far field ground motions scaled to the MCE_R hazard level for regions of high seismicity.

For each archetype, the IDAs were conducted for intensity stripes starting at S_T equal to 0.1g. The intensity was increased by increments of 0.1g, up to an intensity level for which all ground motions in the record set caused collapse of the building model. For each intensity stripe, three-dimensional IDAs were conducted by applying the 22 FEMA P-695 far-field (FF) records (two components each) to the archetype model in two orthogonal orientations (i.e., NS-EW and EW-NS orientations) generating 44 response data for each response parameter of interest. Therefore, the collapse statistics were based on 44 analyses.

Because hysteretic energy dissipation was included for all vertical walls (structural and nonstructural) over the entire range of deformation, only a small amount of inherent viscous damping needed to be introduced. In this study, to represent realistic dynamic response and collapse behavior at large displacements, zero inherent viscous damping was introduced in the archetype models, except for those analyzed in the SSI and foundation flexibility parametric study. From preliminary analysis results, it was found that even a small amount of viscous damping generated significant artificial (and unrealistic) restoring damping forces once the hysteretic damping from wall building blocks was nearly exhausted as they approached collapse. The inclusion of zero viscous damping in this study was different from prior FEMA P-695 studies on wood light-frame systems (FEMA, 2009b), which considered 1% of critical Rayleigh-type damping based on the first two elastic modes of vibration in each building model. Inclusion of zero viscous damping may have contributed to a moderate reduction (less than 10 percent change) in the collapse capacity of building models considered in this study, particularly for those not including nonstructural wall finishes. The effect of viscous damping on the collapse capacities of one-story commercial building baseline archetypes was investigated in Appendix C.

Previous studies have shown that the median collapse intensity resulting from three-dimensional analyses is, on average, approximately 20 percent less than the median collapse intensity resulting from two-dimensional analyses (FEMA, 2009b). The application of pairs of ground motion records in three-dimensional analyses introduces a conservative bias as compared to results from two-dimensional analyses. Three-dimensional IDAs were conducted in this study, and to achieve parity with previous two-dimensional analyses, the calculated median collapse intensities were multiplied by a factor of 1.2 per the FEMA P-695 methodology.

Because the displacement capacities of the backbone curves shown in Figure 4-9 and Figure 4-10 were much larger than those assumed in the FEMA P-695 methodology (i.e., collapse at 80 percent of peak strength on the post-

capping branch), the period based ductility factor, μ_T , used to define spectral shape factors (SSF) was considered unrealistically low. Therefore, the maximum SSF values (based on the code fundamental period for each archetype model) were used to multiply median collapse intensities. For short period building models ($T_1 < 0.5$ seconds), the maximum SSF value is 1.33.

To consider sources of uncertainty beyond the record-to-record uncertainty captured in IDAs, a dispersion factor (standard deviation of the logarithmic values of collapse statistics), $\beta = 0.50$, was used to define all adjusted collapse fragility curves.

Previous studies on wood light-frame buildings have defined collapse using a non-simulated criterion based on when a pre-determined peak story drift was exceeded. In prior FEMA P-695 studies, collapse was defined when IDA plots reached a nearly horizontal slope, or when a peak story drift of 7 percent was exceeded in any wall in the model. In this study, sidesway collapse was explicitly simulated using *Timber3D*, and collapse was defined when a control node on the roof of a building model achieved a vertical displacement equal to the first story height.

The collapse margin ratio (*CMR*) is the ratio of the median 5%-damped spectral acceleration of the collapse level ground motions to the 5%-damped spectral acceleration of the MCE_R ground motions at the fundamental period of the seismic-force-resisting system. The FEMA P-695 methodology requires comparison of an adjusted collapse margin ratio (*ACMR*) with an acceptable *ACMR*. The *ACMR* is obtained by correcting the collapse margin ratio by the SSF value defined above. The acceptable *ACMR* is determined from the composite uncertainty and the acceptable conditional probability of collapse (typically 10%) under MCE_R ground motions. In this study, however, FEMA P-695 analysis methods are used to calculate the probability of collapse rather than collapse margin ratio, which is beyond the requirements of the FEMA P-695 methodology.

As an illustrative example, Figure 4-16 shows IDA results for the baseline one-story commercial building archetype model (COM1B in Tables 4-10 and 4-13). Peak roof drift was selected as the parameter used to quantify the displacement capacity, and the red markers in the figure indicate points of incipient collapse. Also shown in the figure is the fitted lognormal probability density functions (PDFs) of peak roof drift and S_{MT} at incipient collapse.

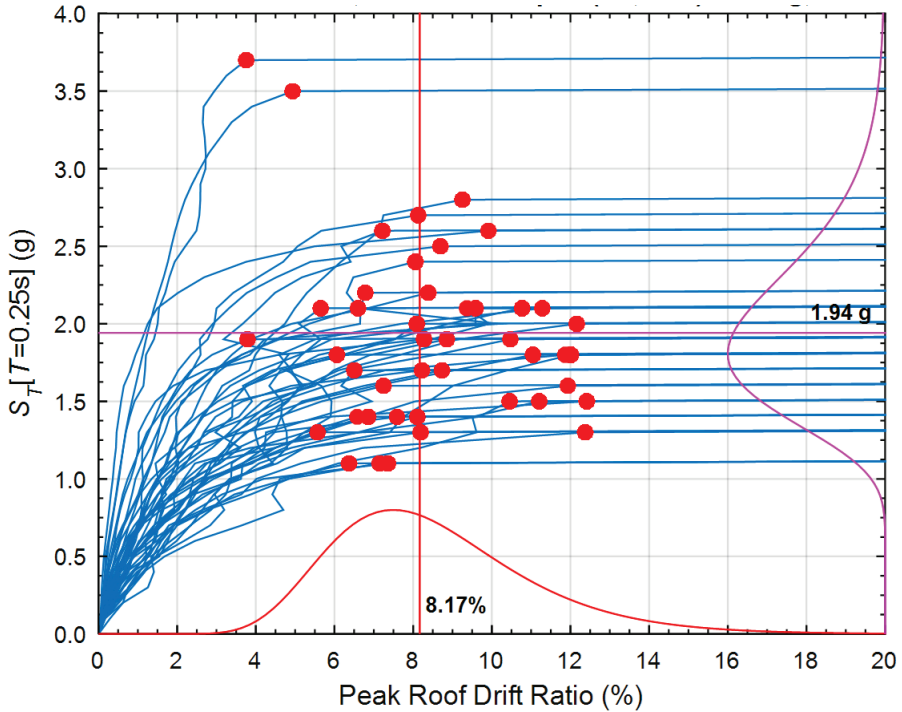


Figure 4-16 IDA curves and probability density functions (PDFs) of peak roof drift and S_{MT} at incipient collapse for the baseline one-story commercial building archetype model (COM1B).

Figure 4-17 illustrates the FEMA P-695 methods used to evaluate collapse performance using the example set of IDA results for COM1B shown in Figure 4-16. The COM1B model has a period of $T = 0.25$ seconds, and was evaluated for 40 increments of ground motion scaled from 0.1g to 4.0g of 0.25-second response spectral acceleration. Collapse fractions are shown in terms of 0.25-second response spectral acceleration factored by 1.2 for consistency with the adjustment of CMR for three-dimensional analysis effects (i.e., CMR_{3D}). In this example, the COM1B archetype was designed for SDC D ground motions corresponding to a 0.25-second MCE_R response spectral acceleration, $S_{MT} = 1.5\text{g}$.

In Figure 4-16, a median collapse intensity, $\hat{S}_{CT} = 1.94\text{g}$, was determined from the IDA results, which corresponds to 2.33g (dashed red line in Figure 4-17) after applying the 1.2 factor for three-dimensional effects. The collapse margin ratio (with adjustment for three-dimensional effects) is calculated as: $CMR_{3D} = 1.2 \times \hat{S}_{CT}/S_{MT} = 1.2 \times 1.94\text{g}/1.5\text{g} = 1.55$. This indicates that the median collapse intensity is about 1.5 times the MCE_R ground motion intensity used as the basis for design of the archetype, before adjustment by the spectrum shape factor (SSF). In this example, the archetype model exhibits significant period-based ductility (i.e., $\mu_T \geq 8$), and the corresponding value of 1.33 for SSF (from Table 7-1b of FEMA P-695),

is justified. The adjusted collapse margin ratio is calculated as: $ACMR = SSF \times CMR_{3D} = 1.33 \times 1.55 = 2.07$. This indicates that median collapse is about 2 times the MCE_R ground motion intensity, after adjustment by the SSF.

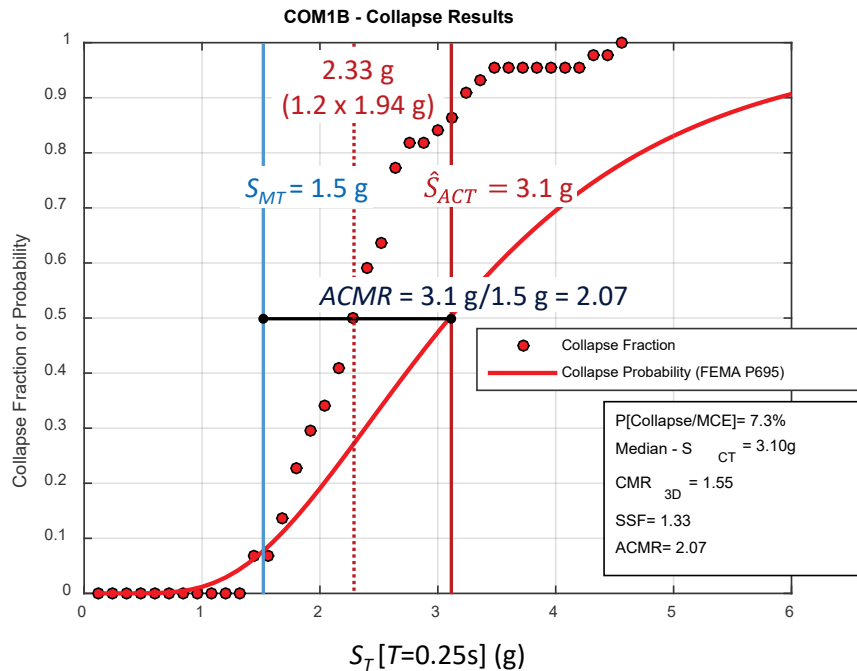


Figure 4-17 Illustration of IDA results (collapse fractions) and FEMA P-695 collapse fragility, based on median collapse $\hat{S}_{CT} = 3.1$ g, derived from the IDA results and an assumed lognormal standard deviation of $\beta_{TOT} = 0.5$, for the baseline one-story commercial archetype model (COM1B). Collapse fractions are plotted in terms of S_T factored by 1.2 for consistency with the value of CMR adjusted for three-dimensional analysis effects (CMR_{3D}).

The probability of collapse as a function of ground motion intensity (at the period, T , of the archetype model) is assumed to be lognormally distributed with an adjusted median, \hat{S}_{ACT} (i.e., $ACMR \times S_{MT}$), and a lognormal standard deviation, β_{TOT} , that accounts for total collapse uncertainty related to:

- (1) record-to-record variability; (2) design requirements (for the SFRS of interest); (3) test data (used to establish nonlinear properties); and
- (4) modeling methods, as described in Section 7.3 of FEMA P-695.

Tables 7-2a to 7-2d of FEMA P-695 specify values of β_{TOT} based on a subjective evaluation of the “quality” of the design requirements, test data, and modeling methods, respectively. Reasonably well-defined archetype models have total collapse uncertainty values of $\beta_{TOT} = 0.50$ to 0.60. For comparison, Section 21.2.1.2 (Method 2) of ASCE/SEI 7-10 specifies a lognormal standard deviation value of 0.6 for the development of site-specific probabilistic MCE_R ground motions (i.e., same value used by the

USGS to develop the MCE_R ground motion maps of Chapter 22 of ASCE/SEI 7-10). As shown in Figure 4-17, the MCE_R collapse probability is 7.3% for the COM1B model, based on a value of $\beta_{TOT} = 0.50$ (and an adjusted median collapse intensity, $\hat{S}_{ACT} = 3.1 \text{ g}$).

4.8.5 Peak Response Calculations

A number of response parameters of interest (stripe statistics) were post-processed and archived at each intensity strip to determine the statistics of peak response for each archetype. Table 4-18 lists the stripe statistics that were archived for each orthogonal (NS and EW) direction of each archetype model. For each IDA, an Excel spreadsheet containing these response parameters for all intensity stripes was automatically generated and archived (see Appendix B).

Table 4-18 Description of Response Parameters Archived for Each Orthogonal Direction (EW and NS) for Numerical Models of Wood Light-Frame Archetypes

Statistic Type	Response Parameters	Statistical Values
Peak Relative Displacement	Peak Roof Relative Displacement Peak Roof Drift Ratio Peak Story Drift Ratio ⁽⁵⁾	Median ⁽¹⁾ Mean of Survivors ⁽²⁾ Overall Mean ⁽³⁾ Overall Beta ⁽⁴⁾ Minimum Maximum
Peak Relative Velocity	Peak Roof Relative Velocity Peak Floor Relative Velocity	
Peak Absolute Acceleration	Peak Roof Absolute Acceleration Peak Floor Absolute Acceleration	
Residual Relative Displacement	Residual Roof Displacement Residual Roof Drift Ratio Residual Story Drift Ratio	
Collapse	All Records Collapse Cases	Number Percentage
	Individual Record Collapse Cases	If “No,” Peak Roof Displacement If “Yes,” Peak Roof Displacement at last surviving intensity, floor level initiating collapse, and collapse direction

⁽¹⁾ Calculated median = fitted lognormal based on all 44 earthquake records with last values of non-surviving records (i.e., records causing collapse).

⁽²⁾ Mean value of surviving earthquake records only (i.e., records not causing collapse).

⁽³⁾ Mean of all 44 earthquake records with last values for non-surviving records.

⁽⁴⁾ Beta is the lognormal standard deviation of all 44 earthquake records with last values of non-surviving records.

⁽⁵⁾ Calculated for each floor of multi-story archetypes.

Chapter 5

Numerical Results of Parametric Studies

This chapter presents the results of parametric studies of wood light-frame building archetypes developed in Chapter 3. All archetypes were modeled using the *Timber 3D* analysis program, as described in Chapter 4.

The nomenclature identifying each archetype model and the variants developed for each parametric study are provided in the sections that follow. For each archetype, the results of free vibration analyses, nonlinear static analyses, and incremental dynamic analyses (IDAs) are presented, along with a discussion of key behaviors. Free vibration analyses were used to determine the natural periods and mode shapes, nonlinear static pushover analyses were used to estimate peak strength and ductility, and IDAs were used to compute collapse probabilities consistent with the FEMA P-695 methodology.

5.1 Overview of Results

Each parametric study evaluates the response behavior and collapse performance characteristics of a set of numerical models of representative archetypes of wood light-frame buildings with variations in selected parameters of interest that are specific to each study. A brief summary of the parametric studies, and their results, is as follows:

- **Baseline Configuration.** Baseline configuration studies provided the primary basis for evaluating response behavior and collapse performance of wood light-frame buildings as a function of building period (i.e., building height), typical configuration (i.e., occupancy), and region of seismicity (i.e., seismic design level). This study considered differences in archetype configurations compared with those of previous FEMA P-695 collapse evaluations, and compared modeled baseline collapse performance to observed earthquake data. In addition, baseline models considered the results of other parametric studies, and incorporated a best estimate for each parameter to provide an overall best estimate of the simulated response of short-period wood light-frame buildings.

Baseline configuration studies showed that the trends observed in prior analytical studies are reversed (i.e., collapse probabilities of short-period wood light-frame buildings do not increase as the period decreases), and that overall collapse probabilities predicted in numerical analyses, including selected modeling enhancements, are aligned with benchmark collapse performance statistics from past earthquakes.

- **Collapse Displacement Capacity.** Analyses of archetypes with different residual strength ratios provided the basis for evaluating the effects of residual post-capping strength and ultimate displacement capacity on response behavior and collapse performance. In this study, models with six levels of residual post-capping strength (i.e., 0 percent, 10 percent, 20 percent, 40 percent, 50 percent, and 60 percent) were compared with baseline models incorporating 30 percent. In addition to capturing nonlinear properties of the wood shear wall elements themselves, residual strength ratios were also used as a proxy for incorporating non-simulated sources of residual strength in wood light-frame systems. All models assumed that the ultimate displacement was unlimited (i.e., $\delta_u = \infty$).

Collapse displacement capacity studies confirmed that higher residual strengths and larger ultimate displacement capacities improve collapse performance (i.e., reduce collapse probabilities). In general, a residual strength of 30 percent resulted in the best match between numerical models and observations from past earthquakes or shake table tests.

- **Nonstructural Interior and Exterior Wall Finishes.** Analyses of archetypes without wall finishes provided the basis for evaluating the effects of nonstructural interior and exterior wall finishes on response behavior and collapse performance. In this study, archetypes were modified to remove all nonstructural interior and exterior wall finishes, and were compared to the results of corresponding baseline archetype models including wall finishes.

Results of this study showed that nonstructural interior and exterior wall finishes have a significant impact on the strength and stiffness of wood light-frame buildings, the presence of nonstructural wall finishes improves collapse performance (i.e., reduces collapse probabilities), and that consideration of nonstructural wall finishes is necessary for matching observed behavior in past earthquakes or shake table tests.

- **Soil-Structure Interaction and Foundation Flexibility.** Analyses of archetypes with flexible foundations provided the basis for evaluating the effects of soil-structure interaction and foundation flexibility on

response behavior and collapse performance. In this study, archetypes were modified to include nonlinear soil springs representing two different site conditions (i.e., stiff and soft soil sites), and were compared to the results of corresponding baseline archetype models with rigid foundations.

SSI effects on wood light-frame archetypes were expected to be minimal, and the results of this study confirmed that modeling of soil-structure interaction and foundation flexibility has a negligible impact on the response behavior and collapse performance of wood light-frame buildings.

- **Backbone Curve Shape.** Analyses of archetypes with different backbone parameters provided the basis for evaluating the effects of backbone curve shape on response behavior and collapse performance. In this study, archetypes were modified to include different assumptions for peak strength, drift ratio at peak strength, and slope of the post-peak curve, and were compared to the results of corresponding baseline archetype models using best estimate properties of backbone parameters from applicable test data. This study also included consideration of backbone shape in combination with the effects of nonstructural wall finishes (i.e., both with and without nonstructural finishes) and varying assumptions on residual post-capping strength ratios (i.e., 0, 30, and 60 percent).

Results of this study showed that peak strength has a significant impact on response and collapse performance. Higher peak strengths resulted in lower collapse probabilities, and the overstrength ratio of wood structural panels was shown to have a significant influence on collapse probabilities. Results also showed that archetypes with different backbone curve shapes, but comparable values of peak strength and displacement capacity, have similar collapse performance

Detailed numerical results for each study are presented in the sections that follow.

5.2 Baseline Configuration Parametric Study

Baseline configuration studies evaluated response behavior and collapse performance of wood light-frame buildings as a function of building period (i.e., building height), typical configuration (i.e., occupancy), and region of seismicity (i.e., seismic design level). In addition, baseline models considered the results of other parametric studies, and incorporated a best

estimate for each parameter to provide an overall best estimate of the simulated response of short-period wood light-frame buildings.

5.2.1 Baseline Configuration Archetypes and Variants

Baseline archetypes were developed for three building heights (one, two, and four stories), three occupancies (commercial buildings, multi-family dwellings, and single-family dwellings), and three seismic design levels (high seismic, very high seismic, and moderate seismic). Baseline archetypes also included best estimate properties for shear wall components, residual post-capping strength of 30 percent of peak strength, and typical types and configurations of nonstructural wall components. Baseline archetypes did not include consideration of soil-structure interaction or foundation flexibility.

A total of 28 baseline archetype models were developed representing different combinations of building height, occupancy, and seismic design level. The baseline archetype models are identified in Chapter 3, Table 3-5. Archetypes are identified using the following nomenclature: commercial buildings (COM), multi-family dwellings (MFD), single-family dwellings (SFD), high seismic design (HS), very high seismic design (VHS), and moderate seismic design. Although 28 baseline archetype models were developed, only the high seismic (HS) and very high seismic (VHS) designs (19 out of 28) were analyzed. Archetype models for moderate seismic design were not analyzed.

5.2.2 Numerical Results

Each baseline archetype model was analyzed as follows:

- Free vibration analyses were conducted to obtain fundamental periods and mode shapes.
- Nonlinear static pushover analyses were conducted to obtain system level (i.e., building) pushover curves in each horizontal direction.
- Nonlinear incremental dynamic analyses (IDAs) were conducted in accordance with the FEMA P-695 methodology to obtain collapse probabilities.

Figure 5-1 shows the undeformed shape of the four-story commercial building archetype model (COM3B) and three mode shapes corresponding to the first three periods obtained from free vibration analyses. The first two modes were translational modes in each lateral direction, and the third mode was a torsional mode. These three modes were typical for all archetype models.

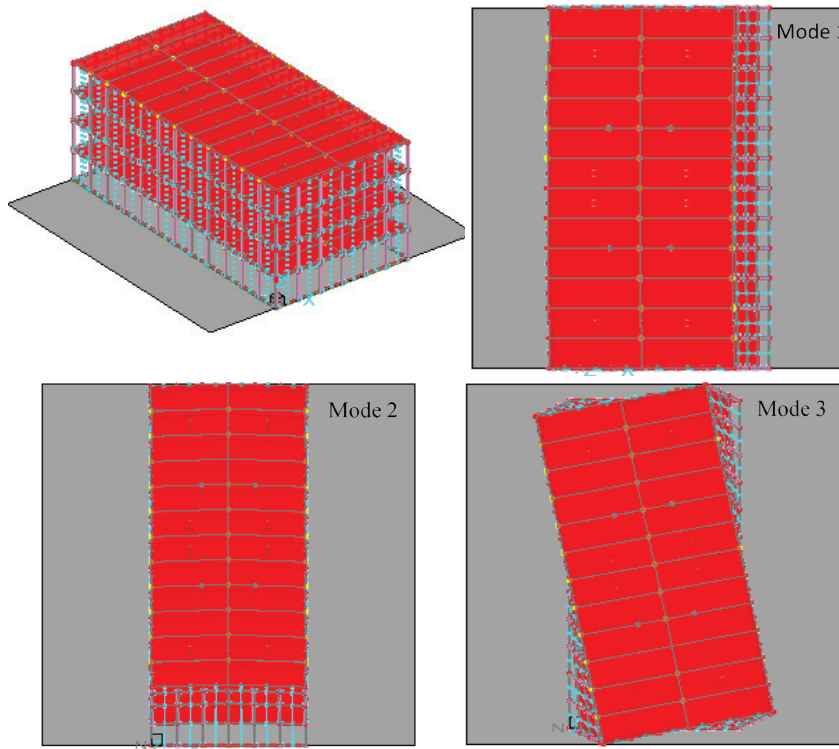


Figure 5-1 Undeformed shape and three mode shapes for the baseline four-story commercial building archetype model (COM3B).

Figure 5-2 through Figure 5-4 show pushover curves for baseline commercial (COM), multi-family dwelling (MFD), and single-family dwelling (SFD) archetype models, respectively, in high seismic (HS) and very high seismic (VHS) regions. Table 5-1 summarizes selected values from free vibration (modal) analysis results (e.g., T_1) and FEMA P-795 pushover analyses.

From Table 3-5, the design base shear coefficients for COM3B (HS design) and COM6B (VHS design) are 0.154 and 0.231, respectively. Although the design base shear for VHS designs is 1.5 times greater than HS designs, the actual strength ratios between VHS and HS archetypes in Table 5-1 are less than this value. Peak strength ratio (V_{\max} / W) is defined as the maximum base shear of the pushover curve normalized by the building weight. In the normalized pushover curves, it can be seen that the peak strength ratios (V_{\max} / W) for all archetypes exceed the design base shear coefficients, and the peak strength ratios for multi-family and single-family dwelling archetypes (Figure 5-3 and Figure 5-4) are significantly higher than peak strength ratios for commercial building archetypes (Figure 5-2). These differences were mainly attributed to the strength contribution from nonstructural wall finishes on interior partitions, which were assumed to be denser in residential configurations than in commercial configurations.

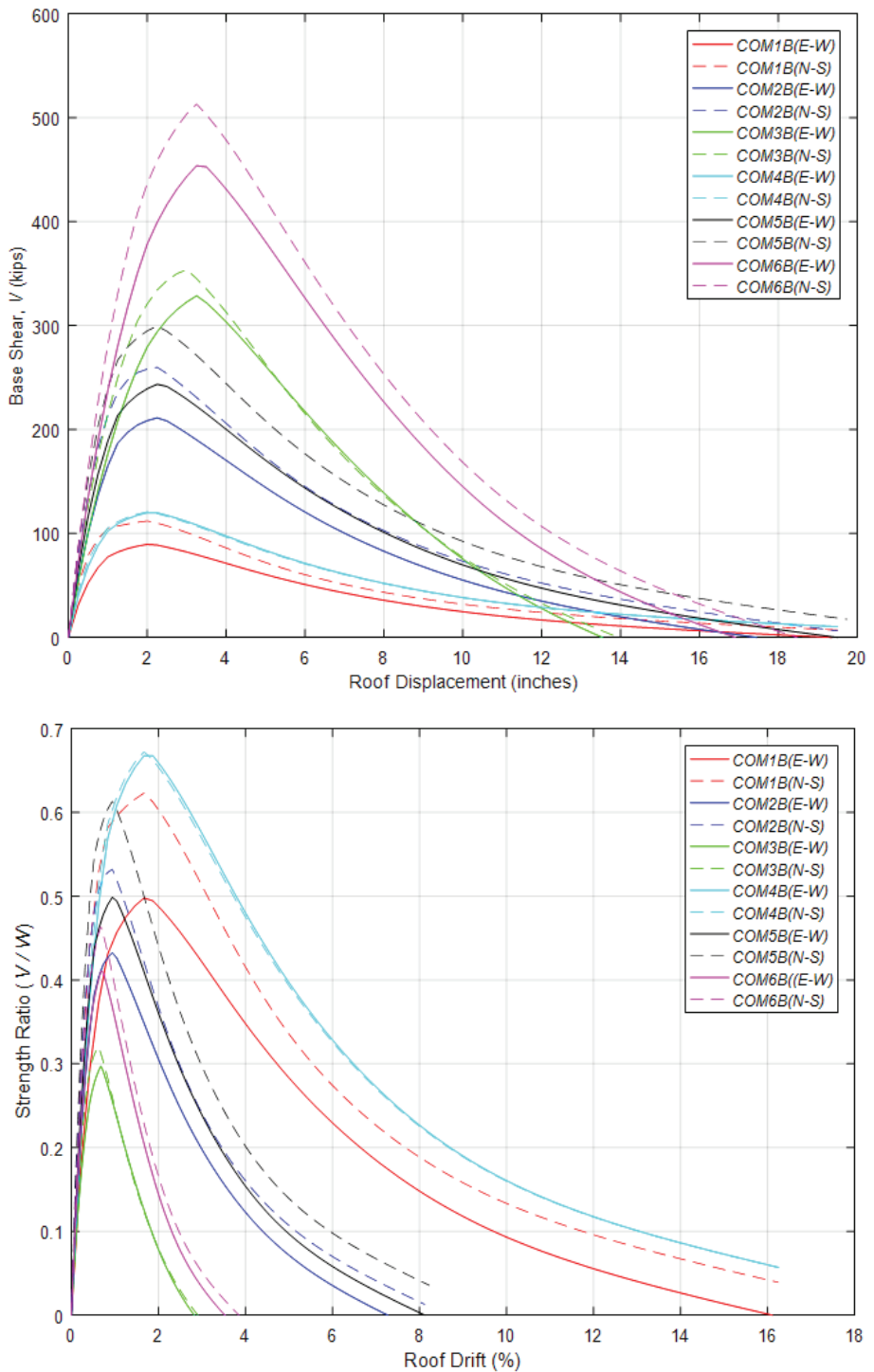


Figure 5-2

Pushover curves for baseline commercial building archetype models (top), and pushover curves normalized by total building seismic weight and roof height (bottom).

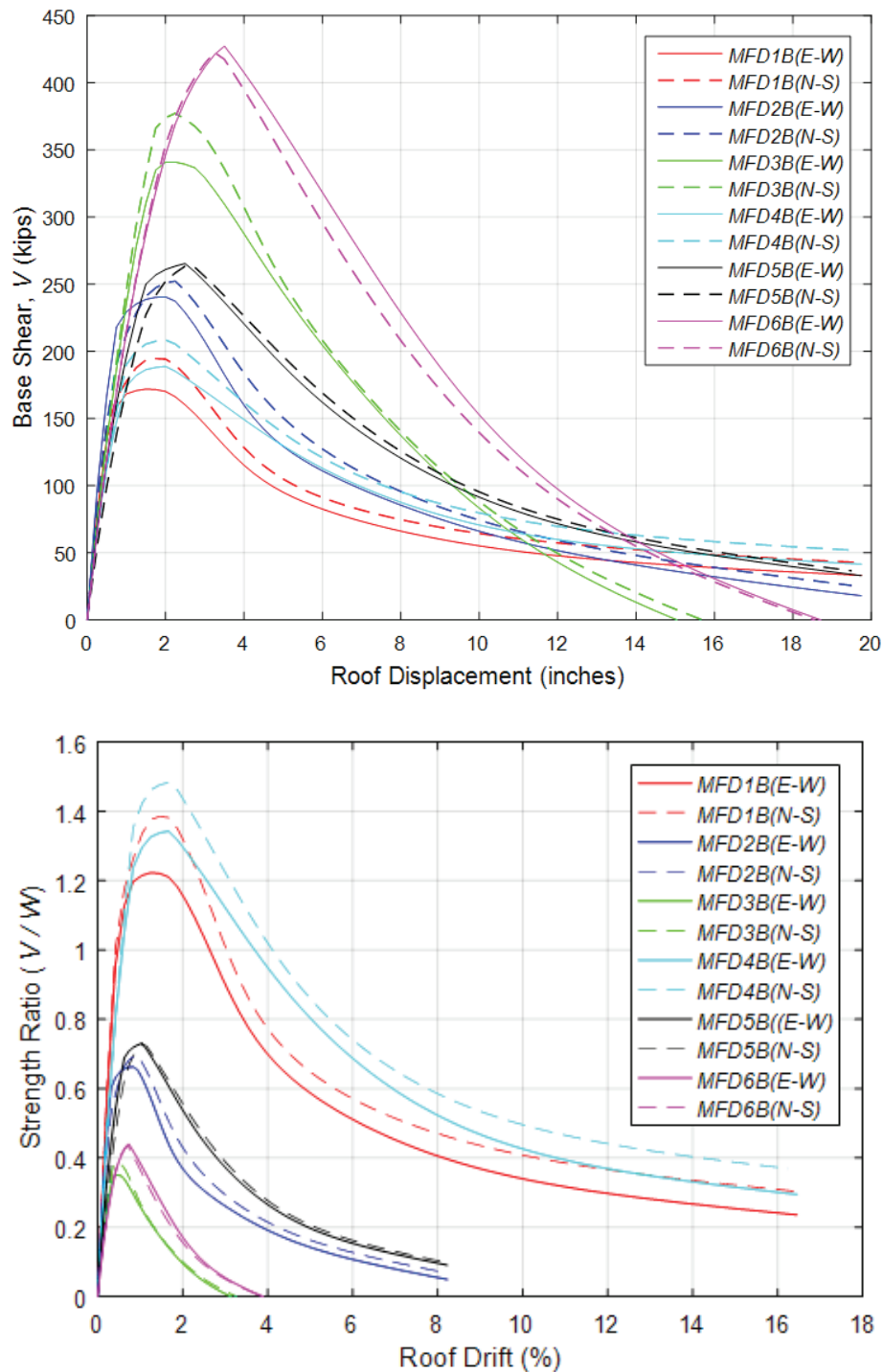


Figure 5-3 Pushover curves for baseline multi-family dwelling archetype models (top), and pushover curves normalized by total building seismic weight and roof height (bottom).

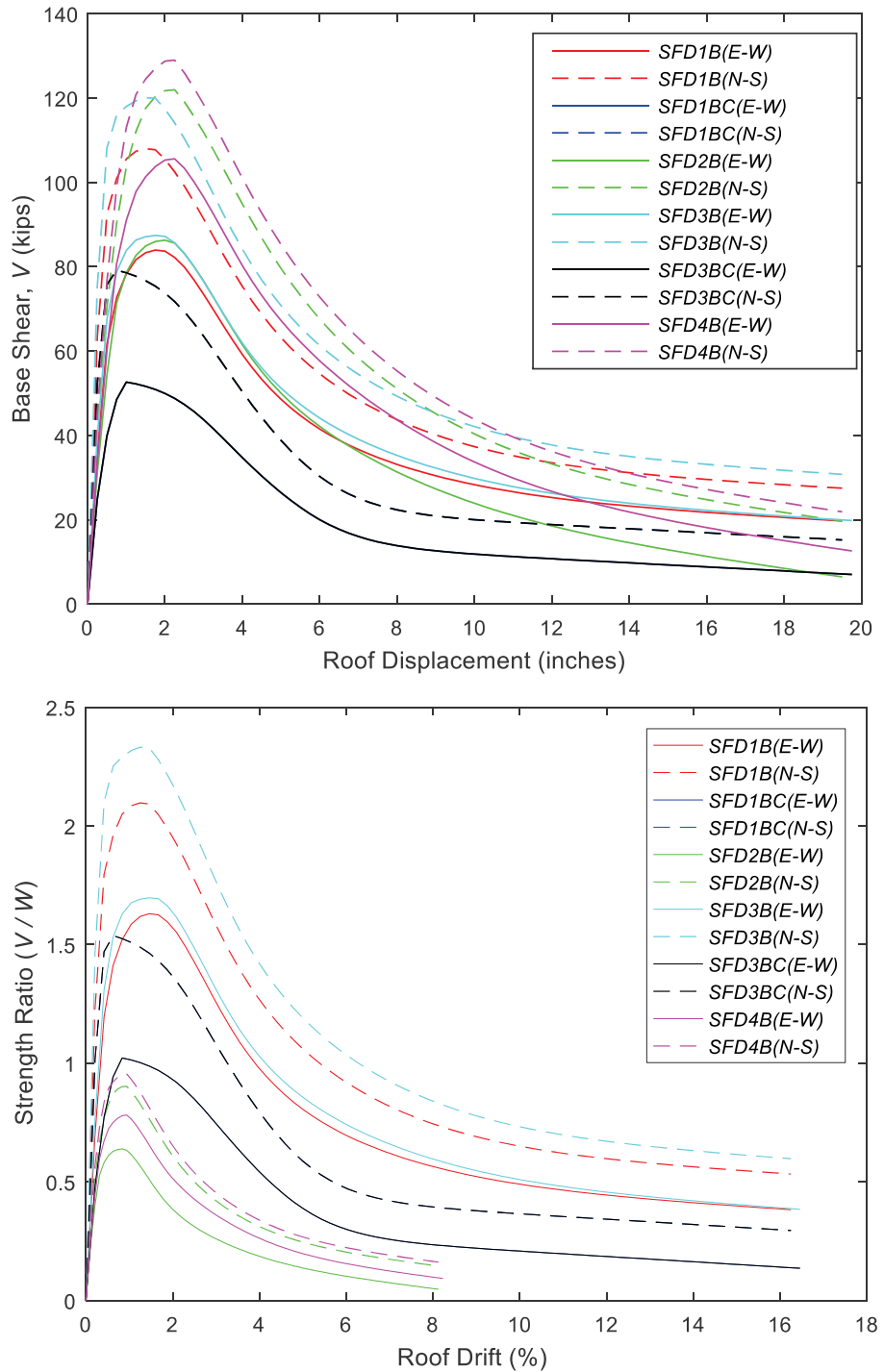


Figure 5-4 Pushover curves for baseline single-family dwelling archetype models (top), and pushover curves normalized by total building seismic weight and roof height (bottom).

Table 5-1 Modal and Pushover Analysis Results for Baseline Archetype Models in the North-South and East-West Directions of Response

Baseline Archetype ID	North-South Direction				East-West Direction			
	T_1 (sec)	V_{max} / W	$\Delta_{U,80}$ (in/in)	$\Delta_{U,max}$ (in/in)	T_1 (sec)	V_{max} / W	$\Delta_{U,80}$ (in/in)	$\Delta_{U,max}$ (in/in)
Commercial Buildings: High Seismic								
COM1B	0.25	0.62	0.03	0.16	0.33	0.50	0.03	0.16
COM2B	0.33	0.53	0.02	0.08	0.39	0.43	0.02	0.07
COM3B	0.54	0.32	0.01	0.03	0.62	0.30	0.01	0.03
Commercial Buildings: Very High Seismic								
COM4B	0.27	0.67	0.03	0.16	0.29	0.67	0.03	0.16
COM5B	0.32	0.61	0.02	0.08	0.37	0.50	0.02	0.08
COM6B	0.49	0.46	0.01	0.04	0.54	0.41	0.01	0.03
Multi-Family Dwellings: High Seismic								
MFD1B	0.18	1.39	0.03	0.16	0.19	1.22	0.03	0.16
MFD2B	0.27	0.70	0.01	0.08	0.29	0.66	0.01	0.08
MFD3B	0.51	0.39	0.01	0.03	0.51	0.35	0.01	0.03
Multi-Family Dwellings: Very High Seismic								
MFD4B	0.18	1.48	0.03	0.16	0.16	1.34	0.03	0.16
MFD5B	0.37	0.73	0.02	0.08	0.32	0.73	0.02	0.08
MFD6B	0.54	0.44	0.01	0.04	0.55	0.44	0.01	0.04
Single-Family Dwellings: High Seismic								
SFD1B	0.14	2.10	0.03	0.16	0.17	1.63	0.03	0.16
SFD1BC	0.11	1.54	0.03	0.16	0.19	1.02	0.03	0.16
SFD2B	0.24	0.90	0.02	0.08	0.28	0.64	0.01	0.08
SFD2BC	0.21	0.96	0.02	0.08	0.29	0.56	0.02	0.08
Single-Family Dwellings: Very High Seismic								
SFD3B	0.13	2.33	0.03	0.16	0.16	1.70	0.03	0.16
SFD3BC	0.12	1.54	0.03	0.16	0.19	1.02	0.03	0.16
SFD4B	0.24	0.95	0.02	0.08	0.27	0.78	0.02	0.08

The pushover curves of some models exhibit “kinks” in the ascending branch of the curve, which was mainly attributed to differences among the displacements at peak strength of dissimilar materials in the wall building blocks (e.g., gypsum wallboard versus wood structural panels). Ultimate roof displacements, defined as the point where the descending branch of the pushover curve drops to zero force, are generally less for taller archetypes than for shorter archetypes, which was attributed to P-Delta effects.

Figure 5-5 through Figure 5-7 present the collapse rates from IDAs and collapse fragility curves determined using the FEMA P-695 methodology for these same archetype models. Unadjusted collapse rates (circular markers shown in the figures) are typically higher than fragility curves obtained using the FEMA P-695 methodology because the unadjusted collapse rates contain only record-to-record uncertainty while the FEMA P-695 fragility curves include other relevant uncertainties (e.g., test data and modeling uncertainties).

In terms of collapse probability, shorter archetypes generally performed better than corresponding taller archetypes. This can be observed in Figure 5-5, where the fragility curves of four-story COM3B and COM6B archetypes are located to the left of curves for the one-story COM1B and COM4B archetypes, which indicates that the taller archetypes tended to collapse at lower intensities than the shorter archetypes. Comparing fragility curves of the VHS and HS archetypes for a given building height and occupancy type, the fragility curves of VHS archetypes were always located to the left of the HS archetypes, indicating that VHS archetypes collapse at lower intensities than HS archetypes, suggesting that buildings located in regions of very high seismicity have higher collapse risks than those located in regions of high seismicity.

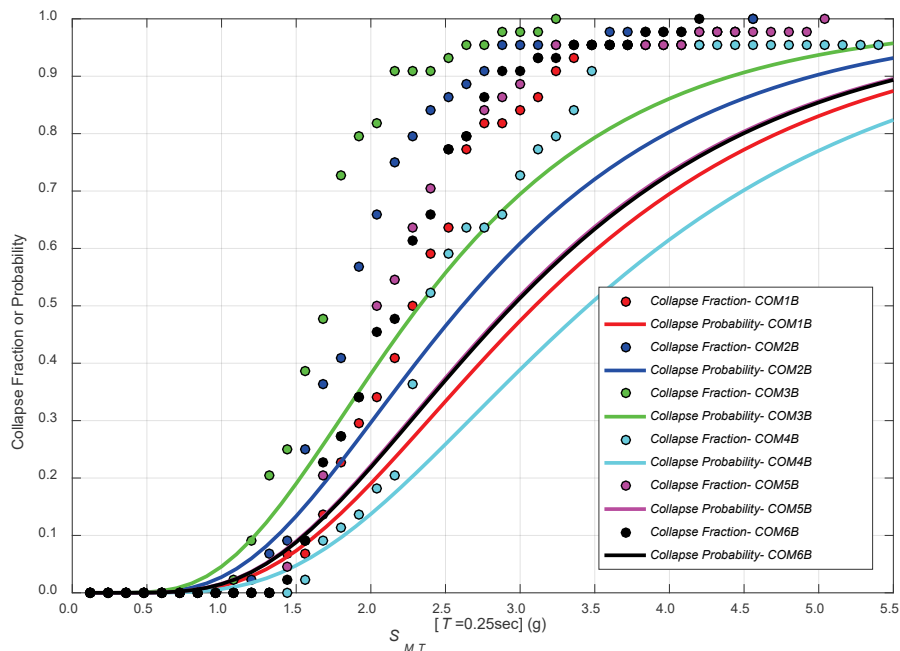


Figure 5-5 Collapse rates from IDA and FEMA P-695 collapse fragility curves for baseline commercial building archetype models.

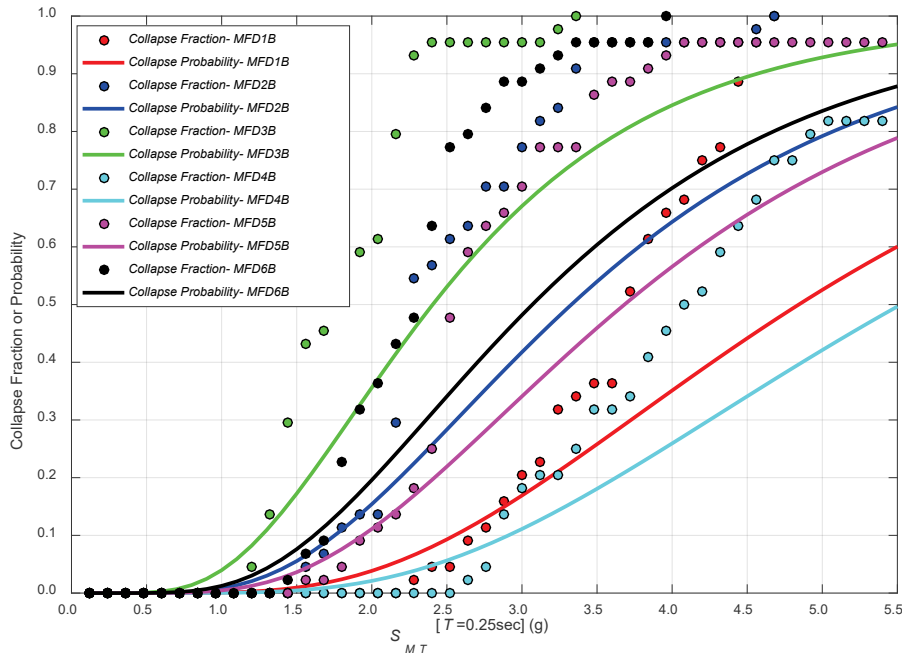


Figure 5-6 Collapse rates from IDA and FEMA P-695 collapse fragility curves for baseline multi-family dwelling archetype models.

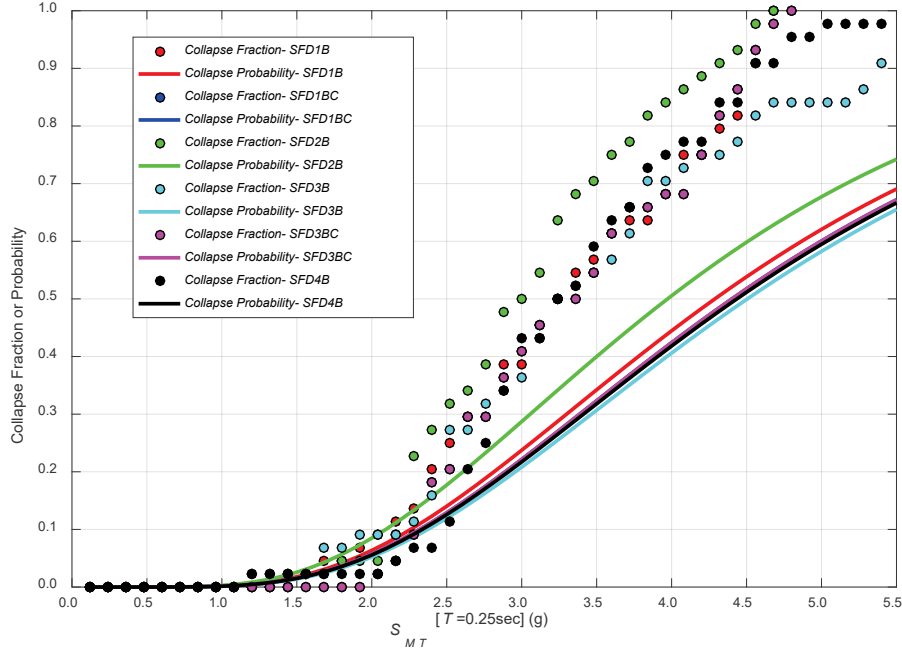


Figure 5-7 Collapse rates from IDA and FEMA P-695 collapse fragility curves for baseline single-family dwelling archetype models.

Table 5-2 summarizes values of various response and collapse parameters of the FEMA P-695 static pushover and IDA for each archetype. Nonlinear IDA results presented in Table 5-2 and Figure 5-5 through Figure 5-7 show that the MCE_R collapse probability increases as the number of stories increases. This trend was observed across all three occupancy types (COM,

MFD, and SFD), and was mainly attributed to P-Delta effects. This can also be seen in the pushover curves shown in Figure 5-2 through Figure 5-4, where taller archetypes have lower ultimate roof displacements due to P-Delta effects.

Table 5-2 Pushover and Collapse Analysis Results for Baseline Archetype Models

Baseline Archetype ID	Pushover Analysis *			Collapse Analysis				
	V_{\max} / W	Ω	μ_r	S_{CT} (g)	CMR _{3D}	SSF	ACMR	P[C MCE _R]
Commercial Buildings: High Seismic								
COM1B	0.56	3.64	>8	3.10	1.55	1.33	2.07	7.3%
COM2B	0.48	3.13	>8	2.61	1.31	1.33	1.74	13.4%
COM3B	0.31	2.00	>8	2.33	1.15	1.35	1.55	19.0%
Commercial Buildings: Very High Seismic								
COM4B	0.67	2.90	>8	3.45	1.15	1.33	1.54	19.0%
COM5B	0.56	2.41	>8	2.93	0.98	1.33	1.30	29.0%
COM6B	0.44	1.89	>8	2.95	0.98	1.34	1.31	28.6%
Multi-Family Dwellings: High Seismic								
MFD1B	1.30	8.47	>8	4.84	2.43	1.33	3.23	1.0%
MFD2B	0.68	4.41	>8	3.33	1.67	1.33	2.22	5.5%
MFD3B	0.37	2.40	>8	2.41	1.20	1.33	1.60	17.2%
Multi-Family Dwellings: Very High Seismic								
MFD4B	1.41	6.12	>8	5.52	1.85	1.33	2.45	3.5%
MFD5B	0.73	3.15	>8	3.68	1.23	1.33	1.64	15.7%
MFD6B	0.44	1.89	>8	3.07	1.02	1.34	1.36	26.0%
Single-Family Dwellings: High Seismic								
SFD1B	1.86	12.10	>8	4.29	2.15	1.33	2.86	1.8%
SFD1BC	1.28	8.31	>8	4.40	2.21	1.33	2.93	1.6%
SFD2B	0.77	5.00	>8	3.97	1.99	1.33	2.65	2.6%
SFD2BC	0.76	4.93	>8	3.84	1.92	1.33	2.56	3.0%
Single-Family Dwellings: Very High Seismic								
SFD3B	2.01	8.72	>8	4.51	1.51	1.33	2.00	7.9%
SFD3BC	1.28	5.54	>8	4.40	1.47	1.33	1.96	8.6%
SFD4B	0.87	3.76	>8	4.44	1.48	1.33	1.97	8.4%

* Pushover analysis results represent average response in the North-South and East-West directions.

Table 5-3 summarizes median and lognormal standard deviation values of peak roof drift ratio, peak first-story drift ratio, and corresponding response spectral acceleration at incipient collapse. Based on median values of peak drift ratio at the roof and first stories of two-story and four-story archetypes,

it can be observed that displacement at incipient collapse occurs primarily in the first story of multi-story archetypes. For example, the peak roof displacement for the COM2B archetype model is approximately 8.4 inches (i.e., 0.035×240 inches) at incipient collapse, whereas the peak first-story displacement of this model is approximately 8.0 inches (i.e., 0.067×120 inches) at incipient collapse.

Table 5-3 Median and Lognormal Standard Deviation Values of Peak Drift Ratio and Response Spectral Acceleration at Incipient Collapse for Baseline Archetype Models

Baseline Archetype ID	Peak Drift Ratio at Incipient Collapse				Response Spectral Acceleration at Incipient Collapse S_T (g)	
	Roof		First Story			
	Median	β	Median	β	Median	β
Commercial Buildings: High Seismic						
COM1B	0.082	0.29	0.082	0.29	1.94	0.27
COM2B	0.035	0.33	0.067	0.35	1.64	0.26
COM3B	0.016	0.18	0.046	0.29	1.43	0.23
Commercial Buildings: Very High Seismic						
COM4B	0.088	0.22	0.088	0.22	2.16	0.28
COM5B	0.038	0.30	0.074	0.32	1.84	0.27
COM6B	0.020	0.18	0.058	0.25	1.84	0.25
Multi-Family Dwellings: High Seismic						
MFD1B	0.071	0.88	0.071	0.88	3.03	0.19
MFD2B	0.046	0.35	0.090	0.37	2.09	0.25
MFD3B	0.016	0.21	0.052	0.31	1.51	0.25
Multi-Family Dwellings: Very High Seismic						
MFD4B	0.101	0.33	0.101	0.33	3.46	0.27
MFD5B	0.053	0.36	0.099	0.43	2.31	0.26
MFD6B	0.022	0.21	0.054	0.37	1.90	0.23
Single-Family Dwellings: High Seismic						
SFD1B	0.022	1.01	0.022	1.01	2.69	0.30
SFD1BC	0.066	0.68	0.066	0.68	2.76	0.26
SFD2B	0.058	0.41	0.117	0.38	2.49	0.28
SFD2BC	0.049	0.43	0.096	0.45	2.40	0.28
Single-Family Dwellings: Very High Seismic						
SFD3B	0.028	1.05	0.028	1.05	2.82	0.38
SFD3BC	0.066	0.68	0.066	0.68	2.76	0.26
SFD4B	0.066	0.53	0.148	0.24	2.78	0.29

Table 5-4 summarizes raw collapse statistics (i.e., without the 1.2 factor for three-dimensional analysis effects) and mean peak first-story drift ratios for each archetype, for ground motions scaled to MCE_R and 0.5 × MCE_R intensity levels.

Table 5-4 Collapse Rates and Mean Peak First-Story Drift Ratios for Baseline Archetype Models at MCE_R and 50-Percent of MCE_R Ground Motion Intensities

Baseline Archetype Model ID	MCE _R Collapse Rate (out of 44)		Mean Peak First-Story Drift Ratio of Survivors (%)			
	0.5 × MCE _R	1.0 × MCE _R	0.5 × MCE _R		MCE _R	
			East-West Direction	North-South Direction	East-West Direction	North-South Direction
Commercial Buildings: High Seismic						
COM1B	0	3	1.00	0.58	3.06	2.22
COM2B	0	8	1.11	0.84	3.27	2.82
COM3B	0	14	0.82	0.84	2.39	2.48
Commercial Buildings: Very High Seismic						
COM4B	0	8	1.54	1.43	4.24	4.03
COM5B	0	14	1.93	1.54	4.47	3.32
COM6B	0	13	1.24	1.14	3.12	2.82
Multi-Family Dwellings: High Seismic						
MFD1B	0	0	0.23	0.21	0.72	0.66
MFD2B	0	1	0.63	0.69	2.21	2.37
MFD3B	0	16	0.78	0.73	2.27	2.42
Multi-Family Dwellings: Very High Seismic						
MFD4B	0	0	0.56	0.57	2.31	2.23
MFD5B	0	4	0.82	1.20	3.47	3.75
MFD6B	0	11	1.06	1.17	2.76	3.09
Single-Family Dwellings: High Seismic						
SFD1B	0	1	0.19	0.11	0.52	0.32
SFD1BC	0	0	0.28	0.10	1.18	0.47
SFD2B	0	1	0.56	0.36	2.41	1.39
SFD2BC	0	0	0.63	0.27	2.46	1.00
Single-Family Dwellings: Very High Seismic						
SFD3B	0	3	0.34	0.19	1.19	0.54
SFD3BC	0	2	0.57	0.21	2.92	1.25
SFD4B	0	2	1.01	0.72	4.42	3.19

The $0.5 \times MCE_R$ intensity level is considered an intensity that better represents a median estimate of design ground motions. In multi-story wood light-frame buildings, due to design constraints, capacity-to-demand ratios are typically much lower in the first story than in the upper stories, resulting in displacement demands that are concentrated mainly in the first story. Hence, peak first-story transient drift ratios are reported in lieu of roof drift ratios in Table 5-4. Peak transient drifts in VHS archetypes are higher than those of HS archetypes, which suggests that buildings in regions of very high seismicity are more prone to damage than buildings in regions of high seismicity. At the MCE_R intensity level, all archetypes with peak story drift ratios greater than 2 percent would be expected to suffer significant damage (except for one-story SFD and MFD high seismic archetypes).

At the MCE_R intensity level, taller archetypes have more collapses (out of 44 ground motions) than shorter archetypes. This is consistent with results from pushover analyses, in which the normalized peak strength ratio (V_{max} / W) and displacement capacity of multi-story archetypes were found to be generally lower than the corresponding one-story archetypes. No collapses were observed in any baseline archetype model at the $0.5 \times MCE_R$ intensity level.

5.2.3 Interpretation of Results

Figure 5-8 shows a strong inverse relationship (negative correlation) between MCE_R collapse probability and the peak strength ratio (V_{max} / W) (average of E-W and N-S directions). In the figure, MCE_R collapse probability decreases as V_{max} / W increases. Among the three occupancy types, COM archetypes were the most susceptible to collapse at MCE_R intensities, followed by MDF archetypes. In general, SFD archetypes had the lowest MCE_R collapse probabilities, which was attributed to their relatively low seismic weight.

Figure 5-9 compares the seismic performance of wood light-frame buildings located in high seismic and very high seismic regions. The MCE_R collapse probabilities of VHS archetypes (right bar in each pair) are higher than corresponding HS archetypes (left bar in each pair). This was mainly attributed to a disparity in the percentage of total lateral strength contributed by nonstructural interior and exterior wall finishes in VHS versus HS archetypes. In VHS archetypes, the additional lateral strength contributed by nonstructural wall finishes is less significant, and, thus, is less beneficial than the strength contributed by the presence of nonstructural wall finishes in HS archetypes.

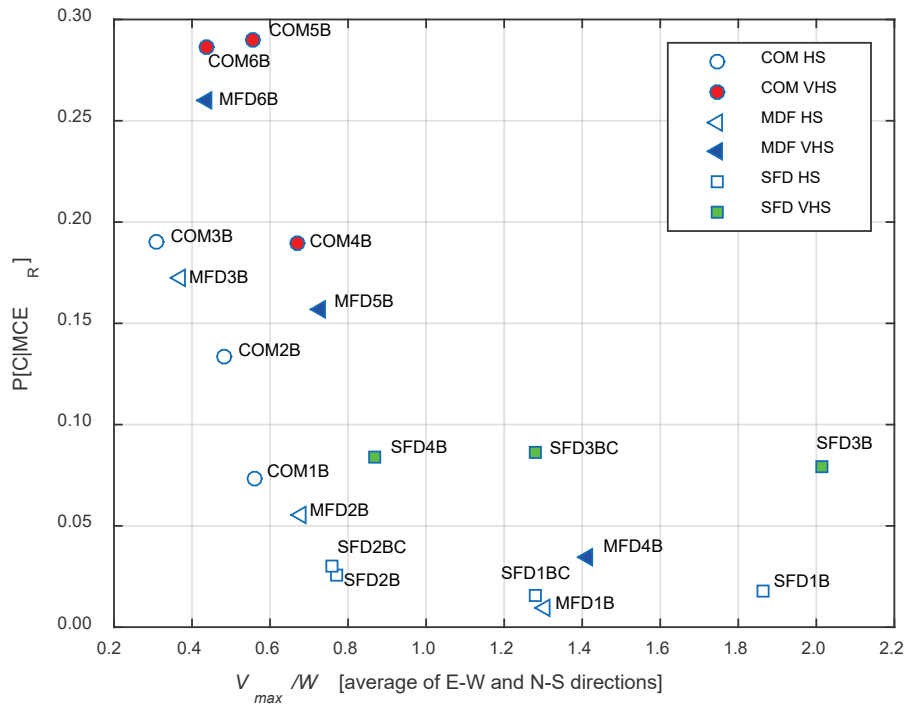


Figure 5-8 MCE_R collapse probability versus peak strength ratio (V_{max} / W) for baseline archetype models.

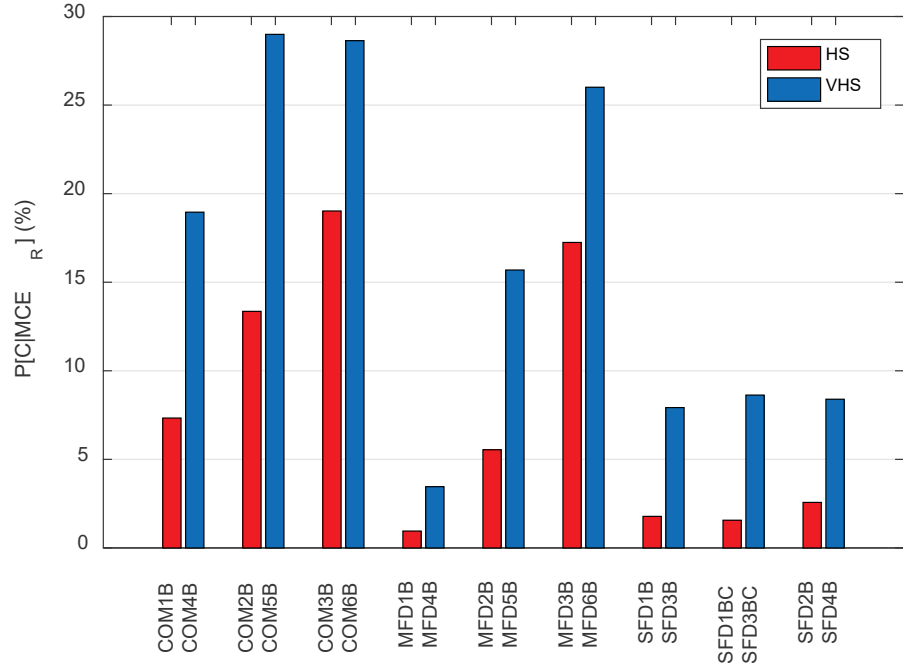


Figure 5-9 MCE_R collapse probabilities for baseline archetype models located in high seismic (HS) and very high seismic (VHS) regions.

In terms of the spectral acceleration at 0.25-second period, the demand at the MCE_R intensity level in very high seismic regions is 1.5 times that of high seismic regions (i.e., $S_{MS}[0.25 \text{ second}] = 2.25\text{g}$ versus 1.5g). Although the corresponding code-required design base shear coefficient for VHS archetypes is also 1.5 times that of HS archetypes (i.e., $C_s = 0.231$ versus $C_s = 0.154$), peak strength ratios (V_{max} / W) for baseline VHS archetypes are less than 1.5 times the peak strength ratios for HS archetypes.

Figure 5-10 shows the relative contributions of wood structural panels (red bars) and nonstructural interior and exterior wall finishes (blue bars) to V_{max} / W . Horizontal dashed lines (green and red) indicate the design base shear coefficients for HS archetypes ($C_s = 0.154$) and VHS archetypes ($C_s = 0.231$), respectively. In both cases, the contributions from wood structural panels exceed the required base shear strength.

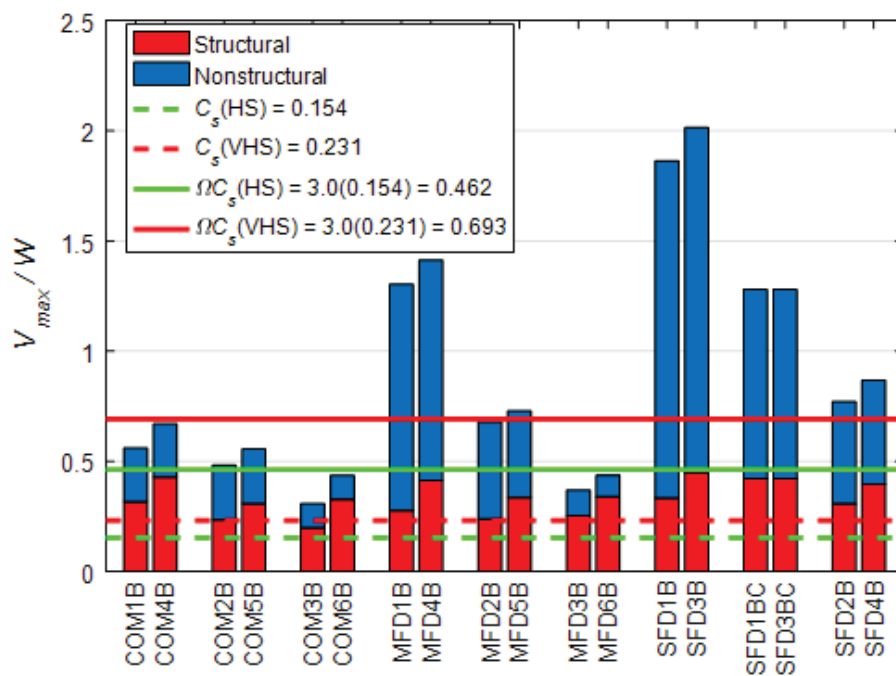


Figure 5-10 Relative strength contributions of structural and nonstructural wall finishes for baseline archetype models located in high seismic (HS) and very high seismic (VHS) regions.

The expected ultimate strength of code compliant buildings, including an overstrength factor, $\Omega = 3.0$ (ASCE, 2010), are indicated by solid horizontal lines (green and red) for HS and VHS archetypes, respectively. Although wood structural panels in VHS archetypes are stronger than HS archetypes, the contribution from nonstructural wall finishes is the same, so the overall capacity-to-demand ratios for HS archetypes are higher than VHS archetypes. For archetypes with V_{max} / W greater than one, MCE_R collapse probabilities correspond with observed red tag collapse rates reported in Chapter 2.

Higher MCE_R collapse probabilities were observed in multi-story archetype models relative to one-story archetype models. This was attributed to code design procedures and typical design practices related to how design strengths in each story are proportioned relative to the vertical distribution of design story shears. The overstrength present in the first story of multi-story buildings (strength provided/strength required) is often lower than the overstrength present in upper stories (or provided in one-story buildings). Because story shears are lower in the upper stories of multi-story buildings, and the strength provided by nonstructural walls and wall finishes is often more significant in the upper stories, additional overstrength present in the upper stories can become even more pronounced, resulting in the formation of a first-story mechanism and higher MCE_R collapse probabilities in multi-story archetypes.

In Figure 5-11, MCE_R collapse probability is plotted versus fundamental period for wood light-frame archetypes. In the figure, MCE_R collapse probabilities are shown to increase with increases in period. This is a reversal of the trend observed in prior FEMA P-695 studies (shown in Figure 1-1) in which short-period buildings ($T_1 < 0.5$ seconds) had higher MCE_R collapse probabilities than longer period buildings (T_1 greater than 0.5 seconds).

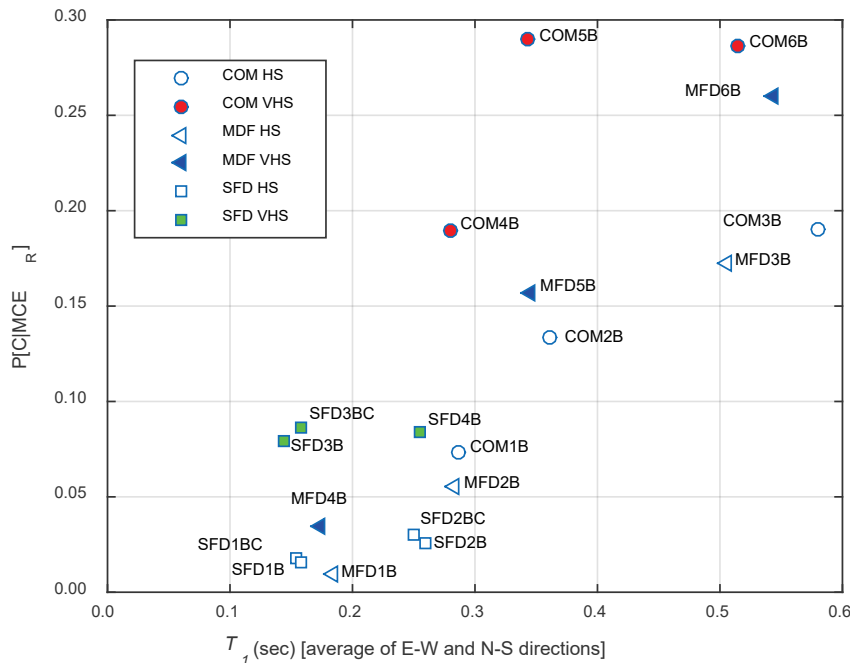


Figure 5-11 MCE_R collapse probability versus fundamental period (T_1) for baseline archetype models.

Reversal of the prior trend in MCE_R collapse probability versus period was mainly attributed to differences in numerical modeling between the current study and prior FEMA P-695 studies. In the FEMA P-695 methodology, nonstructural wall finishes are not considered, and in prior studies, P-Delta effects were not modeled, which led to conservative assumptions related to residual strength and ultimate displacement capacity.

5.3 Collapse Displacement Capacity Parametric Study

Collapse displacement capacity studies investigated the effects of residual post-capping strength and ultimate displacement capacity on response behavior and collapse performance. Based on test data available at the time, prior FEMA P-695 studies limited displacement capacities to the displacement corresponding to a post-peak strength of $0.8V_{\max}$, and “collapse” was assumed to occur when the displacement exceeded 7 percent of the story height. In this study, models with six levels of residual post-capping strength (i.e., 0 percent, 10 percent, 20 percent, 40 percent, 50 percent, and 60 percent) were compared with baseline models incorporating 30 percent. In addition to capturing nonlinear properties of the wood shear wall elements themselves, residual strength ratios were also used as a proxy for incorporating non-simulated sources of residual strength in wood light-frame systems. Based on information from full-scale shake table tests of wood light-frame buildings (e.g., Isoda et al., 2008), all models assumed that the ultimate displacement was unlimited (i.e., $\delta_u = \infty$), although P-Delta effects resulted in lateral instability at finite lateral displacements.

5.3.1 Collapse Displacement Capacity Archetypes and Variants

Table 5-5 to Table 5-7 summarize key design properties and post-capping modeling criteria for the COM, MFD, and SFD archetypes used in collapse displacement capacity studies. Three high-seismic, two-story baseline archetypes (i.e., COM2B, MFD2B, and SFD2B) were modified to include six variants of baseline residual post-capping strength. Three high seismic, one-story baseline archetypes (i.e., COM1B, MFD1B, and SFD1B) were also modified to include three variants of baseline residual post-capping strength.

The post-capping collapse displacement capacity is controlled by the residual strength ratio parameter (f_3 in Figure 4-3) of the individual vertical wall building blocks with the displacement capacity proportional to the residual strength ratio. Variants designated “C0” have zero residual strength, “C1” have 10% residual strength, “C2” have 20% residual strength, “C3 or blank” have baseline 30% residual strength, “C4” have 40% residual strength, and “C6” have 60% residual strength.

Table 5-5 Commercial Building Archetype Models Used to Investigate Collapse Displacement Capacity

Baseline Archetype ID	No. of Stories	W (kips)	Key Archetype Modeling and Design Criteria ⁽¹⁾					$S_{MT}[T]$ (g)	
			Post-Capping Control Points ⁽²⁾		Residual Strength Plateau				
			Drift Ratio at $0.8V_{max}$ (%)	Force / V_{max} (%)	Drift Ratio Range				
Commercial Buildings: High Seismic									
COM1B-C0	1	180	4	0	10	15	1.5		
COM1B-C1	1	180	4	10	10	15	1.5		
COM1B-C2	1	180	4	20	10	15	1.5		
COM1B	1	180	4	30	10	15	1.5		
COM2B-C0	2	488	4	0	10	15	1.5		
COM2B-C1	2	488	4	10	10	15	1.5		
COM2B-C2	2	488	4	20	10	15	1.5		
COM2B	2	488	4	30	10	15	1.5		
COM2B-C4	2	488	4	40	10	15	1.5		
COM2B-C5	2	488	4	50	10	15	1.5		
COM2B-C6	2	488	4	60	10	15	1.5		

⁽¹⁾ See Table 4-13 for additional archetype design criteria for COM archetypes.

⁽²⁾ Applies to OSB building blocks, which dominate the hysteretic properties. See Chapter 4 for other building block materials.

Table 5-6 Multi-Family Dwelling Archetype Models Used to Investigate Collapse Displacement Capacity

Baseline Archetype ID	No. of Stories	W (kips)	Key Archetype Modeling and Design Criteria ⁽¹⁾					$S_{MI}[T]$ (g)	
			Post-Capping Control Points ⁽²⁾		Residual Strength Plateau				
			Drift Ratio at $0.8V_{max}$ (%)	Force / V_{max} (%)	Drift Ratio Range				
Multi-Family Dwellings: High Seismic									
MFD1B-C0	1	141	4	0	10	15	1.5		
MFD1B-C1	1	141	4	10	10	15	1.5		
MFD1B-C2	1	141	4	20	10	15	1.5		
MFD1B	1	141	4	30	10	15	1.5		
MFD2B-C0	2	363	4	0	10	15	1.5		
MFD2B-C1	2	363	4	10	10	15	1.5		
MFD2B-C2	2	363	4	20	10	15	1.5		
MFD2B	2	363	4	30	10	15	1.5		
MFD2B-C4	2	363	4	40	10	15	1.5		
MFD2B-C5	2	363	4	50	10	15	1.5		
MFD2B-C6	2	363	4	60	10	15	1.5		

⁽¹⁾ See Table 4-14 for additional archetype design criteria for MFD archetypes.

⁽²⁾ Applies to OSB building blocks, which dominate the hysteretic properties. See Chapter 4 for other building block materials.

Table 5-7 Single-Family Dwelling Archetype Models Used to Investigate Collapse Displacement Capacity

Baseline Archetype ID	No. of Stories	W (kips)	Key Archetype Modeling and Design Criteria ⁽¹⁾				
			Post-Capping Control Points ⁽²⁾		Residual Strength Plateau	S _{MTL} [T] (g)	
			Drift Ratio at 0.8V _{max} (%)	Force / V _{max} (%)			
Single-Family Dwellings: High Seismic							
SFD1B-C0	1	52	4	0	10	15	1.5
SFD1B-C1	1	52	4	10	10	15	1.5
SFD1B-C2	1	52	4	20	10	15	1.5
SFD1B	1	52	4	30	10	15	1.5
SFD2B-C0	2	135	4	0	10	15	1.5
SFD2B-C1	2	135	4	10	10	15	1.5
SFD2B-C2	2	135	4	20	10	15	1.5
SFD2B	2	135	4	30	10	15	1.5
SFD2B-C4	2	135	4	40	10	15	1.5
SFD2B-C5	2	135	4	50	10	15	1.5
SFD2B-C6	2	135	4	60	10	15	1.5

⁽¹⁾ See Table 4-15 for additional archetype design criteria for SFD archetypes.

⁽²⁾ Applies to OSB building blocks, which dominate the hysteretic properties. See Chapter 4 for other building block materials.

5.3.2 Numerical Results

Figure 5-12 through Figure 5-17 show pushover curves for commercial, multi-family dwelling, and single-family dwelling wood light-frame building archetype models in high seismic regions. The peak strengths of the pushover curves vary somewhat for different residual strengths. This was attributed to an artifact of using an S-shaped curve to model the post-capping branch of the backbone curves (shown in Figure 4-3).

The post-peak residual strength level is shown to have a direct impact on pushover collapse displacement capacity. In Figure 5-13, for example, the two-story commercial building archetype with zero residual strength (COM2B-C0) has a static collapse roof drift ratio of about 4 percent, while baseline archetype with 30 percent post-peak residual strength (COM2B or COM2B-C3) has a static collapse roof drift ratio exceeding 7 percent, which is about 1.75 times of that of the model with zero residual strength.

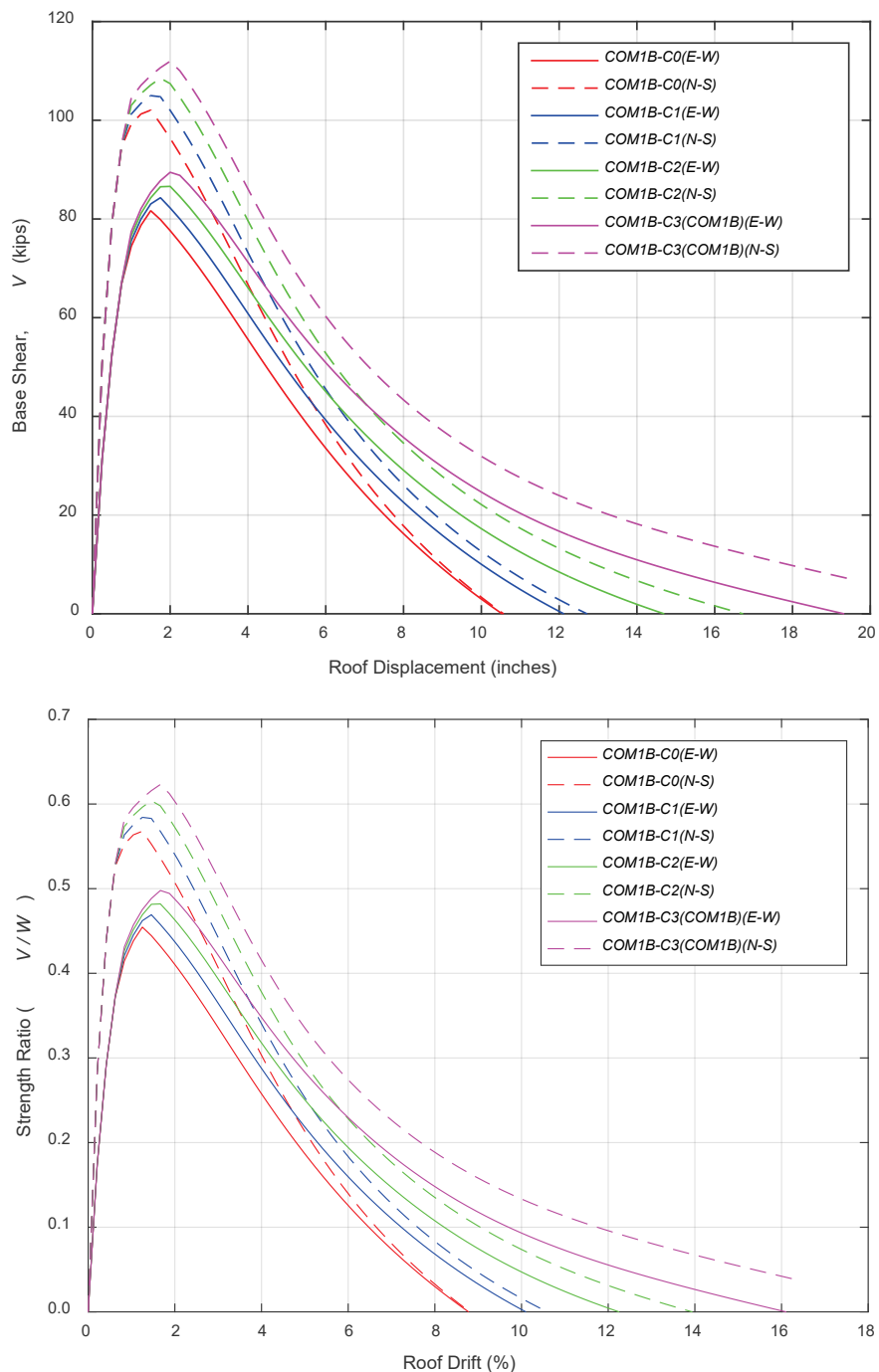


Figure 5-12 Pushover curves for one-story commercial building archetype models in collapse displacement capacity studies (top), and pushover curves normalized by total building seismic weight and roof height (bottom).

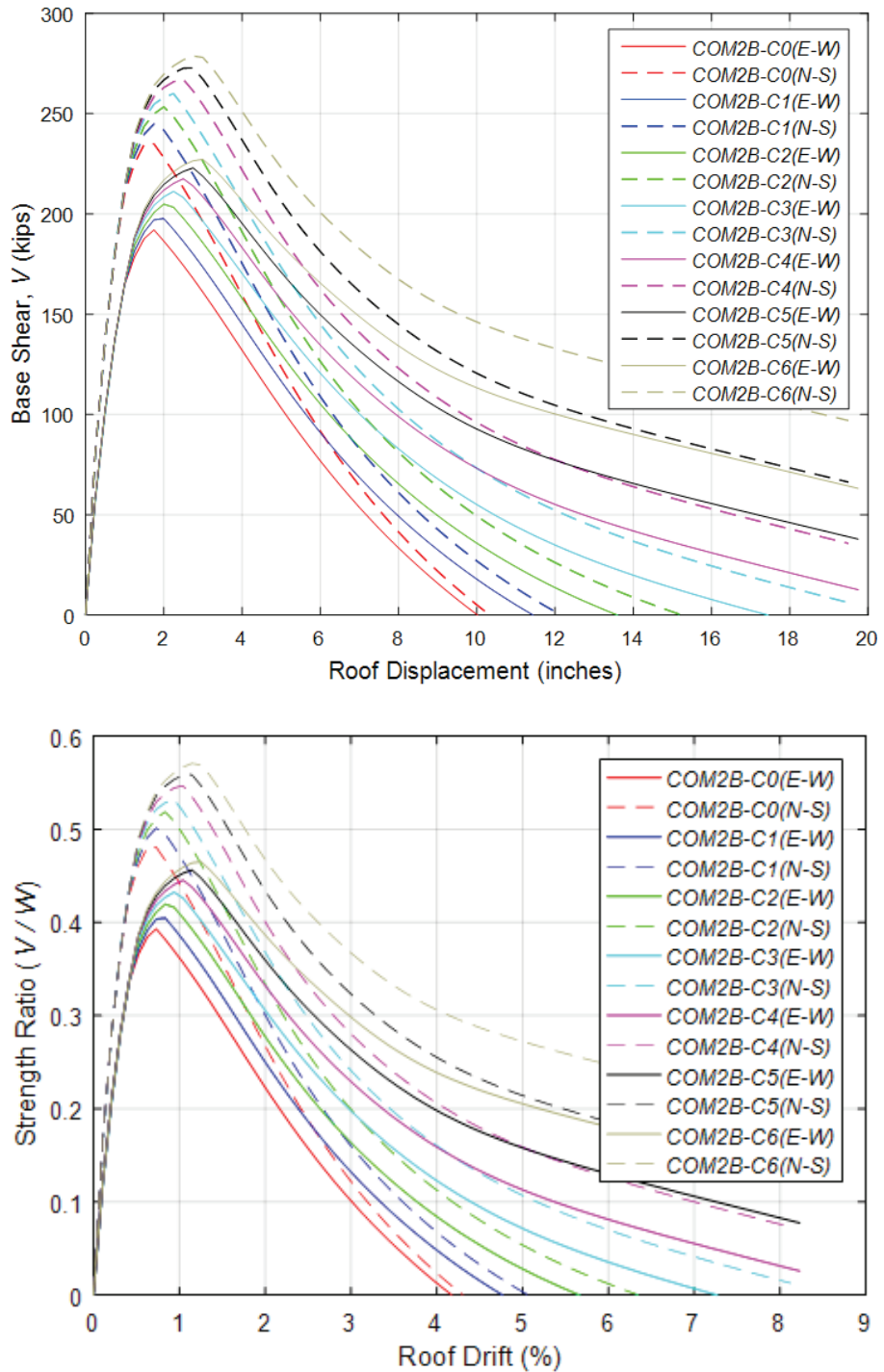


Figure 5-13 Pushover curves for two-story commercial building archetype models in collapse displacement capacity studies (top), and pushover curves normalized by total building seismic weight and roof height (bottom).

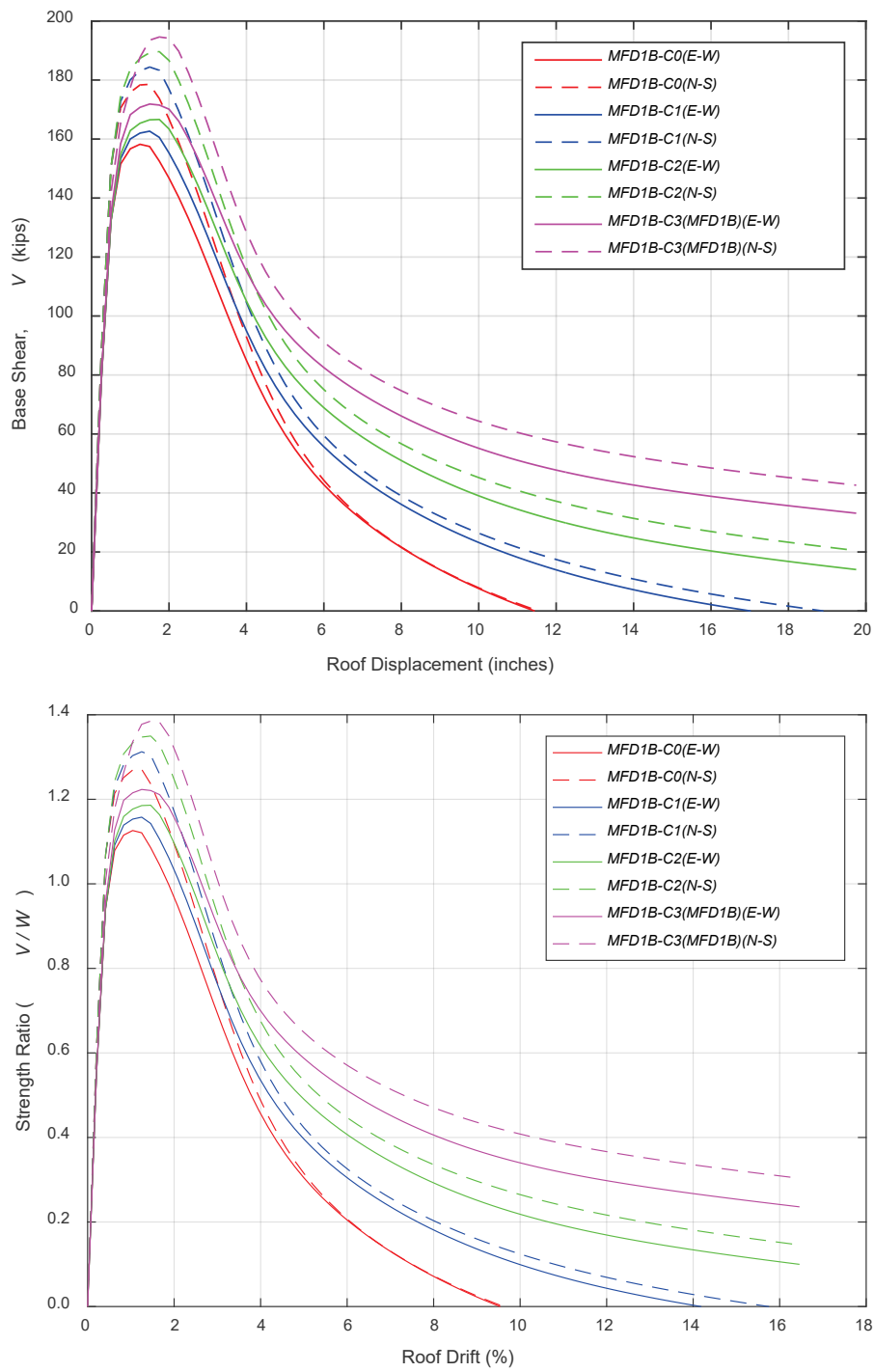


Figure 5-14 Pushover curves for one-story multi-family dwelling archetype models in collapse displacement capacity studies (top), and pushover curves normalized by total building seismic weight and roof height (bottom).

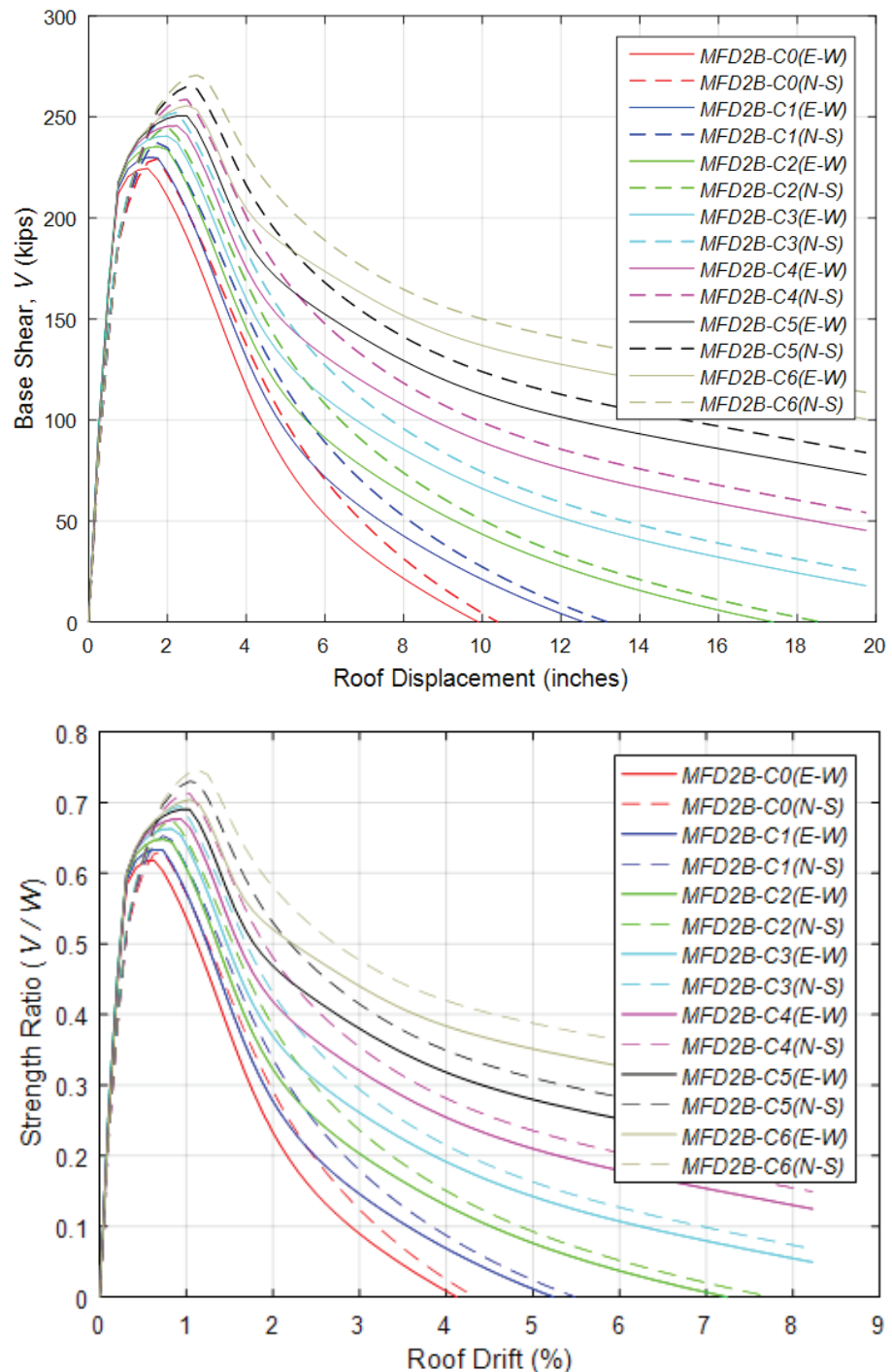


Figure 5-15 Pushover curves for two-story multi-family dwelling archetype models in collapse displacement capacity studies (top), and pushover curves normalized by total building seismic weight and roof height (bottom).

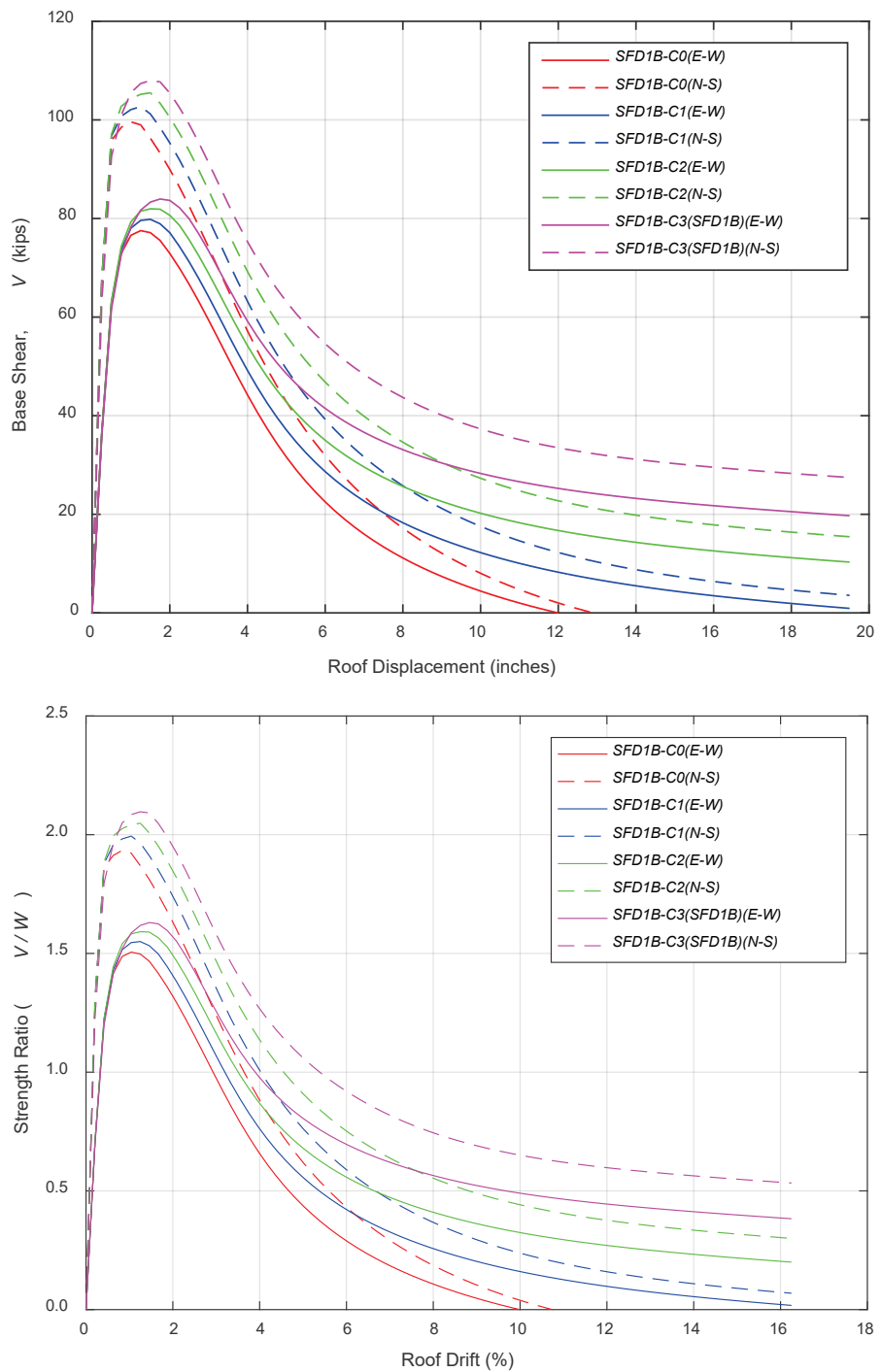


Figure 5-16 Pushover curves for one-story single-family dwelling archetype models in collapse displacement capacity studies (top), and pushover curves normalized by total building seismic weight and roof height (bottom).

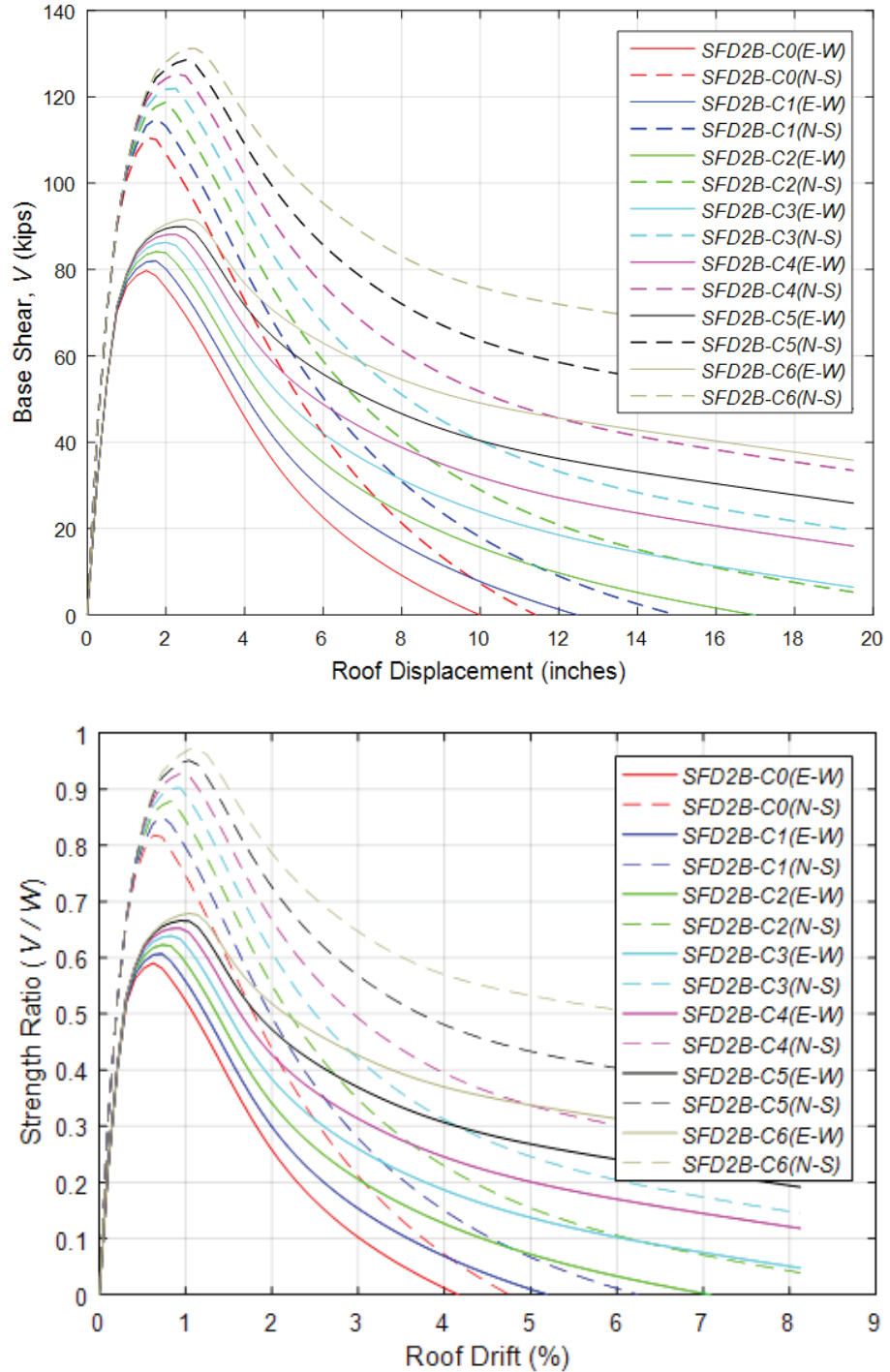


Figure 5-17 Pushover curves for two-story single-family dwelling archetype models in collapse displacement capacity studies (top), and pushover curves normalized by total building seismic weight and roof height (bottom).

Results from free vibration (modal) analysis (T_1) and nonlinear static pushover analyses for the 33 baseline and variant models used in collapse displacement capacity studies are summarized in Table 5-8, Table 5-9, and Table 5-10 for commercial buildings, multi-family dwellings, and single-family-dwellings, respectively. As expected, the fundamental periods in both lateral directions were not affected by values of residual post-peak strength. As observed in the pushover curves in Figure 5-12 through Figure 5-17, the peak strength ratios (V_{max} / W) shown in the tables vary somewhat for different residual strength ratios as an artifact of using an S-shaped curve to model the post-capping branch of the backbone curves.

Table 5-8 Modal and Pushover Analysis Results for Commercial Building Archetype Models Used to Investigate Collapse Displacement Capacity

Archetype ID	North-South Direction				East-West Direction			
	T_1 (sec)	V_M / W	$\Delta_{U,80}$ (in/in)	$\Delta_{U,max}$ (in/in)	T_1 (sec)	V_M / W	$\Delta_{U,80}$ (in/in)	$\Delta_{U,max}$ (in/in)
Commercial Buildings: High Seismic								
COM1B-C0	0.25	0.57	0.027	0.088	0.33	0.45	0.027	0.087
COM1B-C1	0.25	0.58	0.029	0.104	0.33	0.47	0.029	0.100
COM1B-C2	0.25	0.60	0.031	0.138	0.33	0.48	0.031	0.121
COM1B	0.25	0.62	0.033	0.163	0.33	0.50	0.033	0.160
COM2B-C0	0.33	0.48	0.014	0.043	0.39	0.39	0.014	0.042
COM2B-C1	0.33	0.50	0.015	0.050	0.39	0.40	0.015	0.047
COM2B-C2	0.33	0.52	0.016	0.063	0.39	0.42	0.016	0.056
COM2B	0.33	0.53	0.017	0.081	0.39	0.43	0.017	0.072
COM2B-C4	0.33	0.55	0.018	0.081	0.39	0.45	0.018	0.082
COM2B-C5	0.33	0.56	0.020	0.081	0.39	0.46	0.020	0.082
COM2B-C6	0.33	0.57	0.021	0.081	0.39	0.47	0.022	0.082

Table 5-9 Modal and Pushover Analysis Results for Multi-Family Dwelling Archetype Models Used to Investigate Collapse Displacement Capacity

Archetype ID	North-South Direction				East-West Direction			
	T_1 (sec)	V_M / W	$\Delta_{U,80}$ (in/in)	$\Delta_{U,\max}$ (in/in)	T_1 (sec)	V_M / W	$\Delta_{U,80}$ (in/in)	$\Delta_{U,\max}$ (in/in)
Multi-Family Dwellings: High Seismic								
MFD1B-C0	0.18	1.27	0.023	0.096	0.19	1.13	0.023	0.094
MFD1B-C1	0.18	1.31	0.025	0.156	0.19	1.16	0.025	0.142
MFD1B-C2	0.18	1.35	0.025	0.165	0.19	1.19	0.025	0.165
MFD1B	0.18	1.39	0.027	0.165	0.19	1.22	0.027	0.165
MFD2B-C0	0.27	0.63	0.013	0.043	0.29	0.62	0.011	0.041
MFD2B-C1	0.27	0.65	0.014	0.054	0.29	0.63	0.012	0.052
MFD2B-C2	0.27	0.68	0.014	0.077	0.29	0.65	0.012	0.072
MFD2B	0.27	0.70	0.018	0.081	0.29	0.66	0.016	0.082
MFD2B-C4	0.27	0.71	0.016	0.082	0.29	0.68	0.015	0.082
MFD2B-C5	0.27	0.73	0.018	0.082	0.29	0.69	0.016	0.082
MFD2B-C6	0.27	0.75	0.020	0.082	0.29	0.70	0.017	0.082

Table 5-10 Modal and Pushover Analysis Results for Single-Family Dwelling Archetype Models Used to Investigate Collapse Displacement Capacity

Archetype ID	North-South Direction				East-West Direction			
	T_1 (sec)	V_M / W	$\Delta_{U,80}$ (in/in)	$\Delta_{U,\max}$ (in/in)	T_1 (sec)	V_M / W	$\Delta_{U,80}$ (in/in)	$\Delta_{U,\max}$ (in/in)
Single-Family Dwellings: High Seismic								
SFD1B-C0	0.14	1.93	0.023	0.106	0.17	1.51	0.025	0.098
SFD1B-C1	0.14	1.99	0.025	0.163	0.17	1.55	0.025	0.163
SFD1B-C2	0.14	2.05	0.027	0.163	0.17	1.59	0.027	0.163
SFD1B	0.14	2.10	0.029	0.163	0.17	1.63	0.029	0.163
SFD2B-C0	0.24	0.82	0.014	0.047	0.28	0.59	0.013	0.041
SFD2B-C1	0.24	0.85	0.015	0.061	0.28	0.61	0.013	0.051
SFD2B-C2	0.24	0.88	0.016	0.081	0.28	0.62	0.014	0.070
SFD2B	0.24	0.90	0.017	0.081	0.28	0.64	0.015	0.081
SFD2B-C4	0.24	0.93	0.019	0.081	0.28	0.65	0.016	0.081
SFD2B-C5	0.24	0.95	0.020	0.081	0.28	0.67	0.017	0.081
SFD2B-C6	0.24	0.97	0.023	0.081	0.28	0.68	0.019	0.081

Nonlinear IDA results are summarized in Figure 5-18 through Figure 5-23, which present IDA collapse rates and FEMA P-695 fragility curves. Table 5-11 summarizes values of various response and collapse parameters from FEMA P-695 static pushover and nonlinear incremental dynamic collapse analyses for each archetype. Although pushover analyses were performed on all 33 archetype models, IDAs were only conducted on 26 of the 33 models.

Pushover analyses were conducted to investigate the effect of residual strength ratio on the displacement capacity of individual building archetypes. Because of computational demands, however, IDAs were only performed on those archetype models deemed necessary for understanding the relationship between MCE_R collapse probability and collapse displacement capacity. As can be observed in Table 5-11, for a given baseline archetype model, the MCE_R collapse probability decreases as the residual post-capping strength increases. In the case of the one-story single-family dwelling archetype (SFD1B), the influence of post-peak residual strength on MCE_R collapse probability is less significant because the one-story single-family dwelling has a high peak strength ratio and is relatively light.

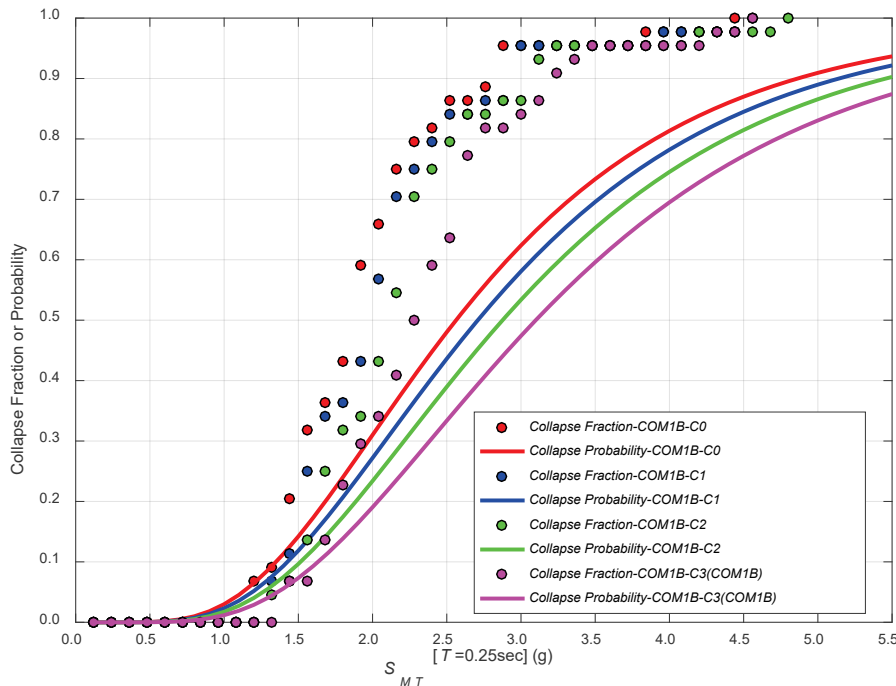


Figure 5-18 Collapse rates from IDA and FEMA P-695 collapse fragility curves for one-story commercial building archetype models in collapse displacement capacity studies.

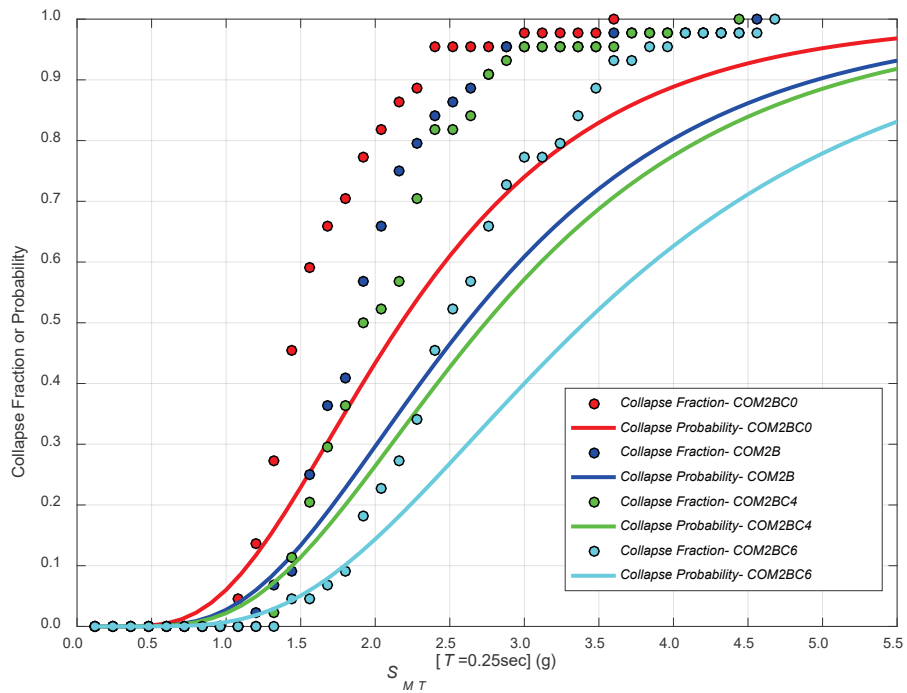


Figure 5-19 Collapse rates from IDA and FEMA P-695 collapse fragility curves for two-story commercial building archetype models in collapse displacement capacity studies.

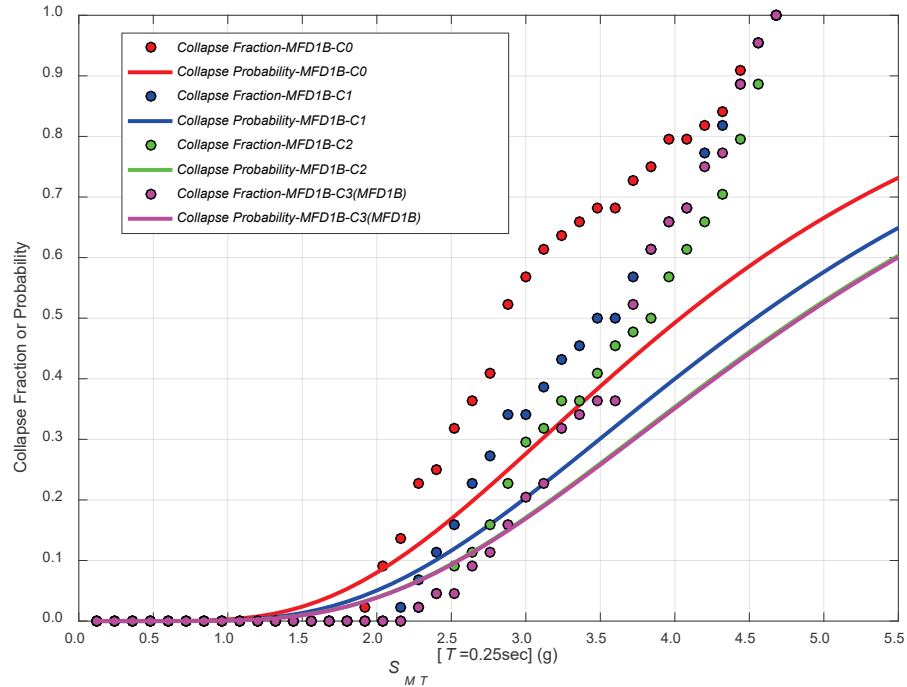


Figure 5-20 Collapse rates from IDA and FEMA P-695 collapse fragility curves for one-story multi-family dwelling archetype models in collapse displacement capacity studies.

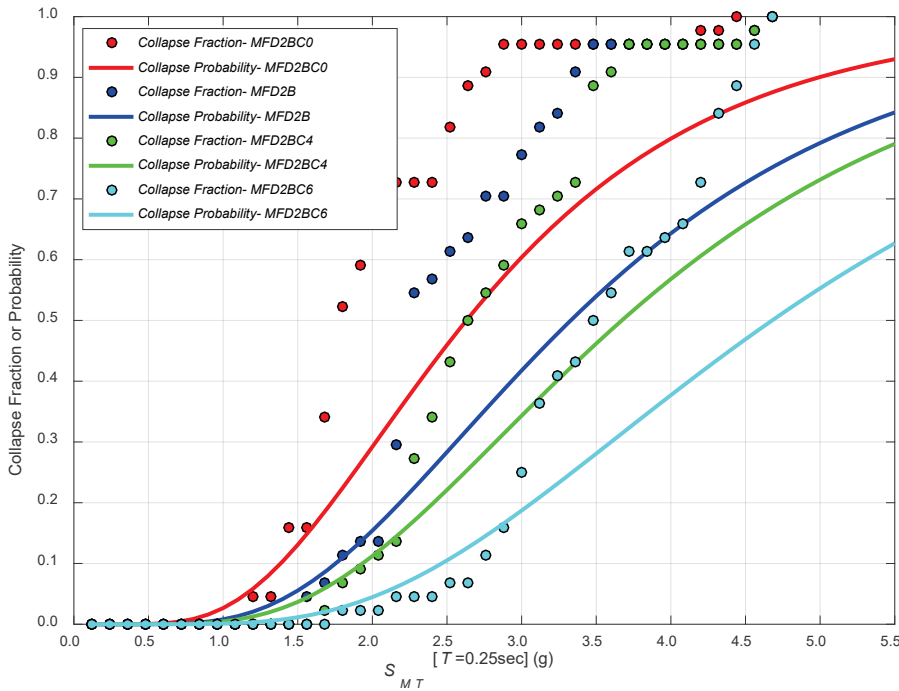


Figure 5-21 Collapse rates from IDA and FEMA P-695 collapse fragility curves for two-story multi-family dwelling archetype models in collapse displacement capacity studies.

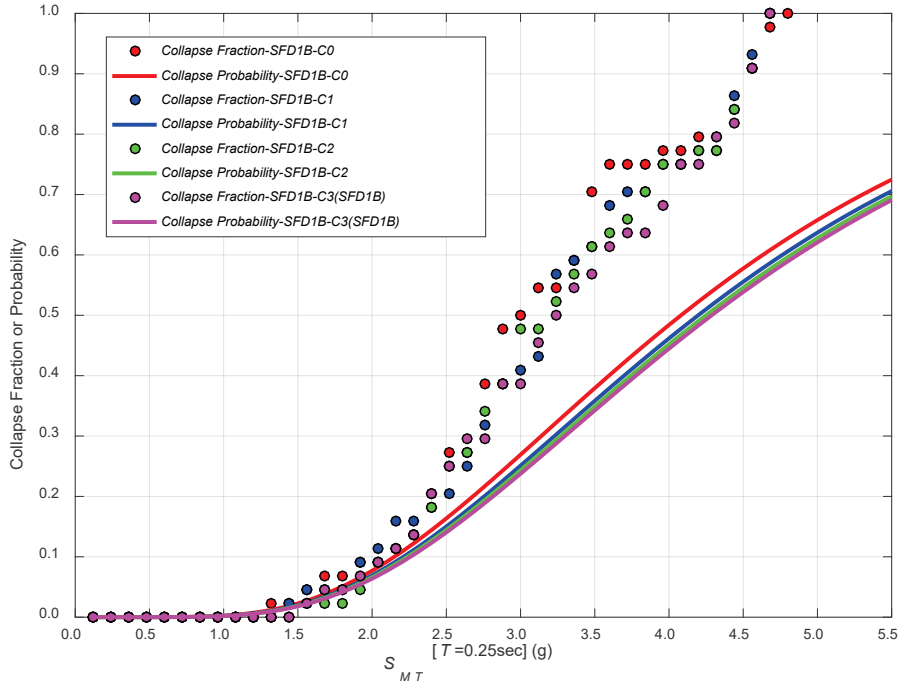


Figure 5-22 Collapse rates from IDA and FEMA P-695 collapse fragility curves for one-story single-family dwelling archetype models in collapse displacement capacity studies.

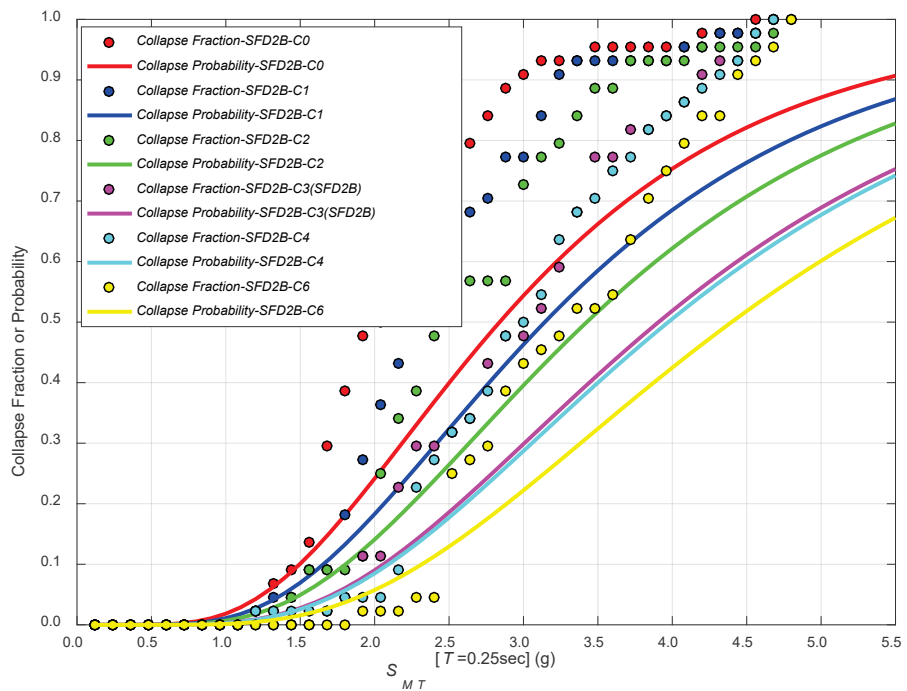


Figure 5-23 Collapse rates from IDA and FEMA P-695 collapse fragility curves for two-story single-family dwelling archetype models in collapse displacement capacity studies.

Table 5-12 summarizes median and lognormal standard deviation values of peak roof drift ratio, peak first-story drift ratio, and corresponding response spectral acceleration at incipient collapse. Values at incipient collapse are extracted from data corresponding to the last survival intensity for individual ground motions. Roof and first-story drift ratios at incipient collapse increase, and the median spectral acceleration at incipient collapse increases, as the residual post-capping strength ratio increases.

Table 5-13 summarizes raw collapse statistics and mean peak first-story drift ratios for each archetype for ground motions scaled to MCE_R and $0.5 \times MCE_R$ intensity levels. No collapses were observed at the $0.5 \times MCE_R$ intensity level. For baseline archetypes with relatively high collapse rates (e.g., COM1B and COM2B archetypes), the number of collapses at the MCE_R intensity level decreases as the residual post-capping strength ratio increases. For baseline archetypes with relatively high peak strength ratios (V_{max}/W) (e.g., SFD1B and MFD1B), the collapse rates at the MCE_R level are not significantly affected by changes in the residual post-capping strength ratio.

Table 5-11 Pushover and Collapse Analysis Results for Archetype Models Used to Investigate Collapse Displacement Capacity

Archetype ID	Pushover Analysis *			Collapse Analysis				
	V_{\max} / W	Ω	μ_T	S_{CT} (g)	CMR _{3D}	SSF	ACMR	P[C] MCE _R]
Commercial Buildings: High Seismic								
COM1B-C0	0.51	3.32	>8	2.56	1.28	1.33	1.71	14.2%
COM1B-C1	0.53	3.42	>8	2.71	1.36	1.33	1.81	11.9%
COM1B-C2	0.54	3.53	>8	2.88	1.44	1.33	1.92	9.7%
COM1B	0.56	3.64	>8	3.10	1.55	1.33	2.07	7.3%
COM2B-C0	0.44	2.84	>8	2.17	1.09	1.33	1.45	22.9%
COM2B	0.48	3.13	>8	2.61	1.31	1.33	1.74	13.4%
COM2B-C4	0.50	3.22	>8	2.74	1.37	1.33	1.83	11.4%
COM2B-C6	0.52	3.36	>8	3.40	1.71	1.33	2.27	5.1%
Multi-Family Dwellings: High Seismic								
MFD1B-C0	1.20	7.78	>8	4.04	2.02	1.33	2.69	2.4%
MFD1B-C1	1.24	8.02	>8	4.54	2.28	1.33	3.03	1.3%
MFD1B-C2	1.27	8.23	>8	4.83	2.42	1.33	3.22	1.0%
MFD1B	1.30	8.47	>8	4.84	2.43	1.33	3.23	1.0%
MFD2B-C0	0.63	4.06	>8	2.63	1.32	1.33	1.75	13.1%
MFD2B	0.68	4.41	>8	3.33	1.67	1.33	2.22	5.5%
MFD2B-C4	0.69	4.51	>8	3.67	1.84	1.33	2.45	3.7%
MFD2B-C6	0.73	4.71	>8	4.68	2.35	1.33	3.12	1.1%
Single-Family Dwellings: High Seismic								
SFD1B-C0	1.72	11.17	>8	4.08	2.05	1.33	2.72	2.3%
SFD1B-C1	1.77	11.51	>8	4.20	2.10	1.33	2.80	2.0%
SFD1B-C2	1.82	11.82	>8	4.25	2.13	1.33	2.83	1.9%
SFD1B	1.86	12.10	>8	4.29	2.15	1.33	2.86	1.8%
SFD2B-C0	0.70	4.57	>8	2.84	1.42	1.33	1.89	10.1%
SFD2B-C1	0.73	4.73	>8	3.14	1.58	1.33	2.10	7.0%
SFD2B-C2	0.75	4.88	>8	3.43	1.72	1.33	2.28	4.9%
SFD2B	0.77	5.00	>8	3.97	1.99	1.33	2.65	2.6%
SFD2B-C4	0.79	5.13	>8	3.91	1.96	1.33	2.60	2.8%
SFD2B-C6	0.82	5.36	>8	4.40	2.20	1.33	2.93	1.6%

* Pushover analysis results represent average response in the North-South and East-West directions.

Table 5-12 Median and Lognormal Standard Deviation Values of Peak Drift Ratio and Response Spectral Acceleration at Incipient Collapse for Archetype Models Used to Investigate Collapse Displacement Capacity

Baseline Archetype ID	Peak Drift Ratio at Incipient Collapse				Response Spectral Acceleration at Incipient Collapse S_T (g)	
	Roof		First Story			
	Median	β	Median	β	Median	β
Commercial Buildings: High Seismic						
COM1B-C0	0.051	0.21	0.051	0.21	1.61	0.29
COM1B-C1	0.059	0.21	0.059	0.21	1.70	0.28
COM1B-C2	0.067	0.25	0.067	0.25	1.80	0.28
COM1B	0.082	0.29	0.082	0.29	1.94	0.27
COM2B-C0	0.024	0.20	0.046	0.23	1.36	0.27
COM2B	0.035	0.33	0.067	0.35	1.64	0.26
COM2B-C4	0.044	0.40	0.084	0.43	1.72	0.26
COM2B-C6	0.072	0.43	0.142	0.46	2.13	0.26
Multi-Family Dwellings: High Seismic						
MFD1B-C0	0.045	0.62	0.045	0.62	2.53	0.27
MFD1B-C1	0.067	0.76	0.067	0.76	2.85	0.24
MFD1B-C2	0.075	0.82	0.075	0.82	3.02	0.22
MFD1B	0.071	0.88	0.071	0.88	3.03	0.19
MFD2B-C0	0.026	0.17	0.050	0.19	1.66	0.28
MFD2B	0.046	0.35	0.090	0.37	2.09	0.25
MFD2B-C4	0.065	0.48	0.128	0.50	2.30	0.24
MFD2B-C6	0.095	0.47	0.187	0.50	2.93	0.22
Single-Family Dwellings: High Seismic						
SFD1B-C0	0.022	0.89	0.022	0.89	2.56	0.31
SFD1B-C1	0.021	0.90	0.021	0.90	2.63	0.30
SFD1B-C2	0.021	0.94	0.021	0.94	2.66	0.29
SFD1B	0.022	1.01	0.022	1.01	2.69	0.30
SFD2B-C0	0.029	0.23	0.056	0.25	1.78	0.30
SFD2B-C1	0.030	0.24	0.030	0.24	1.97	0.29
SFD2B-C2	0.041	0.39	0.041	0.39	2.15	0.30
SFD2B	0.058	0.41	0.117	0.38	2.49	0.28
SFD2B-C4	0.065	0.46	0.128	0.48	2.45	0.28
SFD2B-C6	0.078	0.49	0.153	0.52	2.76	0.24

Table 5-13 Collapse Rates and Mean Peak First-Story Drift Ratios at MCE_R and 50-Percent of MCE_R Ground Motion Intensities for Archetype Models Used to Investigate Collapse Displacement Capacity

Archetype ID	MCE _R Collapse Rate (out of 44)		Mean Peak First-Story Drift Ratio of Survivors (%)			
	0.5 × MCE _R	1.0 × MCE _R	0.5 × MCE _R		MCE _R	
			East-West Direction	North-South Direction	East-West Direction	North-South Direction
Commercial Buildings: High Seismic						
COM1B-C0	0	12	1.02	0.58	2.75	2.05
COM1B-C1	0	8	1.01	0.58	2.92	2.12
COM1B-C2	0	5	1.00	0.58	3.08	2.14
COM1B	0	3	1.00	0.58	3.06	2.22
COM2B-C0	0	23	1.22	1.02	2.52	2.28
COM2B	0	8	1.11	0.84	3.27	2.82
COM2B-C4	0	7	1.19	0.99	3.44	3.06
COM2B-C6	0	2	1.14	0.96	3.32	2.74
Multi-Family Dwellings: High Seismic						
MFD1B-C0	0	0	0.23	0.20	0.77	0.62
MFD1B-C1	0	0	0.23	0.20	0.75	0.62
MFD1B-C2	0	0	0.23	0.20	0.74	0.62
MFD1B	0	0	0.23	0.21	0.72	0.66
MFD2B-C0	0	7	0.67	0.75	2.24	2.44
MFD2B	0	1	0.63	0.69	2.21	2.37
MFD2B-C4	0	0	0.67	0.74	2.18	2.12
MFD2B-C6	0	0	0.67	0.73	2.15	2.22
Single-Family Dwellings: High Seismic						
SFD1B-C0	0	2	0.19	0.11	0.53	0.29
SFD1B-C1	0	2	0.19	0.11	0.48	0.29
SFD1B-C2	0	1	0.19	0.11	0.51	0.29
SFD1B	0	1	0.19	0.11	0.52	0.32
SFD2B-C0	0	5	0.81	0.49	2.75	1.64
SFD2B-C1	0	3	0.56	0.34	2.26	1.49
SFD2B-C2	0	3	0.56	0.34	2.15	1.40
SFD2B	0	1	0.56	0.36	2.41	1.39
SFD2B-C4	0	0	0.77	0.48	2.64	1.57
SFD2B-C6	0	0	0.77	0.48	2.42	1.51

5.3.3 Interpretation of Results

The results presented in Table 5-11 and shown in Figure 5-18 through Figure 5-23 show that the MCE_R collapse probability decreases with an increase in residual post-capping strength ratio (and displacement capacity).

Example IDA curves are shown in Figure 5-24 for a two-story single-family dwelling archetype with zero residual strength (SFD2B-C0) and the baseline two-story single-family dwelling archetype with 30% residual strength (SFD2B). Also shown in the figure are the distributions of peak first-story drift and spectral acceleration at incipient collapse. The archetype with zero residual strength (SFD2B-C0) has a very low median drift at incipient collapse (5.64 percent), with all 44 ground motions causing collapse at a peak story drift of less than 9 percent. In contrast, the baseline archetype with 30 percent residual strength (SFD2B) has a median drift at incipient collapse of 11.74 percent, which more closely matches collapse drifts observed in full shake table tests (Isoda et al., 2008).

Figure 5-25 shows the relationship between median drift at incipient collapse and residual strength ratio. Except for the one-story single-family dwelling archetype, which is very strong (i.e., V_{max} / W greater than the $MCE_R S_T$ of 1.5g), the displacement capacity of all other archetypes is proportional to the residual strength ratio. Further, the median first-story drift at incipient collapse for all COM and MFD archetypes with residual post-capping strength ratios of 30 percent, or higher, ranged from about 7 percent to 19 percent. These levels of median collapse drift are more closely aligned with collapse drifts observed in shake table tests (Isoda et al., 2008).

Figure 5-26 shows the trends between MCE_R collapse probability and residual strength ratio. The inverse relationship (negative correlation) between MCE_R collapse probability and residual strength is seen in each of the three occupancy types (i.e., COM, MFD, and SFD). For the one-story single-family dwelling (SFD1B) and one-story multi-family dwelling (MFD1B) archetype models, which are very strong (i.e., high V_{max} / W ratios), MCE_R collapse probabilities remain nearly constant regardless of the residual strength ratio.

Figure 5-27 shows the relationship between MCE_R collapse probability and the median first-story drift at incipient collapse. Prior FEMA P-695 studies assumed collapse occurred at a displacement corresponding to 7 percent of story height. The relatively large displacement capacities (more than 10 to 15 percent story drift) observed in many full-scale wood light-frame building shake table tests (Isoda et al., 2008), have shown that this assumption is overly conservative.

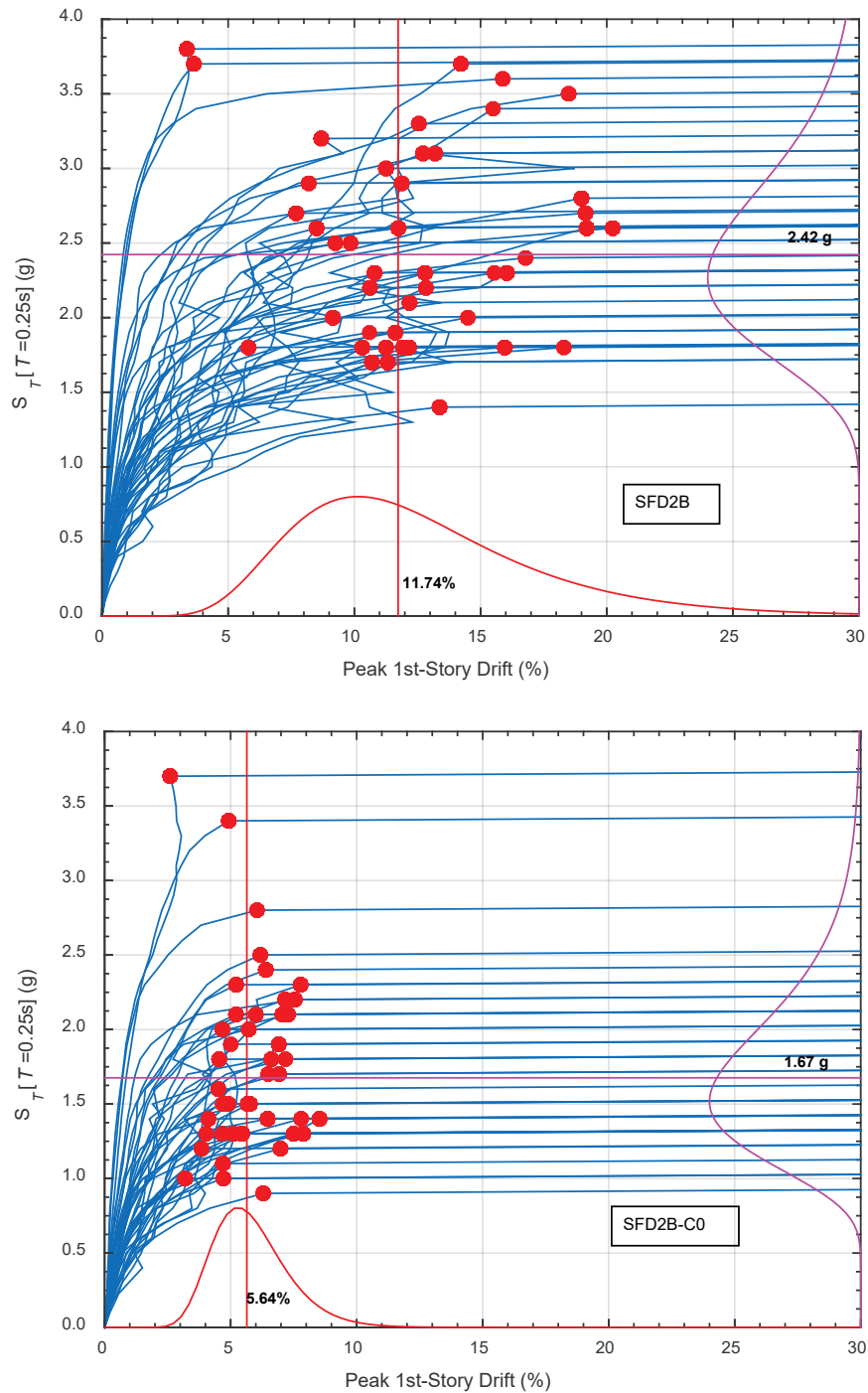


Figure 5-24 IDA curves and incipient collapse points for two-story single-family wood light-frame building archetype models: 30 percent residual strength (top); and 0 percent residual strength (bottom).

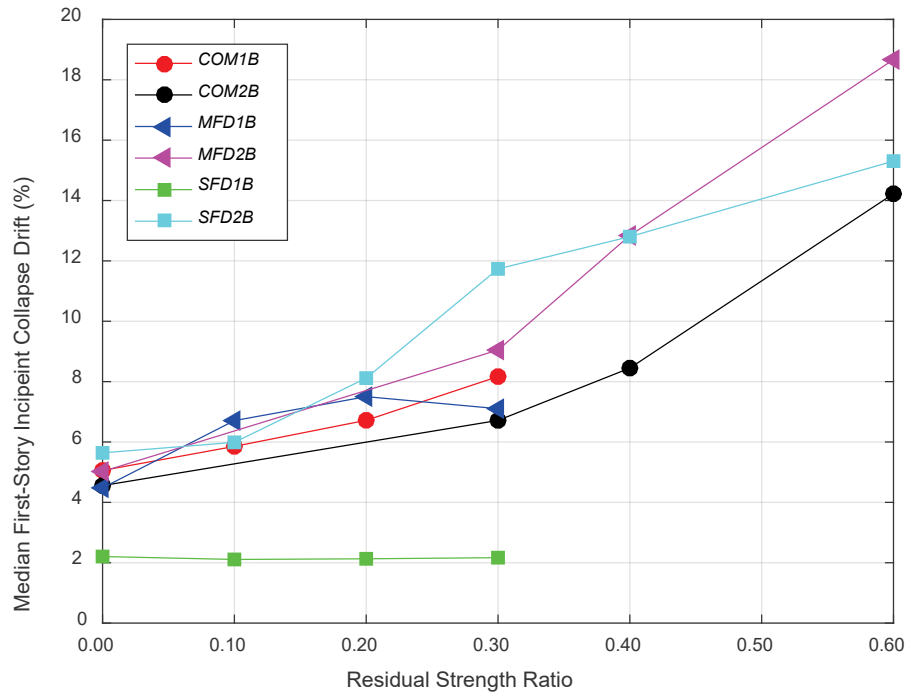


Figure 5-25 Median first-story drift at incipient collapse versus residual strength ratio for archetype models used in collapse displacement capacity studies.

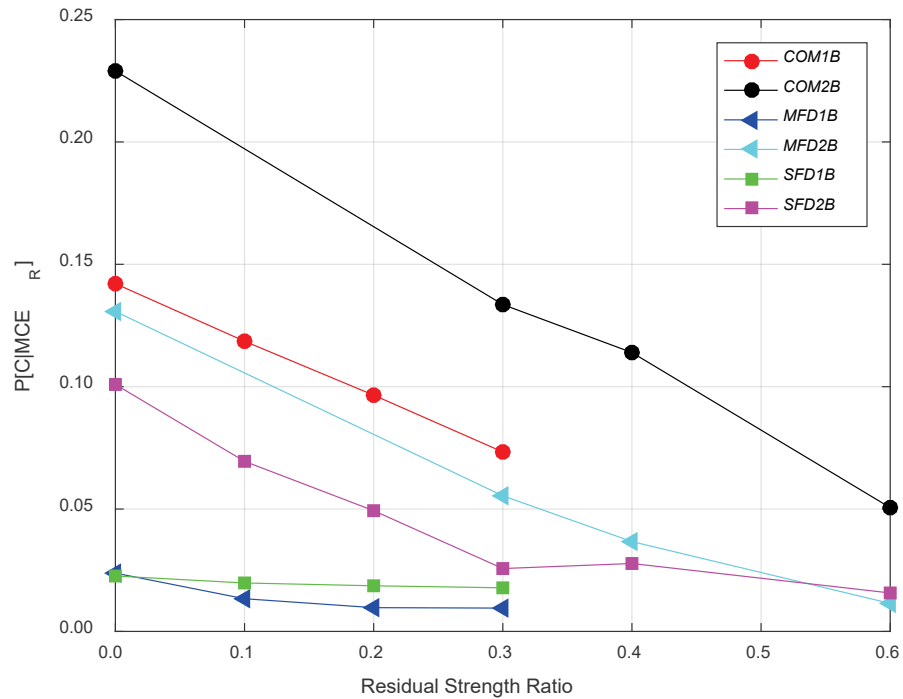


Figure 5-26 MCE_R collapse probability versus residual strength ratio for archetype models used in collapse displacement capacity studies.

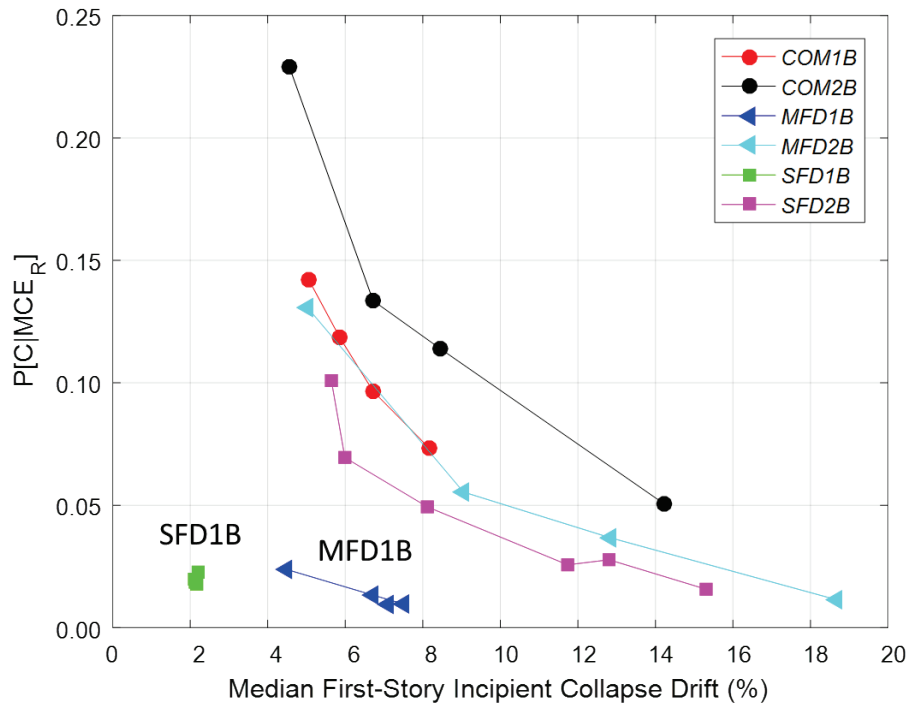


Figure 5-27 MCE_R collapse probability versus median first-story drift at incipient collapse for archetype models used in collapse displacement capacity studies.

The collective information presented in Figure 5-25 to Figure 5-27 demonstrates that peak strength ratio (V_{\max} / W) and collapse displacement capacity (or residual strength) are key parameters determining the collapse performance of wood light-frame buildings in earthquakes.

5.4 Nonstructural Interior and Exterior Wall Finishes Parametric Study

Nonstructural interior and exterior wall finish studies investigated the effects of wall finishes on response behavior and collapse performance. Wall finishes such as gypsum wallboard, stucco, and horizontal wood siding are considered to be nonstructural, and are typically not considered in the design of the seismic force-resisting system. However, full-scale wood light-frame building shake table tests (e.g., Christovasilis et al., 2007; van de Lindt et al., 2012) have shown that nonstructural wall finishes can significantly influence response and behavior. In this study, archetypes were modified to remove all nonstructural interior and exterior wall finishes, and were compared to the results of corresponding baseline archetype models including wall finishes.

5.4.1 Nonstructural Interior and Exterior Wall Finish Archetypes and Variants

Table 5-14 summarizes key properties and structural design criteria for the COM, MFD, and SFD archetypes used in nonstructural interior and exterior wall finish studies. Seven baseline archetype models (COM2B, COM3B, MFD2B, SFD1B, SFD1BC, SFD2B, and SFD2BC) were modified by removing nonstructural interior and exterior wall finishes from the models, designated by “NS” in the table.

Table 5-14 Commercial Building, Multi-Family Dwelling, and Single-Family Dwelling Archetype Models Used to Investigate Nonstructural Interior and Exterior Wall Finishes

Baseline Archetype Model ID	No. of Stories	W (kips)	Key Archetype Modeling and Design Criteria				
			Inclusion of Nonstructural Walls	Design Criteria			S_{MT}/T (g)
				R	T (sec)	C _s	
Commercial Buildings: High Seismic							
COM2B	2	488	Yes	6.5	0.26	0.154	1.5
COM2B-NS	2	488	No	6.5	0.26	0.154	1.5
COM3B	4	1106	Yes	6.5	0.26	0.154	1.5
COM3B-NS	4	1106	No	6.5	0.26	0.154	1.5
Multi-Family Dwellings: High Seismic							
MFD2B	2	363	Yes	6.5	0.26	0.154	1.5
MFD2B-NS	2	363	No	6.5	0.26	0.154	1.5
Single-Family Dwellings: High Seismic							
SFD1B	1	52	Yes	6.5	0.25	0.154	1.5
SFD1B-NS	1	52	No	6.5	0.25	0.154	1.5
SFD1B-NSP	1	52	Yes + Wood Siding	6.5	0.25	0.154	1.5
SFD1BC	1	52	Yes	6.5	0.25	0.154	1.5
SFD1BC-NS	1	52	No	6.5	0.25	0.154	1.5
SFD1BC-NSP	1	52	Yes + Wood Siding	6.5	0.25	0.154	1.5
SFD2B	2	135	Yes	6.5	0.45	0.154	1.5
SFD2B-NS	2	135	No	6.5	0.45	0.154	1.5
SFD2B-NSP	2	135	Yes + Wood Siding	6.5	0.45	0.154	1.5
SFD2BC	2	135	Yes	6.5	0.45	0.154	1.5
SFD2BC-NS	2	135	No	6.5	0.45	0.154	1.5
SFD2BC-NSP	2	135	Yes + Wood Siding	6.5	0.45	0.154	1.5

In addition to variants without wall finishes, an additional variant was created for each of the four single-family dwelling archetypes by replacing the exterior stucco wall finish with horizontal wood siding while still retaining interior gypsum wallboard finishes. This variant is designated by “NSP” in the table. A total of 18 models were utilized in this study, including seven (7) baseline models, seven (7) variant models without nonstructural interior and exterior wall finishes, and four (4) single-family dwelling models with horizontal wood siding. Single-family dwelling archetypes in this study included both engineered and conventional construction archetypes (designated by “C” in the table).

5.4.2 Numerical Results

Figure 5-28 and Figure 5-29 compare the nonlinear static pushover curves of two-story commercial (COM2B) and two-story multi-family dwelling (MFD2B) archetypes, both with and without interior and exterior wall finishes. Table 5-15 summarizes selected values of free vibration (modal) analysis results (T_I) and FEMA P-795 pushover analyses.

The peak strength ratios (V_{\max} / W) of the baseline COM2B model (with wall finishes) are 0.43 and 0.53 in the E-W direction and N-S directions, respectively. Without nonstructural wall finishes, the normalized peak strength ratios are 0.24 and 0.23 in the E-W direction and N-S directions, respectively. Although these values are significantly lower than the baseline archetypes with nonstructural wall finishes, they exceed the required design base shear coefficient of 0.154. For the COM2B model, nonstructural wall finishes account for 44 percent and 57 percent of the total peak strength of the building in the transverse direction and longitudinal directions, respectively. The contribution of nonstructural wall finishes is even more visible in pushover curves for the two-story multi-family dwelling archetype (i.e., more than 62 percent contribution to total peak strength), because the MFD2B archetype has more interior partition walls.

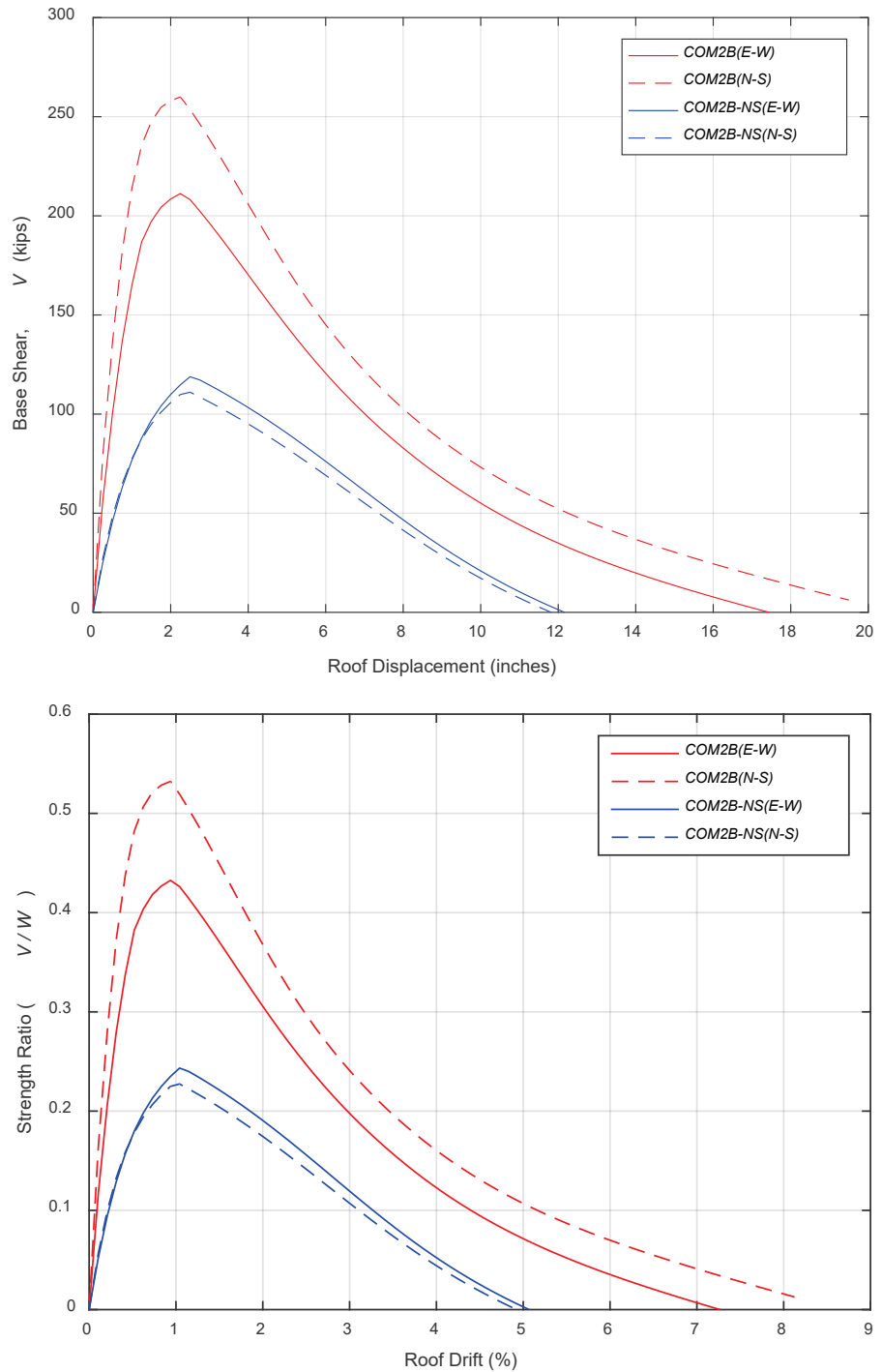


Figure 5-28 Pushover curves for two-story commercial building archetype models in nonstructural interior and exterior wall finish studies (top), and pushover curves normalized by total building seismic weight and roof height (bottom).

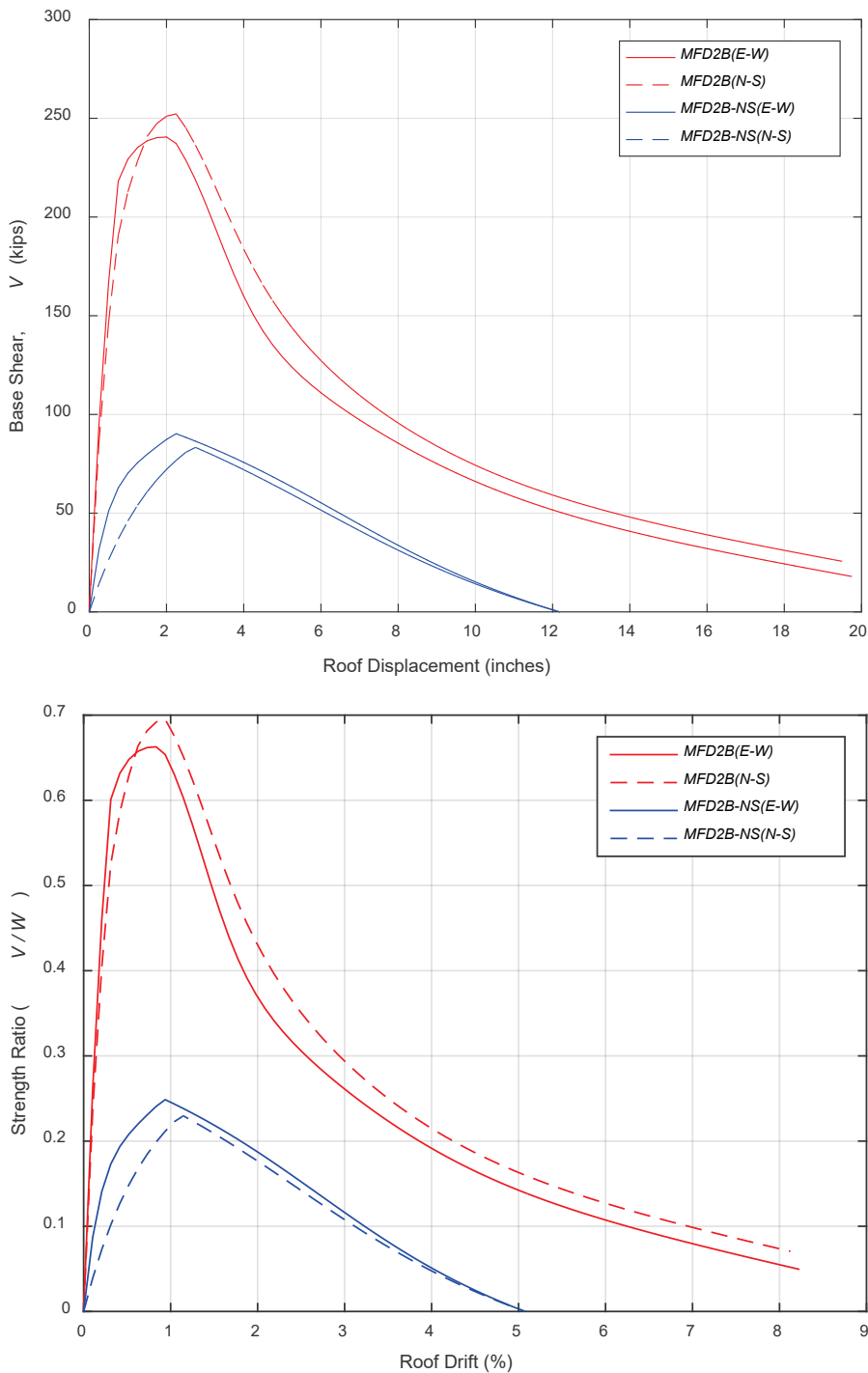


Figure 5-29 Pushover curves for two-story multi-family dwelling archetype models in nonstructural interior and exterior wall finish studies (top), and pushover curves normalized by total building seismic weight and roof height (bottom).

Table 5-15 Modal and Pushover Analysis Results for Archetype Models Used to Investigate Nonstructural Interior and Exterior Wall Finishes

Baseline Archetype ID	North-South Direction				East-West Direction			
	T_1 (sec)	V_M/W	$\Delta_{U,80}$ (in/in)	$\Delta_{U,\max}$ (in/in)	T_1 (sec)	V_M/W	$\Delta_{U,80}$ (in/in)	$\Delta_{U,\max}$ (in/in)
Commercial Buildings: High Seismic								
COM2B	0.33	0.53	0.02	0.08	0.39	0.43	0.02	0.07
COM2B-NS	0.58	0.23	0.02	0.05	0.57	0.24	0.02	0.05
COM3B	0.54	0.32	0.01	0.03	0.62	0.30	0.01	0.03
COM3B-NS	0.81	0.18	0.03	0.08	0.82	0.21	0.04	0.09
Multi-Family Dwellings: High Seismic								
MFD2B	0.27	0.70	0.02	0.08	0.29	0.66	0.02	0.08
MFD2B-NS	0.71	0.23	0.02	0.05	0.44	0.25	0.02	0.05
Single-Family Dwellings: High Seismic								
SFD1B	0.14	2.10	0.03	0.16	0.17	1.63	0.03	0.16
SFD1B-NS	0.22	0.96	0.04	0.16	0.31	0.64	0.04	0.16
SFD1B-NSP	0.19	1.51	0.04	0.16	0.20	1.18	0.03	0.16
SFD1BC	0.11	1.54	0.03	0.16	0.19	1.02	0.03	0.16
SFD1BC-NS	0.36	0.51	0.03	0.14	0.37	0.34	0.02	0.10
SFD1BC-NSP	0.34	0.56	0.03	0.16	0.36	0.37	0.03	0.14
SFD2B	0.24	0.90	0.02	0.08	0.28	0.64	0.01	0.08
SFD2B-NS	0.42	0.43	0.03	0.07	0.51	0.25	0.02	0.05
SFD2B-NSP	0.31	0.68	0.02	0.08	0.34	0.50	0.02	0.08
SFD2BC	0.21	0.96	0.02	0.08	0.29	0.56	0.02	0.08
SFD2BC-NS	0.41	0.52	0.01	0.07	0.44	0.34	0.01	0.05
SFD2BC-NSP	0.38	0.60	0.02	0.08	0.43	0.39	0.02	0.08

Nonlinear IDA results are summarized in Figure 5-30 through Figure 5-33, which present IDA collapse rates and FEMA P-695 fragility curves. In the figures, fragility curves for archetypes without nonstructural wall finishes (e.g., COM2B-NS) are located to the left of curves for baseline archetypes with nonstructural wall finishes (e.g., COM2B), which indicates that the archetypes without nonstructural wall finishes tended to collapse at lower intensities.

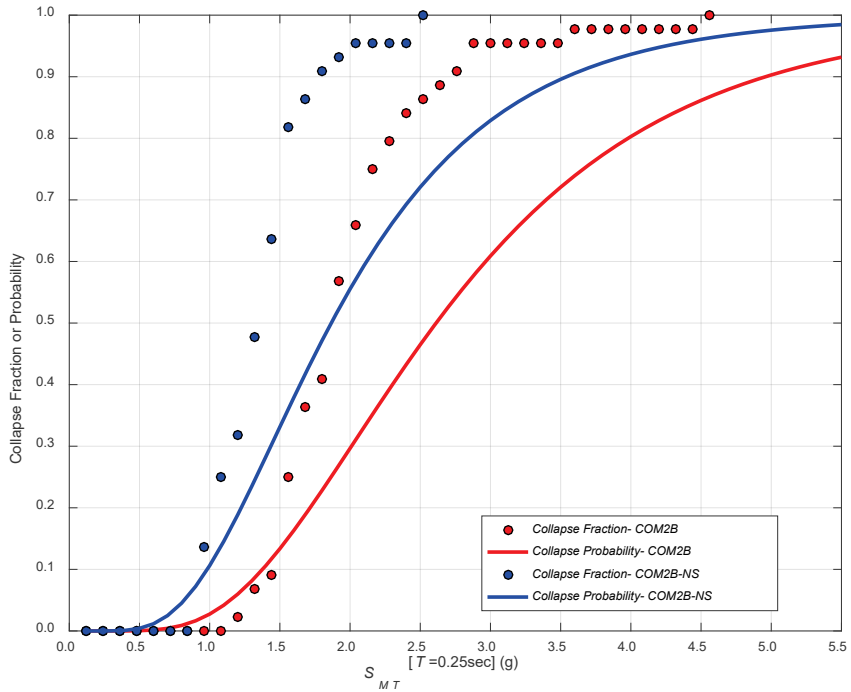


Figure 5-30 Collapse rates from IDA and FEMA P-695 collapse fragility curves for two-story commercial building archetype models in nonstructural interior and exterior wall finish studies.

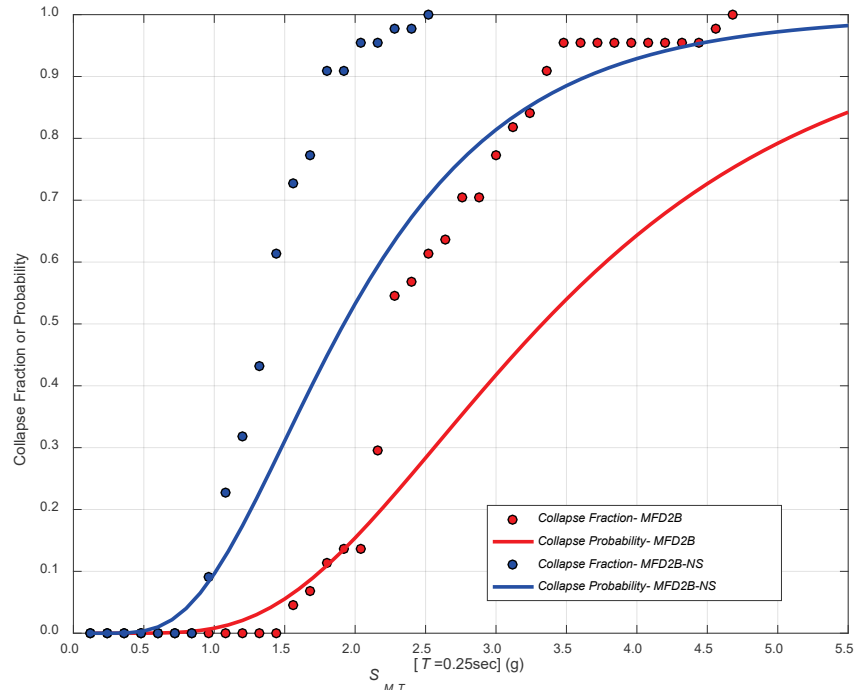


Figure 5-31 Collapse rates from IDA and FEMA P-695 collapse fragility curves for two-story multi-family dwelling archetype models in nonstructural interior and exterior wall finish studies.

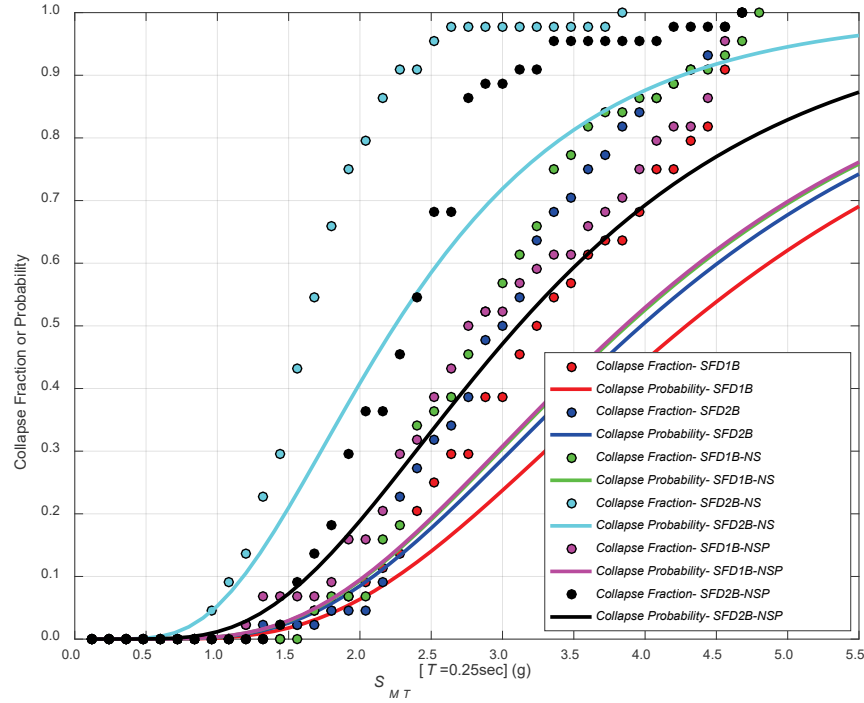


Figure 5-32 Collapse rates from IDA and FEMA P-695 collapse fragility curves for engineered one-story single-family dwelling archetype models in nonstructural interior and exterior wall finish studies.

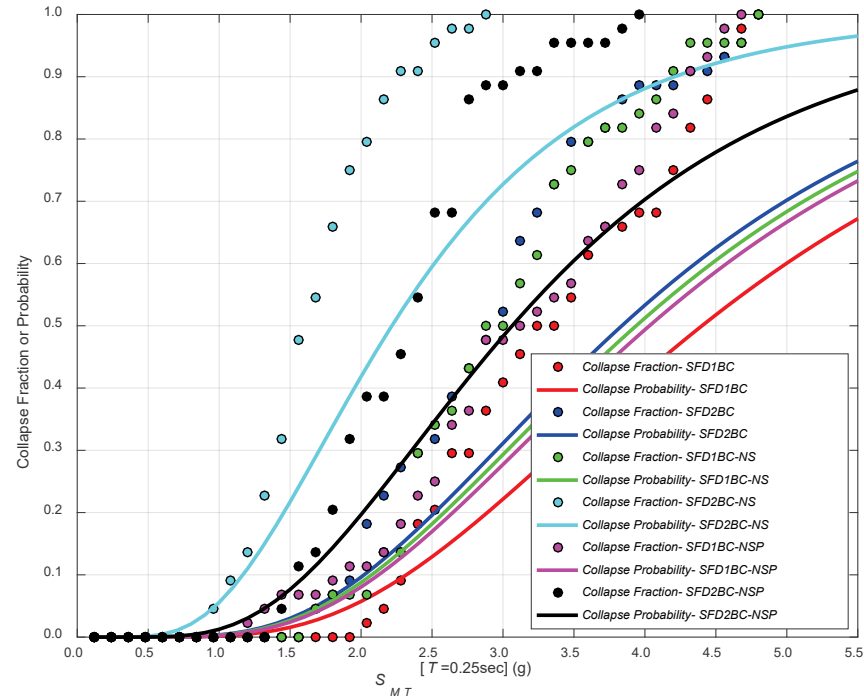


Figure 5-33 Collapse rates from IDA and FEMA P-695 collapse fragility curves for conventional construction one-story single-family dwelling archetype models in nonstructural interior and exterior wall finish studies.

Table 5-16 summarizes values of various response and collapse parameters from FEMA P-695 static pushover and nonlinear incremental dynamic collapse analyses for each archetype. Differences in MCE_R collapse probabilities between models with and without nonstructural wall finishes reported in the table are significant in all cases, but especially significant in MFD and SFD archetypes, which include more interior partition walls.

Table 5-16 Pushover and Collapse Analysis Results for Archetype Models Used to Investigate Nonstructural Interior and Exterior Wall Finishes

Archetype ID	Pushover Analysis *			Collapse Analysis				
	V_{\max} / W	Ω	μ_r	S_{CT} (g)	CMR _{3D}	SSF	ACMR	P[C MCE _R]
Commercial Buildings: High Seismic								
COM2B	0.48	3.13	>8	2.61	1.31	1.33	1.74	13.4%
COM2B-NS	0.24	1.53	>8	1.87	0.92	1.35	1.24	33.1%
COM3B	0.31	2.00	>8	2.33	1.15	1.35	1.55	19.0%
COM3B-NS	0.20	1.29	>8	2.18	1.03	1.41	1.45	22.7%
Multi-Family Dwellings: High Seismic								
MFD2B	0.68	4.41	>8	3.33	1.67	1.33	2.22	5.5%
MFD2B-NS	0.24	1.55	>8	1.92	0.94	1.36	1.28	31.1%
Single-Family Dwellings: High Seismic								
SFD1B	1.86	12.10	>8	4.29	2.15	1.33	2.86	1.8%
SFD1B-NS	0.80	5.18	>8	3.87	1.94	1.33	2.58	2.9%
SFD1B-NSP	1.34	8.73	>8	3.86	1.93	1.33	2.57	2.9%
SFD1BC	1.28	8.31	>8	4.40	2.21	1.33	2.93	1.6%
SFD1BC-NS	0.42	2.73	>8	2.22	1.11	1.33	1.48	21.6%
SFD1BC-NSP	0.46	3.02	>8	4.00	2.01	1.33	2.67	2.5%
SFD2B	0.77	5.00	>8	3.97	1.99	1.33	2.65	2.6%
SFD2B-NS	0.34	2.22	>8	2.25	1.12	1.33	1.50	21.0%
SFD2B-NSP	0.59	3.82	>8	3.11	1.56	1.33	2.07	7.2%
SFD2BC	0.76	4.93	>8	3.84	1.92	1.33	2.56	3.0%
SFD2BC-NS	0.43	2.79	>8	2.22	1.11	1.33	1.48	21.7%
SFD2BC-NSP	0.49	3.21	>8	3.06	1.54	1.33	2.04	7.7%

* Pushover analysis results represent average response in the North-South and East-West directions.

Table 5-17 summarizes median and lognormal standard deviation values of peak roof drift ratio, peak first-story drift ratio, and corresponding response spectral acceleration at incipient collapse. Roof and first-story drift ratios, and the median spectral acceleration at incipient collapse, decrease in all

cases without nonstructural wall finishes when compared to baseline archetypes with nonstructural wall finishes.

Table 5-17 Median and Lognormal Standard Deviation Values of Peak Drift Ratio and Response Spectral Acceleration at Incipient Collapse for Archetype Models Used to Investigate Nonstructural Interior and Exterior Wall Finishes

Archetype ID	Peak Drift Ratio at Incipient Collapse				Response Spectral Acceleration at Incipient Collapse S_T (g)	
	Roof		First Story		Median	β
	Median	β	Median	β		
Commercial Buildings: High Seismic						
COM2B	0.035	0.33	0.067	0.35	1.64	0.26
COM2B-NS	0.028	0.18	0.047	0.25	1.15	0.24
COM3B	0.016	0.18	0.046	0.29	1.43	0.23
COM3B-NS	0.019	0.21	0.047	0.26	1.28	0.25
Multi-Family Dwellings: High Seismic						
MFD2B	0.046	0.35	0.090	0.37	2.09	0.25
MFD2B-NS	0.029	0.17	0.047	0.25	1.18	0.24
Single-Family Dwellings: High Seismic						
SFD1B	0.022	1.01	0.022	1.01	2.69	0.30
SFD1B-NS	0.090	0.30	0.090	0.30	2.43	0.27
SFD1B-NSP	0.032	0.92	0.032	0.92	2.42	0.37
SFD1BC	0.066	0.68	0.066	0.68	2.76	0.26
SFD1BC-NS	0.084	0.34	0.084	0.34	1.39	0.23
SFD1BC-NSP	0.035	1.01	0.035	1.01	2.53	0.34
SFD2B	0.058	0.41	0.117	0.38	2.49	0.28
SFD2B-NS	0.030	0.25	0.056	0.27	1.41	0.28
SFD2B-NSP	0.041	0.38	0.088	0.35	1.95	0.26
SFD2BC	0.049	0.43	0.096	0.45	2.40	0.28
SFD2BC-NS	0.025	0.27	0.046	0.31	1.39	0.26
SFD2BC-NSP	0.035	0.41	0.075	0.40	1.92	0.25

Table 5-18 summarizes raw collapse statistics and mean peak first-story drift ratios for each archetype at ground motions scaled to MCE_R and 0.5 × MCE_R intensity levels. No collapses were observed at the 0.5 × MCE_R intensity level. In general, collapse rates at the MCE_R intensity level significantly increase for archetypes without nonstructural wall finishes when compared to baseline archetypes with nonstructural wall finishes.

Table 5-18 Collapse Rates and Mean Peak First-Story Drift Ratios at MCE_R and 50-Percent of MCE_R Ground Motion Intensities for Archetype Models Used to Investigate Nonstructural Interior and Exterior Wall Finishes

Archetype ID	MCE _R Collapse Rate (out of 44)		Mean Peak First-Story Drift Ratio of Survivors (%)			
	0.5 × MCE _R	1.0 × MCE _R	0.5 × MCE _R		MCE _R	
			East-West Direction	North-South Direction	East-West Direction	North-South Direction
Commercial Buildings: High Seismic						
COM2B	0	8	1.11	0.84	3.27	2.82
COM2B-NS	0	32	1.40	1.46	3.23	2.74
COM3B	0	14	0.82	0.84	2.39	2.48
COM3B-NS	0	21	1.26	1.41	3.50	3.42
Multi-Family Dwellings: High Seismic						
MFD2B	0	1	0.63	0.69	2.21	2.37
MFD2B-NS	0	30	1.28	1.60	3.82	2.79
Single-Family Dwellings: High Seismic						
SFD1B	0	1	0.19	0.11	0.52	0.32
SFD1B-NS	0	0	0.79	0.36	2.41	1.27
SFD1B-NSP	0	3	0.30	0.24	0.87	0.56
SFD1BC	0	0	0.28	0.10	1.18	0.47
SFD1BC-NS	0	17	1.04	0.84	2.42	2.43
SFD1BC-NSP	0	3	0.27	0.22	0.78	0.51
SFD2B	0	1	0.56	0.36	2.41	1.39
SFD2B-NS	0	16	1.46	1.01	3.35	2.94
SFD2B-NSP	0	3	0.84	0.61	3.05	2.12
SFD2BC	0	0	0.63	0.27	2.46	1.00
SFD2BC-NS	0	18	1.25	0.87	2.75	2.37
SFD2BC-NSP	0	4	0.74	0.53	2.63	1.83

5.4.3 Interpretation of Results

The results presented in Tables 5-15 through 5-18, and shown in Figures 5-28 through 5-33, show that nonstructural interior and exterior wall finishes significantly influence the stiffness and strength of wood light-frame archetypes, and have a significant impact on response behavior and collapse performance.

In Table 5-15, the fundamental periods of archetypes without nonstructural wall finishes are almost double those of baseline archetypes with nonstructural wall finishes. Figure 5-28 and Figure 5-29 show that the peak strength ratio V_{max} / W is reduced by 50 percent or more when the contributions of nonstructural wall finishes are ignored.

Results presented in Table 5-16 and plotted in Figure 5-34 summarize MCE_R collapse probabilities for all archetypes considered in nonstructural interior and exterior wall finish studies. As shown in the figure, MCE_R collapse probabilities increase significantly when nonstructural wall finishes are removed (hollow markers). The effect is especially pronounced in commercial building, multi-family dwelling, and two-story single-family dwelling archetypes, and is less pronounced in single-family dwelling archetypes with relatively low seismic weights.

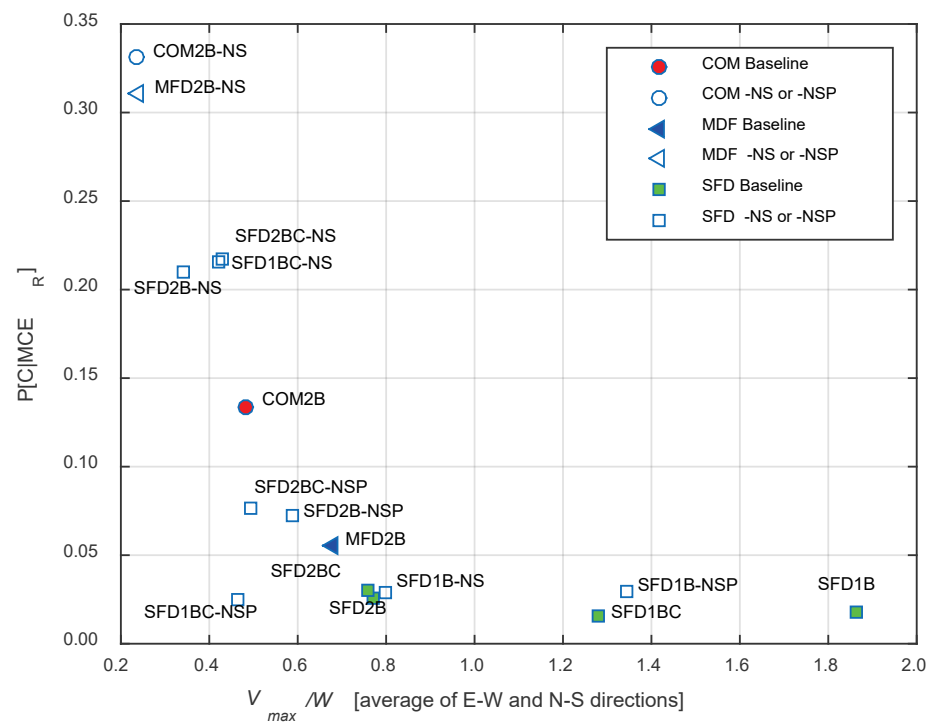


Figure 5-34 MCE_R collapse probability versus peak strength ratio (V_{max} / W) for archetype models used in nonstructural interior and exterior wall finish studies.

5.5 Soil-Structure Interaction and Foundation Flexibility Parametric Study

Soil-structure interaction (SSI) and foundation flexibility studies investigated the effects of non-rigid foundations on response behavior and collapse performance. SSI effects on wood light-frame archetypes were expected to be minimal. In this study, archetypes were modified to include

nonlinear soil springs representing two different site conditions (i.e., stiff and soft soil sites), and were compared to the results of corresponding baseline archetype models with rigid foundations.

5.5.1 Soil-Structure Interaction and Foundation Flexibility Archetypes and Variants

Table 5-19 summarizes key design properties, including shear-wave velocity, for COM and MFD archetypes used in SSI and foundation flexibility studies. Six high seismic archetypes (COM1B, COM2B, COM3B, MFD1B, MFD2B, and MFD3B) were each modified to include nonlinear soil springs for both soft (DE) and stiff (CD) soil sites. A total of 12 archetype variants were considered.

Table 5-19 Commercial Building and Multi-Family Dwelling Archetype Models Used to Investigate SSI and Foundation Flexibility

Archetype ID	No. of Stories	W (kips)	Key Archetype Design Criteria				
			Seismic Design Criteria			$S_{MI}[T]$ (g)	
			R	v_{s30} (ft/sec)	T (sec)	C_s	
Commercial Buildings: High Seismic							
COM1B	1	180	6.5	-	0.25	0.154	1.5
COM1B-F-DE	1	180	6.5	590	0.25	0.154	1.5
COM1B-F-CD	1	180	6.5	1180	0.25	0.154	1.5
COM2B	2	488	6.5	-	0.26	0.154	1.5
COM2B-F-DE	2	488	6.5	590	0.26	0.154	1.5
COM2B-F-CD	2	488	6.5	1180	0.26	0.154	1.5
COM3B	4	1106	6.5	-	0.45	0.154	1.5
COM3B-F-DE	4	1106	6.5	590	0.45	0.154	1.5
COM3B-F-CD	4	1106	6.5	1180	0.45	0.154	1.5
Multi-Family Dwellings: High Seismic							
MFD1B	1	141	6.5	-	0.25	0.154	1.5
MFD1B-F-DE	1	141	6.5	590	0.25	0.154	1.5
MFD1B-F-CD	1	141	6.5	1180	0.25	0.154	1.5
MFD2B	2	363	6.5	-	0.26	0.154	1.5
MFD2B-F-DE	2	363	6.5	590	0.26	0.154	1.5
MFD2B-F-CD	2	363	6.5	1180	0.26	0.154	1.5
MFD3B	4	971	6.5	-	0.45	0.154	1.5
MFD3B-F-DE	4	971	6.5	590	0.45	0.154	1.5
MFD3B-F-CD	4	971	6.5	1180	0.45	0.154	1.5

Because SSI and foundation flexibility effects were expected to be more significant in larger, heavier structures, SFD archetypes were excluded from consideration. To achieve convergence and numerical stability in incremental dynamic analyses, a 0.1 percent damping ratio was used in all models, as discussed in Section 4.6.1, resulting in values for baseline archetypes in this parametric study that are different from results for baseline archetypes reported elsewhere in this chapter.

5.5.2 Numerical Results

Figure 5-35 and Figure 5-36 compare the nonlinear static pushover curves of commercial (COM) and multi-family dwelling (MFD) archetypes, both with and without nonlinear soil springs. Table 5-20 summarizes selected values of free vibration (modal) analysis results (T_1) and FEMA P-795 pushover analyses.

For the COM archetypes shown in Figure 5-35, the pushover curves for each variant at the same building height are nearly identical. Thus, there appears to be only three pairs of identifiable lines: four-story models (top pair in top figure and bottom pair in lower figure), two-story models (central pair in both figures), and one-story models (bottom pair in upper figure and top pair in bottom figure). The pushover curves for MFD archetypes shown in Figure 5-36 exhibit a similar pattern.

Modal analysis results in Table 5-20 show that the fundamental periods for models with and without nonlinear soil springs are nearly identical, and the effects associated with period lengthening due to foundation flexibility are modest, even on a soft soil site. Similarly, the inclusion of nonlinear soil springs has little effect on the overall dynamic response of wood light-frame buildings. This was attributed to the high unit stiffness of soil springs (e.g., 27.7 kips/inch/foot for a soft soil site, from Table 4-17) in comparison with the unit stiffness of wood shear walls (e.g., 2 kips/inch/foot for OSB-High, 4-foot width, from Table 4-6).

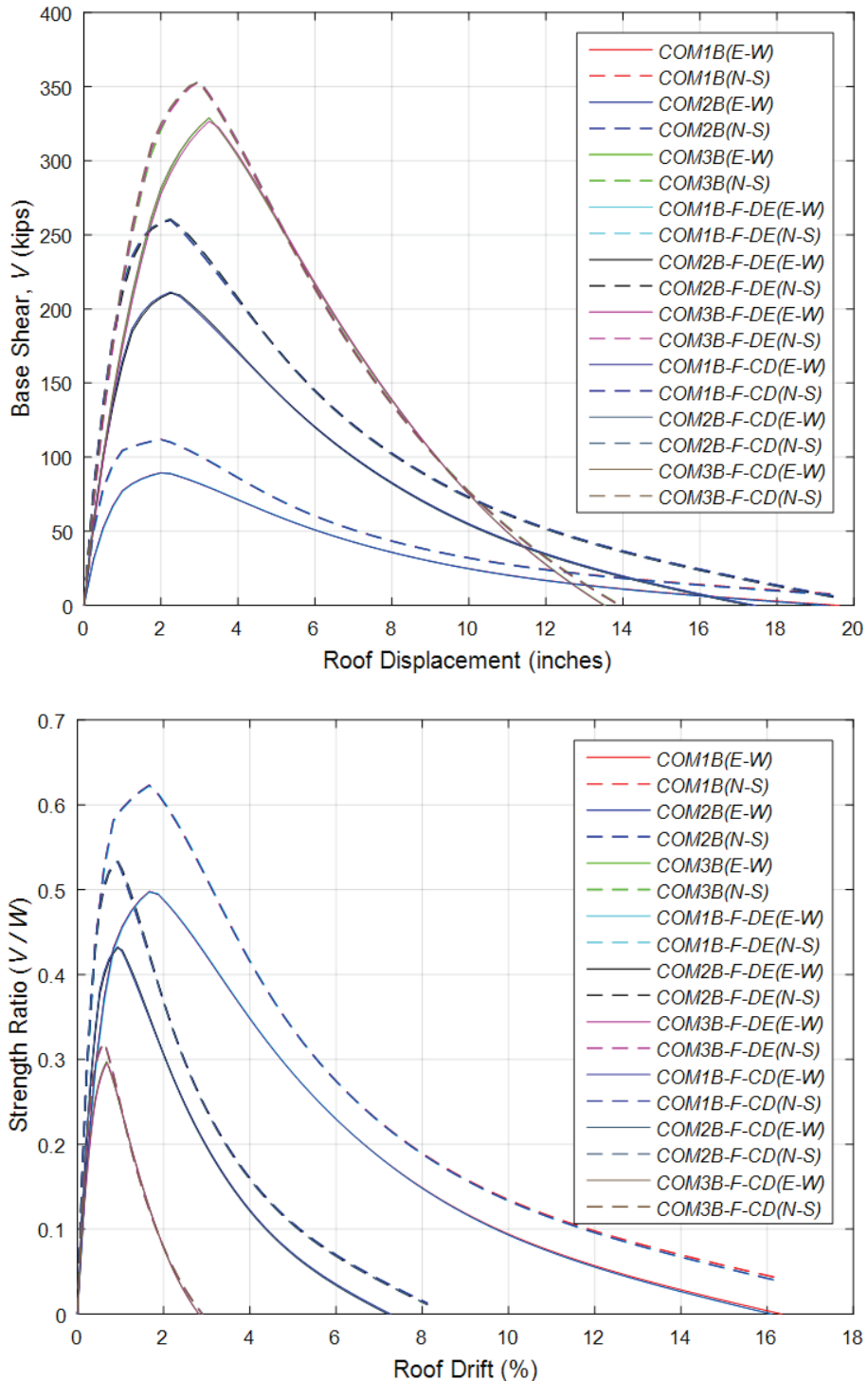


Figure 5-35 Pushover curves for commercial building archetypes in SSI and foundation flexibility studies (top), and pushover curves normalized by total building seismic weight and roof height (bottom).

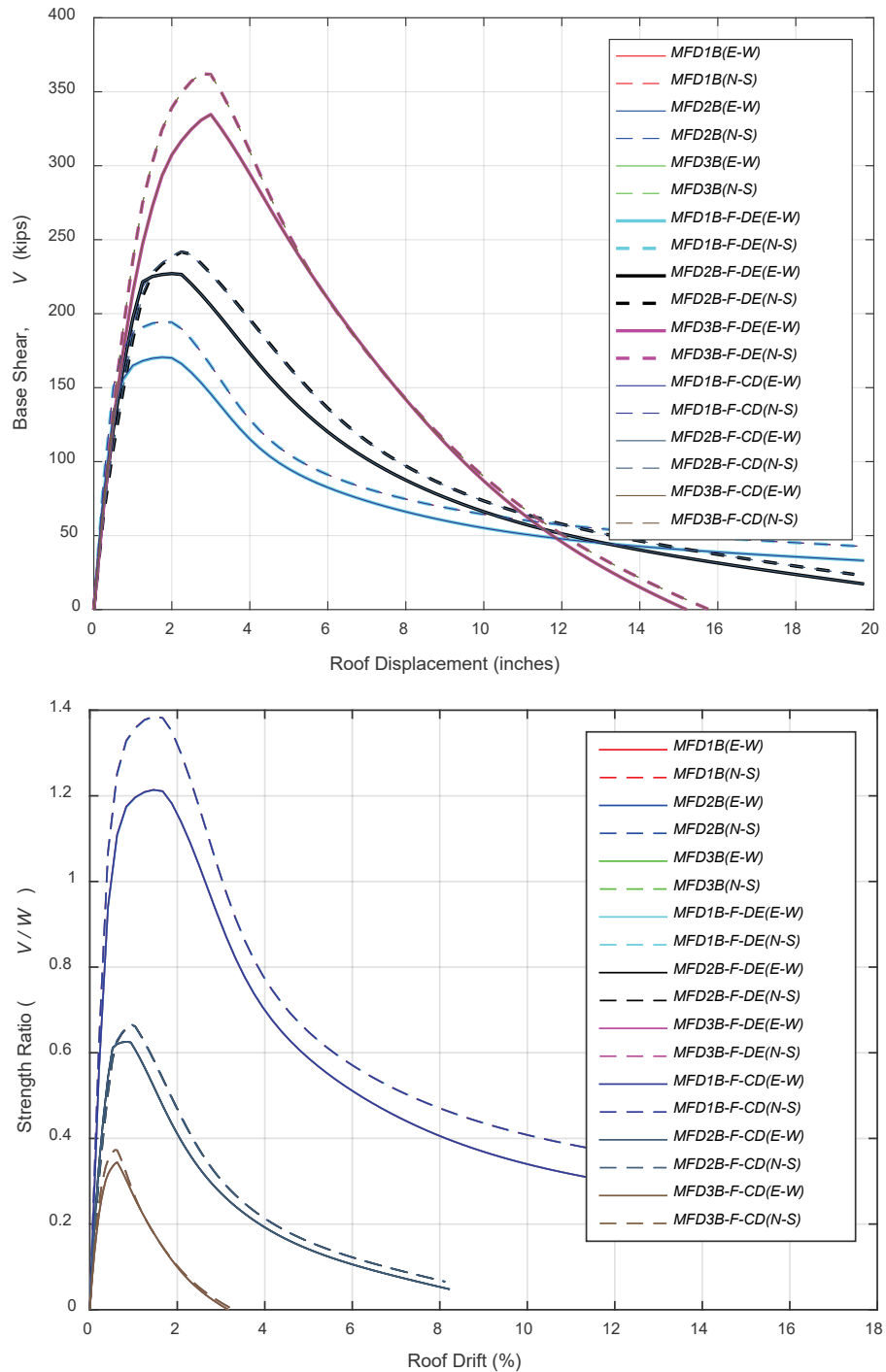


Figure 5-36 Pushover curves for multi-family dwelling archetypes in SSI and foundation flexibility studies (top), and pushover curves normalized by total building seismic weight and roof height (bottom).

Table 5-20 Modal and Pushover Analysis Results for Archetype Models Used to Investigate SSI and Foundation Flexibility *

Baseline Archetype ID	North-South Direction				East-West Direction			
	T_1 (sec)	V_M / W	$\Delta_{U,80}$ (in/in)	$\Delta_{U,max}$ (in/in)	T_1 (sec)	V_M / W	$\Delta_{U,80}$ (in/in)	$\Delta_{U,max}$ (in/in)
Commercial Buildings: High Seismic								
COM1B	0.25	0.62	0.03	0.16	0.33	0.50	0.03	0.16
COM1B-F-DE	0.26	0.62	0.03	0.16	0.33	0.50	0.03	0.16
COM1B-F-CD	0.25	0.62	0.03	0.16	0.33	0.50	0.03	0.16
COM2B	0.33	0.53	0.02	0.08	0.39	0.53	0.02	0.08
COM2B-F-DE	0.34	0.53	0.02	0.08	0.40	0.43	0.02	0.07
COM2B-F-CD	0.33	0.53	0.02	0.08	0.39	0.43	0.02	0.07
COM3B	0.54	0.32	0.01	0.03	0.62	0.30	0.01	0.03
COM3-F-DE	0.56	0.32	0.01	0.03	0.64	0.30	0.01	0.03
COM3B-F-CD	0.54	0.32	0.01	0.03	0.62	0.30	0.01	0.03
Multi-Family Dwellings: High Seismic								
MFD1B	0.18	1.39	0.03	0.16	0.19	1.21	0.03	0.16
MFD1B-F-DE	0.18	1.38	0.03	0.16	0.19	1.21	0.03	0.16
MFD1B-F-CD	0.18	1.38	0.03	0.16	0.19	1.21	0.03	0.16
MFD2B	0.27	0.67	0.02	0.08	0.29	0.63	0.02	0.08
MFD2B-F-DE	0.28	0.67	0.02	0.08	0.29	0.63	0.02	0.08
MFD2B-F-CD	0.27	0.67	0.02	0.08	0.29	0.63	0.02	0.08
MFD3B	0.51	0.37	0.01	0.03	0.51	0.34	0.01	0.03
MFD3B-F-DE	0.51	0.37	0.01	0.03	0.51	0.34	0.01	0.03
MFD3B-F-CD	0.51	0.37	0.01	0.03	0.51	0.34	0.01	0.03

* Rayleigh damping equal to 0.1% assigned to first and second modes was used in these analyses.

Nonlinear IDA results are summarized in Figure 5-37 and Figure 5-38, which present IDA collapse rates and FEMA P-695 fragility curves for COM and MFD archetypes, both with and without nonlinear soil springs. Table 5-21 summarizes values of various response and collapse parameters from FEMA P-695 static pushover and nonlinear incremental dynamic collapse analyses for each archetype. Although the MCE_R collapse probabilities for each group of baseline and variant archetype models are not identical, the differences are very small. This can be seen in the overlapping fragility curves shown in the figures and nearly identical values reported in the table.

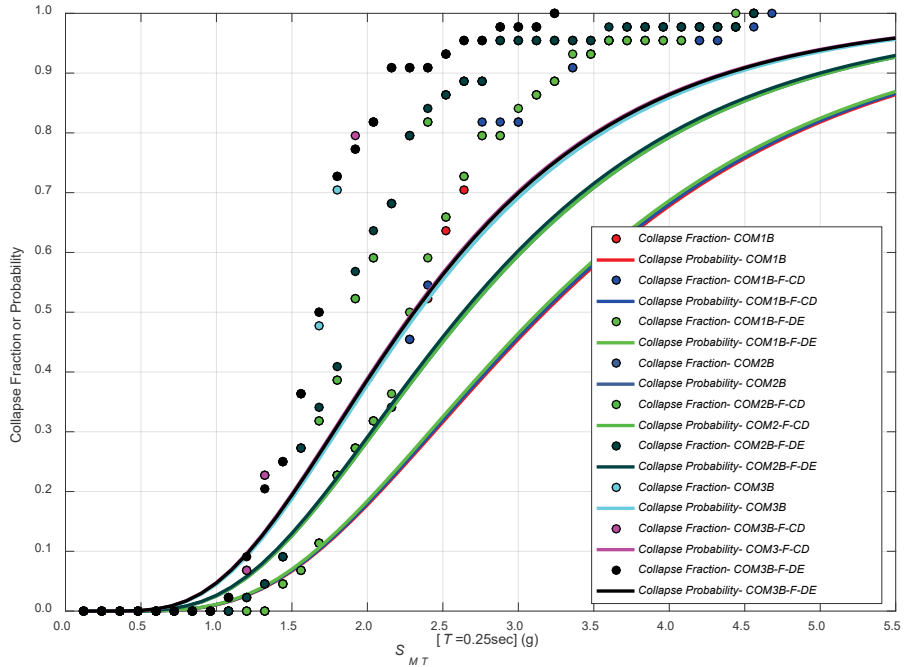


Figure 5-37 Collapse rates from IDA and FEMA P-695 collapse fragility curves for commercial building archetypes in SSI and foundation flexibility studies.

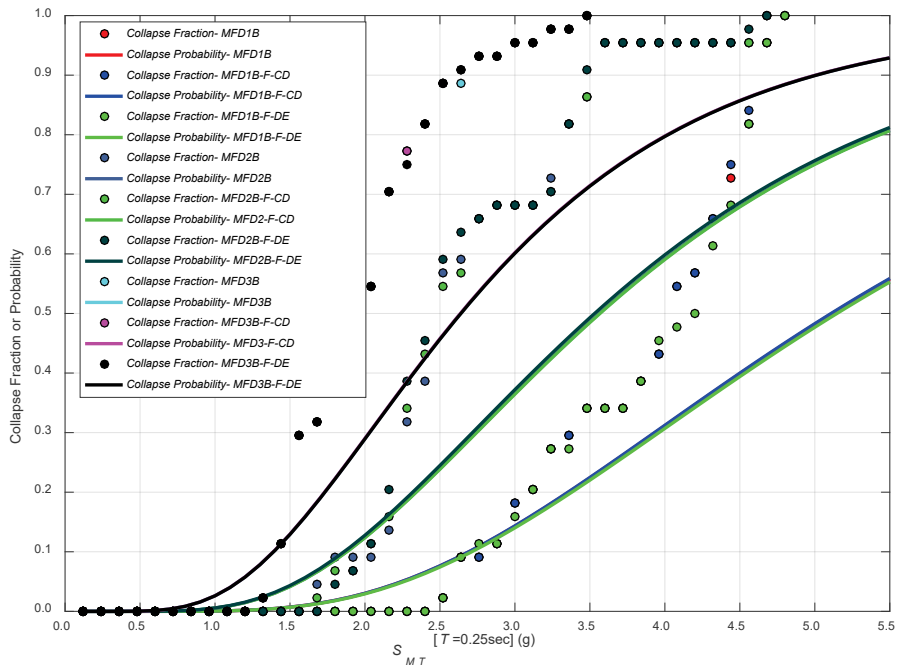


Figure 5-38 Collapse rates from IDA and FEMA P-695 collapse fragility curves for multi-family dwelling archetypes in SSI and foundation flexibility studies.

Table 5-21 Pushover and Collapse Analysis Results for Archetype Models Used to Investigate SSI and Foundation Flexibility

Baseline Archetype ID	Pushover Analysis ⁽¹⁾ ⁽²⁾			Collapse Analysis ⁽²⁾				
	V_{\max} / W	Ω	μ_r	S_{CT} (g)	CMR _{3D}	SSF	ACMR	$P[C MCE_R]$
Commercial Buildings: High Seismic								
COM1B	0.56	3.64	>8	3.18	1.59	1.33	2.12	6.7%
COM1B-F-DE	0.56	3.63	>8	3.14	1.57	1.33	2.09	7.0%
COM1B-F-CD	0.56	3.64	>8	3.16	1.58	1.33	2.11	6.8%
COM2B	0.53	3.46	>8	2.66	1.33	1.33	1.77	12.6%
COM2B-F-DE	0.48	3.13	>8	2.63	1.32	1.33	1.76	13.0%
COM2B-F-CD	0.48	3.14	>8	2.66	1.33	1.33	1.77	12.6%
COM3B	0.31	2.00	>8	2.34	1.15	1.35	1.56	18.8%
COM3B-F-DE	0.31	2.00	>8	2.31	1.15	1.34	1.54	19.4%
COM3B-F-CD	0.31	2.00	>8	2.30	1.15	1.34	1.53	19.6%
Multi-Family Dwellings: High Seismic								
MFD1B	1.30	8.44	>8	5.11	2.56	1.33	3.41	0.7%
MFD1B-F-DE	1.30	8.43	>8	5.15	2.58	1.33	3.43	0.7%
MFD1B-F-CD	1.30	8.44	>8	5.11	2.56	1.33	3.41	0.7%
MFD2B	0.65	4.20	>8	3.56	1.79	1.33	2.37	4.2%
MFD2B-F-DE	0.65	4.19	>8	3.53	1.77	1.33	2.35	4.3%
MFD2B-F-CD	0.65	4.20	>8	3.57	1.79	1.33	2.38	4.2%
MFD3B	0.36	2.33	>8	2.64	1.32	1.33	1.76	12.9%
MFD3B-F-DE	0.36	2.33	>8	2.64	1.32	1.33	1.76	12.9%
MFD3B-F-CD	0.36	2.33	>8	2.64	1.32	1.33	1.76	13.0%

⁽¹⁾ Pushover analysis results represent average response in the North-South and East-West directions.

⁽²⁾ Rayleigh damping equal to 0.1% assigned to first and second modes was used in these analyses.

Table 5-22 summarizes median and lognormal standard deviation values of peak roof drift ratio, peak first-story drift ratio, and corresponding response spectral acceleration at incipient collapse, for COM and MFD archetypes, both with and without nonlinear soil springs. Median peak first-story and roof drift ratios, as well as the median response spectral acceleration at incipient collapse, are nearly identical for archetypes on rigid foundations and archetypes with springs representing soft or stiff soil sites.

Table 5-22 Median and Lognormal Standard Deviation Values of Peak Drift Ratio and Response Spectral Acceleration at Incipient Collapse for Archetype Models Used to Investigate SSI and Foundation Flexibility *

Archetype ID	Peak Drift Ratio at Incipient Collapse				Response Spectral Acceleration at Incipient Collapse S_T (g)	
	Roof		First Story			
	Median	β	Median	β	Median	β
Commercial Buildings: High Seismic						
COM1B	0.082	0.25	0.082	0.25	1.99	0.27
COM1B-F-DE	0.079	0.26	0.079	0.26	1.96	0.26
COM1B-F-CD	0.082	0.27	0.082	0.27	1.98	0.27
COM2B	0.034	0.31	0.066	0.33	1.67	0.27
COM2B-F-DE	0.033	0.28	0.065	0.30	1.65	0.26
COM2B-F-CD	0.035	0.35	0.068	0.37	1.67	0.27
COM3B	0.016	0.18	0.045	0.25	1.44	0.23
COM3B-F-DE	0.016	0.17	0.047	0.24	1.43	0.24
COM3B-F-CD	0.016	0.19	0.044	0.27	1.43	0.23
Multi-Family Dwellings: High Seismic						
MFD1B	0.071	0.90	0.071	0.90	3.20	0.19
MFD1B-F-DE	0.073	0.86	0.073	0.86	3.22	0.20
MFD1B-F-CD	0.074	0.86	0.074	0.86	3.20	0.19
MFD2B	0.059	0.47	0.116	0.48	2.23	0.24
MFD2B-F-DE	0.056	0.43	0.109	0.44	2.21	0.23
MFD2B-F-CD	0.058	0.45	0.115	0.46	2.23	0.24
MFD3B	0.018	0.27	0.052	0.40	1.65	0.24
MFD3B-F-DE	0.018	0.19	0.051	0.34	1.65	0.24
MFD3B-F-CD	0.018	0.19	0.050	0.32	1.65	0.24

* Rayleigh damping equal to 0.1% assigned to first and second modes was used in these analyses.

Table 5-23 summarizes raw collapse statistics and mean peak first-story drift ratios for each archetype at ground motions scaled to MCE_R and 0.5 × MCE_R intensity levels. No collapses were observed at the 0.5 × MCE_R intensity level. At the MCE_R intensity level, the number of collapses for COM1B and COM2B archetypes with nonlinear soil springs are lower than the number of collapses in corresponding baseline archetypes (without soil springs). However, because the median response spectral acceleration values at incipient collapse are nearly identical (as shown in Table 5-22), the final adjusted collapse margin ratio (*ACMR*) and MCE_R collapse probabilities computed per the FEMA P-695 methodology are nearly identical (as shown in Table 5-21).

Table 5-23 Collapse Rates and Mean Peak First-Story Drift Ratios at MCE_R and 50-Percent of MCE_R Ground Motion Intensities for Archetype Models Used to Investigate SSI and Foundation Flexibility *

Archetype ID	MCE _R Collapse Rate (out of 44)		Mean Peak First-Story Drift Ratio of Survivors (%)			
	0.5 × MCE _R	1.0 × MCE _R	0.5 × MCE _R		MCE _R	
			East-West Direction	North-South Direction	East-West Direction	North-South Direction
Commercial Buildings: High Seismic						
COM1B	0	3	0.98	0.57	3.03	2.13
COM1B-F-DE	0	1	0.95	0.56	2.98	1.94
COM1B-F-CD	0	1	0.93	0.54	2.97	1.91
COM2B	0	8	1.05	0.80	3.12	2.68
COM2B-F-DE	0	5	1.03	0.78	3.12	2.58
COM2B-F-CD	0	5	1.00	0.75	3.01	2.56
COM3B	0	14	0.81	0.84	2.32	2.48
COM3B-F-DE	0	14	0.87	0.88	2.47	2.53
COM3B-F-CD	0	14	0.82	0.85	2.33	2.48
Multi-Family Dwellings: High Seismic						
MFD1B	0	0	0.23	0.20	0.72	0.60
MFD1B-F-DE	0	0	0.23	0.20	0.72	0.61
MFD1B-F-CD	0	0	0.23	0.20	0.72	0.60
MFD2B	0	0	0.63	0.59	2.48	2.04
MFD2B-F-DE	0	0	0.57	0.61	1.96	2.00
MFD2B-F-CD	0	0	0.55	0.62	1.90	2.04
MFD3B	0	9	0.70	0.67	2.19	2.10
MFD3B-F-DE	0	9	0.71	0.67	2.20	2.10
MFD3B-F-CD	0	9	0.70	0.67	2.19	2.09

* Rayleigh damping equal to 0.1% assigned to first and second modes was used in these analyses.

5.5.3 Interpretation of Results

Figure 5-39 presents maximum horizontal and vertical stresses along the four perimeter foundation beams in the one-story commercial archetype on a soft soil site (COM1B-F-DE). The maximum stress distribution was obtained from one of the 22 pairs of FEMA P-695 ground motions, scaled to incipient collapse (i.e., the Northridge Beverly Hills ground motion scaled to $S_T(0.25 \text{ second}) = 1.9g$). The soil springs are spaced at 2-foot on-center along the bottom of each foundation beam, and the width of the foundation beam (B) is 8 inches. For computing the maximum vertical stress, the peak

force in each of the vertical springs is divided by $2B$ times the spacing of the soil springs ($2 \times B \times 2$ feet) to obtain the maximum stress profiles shown in the figure. The peak vertical stresses ranged from 3.4 psi to 4.8 psi, which is significantly below the bearing capacity of the soil (160 kPa, or 23.2 psi). Integrating the stress profiles along the length of the foundation beams and summing the forces produced a peak vertical force of 208.6 kips, which is about 1.15 times the self-weight of the baseline one-story commercial building (i.e., 180 kips).

Figure 5-40 shows the distribution of the soil spring vertical forces in the four-story multi-family dwelling model on soft soil (MFD3D-F-DE). Under gravity load, the soil spring forces are symmetrical about both the North-South (Y) and East-West (X) directions (top image in the figure). For the X-direction pushover analysis, the deformed shape of the building (bottom image in the figure) and the distribution of soil spring vertical forces (middle image in the figure) are shown. At the peak strength of the X-direction pushover analysis, the maximum soil spring forces are shifted to one side (i.e., the East side) of the building, but all foundation beams remained under compression.

The results presented in Tables 5-20 through 5-23, and shown in Figures 5-35 through 5-38, show that inclusion of nonlinear soil springs does not significantly impact the response behavior and collapse performance of wood light-frame archetypes. This was mainly attributed to the lightweight nature of wood light-frame construction (relative to other construction materials).

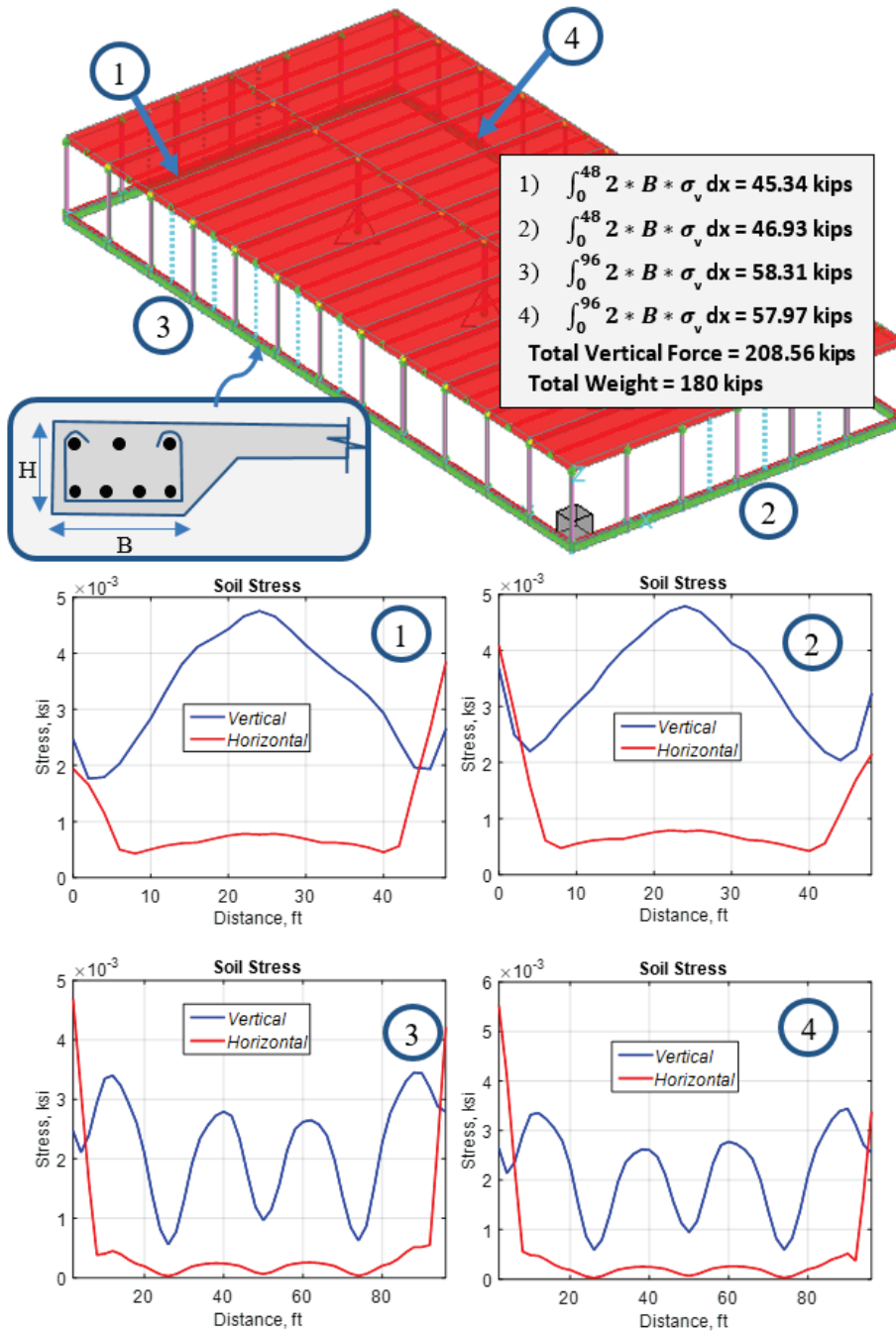


Figure 5-39 Maximum foundation stresses in the COM1B-F-DE archetype model subjected to the Northridge Beverly Hills ground motion scaled to $S_T = 1.9g$.

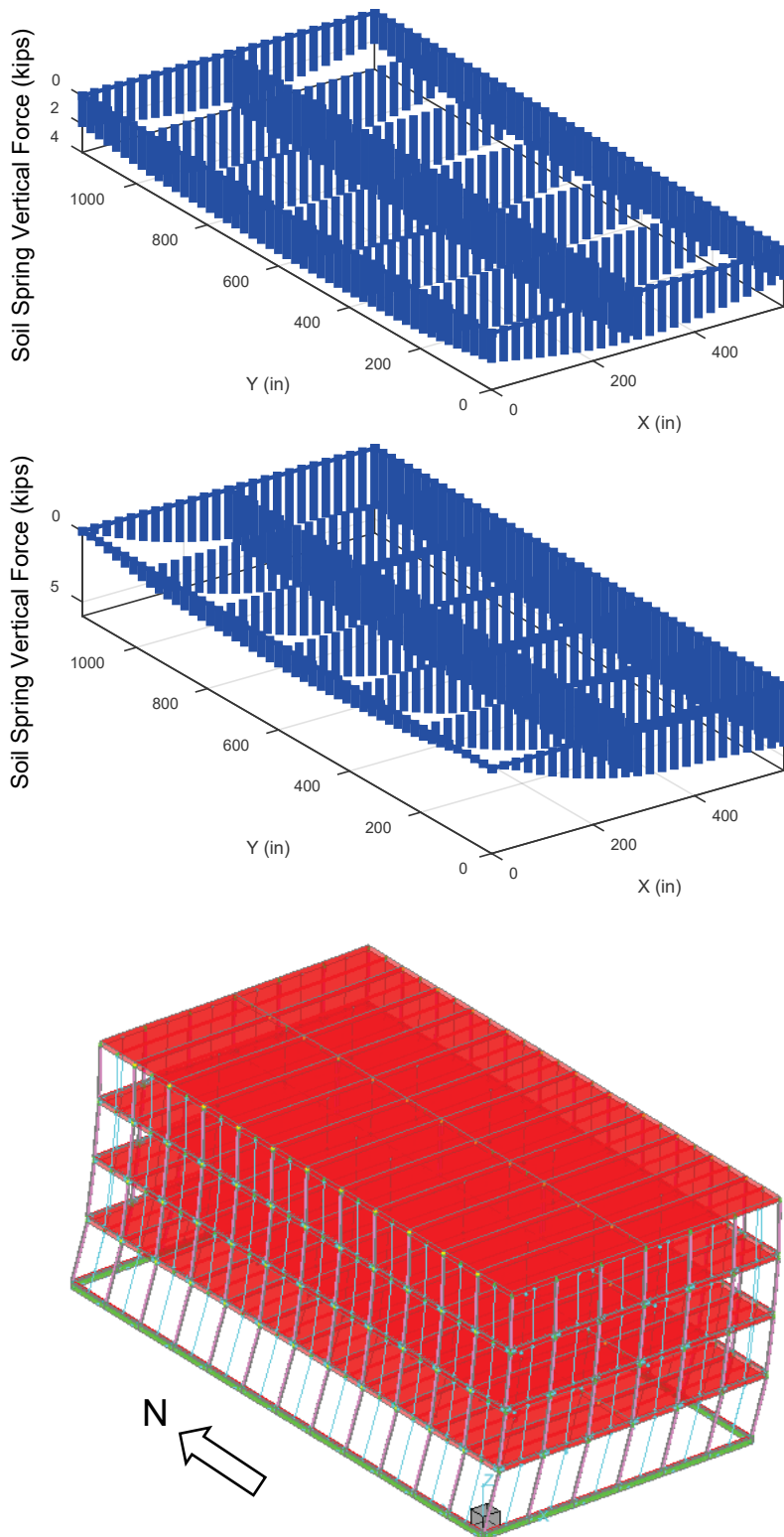


Figure 5-40 Distribution of soil spring vertical forces in the MFD3B-F-DE archetype model under gravity load (top); and at peak strength in the X-direction pushover (middle); and deformed shaped of model in the X-direction pushover (bottom).

5.6 Backbone Curve Shape Parametric Study

Backbone curve shape studies investigated the effects of backbone shape parameters on response behavior and collapse performance. In this study, archetypes were modified to include different assumptions for peak strength, drift ratio at peak strength, and slope of the post-peak curve, and were compared to the results of corresponding baseline archetype models using best estimate properties of backbone parameters from applicable test data. This study also included consideration of backbone shape in combination with the effects of nonstructural wall finishes (i.e., both with and without nonstructural finishes) and varying assumptions on residual post-capping strength ratios (i.e., 0, 30, and 60 percent).

5.6.1 Backbone Curve Shape Archetypes and Variants

Table 5-24 identifies modeling variables considered in each of four-story commercial building (COM3B) archetypes included in backbone curve shape studies. A total of the 14 archetypes were considered, including two baseline archetypes and 12 variants.

Table 5-24 Commercial Building Archetype Models Used to Investigate Backbone Curve Shape

Archetype ID	Modeling Variables		
	WSP Hysteresis Model	Residual Strength (% of Peak-Strength)	Contribution of Nonstructural Wall Finishes
COM3B	Baseline	30	Yes
COM3B-BSR1	R1	30	Yes
COM3B-BSR1-NS	R1	30	No
COM3B-BSR2	R2	30	Yes
COM3B-BSR2-NS	R2	30	No
COM3B-BSR1-C0	R1	0	Yes
COM3B-BSR1-C0-NS	R1	0	No
COM3B-BSR2-C0	R2	0	Yes
COM3B-BSR2-C0-NS	R2	0	No
COM3B-BSR1-C6	R2	60	Yes
COM3B-BSR1-C6-NS	R2	60	No
COM3B-BSR2-C6	R2	60	Yes
COM3B-BSR2-C6-NS	R2	60	No
COM3B-NS	Baseline	30	No

Three sets of backbone parameters for wood structural panels (WSP) were considered: baseline (best estimate), R1 (based on an actual shear wall test for the configuration of interest), and R2 (based on mean allowable strength with an overstrength factor of 3.0). Archetypes with alternative backbone parameters are identified by “R1” or “R2” in the table. Archetypes without nonstructural wall finishes are identified by “NS,” and archetypes with different levels of residual strength are identified by “C0” (zero residual strength) and “C6” (60% residual strength). Baseline archetypes included nonstructural wall finishes and 30% residual strength.

5.6.2 Numerical Results

Figure 5-41, Figure 5-42, and Figure 5-43 show pushover curves for the baseline and variant models with 30-percent, 0-percent, and 60-percent residual post-capping strengths, respectively. Table 5-25 summarizes the results of free vibration (modal) analyses and FEMA P-795 nonlinear static pushover analyses.

From the pushover curves, it can be observed that archetypes with R2 parameters (i.e., the peak strength of the wood structural panel scaled to three times ASD values) have the largest peak strengths, while R1 and baseline archetype models have approximately the same peak strength. However, the displacements at peak strength for both the R1 and R2 archetypes are larger than the displacements at peak strength for the baseline archetype.

With a 30-percent residual post-capping strength (Figure 5-41), the pushover collapse drifts for all three backbone variants (baseline, R1, and R2) fall within the range of 1.5 percent to 3 percent roof drift. Because displacement demands are mainly concentrated in the first story, the static collapse capacities in terms of story drifts range from about 6 percent to 12 percent, which are representative of the collapse drifts observed in full-scale building shake table tests. When the residual post-capping strength was reduced to 0 percent (Figure 5-42), the static collapse drifts for all models fell within a very narrow range of 1.6 percent to 2 percent roof drift (or about 6 percent to 7.5 percent story drift), regardless of the backbone curve shape.

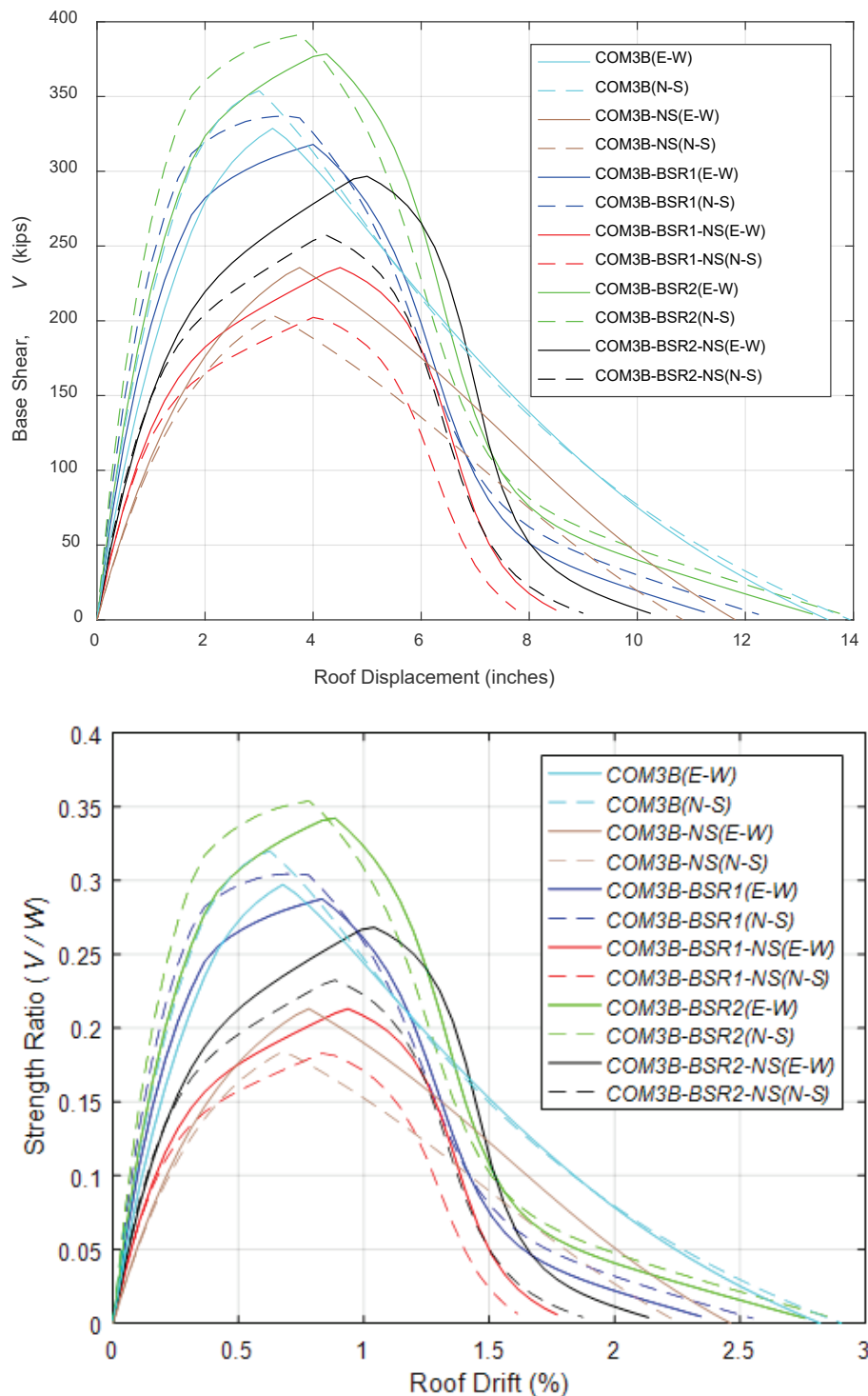


Figure 5-41 Pushover curves for commercial building archetypes with 30-percent residual strength in backbone curve shape studies (top), and pushover curves normalized by total building seismic weight and roof height (bottom).

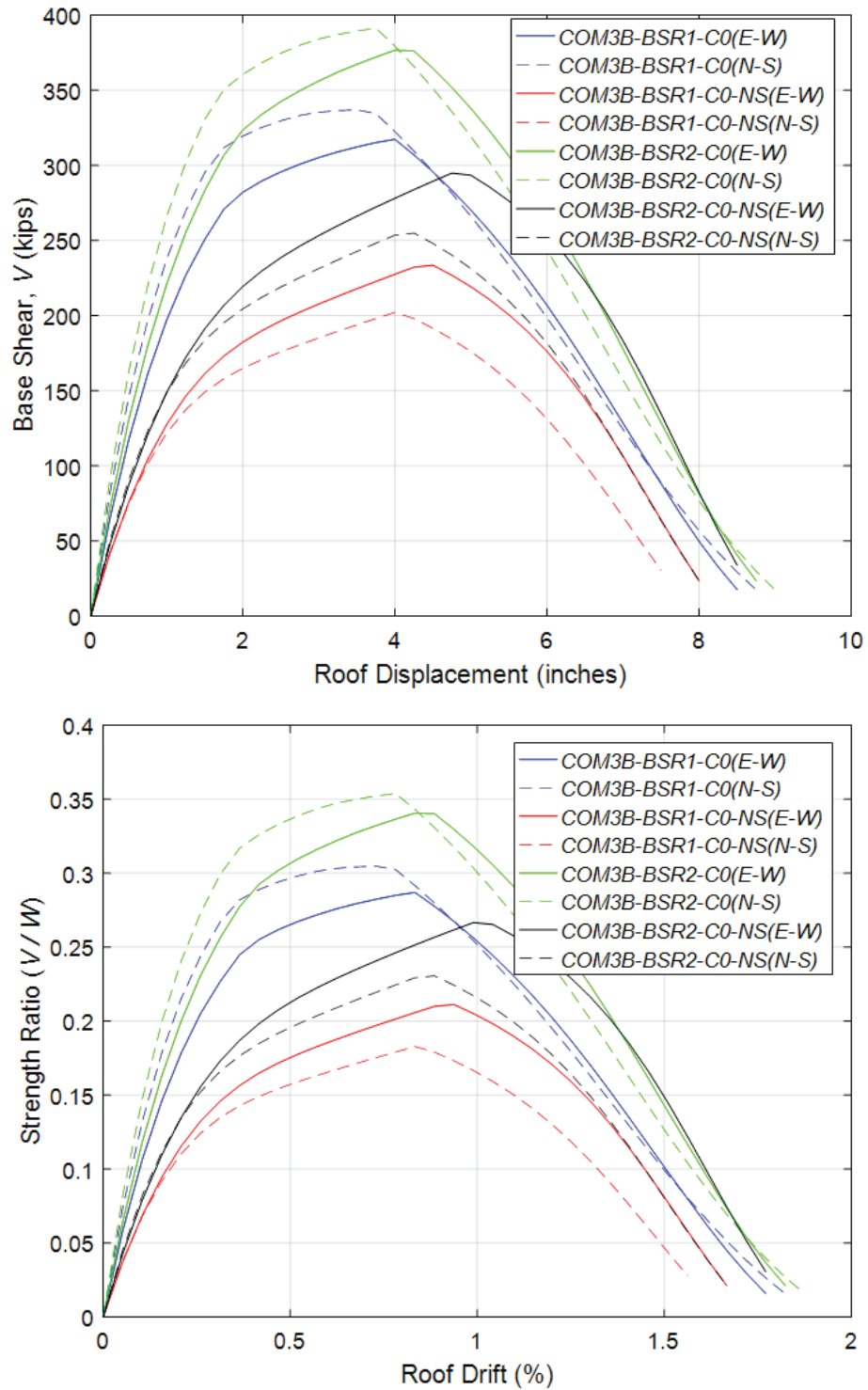


Figure 5-42 Pushover curves for commercial building archetypes with 0-percent residual strength in backbone curve shape studies (top), and pushover curves normalized by total building seismic weight and roof height (bottom).

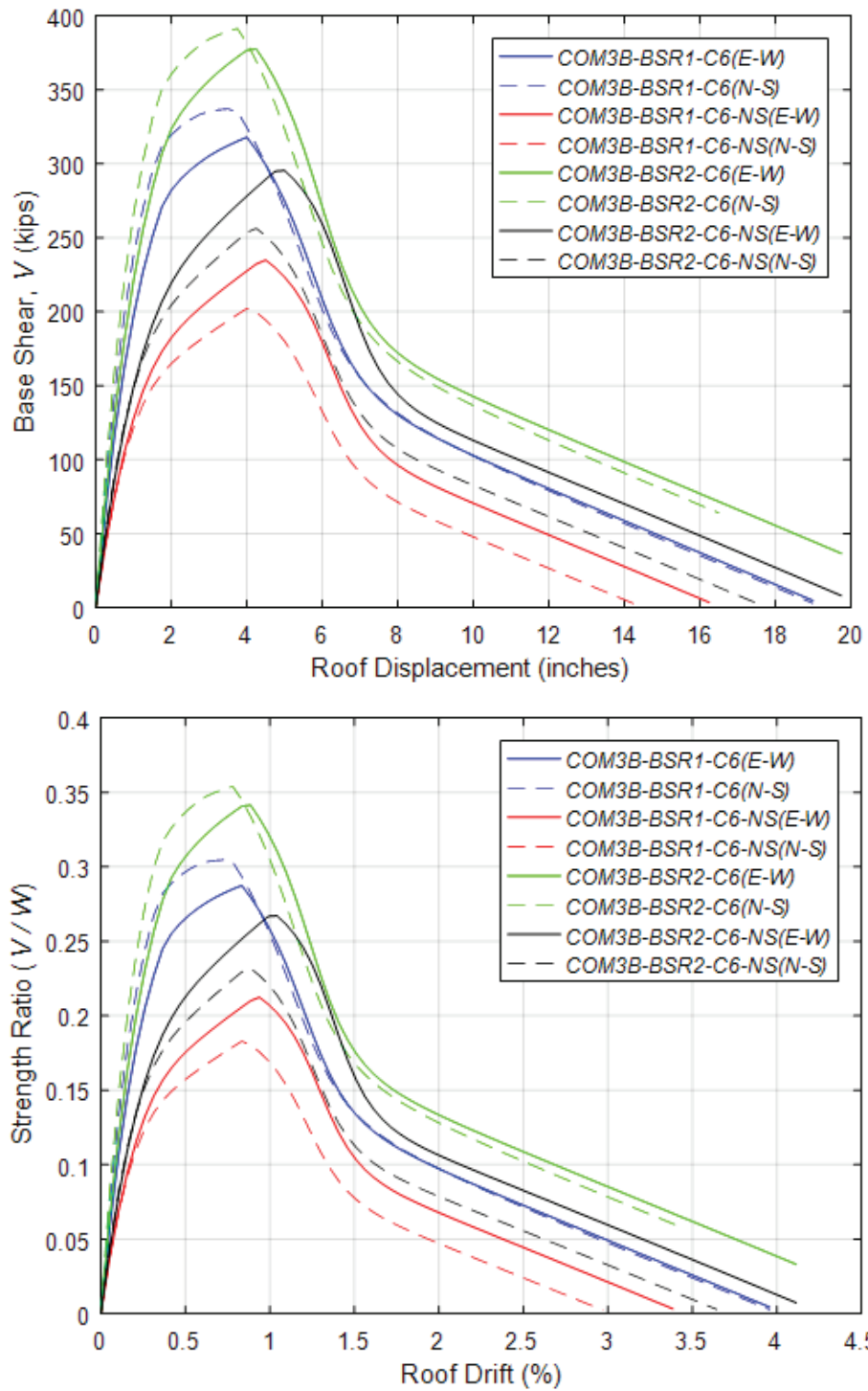


Figure 5-43 Pushover curves for commercial building archetypes with 60-percent residual strength in backbone curve shape studies (top), and pushover curves normalized by total building seismic weight and roof height (bottom).

Table 5-25 Modal Pushover Analysis Results for Commercial Building Archetype Models Used to Investigate Backbone Curve Shape

Baseline Archetype ID	North-South Direction				East-West Direction			
	T_1 (sec)	V_{\max} / W	$\Delta U_{,80}$ (in/in)	$\Delta U_{,\max}$ (in/in)	T_1 (sec)	V_{\max} / W	$\Delta U_{,80}$ (in/in)	$\Delta U_{,\max}$ (in/in)
Commercial Buildings: High Seismic, Baseline Backbone Curve								
COM3B	0.54	0.32	0.01	0.03	0.62	0.30	0.01	0.03
COM3B-NS	0.81	0.18	0.03	0.08	0.82	0.21	0.04	0.09
Commercial Buildings: High Seismic, Alternative Backbone Curve R1								
COM3B-BSR1-C0	0.50	0.30	0.04	0.07	0.56	0.29	0.04	0.07
COM3B-BSR1	0.50	0.30	0.04	0.10	0.56	0.29	0.01	0.09
COM3B-BSR1-C6	0.50	0.30	0.04	0.16	0.56	0.29	0.04	0.16
COM3B-BSR1-C0-NS	0.69	0.18	0.04	0.06	0.70	0.21	0.04	0.06
COM3B-BSR1-NS	0.69	0.18	0.04	0.06	0.70	0.21	0.01	0.07
COM3B-BSR1-C6-NS	0.69	0.18	0.04	0.11	0.70	0.21	0.04	0.13
Commercial Buildings: High Seismic, Alternative Backbone Curve R2								
COM3B-BSR2-C0	0.47	0.35	0.04	0.07	0.53	0.34	0.04	0.07
COM3B-BSR2	0.47	0.35	0.04	0.11	0.53	0.34	0.01	0.11
COM3B-BSR2-C6	0.47	0.35	0.04	0.13	0.53	0.34	0.04	0.16
COM3B-BSR2-C0-NS	0.63	0.23	0.04	0.06	0.65	0.27	0.04	0.06
COM3B-BSR2-NS	0.63	0.23	0.04	0.07	0.65	0.27	0.01	0.08
COM3B-BSR2-C6-NS	0.63	0.23	0.04	0.14	0.65	0.27	0.04	0.16

Nonlinear IDA results are summarized in Figure 5-44 and Figure 5-45, which present IDA collapse rates and FEMA P-695 fragility curves for archetypes with baseline, R1, and R2 backbone parameters. Table 5-26 summarizes values of various response and collapse parameters from FEMA P-695 static pushover and nonlinear incremental dynamic collapse analyses for each archetype.

Values in Table 5-26 show that the peak strength ratio (V_{\max} / W) for the R2 archetype without nonstructural wall finishes (COM3B-BSR2-NS) is about 28 percent greater than the baseline model without nonstructural wall finishes (COM3B-NS) in both lateral directions. When nonstructural wall finishes are considered, the percentage difference drops to about 10 percent.

Also shown in Table 5-26, MCE_R collapse probabilities for baseline (COM3B) and R1 (COM3B-BSR1) archetypes are on the same order of magnitude (19.0 percent versus 15.7 percent). This was mainly attributed to the similar peak strength ratios (V_{\max} / W) between the two models. In the

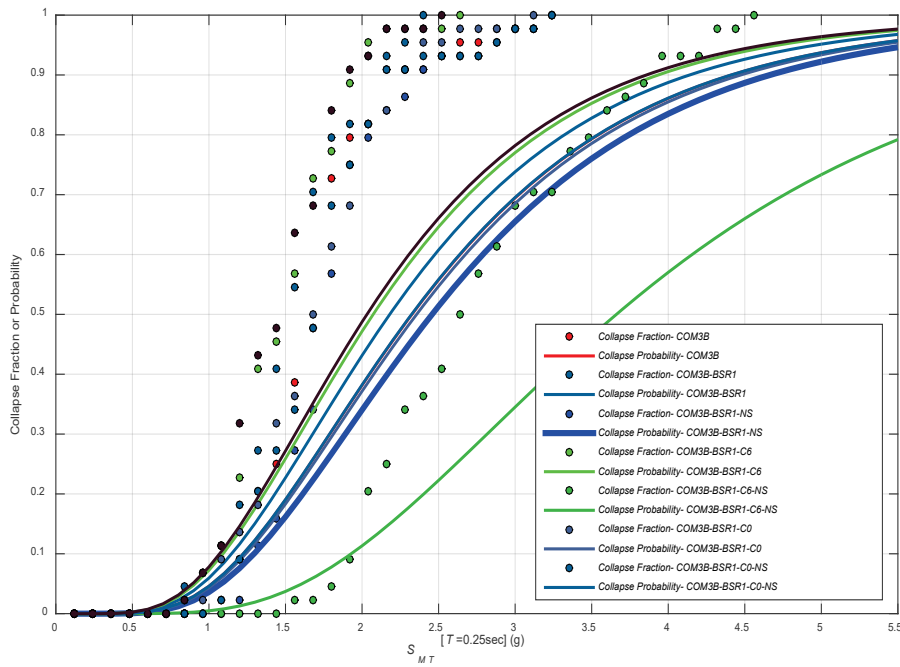


Figure 5-44 Collapse rates from IDA and FEMA P-695 collapse fragility curves for commercial building archetype models with R1 backbone parameters used in backbone curve shape studies.

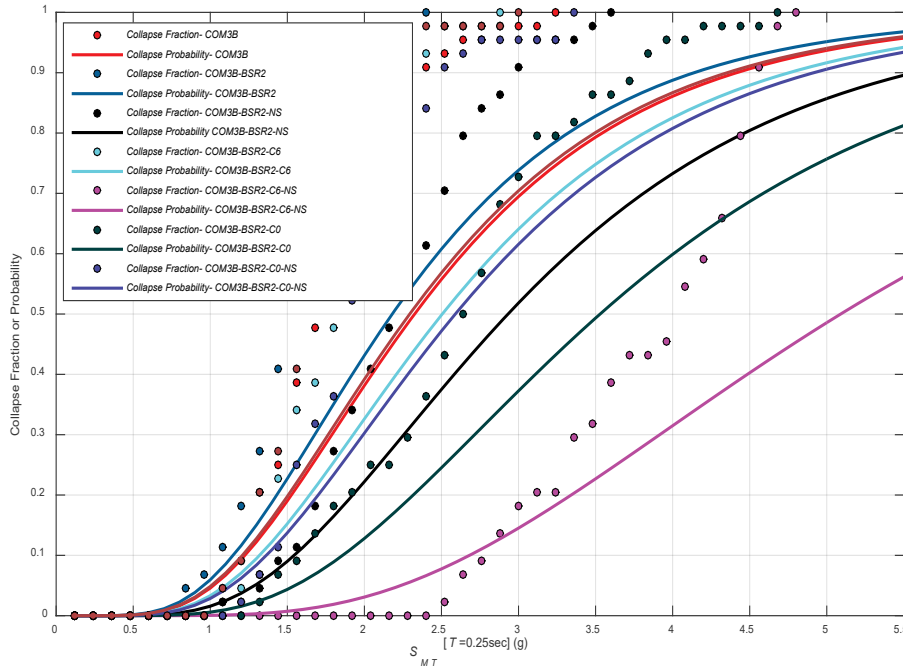


Figure 5-45 Collapse rates from IDA and FEMA P-695 collapse fragility curves for commercial building archetype models with R2 backbone parameters used in backbone curve shape studies.

Table 5-26 Pushover and Collapse Analysis Results for Commercial Building Archetype Models Used to Investigate Backbone Curve Shape

Baseline Archetype ID	Pushover Analysis *			Collapse Analysis				
	V_{max} / W	Ω	μ_f	S_{CT} (g)	CMR _{3D}	SSF	ACMR	P[C] MCE _R]
Commercial Buildings: High Seismic								
COM3B	0.31	2.0	>8	2.33	1.15	1.35	1.55	19.0%
COM3B-NS	0.20	1.3	>8	2.18	1.03	1.41	1.45	22.7%
Commercial Buildings: High Seismic, Alternative Backbone Curve R1								
COM3B-BSR1-C0	0.30	1.9	>8	2.32	1.16	1.34	1.55	19.1%
COM3B-BSR1	0.30	1.9	>8	2.48	1.22	1.35	1.65	15.7%
COM3B-BSR1-C6	0.30	1.9	>8	3.66	1.82	1.34	2.44	3.7%
COM3B-BSR1-C0-NS	0.20	1.3	>8	2.03	0.98	1.38	1.35	27.2%
COM3B-BSR1-NS	0.20	1.3	>8	2.03	1.00	1.35	1.36	27.1%
COM3B-BSR1-C6-NS	0.20	1.3	>8	2.36	1.14	1.38	1.57	18.3%
Commercial Buildings: High Seismic, Alternative Backbone Curve R2								
COM3B-BSR2-C0	0.35	2.3	>8	2.59	1.29	1.34	1.73	13.7%
COM3B-BSR2	0.35	2.3	>8	2.97	1.46	1.35	1.98	8.6%
COM3B-BSR2-C6	0.35	2.3	>8	5.09	2.54	1.34	3.39	0.7%
COM3B-BSR2-C0-NS	0.25	1.6	>8	2.29	1.12	1.37	1.53	19.8%
COM3B-BSR2-NS	0.25	1.6	>8	2.48	1.22	1.35	1.65	15.8%
COM3B-BSR2-C6-NS	0.25	1.6	>8	3.53	1.72	1.37	2.35	4.4%

* Pushover analysis results represent average response in the North-South and East-West directions.

case of the R2 archetype (COM3B-BSR2), however, the MCE_R collapse probability was significantly lower (8.6 percent). This suggests that the overstrength ratio of the wood structural panels has a significant influence on MCE_R collapse probabilities in wood light-frame buildings.

Table 5-27 summarizes median and lognormal standard deviation values of peak roof drift ratio, peak first-story drift ratio, and corresponding response spectral acceleration at incipient collapse, for COM archetypes used to investigate the effects of backbone curve shape. The better post-peak displacement capacity of R2 archetypes observed in pushover analyses (Figures 5-41 to 5-43) are also reflected in the nonlinear IDA results summarized in the table. For example, the median peak first-story drift ratio for COM3B-BSR2 (10.7%) is significantly higher than the drift ratio for the COM3B baseline archetype (4.6%). An increase in both the peak strength (V_{max}/W) and post-peak displacement capacity of the COM3B-BSR2 model contributes to the reduction in MCE_R collapse probability when compared to the baseline COM3B model (i.e., from 19 percent to 8.6 percent).

Table 5-28 summarizes raw collapse statistics and mean peak first-story drift ratios for each archetype at ground motions scaled to MCE_R and 0.5 × MCE_R intensity levels. No collapses were observed at the 0.5 × MCE_R intensity level. At the MCE_R intensity level, the number of collapses for decreases from 14 to 5 when R2 backbone parameters are used (COM3B-BSR2) instead of baseline best-estimate backbone parameters (COM3B).

Table 5-27 Median and Lognormal Standard Deviation Values of Peak Drift Ratio and Response Spectral Acceleration at Incipient Collapse for Commercial Building Archetype Models Used to Investigate Backbone Curve Shape

Archetype ID	Peak Drift Ratio at Incipient Collapse				Response Spectral Acceleration at Incipient Collapse S_T (g)	
	Roof		First Story			
	Median	β	Median	β	Median	β
Commercial Buildings: High Seismic						
COM3B	0.016	0.18	0.046	0.29	1.43	0.23
COM3B-NS	0.019	0.21	0.047	0.26	1.28	0.25
Commercial Buildings: High Seismic, Alternative Backbone Curve R1						
COM3B-BSR1-C0	0.017	0.22	0.045	0.27	1.45	0.24
COM3B-BSR1	0.023	0.54	0.073	0.73	1.53	0.22
COM3B-BSR1-C6	0.046	0.41	0.165	0.45	2.28	0.26
COM3B-BSR1-C0-NS	0.017	0.26	0.035	0.23	1.23	0.24
COM3B-BSR1-NS	0.018	0.40	0.041	0.44	1.25	0.24
COM3B-BSR1-C6-NS	0.026	0.48	0.076	0.64	1.42	0.26
Commercial Buildings: High Seismic, Alternative Backbone Curve R2						
COM3B-BSR2-C0	0.019	0.29	0.055	0.47	1.62	0.23
COM3B-BSR2	0.032	0.50	0.107	0.66	1.83	0.26
COM3B-BSR2-C6	0.058	0.26	0.211	0.32	3.18	0.19
COM3B-BSR2-C0-NS	0.021	0.32	0.045	0.40	1.40	0.21
COM3B-BSR2-NS	0.025	0.46	0.059	0.61	1.53	0.22
COM3B-BSR2-C6-NS	0.043	0.43	0.136	0.59	2.15	0.30

Table 5-28 Collapse Rates and Mean Peak First-Story Drift Ratios at MCE_R and 50-Percent of MCE_R Ground Motion Intensities for Commercial Building Archetype Models Used to Investigate Backbone Curve Shape

Archetype ID	MCE _R Collapse Rate (out of 44)		Mean Peak First-Story Drift Ratio of Survivors (%)			
	0.5 × MCE _R	1.0 × MCE _R	0.5 × MCE _R		MCE _R	
			East-West Direction	North-South Direction	East-West Direction	North-South Direction
Commercial Buildings: High Seismic						
COM3B	0	14	0.82	0.84	2.39	2.48
COM3B-NS	0	21	1.26	1.41	3.50	3.42
Commercial Buildings: High Seismic, Alternative Backbone Curve R1						
COM3B-BSR1-C0	0	14	0.86	0.87	2.58	2.67
COM3B-BSR1	0	10	0.77	0.82	2.66	3.29
COM3B-BSR1-C6	0	1	0.82	0.83	2.79	3.35
COM3B-BSR1-C0-NS	0	25	1.20	1.34	3.19	3.28
COM3B-BSR1-NS	0	23	1.07	1.26	3.79	3.39
COM3B-BSR1-C6-NS	0	16	1.16	1.30	3.92	3.76
Commercial Buildings: High Seismic, Alternative Backbone Curve R2						
COM3B-BSR2-C0	0	8	0.77	0.78	2.45	2.50
COM3B-BSR2	0	5	0.81	0.81	2.51	2.63
COM3B-BSR2-C6	0	0	0.75	0.77	2.64	2.83
COM3B-BSR2-C0-NS	0	16	1.21	1.30	3.00	3.50
COM3B-BSR2-NS	0	13	1.11	1.20	3.47	3.61
COM3B-BSR2-C6-NS	0	4	1.12	1.20	3.52	3.96

5.6.3 Interpretation of Results

Figure 5-46 plots MCE_R collapse probabilities from Table 5-26 versus peak strength ratio (V_{max} / W). For purposes of comparison, results from baseline archetype models shown in Figure 5-8 are also plotted in Figure 5-46. In the figure, circular, triangular, and rectangular markers denote the baseline, R1 and R2 backbone archetypes, respectively. Hollow markers represent models without nonstructural wall finishes, and C0 and C6 represent the models with 0 percent and 60 percent residual strengths, respectively.

The data show a strong inverse relationship (negative correlation) between MCE_R collapse probability and V_{max} / W (i.e., collapse probability decreases as V_{max} / W ratio increases). The data in Figure 5-46 also show that the MCE_R collapse probability of COM3B archetypes with different backbone

parameters follow the same overall pattern exhibited by other wood light-frame archetype models. For example, for a given backbone curve shape and V_{max} / W , archetypes with zero residual strength (C0) have significantly higher collapse probabilities when compared to corresponding archetypes with high residual strength (60 percent). This trend is consistent with findings from the displacement capacity parametric study.

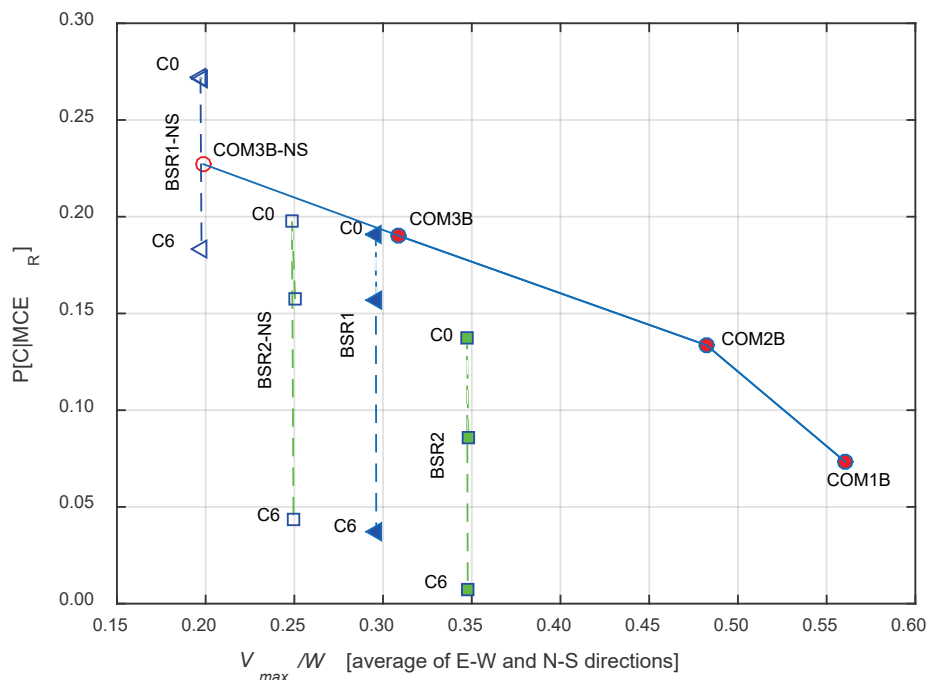


Figure 5-46 MCE_R collapse probability versus peak strength ratio (V_{max} / W) for commercial building archetype models used in backbone curve shape studies.

5.7 Overarching Findings on Parametric Studies

Across all parametric studies, the peak strength ratio (V_{max} / W) and residual strength ratio were found to be the two factors that consistently impacted the collapse probability of wood light-frame buildings. Overall results from the five parametric studies are graphically summarized in Figure 5-47. This figure demonstrates the strong inverse relationship (negative correlation) between MCE_R collapse probability and V_{max} / W across all archetypes.

Figure 5-48 is a three-dimensional plot of MCE_R collapse probability versus V_{max} / W and residual strength ratio. The three-dimensional surface was fitted using selected results from wood light-frame archetype models evaluated in the parametric studies. This figure demonstrates the strong inverse relationship among MCE_R collapse probability, peak strength ratio (V_{max} / W), and residual post-capping strength ratio.

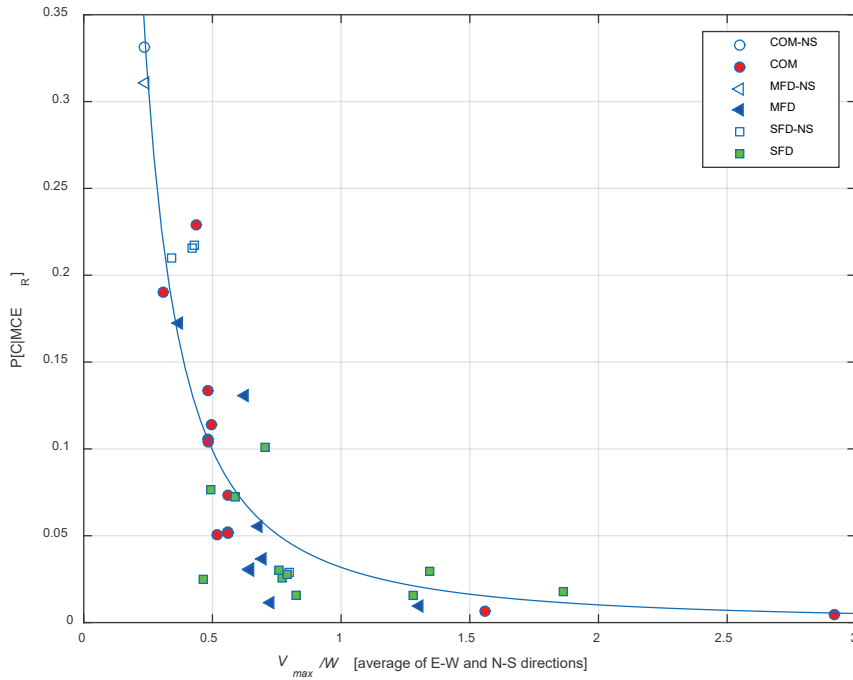


Figure 5-47 MCE_R collapse probability versus peak strength ratio (V_{\max} / W) for all wood light-frame building archetype models used in parametric studies.

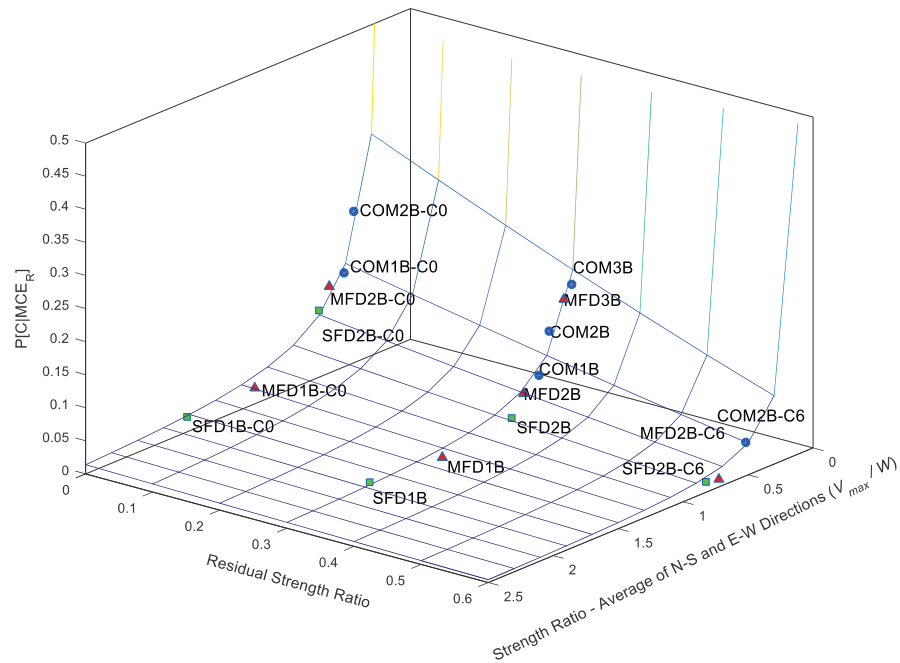


Figure 5-48 Three-dimensional plot of MCE_R collapse probability versus peak strength ratio (V_{\max} / W) and residual strength ratio, for selected wood light-frame building archetype models used in parametric studies.

Detailed findings, conclusions, and recommendations resulting from the five parametric studies are discussed in Chapter 6.

Chapter 6

Findings, Conclusions, and Recommendations

6.1 Introduction

This chapter summarizes key findings, conclusions, and recommendations arising from the parametric studies conducted on wood light-frame building archetypes. In preceding chapters, the following topics were addressed:

- Estimation of target collapse performance benchmarks for wood light-frame buildings based on observations of response and collapse performance in past earthquakes and shake table tests (Chapter 2);
- Identification of representative wood light-frame building archetype configurations and development of detailed designs in accordance with current seismic code requirements (Chapter 3);
- Transformation of wood light-frame archetype designs into nonlinear numerical models including variation on several parameters in the models (Chapter 4); and
- Conduct of free vibration, nonlinear static (pushover), and nonlinear response history (incremental dynamic) analyses of numerical models to evaluate the relative importance of modeling assumptions and varying parameters on wood light-frame building response behavior and collapse performance (Chapter 5).

6.2 Key Findings of the Parametric Studies

Key findings of the parametric studies are summarized and discussed in the following sections. A table is provided with each parametric study, summarizing key archetype model properties (i.e., number of stories, fundamental-mode period (T_1), overstrength (Ω), normalized peak strength ratio (V_{max}/W), and key collapse results (i.e., roof and 1st-story drift ratios at the point of incipient collapse, collapse margin ratio (CMR_{3D}) and MCE_R collapse probabilities. The target range of benchmark collapse probabilities are also provided in each table for comparison with numerical results from high-seismic archetypes models. Values of fundamental-mode period, overstrength, and pushover strength provided in these tables, represent the average value of these parameters in the two horizontal directions of response.

6.2.1 Baseline Configuration Study

Baseline configuration studies evaluated response behavior and collapse performance of wood light-frame buildings as a function of building period (i.e., building height), typical configuration (i.e., occupancy), and region of seismicity (i.e., seismic design level). In addition, baseline models considered the results of other parametric studies, and incorporated a best estimate for each parameter to provide an overall best estimate of the simulated response of short-period wood light-frame buildings.

Key model properties and collapse results for each of the 19 baseline archetypes are summarized in Table 6-1. In this table, and throughout the balance of this chapter, model names ending in “B” (e.g., COM1B, MFD1B, SFD1B) indicate a baseline model designed to meet 2015 IBC (ASCE/SEI 7-10) requirements, and model names ending in “BC” (e.g., SFD1BC) indicate a baseline SFD model configured to meet the conventional construction provisions of the 2015 IRC.

In Figure 6-1, the average horizontal fundamental periods of the ten high seismic baseline configurations of wood light-frame building archetype models are compared with the benchmark periods developed from observations of the response of wood light-frame buildings and the approximate fundamental-period formula, $T = C_u T_a$, of ASCE/SEI 7-10. Building archetype models, COM1BT1 and COM1BT2 represent the north wing of the Templeton Hospital building (described in Appendix D) modeled with the actual strength and stiffness (Koliou et al., 2017) of the building and with bounding values of building weight, which is not precisely known. Because of the additional seismic force required for design of essential facilities, as well as conservatism present in the design, the strength and stiffness of the Templeton Hospital building is much greater than that of the one-story baseline commercial building archetype (i.e., COM1B) of this study.

The finding that the baseline MFD and SFD archetype models have fundamental-mode periods that are similar to measured periods of wood light-frame buildings of comparable height is confirmed in Figure 6-1. Modeled periods, however, would not be similar to measured periods without incorporation of nonstructural wall finishes in the baseline archetype models. The idea that baseline COM archetype models (even with nonstructural wall finishes) have fundamental periods that are consistently greater than those of other wood light-frame buildings of comparable height is also shown in Figure 6-1. The difference in fundamental periods between baseline COM archetype models and measured building periods is primarily attributed to the

Table 6-1 Summary of Key Properties and Collapse Results for High-Seismic and Very High-Seismic Baseline Archetype Models

Archetype Model ID	Model Properties				Collapse Results				Benchmark Collapse Probability (%)
	No. of Stories	Period T_1 (sec)	Strength		Drift Ratio*		CMR_{3D}	P[COL MCE _R] (%)	
Commercial Building High-Seismic ($S_{MS} = 1.5$ g) Baseline Archetype Models									
COM1B	1	0.29	3.6	0.56	0.082	0.082	1.55	7.3%	0 to 2%
COM2B	2	0.36	3.1	0.48	0.035	0.067	1.31	13.4%	0 to 5%
COM3B	4	0.58	2.0	0.31	0.016	0.046	1.15	19.0%	0 to 5%
Commercial Building Very High-Seismic ($S_{MS} = 2.25$ g) Baseline Archetype Models									
COM4B	1	0.28	2.9	0.67	0.088	0.088	1.15	19.0%	NA
COM5B	2	0.35	2.4	0.56	0.038	0.074	0.98	29%	NA
COM6B	4	0.52	1.9	0.44	0.020	0.058	0.98	29%	NA
Multi-Family-Dwelling High-Seismic ($S_{MS} = 1.5$ g) Baseline Archetype Models									
MFD1B	1	0.19	8.5	1.30	0.071	0.071	2.43	1.0%	0 to 2%
MFD2B	2	0.28	4.4	0.68	0.046	0.091	1.67	5.5%	0 to 5%
MFD3B	4	0.51	2.4	0.37	0.0164	0.052	1.2	17.2%	0 to 5%
Multi-Family Dwelling Very High-Seismic ($S_{MS} = 2.25$ g) Baseline Archetype Models									
MFD4B	1	0.17	6.1	1.41	0.102	0.102	1.85	3.5%	NA
MFD5B	2	0.35	3.2	0.73	0.053	0.099	1.23	15.7%	NA
MFD6B	4	0.54	1.9	0.44	0.022	0.054	1.02	26%	NA
Single-Family Dwelling High-Seismic ($S_{MS} = 1.5$ g) Baseline Archetype Models									
SFD1B	1	0.16	12.1	1.86	0.022	0.022	2.15	1.8%	0 to 2%
SFD1BC	1	0.15	8.3	1.28	0.066	0.066	2.21	1.6%	0 to 2%
SFD2B	2	0.26	5.0	0.77	0.058	0.117	1.99	2.6%	0 to 5%
SFD2BC	2	0.25	4.9	0.76	0.049	0.096	1.92	3.0%	0 to 5%
Single-Family Dwelling Very High-Seismic ($S_{MS} = 2.25$ g) Baseline Archetype Models									
SFD3B	1	0.15	8.7	2.01	0.028	0.028	1.51	7.9%	NA
SFD3BC	1	0.16	5.5	1.28	0.066	0.066	1.47	8.6%	NA
SFD4B	2	0.26	3.8	0.87	0.066	0.148	1.48	8.4%	NA

* Median drift ratio at incipient collapse.

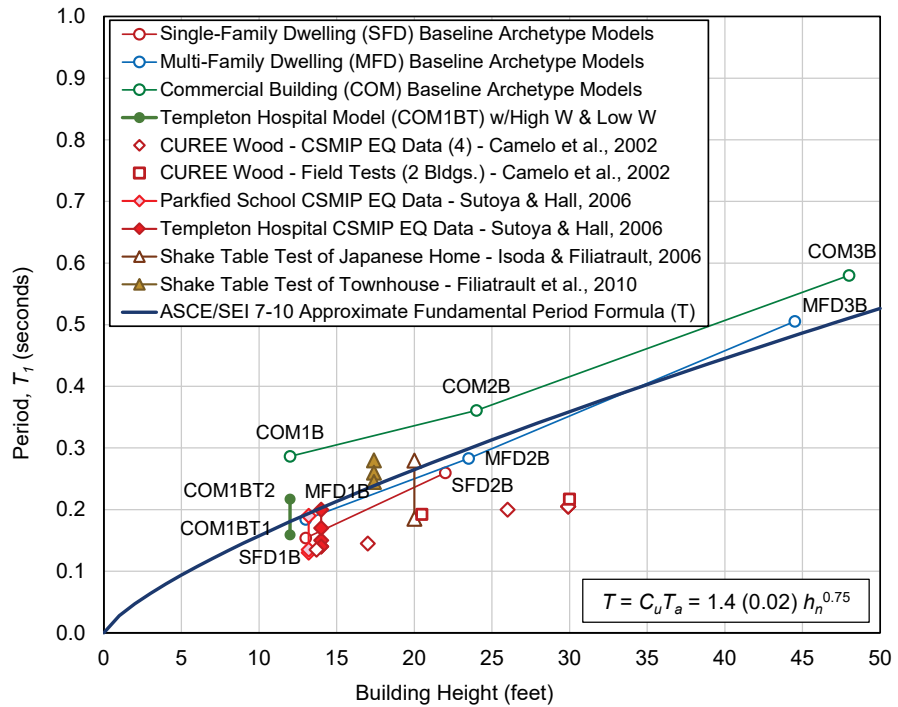


Figure 6-1 Fundamental-mode periods (T_f) of baseline archetype models, measured periods of wood light-frame buildings obtained from earthquake records, forced-vibration testing, and shake table tests, and the approximate fundamental-period ($T = C_u T_a$) from ASCE/SEI 7-10.

assumed archetype configuration. One-story COM archetype models have relatively large plan dimensions with significant window and door openings in the exterior walls, no interior structural shear walls, and a limited number of nonstructural partition walls. The numerical periods of the Templeton Hospital building (COM1BT1 and COM1BT2), modeled with the actual stiffness (including nonstructural wall finishes), are similar to the measured periods of this building (Sutoya and Hall, 2006).

Values of MCE_R collapse probability for the ten high seismic baseline archetype models plotted as a function of building period are shown in Figure 6-2. MCE_R collapse probabilities are low (i.e., 1 percent to 3 percent) at very short periods (i.e., 0.15 seconds to 0.25 seconds), and increase with period, representing a reversal of the trend observed in the collapse performance of short-period buildings in prior FEMA P-695 studies (see Figure 1-1). In all cases, collapse of these models occurred due to lateral instability in the first story caused by P-Delta effects.

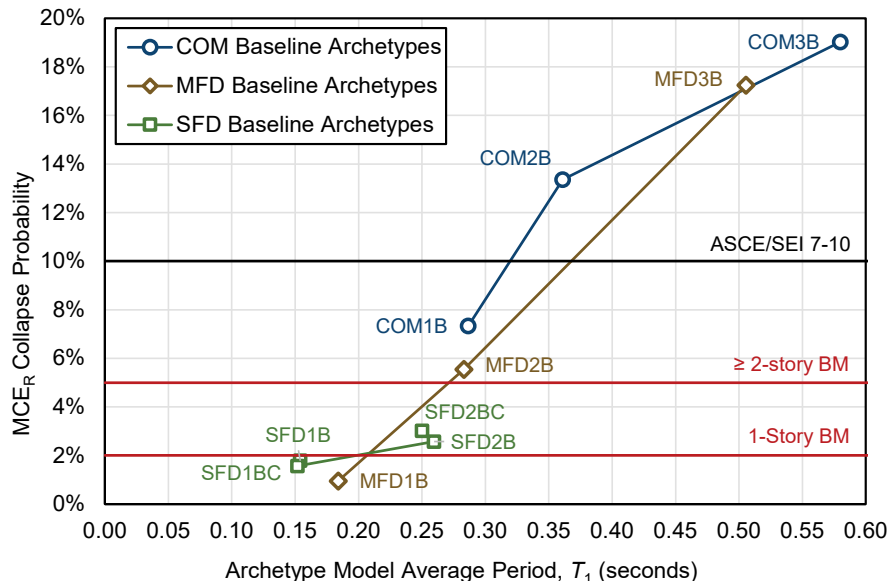


Figure 6-2 MCE_R collapse probability versus average model period (T_1), including benchmark (BM) collapse probabilities from historical earthquake data (Chapter 2) and ASCE/SEI 7-10, for high seismic baseline archetype models.

For purposes of comparison, horizontal lines are included in Figure 6-2 (and in subsequent figures of this chapter) to indicate: (1) the 2-percent benchmark collapse probability for one-story high-seismic archetype models based on historical earthquake data presented in Chapter 2; (2) the 5-percent benchmark collapse probability for two-story and taller high-seismic archetype models, also based on historical earthquake data; and (3) the 10 percent collapse safety objective of ASCE/SEI 7-10. As shown in the figure, collapse probabilities for one-story and two-story SFD and MFD archetypes conform to benchmark collapse rates based on red-tag data (except for the two-story MFD archetype), whereas, the taller (i.e., longer period) four-story MFD archetype, and all COM archetypes, do not conform. It should also be noted that two-story and taller archetypes consistently have a greater MCE_R collapse probability than one-story archetypes of the same system, which is consistent with the observation that two-story and taller wood light-frame buildings are about 2.5 times more likely (on average) than one-story wood light-frame buildings to receive a red tag following an earthquake.

The trend of increasing probability of collapse with period shown in Figure 6-2 is not directly related to building period. Rather, the increase in the probability of collapse in taller archetypes is a function of P-Delta failure mechanisms in the first story of multi-story archetypes, and reduced archetype model overstrength, as illustrated in Figure 6-3.

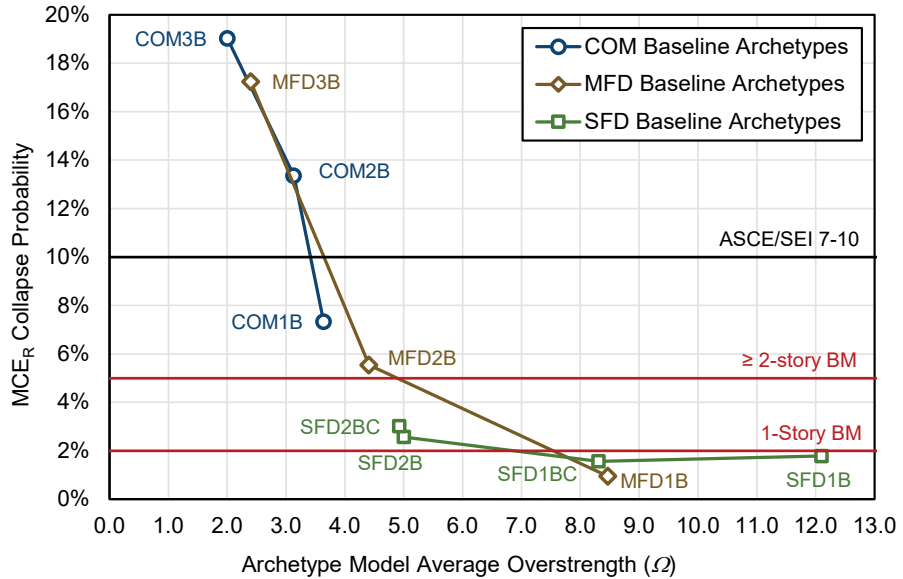


Figure 6-3 MCE_R collapse probability versus archetype model overstrength (Ω), including benchmark (BM) collapse probabilities from historical earthquake data (Chapter 2) and ASCE/SEI 7-10, for high seismic baseline archetype models.

In Figure 6-3, MCE_R collapse probabilities for the ten high seismic baseline archetype models, plotted as a function of average (of N-S and E-W) building archetype model overstrength (Ω), show that the probability of collapse decreases with increased archetype model overstrength. Archetype models with overstrength (Ω) of about 4.0 have collapse probabilities that conform (or almost conform) to benchmark collapse rates based on red-tag data. In contrast, weaker COM and MFD archetypes have significantly higher collapse probabilities, and collapse probability increases significantly for archetype model overstrengths below about 4.0.

The MCE_R collapse probabilities for the nine very high seismic baseline archetype models, plotted as a function of building period, are shown in Figure 6-4. Trends in collapse performance for very high seismic archetypes are similar to trends observed in Figure 6-2 for high seismic archetypes, although collapse probabilities are significantly higher. For example, collapse probabilities for the very high seismic one-story and two-story SFD archetypes are about 8 percent; whereas, collapse probabilities for the corresponding high seismic SFD archetypes shown in Figure 6-2 are only about 2 percent. It should be noted that target benchmark collapse probabilities based on red-tag data are not shown in Figure 6-4 because these targets do not apply to the very high seismic ground motion intensity, due to a lack of empirical data.

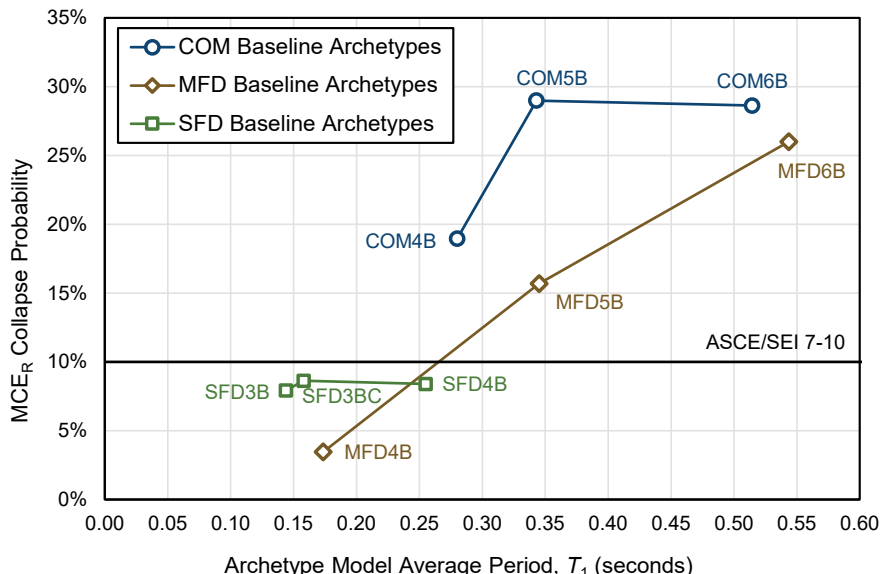


Figure 6-4 MCE_R collapse probability versus average model period (T_1), including the benchmark collapse probability from ASCE/SEI 7-10, for very high seismic baseline archetype models.

MCE_R collapse probabilities for the same nine very high seismic baseline archetype models, plotted as a function of archetype model overstrength (Ω), are shown in Figure 6-5. The trends for very high seismic archetypes are similar to trends observed in Figure 6-3 for high seismic archetypes. As shown in Figure 6-5, collapse probability increases as the archetype model overstrength decreases, and exceeds 10 percent when archetype model overstrength drops below about 4.0.

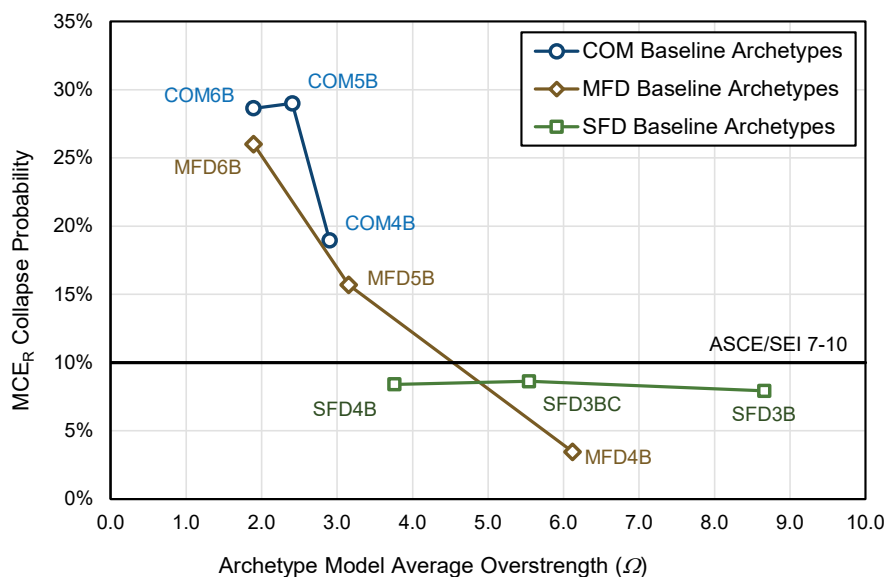


Figure 6-5 MCE_R collapse probability versus archetype model overstrength (Ω), including the benchmark collapse probability from ASCE/SEI 7-10, for very high seismic baseline archetype models.

Differences in collapse performance between high seismic and very high seismic archetypes are due to the relative contribution of: (1) the seismic force-resisting system (SFRS); and (2) other structural elements and nonstructural components that contribute to the total strength of the building. Conceptually, if the SFRS provided 100 percent of the lateral strength in a building, then a very high seismic archetype that was designed for 50 percent more base shear would have the same MCE_R collapse probability as the high seismic archetype (i.e., a 50-percent increase in design strength would be sufficient to accommodate a 50-percent increase in MCE_R ground motion intensity without a reduction in collapse performance).

For wood light-frame buildings, however, the total seismic force resistance is a combination of the strength of the SFRS and contributions from nonstructural interior and exterior wall finishes. Although the SFRS in very high seismic archetypes is required to be 50 percent stronger, nonstructural wall finishes are not, and provide a smaller percentage contribution to the overall strength of the building. A similar observation was made in prior FEMA P-695 studies (FEMA, 2009b; NIST, 2010), in which collapse performance was influenced by the relative contributions between seismic and gravity design loads to the resulting archetype strength.

Overall findings of the parametric study on baseline configurations of wood light-frame building archetype models include:

1. **Building Period.** Fundamental periods of baseline SFD and MFD archetype models are consistent with measured periods in actual wood light-frame buildings. Fundamental periods of COM building archetype models are somewhat longer than measured periods. Fundamental building periods are consistent with the measured periods in the Templeton Hospital building when model stiffness properties are based on actual building stiffness (i.e., COM1BT1 and COMB1T2). Including the stiffness contributions from nonstructural wall finishes is necessary for modeled periods to approximately match measured periods.
2. **Collapse Failure Modes.** Simulated collapse of all baseline archetype models was due to sideway collapse in the first story, caused by P-Delta effects. This is consistent with collapse modes observed in wood light-frame buildings in historic earthquakes and full-scale shake table tests.
3. **Collapse Probabilities.** MCE_R collapse probabilities calculated for one-story and two-story SFD and MFD baseline archetype models (high seismic design) are consistent with collapse rates based on red-tag data for wood light-frame buildings in areas that experienced MCE_R ground motions during the 1994 Northridge earthquake. Collapse probabilities

of (weaker) two-story COM, and (weaker) four-story MFD and COM archetype models, are much larger than collapse rates based on red-tag data, and exceed the 10-percent probability of collapse safety objective in ASCE/SEI 7-10.

Although the trend of larger collapse probabilities for taller archetypes is supported by the red-tag data presented in Chapter 2 (i.e., the likelihood of a two-story and taller wood light-frame building receiving a red tag was about 2.5 times that of one-story wood light-frame building), collapse probabilities above 5 percent are suspect. Possible explanations include limitations in available earthquake data (i.e., red-tag data are insufficient to accurately determine possible differences in collapse performance of multi-story buildings by height) and design and modeling assumptions, which may be pessimistic for taller wood light-frame buildings employing nailed wood structural panel shear walls.

4. **Collapse Trend with Building Height.** The probability of collapse in wood light-frame baseline archetype models increases with height, all else being equal. This trend is most likely due to differences in archetype model overstrength (Ω), which tends to decrease with height, and P-Delta collapse in the first story, which becomes more critical with height.
5. **Strength.** Collapse of wood light-frame baseline archetype models is strongly influenced by archetype strength. The stronger the archetype model, the better the collapse performance, all else being equal.
6. **P-Delta Effects.** Collapse of wood light-frame archetype models is strongly influenced by P-Delta effects. In general, the weaker the archetype model, the more that P-Delta effects detrimentally affect collapse performance, all else being equal.
7. **Very High Seismic (Near Fault) Collapse Performance.** The probability of collapse for very high seismic archetype models is larger than corresponding high seismic archetype models, even when the SFRS is designed for proportionally larger seismic forces. A 50-percent increase in the strength of the SFRS does not result in a 50-percent increase in normalized peak strength ratio (V_{max}/W) in very high seismic archetypes because the relative contribution from nonstructural wall finishes is not similarly increased.

Collapse performance of very high seismic designs was evaluated for MCE_R ground motions ($S_{MS} = 2.25$ g) that represent a ground motion intensity typical of sites relatively close to an active fault (i.e., an intensity 50 percent greater than that of high seismic ground motions). Analyses

was performed using ground motions recorded at far-field sites, but the amplitudes were scaled up based upon design as $S_{MS} = 2.25g$.

6.2.2 Collapse Displacement Capacity Parametric Study

Collapse displacement capacity studies investigated the effects of residual post-capping strength and ultimate displacement capacity on response behavior and collapse performance. Based on test data available at the time, prior FEMA P-695 studies limited displacement capacities to the displacement corresponding to a post-peak strength of $0.8V_{max}$, and “collapse” was assumed to occur when the displacement exceeded 7 percent of the story height. In this study, models with six levels of residual post-capping strength (i.e., 0 percent, 10 percent, 20 percent, 40 percent, 50 percent, and 60 percent) were compared with baseline models incorporating 30 percent. In addition, residual strength ratios were also used as a proxy for incorporating non-simulated sources of residual strength in wood light-frame systems, and all models assumed that the ultimate displacement was unlimited (i.e., $\delta_u = \infty$).

Key model properties and collapse results of the archetypes used in the collapse displacement parametric study are summarized in Table 6-2. Variants designated “C0” have zero residual strength, “C1” have 10% residual strength, “C2” have 20% residual strength, “C3 or blank” have baseline 30% residual strength, “C4” have 40% residual strength, and “C6” have 60% residual strength.

MCE_R collapse probabilities for two-story baseline and variant archetypes, plotted as a function of collapse displacement characterized by first-story median drift ratio at incipient collapse, are shown in Figure 6-6. The figure illustrates two strong trends: (1) collapse displacement capacity increases with residual strength; and (2) collapse probabilities decrease with increases in collapse displacement capacity.

First-story median drift ratios at incipient collapse range from about 6 percent for the COM2B archetype model, to about 9 percent for the MFD2B archetype model, and about 12 percent for SFD2B archetype model, following the trend in archetype model strength (i.e., the SFD2B archetype is stronger than the MFD2B archetype, which is stronger than the COM2B archetype). The first-floor median drift ratio of about 12 percent for the SFD2B baseline archetype model (with 30-percent residual strength) is larger than the drift ratio of 8 percent for the SFD2B-C2 archetype (with 20-percent residual strength), and the probability of collapse for this archetype decreases from about 5 percent to about 2.5 percent. In this case, the relatively strong, two-story SFD archetype does not require as much collapse displacement

Table 6-2 Summary of Key Properties and Collapse Results for Archetype Models used in the Displacement Capacity Parametric Study

Archetype Model ID	Model Properties				Collapse Results				Benchmark Collapse Probability (%)
	No. of Stories	Period T_1 (sec)	Strength		Drift Ratio *		CMR_{3D}	P[COL MCE _R] (%)	
One-story Commercial Building High-Seismic ($S_{MS} = 1.5$ g) Archetype Models									
COM1B-C0	1	0.29	3.3	0.51	0.051	0.051	1.28	14.2%	0 to 2%
COM1B-C1	1	0.29	3.4	0.53	0.059	0.059	1.36	11.9%	0 to 2%
COM1B-C2	1	0.29	3.5	0.54	0.067	0.067	1.44	9.7%	0 to 2%
COM1B	1	0.29	3.6	0.56	0.082	0.082	1.55	7.3%	0 to 2%
Two-Story Commercial Building High-Seismic ($S_{MS} = 1.5$ g) Archetype Models									
COM2B-C0	2	0.36	2.8	0.44	0.024	0.046	1.09	23%	0 to 5%
COM2B	2	0.36	3.1	0.48	0.035	0.067	1.31	13.4%	0 to 5%
COM2B-C4	2	0.36	3.2	0.50	0.044	0.085	1.37	11.4%	0 to 5%
COM2B-C6	2	0.36	3.4	0.52	0.072	0.142	1.71	5.1%	0 to 5%
One-Story Multi-Family-Dwelling High-Seismic ($S_{MS} = 1.5$ g) Archetype Models									
MFD1B-C0	1	0.19	7.8	1.20	0.045	0.045	2.02	2.4%	0 to 2%
MFD1B-C1	1	0.19	8.0	1.24	0.067	0.067	2.28	1.3%	0 to 2%
MFD1B-C2	1	0.19	8.2	1.27	0.075	0.075	2.42	1.0%	0 to 2%
MFD1B	1	0.19	8.5	1.30	0.071	0.071	2.43	1.0%	0 to 2%
Two-Story Multi-Family-Dwelling High-Seismic ($S_{MS} = 1.5$ g) Archetype Models									
MFD2B-C0	2	0.28	4.1	0.63	0.026	0.050	1.32	13.1%	0 to 5%
MFD2B	2	0.28	4.2	0.68	0.046	0.091	1.67	5.5%	0 to 5%
MFD2B-C4	2	0.28	4.5	0.69	0.065	0.128	1.84	3.7%	0 to 5%
MFD2B-C6	2	0.28	4.7	0.73	0.095	0.187	2.35	1.1%	0 to 5%
One-Story Single-Family Dwelling High-Seismic ($S_{MS} = 1.5$ g) Archetype Models									
SFD1B-C0	1	0.16	11.2	1.72	0.022	0.022	2.05	2.3%	0 to 2%
SFD1B-C1	1	0.16	11.5	1.77	0.021	0.021	2.10	2.0%	0 to 2%
SFD1B-C2	1	0.16	11.8	1.82	0.021	0.021	2.13	1.9%	0 to 2%
SFD1B	1	0.16	12.1	1.86	0.022	0.022	2.15	1.8%	0 to 2%
Two-Story Single-Family Dwelling High-Seismic ($S_{MS} = 1.5$ g) Archetype Models									
SFD2B-C0	2	0.26	4.6	0.70	0.029	0.056	1.42	10.1%	0 to 5%
SFD2B-C1	2	0.26	4.7	0.73	0.030	0.060	1.58	7.0%	0 to 5%
SFD2B-C2	2	0.26	4.9	0.75	0.041	0.081	1.72	4.9%	0 to 5%
SFD2B	2	0.26	5.0	0.77	0.058	0.117	1.99	2.6%	0 to 5%
SFD2B-C4	2	0.26	5.1	0.79	0.065	0.128	1.96	2.8%	0 to 5%
SFD2B-C6	2	0.26	5.4	0.82	0.078	0.153	2.20	1.6%	0 to 5%

* Median drift ratio at incipient collapse.

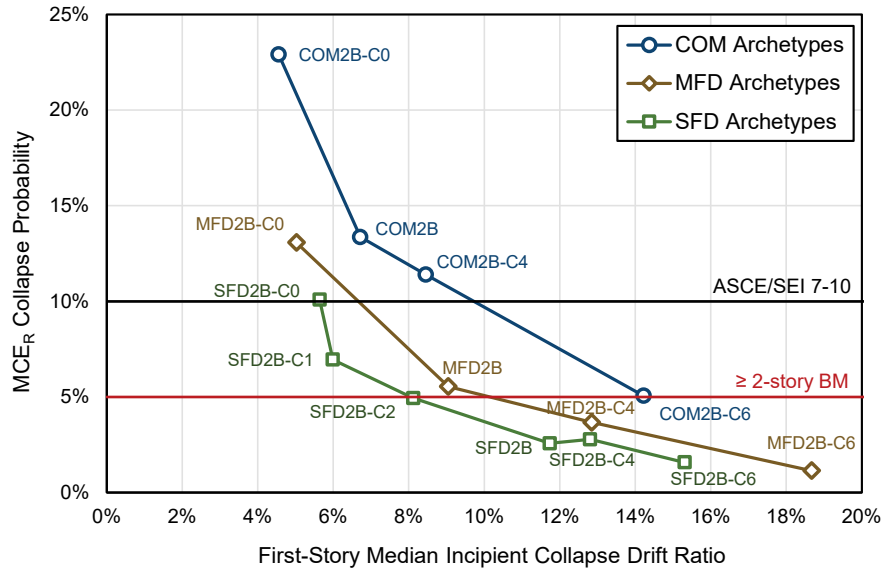


Figure 6-6 MCE_R collapse probability versus first story median drift ratio at incipient collapse, including benchmark (BM) collapse probabilities from historical earthquake data (Chapter 2) and ASCE/SEI 7-10, for two-story archetype models used in the displacement capacity parametric study.

capacity (i.e., residual strength) to be consistent with the observed collapse performance suggested by red-tag data.

MCE_R collapse probabilities for one-story baseline and variant archetypes, plotted as a function of collapse displacement characterized by first-story median drift ratio at incipient collapse, are shown in Figure 6-7. This group of archetypes includes relatively pessimistic assumptions of collapse displacement capacity characterized by residual strengths of 0 percent, 10 percent and 20 percent. Although basic trends are similar to those observed in Figure 6-6 for two-story COM archetypes, they are less pronounced for MFD archetypes, and essentially independent of collapse displacement capacity for SFD archetypes.

In the case of single-family dwellings, one-story archetypes are so strong that they do not require large displacement capacities to perform well. The very low first-story median drift ratio at incipient collapse (i.e., about 2 percent for all one-story SFD archetypes) is the result of rapid and complete failure when dynamic response reaches the full strength of the archetype (at a very high level of response). As illustrated in Figure 6-7, trends in the collapse performance of one-story SFD and MFD baseline archetype models would not have changed significantly, if, for example, residual post-capping strength ratios were assumed to be 10 percent, rather than 30 percent of peak strength.

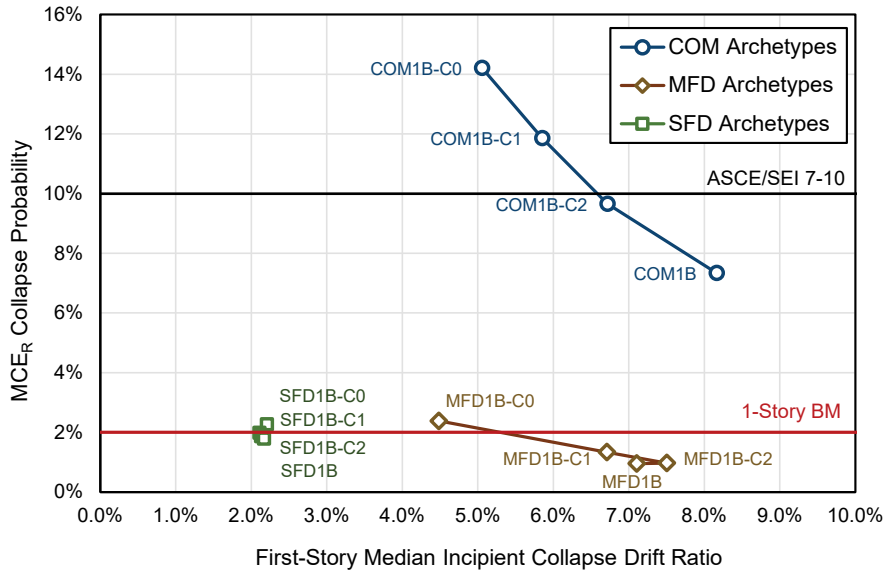


Figure 6-7 MCE_R collapse probability versus first story median drift ratio at incipient collapse, including benchmark (BM) collapse probabilities from historical earthquake data (Chapter 2) and ASCE/SEI 7-10, for one-story archetype models used in the displacement capacity parametric study.

Overall findings of the parametric study on collapse displacement capacity include:

- Response Behavior.** Qualitatively, earthquake response of archetype models with some level of residual strength better emulate period lengthening, displacement capacity, and first-story collapse failure mechanisms observed during shake table testing of full-scale wood light-frame buildings.
- Collapse Probabilities.** MCE_R collapse probabilities calculated for relatively strong one-story and two-story SFD and MFD archetypes with 30 percent (or less) residual strength compare well with collapse rates based on red-tag data. Weaker, two-story COM archetypes would require more than the baseline assumption of 30 percent residual strength to have collapse performance consistent with red-tag data.
- Collapse Displacement Capacity.** Collapse of weaker archetype models is strongly influenced by post-capping collapse displacement capacity. The greater the collapse displacement capacity in the archetype model, the better the collapse performance, all else being equal.

6.2.3 Nonstructural Interior and Exterior Wall Finishes Parametric Study

Nonstructural interior and exterior wall finish studies investigated the effects of wall finishes on response behavior and collapse performance. Wall finishes such as gypsum wallboard, stucco, and horizontal wood siding) are considered to be nonstructural, and are typically not considered in the design of the seismic force-resisting system. In this study, archetypes were modified to remove all nonstructural interior and exterior wall finishes, and were compared to the results of corresponding baseline archetype models including wall finishes.

Key model properties and collapse results for the baseline and variant archetype models are summarized in Table 6-3. Archetypes with nonstructural wall finishes removed are designated by “NS” in the table. Archetypes with exterior stucco finishes replaced by horizontal wood siding are designated by “NSP” in the table.

MCE_R collapse probabilities for the six high seismic archetype models without wall finishes and the corresponding baseline archetype models (with nonstructural wall finishes) are plotted as a function of average building overstrength (Ω) in Figure 6-8. The trend of probability of collapse decreasing with increasing archetype model overstrength is similar to the trend observed in Figure 6-3, except that the probability of collapse is typically much higher for archetypes without nonstructural wall finishes than for the corresponding baseline archetypes with wall finishes. Archetype models with overstrength (Ω) of about 4.0 have collapse probabilities that conform (or almost conform) to benchmark collapse rates based on red-tag data. In contrast, weaker archetypes have significantly higher collapse probabilities, and collapse probability increases significantly for archetype model overstrengths below about 4.0.

Overall findings of the parametric study on nonstructural interior and exterior wall finishes include:

1. **Building Period.** Fundamental periods of archetype models without nonstructural wall finishes are much longer and inconsistent with the measured periods of actual buildings.
2. **Collapse Probabilities.** MCE_R collapse probabilities calculated for archetype models without nonstructural wall finishes are typically higher than, and inconsistent with, collapse rates based on red-tag data. Differences are more significant in two-story archetype models.

Table 6-3 Summary of Key Properties and Collapse Results for Archetype Models used in the Nonstructural Wall Finishes Parametric Study

Archetype Model ID	Model Properties			Collapse Results				P[COL MCE _R] (%)	Benchmark Collapse Probability (%)
	No. of Stories	Period T_1 (sec)	Strength		Drift Ratio *		CMR _{3D}		
			Ω	V_{\max}/W	Roof	1 st -Story			
2-Story Commercial Building High-Seismic ($S_{MS} = 1.5$ g) Archetype Models									
COM2B	2	0.36	3.1	0.48	0.035	0.067	1.31	13.4%	0 to 5%
COM2B-NS	2	0.58	1.53	0.24	0.028	0.046	0.92	33%	0 to 5%
2-Story Multi-Family-Dwelling High-Seismic ($S_{MS} = 1.5$ g) Archetype Models									
MFD2B	2	0.28	4.4	0.68	0.046	0.091	1.67	5.5%	0 to 5%
MFD2B-NS	2	0.58	1.55	0.24	0.029	0.047	0.94	31%	0 to 5%
One-Story Single-Family Dwelling High-Seismic ($S_{MS} = 1.5$ g) Archetype Models									
SFD1B	1	0.16	12.1	1.86	0.022	0.022	2.15	1.8%	0 to 2%
SFD1B-NS	1	0.27	5.2	0.80	0.022	0.022	1.94	2.9%	0 to 2%
SFD1B-NSP	1	0.20	8.7	1.34	0.090	0.090	1.93	2.9%	0 to 2%
SFD1BC	1	0.15	8.3	1.28	0.033	0.033	2.21	1.6%	0 to 2%
SFD1BC-NS	1	0.37	2.7	0.42	0.066	0.066	1.11	21.6%	0 to 2%
SFD1BC-NSP	1	0.35	3.0	0.46	0.084	0.084	2.01	2.5%	0 to 2%
2-Story Single-Family Dwelling High-Seismic ($S_{MS} = 1.5$ g) Archetype Models									
SFD2B	2	0.26	5.0	0.77	0.058	0.117	1.99	2.6%	0 to 5%
SFD2B-NS	2	0.27	2.2	0.34	0.030	0.056	1.12	21%	0 to 5%
SFD2B-NSP	2	0.33	3.8	0.59	0.042	0.088	1.56	7.2%	0 to 5%
SFD2BC	2	0.25	4.9	0.76	0.049	0.096	1.92	3.0%	0 to 5%
SFD2BC-NS	2	0.43	2.8	0.43	0.025	0.046	1.11	22%	0 to 5%
SFD2BC-NSP	2	0.41	3.2	0.49	0.035	0.075	1.54	7.7%	0 to 5%

* Median drift ratio at incipient collapse.

3. **Multi-Story Buildings.** Without the added stiffness and strength from nonstructural wall finishes, MCE_R collapse probabilities for two-story archetype models increase significantly. For example, MCE_R collapse probabilities increase from 13.4 percent to 33.1 percent for two-story commercial building archetypes (COM2B and COM2B-NS), from 5.5 percent to 31.3 percent for multi-family dwelling archetypes (MFD2B and MFD2B-NS), from 2.6 percent to 21 percent for two-story single-family dwelling archetypes (SFD2B and SFD2B-NS), and from 3.0 percent to 21 percent for single-family dwelling conventional construction archetypes (SFD2BC and SFD2B-NS). These results suggest that nonstructural wall finishes can be as important to collapse performance of multi-story wood light-frame buildings as the wood structural panel sheathing.

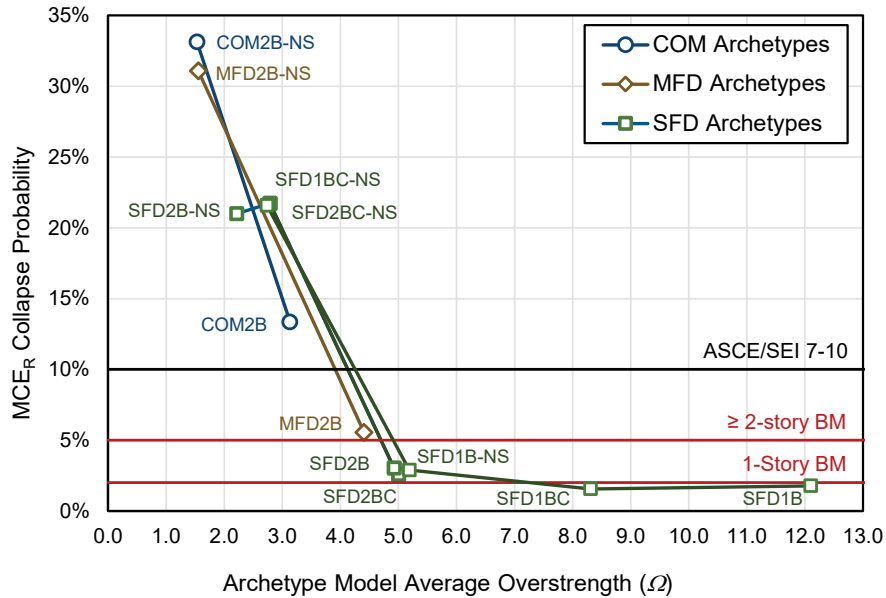


Figure 6-8 MCE_R collapse probability versus archetype model overstrength (Ω), including benchmark (BM) collapse probabilities from historical earthquake data (Chapter 2) and ASCE/SEI 7-10, for archetype models used in the nonstructural wall finishes parametric study.

6.2.4 Soil-Structure Interaction and Foundation Flexibility Parametric Study

Soil-structure interaction (SSI) and foundation flexibility studies investigated the effects of non-rigid foundations on response behavior and collapse performance. SSI effects on wood light-frame archetypes were expected to be minimal. In this study, archetypes were modified to include nonlinear soil springs representing two different site conditions (i.e., stiff and soft soil sites), and were compared to the results of corresponding baseline archetype models with rigid foundations.

Key model properties and collapse results for baseline and variant archetype models are summarized in Table 6-4. Archetypes with springs representing a stiffer (CD boundary) site are designated by “CD” and archetypes with springs representing a softer (DE boundary) site are designated by “DE” in the table.

Overall findings of the parametric study on SSI and foundation flexibility include:

- 1. Nonlinear Static (Pushover) Response.** In all cases, nonlinear static (pushover) curves for archetype models with nonlinear soil springs were found to be virtually identical to pushover curves for corresponding baseline archetype models with rigid foundations.

Table 6-4 Summary of Key Properties and Collapse Results for Archetype Models used in the Soil-Structure Interaction and Foundation Flexibility Parametric Study

Archetype Model ID	Model Properties			Collapse Results ⁽¹⁾				Benchmark Collapse Probability (%)	
	No. of Stories	Period T_1 (sec)	Strength ⁽¹⁾		Drift Ratio ⁽²⁾		$P[COL MCE_R]$ (%)		
			Ω	V_{max}/W	Roof	1st-Story			
Commercial Building High-Seismic ($S_{MS} = 1.5$ g) Archetype Models									
COM1B	1	0.29	3.6	0.56	0.083	0.083	1.59	6.7%	
COM1B-CD	1	0.29	3.6	0.56	0.082	0.082	1.57	6.8%	
COM1B-DE	1	0.29	3.6	0.56	0.079	0.079	1.58	7.0%	
COM2B	2	0.36	3.5	0.53	0.034	0.066	1.33	12.6%	
COM2B-CD	2	0.36	3.1	0.48	0.035	0.068	1.32	12.6%	
COM2B-DE	2	0.36	3.1	0.48	0.034	0.065	1.33	13.0%	
COM3B	4	0.58	2.0	0.31	0.016	0.045	1.15	18.8%	
COM3B-CD	4	0.58	2.0	0.31	0.016	0.045	1.15	19.6%	
COM3B-DE	4	0.58	2.0	0.31	0.016	0.047	1.15	19.4%	
Multi-Family Dwelling Building High-Seismic ($S_{MS} = 1.5$ g) Archetype Models									
MFD1B	1	0.19	8.4	1.30	0.071	0.071	2.56	1.00.7%	
MFD1-CD	1	0.19	8.4	1.30	0.074	0.074	2.58	0.7%	
MFD1-DE	1	0.19	8.4	1.30	0.073	0.073	2.56	0.7%	
MFD2B	2	0.28	4.2	0.65	0.059	0.116	1.79	4.2%	
MFD2-CD	2	0.28	4.2	0.65	0.058	0.115	1.77	4.2%	
MFD2-DE	2	0.28	4.2	0.65	0.056	0.109	1.79	4.3%	
MFD3B	4	0.51	2.3	0.36	0.018	0.052	1.32	17.22.9%	
MFD3-CD	4	0.51	2.3	0.36	0.018	0.050	1.32	13.0%	
MFD3-DE	4	0.51	2.3	0.36	0.018	0.051	1.32	12.9%	

⁽¹⁾ Rayleigh damping equal to 0.1% assigned to first and second modes was used in these analyses.

⁽²⁾ Median drift ratio at incipient collapse.

- Collapse Probabilities.** In all cases, MCE_R collapse probabilities calculated for archetype models with nonlinear soil springs were found to be essentially the same as the corresponding baseline archetype models with rigid foundations.
- Soil Springs and Foundation Flexibility.** Flexible foundation elements and nonlinear soil springs are an unnecessary modeling enhancement for low-rise wood light-frame buildings, which typically do not have the requisite foundation size and depth, or building weight, to significantly impact building response and collapse performance.

6.2.5 Backbone Curve Shape Parametric Study

Backbone curve shape studies investigated the effects of backbone shape parameters on response behavior and collapse performance. In this study, archetypes were modified to include different assumptions for peak strength, drift ratio at peak strength, and slope of the post-peak curve, and were compared to the results of corresponding baseline archetype models using best estimate properties of backbone parameters from applicable test data. This study also included consideration of backbone shape in combination with the effects of nonstructural wall finishes (i.e., both with and without nonstructural finishes) and varying assumptions on residual post-capping strength ratios (i.e., 0, 30, and 60 percent).

Key model properties and collapse results for baseline and variant archetype models are summarized in table 6-5. Archetypes with alternative backbone parameters are identified by “R1” or “R2” in the table. Archetypes without nonstructural wall finishes are identified by “NS,” and archetypes with different levels of residual strength are identified by “C0” (zero residual strength) and “C6” (60% residual strength). Baseline archetypes included nonstructural wall finishes and 30% residual strength.

MCE_R collapse probabilities for each of the fourteen four-story commercial building archetype models are plotted as a function of average building overstrength (\mathcal{Q}) in Figure 6-9. Results are plotted for each archetype configuration, both with and without nonstructural wall finishes. Baseline and R1 archetypes have comparable backbone strength, while R2 archetype models have about 25 percent more strength in the wood structural panel shear walls.

MCE_R collapse probabilities for archetypes with baseline and R1 backbone parameters, both with and without nonstructural wall finishes are comparable (i.e., a 19 percent collapse probability for COM3B compared to a 19 percent collapse probability for COM3B-BSR1; and a 23 percent collapse probability for COM3B-NS compared to a 27 percent collapse probability for COM3B-BSR1-NS). MCE_R collapse probabilities for archetypes with R2 backbone parameters are significantly lower by comparison (i.e., 8.6% for COM3B-BSR2 with nonstructural wall finishes, and 16% collapse probability for COM3B-BSR2-NS with nonstructural wall finishes).

Table 6-5 Summary of Key Properties and Collapse Results for Archetype Models used in the Backbone Curve Shape Parametric Study

Archetype Model ID	Model Properties			Collapse Results				Benchmark Collapse Probability (%)	
	No. of Stories	Period T_1 (sec)	Strength		Drift Ratio *		$P[COL MCE_R]$ (%)		
			Ω	V_{max}/W	Roof	1 st -Story			
Baseline Backbone Curve – 4-Story Commercial Building High-Seismic ($S_{MS} = 1.5$ g) Archetype Models									
COM3B	4	0.58	2.0	0.31	0.016	0.046	1.15	19.0%	
COM3B-NS	4	0.82	1.3	0.20	0.019	0.047	1.03	22.7%	
Alternative Backbone Curve R1 – 4-Story Commercial Building High-Seismic ($S_{MS} = 1.5$ g) Archetype Models									
COM3B-BSR1-C0	4	0.53	1.9	0.30	0.017	0.045	1.16	19.1%	
COM3B-BSR1	4	0.53	1.9	0.30	0.023	0.073	1.22	15.7%	
COM3B-BSR1-C6	4	0.53	1.9	0.30	0.046	0.165	1.82	3.7%	
COM3B-BSR1-C0-NS	4	0.70	1.3	0.20	0.017	0.035	0.98	27.2%	
COM3B-BSR1-NS	4	0.70	1.3	0.20	0.018	0.041	1.00	27.1%	
COM3B-BSR1-C6-NS	4	0.70	1.3	0.20	0.026	0.076	1.14	18.3%	
Alternative Backbone Curve R2 – 4-Story Commercial Building High-Seismic ($S_{MS} = 1.5$ g) Archetype Models									
COM3B-BSR2-C0	4	0.50	2.3	0.35	0.019	0.055	1.29	13.7%	
COM3B-BSR2	4	0.50	2.3	0.35	0.032	0.107	1.46	8.6%	
COM3B-BSR2-C6	4	0.50	2.3	0.35	0.058	0.211	2.54	0.7%	
COM3B-BSR2-C0-NS	4	0.64	1.6	0.25	0.021	0.045	1.12	19.8%	
COM3B-BSR2-NS	4	0.64	1.6	0.25	0.026	0.059	1.22	15.8%	
COM3B-BSR2-C6-NS	4	0.64	1.6	0.25	0.043	0.136	1.72	4.4%	

* Median drift ratio at incipient collapse.

MCE_R collapse probabilities are plotted as a function of the first-story median drift ratio at incipient collapse in Figure 6-10. Results are plotted for each archetype configuration, both with and without nonstructural wall finishes, and indicate a strong trend in collapse performance with collapse displacement capacity. In the figure, MCE_R collapse probabilities decrease with increases in first-story median drift ratio at incipient collapse.

MCE_R collapse probabilities for R1 and R2 archetypes with 0-percent residual strength likely overestimate collapse risk by understating collapse displacement capacity; whereas, MCE_R collapse probabilities for R1 and R2 archetypes with 60-percent residual strength likely underestimate collapse risk by overstating collapse displacement capacity. For example, the MCE_R collapse probability for the R2 model, with nonstructural wall finishes, and 60 percent residual strength (COM3B-BSR2-C6) has a very low collapse probability of less than 1 percent, with an unrealistically large first-story median collapse drift ratio of 21 percent.

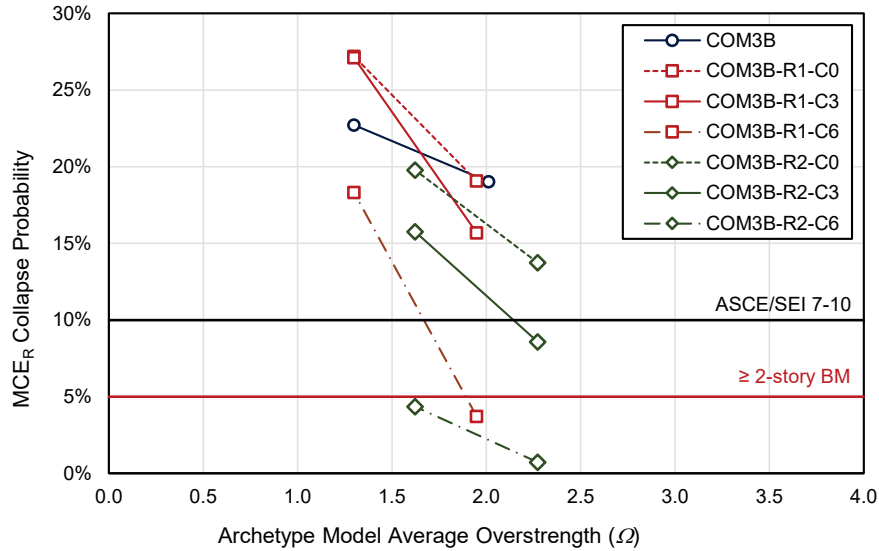


Figure 6-9 MCE_R collapse probability versus archetype model overstrength (Ω), including benchmark (BM) collapse probabilities from historical earthquake data (Chapter 2) and ASCE/SEI 7-10, for commercial building archetype models, with and without nonstructural wall finishes, used in the backbone curve shape parametric study.

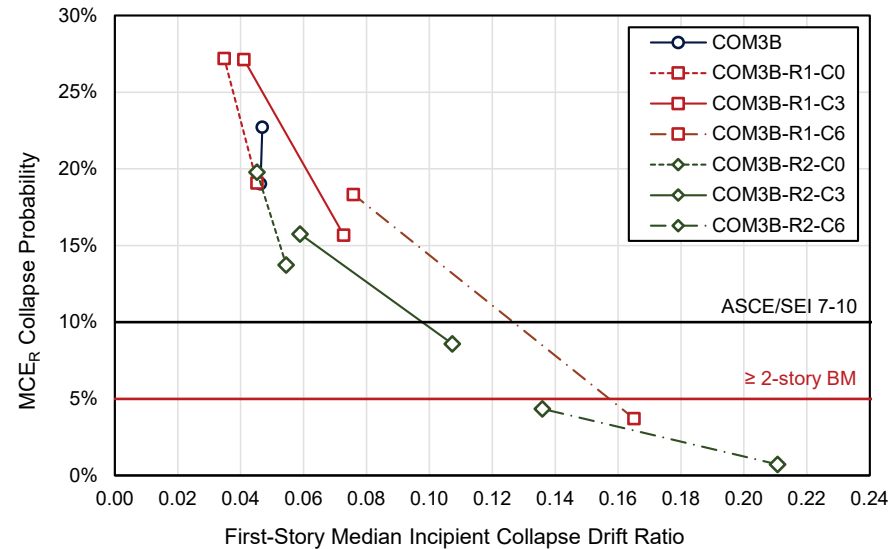


Figure 6-10 MCE_R collapse probability versus first story median drift ratio at incipient collapse, including benchmark (BM) collapse probabilities from historical earthquake data (Chapter 2) and ASCE/SEI 7-10, for commercial building archetype models, with and without nonstructural wall finishes, used in the backbone curve shape parametric study.

Overall findings of the parametric study on backbone curve shape include the following:

1. **Trends in MCE_R Collapse Performance.** MCE_R collapse probabilities for baseline, R1, and R2 archetypes with different backbone curve shapes show trends of improved collapse performance with increases in peak strength and collapse displacement that are consistent with trends observed in other wood light-frame building archetypes.
2. **Backbone Curve Shape.** MCE_R collapse probabilities were influenced by backbone shape parameters. Baseline and R1 archetypes, with different backbone curve shapes, but similar peak strengths and collapse displacement capacities (e.g., residual strength) were found to have comparable MCE_R collapse probabilities. R2 archetypes, with higher peak strengths, had lower MCE_R collapse probabilities. Increases in peak strength reduced the need for large collapse displacement capacities.

6.3 Conclusions and Recommendations

Prior FEMA P-695 collapse performance studies on a variety of structural systems over a range of periods have suggested that, for systems with design periods less than about 0.5 seconds, the probability of collapse given MCE_R ground motions increases significantly as the design period decreases.

Trends in observed earthquake damage of short-period buildings, however, do not support the high collapse probabilities predicted by numerical analysis. The apparent discrepancy between analytical prediction of collapse performance and the opinions and observations of structural engineers has been designated the *short-period building seismic performance paradox*.

With improved numerical modeling and representative wood light-frame building archetypes, this study has shown that MCE_R collapse probabilities decrease as the design period decreases, which is a reversal of the trend observed in prior FEMA P-695 studies. Further, numerical analyses of short-period wood light-frame buildings designed and evaluated for high seismic loads ($S_{MS} = 1.5$ g), resulted in low collapse probabilities for MCE_R ground motions, consistent with the collapse rates inferred by the observed performance of low-rise wood light-frame buildings in past earthquakes (e.g., red-tag data from the 1994 Northridge earthquake). As a result, this study has solved the short-period building seismic performance paradox for wood light-frame systems.

Numerical investigations conducted in this study provide valuable insights into the collapse performance of wood light-frame buildings that should be of

importance to seismic code development committees, engineering practitioners, and researchers. In the sections that follow, results from this study are compared to prior FEMA P-695 studies on wood light-frame buildings, and recommendations are provided in the following areas:

- Improved Seismic Design Codes and Standards
- Advanced Seismic Design and Analysis Practice
- Enhanced Modeling and Testing

6.3.1 Comparison with Prior FEMA P-695 Collapse Studies

Prior studies on wood light-frame systems were conducted as part of the FEMA P-695 methodology development and were presented as an example application in Section 9.4 of FEMA P-695 (FEMA, 2009b). Archetype configurations in that example included two performance groups for short-period wood light-frame buildings designed and evaluated for high seismic (SDC D_{max}) ground motions:

- Performance Group PG-1: one-story, two-story and three-story commercial buildings with low aspect ratio walls
- Performance Group PG-9: one-story and two-story single-family dwellings, and three-story, four-story, and five-story multi-family dwellings with high aspect ratio walls

Key model properties and collapse results for archetypes in Performance Groups PG-1 and PG-9 are summarized in Table 6-6. Information similar to that provided in Tables 6-1 to 6-5 of this report are provided in Table 6-6, with the following differences:

- The design period, T , (as well as the model period, T_l) is reported for comparison with the collapse probabilities plotted in Figure 1-1 of this report.
- Drift ratios at incipient collapse are not provided in the FEMA P-695 report. In that study, backbone curves have a descending slope beyond a story drift ratio of about 0.03, causing collapse at or before a story drift ratio of 0.07 (i.e., non-simulated failure).
- The collapse margin ratio, CMR , is based on incremental dynamic analyses of two-dimensional analytical models because two-dimensional (planar) models of shear walls were used in prior studies of wood light-frame buildings.

Table 6-6 Summary of Key Properties and Collapse Results for High Seismic Archetype Models from Prior FEMA P-695 Studies on Wood Light-Frame Buildings (FEMA, 2009b)

Archetype Model ID	Model Properties				Collapse Results				
	No. of Stories	Period T (sec)	Period T_1 (sec)	Strength		Drift Ratio*		CMR	P[COL MCE _R] (%)
				Ω	V_{max}/W	Roof	1 st -Story		
PG-1 – High Seismic ($S_{MS} = 1.5$ g) with Low Aspect Ratio Walls									
1	1	0.25	0.40	2.0	0.33	≤ 0.07	≤ 0.07	1.34	12.4%
5	2	0.26	0.46	2.5	0.42		≤ 0.07	1.49	9.1%
9	3	0.36	0.58	2.0	0.33		≤ 0.07	1.45	9.4%
PG-1	All	0.29	0.48	2.2	0.36		≤ 0.07	1.43	10.1%
PG-9 – High Seismic ($S_{MS} = 1.5$ g) with High Aspect Ratio Walls									
2	1	0.25	0.29	4.1	0.68	≤ 0.07	≤ 0.07	1.94	8.1%
6	2	0.26	0.37	3.8	0.63		≤ 0.07	2.14	6.1%
10	3	0.36	0.44	3.7	0.62		≤ 0.07	1.91	8.4%
13	4	0.45	0.53	2.9	0.48		≤ 0.07	1.73	12.0%
15	5	0.53	0.62	2.6	0.43		≤ 0.07	1.78	11.4%
PG-9	All	0.37	0.45	3.4	0.57		≤ 0.07	1.90	8.9%

* Drift ratios at incipient collapse are not provided in the FEMA P-695 report. In that study, backbone curves have a relatively steep descending slope beyond a story drift ratio of about 0.03, resulting in collapse at or before a story drift ratio of about 0.07.

Collapse results for short-period wood light-frame shear wall systems plotted in Figure 1-1 of this report represent the average values for PG-1 (low aspect ratio shear walls) and PG-9 (high aspect ratio shear walls) shown in the table. For example, PG-1 was plotted with a 10.1 percent average probability of collapse for an average period of $T = 0.29$ seconds, and PG-9 was plotted with an 8.9 percent average probability of collapse for an average period of $T = 0.37$ seconds. Collapse probabilities for individual archetypes ranged from 6.1 percent to 12.4 percent.

Archetypes in the prior FEMA P-695 study were designed in accordance with ASCE/SEI 7-05, except seismic design forces were based on a value of $R = 6$, rather than the current required value of $R = 6.5$. Archetypes with high aspect ratio walls were designed for reduced allowable shear capacity in accordance with the ANSI/AF&PA SDPWS strength adjustment factor for shear walls with aspect ratios greater than 2. This design adjustment effectively increased the strength of PG-9 archetypes by a range of about 35 percent to 65 percent over unreduced design strengths for low aspect ratio shear walls in PG-1. Walls were proportioned using ASD design, which requires approximately 12% longer shear walls relative to LRFD design, and

archetypes did not include the strength and stiffness of nonstructural interior and exterior walls and wall finishes.

There was an important difference in the calculation of the probability of collapse for PG-1 versus PG-9 archetypes. Due to greater uncertainty in the modeling of taller shear walls, a larger value of the total system collapse uncertainty factor, $\beta_{TOT} = 0.675$, was used to evaluate the collapse performance of PG-9 archetypes. A smaller value, $\beta_{TOT} = 0.50$, was used to evaluate the collapse performance of PG-1 archetypes. Hypothetically, if a lower value of $\beta_{TOT} = 0.50$ had been considered appropriate for the evaluation of PG-9 archetypes (e.g., due to improved modeling methods), then the collapse probabilities of PG-9 archetypes would have been about one-half of the values shown in Table 6-6, all else equal.

In Figure 6-11, collapse probabilities for eight archetype models from the prior FEMA P-695 study (shown in Table 6-6) are compared with six archetype models from this study with nonstructural exterior and interior wall finishes removed (shown in Table 6-3), and plotted as a function of normalized peak strength ratio (V_{max}/W).

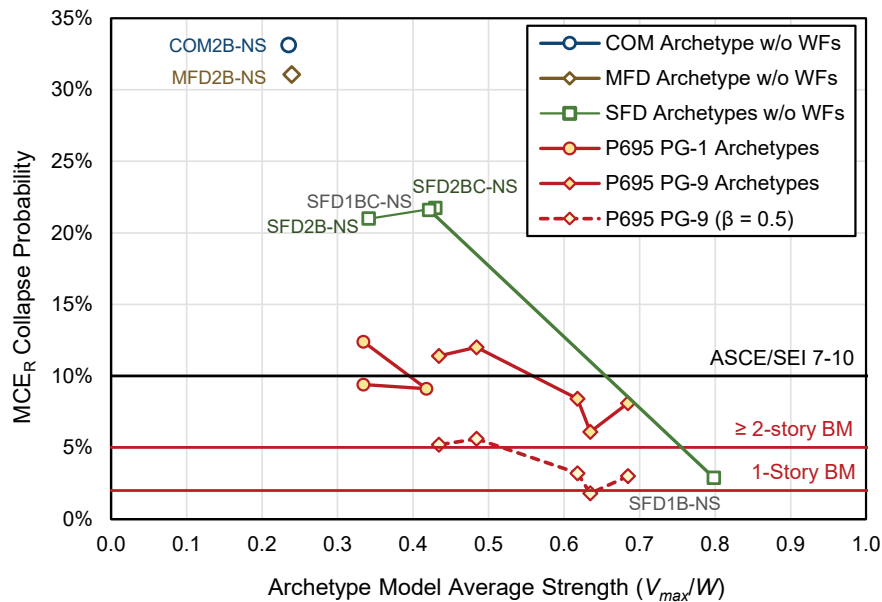


Figure 6-11 Comparison of MCE_R collapse probabilities for six COM, MFD and SFD archetypes without nonstructural wall finishes (WFs) from this study with eight PG-1 and PG-9 archetypes from a prior FEMA P-695 study, including adjusted collapse probabilities for PG-9 archetypes assuming a lognormal standard deviation of $\beta_{TOT} = 0.5$.

Adjusted values for PG-9 assuming $\beta_{TOT} = 0.50$ consistent with PG-1 are included in the figure for comparison with results from this study.

Normalized pushover strength (V_{max}/W), rather than overstrength (Ω), is used in the figure to compare the collapse performance of archetypes designed for different values of R . Horizontal lines indicating benchmark (BM) collapse probabilities from historical earthquake data (Chapter 2) and ASCE/SEI 7-10 are provided to compare overall results with established benchmarks.

Similarities or differences in collapse probabilities between this study and the prior FEMA P-695 study are related to the strength and collapse displacement capacities provided in the archetype models. Considering archetype strength, collapse probabilities from the prior FEMA P-695 study are generally consistent with the collapse probabilities from this study in the case of archetype models without nonstructural wall finishes. Better collapse performance of one-story archetypes in this study is attributed to more realistic modeling of the post-peak displacement capacity of wood light-frame buildings and increased strength associated with nonstructural wall finishes.

Overall, collapse probabilities for archetypes from both studies exceed the benchmark collapse rates established from historical earthquake data. One of the primary conclusions from this comparison is that archetype models without nonstructural wall finishes cannot, in general, explain the observed performance of short-period wood light-frame buildings in past earthquakes or full-scale shake table tests.

6.3.2 Recommendations for Improved Seismic Design Codes and Standards

Recommendations for improved codes and standards are considered applicable to seismic code development committees, including the Provisions Update Committee of the Building Seismic Safety Council, the Seismic Subcommittee of ASCE 7, and the ASCE 41 Standards Committee on Seismic Evaluation and Retrofit of Existing Buildings where applicable, as well as the Wood Design Standards Committee of the American Wood Council and other wood standards committees. It is recognized that code committees have limited resources, and recommended studies would, in most cases, require a funded project to develop the requisite technical basis for proposals to improve current codes or standards.

Improved Collapse Performance. In all cases, collapse of archetype models occurred due to sidesway failure of first-story walls. Increasing the strength and stiffness in the first-story of multi-story wood light-frame buildings could significantly improve the collapse performance of multi-

story buildings, which, in some cases, were found to have MCE_R collapse probabilities exceeding the collapse safety objectives of ASCE/SEI 7-10.

A study is recommended to develop code or standard changes (e.g., revisions to the vertical distribution of seismic design loads, or incorporation of nonstructural wall finishes) that would reduce the susceptibility of multi-story wood light-frame buildings to first-story failure and improve collapse performance.

Nonstructural Wall Finishes as Part of the Seismic-Force-Resisting System. Although not currently part of the designated seismic-force-resisting system for nailed wood structural panel shear walls, nonstructural wall finishes were found to significantly improve the collapse performance of wood light-frame buildings.

A study is recommended to develop code or standard changes that would incorporate nonstructural wall finishes in the seismic force resisting system of wood light-frame buildings. Although design procedures and nominal capacities are provided for some of these materials in the current wind and seismic design standard (AWC, 2015), a number of obstacles inhibit their use in typical design practice. Because incorporation of these materials would involve a significant revision to seismic design practice, exploration of this direction in a design example or guideline format might be considered as a first step. Consideration should include both design of new structures and evaluation and retrofit of existing structures.

Irregularity due to Nonstructural Wall Finishes. Nonstructural wall finishes above the first story can precipitate premature failure in the first-story, and adversely impact the collapse performance of certain wood light-frame building configurations.

A study is recommended to develop code or standard changes that would require checking and mitigating the potential for adverse impacts associated with building irregularity caused by the effects of nonstructural wall finishes.

SSI Reduction of Equivalent Lateral Force (ELF) Base Shear. The parametric study on SSI and foundation flexibility demonstrated that collapse performance was essentially the same for wood light-frame archetypes on a rigid base or modeled with a flexible foundation on nonlinear soil springs. The provisions of Section 19.2.1 of ASCE/SEI 7 permit a reduction in the equivalent lateral force (ELF) procedure design base shear to account for the soil damping effects of SSI.

Seismic code or standard committees should consider prohibiting this reduction for short-period wood light-frame buildings. This recommendation is based on investigations of wood light-frame collapse performance, but these findings may apply to other short-period building systems that depend on significant ductility in resisting earthquake ground motions.

Deformation Compatibility of Components Not Part of the Seismic-Force-Resisting System. Analytical results from this study have demonstrated that drift ratios experienced by short-period wood light-frame structures prior to collapse can be significantly larger than those currently used in ASCE/SEI 7 checks for deformation compatibility of components not part of the seismic-force-resisting system. This is of concern because the collapse probabilities presented herein assume that the gravity system can maintain gravity load support out to drifts at incipient collapse.

A study is recommended to determine whether current ASCE/SEI 7 provisions for deformation compatibility checks are adequate for protecting the gravity system and other components given the potentially large drifts expected at incipient collapse.

Very High Seismic Collapse Potential. The collapse probabilities of two-story and four-story archetypes designed and evaluated for very high seismic loads (i.e., 1.5 x high seismic, SDC D_{max} criteria of FEMA P-695) exceed the 10 percent collapse safety objective of ASCE/SEI 7 for Risk Category II structures, often by a substantial amount. Collapse performance is, in all cases, substantially worse for an archetype designed and evaluated for very high seismic criteria, as compared to the same archetype designed and evaluated for high seismic criteria. This trend is attributed to the influence of nonstructural wall finishes on the strength of wood light-frame buildings, which is not in proportion to the seismic design load. An increase in the probability of collapse given MCE_R ground motions was also observed in a study documented in FEMA P-695 for reinforced concrete moment frame systems. There is a consistent trend of collapse probabilities exceeding the 10 percent collapse safety objective of ASCE/SEI 7 in regions of very high seismicity, which is not unique to short-period wood buildings.

A study is recommended to quantify the potential increase in the conditional probability of collapse given MCE_R ground motions (i.e., above the 10 percent target of ASCE/SEI -7 for Risk Category II structures) and the associated increase in collapse risk (i.e., annual probability of collapse) for building archetypes of common seismic force resisting systems on sites located in regions of very high seismicity (i.e., $S_{MS} \geq 1.5$ g).

FEMA P-695 Seismic Criteria Update. The seismic criteria of FEMA P-695 are based on the “Zone 4” seismic criteria of the 1994 *Uniform Building Code* (ICBO, 1994), as embodied in the deterministic lower limit (DLL) seismic criteria of Section 21.2.2 of ASCE/SEI 7-05. The seismic criteria of FEMA P-695 are out-of-date with respect to the current seismic criteria of ASCE/SEI 7-16 and ASCE/SEI 7-22, as proposed. At short periods (i.e., the acceleration domain), the seismic criteria of FEMA P-695 are either the same as the DLL of ASCE/SEI 7-16, or about 10 percent less than those proposed for ASCE/SEI 7-22. In the velocity domain (i.e., periods greater than 1.0 second for Site Class D site conditions) the seismic criteria of FEMA P-695 are about 60 percent of those of ASCE/SEI 7-16 and somewhat less than those proposed for ASCE/SEI 7-22. Updating the seismic criteria of FEMA P-695 would not significantly affect the collapse evaluation of short-period buildings (or the findings of this study on wood light-frame buildings), but could be of importance to the collapse evaluation of taller buildings with longer periods.

As per the original “Zone 4” approach of FEMA P-695, all of the ground motions represent “far-field” sites, and purposely ignore higher levels of ground shaking typical of sites closer to the fault(s) governing site seismic hazard. Accordingly, FEMA P-695 implicitly permits MCE_R collapse probabilities greater than 10 percent for structures at sites where ground motions are greater than those of the “far-field” SDC D_{max} seismic criteria; whereas, the 10 percent collapse objective of Section 1.3.1.3 (Performance-Based Procedures) and Section 12.2.1.1 (Alternate Structural Systems) of ASCE/SEI 7-16 applies to all sites, regardless of their proximity to fault rupture, and the commentary to Section 12.2.1.1 identifies FEMA P-695 as the preferred methodology for verifying compliance with the 10 percent collapse objective. As shown by comparison of the collapse performance of high seismic and very high seismic archetype models in this study, very different conclusions could be reached if MCE_R ground motions greater than those of the “far-field” SDC D_{max} of FEMA P-695 were required for collapse evaluation. The fundamental question is whether the 10 percent collapse safety target of ASCE/SEI 7-16 applies to buildings at all possible sites, or only to those sites that are not “near-source.”

A study is recommended to determine what, if any, updates should be made to the FEMA P-695 methodology to: (1) incorporate current ASCE/SEI 7-16 (or future ASCE/SEI 7-22) ground motion criteria; and (2) address the apparent discrepancy between acceptance criteria of FEMA P-695 and those of Section 12.2.1.1 of ASCE/SEI 7-16.

6.3.3 Recommendations for Advanced Seismic Design and Analysis Practices

Recommendations for advanced seismic design and analysis practices are considered applicable to design and analysis practitioners, particularly those interested in performance-based design of new wood light-frame buildings, or seismic retrofit of existing wood light-frame buildings. It is recognized that performance-based design procedures are not commonly used for design of low-rise buildings, and that nonlinear response history analysis is not yet practical for implementation in design by most practitioners. Such changes would likely require funded projects to develop practical methods of application.

Performance-Based Design Based on Pushover Strength. The analytical methods, numerical models, and results of this study, which better represent the observed collapse performance of wood light-frame buildings may be of interest to practitioners seeking to implement performance-based design for wood light-frame buildings. The collapse analyses of this study show a strong correlation between collapse probability and the strength of the archetype model, as determined by nonlinear (static) pushover analysis. The shear wall “building blocks” of this study (Chapter 4) provide pushover models for a variety of configurations of different structural and nonstructural wall components.

Additional study is recommended to incorporate the lessons learned from this study into a complete performance-based design methodology for new buildings, or to augment the current performance-based methods of ASCE/SEI 41 for retrofit of existing buildings.

Performance-Based Design Criteria (Collapse Surface). Collapse results from baseline archetype models show a strong relationship among MCE_R collapse probability, strength, and displacement capacity. This relationship is depicted in Figure 6-12, which is a three-dimensional plot of MCE_R collapse probability versus normalized peak strength ratio (V_{max} / W) and first-story drift ratio at incipient collapse (as a measure of displacement capacity). The “best fit” through these data points is a notional collapse surface describing the relationship.

Additional study is recommended to determine how the trends embodied in the collapse surface could be used to establish performance-based design criteria for wood light-frame buildings. For example, given an amount of displacement capacity (e.g., one of the red lines in Figure 6-12), the surface could be used to estimate the normalized pushover strength (V_{max}/W) that would be required for a wood light-frame building to achieve a desired

collapse performance objective (e.g., 5 percent probability of collapse given MCE_R ground motions).

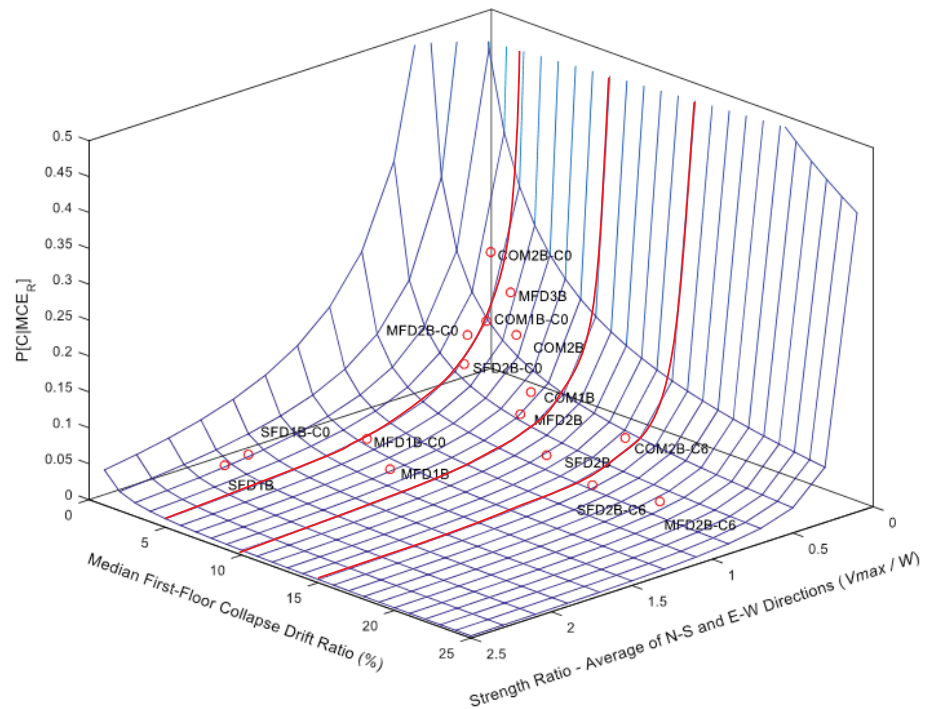


Figure 6-12 Three-dimensional plot of collapse probability as a function of normalized peak strength ratio (V_{max} / W) and displacement capacity in terms of median first-floor drift ratio at incipient collapse, for high seismic wood light frame building archetypes.

Damage and Loss Estimation. The analytical methods, numerical models, and results of this study, which include consideration of nonstructural wall finishes and better represent the observed collapse performance of wood light-frame buildings, may be of interest to practitioners seeking to improve estimates of earthquake damage and loss using, for example, the FEMA P-58 methodology (FEMA, 2018b), or other methods, such as those of the insurance industry. Probability of collapse is an important element of building damage and loss estimation, and the improved models and methods of this study would provide a more reliable characterization of the earthquake collapse risk of wood light-frame buildings.

Best Practice Design Recommendations. Results of this study show that, where performance-based methods are used for design of wood light-frame buildings to meet specific MCE_R collapse objectives (e.g., 10 percent probability of collapse given MCE_R ground motions of ASCE/SEI 7-10), the actual strength (not design strength) of the building, expressed as a fraction of the seismic weight, can be a simple and useful criterion. Where buildings are similar to the baseline archetypes of this study, specifically with respect

to the story drift at which P-Delta causes lateral instability, the values listed in Table 6-7 are recommended.

Values in Table 6-7 apply to the combined strength of the seismic force-resisting system and nonstructural interior and exterior wall finishes.

Information from this study was insufficient for recommending design strength values for very high seismic design of wood light-frame buildings at MCE_R collapse objectives other than 10 percent.

Table 6-7 Recommended Design Strength for Wood Light-Frame Buildings Designed for High Seismic or Very High Seismic Loads to Meet Specific MCE_R Collapse Objectives

Design Strength		MCE _R Collapse Objective		
Parameter	Symbol	2 Percent	5 Percent	10 Percent
High Seismic Design ($S_{MS} = 1.5 \text{ g}$)				
Pushover Strength	V_{max}/W	1.0	0.75	0.50
Overshoot ($R = 6.5$)	Ω	6.5	5.0	3.3
Very High Seismic Design ($S_{MS} = 2.25 \text{ g}$)				
Pushover Strength	V_{max}/W			0.90
Overshoot ($R = 6.5$)	Ω			4.0

Best Practice Analysis Recommendations. Results of this study show that, where nonlinear models are used to evaluate the collapse potential of wood light-frame buildings, the following should be implemented to improve the reliability of models:

- Include nonstructural interior and exterior wall finishes.
- Incorporate realistic collapse displacement capacities for the seismic force-resisting system (accomplished in this study through the use of a residual strength plateau).
- Explicitly model P-Delta effects.

Conversely, nonlinear models of wood light-frame buildings need not incorporate flexible foundations or the effects of SSI to reliably calculate the probability of collapse. Inclusion of nonstructural interior and exterior wall finishes will also improve the strength, stiffness, and period of vibration resulting from linear analyses of wood light-frame buildings.

6.3.4 Recommendations for Enhanced Modeling and Testing

Recommendations for enhanced modeling and testing are considered applicable to engineers and academics interested in research related to wood light-frame buildings. In this context, modeling recommendations apply to

sophisticated or complex modeling of wood light-frame building systems, and testing recommendations apply to monotonic- and cyclic-load testing of wood shear walls, or shake table testing of large-scale specimens.

Cyclic-Load Testing Protocol. There are a number of cyclic-load testing protocols available, which have been used to develop hysteretic backbone characterizations of structural and nonstructural elements of buildings. For the cyclic testing of wood light-frame assemblies, for example, the CUREE protocol (Krawinkler et al., 2000) has been used extensively. Many of these testing protocols are dated, and not necessarily appropriate for measuring nonlinear behavior at very large displacements.

A study is recommended to review and update existing cyclic-load testing protocols to better measure the nonlinear behavior of structural and nonstructural elements at very large displacements, considering potential differences in the frequency content and duration of earthquake ground motions. Detailed time-history responses from archetype models archived in this project could be mined for first-story displacement response, for each archetype model under each ground motion. Statistical measures (e.g., 84th percentile) of first-story displacement excursions could then be used to develop a more realistic loading protocol up to the level of first floor collapse drift ratios. Alternatively, new nonlinear response history analyses could be conducted with improved single-degree-of-freedom models using the modeling enhancements of this study.

Shear Wall System Testing to Large Displacements. Additional cyclic and monotonic testing of shear wall systems is recommended to provide insight into potential improved response behavior and ability to sustain large displacements. Tests should incorporate features and boundary conditions that are more representative of modern end-use conditions (e.g., with and without application of vertical load in combination with in-plane shear loading, presence of continuous framing adjacent to the shear wall sheathing, presence of perpendicular walls, and presence of sheathing above and below openings) relative to industry standard isolated 8 foot by 8 foot wall tests. Such testing should make use of new or revised cyclic-load testing protocols, and should address strength and stiffness effects of nonstructural finishes alone, and in combination with structural sheathing, to assess individual and combined strength rules.

Numerical Modeling of Nonlinear Behavior at Large Displacements.

Modeling of residual strength at large displacements in wood light-frame archetypes in this study assumed a plateau equal to 30 percent of peak strength (i.e., $0.3V_{max}$) in the direction of interest. Residual strength is

intended to incorporate the resistance provided by out-of-plane walls and other “system” effects. The 30 percent value was used for all baseline archetypes regardless of their strength. For relatively strong archetypes ($V_{\max}/W > 1.0$ g), the 30 percent assumption likely overestimates residual strength and for relatively weak archetypes ($V_{\max}/W < 0.33$ g), the 30 percent assumption likely underestimates residual strength.

Additional study is recommended to develop guidance on the percent of residual strength that should be assigned in a wood light-frame building as a function of the absolute value of its peak strength. Development of this guidance would require the identification of sources of residual strength in wood light-frame buildings and the absolute magnitude of the strength of these sources. Alternatively, detailed numerical models could be used that explicitly consider connection details for out-of-plane walls, composite actions between walls and floor diaphragms, and other aspects of system response. Such an approach would likely require a combination of numerical analyses and experimental studies.

Damping Model. In numerical modeling, the global stiffness and mass matrices of the governing equation of motion may be computed with reasonable accuracy by estimating the properties of individual building components. Unlike the mass and stiffness matrices, an equivalent viscous damping model such as the Rayleigh model is recommended, since it is generally not practical and not accurate to define the global damping matrix from the properties of individual building components. However, since damping force is proportional to the velocity of building components at the point of incipient collapse, the velocity of the vertical degree of freedom often increases rapidly as the building is collapsing. For a non-zero constant Raleigh damping matrix, the increase in restoring forces due to damping may result in unrealistically high damping forces.

To properly simulate collapse, a relatively small viscous damping ratio, on the order of 0.1 percent or less of the critical damping, is recommended in nonlinear dynamic analyses of wood light-frame buildings (see Appendix C).

Effective Properties for Equivalent Linear Analyses. Novel seismic design procedures for building systems, such as Direct-Displacement Based Design (DDBD), are slowly making their way into modern building codes. The DDBD procedure, for example, makes use of an equivalent linear model of the building structure through an equivalent (secant) stiffness (period) and viscous damping at the design displacement. In this case, the level of equivalent viscous damping must be higher than that used in nonlinear dynamic analyses to capture the amount of hysteretic energy dissipated.

Additional study is recommended to mine the large number of hysteretic responses (i.e., base shear versus roof drift ratio) for the archetype models archived in this project, to develop empirical relationships between the equivalent secant period and displacement, and between the equivalent viscous damping and displacement, for equivalent linear modeling of wood light-frame buildings.

Simulated Collapse Model. In prior FEMA P-695 collapse studies, non-simulated collapse models were used. This resulted in conservative estimates of when collapse was assumed to occur. Full scale shake table testing has shown that wood light-frame buildings can experience very large displacements at collapse, indicating that prior non-simulated collapse models were overconservative. In this study, side-sway collapse was explicitly simulated using a three-dimensional numerical model in which collapse was defined when a controlling node on the roof experienced a vertical drop (displacement) equal to the first story height.

Results of this study show that explicit simulation of collapse, and consideration of P-Delta effects were critical for matching calculated collapse performance to observed performance in past earthquakes or shake table tests.

Shake Table Testing to Collapse. Shake table testing of full-scale wood light-frame test buildings, such as those described in Section 2.7 of this report, provide valuable insight into the response behavior and collapse performance of wood light-frame buildings. It is recommended that large-scale shake table testing be performed for additional test buildings, including taller configurations, which were found to be more vulnerable than shorter configurations.

Appendix A

Archetype Design Criteria and Details

A.1 Introduction

The development of commercial, multi-family dwelling, and single-family dwelling wood light-frame building archetypes is described in Chapter 3. This appendix provides details for the design of the shear walls and foundations for the seismic-force-resisting system of each wood light-frame building archetype. This information was used in the development of numerical models for each of the parametric studies.

A.2 Design of Wood Light-Frame Archetypes

Engineered archetypes were designed in accordance with ASCE/SEI 7-10, *Minimum Design Loads for Buildings and Other Structures* (ASCE, 2010), ANSI/AWC *National Design Standard for Wood Construction* (AWC, 2012), and ANSI/AWC Special Design Provisions for Wind and Seismic (AWC, 2008). Conventional construction archetypes were designed in accordance with the 2015 *International Residential Code* (ICC, 2015b).

Each archetype was designed for three levels of seismic hazard, which are described in Chapter 3 and summarized in Table A-1.

Table A-1 Basic Design Criteria for Wood Light-Frame Archetypes

Building Type	Seismic Design Level	Seismic Design Category (SDC)	MCE _R Ground Motions				Design Criteria	
			S_I (g)	S_S (g)	F_a	S_{MS} (g)	S_{DS} (g)	C_s
Engineered COM, MFD, and SFD (ASCE/SEI 7-10)	Very High	E	0.9	2.25	1.0	2.25	1.5	0.231
	High	D	0.6	1.5	1.0	1.5	1.0	0.154
	Moderate	C	0.132	0.55	1.36	0.75	0.5	0.077
Conventional Construction SFD (2015 IRC)	Very High	E	0.9	2.25	1.0	2.25	1.5	NA
	High	D ₂	0.6	1.5	1.0	1.5	1.0	NA
	Moderate	C	0.132	0.55	1.36	0.75	0.5	NA

A.2.1 Structural Properties for Engineered Designs

The seismic-force-resisting system in each building archetype utilizes oriented strand board (OSB) and/or gypsum wallboard shear walls. Three different OSB shear wall strengths are considered (i.e., “OSB-Low,” “OSB-Medium,” and “OSB-High”), and two gypsum wallboard strengths are considered (i.e., “Max-Gyp” and “Min-Gyp”). Table A-2 contains brief descriptions for each wall type.

Table A-2 Description of Wall Types for Wood Light-Frame Archetypes

Wall Type	Description	Nominal Strength (plf)
OSB-Low	$\frac{7}{16}$ -inch structural panels with 8d common nails at 6 inches o.c. on edges into Douglas Fir framing	520
OSB-Med	$\frac{7}{16}$ -inch structural panels with 8d common nails at 3 inches o.c. on edges into Douglas Fir framing	980
OSB-High	$\frac{19}{32}$ -inch ($\frac{5}{8}$ -inch) structural panels with 10d common nails at 2 inches o.c. on edges into Douglas Fir framing	1740
Min-Gyp	$\frac{1}{2}$ -inch gypsum board with 5d cooler nails at 7 inches o.c. on edges, no blocked joints, studs at 16 inches o.c.	200
Max-Gyp	$\frac{5}{8}$ -inch gypsum board with 6d cooler nails at 4 inches o.c. on edges, blocked joints, studs at 16 inches o.c.	350
Exterior Nonstructural	Non-SFRS exterior walls with nonstructural $\frac{7}{16}$ -inch OSB, unblocked, with 8d nails at 6 inches o.c., on edges, nonstructural $\frac{1}{2}$ -inch GWB with drywall screws at 12 inches o.c. on inside face, plus stucco on the outside face	Not used in design
Interior Nonstructural	Nonstructural interior partition walls with $\frac{1}{2}$ -inch GWB and drywall screws at 12 inches o.c., both faces	Not used in design

In addition to the structural wall types listed above, nonstructural exterior and interior wall types are also included in the table. Although nonstructural wall types are not used in the design of the seismic-force-resisting system (SFRS), they are included in the numerical models to consider the participation of nonstructural walls in evaluating response and collapse performance of wood light-frame buildings. Properties of each wall type, including design strengths, are listed in Table A-3 and Table A-4.

When overturning forces generated by the design shear in a wall are greater than the resistance provided by dead loads acting on the wall, hold-down anchorage is designed. One-story and two-story archetypes use hold-downs listed in Table A-5. Four-story archetypes use an anchor tie-down system comparable to a Simpson Strong-Rod (SST, 2015). Anchor tie-down systems consist of a threaded rod that is embedded into the foundation and runs up the height of the building. A nut (or similar device) and washer, with a spring to compensate for wood shrinkage, are installed at the top of each

wall to restrain it from overturning. Hold-down and anchor tie-down properties are specific to each archetype and are tabulated in the sections that follow. Hold-down and tie-down systems have been designed for the purpose of completing the archetype designs, however, these systems were not explicitly included in the numerical models used in parametric studies.

Table A-3 Wall Framing Properties for Wood Light-Frame Archetypes

Wall Type	Design Shear * (plf)	Lumber Size	Bottom Plate	Top Plate
OSB-Low	520×0.8	See Structural Wall Property Table for each Archetype	Single 2×	Double 2×
OSB-Med	980×0.8		Single 3×	
OSB-High	1740×0.8			
Min-Gyp	200×0.8			Single 2×
Max-Gyp	350×0.8			
Exterior Nonstructural	NA	2×6		
Interior Nonstructural		2×4		

* Design shears are LRFD values, which are adjusted by a 0.8 strength reduction factor (ϕ).

Table A-4 Bottom Plate Fastening Schedule for Wood Light-Frame Archetypes

Wall Type	Anchor Bolts at Foundation			Sill Nails	
	Diameter (in)	Spacing * (in)	Washer	Size	Spacing (in)
OSB-Low	5/8	48	3"×3" for 4× walls and 4.5"×3" for 6× walls	16d common	8
OSB-Med	5/8	40		20d box	4
OSB-High	3/4	24		30d common	3 (staggered)
OSB-Low × 2	5/8	24		16d common	4
OSB-Med × 2	5/8	20		20d box	2
OSB-High × 2	3/4	12		30d common	1-1/2 (staggered)
Min-Gyp	1/2	48			16
Max-Gyp	1/2	40			16
Exterior Nonstructural	1/2	72	Standard 1 1/16" dia.	16d common	16
Interior Nonstructural	0.145" diameter shot pin at 16" o.c.				16

* Must have anchor bolt within 1 foot at each end of wall unless there is a hold-down.

Table A-5 Hold-Downs and Straps for Two-Story and Four-Story for Wood Light-Frame Archetypes

Hold-Down ID	Hold-Down Type	ASD Capacity (kip)	LRFD Capacity (kip)
HDU2	Wall-to-Foundation	3.08	4.15
HDU8	Wall-to-Foundation	7.87	10.62
HDU14	Wall-to-Foundation	14.45	19.50
MSTC28 *	Wall-to-Wall	1.16	1.56
MSTC40 *	Wall-to-Wall	2.70	3.64
MSTC52 *	Wall-to-Wall	4.24	5.72

* Strap capacities are based on 18" deep structure between stories.

A.2.2 Wall Locations and Configurations

The location, length, and type of shear walls are described in a plan layout for each class of archetype (e.g., four-story, multi-family dwellings), showing all potential shear wall locations, accompanied by a table listing shear wall properties for each wall, including hold-down devices and the number of studs at each end of each wall.

In addition to plans showing shear wall locations, a second set of plans showing interior partitions for each class of archetype are provided in Chapter 3. Nonstructural interior partitions are not considered in the design of the seismic-force-resisting system, but they are considered in numerical models for the purpose of evaluating their impact on response and performance.

A.3 Commercial Building Shear Wall Designs

Shear walls are provided around the perimeter of commercial building archetypes. Shear wall locations are identified in Figure A-1. Table A-6 provides design information for each commercial building archetype including the assumed seismic weight at each level along with the design story shear.

Table A-7 provides the details of shear wall designs for commercial building archetypes. Shear wall lengths were set to provide as little overstrength as possible based on the unit strength of each shear wall type.

Table A-8 provides information on traditional hold-downs used in for the one-story and two-story commercial archetypes, including the size of the stud pack at each end of the shear walls where the hold-downs are located, while Table A-9 provides information about the anchor rod tie-downs used in four-story commercial archetypes. Hold-downs or tie-downs were not specified if the dead load was sufficient to prevent uplift.

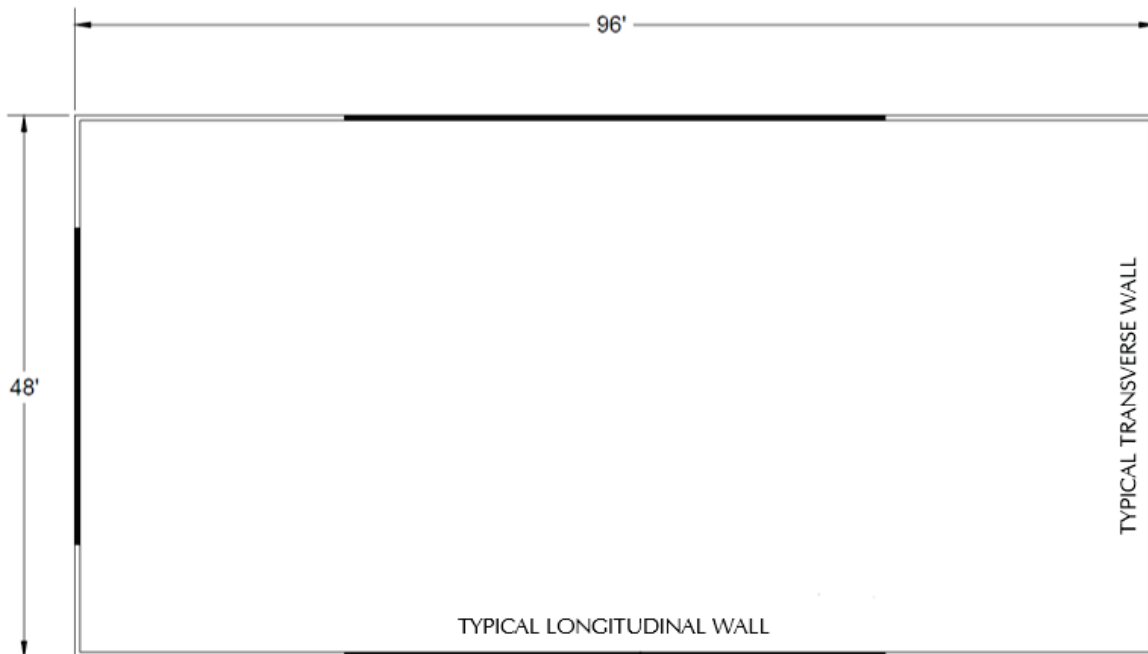


Figure A-1 Typical plan showing perimeter shear wall locations in commercial building archetypes.

Table A-6 General Design Information for Commercial Building Archetypes

Archetype ID	No. of Stories	SDC	Story	Story Weight (kips)	Story Shear (kips)
Commercial Buildings: High Seismic					
COM1	1	D	1 st	180	27.6
COM2	2	D	1 st	263	68.1
			2 nd	180	39.3
COM3	4	D	1 st	263	148.9
			2 nd	263	131.8
			3 rd	263	97.8
			4 th	180	46.6
Commercial Buildings: Very High Seismic					
COM4	1	E	1 st	180	41.5.
COM5	2	E	1 st	263	102.1
			2 nd	180	59.0
COM6	4	E	1 st	263	223.3
			2 nd	263	197.8
			3 rd	263	146.6
			4 th	180	70.0
Commercial Buildings: Moderate Seismic					
COM7	1	C	1 st	180	13.8
COM8	2	C	1 st	263	34.0
			2 nd	180	19.7
COM9	4	C	1 st	263	174.4
			2 nd	263	65.9
			3 rd	263	48.9
			4 th	180	23.3

Table A-7 Shear Wall Schedule for Commercial Building Archetypes

Archetype ID	Story	Transverse Shear Walls			Longitudinal Shear Walls		
		Wall Type	Length (feet)	Design Overstrength (%)	Wall Type	Length (feet)	Design Overstrength (%)
Commercial Buildings: High Seismic							
COM1	1 st	OSB-Med	24	36	OSB-Low	40	20
COM2	1 st	OSB-High	32	31	OSB-Med	48	11
	2 nd	OSB-Med	32	28	OSB-Low	48	2
COM3	1 st	OSB-High × 2	32	20	OSB-High	56	5
	2 nd	OSB-High × 2	32	35	OSB-High	56	18
	3 rd	OSB-Med × 2	32	3	OSB-High	56	59
	4 th	OSB-Low × 2	32	14	OSB-Low	56	0
Commercial Buildings: Very High Seismic							
COM4	1 st	OSB-Med	32	21	OSB-Med	32	21
COM5	1 st	OSB-High	40	9	OSB-High	40	9
	2 nd	OSB-Med	40	6	OSB-Med	40	6
COM6	1 st	OSB-High × 2	48	20	OSB-High × 2	48	20
	2 nd	OSB-High × 2	48	35	OSB-High × 2	48	35
	3 rd	OSB-Med × 2	48	3	OSB-Med × 2	48	3
	4 th	OSB-Low × 2	48	14	OSB-Low × 2	48	14
Commercial Buildings: Moderate Seismic							
COM7	1 st	OSB-Low	24	44	OSB-Low	24	44
COM8	1 st	OSB-Med	24	11	OSB-Low	48	17
	2 nd	OSB-Low	24	2	OSB-Low	48	103
COM9	1 st	OSB-High	32	20	OSB-Med	48	1
	2 nd	OSB-High	32	35	OSB-Med	48	14
	3 rd	OSB-Med	32	3	OSB-Med	48	54
	4 th	OSB-Low	32	14	OSB-Low	48	71

Table A-8 Hold-Down Schedule for One-Story and Two-Story Commercial Building Archetypes

Archetype ID	Story	Transverse Shear Walls		Longitudinal Shear Walls	
		Hold-Down	2×6 Stud Pack	Hold-Down	2×6 Stud Pack
Commercial Buildings: High Seismic					
COM1	1 st	HDU2	2	NA	2
COM2	1 st	HDU8	3	NA	2
	2 nd	MSTC28	2	NA	2
Commercial Buildings: Very High Seismic					
COM4	1 st	HDU2	2	HDU2	2
COM5	1 st	HDU8	3	HDU14	3
	2 nd	MSTC40	2	MSTC40	2
Commercial Buildings: Moderate Seismic					
COM7	1 st	NA	2	NA	2
COM8	1 st	HDU2	2	NA	2
	2 nd	NA	2	NA	2

Table A-9 Anchor Rod Tie-Down Schedule for Four-Story Commercial Building Archetypes

Archetype ID	Story	Transverse Shear Walls				Longitudinal Shear Walls			
		Rod Diameter (in)	Terminate at Top of Story	Washer Area (in ²)	2×6 Stud Pack	Rod Diameter (in)	Terminate at Top of Story	Washer Area (in ²)	2×6 Stud Pack
Commercial Buildings: High Seismic									
COM3	1 st	1.375	4 th	18	7	0.625	2 nd	11	5
	2 nd				5				3
	3 rd				3				2
	4 th				2				2
Commercial Buildings: Very High Seismic									
COM6	1 st	1.25	4 th	13.5	7	1.5	4 th	22	9
	2 nd				5				6
	3 rd				3				3
	4 th				2				2
Commercial Buildings: Moderate Seismic									
COM9	1 st	0.625	2 nd	9	4	NA	NA	NA	3
	2 nd				3				2
	3 rd				2				2
	4 th				2				2

A.4 Multi-Family Dwelling Shear Wall Designs

Shear walls in all in multi-family dwelling archetypes are provided around the perimeter and at selected interior wall lines. Table A-10 provides design information for each multi-family dwelling archetype including the assumed seismic weight at each level along with the design story shear.

Table A-10 General Design Information for Multi-Family Dwelling Archetypes

Archetype ID	No. of Stories	SDC	Story	Story Weight (kips)	Story Shear (kips)
Multi-Family Dwellings: High Seismic					
MFD1	1	D	1 st	141	21.6
MFD2	2	D	1 st	182	50.2
			2 nd	144	30.7
MFD3	4	D	1 st	237	132.4
			2 nd	237	116.8
			3 rd	237	85.7
			4 th	149	39.0
			Multi-Family Dwellings: Very High Seismic		
MFD4	1	E	1 st	141	32.4
MFD5	2	E	1 st	182	75.2
			2 nd	144	46.1
MFD6	4	E	1 st	237	198.6
			2 nd	237	175.2
			3 rd	237	128.5
			4 th	149	58.5
Multi-Family Dwellings: Moderate Seismic					
MFD7	1	C	1 st	141	10.8
MFD8	2	C	1 st	182	25.1
			2 nd	144	15.4
MFD9	4	C	1 st	237	66.2
			2 nd	237	58.4
			3 rd	237	42.8
			4 th	149	19.5

A.4.1 One-Story Multi-Family Dwelling Shear Walls

Shear wall locations in one-story multi-family dwelling archetypes are identified in Figure A-2.

Table A-11, Table A-12, and Table A-13 provide the details of shear wall and hold-down designs, including the size of the stud pack at each end of the shear walls, for high, very high, and moderate seismic archetypes, respectively.

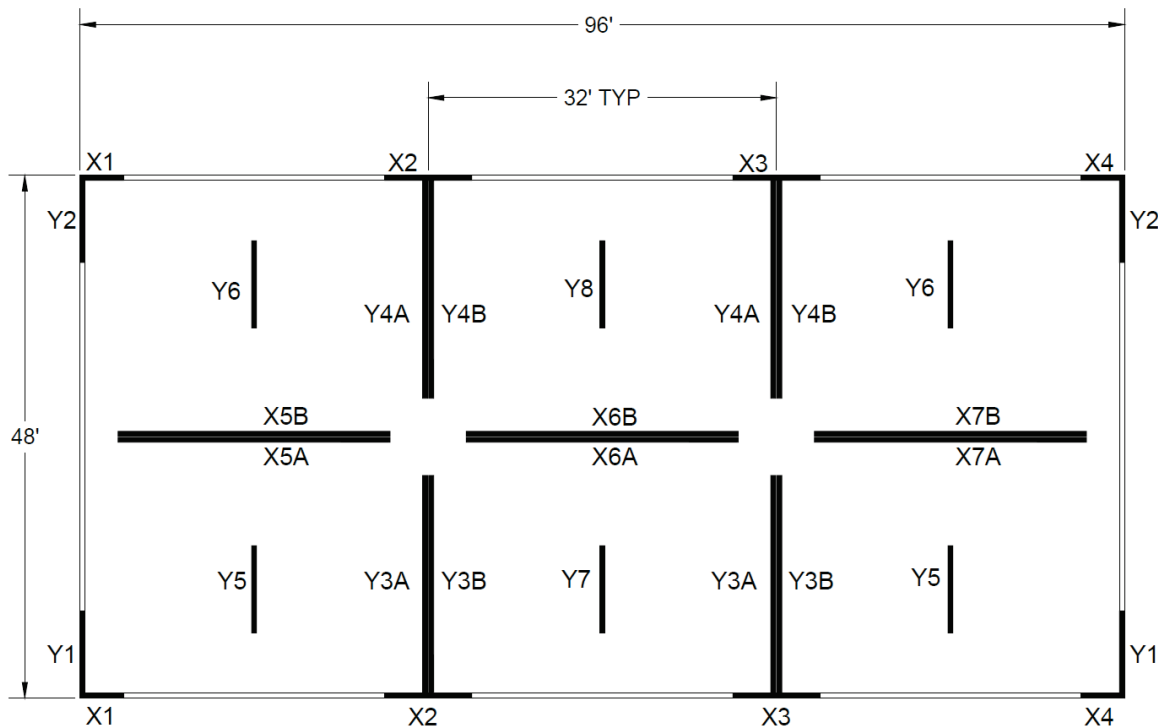


Figure A-2 Typical plan showing perimeter and interior shear wall locations in one-story multi-family dwelling archetypes.

Table A-11 Shear Wall and Hold-Down Schedule for the One-Story, Multi-Family Dwelling, High Seismic Archetype

Archetype ID	Property / Description			1 st Story			
Multi-Family Dwellings: High Seismic							
	Wall	No. of Locs	Framing Size	Wall Type	Length (feet)	Hold-Down	Stud Pack
	X1	2	2×6	Non-SFRS Wall			
	X2	2	2×6	Med-OSB	8	HDU8	3
	X3	2	2×6	Med-OSB	8	HDU8	3
	X4	2	2×6	Non-SFRS Wall			
MFD1	Design Overstrength			16%			
	Wall	No. of Locs	Framing Size	Wall Type	Length (feet)	Hold-Down	Stud Pack
	Y1	2	2×6	Low-OSB	4	HDU2	2
	Y2	2	2×6	Low-OSB	4	HDU2	2
	Y3A	2	2×4	Low-OSB	12	HDU2	2
	Y3B	2	2×4	Non-SFRS Wall			
	Y4A	2	2×4	Low-OSB	8	HDU2	2
	Y4B	2	2×4	Non-SFRS Wall			
	Y5	2	2×6	Non-SFRS Wall			
	Y6	2	2×6	Non-SFRS Wall			
	Y7	1	2×6	Non-SFRS Wall			
	Y8	1	2×6	Non-SFRS Wall			
	Design Overstrength			4%			

Table A-12 Shear Wall and Hold-Down Schedule for the One-Story, Multi-Family Dwelling, Very High Seismic Archetype

Archetype ID	Property / Description			1 st Story			
	Multi-Family Dwellings: Very High Seismic						
MFD4	Wall	No. of Locs	Framing Size	Wall Type	Length (feet)	Hold-Down	Stud Pack
	X1	2	2×6	Med-OSB	4	HDU8	3
	X2	2	2×6	Med-OSB	8	HDU8	3
	X3	2	2×6	Med-OSB	8	HDU8	3
	X4	2	2×6	Med-OSB	4	HDU8	3
	Design Overstrength			12%			
	Wall	No. of Locs	Framing Size	Wall Type	Length (feet)	Hold-Down	Stud Pack
	Y1	2	2×6	Low-OSB	4	HDU2	2
	Y2	2	2×6	Low-OSB	4	HDU2	2
	Y3A	2	2×4	Low-OSB	8	HDU2	2
	Y3B	2	2×4	Low-OSB	8	HDU2	2
	Y4A	2	2×4	Low-OSB	8	HDU2	2
	Y4B	2	2×4	Low-OSB	8	HDU2	2
	Y5	2	2×6	Non-SFRS Wall			
	Y6	2	2×6	Non-SFRS Wall			
	Y7	1	2×6	Non-SFRS Wall			
	Y8	1	2×6	Non-SFRS Wall			
	Design Overstrength			0%			

Table A-13 Shear Wall and Hold-Down Schedule for the One-Story, Multi-Family Dwelling, Moderate Seismic Archetype

Archetype ID	Property / Description			1 st Story			
Multi-Family Dwellings: Moderate Seismic							
	Wall	No. of Locs	Framing Size	Wall Type	Length (feet)	Hold-Down	Stud Pack
MFD7	X1	2	2×6	Non-SFRS Wall			
	X2	2	2×6	Low-OSB	8	HDU2	2
	X3	2	2×6	Low-OSB	8	HDU2	2
	X4	2	2×6	Non-SFRS Wall			
	Design Overstrength			23%			
	Wall	No. of Locs	Framing Size	Wall Type	Length (feet)	Hold-Down	Stud Pack
	Y1	2	2×6	Low-OSB	4	HDU2	2
	Y2	2	2×6	Non-SFRS Wall			2
	Y3A	2	2×4	Max-Gyp	20	HDU2	2
	Y3B	2	2×4	Max-Gyp	20	HDU2	2
	Y4A	2	2×4	Min-Gyp	20	HDU2	2
	Y4B	2	2×4	Min-Gyp	20	HDU2	2
	Y5	2	2×6	Non-SFRS Wall			
	Y6	2	2×6	Non-SFRS Wall			
	Y7	1	2×6	Non-SFRS Wall			
	Y8	1	2×6	Non-SFRS Wall			
	Design Overstrength			9%			

A.4.2 Two-Story Multi-Family Dwelling Shear Walls

Shear wall locations in two-story multi-family dwelling archetypes are identified in Figure A-3. Table A-14 provides general wall properties for the two-story multi-family dwelling archetypes.

Table A-15, Table A-16, and Table A-17 provide the details of shear wall and hold-down designs, including the size of the stud pack at each end of the shear walls, for high, very high, and moderate seismic archetypes, respectively. Where the shear wall configuration results in a design overstrength, the percentage of overstrength is provided in the tables.

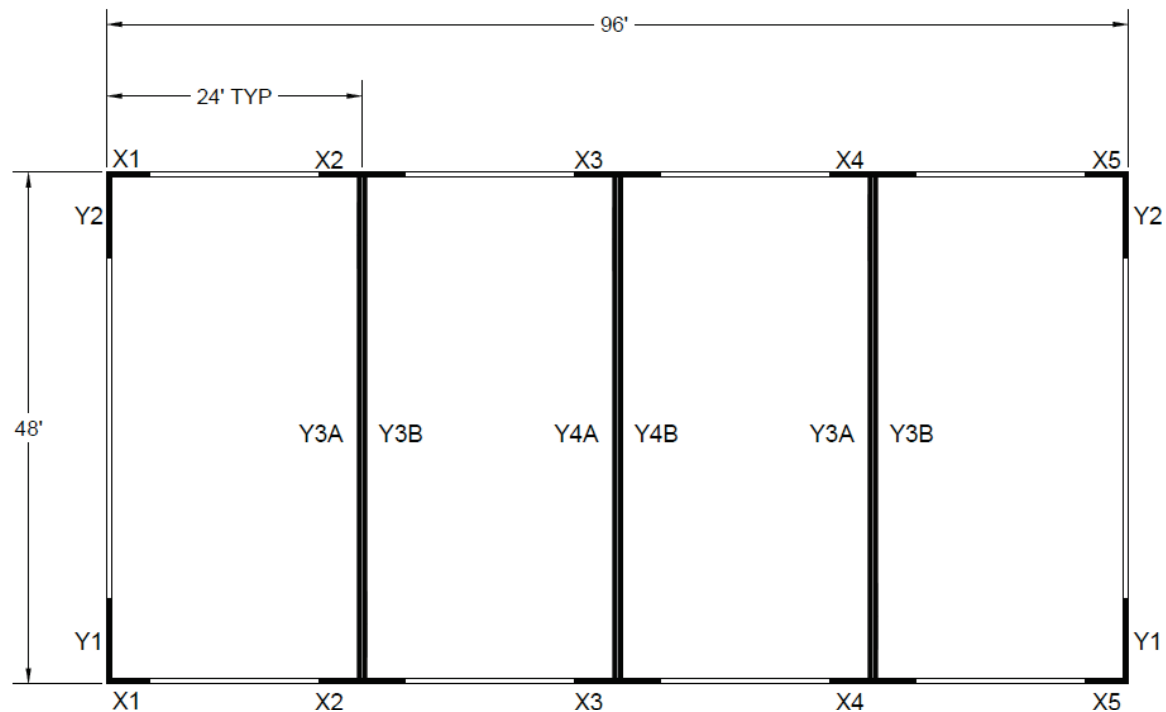


Figure A-3 Typical plan showing perimeter and interior shear wall locations in two-story multi-family dwelling archetypes.

Table A-14 General Wall Properties for Two-Story Multi-Family Dwelling Archetypes

Archetype ID	SDC	Longitudinal Property / Description			Transverse Property / Description		
		Wall	No. of Locs	Framing Size	Wall	No. of Locs	Framing Size
MFD2, MFD5, or MFD8	C, D, or E	X1	2	2×6	Y1	2	2×6
		X2	2	2×6	Y2	2	2×6
		X3	2	2×6	Y3A	2	2×4
		X4	2	2×6	Y3B	2	2×4
		X5	2	2×6	Y4A	1	2×4
		NA			Y4B	1	2×4

Table A-15 Shear Wall and Hold-Down Schedule for the Two-Story, Multi-Family Dwelling, High Seismic Archetype

Archetype ID	Property / Description		1 st Story			2 nd Story			
Multi-Family Dwellings: High Seismic									
MFD2	Wall	Wall Type	Length (feet)	Hold-Down	Stud Pack	Wall Type	Length (feet)	Hold-Down	Stud Pack
	X1	Med-OSB	4	HDU8	3	Low-OSB	4	MSTC40	2
	X2	High-OSB	8	HDU14	3	Med-OSB	8	MSTC52	3
	X3	Med-OSB	8	HDU8	3	Low-OSB	8	MSTC40	2
	X4	Med-OSB	8	HDU8	3	Low-OSB	8	MSTC40	2
	X5	Low-OSB	4	HDU8	3	Low-OSB	4	MSTC40	2
	Design Overstrength	9%				3%			
	Wall	Wall Type	Length (feet)	Hold-Down	Stud Pack	Wall Type	Length (feet)	Hold-Down	Stud Pack
	Y1	Low-OSB	8	HDU8	3	Low-OSB	8	MSTC40	2
	Y2	Low-OSB	8	HDU2	2	Non-SFRS Wall			
MFD2	Y3A	Low-OSB	48	HDU2	2	Low-OSB	48	MSTC40	2
	Y3B	Non-SFRS Wall				Non-SFRS Wall			
	Y4A	Non-SFRS Wall				Non-SFRS Wall			
	Y4B	Non-SFRS Wall				Non-SFRS Wall			
Design Overstrength		6%				52%			

Table A-16 Shear Wall and Hold-Down Schedule for the Two-Story, Multi-Family Dwelling, Very High Seismic Archetype

Archetype ID	Property / Description	1 st Story				2 nd Story			
Multi-Family Dwellings: Very High Seismic									
	Wall	Wall Type	Length (feet)	Hold-Down	Stud Pack	Wall Type	Length (feet)	Hold-Down	Stud Pack
	X1	Med-OSB	4	HDU14	3	Med-OSB	4	MSTC52	3
	X2	High-OSB	8	HDU14	3	Med-OSB	8	MSTC52	3
	X3	High-OSB	8	HDU14	3	Med-OSB	8	MSTC52	3
	X4	High-OSB	8	HDU14	3	Med-OSB	8	MSTC52	3
	X5	Med-OSB	4	HDU14	3	Med-OSB	4	MSTC52	3
MFD5	Design Overstrength	2%				6%			
	Wall	Wall Type	Length (feet)	Hold-Down	Stud Pack	Wall Type	Length (feet)	Hold-Down	Stud Pack
	Y1	Low-OSB	8	HDU8	3	Low-OSB	8	MSTC40	2
	Y2	Low-OSB	12	HDU2	2	Non-SFRS Wall			
	Y3A	Low-OSB	48	HDU2	2	Low-OSB	48	MSTC40	2
	Y3B	Non-SFRS Wall				Non-SFRS Wall			
	Y4A	Low-OSB	48	None	2	Non-SFRS Wall			
	Y4B	Non-SFRS Wall				Non-SFRS Wall			
	Design Overstrength	2%				1%			

Table A-17 Shear Wall and Hold-Down Schedule for the Two-Story, Multi-Family Dwelling, Moderate Seismic Archetype

Archetype ID	Property / Description		1 st Story			2 nd Story			
Multi-Family Dwellings: Moderate Seismic									
	Wall	Wall Type	Length (feet)	Hold-Down	Stud Pack	Wall Type	Length (feet)	Hold-Down	Stud Pack
	X1	Med-OSB	4	HDU8	3	Low-OSB	4	MSTC40	2
	X2	Low-OSB	8	HDU8	3	Low-OSB	8	MSTC40	2
	X3	Low-OSB	8	HDU2	2	Non-SFRS Wall			
	X4	Low-OSB	8	HDU8	3	Low-OSB	8	MSTC40	2
	X5	Low-OSB	4	HDU2	2	Non-SFRS Wall			
MFD8	Design Overstrength	9%				6%			
	Wall	Wall Type	Length (feet)	Hold-Down	Stud Pack	Wall Type	Length (feet)	Hold-Down	Stud Pack
	Y1	Low-OSB	8	HDU8	3	Low-OSB	8	MSTC40	2
	Y2	Non-SFRS Wall				Non-SFRS Wall			
	Y3A	Max-Gyp	48	None	2	Min-Gyp	48	MSTC28	2
	Y3B	Max-Gyp	48	None	2	Min-Gyp	48	MSTC28	2
	Y4A	Max-Gyp	48	None	2	Min-Gyp	48	MSTC28	2
	Y4B	Max-Gyp	48	None	2	Min-Gyp	48	MSTC28	2
	Design Overstrength	7%				6%			

A.4.3 Four-Story Multi-Family Dwelling Shear Walls

Shear wall locations in four-story multi-family dwelling archetypes are identified in Figure A-4. Table A-18 provides general wall properties for the four-story multi-family dwelling archetypes.

Table A-15, Table A-16, and Table A-17 provide the details of shear wall and hold-down designs, including the size of the stud pack at each end of the shear walls, for high, very high, and moderate seismic archetypes, respectively. Where the shear wall configuration results in a design overstrength, the percentage of overstrength is provided in the tables.

Table A-19, Table A-20, and Table A-21 provide the details of shear wall designs for the four-story multi-family dwelling archetype for high, very high, and moderate seismic designs, respectively. Table A-19, Table A-20, and Table A-21 also provide the design overstrengths for each direction. Table A-22, Table A-23, and Table A-24 provide the details of anchor rod tie-down designs, including the size of the stud pack needed at end of the

shear wall where the tie-down is located, for the four-story multi-family dwelling archetype for high, very high, and moderate seismic design, respectively.

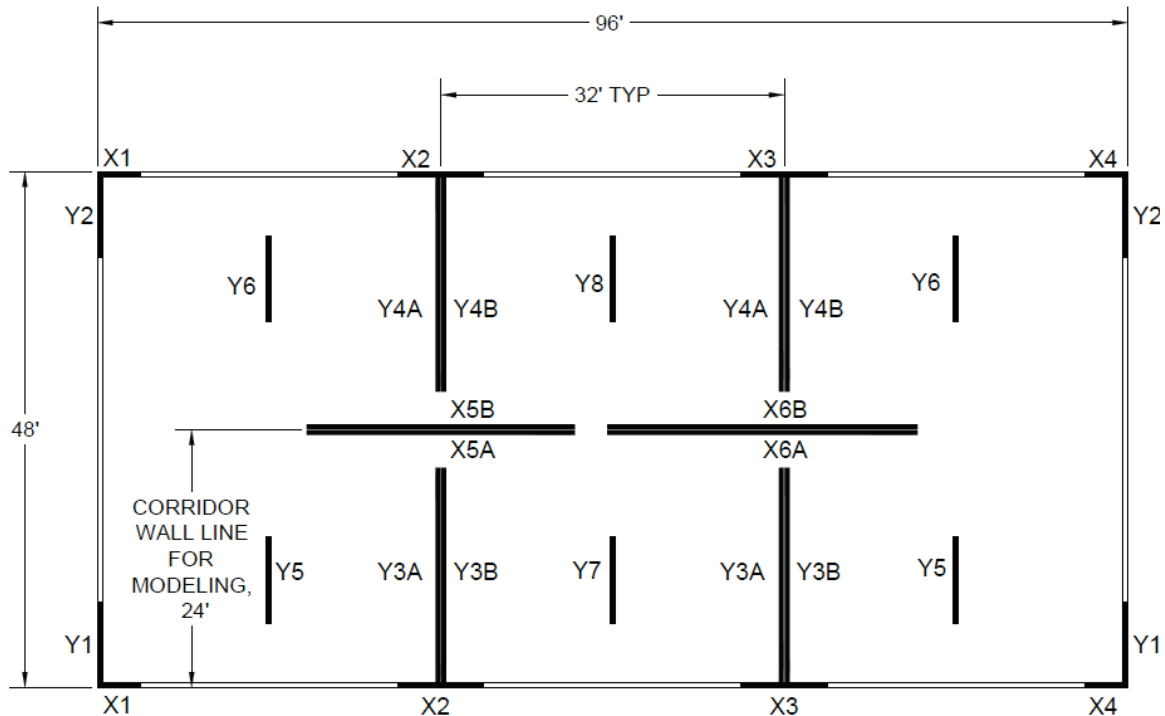


Figure A-4 Typical plan showing perimeter and interior shear wall locations in four-story multi-family dwelling archetypes.

Table A-18 General Wall Properties for Four-Story Multi-Family Dwelling Archetypes

Archetype ID	SDC	Longitudinal Property / Description			Transverse Property / Description		
		Wall	No. of Locs	Framing Size	Wall	No. of Locs	Framing Size
MFD3, MFD6, or MFD9	C, D, or E	X1	2	2×6	Y1	2	2×6
		X2	2	2×6	Y2	2	2×6
		X3	2	2×6	Y3A	2	2×4
		X4	2	2×6	Y3B	2	2×4
		X5A	1	2×4	Y4A	2	2×4
		X5B	1	2×4	Y4B	2	2×4
		X6A	1	2×4	Y5	2	2×6
		X6B	1	2×4	Y6	2	2×6
		NA			Y7	1	2×6
		NA			Y8	1	2×6

Table A-19 Shear Wall Schedule for the Four-Story, Multi-Family Dwelling, High Seismic Archetype

Archetype ID	Property / Description		1 st Story		2 nd Story		3 rd Story		4 th Story	
Multi-Family Dwellings: High Seismic										
MFD3	Wall	No. of Locs	Wall Type	Length (feet)						
	X1	2	Low-OSB	4	Low-OSB	4	Non-SFRS Wall		Non-SFRS Wall	
	X2	2	Low-OSB	8	Low-OSB	8	Low-OSB	8	Low-OSB	8
	X3	2	Low-OSB	8	Low-OSB	8	Low-OSB	8	Non-SFRS Wall	
	X4	2	Low-OSB	4	Low-OSB	4	Low-OSB	4	Non-SFRS Wall	
	X5A	1	Med-OSB	24	Med-OSB	24	Low-OSB	24	Low-OSB	24
	X5B	1	High-OSB	24	High-OSB	24	Med-OSB	24	Non-SFRS Wall	
	X6A	1	High-OSB	28	Med-OSB	28	Med-OSB	28	Low-OSB	28
	X6B	1	High-OSB	28	High-OSB	28	Med-OSB	28	Low-OSB	28
	Design Overstrength		12%		13%		3%		2%	
	Wall	No. of Locs	Wall Type	Length (feet)						
	Y1	2	Med-OSB	8	Low-OSB	8	Low-OSB	8	Low-OSB	8
	Y2	2	Med-OSB	8	Low-OSB	8	Low-OSB	8	Non-SFRS Wall	
	Y3A	2	Low-OSB	20	Low-OSB	20	Low-OSB	20	Low-OSB	20
	Y3B	2	Med-OSB	20	Med-OSB	20	Low-OSB	20	Non-SFRS Wall	
	Y4A	2	Low-OSB	20	Low-OSB	20	Low-OSB	20	Low-OSB	20
	Y4B	2	Med-OSB	20	Med-OSB	20	Low-OSB	20	Non-SFRS Wall	
	Y5	2	Low-OSB	8	Low-OSB	8	Low-OSB	8	Non-SFRS Wall	
	Y6	2	Low-OSB	8	Low-OSB	8	Low-OSB	8	Non-SFRS Wall	
	Y6	2	Low-OSB	8	Low-OSB	8	Low-OSB	8	Non-SFRS Wall	
	Y7	1	Low-OSB	8	Low-OSB	8	Low-OSB	8	Non-SFRS Wall	
	Y8	1	Low-OSB	8	Low-OSB	8	Low-OSB	8	Non-SFRS Wall	
	Design Overstrength		7%		11%		17%		2%	

Table A-20 Shear Wall Schedule for the Four-Story, Multi-Family Dwelling, Very High Seismic Archetype

Archetype ID	Property / Description		1 st Story		2 nd Story		3 rd Story		4 th Story	
Multi-Family Dwellings: Very High Seismic										
MFD6	Wall	No. of Locs	Wall Type	Length (feet)						
	X1	2	Med-OSB	4	Med-OSB	4	Low-OSB	4	Low-OSB	4
	X2	2	High-OSB	8	Med-OSB	8	Low-OSB	8	Low-OSB	8
	X3	2	High-OSB	8	Med-OSB	8	Low-OSB	8	Low-OSB	8
	X4	2	High-OSB	4	Med-OSB	4	Low-OSB	4	Low-OSB	4
	X5A	1	High-OSB	24	High-OSB	24	Med-OSB	24	Low-OSB	24
	X5B	1	High-OSB	24	High-OSB	24	Med-OSB	24	Low-OSB	24
	X6A	1	High-OSB	28	High-OSB	28	High-OSB	28	Low-OSB	28
	X6B	1	High-OSB	28	High-OSB	28	High-OSB	28	Low-OSB	28
	Design Overstrength		2%		2%		4%		7%	
	Wall	No. of Locs	Wall Type	Length (feet)						
	Y1	2	Med-OSB	8	Med-OSB	8	Low-OSB	8	Low-OSB	8
	Y2	2	Med-OSB	8	Med-OSB	8	Low-OSB	8	Low-OSB	8
	Y3A	2	Med-OSB	20	Med-OSB	20	Med-OSB	20	Low-OSB	20
	Y3B	2	Med-OSB	20	Med-OSB	20	Med-OSB	20	Non-SFRS Wall	
	Y4A	2	Med-OSB	20	Med-OSB	20	Med-OSB	20	Low-OSB	20
	Y4B	2	Med-OSB	20	Med-OSB	20	Med-OSB	20	Low-OSB	20
	Y5	2	High-OSB	8	Med-OSB	8	Non-SFRS Wall		Non-SFRS Wall	
	Y6	2	High-OSB	8	Low-OSB	8	Non-SFRS Wall		Non-SFRS Wall	
	Y7	1	High-OSB	8	Low-OSB	8	Non-SFRS Wall		Non-SFRS Wall	
	Y8	1	High-OSB	8	Low-OSB	8	Non-SFRS Wall		Non-SFRS Wall	
	Design Overstrength		9%		1%		8%		8%	

Table A-21 Shear Wall Schedule for the Four-Story, Multi-Family Dwelling, Moderate Seismic Archetype

Archetype ID	Property / Description		1 st Story		2 nd Story		3 rd Story		4 th Story	
Multi-Family Dwellings: Moderate Seismic										
MFD9	Wall	No. of Locs	Wall Type	Length (feet)						
	X1	2	Low-OSB	4	Low-OSB	4	Non-SFRS Wall		Non-SFRS Wall	
	X2	2	Low-OSB	8	Low-OSB	8	Low-OSB	8	Low-OSB	8
	X3	2	Med-OSB	8	Low-OSB	8	Low-OSB	8	Non-SFRS Wall	
	X4	2	Low-OSB	4	Low-OSB	4	Non-SFRS Wall		Non-SFRS Wall	
	X5A	1	Low-OSB	24	Low-OSB	24	Low-OSB	24	Low-OSB	24
	X5B	1	Low-OSB	24	Low-OSB	24	Low-OSB	24	Low-OSB	24
	X6A	1	Low-OSB	28	Low-OSB	28	Low-OSB	28	Non-SFRS Wall	
	X6B	1	Low-OSB	28	Low-OSB	28	Non-SFRS Wall		Non-SFRS Wall	
	Design Overstrength		2%		6%		5%		37%	
	Wall	No. of Locs	Wall Type	Length (feet)						
	Y1	2	Low-OSB	8	Low-OSB	8	Low-OSB	8	Low-OSB	8
	Y2	2	Low-OSB	8	Low-OSB	8	Low-OSB	8	Low-OSB	8
	Y3A	2	Low-OSB	12	Low-OSB	12	Low-OSB	12	Low-OSB	12
	Y3B	2	Low-OSB	12	Low-OSB	12	Non-SFRS Wall		Non-SFRS Wall	
	Y4A	2	Low-OSB	12	Low-OSB	12	Low-OSB	12	Non-SFRS Wall	
	Y4B	2	Low-OSB	12	Low-OSB	12	Low-OSB	12	Non-SFRS Wall	
	Y5	2	Low-OSB	8	Low-OSB	8	Non-SFRS Wall		Non-SFRS Wall	
	Y6	2	Low-OSB	8	Non-SFRS Wall		Non-SFRS Wall		Non-SFRS Wall	
	Y7	1	Non-SFRS Wall		Non-SFRS Wall		Non-SFRS Wall		Non-SFRS Wall	
	Y8	1	Non-SFRS Wall		Non-SFRS Wall		Non-SFRS Wall		Non-SFRS Wall	
	Design Overstrength		1%		3%		1%		19%	

Table A-22 Tie-Down Schedule for the Four-Story, Multi-Family Dwelling, High Seismic Archetype

Archetype ID	Tie-Down Rods							
	Multi-Family Dwellings: High Seismic							
MFD3	Wall	Diameter (in)	Terminate at Top of Story	Washer Area (in ²)	1 st Story Stud Pack	2 nd Story Stud Pack	3 rd Story Stud Pack	4 th Story Stud Pack
	X1	0.5	2	9	2	2	2	2
	X2	0.75	4	9	2	2	2	2
	X3	0.625	3	9	2	2	2	2
	X4	0.5	3	9	2	2	2	2
	X5A	0.75	4	5	4	3	2	2
	X5B	1	3	10	5	3	2	2
	X6A	0.875	4	10	5	3	2	2
	X6B	1	4	5	6	4	2	2
	Y1	0.75	4	9	2	2	2	2
	Y2	0.75	3	9	2	2	2	2
	Y3A	0.625	4	5	3	2	2	2
	Y3B	0.75	3	5	3	2	2	2
	Y4A	0.625	4	5	3	2	2	2
	Y4B	0.75	3	5	3	2	2	2
	Y5	0.5	3	9	2	2	2	2
	Y6	0.5	3	9	2	2	2	2
	Y7	0.5	3	9	2	2	2	2
	Y8	0.5	3	9	2	2	2	2

Table A-23 Tie-Down Schedule for the Four-Story, Multi-Family Dwelling, Very High Seismic Archetype

Archetype ID	Tie-Down Rods							
	Multi-Family Dwellings: Very High Seismic							
MFD6	Wall	Diameter (in)	Terminate at Top of Story	Washer Area (in ²)	1 st Story Stud Pack	2 nd Story Stud Pack	3 rd Story Stud Pack	4 th Story Stud Pack
	X1	0.875	4	9	2	2	2	2
	X2	1	4	13.5	3	2	2	2
	X3	1	4	13.5	3	2	2	2
	X4	0.875	4	9	3	2	2	2
	X5A	1.125	4	10	6	4	2	2
	X5B	1.125	4	10	6	4	2	2
	X6A	1.25	4	10	7	5	3	2
	X6B	1.25	4	5	7	5	3	2
	Y1	0.875	4	9	3	2	2	2
	Y2	0.875	4	9	3	2	2	2
	Y3A	0.875	4	5	4	3	2	2
	Y3B	0.875	3	5	4	3	2	2
	Y4A	0.875	4	5	4	3	2	2
	Y4B	0.875	4	5	4	3	2	2
	Y5	0.875	2	13.5	2	2	2	2
	Y6	0.75	2	9	2	2	2	2
	Y7	0.75	2	9	2	2	2	2
	Y8	0.75	2	9	2	2	2	2

Table A-24 Tie-Down Schedule for the Four-Story, Multi-Family Dwelling, Moderate Seismic Archetype

Archetype ID	Tie-Down Rods							
	Multi-Family Dwellings: Moderate Seismic							
Wall	Diameter (in)	Terminate at Top of Story	Washer Area (in ²)	1 st Story Stud Pack	2 nd Story Stud Pack	3 rd Story Stud Pack	4 th Story Stud Pack	
MFD9	X1	0.5	2	9	2	2	2	2
	X2	0.75	4	9	2	2	2	2
	X3	0.75	3	9	2	2	2	2
	X4	0.5	2	9	2	2	2	2
	X5A	0.5	3	5	3	2	2	2
	X5B	0.5	3	5	3	2	2	2
	X6A	0.5	1	5	2	2	2	2
	X6B	No Tie-Down			2	2	2	2
	Y1	0.75	4	9	2	2	2	2
	Y2	0.75	4	9	2	2	2	2
	Y3A	0.75	4	5	3	2	2	2
	Y3B	0.5	2	5	2	2	2	2
	Y4A	0.625	3	5	2	2	2	2
	Y4B	0.625	3	5	2	2	2	2
	Y5	0.5	1	9	2	2	2	2
	Y6	No Tie-Down			2	2	2	2
	Y7	No Tie-Down			2	2	2	2
	Y8	No Tie-Down			2	2	2	2

A.5 Single-Family Dwelling Engineered Shear Wall Designs

Shear walls in all in single-family dwelling archetypes are provided around the perimeter and at selected interior wall lines. Shear wall locations in one-story and two-story single-family dwelling archetypes are identified in Figure A-5. Table A-25 provides design information for each single-family dwelling archetype including the assumed seismic weight at each level along with the design story shear.

Table A-26, Table A-27, and Table A-28 provide the details of shear wall and hold-down designs for one-story single-family dwelling archetypes, including the size of the stud pack at each end of the shear walls, for high, very high, and moderate seismic designs, respectively. Table A-29, Table A-30, and Table A-31 provide the details of the shear wall and hold-down designs for two-story single-family dwelling archetypes, for high, very high, and moderate seismic designs, respectively. Where the shear wall configuration results in a design overstrength, the percentage of overstrength is provided in the tables.

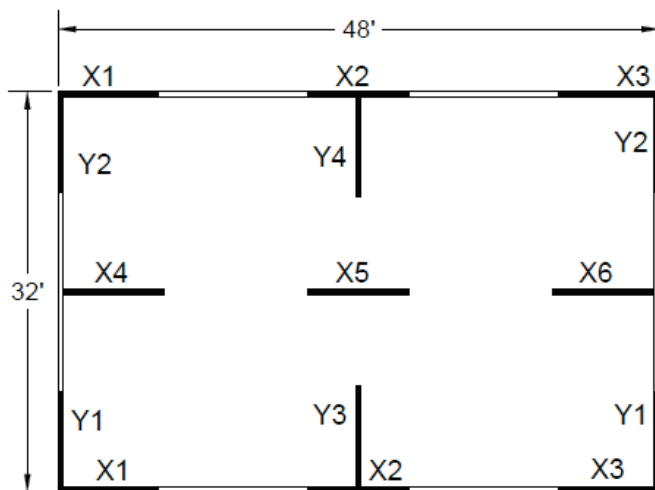


Figure A-5 Typical plan showing perimeter and interior shear wall locations in one-story and two-story single-family dwelling archetypes.

Table A-25 General Design Information for Engineered Single-Family Dwelling Archetypes

Archetype ID	No. of Stories	SDC	Story	Story Weight (kips)	Story Shear (kips)
Single-Family Dwellings: High Seismic					
SFD1	1	D	1 st	51	7.9
SFD2	2	D	1 st	70	18.9
			2 nd	53	11.4
Single-Family Dwellings: Very High Seismic					
SFD3	1	E	1 st	51	11.9
SFD4	2	E	1 st	70	28.4
			2 nd	53	17.0
Single-Family Dwellings: Moderate Seismic					
SFD5	1	C	1 st	51	4.0
SFD6	2	C	1 st	70	9.5
			2 nd	53	5.7

Table A-26 Shear Wall and Hold-Down Schedule for the Engineered, One-Story, Single-Family Dwelling, High Seismic Archetype

Archetype ID	Property / Description *		1 st Story			
Single-Family Dwellings: High Seismic						
SFD1	Wall	No. of Locs	Framing Size	Wall Type	Length (feet)	Hold-Down
	X1	2	2×6	Low-OSB	4	HDU2
	X2	2	2×6	Low-OSB	4	HDU2
	X3	2	2×6	Low-OSB	4	HDU2
	X4	1	2×4	Non-SFRS Wall		
	X5	1	2×4	Non-SFRS Wall		
	X6	1	2×4	Non-SFRS Wall		
	Design Overstrength		12%			
	Wall	No. of Locs	Framing Size	Wall Type	Length (feet)	Hold-Down
	Y1	2	2×6	Low-OSB	8	HDU2
	Y2	2	2×6	Low-OSB	4	HDU2
	Y3	1	2×4	Non-SFRS Wall		
	Y4	1	2×4	Non-SFRS Wall		
	Design Overstrength		21%			

* All walls have double end studs (i.e., the stud pack at the end has two king studs).

Table A-27 Shear Wall and Hold-Down Schedule for the Engineered, One-Story, Single-Family Dwelling, Very High Seismic Archetype

Archetype ID	Property / Description *			1 st Story		
	Single-Family Dwellings: Very High Seismic					
SFD3	Wall	No. of Locs	Framing Size	Wall Type	Length (feet)	Hold-Down
	X1	2	2×6	Low-OSB	4	HDU2
	X2	2	2×6	Low-OSB	8	HDU2
	X3	2	2×6	Low-OSB	4	HDU2
	X4	1	2×4	Non-SFRS Wall		
	X5	1	2×4	Non-SFRS Wall		
	X6	1	2×4	Non-SFRS Wall		
	Design Overstrength			6%		
	Wall	No. of Locs	Framing Size	Wall Type	Length (feet)	Hold-Down
	Y1	2	2×6	Low-OSB	8	HDU2
	Y2	2	2×6	Low-OSB	8	HDU2
	Y3	1	2×4	Non-SFRS Wall		
	Y4	1	2×4	Non-SFRS Wall		
	Design Overstrength			12%		

* All walls have double end studs (i.e., the stud pack at the end has two king studs).

Table A-28 Shear Wall and Hold-Down Schedule for the Engineered, One-Story, Single-Family Dwelling, Moderate Seismic Archetype

Archetype ID	Property / Description *		1 st Story			
	Single-Family Dwellings: Moderate Seismic					
SFD5	Wall	No. of Locs	Framing Size	Wall Type	Length (feet)	Hold-Down
	X1	2	2×6	Low-OSB	4	HDU2
	X2	2	2×6	Non-SFRS Wall		
	X3	2	2×6	Low-OSB	4	HDU2
	X4	1	2×4	Non-SFRS Wall		
	X5	1	2×4	Non-SFRS Wall		
	X6	1	2×4	Non-SFRS Wall		
	Design Overstrength		49%			
	Wall	No. of Locs	Framing Size	Wall Type	Length (feet)	Hold-Down
	Y1	2	2×6	Low-OSB	4	HDU2
	Y2	2	2×6	Low-OSB	4	HDU2
	Y3	1	2×4	Non-SFRS Wall		
	Y4	1	2×4	Non-SFRS Wall		
	Design Overstrength		49%			

* All walls have double end studs (i.e., the stud pack at the end has two king studs).

Table A-29 Shear Wall and Hold-Down Schedule for the Engineered, Two-Story, Single-Family Dwelling, High Seismic Archetype

Archetype ID	Property / Description *			1 st Story			2 nd Story		
Single-Family Dwellings: High Seismic									
SFD2	Wall	No. of Locs	Framing Size	Wall Type	Length (feet)	Hold-Down	Wall Type	Length (feet)	Hold-Down
	X1	2	2×6	Med-OSB	4	HDU8	Non-SFRS Wall		
	X2	2	2×6	Med-OSB	8	HDU14	Med-OSB	8	MSTC52
	X3	2	2×6	Low-OSB	4	HDU2	Non-SFRS Wall		
	X4	1	2×6	Non-SFRS Wall			Non-SFRS Wall		
	X5	1	2×6	Non-SFRS Wall			Non-SFRS Wall		
	X6	1	2×6	Non-SFRS Wall			Non-SFRS Wall		
	Design Overstrength			11%			10%		
	Wall	No. of Locs	Framing Size	Wall Type	Length (feet)	Hold-Down	Wall Type	Length (feet)	Hold-Down
	Y1	2	2×6	Med-OSB	8	HDU14	Med-OSB	8	HDU8
	Y2	2	2×6	Low-OSB	8	HDU2	Non-SFRS Wall		
	Y3	1	2×4	Non-SFRS Wall			Non-SFRS Wall		
	Y4	1	2×4	Non-SFRS Wall			Non-SFRS Wall		
	Design Overstrength			2%			10%		

* All walls have double end studs (i.e., the stud pack at the end has two king studs).

Table A-30 Shear Wall and Hold-Down Schedule for the Engineered, Two-Story, Single-Family Dwelling, Very High Seismic Archetype

Archetype ID	Property / Description *			1 st Story			2 nd Story		
	Single-Family Dwellings: Very High Seismic								
SFD4	Wall	No. of Locs	Framing Size	Wall Type	Length (feet)	Hold-Down	Wall Type	Length (feet)	Hold-Down
	X1	2	2×6	Med-OSB	4	HDU8	Low-OSB	4	MSTC40
	X2	2	2×6	High-OSB	8	HDU14	Med-OSB	8	MSTC52
	X3	2	2×6	Low-OSB	4	HDU8	Low-OSB	4	MSTC40
	X4	1	2×6	Non-SFRS Wall			Non-SFRS Wall		
	X5	1	2×6	Non-SFRS Wall			Non-SFRS Wall		
	X6	1	2×6	Non-SFRS Wall			Non-SFRS Wall		
	Design Overstrength			9%			8%		
	Wall	No. of Locs	Framing Size	Wall Type	Length (feet)	Hold-Down	Wall Type	Length (feet)	Hold-Down
	Y1	2	2×6	Med-OSB	8	HDU8	Low-OSB	8	MSTC40

* All walls have double end studs (i.e., the stud pack at the end has two king studs).

Table A-31 Shear Wall and Hold-Down Schedule for the Engineered, Two-Story, Single-Family Dwelling, Moderate Seismic Archetype

Archetype ID	Property / Description *			1 st Story			2 nd Story		
Single-Family Dwellings: Moderate Seismic									
SFD6	Wall	No. of Locs	Framing Size	Wall Type	Length (feet)	Hold-Down	Wall Type	Length (feet)	Hold-Down
	X1	2	2×6	Low-OSB	4	HDU2	Non-SFRS Wall		
	X2	2	2×6	Low-OSB	8	HDU8	Low-OSB	8	MSTC40
	X3	2	2×6	Non-SFRS Wall			Non-SFRS Wall		
	X4	1	2×6	Non-SFRS Wall			Non-SFRS Wall		
	X5	1	2×6	Non-SFRS Wall			Non-SFRS Wall		
	X6	1	2×6	Non-SFRS Wall			Non-SFRS Wall		
	Design Overstrength			2%			17%		
	Wall	No. of Locs	Framing Size	Wall Type	Length (feet)	Hold-Down	Wall Type	Length (feet)	Hold-Down
	Y1	2	2×6	Med-OSB	8	HDU8	Low-OSB	8	MSTC40
	Y2	2	2×6	Non-SFRS Wall			Non-SFRS Wall		
	Y3	1	2×4	Non-SFRS Wall			Non-SFRS Wall		
	Y4	1	2×4	Non-SFRS Wall			Non-SFRS Wall		
	Design Overstrength			33%			17%		

* All walls have double end studs (i.e., the stud pack at the end has two king studs).

A.6 Single-Family Dwelling Conventional Construction Shear Wall Designs

Shear walls in all in single-family dwelling archetypes are provided around the perimeter and at selected interior wall lines. Shear wall locations in conventional construction single-family dwelling archetypes are the same as those used in engineered construction, and are identified in Figure A-5.

Table A-32 provides design information for each single-family dwelling archetype, including, for comparison, the assumed seismic weight and design story shear at each level, although this information is not used in conventional construction design. Table A-33 describes the wall types and sheathing configurations used for conventional construction design.

Table A-34 provides the details of shear wall designs for conventional construction, one-story single-family dwelling archetypes, for high and very high seismic designs. Table A-35 provides details of the shear wall design for the conventional construction, two-story single-family dwelling archetype, for high seismic design. Conventional construction does not require hold-downs at the ends of shear walls.

Table A-32 General Design Information for Conventional Construction Single-Family Dwelling Archetypes

Archetype ID	No. of Stories	SDC	Story	Story Weight (kips)	Story Shear (kips)
Single-Family Dwellings: High Seismic					
SFD1C	1	D ₂	1 st	51	7.9
SFD2C	2	D ₂	1 st	70	18.9
			2 nd	53	11.4
Single-Family Dwellings: Very High Seismic					
SFD3C	1	E	1 st	51	11.9

Table A-33 Wall Types for Conventional Construction Single-Family Dwelling Archetypes

Wall Type	Description
GB	½-inch gypsum wallboard on both faces of framing, with 1½-inch long nails or screws at 7inches on center to studs, plates, and sills.
ST	Stucco on exterior, 1½-inch long nails at 6 inches on-center to studs, plates, and sills.
OSB	7/16-inch OSB with 6d common nails at 6 inches on-center along panel edges and 12 inches on-center in field.

Table A-34 Shear Wall Schedule for Conventional Construction, One-Story, Single-Family Dwelling, High and Very High Seismic Archetypes

Archetype ID	Property / Description		1 st Story		
Single-Family Dwellings: High and Very High Seismic					
SFD1C or SFD3C	Wall	No. of Locs.	Framing Size	Wall Type	Length (feet)
	X1	2	2×6	ST	8
	X2	2	2×6	ST	8
	X3	2	2×6	ST	8
	X4	1	2×4	GB	8
	X5	1	2×4	GB	8
	X6	1	2×4	GB	8
	Y1	2	2×6	ST	8
	Y2	2	2×6	ST	8
	Y3	1	2×4	GB	8
	Y4	1	2×4	GB	8

Table A-35 Shear Wall Schedule for the Conventional Construction, Two-Story, Single-Family Dwelling, High Seismic Archetype

Archetype ID	Property / Description			1 st Story		2 nd Story	
Single-Family Dwellings: High Seismic							
SFD2C	Wall	No. of Locs.	Framing Size	Wall Type	Length (feet)	Wall Type	Length (feet)
	X1	2	2×6	OSB	12	ST	8
	X2	2	2×6	OSB	8	ST	8
	X3	2	2×6	OSB	12	ST	8
	X4	1	2×4	GB	8	GB	8
	X5	1	2×4	GB	24	GB	8
	X6	1	2×4	GB	8	GB	8
	Y1	2	2×6	OSB	12	ST	8
	Y2	2	2×6	OSB	8	ST	8
	Y3	1	2×4	GB	12	GB	8
	Y4	1	2×4	GB	8	GB	8

A.7 Foundation Designs for Wood Light-Frame Building Archetypes

Foundation design considered gravity load combinations as well as seismic load combinations. The foundations for all archetypes consist of slabs-on-grade with edge footings formed by thickening of the slab. Slabs-on-grade are also thickened, as needed, under interior shear walls and bearing walls. Many of the foundation designs were controlled by gravity load, except seismic loading controlled taller buildings in locations of higher seismic demand. Where overturning demands were significant, a beam on compression spring analysis was used for design. Consistent with common practice, the spring stiffness assumed for design of the foundations was softer than the springs used for consideration of soil-structure interaction in the parametric studies. An assumption of softer springs results in larger flexural demands on concrete foundations, which is conservative for design.

Plan views of the foundations for COM, MFD (one-story or four-story), MFD (two-story), and SFD buildings are shown in Figure A-6 through Figure A-9. A typical section through an edge footing and an interior footing are shown in Figure A-10 and Figure A-11, respectively. Foundation reinforcement is specified as follows:

- The reinforcement schedule for footings in all commercial building archetypes is provided in Table A-36.
- The reinforcement schedule for footings in multi-family dwelling archetypes is provided in Table A-37, Table A-38, and Table A-39 for high seismic, very high seismic, and moderate seismic design levels, respectively.
- The reinforcement schedule for footings in all single-family dwelling archetypes is provided in Table A-40 for high seismic, very high seismic, and moderate seismic design levels.

Slab-on-grade thickness and reinforcement for all archetypes is noted in the footnotes to Table A-36 through Table A-40.

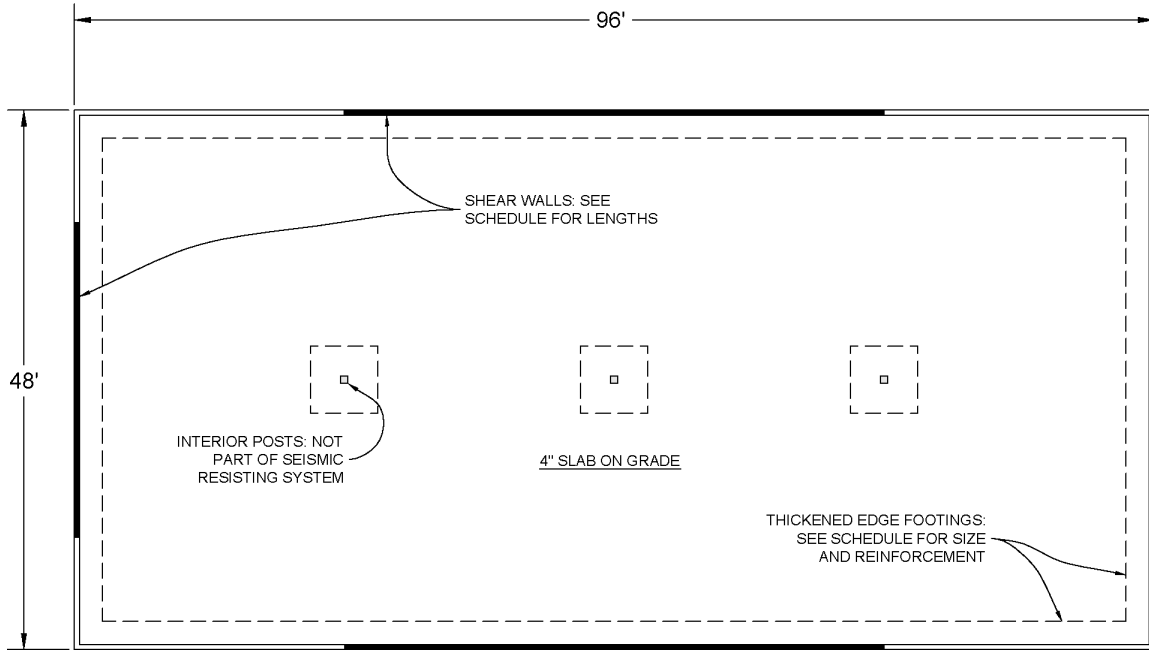


Figure A-6 Foundation plan for commercial building archetypes.

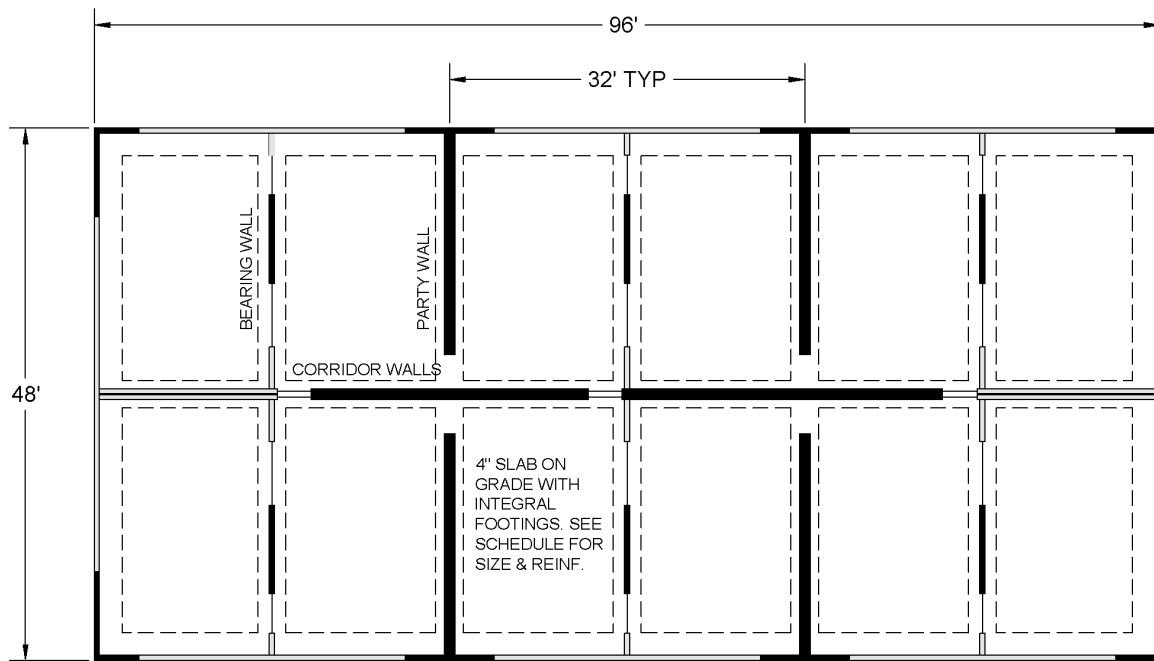


Figure A-7 Foundation plan for one-story and four-story multi-family dwelling archetypes.

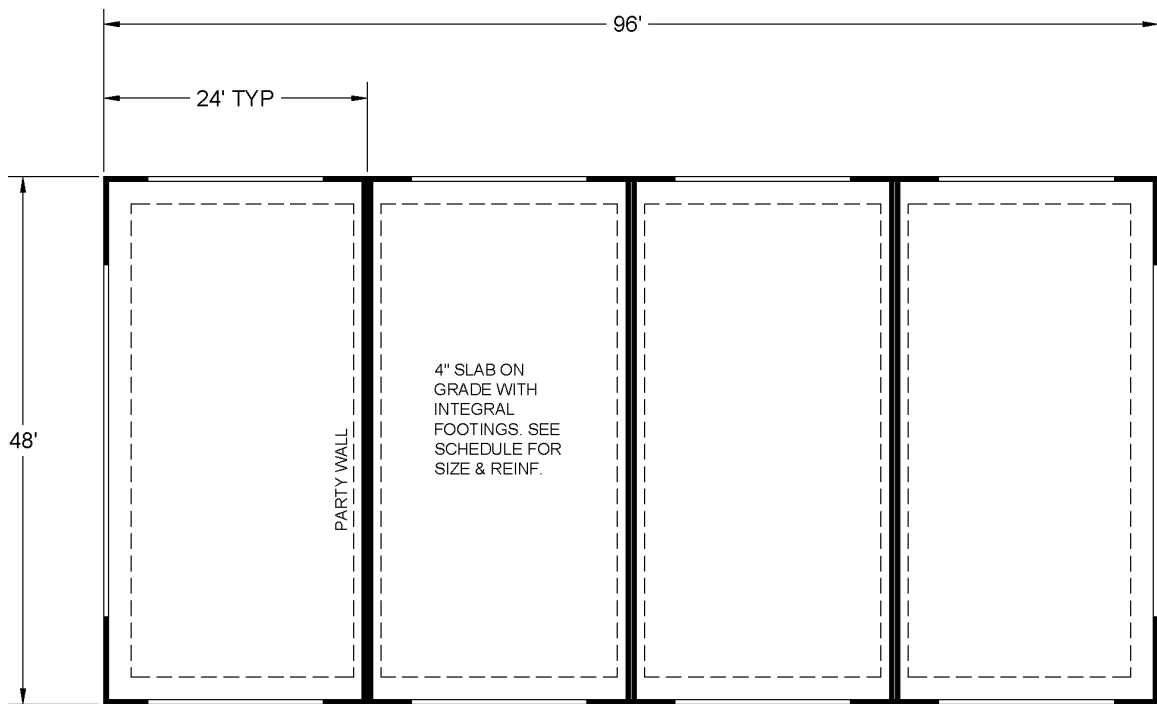


Figure A-8 Foundation plan for two-story multi-family dwelling archetypes.

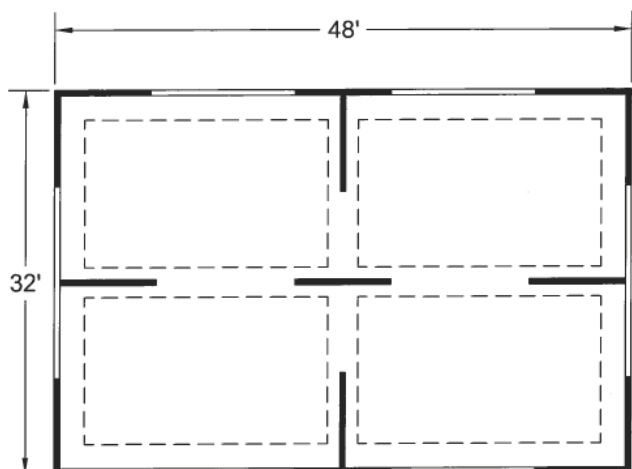


Figure A-9 Foundation plan for one-story and two-story single-family dwelling archetypes.

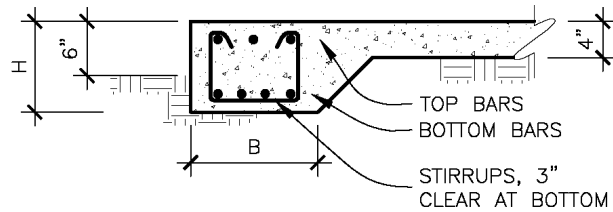


Figure A-10 Section through a typical edge footing (thickened slab).

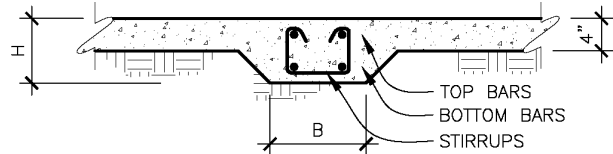


Figure A-11 Section through a typical interior footing (thickened slab).

Table A-36 Foundation Schedule for Commercial Building Archetypes⁽¹⁾

Archetype ID	No. of Stories	Wall	Width B (in)	Height H (in)	Bottom Bars	Top Bars	Stirrups ⁽²⁾
Commercial Buildings: High Seismic							
COM1	1	Transverse	16	12	2-#5	2-#5	None
		Longitudinal	16	12	4-#5	2-#5	#3@4"
COM2	2	Transverse	16	12	4-#5	4-#6	None
		Longitudinal	24	16	5-#6	4-#5	#3@6"
COM3	4	Transverse	36	20	6-#8	6-#7	#4@8"
		Longitudinal	36	20	6-#7	5-#6	#4@8"
Commercial Buildings: Very High Seismic							
COM4	1	Transverse	16	12	2-#5	2-#5	None
		Longitudinal	16	12	4-#5	2-#5	#3@4"
COM5	2	Transverse	16	12	4-#5	4-#5	None
		Longitudinal	24	16	5-#6	5-#5	#3@6"
COM6	4	Transverse	48	30	6-#8	6-#8	#4@10"
		Longitudinal	36	20	6-#9	6-#7	#4@8"
Commercial Buildings: Moderate Seismic							
COM7	1	Transverse	16	12	2-#5	2-#5	None
		Longitudinal	16	12	4-#5	2-#5	#3@4"
COM8	2	Transverse	16	12	4-#5	3-#5	None
		Longitudinal	24	16	5-#6	4-#5	#3@6"
COM9	4	Transverse	30	16	5-#6	5-#5	#3@6"
		Longitudinal	36	20	6-#7	5-#6	#4@8"

⁽¹⁾ Slab on grade is 4 inches thick, except as noted, and is reinforced with 6x6-W1.9 WWF.

⁽²⁾ Stirrups are only adjacent to columns and at the ends of shear walls.

Table A-37 Foundation Schedule for Multi-Family Dwelling High Seismic Archetypes*

Archetype ID	No. of Stories	Wall	Width B (in)	Height H (in)	Bottom Bars	Top Bars
Multi-Family Dwellings: High Seismic						
MFD1	1	Transverse	16	12	2-#5	2-#5
		Longitudinal	16	12	2-#5	2-#5
		Party	16	10	3-#5	3-#5
MFD2	2	Transverse	16	12	4-#5	3-#4
		Longitudinal	20	12	4-#6	4-#6
		Party	16	12	3-#5	3-#4
MFD3	4	Transverse	20	16	5-#6	5-#6
		Longitudinal	16	12	4-#6	3-#6
		Corridor	40	16	5-#8	5-#8
		Party	36	16	6-#7	5-#7
		Bearing	30	16	6-#6	6-#6

* Slab on grade is 4 inches thick, except as noted, and is reinforced with 6x6-W1.9 WWF.

Table A-38 Foundation Schedule for Multi-Family Dwelling Very High Seismic Archetypes*

Archetype ID	No. of Stories	Wall	Width B (in)	Height H (in)	Bottom Bars	Top Bars
Multi-Family Dwellings: Very High Seismic						
MFD4	1	Transverse	16	12	2-#5	2-#5
		Longitudinal	16	12	2-#5	2-#5
		Party	16	10	3-#5	3-#5
MFD5	2	Transverse	16	12	4-#4	4-#5
		Longitudinal	20	12	4-#6	4-#6
		Party	16	12	4-#5	3-#4
MFD6	4	Transverse	20	16	5-#7	4-#7
		Longitudinal	20	16	4-#6	4-#6
		Corridor	60	16	8-#8	8-#8
		Party	48	20	10-#8	5-#6
		Bearing	30	16	6-#6	6-#6

* Slab on grade is 4 inches thick, except as noted, and is reinforced with 6x6-W1.9 WWF.

Table A-39 Foundation Schedule for Multi-Family Dwelling Moderate Seismic Archetypes *

Archetype ID	No. of Stories	Wall	Width B (in)	Height H (in)	Bottom Bars	Top Bars
Multi-Family Dwellings: Moderate Seismic						
MFD7	1	Transverse	16	12	2-#5	2-#5
		Longitudinal	16	10	2-#5	2-#5
		Party	16	12	3-#5	3-#5
MFD8	2	Transverse	16	12	4-#5	3-#4
		Longitudinal	16	12	4-#5	3-#4
		Party	16	12	3-#5	3-#4
MFD9	4	Transverse	20	16	4-#6	4-#6
		Longitudinal	16	12	3-#6	3-#6
		Corridor	40	12	4-#6	5-#6
		Party	36	16	6-#6	6-#7
		Bearing	30	16	6-#6	6-#6

* Slab on grade is 4 inches thick, except as noted, and is reinforced with 6x6-W1.9 WWF.

Table A-40 Foundation Schedule for Single-Family Dwelling Archetypes *

Archetype ID	No. of Stories	Wall	Width B (in)	Height H (in)	Bottom Bars	Top Bars
Single-Family Dwellings: High Seismic						
SFD1	1	Perimeter	16	12	2-#5	2-#5
SFD2	2	Perimeter	16	12	2-#5	2-#5
Single-Family Dwellings: Very High Seismic						
SFD3	1	Perimeter	16	12	2-#5	2-#5
SFD4	2	Perimeter	16	12	2-#5	2-#5
Single-Family Dwellings: Moderate Seismic						
SFD5	1	Perimeter	16	12	2-#5	2-#5
SFD6	1	Perimeter	16	12	2-#5	2-#5

* Slab on grade is 4 inches thick, except as noted, and is reinforced with 6x6-W1.9 WWF.

Appendix B

Archive of Peak Response Calculations

B.1 Peak Response Calculations from Parametric Studies

Response parameters of interest (stripe statistics) were post-processed and archived at each intensity stripe to determine the statistics of peak response for each archetype. Stripe statistics were archived for each orthogonal direction (E-W and N-S) of each archetype numerical model. A spreadsheet for each incremental dynamic analysis (IDA) containing response parameters for all intensity stripes was developed. The names of the archiving files for each commercial building (COM), multi-family dwelling (MFD), and single-family dwelling (SFD) archetype are listed in Table B-1, Table B-2, and Table B-3, respectively. The archives for all stripe statistics are available at <https://femap2139.atcouncil.org/>.

B.2 Peak Response Calculations from the Study on Effect of Viscous Damping

In the soil-structure interaction (SSI) and foundation flexibility parametric study, an asymmetrical bilinear spring was utilized to model vertical response of the foundation. An asymmetrical foundation soil spring has zero tension stiffness (i.e., the building model is not restrained vertically against uplift). Numerical instability can arise during the iterative process of numerical integration if transient vertical displacements occur in the soil spring. To avoid convergence issues, very small viscous damping (between 0.1 to 5 percent) was assigned to the models. Table B-4 shows the models used in a sensitivity study conducted to determine the influence of viscous damping on the MCE_R collapse probability (see Appendix C).

B.3 Response Parameters Archived for Each Model

Selected key response parameters (e.g., peak relative roof displacement) from incremental dynamic analyses (IDAs) were archived. Table B-5 provides the list of response parameters available in each of the data archiving files.

Table B-1 Parametric Studies and Peak Response Archiving Files for Numerical Models of Commercial Building Archetypes

Archetype ID	No. of Stories	Seismic Design Level	Parametric Study	Peak Response Archiving Files
COM1B	1	High	Baseline	Stripe_Statistics_ATC116_COM1B
COM1B-T	1	High	Weight Study ⁽¹⁾	Stripe_Statistics_ATC116_COM1B-T1 Stripe_Statistics_ATC116_COM1B-T2
COM1B-F	1	High	SSI/Foundation Flexibility ⁽³⁾	Stripe_Statistics_ATC116_COM1B-F-CD Stripe_Statistics_ATC116_COM1B-F-DE
COM2B	2	High	Baseline	Stripe_Statistics_ATC116_COM2B
COM2B-C	2	High	Collapse Displacement Capacity ⁽²⁾	Stripe_Statistics_ATC116_COM2BC0 Stripe_Statistics_ATC116_COM2BC4 Stripe_Statistics_ATC116_COM2BC6
COM2B-NS	2	High	Wall Finishes	Stripe_Statistics_ATC116_COM2B-NS
COM2B-F	2	High	SSI/Foundation Flexibility ⁽³⁾	Stripe_Statistics_ATC116_COM2B-F-CD Stripe_Statistics_ATC116_COM2B-F-DE
COM3B	4	High	Baseline	Stripe_Statistics_ATC116_COM3B
COM3B-F	4	High	SSI/Foundation Flexibility ⁽³⁾	Stripe_Statistics_ATC116_COM3B-F-CD Stripe_Statistics_ATC116_COM3B-F-DE
COM3B-BS	4	High	Backbone Shape	Stripe_Statistics_ATC116_COM3B-BSR1 Stripe_Statistics_ATC116_COM3B-BSR1-NS Stripe_Statistics_ATC116_COM3B-BSR2 Stripe_Statistics_ATC116_COM3B-BSR2-NS Stripe_Statistics_ATC116_COM3B-BSR1-C0 Stripe_Statistics_ATC116_COM3B-BSR1-C0-NS Stripe_Statistics_ATC116_COM3B-BSR2-C0 Stripe_Statistics_ATC116_COM3B-BSR2-C0-NS Stripe_Statistics_ATC116_COM3B-BSR1-C6 Stripe_Statistics_ATC116_COM3B-BSR1-C6-NS Stripe_Statistics_ATC116_COM3B-BSR2-C6 Stripe_Statistics_ATC116_COM3B-BSR2-C6-NS
COM4B	1	Very High	Baseline	Stripe_Statistics_ATC116_COM4B
COM5B	2	Very High	Baseline	Stripe_Statistics_ATC116_COM5B
COM6B	4	Very High	Baseline	Stripe_Statistics_ATC116_COM6B

⁽¹⁾ Two types of weight.

⁽²⁾ Six residual strength levels: from 10 percent to 60 percent of peak strength with four of them used in IDAs.

⁽³⁾ Two soil sites: soft (DE) site and stiff (CD) site.

Table B-2 Parametric Studies and Peak Response Archiving Files for Numerical Models of Multi-Family Dwelling Archetypes

Archetype ID	No. of Stories	Seismic Design Level	Parametric Study	Peak Response Archiving Files
MFD1B	1	High	Baseline	Stripe_Statistics_ATC116_MFD1B
MFD1B-F	1	High	SSI/Foundation Flexibility ⁽¹⁾	Stripe_Statistics_ATC116_MFD1B-F-CD Stripe_Statistics_ATC116_MFD1B-F-DE
MFD2B	2	High	Baseline	Stripe_Statistics_ATC116_MFD2B
MFD2B-F	2	High	SSI/Foundation Flexibility ⁽¹⁾	Stripe_Statistics_ATC116_MFD2B-F-CD Stripe_Statistics_ATC116_MFD2B-F-DE
MFD2B-NS	2	High	Wall Finishes	Stripe_Statistics_ATC116_MFD2B-NS
MFD2B-C	2	High	Collapse Displacement Capacity ⁽²⁾	Stripe_Statistics_ATC116_MFD2B-C0 Stripe_Statistics_ATC116_MFD2B-C4 Stripe_Statistics_ATC116_MFD2B-C6
MFD3B	4	High	Baseline	Stripe_Statistics_ATC116_MFD3B
MFD3B-F	4	High	SSI/Foundation Flexibility ⁽¹⁾	Stripe_Statistics_ATC116_MFD3B-F-CD Stripe_Statistics_ATC116_MFD3B-F-DE
MFD4B	1	Very High	Baseline	Stripe_Statistics_ATC116_MFD4B
MFD5B	2	Very High	Baseline	Stripe_Statistics_ATC116_MFD5B
MFD6B	4	Very High	Baseline	Stripe_Statistics_ATC116_MFD6B
MFD7B	1	Moderate	Baseline	IDAs Not Performed
MFD8B	2	Moderate	Baseline	IDAs Not Performed
MFD9B	4	Moderate	Baseline	IDAs Not Performed

⁽¹⁾ Two soil sites: soft (DE) site and stiff (CD) site.

⁽²⁾ Six residual strength levels: from 10 percent to 60 percent of peak strength with four of them used in IDAs.

Table B-3 Parametric Studies and Peak Response Archiving Files for Numerical Models of Single-Family Dwelling Archetypes

Archetype ID	No. of Stories	Seismic Design Level	Parametric Study	Peak Response Archiving Files
SFD1B	1	High	Baseline	Stripe_Statistics_ATC116_SFD1B
SFD1BC *	1	High	Baseline	Stripe_Statistics_ATC116_SFD1BC
SFD1B-NS	1	High	Wall Finishes	Stripe_Statistics_ATC116_SFD1B-NS Stripe_Statistics_ATC116_SFD1B-NSP
SFD1BC-NS	1	High	Wall Finishes	Stripe_Statistics_ATC116_SFD1BC-NS Stripe_Statistics_ATC116_SFD1BC-NSP
SFD2B	2	High	Baseline	Stripe_Statistics_ATC116_SFD2B
SFD2BC *	2	High	Baseline	Stripe_Statistics_ATC116_SFD2BC
SFD2B-NS	2	High	Wall Finishes	Stripe_Statistics_ATC116_SFD2B-NS Stripe_Statistics_ATC116_SFD2B-NSP
SFD3B	1	Very High	Baseline	Stripe_Statistics_ATC116_SFD3B
SFD3BC *	1	Very High	Baseline	Stripe_Statistics_ATC116_SFD3BC
SFD4B	2	Very High	Baseline	Stripe_Statistics_ATC116_SFD4B
SFD5B	1	Moderate	Baseline	IDAs Not Performed
SFD5BC *	1	Moderate	Baseline	IDAs Not Performed
SFD6B	2	Moderate	Baseline	IDAs Not Performed

* Conventional construction rather than engineered design.

Table B-4 Properties and Peak Response Archiving Files for Equivalent Viscous Damping Study on Wood Light-Frame Archetypes

Archetype ID	No. of Stories	Seismic Design Level	Critical Damping* (%)	Peak Response Archiving Files
COM1B	1	High	0.0	Stripe_Statistics_ATC116_COM1B
COM1B-01D	1	High	0.1	Stripe_Statistics_ATC116_COM1B-01D
COM1B-02D	1	High	0.2	Stripe_Statistics_ATC116_COM1B-02D
COM1B-05D	1	High	0.5	Stripe_Statistics_ATC116_COM1B-05D
COM1B-1D	1	High	1.0	Stripe_Statistics_ATC116_COM1B-1D
COM1B-2D	1	High	2.0	Stripe_Statistics_ATC116_COM1B-2D
COM1B-5D	1	High	5.0	Stripe_Statistics_ATC116_COM1B-5D
COM2B-01D	2	High	0.1	Stripe_Statistics_ATC116_COM2B-01D
COM3B-01D	4	High	0.1	Stripe_Statistics_ATC116_COM3B-01D
MFD1B-01D	1	High	0.1	Stripe_Statistics_ATC116_MFD1B-01D
MFD2B-01D	2	High	0.1	Stripe_Statistics_ATC116_MFD2B-01D
MFD3B-01D	4	High	0.1	Stripe_Statistics_ATC116_MFD3B-01D

* Rayleigh damping is used, and the assigned damping level is applied to the first and second modes of vibration.

Table B-5 Description of Response Parameters Archived for Each Orthogonal Direction (EW and NS) for Numerical Models of Wood Light-Frame Archetypes

Type	Response Parameters	Statistical Values
Peak Relative Displacement	Peak Roof Relative Displacement Peak Roof Drift Ratio Peak Story Drift Ratio ⁽⁵⁾	Median ⁽¹⁾ Mean of Survivors ⁽²⁾ Overall Mean ⁽³⁾ Overall Beta ⁽⁴⁾ Minimum Maximum
Peak Relative Velocity	Peak Roof Relative Velocity Peak Floor Relative Velocity	
Peak Absolute Acceleration	Peak Roof Absolute Acceleration Peak Floor Absolute Acceleration	
Residual Relative Displacement	Residual Roof Displacement Residual Roof Drift Ratio Residual Story Drift Ratio	
	All Records Collapse Cases	Number Percentage
Collapse	Individual Record Collapse Cases	If "No," Peak Roof Displacement If "Yes," Peak Roof Displacement at last surviving intensity, floor level initiating collapse, and collapse direction

⁽¹⁾ Calculated median = fitted lognormal based on all 44 earthquake records with last values of non-surviving records (i.e., records causing collapse).

⁽²⁾ Mean value of surviving earthquake records only (i.e., records not causing collapse).

⁽³⁾ Mean of all 44 earthquake records with last values for non-surviving records.

⁽⁴⁾ Beta is the lognormal standard deviation of all 44 earthquake records with last values of non-surviving records.

⁽⁵⁾ Calculated for each floor of multi-story archetypes.

Appendix C

Effect of Viscous Damping on Collapse Performance of Wood Light-Frame Archetypes

C.1 Introduction

According to a study by Folz and Filiatrault (2004), a relatively small viscous damping ratio (i.e., 1 percent or less of critical damping) may be used for response history analysis of wood light-frame buildings, provided the nonlinear hysteresis behavior of the vertical shear walls is explicitly modeled. Except for the soil-structure interaction and foundation flexibility study, all the parametric studies were conducted using models with zero viscous damping.

In the soil-structure interaction and foundation flexibility study, asymmetric bilinear springs used for modeling the vertical response of the foundation have zero tension stiffness. As a result, numerical instability can occur if the transient vertical displacement, or uplift, occurs in the soil spring during the iterative process of numerical integration. To achieve convergence and numerical stability in nonlinear response history analysis, a very small amount of non-zero viscous damping is needed in the models used to study soil-structure interaction and foundation flexibility.

A sensitivity study was carried out to: (1) investigate the effect of equivalent viscous damping on the collapse performance of wood light-frame archetypes; and (2) determine the maximum value of viscous damping ratio that can be used in soil-structure interaction and foundation flexibility models.

C.2 Equation of Motion and Damping Model

The methods used for modeling the dynamic behavior of wood light-frame archetypes are described in Section 4.3. The equations of motion governing the dynamic behavior of an inelastic system or building are given below:

$$M\ddot{u} + C\dot{u} + f_s(u) = -M\ddot{u}_g \quad (\text{C-1})$$

where \ddot{u} , \dot{u} , and u are the relative acceleration, relative velocity and relative displacement vectors of the degrees of freedom of the building of interest, respectively. Vector i_{ig} contains the ground accelerations, M is the global mass matrix, C is the global damping matrix, and $f_s(u)$ is the resisting force vector of the building components, which include the vertical wood shear walls and roof or floor diaphragms. For a nonlinear system, the resisting force is a function of the displacement response history, u . The parameters that describe the hysteresis responses of the vertical wood shear walls are given in Table 4-3 and Table 4-4. The global mass matrix, M , can be computed with reasonable accuracy by estimating the weights of the building materials. On the other hand, the estimation of the global damping matrix C is not as straightforward as the global mass matrix. Since a significant portion of the damping may come from mechanisms other than the structural elements, unlike the global stiffness or global mass matrix, it is not practical and not accurate to compute the global damping matrix from the structural properties or dimensions of individual building components. Thus, the global damping matrix should be determined from the modal damping ratios of the structure (Chopra, 2011).

C.2.1 Rayleigh Damping Model

In the *Timber3D* software, the Rayleigh damping model is used to construct the global damping matrix, C :

$$C = \alpha_M M + \beta_K K \quad (\text{C-2})$$

where M and K are the mass and stiffness matrices, respectively. The constants α_M and β_K define the mass-proportional and stiffness-proportional contributions of the damping matrix, respectively. For a system that follows Rayleigh damping, the damping ratio (as a fraction of critical damping) for the n^{th} mode of vibration is given below:

$$\xi_n = \frac{\alpha_M}{2\omega_n} + \frac{\beta_K}{2} \omega_n \quad (\text{C-3})$$

The solutions for constants α_M and β_K , which have units of seconds⁻¹ and seconds, respectively, and can be obtained by specifying the damping ratios for the i^{th} and j^{th} modes (ξ_i and ξ_j) and solving for the following system of equations (Chopra, 2011):

$$\frac{1}{2} \begin{bmatrix} \frac{1}{\omega_i} & \omega_i \\ \frac{1}{\omega_j} & \omega_j \end{bmatrix} \begin{Bmatrix} \alpha_M \\ \beta_K \end{Bmatrix} = \begin{Bmatrix} \xi_i \\ \xi_j \end{Bmatrix} \quad (\text{C-4})$$

where ω_i and ω_j are the natural frequencies of the i^{th} and j^{th} modes, respectively, which can be obtained from modal analysis.

To solve for the constants α_M and β_K , one must specify two modes (i.e., the i^{th} and j^{th} modes) and assign an appropriate damping ratio to each of the two modes such that the damping ratios for all the modes contributing to the dynamic response of the structure are reasonable. Note that once the constants α_M and β_K are known, the damping ratios for all modes can be computed using Equation C-3.

C.2.2 Variation of Damping Ratios with Natural Periods

The baseline one-story commercial building archetype (COM1B) was selected for this viscous damping sensitivity study. Figure C-1 shows example curves for the variation of modal damping ratios with natural period, with 1-percent viscous damping assigned to mode 1 and mode 2.

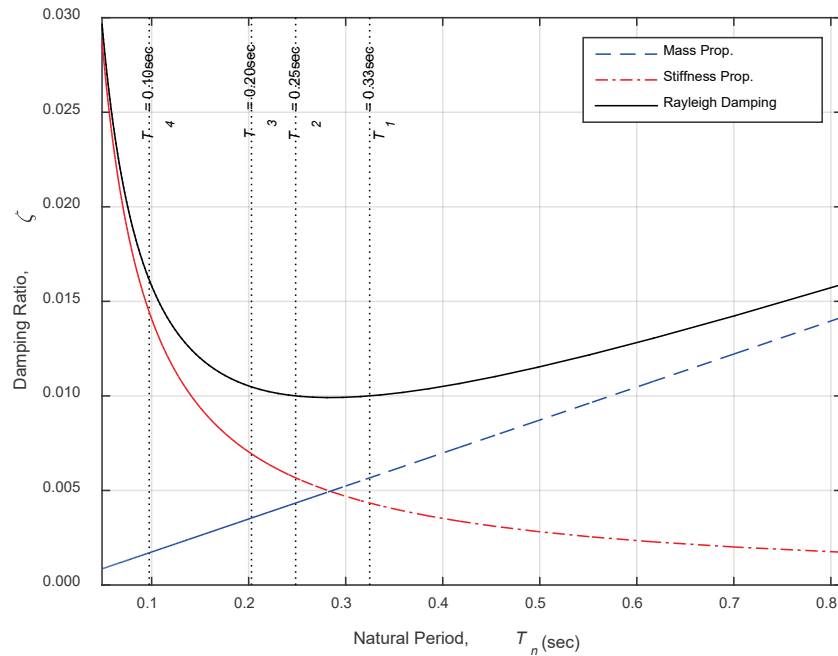


Figure C-1 Variation of modal damping ratios with natural period for COM1B baseline model with 1-percent viscous damping assigned to both mode 1 and mode 2.

The natural periods for the first two modes of the COM1B model are 0.33 second and 0.25 second, respectively. The solid black curve shows the variation of Rayleigh damping ratio as a function of the natural period. The Rayleigh damping can be computed using Equation C-3, as the sum of both the mass-proportional and stiffness-proportional damping ratios. From Figure C-1, it can be seen that the mass-proportional damping (dashed blue curve) is linearly proportional to the natural period, while the stiffness-

proportional damping (dashed-dot red curve) is inversely proportional to the natural period.

In *Timber3D*, the Rayleigh damping matrix (Equation C-2) is computed using the initial stiffness matrix of the undamaged building. As the building is damaged by earthquake shaking, the natural periods of the building will elongate, and modal damping ratios will increase (see Figure C-1). At incipient collapse, the velocity of the vertical degree of freedom increases as the building is collapsing (i.e., the floor or roof diaphragm is falling in the vertical direction). For a non-zero and constant Rayleigh damping matrix, the increased damping forces for vertical degrees of freedom at incipient collapse may result in unrealistically high damping forces, and this may affect the ultimate collapse mechanism.

C.3 Sensitivity Study on Addition of Viscous Damping

A sensitivity study on the addition of viscous damping was conducted to investigate the influence of viscous damping ratio on MCE_R collapse probability, $P[C|MCE_R]$, of wood light-frame building archetypes.

The main contribution of damping in a wood light-frame system comes from the nonlinear force-displacement response of the seismic force resisting system. Since the hysteresis response of the shear walls is explicitly modeled in *Timber3D*, a relatively small viscous damping ratio (i.e., 1 percent or less of critical damping) may be used for time history analysis of wood light-frame buildings, based on a previous study (Folz and Filiatrault, 2004).

To evaluate the effect of damping on MCE_R collapse probability, the baseline COM1B model was modified to have seven levels of equivalent viscous damping (0.0 percent, 0.1 percent, 0.2 percent, 0.5 percent, 1.0 percent, 2.0 percent, and 5.0 percent of critical damping). For each of the seven variant models, an equivalent viscous damping ratio was assigned to the first two modes of the COM1B model.

C.3.1 Modal and Pushover Analyses

Key properties and structural design criteria for the baseline COM1B wood light-frame archetype are reported in Table C-1. More details on the COM1B archetype design may be found in Chapter 3. Design criteria were the same for all COM1B archetype model variants used in the viscous damping study.

Table C-2 summarizes selected values of modal analysis results (T_I) and FEMA P-795 pushover analyses. From Table C-2, it can be seen that the fundamental periods in the two lateral directions, and the pushover

parameters (V_M / W) are essentially identical for all the models (with different viscous damping ratios). This is expected, as the damping matrix has no effect on the results of static pushover analyses.

Table C-1 Design Criteria for the COM1B Wood Light-Frame Building Archetype Used to Investigate the Effects of Viscous Damping

Baseline Archetype Model ID	No. of Stories	W (kips)	Key Archetype Design Criteria					
			Seismic Design Criteria					$S_{MT}[T]$ (g)
			SDC	R	v_{s30} (ft/sec)	T (sec)	C_s	
Commercial Buildings: High Seismic								
COM1B	1	180	D _{max}	6.5	-	0.25	0.154	1.5

Table C-2 Modal and FEMA P-795 Pushover Results for COM1B Archetype Models Used to Investigate the Effects of Viscous Damping

Archetype ID	Viscous Damping (% of Critical)	North-South Direction				East-West Direction			
		T_1 (sec)	V_M / W	$\Delta_{U,80}$ (in/in)	$\Delta_{U,max}$ (in/in)	T_1 (sec)	V_M / W	$\Delta_{U,80}$ (in/in)	$\Delta_{U,max}$ (in/in)
Commercial Buildings: High Seismic									
COM1B	0.0	0.25	0.62	0.03	0.16	0.33	0.50	0.03	0.16
COM1B-01D	0.1	0.25	0.62	0.03	0.16	0.33	0.50	0.03	0.16
COM1B-02D	0.2	0.25	0.62	0.03	0.16	0.33	0.50	0.03	0.16
COM1B-05D	0.5	0.25	0.62	0.03	0.16	0.33	0.50	0.03	0.16
COM1B-1D	1.0	0.25	0.62	0.03	0.16	0.33	0.50	0.03	0.16
COM1B-2D	2.0	0.25	0.62	0.03	0.16	0.33	0.50	0.03	0.16
COM1B-5D	5.0	0.25	0.62	0.03	0.16	0.33	0.50	0.03	0.16

C.3.2 Incremental Dynamic Analyses

Figure C-2 presents collapse rates and FEMA P-695 collapse fragility curves for the COM1B archetype models used to investigate the effects of viscous damping. As the viscous damping ratio increases, the MCE_R collapse fragility curve shifts to the right, which indicates reduced collapse risk. For the COM1B building, which was designed for high seismic regions, the MCE_R spectral acceleration at $T_1 = 0.25$ seconds is 1.5g.

The variation of MCE_R collapse probabilities with viscous damping ratios are summarized in the last column of Table C-3. Also shown in the table are the values of various response and collapse parameters from FEMA P-695 static pushover analyses and nonlinear IDAs for COM1B models with different viscous damping ratios.

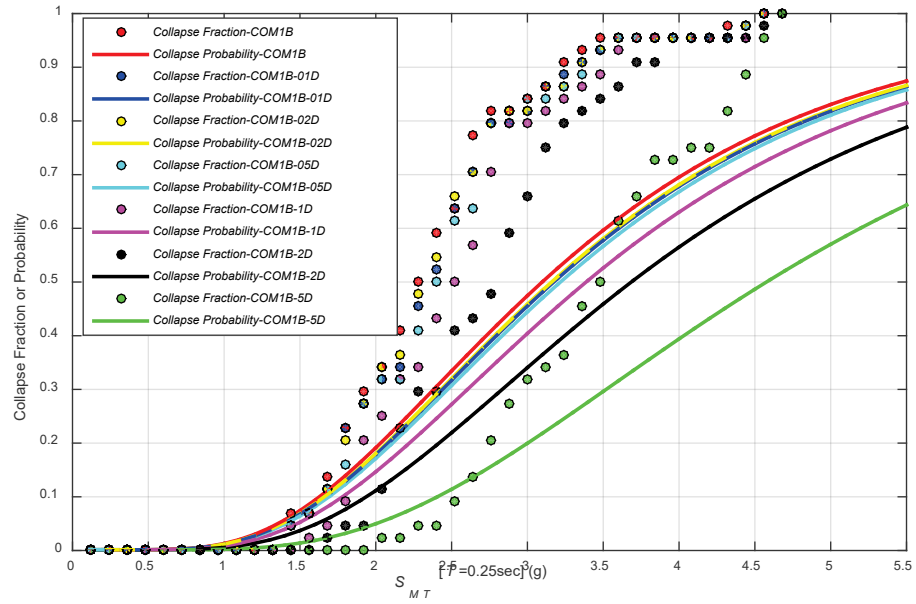


Figure C-2 Collapse rates from IDA and FEMA P-695 collapse fragility curves for COM1B archetype models used to investigate the effects of viscous damping.

Table C-3 FEMA P-695 Pushover and Collapse Analysis Results for COM1B Archetype Models Used to Investigate the Effects of Viscous Damping

Archetype ID	Viscous Damping (% of Critical)	Pushover Analysis			Collapse Analysis				$P[C MCE_R]$ (%)
		V_{max} / W	Ω	μ_r	S_{CT} (g)	CMR_{3D}	SSF	ACMR	
Commercial Buildings: High Seismic									
COM1B	0.0	0.56	3.6	>8	3.10	1.55	1.33	2.1	7.33
COM1B	0.1	0.56	3.6	>8	3.18	1.59	1.33	2.1	6.68
COM1B-01D	0.2	0.56	3.6	>8	3.16	1.58	1.33	2.1	6.80
COM1B-02D	0.5	0.56	3.6	>8	3.22	1.61	1.33	2.1	6.33
COM1B-05D	1.0	0.56	3.6	>8	3.39	1.70	1.33	2.3	5.15
COM1B-1D	2.0	0.56	3.6	>8	3.69	1.85	1.33	2.5	3.61
COM1B-2D	5.0	0.56	3.6	>8	4.58	2.29	1.33	3.1	1.28

C.4 Discussion

Figure C-3 shows the relationship between the $P[C|MCE_R]$ and equivalent viscous damping. From the figure, it can be seen that the MCE_R collapse probability as a function of viscous damping follows an exponential decay function of the form:

$$P[C|MCE_R] = c_0 \exp(-c_1 \xi) \quad (C-5)$$

where ζ is the equivalent damping ratio assigned to mode 1 and mode 2. Constant c_0 is the MCE_R collapse probability at zero percent damping. Constant c_1 is the decay constant that describes the reduction of MCE_R collapse probability with the increase of viscous damping ratio. Based on the trend line shown in Figure C-3, it can be determined that using a damping ratio between 0.0 percent and 0.5 percent has negligible effect on the MCE_R collapse probability.

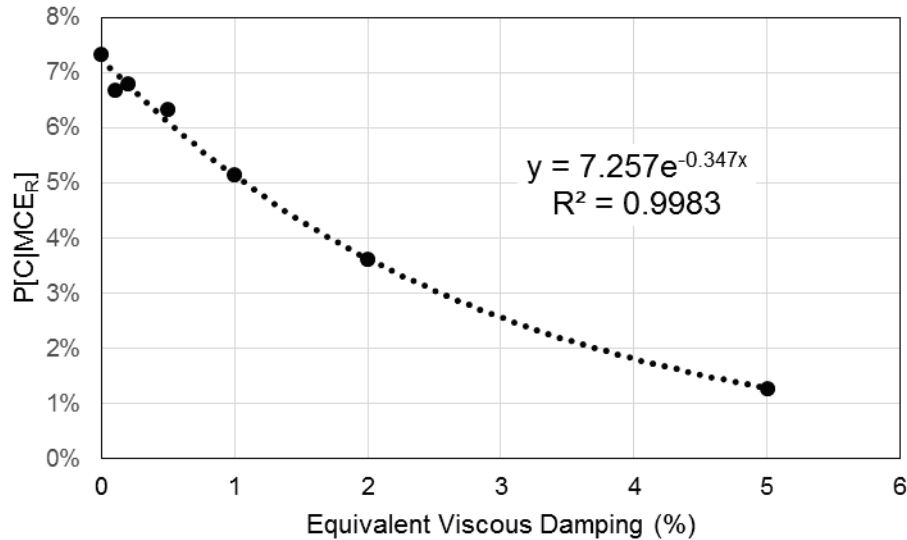


Figure C-3 Variation of MCE_R collapse probability with equivalent viscous damping for COM1B archetype models used to investigate the effects of viscous damping.

Appendix D

Validation Study

D.1 Introduction

The Twin Cities Community Hospital, located in Templeton, California (referred to herein as the Templeton Hospital) is a one-story wood light-frame building that experienced strong shaking during the 2003 San Simeon earthquake, but was not significantly damaged. The building was well-instrumented and building records from the earthquake provide a basis to compare and reconcile observed and simulated behavior using nonlinear response-history analysis.

A study of the Templeton Hospital building was conducted to validate potential numerical modeling approaches. The objectives of this validation study were to:

- **Investigate the Importance of Modeling Techniques.** The study performed preliminary investigations of wood light-frame shear wall and wood light-frame roof diaphragm modeling methods, and demonstrated the importance of diaphragm flexibility in the simulation of the response of the Templeton Hospital recorded during the 2003 San Simeon earthquake. The study also performed FEMA P-695 (FEMA, 2009b) collapse analyses of the Templeton Hospital analytical model.
- **Demonstrate the Use of Past Earthquake Data.** The study collected building inventory, ground motion, and damage data from the 1994 Northridge earthquake, and demonstrated use of these data as benchmarks for evaluation of the accuracy and reliability of FEMA P-695 collapse analyses of the Templeton Hospital building.

D.2 Measured Response Behavior in the 2003 San Simeon Earthquake

The Templeton Hospital, shown in Figure D-1, is irregularly configured in plan, with a main building and north and west wings. The building was designed in 1975 to stringent California “Post-Act” hospital seismic criteria. The plan dimensions of the building are 335 feet by 277 feet. The north (N) wing of the hospital was analyzed in this study as a stand-alone structure. The vertical elements of the seismic force-resisting-system (SFRS) in the north wing structure consist of perimeter wood light-frame shear walls and

interior wood light-frame shear walls in the east-west direction, as illustrated in Figure D-2. The wood light-frame shear walls are made of 2×6 studs at 16 inches on center, sheathed with $\frac{1}{2}$ -inch plywood on the exterior face. The diaphragm in the north wing consists of wood light-framing sheathed with $\frac{1}{2}$ -inch plywood. The building is founded on a 5-inch thick concrete slab-on-grade, cast with shallow continuous concrete footings.



Figure D-1 Templeton Hospital before the 2003 San Simeon earthquake; view looking southwest with north wing shown on the right (CSMIP, 2015).

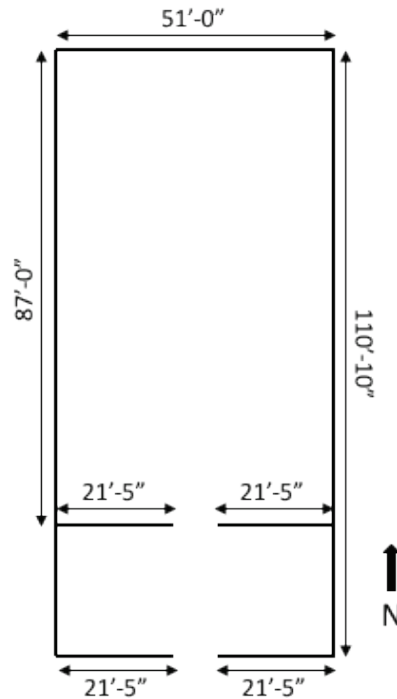


Figure D-2 Vertical elements of the SFRS of the north wing of the Templeton Hospital.

The building has nine channels of strong-motion instrumentation (CSMIP Station No. 36695), with one free-field instrument (CSMIP Station No. 36712) that was added after the 2003 San Simeon earthquake. The Templeton Hospital is part of the CSMIP-OSHPD Seismic Instrumentation Program for Hospital Buildings (Tokas and Lobo, 2012). Figure D-3 shows

the locations of the nine channels of strong motion instrumentation located at the first floor (slab on grade) and roof of the north and west wings. In the north wing, Channel 2 (first floor) and Channel 4, Channel 5, and Channel 6 (roof) are oriented in the east-west direction. Channel 4 and Channel 5 are near the top of shear walls at the north and south boundaries of the north wing. Channel 6 is located on the roof near the mid-point.

Templeton - 1-story Hospital

(CSMIP Station No. 36695)

SENSOR LOCATIONS

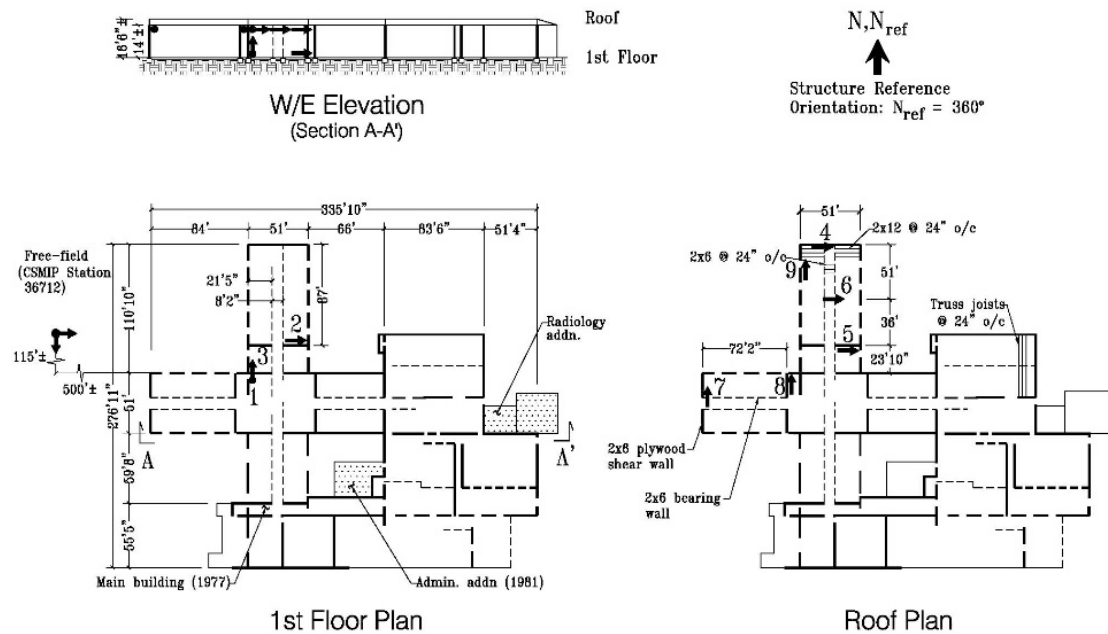


Figure D-3 Location of nine channels of strong motion instrumentation in the Templeton Hospital (CSMIP, 2015).

The CSMIP record sets include processed records, response spectra and Fourier spectra for each record. For example, Figure D-4 shows records of the response of the north wing of the Templeton Hospital recorded during the 2003 San Simeon earthquake, and Figure D-5 shows the 5-percent-damped response spectra of these records (with response spectral acceleration plotted as a function of response spectral displacement). Response recorded in the east-west direction at Channel 6, near the center of the north wing, shows increased response (relative to response in the east-west direction recorded by Channel 4 and Channel 5) indicating that roof diaphragm participated to some degree in the dynamic response (e.g., response is roughly 50 percent greater at center of the diaphragm than at the boundaries of the roof diaphragm). Ratios of Fourier spectra of records of response at different locations may be used to quantify differences in the amplitudes of response at the period of interest.

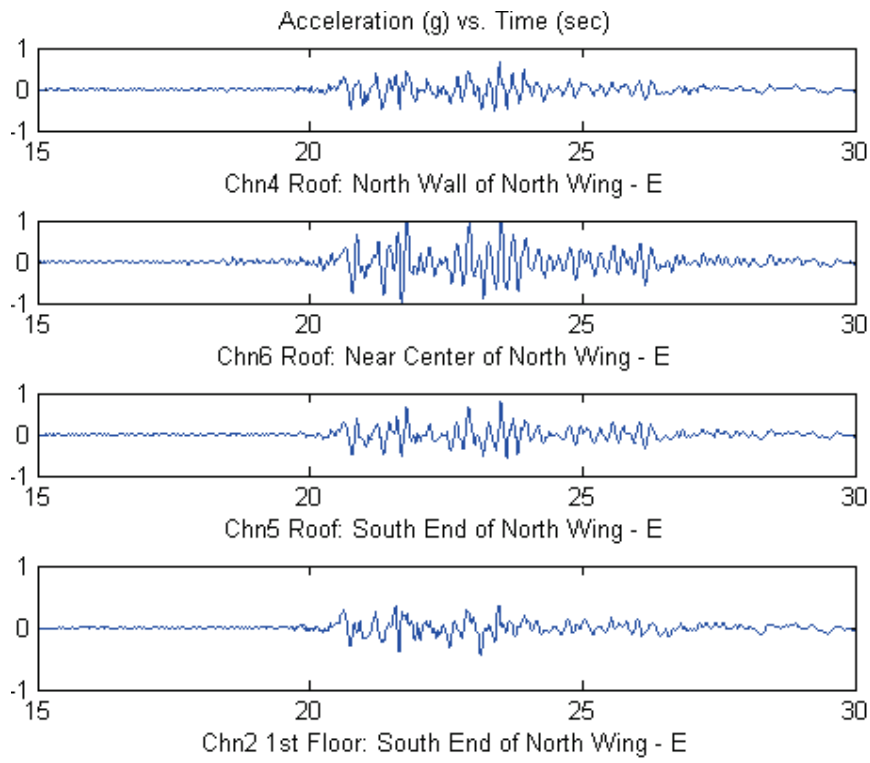


Figure D-4 East-west response of the north wing of the Templeton Hospital (CSMIP, 2015).

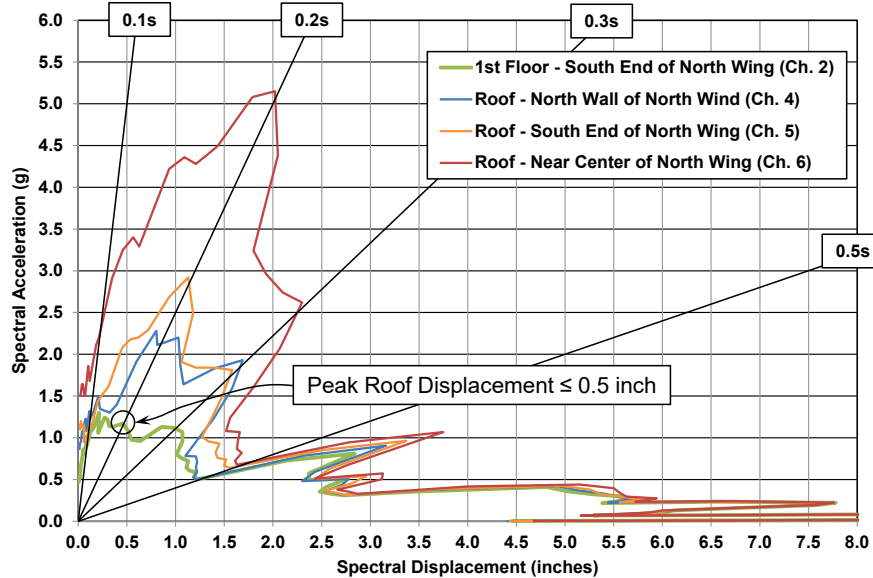


Figure D-5 Roof response spectra (5-percent viscous damping) of the north wing of the Templeton Hospital in the east-west direction.

The roof response spectra of the north wing of the Templeton Hospital in the east-west shown in Figure D-5 (Channel 4, Channel 5, and Channel 6) indicate significant amplification at periods from about 0.1 seconds to about 0.5 second, and a dominant period of roof response in the north wing in the

east-west direction of about 0.2 seconds (5 Hz). The response spectrum of Channel 2 (first floor) in the east-west direction shows a peak spectral acceleration of about 1.2g and a corresponding peak spectral displacement of about 0.5 inches at a period of 0.2 seconds, consistent with the peak roof acceleration of 1.28g and approximate peak roof displacement of 0.5 inches recorded at Channel 6 (i.e., 0.5 inches \approx $((386.4 \text{ in/sec}^2/\text{g})/4\pi^2)(1.28\text{g})(0.2 \text{ sec}^2)$). A peak roof displacement of 0.5 inches (i.e., drift ratio less than about 0.5 percent) is consistent with the observation of no significant damage in the structure of the hospital building.

Although building behavior can be directly observed in the records and response spectra, more sophisticated analyses of the records can be made using system identification techniques. Figure D-6 and Figure D-7 are examples of results from the Sutoyo and Hall (2006) study showing effective viscous damping and effective frequency, respectively, of the Templeton Hospital (north and west wings) calculated at points in time during earthquake shaking. In this case, building frequencies of about 6 Hz to 7 Hz (ignoring the first point of the graph) occur before the strongest shaking occurs, drop to about 5 Hz during the strongest intensity of shaking (i.e., between 20 seconds and 25 seconds), then gradually increase to 6 Hz to 7 Hz as the shaking decreases and returns to ambient conditions. Values of effective viscous damping are about 15 percent, regardless of the amplitude of shaking.

In summary, the response behavior of an analytical model of the north wing of the Templeton Hospital would be deemed valid if calculated response in the east-west direction was mildly nonlinear at a peak roof acceleration of about 1.0g, and the effective period was about 0.2 seconds and the effective viscous damping was about 15 percent at this response level. Similarly, the analytical model would be expected to replicate the records of roof response at Channel 4, Channel 5, and Channel 6 (see Figure D-3) reasonably well, using input motions of the Channel 2 record as a surrogate for free-field ground motions.

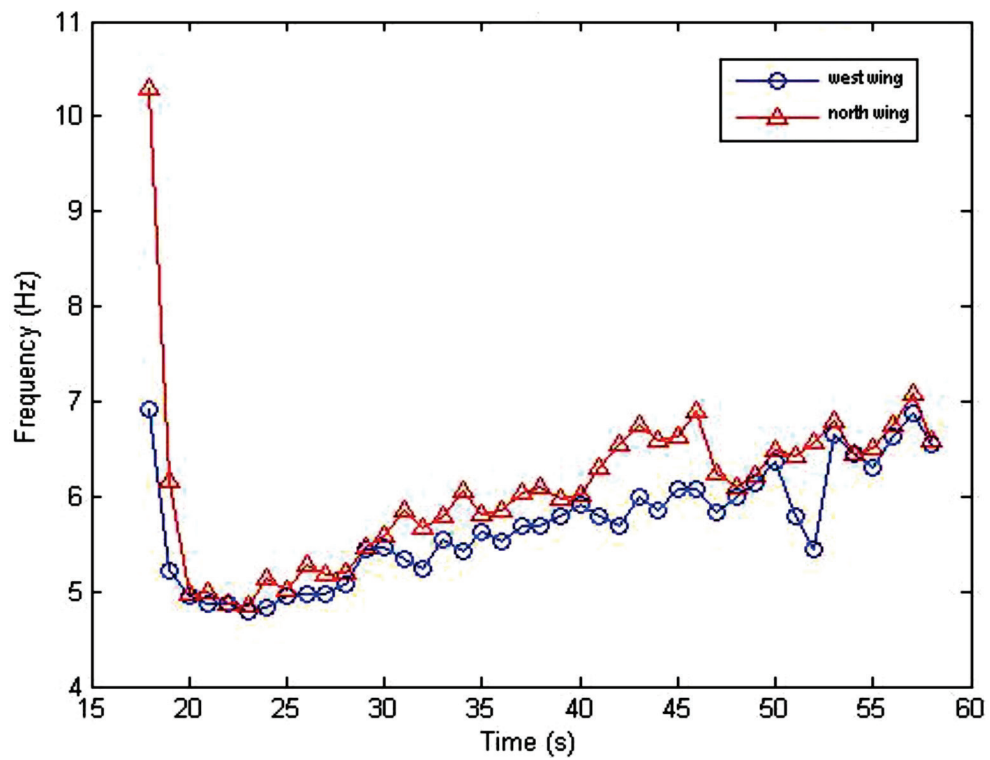


Figure D-6 Measured periods of the Templeton Hospital (Sutoyo and Hall, 2006).

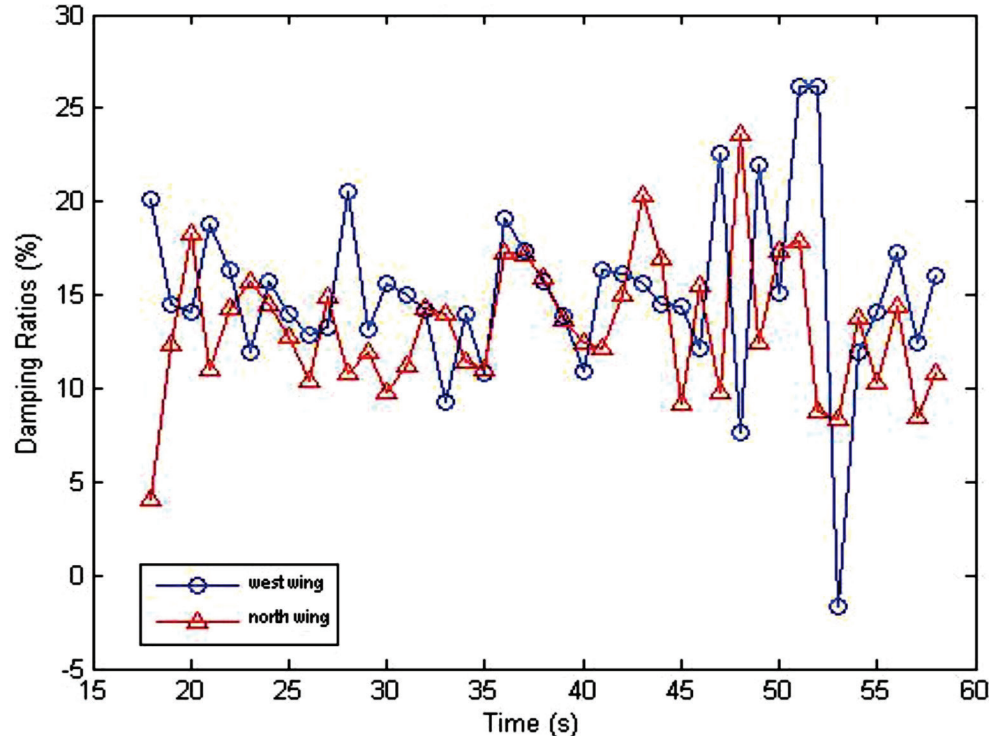


Figure D-7 Measured viscous damping of the Templeton Hospital (Sutoyo and Hall, 2006).

D.3 Validation of Numerical Modeling

The main objective of this study is to evaluate current numerical models of short-period wood light-frame buildings, and to evaluate the effects of more complex modeling on the ability to predict the recorded response and collapse capacity of the Templeton Hospital building. In particular, this study focused on more complex modeling of the wood light-frame diaphragm.

D.3.1 Modeling and Scope

For this study, two nonlinear numerical models of the north wing of the Templeton Hospital building were developed. These two building models incorporated various levels of complex behaviors to evaluate their influence on the level of correlation between predicted and recorded responses. The characteristics of the two models are:

- **Model 1.** A basic model reflecting current modeling practice and considering only the vertical elements (wood light-frame shear walls) of the seismic force-resisting system (SFRS). Vertical elements are assumed rigidly connected to each other and anchored to a rigid foundation. The roof diaphragm is assumed rigid in this model.
- **Model 2.** A modified version of Model 1 including the effects of a non-rigid roof diaphragm. A very small viscous damping ratio of 0.1 percent of critical (nominally zero viscous damping) was introduced in Model 2 because hysteretic response in both the vertical wood light-frame shear walls and horizontal roof diaphragm were explicitly considered.

The development of Model 2 with a non-rigid wood light-frame roof diaphragm used the numerical framework developed by Koliou et al. (2014; 2016) for rigid wall-flexible roof diaphragm structures. The numerical modeling framework is based on a three-step sub-structuring approach including: (1) a hysteretic response database for roof diaphragm connectors; (2) a two-dimensional inelastic roof diaphragm model incorporating hysteretic connector response; and (3) a simplified building model incorporating hysteretic diaphragm model response. RUAUMOKO-2D (Carr, 2007) was used for the development of the simplified building models.

Nonlinear response history analyses were performed for each of the two models under the ground motions recorded at the base of Templeton Hospital (Channel 2 and Channel 3 in Figure D-3) during the 2003 San Simeon earthquake. Comparisons between predicted and recorded acceleration response-histories in various locations of the building were made to evaluate the effects of the different levels of complexity included in the two models.

Incremental dynamic analyses were also conducted using the FEMA P-695 methodology to evaluate the effects of complex behaviors on the collapse capacity of the building. More details on the numerical model and analysis procedures can be found in Koliou et al. (2017).

D.3.2 Main Findings – Model 1

Figure D-8 shows the pushover curves in each principal direction at the center of the north wing predicted by Model 1. The seismic coefficient (base shear normalized by seismic weight) at peak strength is close to 0.9 in both directions, indicating a laterally strong building. The peak strength of the building occurs at a drift ratio of 2.0 percent in the east-west direction, and at 2.2 percent in the north-south direction.

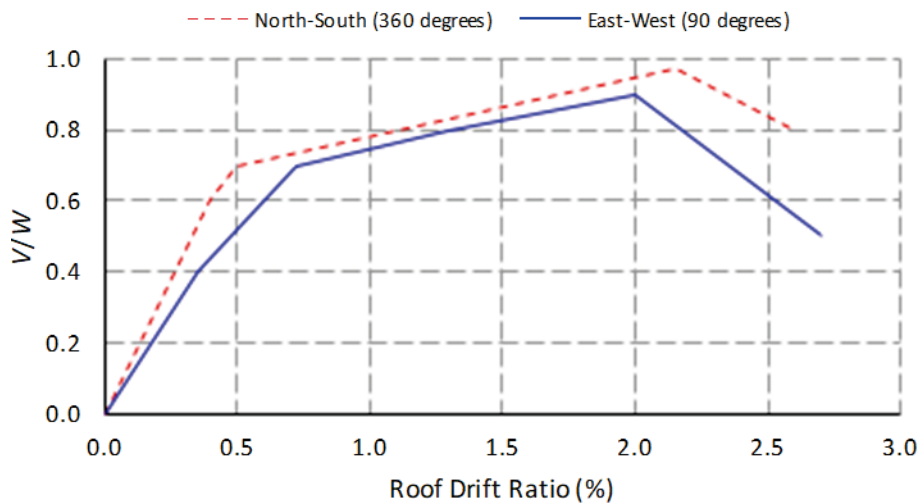


Figure D-8 Pushover curves predicted by Model 1.

Figure D-9 shows the first two natural periods and plan views of the mode shapes of the north wing of the Templeton Hospital predicted by Model 1. The fundamental periods of the building in the east-west and north-south direction are very close to each other. A predicted fundamental period of 0.16 seconds is reasonably close to the dominant period of roof-level response immediately above the shear wall elements (i.e., not within the diaphragm) of the north wing in the east-west direction, about 0.2 seconds (5 Hz), measured during the 2003 San Simeon earthquake.

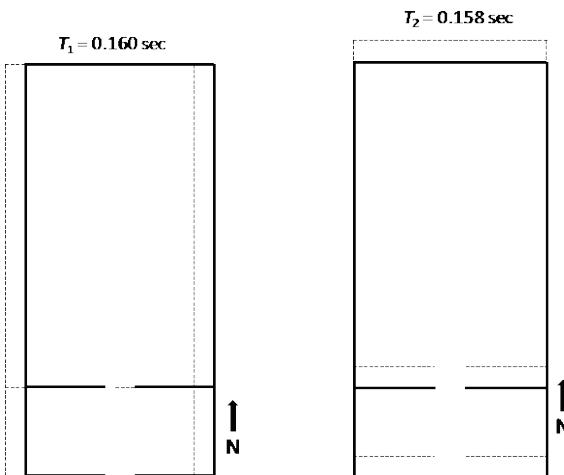


Figure D-9 Natural periods and mode shapes predicted by Model 1.

Figure D-10 compares the time histories of relative roof displacements (drifts) and absolute roof accelerations measured in the east-west direction by Channel 5 (see Figure D-3) during the San Simeon earthquake against the predictions of Model 1. The model underestimates both the measured peak drift and acceleration by approximately 35 percent. Significant differences between predicted and measured response also occur throughout the dynamic response histories.

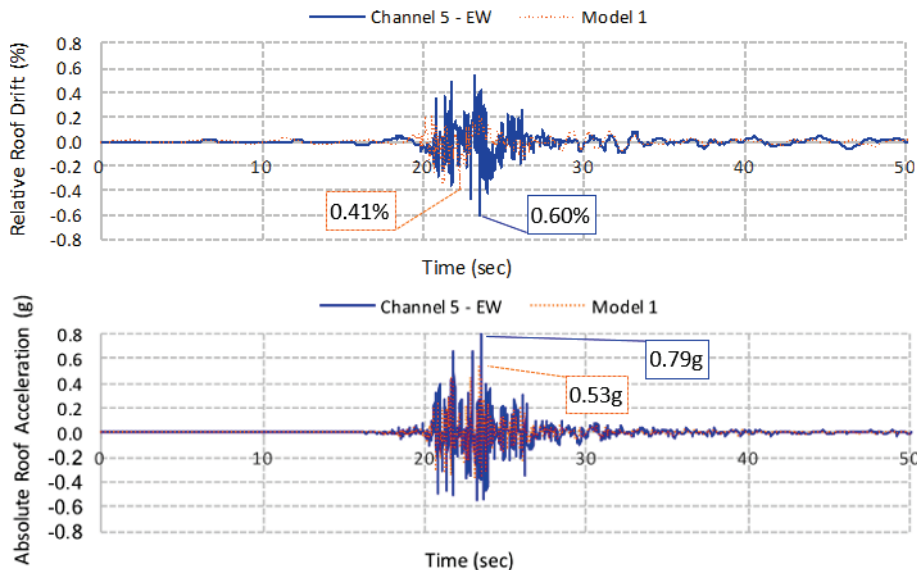


Figure D-10 Measured and predicted east-west response, Model 1, 2003 San Simeon earthquake ground motion.

Figure D-11 compares the time histories of relative roof displacements (drifts) and absolute roof accelerations measured in the north-south direction by Channel 9 (see Figure D-3) during the San Simeon earthquake against the predictions of Model 1. Again, the model significantly underestimates the

measured peak drift and acceleration and is unable to predict accurately the details of the response histories.

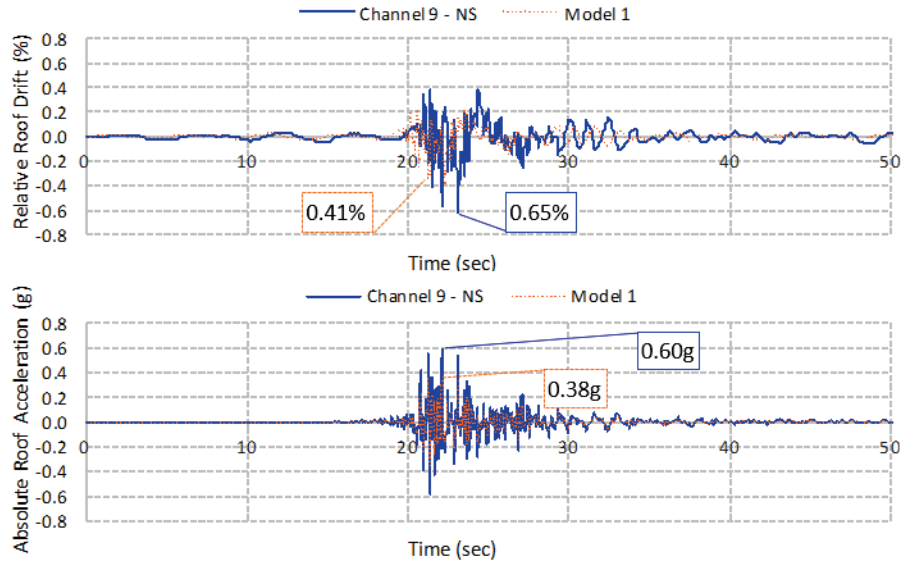


Figure D-11 Measured and predicted north-south response, Model 1, 2003 San Simeon earthquake ground motion.

D.3.3 Main Findings – Model 2

Figure D-12 shows the pushover curves in each principal direction at the center of the roof diaphragm of the north wing of the Templeton Hospital predicted by Model 2. Again, the seismic coefficient (base shear normalized by seismic weight) at peak strength is above 0.9 in both directions indicating a very laterally strong building. Again, the peak strength of the building occurs at a drift ratio at the center of the roof diaphragm of 2.0 percent in the east-west direction and at 2.2 percent in the north-south direction.

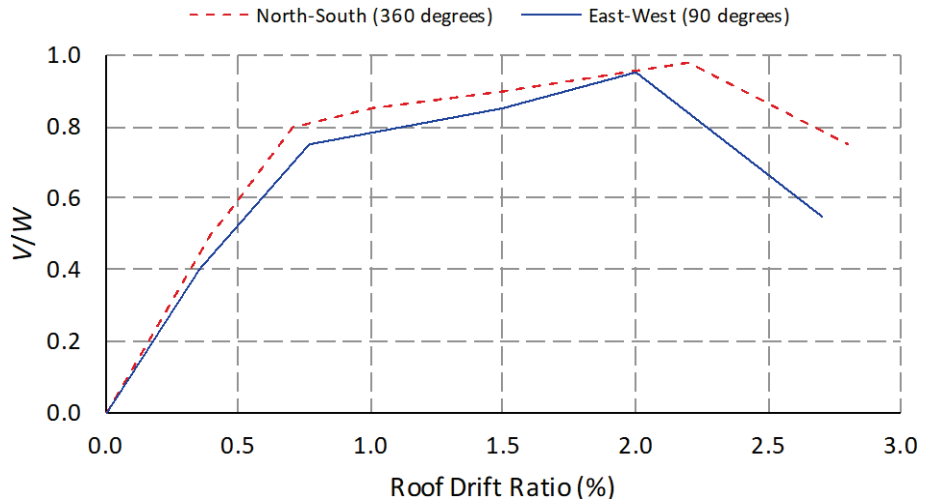


Figure D-12 Pushover curves predicted by Model 2.

Figure D-13 shows the first two natural periods and mode shapes of the north wing of the Templeton Hospital predicted by Model 2. Similar to Model 1, the fundamental periods of the building in the east-west and north-south directions are very close to each other. The fundamental period of 0.19 seconds predicted by Model 2 is almost identical to the dominant period of roof response of the north wing in the east-west direction of about 0.2 seconds (5 Hz) measured during the San Simeon earthquake.

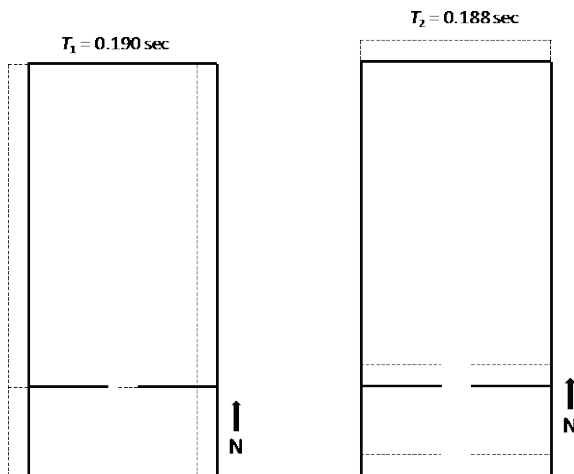


Figure D-13 Natural periods and mode shapes predicted by Model 2.

Figure D-14 compares the central portions (20 seconds to 30 seconds) of time histories of relative roof displacements (drifts) and absolute roof accelerations measured in the east-west direction by Channel 5 (see Figure D-3) during the San Simeon earthquake against the predictions of Model 2. Model 2 almost exactly predicts both the measured peak drift and acceleration. In addition, almost perfect correlation can be observed between the predicted and measured dynamic response histories. This result indicates that the more complex modeling of the in-plane flexibility of the roof diaphragm in Model 2 was an important contributor to the dynamic response of the north wing of the Templeton Hospital during the San Simeon earthquake.

Figure D-15 compares the central portions (20 seconds to 30 seconds) of the time histories of relative roof displacements (drifts) and absolute roof accelerations measured in the north-south direction by Channel 9 during the San Simeon earthquake against the predictions of Model 2. Again, Model 2 almost perfectly predicts the measured drift and acceleration histories. The level of drift level predicted by Model 2 (0.61 percent) is consistent with the observed quasi-elastic response of the building during the San Simeon earthquake.

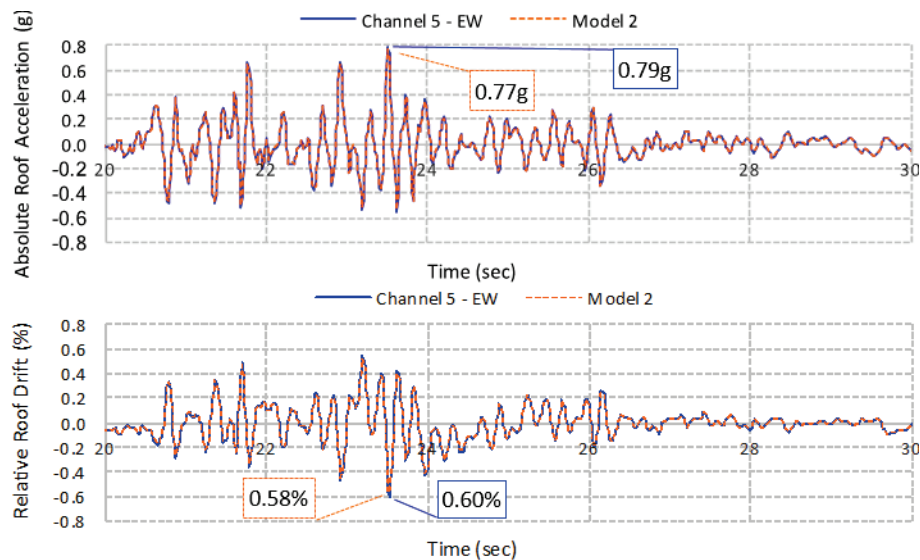


Figure D-14 Measured and predicted east-west response, Model 2, 2003 San Simeon earthquake ground motion.

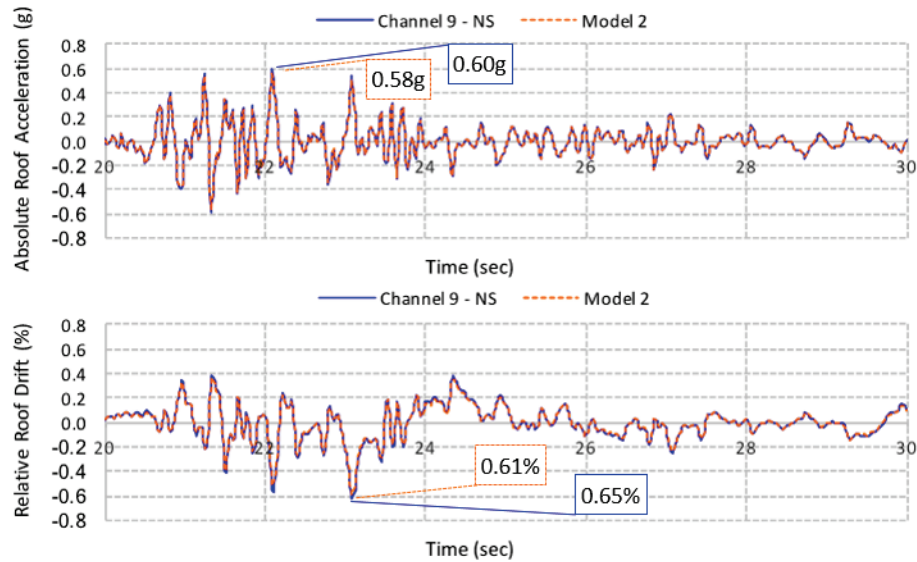


Figure D-15 Measured and predicted north-south response, Model 2, 2003 San Simeon earthquake ground motion.

To evaluate the effects of more complex modeling on predictions of the collapse capacity of the north wing of the Templeton Hospital, bi-directional incremental dynamic analyses (IDAs) were conducted using Model 2. The FEMA P-695 far-field record set was used and each record (i.e., 22 records, 2 horizontal components each) was applied in the two orthogonal orientations relative to the axes of the model (i.e., a NS-EW orientation of the records, which were then rotated 90 degrees in plan to produce an EW-NS orientation). The records were scaled in accordance with Section 6.2.3, Section 6.4.3, and Appendix A of FEMA P-695. The intensity measure was taken as the median spectral acceleration of the record set at a fundamental

period of 0.25 seconds. The collapse capacity of the model was defined as the last survival intensity before P-Delta effects caused numerical instability in the model.

Figure D-16 shows the resulting bi-directional IDA curves and collapse fragility curve predicted by Model 2. The median collapse capacity from the analysis is 2.09g. According to FEMA P-695, this raw collapse capacity should be multiplied by a bi-directional calibration factor of 1.2 to account for bi-directional analysis effects and by a spectral shape factor equal to 1.14 (in this case). The resulting FEMA P-695 median collapse capacity then becomes 2.86g. For seismic design category SDC D_{max}, the associated collapse margin ratio CMR = 1.91 (2.86g / 1.5g).

For an overall dispersion factor $\beta = 0.50$, the probability of collapse at the MCE_R level is just under 10 percent. This is not consistent with the 0 percent to 2 percent probability of collapse that would be expected for one-story buildings given MCE_R ground motions obtained from Office of Emergency Services (OES) red-tag data from the 1994 Northridge earthquake (OES, 1995), as described in Chapter 2.

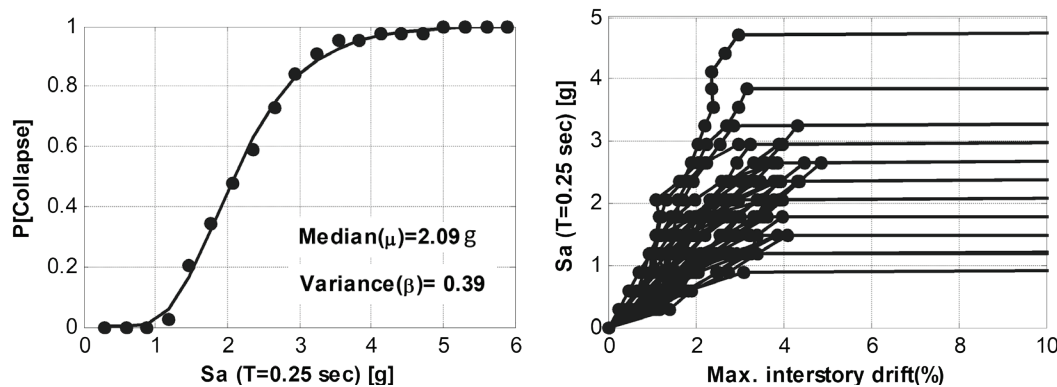


Figure D-16 Bi-directional IDA curves and collapse fragility of the north wing of the Templeton Hospital predicted by Model 2.

D.3.4 Summary of Findings

The validation study conducted on a well-instrumented wing of the Templeton Hospital indicated that more complex modeling of the in-plane diaphragm flexibility is important to predict with accuracy the observed building response during the 2003 San Simeon earthquake. Model 2, which incorporated the in-plane roof diaphragm flexibility, almost perfectly reproduced the quasi-elastic dynamic response characteristics of the Templeton Hospital recorded during the 2003 San Simeon earthquake.

Limited supplementary analyses incorporating nonstructural interior and exterior wall finishes in Model 2 showed very little difference in elastic

dynamic response (Koliou et al., 2017). The small difference in results with and without nonstructural interior and exterior wall finishes can be attributed to the already very high lateral strength and stiffness of the Templeton Hospital building contributed by the wood light-frame shear walls, which overwhelmed the effects of nonstructural interior and exterior wall finishes. It is believed that the effects of nonstructural interior and exterior wall finishes would be more significant in buildings that are more representative of typical of code-compliant designs.

The more complex Model 2 predicted a collapse probability at MCE_R for the Templeton Hospital building that is an order of magnitude higher than what would be expected based on OES red-tag data from the 1994 Northridge earthquake. This suggests that other modeling features not considered in this pilot study (but considered in this report) are important for improving the prediction of collapse probability. More sophisticated modeling (e.g., three-dimensional modeling with more accurate building response characteristics) would need to be developed for this purpose.

References

- AIJ, 1995, *Preliminary Reconnaissance Report of the 1995 Hyogoken-Nanbu Earthquake*, English Edition, Architectural Institute of Japan, Tokyo, Japan.
- ASCE, 2010, *Minimum Design Loads for Buildings and Other Structures*, ASCE/SEI 7-10, American Society of Civil Engineers, Reston, Virginia.
- ASCE, 2013, *Seismic Rehabilitation of Existing Buildings*, ASCE/SEI 41-13, American Society of Civil Engineers, Reston, Virginia.
- ASCE, 2016, *Minimum Design Loads and Associated Criteria for Buildings and Other Structures*, ASCE/SEI 7-16, American Society of Civil Engineers, Reston, Virginia.
- ASCE, 2017, *Seismic Evaluation and Retrofit of Existing Buildings*, ASCE/SEI Standard 41-17, American Society of Civil Engineers, Reston, Virginia.
- ATC, 1985, *Earthquake Damage Evaluation Data for California*, ATC-13, Applied Technology Council, Redwood City, California.
- ATC, 1989, *Procedures for Postearthquake Safety Evaluation of Buildings*, ATC-20, Applied Technology Council, Redwood City, California.
- ATC, 2000, *Database on the Performance of Structures near Strong-Motion Recordings: 1994 Northridge, California, Earthquake*, ATC-38, Applied Technology Council, Redwood City, California.
- ATC, 2005, *Field Manual: Postearthquake Safety Evaluation of Buildings Second Edition*, ATC-20-1, Applied Technology Council, Redwood City, California.
- ATC, 2015, *Roadmap for Solutions to the Issue of Short Period Building Performance*, ATC-116, Applied Technology Council, Redwood City, California.
- AWC, 2008, *Special Design Provisions for Wind and Seismic, 2008 Edition*, ANSI/AF&PA SDPWS-2008, American Wood Council, American Forest & Paper Association, Washington, D.C.

AWC, 2012, *National Design Specification for Wood Construction, 2012 Edition*, ANSI/AWC NDS-2012, American Wood Council, Leesburg, Virginia.

AWC, 2015, *National Design Specification for Wood Construction, 2015 Edition*, ANSI/AWC NDS-2015, American Wood Council, Leesburg, Virginia.

Baker, J.W., 2015, “Efficient analytical fragility function fitting using dynamic structural analysis,” *Earthquake Spectra*, Vol. 31, No.1, pp. 579-599.

Camelo, V.S., Beck, J.L., and Hall, J.F., 2002, *Dynamic Characteristics of Woodframe Buildings*, Final Report for Task 1.3.3 of the CUREE-Caltech Woodframe Project, Report W-11, Consortium of Universities for Research in Earthquake Engineering, Richmond, California.

Carr, A.J., 2007, *RUAUMOKO-2D Manual – Theory*, University of Canterbury Press, Christchurch, New Zealand.

CBSC, 2007, “HAZUS AEBM regulations,” Appendix H to Chapter 6, Administrative Regulations for the Office of Statewide Health Planning and Development (OSHPD), *2007 California Building Standards Code, California Code of Regulations, Title 24, Part 1*, California Building Standards Commission, Sacramento, California.

CEN, 2004, *Eurocode 8: Design of Structures for Earthquake Resistance - Part 1: General Rules, Seismic Actions and Rules for Buildings*, European Committee for Standardization, Brussels, Belgium.

Chopra, A., 2011, *Dynamics of Structures – Theory and Applications to Earthquake Engineering, 4th Edition*, Prentice-Hall International, Upper Saddle River, New Jersey.

Christovasilis, I.P., and Filiatrault, A., 2010, “Two-dimensional seismic analysis of multi-story light-frame wood buildings,” *Proceedings, 9th U.S. National & 10th Canadian Conference on Earthquake Engineering: Reaching Beyond Borders*, Toronto, Canada, Paper No. 69.

Christovasilis, I.P., and Filiatrault, A., 2013, “Numerical framework for non-linear analysis of two-dimensional light-frame wood structures,” *Ingegneria Sismica: International Journal of Earthquake Engineering*, No. 4, pp. 5-25.

Christovasilis, I.P., Filiatrault, A., and Wanitkorkul, A., 2007, *Seismic Testing of a Full-Scale Two Story Light Frame Wood Building: NEESWood Benchmark Test*, Technical Report No. NW-01, University at Buffalo, State University of New York, Buffalo, New York.

Christovasilis, I.P., Filiatrault, A., Constantinou, M.C., and Wanitkorkul, A., 2009, "Incremental dynamic analysis of woodframe buildings," *Earthquake Engineering & Structural Dynamics*, Vol. 38, No. 4, pp. 477-496.

CoLA, 2001, *Report of a Testing Program of Light-Framed Walls with Wood-Sheathed Shear Panels*, Final Report to the City of Los Angeles (CoLA) Department of Building and Safety, Structural Engineers Association of Southern California, COLA-UCI Light Frame Test Committee, University of California, Irvine, California.

CSMIP, 2015, Center for Engineering Strong Motion Data, California Strong Motion Instrumentation Program, California Geological Survey, Sacramento, California, <http://www.strongmotioncenter.org/>, last accessed August 30, 2020.

CUREE, 2010, *General Guidelines for the Assessment and Repair of Earthquake Damage in Residential Woodframe Buildings*, CUREE Publication No. EDA-02, Consortium of Universities for Research in Earthquake Engineering, Richmond, California.

Das, B.M., 2005, *Principles of Geotechnical Engineering*, 6th Edition, CL Engineering.

EERI, 1994, *Expected Seismic Performance of Buildings*, Earthquake Engineering Research Institute, Oakland, California.

FEMA, 2002, *Advanced Engineering Building Module, Multi-Hazard Loss Estimation Methodology Earthquake Model*, HAZUS-MH MR1, prepared by the National Institute of Building Sciences for the Federal Emergency Management Agency, Washington, D.C.

FEMA, 2003, *Multi-hazard Loss Estimation Methodology, Earthquake Model*, HAZUS®MH MR4, Technical Manual, prepared by the National Institute of Building Sciences for the Federal Emergency Management Agency, Washington, D.C.

- FEMA, 2007, *Interim Testing Protocols for Determining the Seismic Performance Characteristics of Structural and Nonstructural Components*, FEMA 461, prepared by the Applied Technology Council for the Federal Emergency Management Agency, Washington, D.C.
- FEMA, 2009a, *NEHRP Recommended Seismic Provisions for New Buildings and Other Structures*, FEMA P-750, prepared by the Building Seismic Safety Council of the National Institute of Building Sciences for the Federal Emergency Management Agency, Washington, D.C.
- FEMA, 2009b, *Quantification of Building Seismic Performance Factors*, FEMA P-695, prepared by the Applied Technology Council for the Federal Emergency Management Agency, Washington, D.C.
- FEMA, 2011, *Quantification of Building Seismic Performance Factors: Component Equivalency Methodology*, FEMA P-795, prepared by the Applied Technology Council for the Federal Emergency Management Agency, Washington, D.C.
- FEMA, 2012a, *Seismic Performance Assessment of Buildings, Volume 1 – Methodology*, FEMA P-58-1, prepared by the Applied Technology Council for the Federal Emergency Management Agency, Washington, D.C.
- FEMA, 2012b, *Seismic Evaluation and Retrofit of Multi-Unit Wood-Frame Buildings with Weak First Stories*, FEMA P-807, prepared by the Applied Technology Council for the Federal Emergency Management Agency, Washington, D.C.
- FEMA, 2015a, *NEHRP Recommended Seismic Provisions for New Buildings and Other Structures*, FEMA P-1050, prepared by the Building Seismic Safety Council of the National Institute of Building Sciences for the Federal Emergency Management Agency, Washington, D.C.
- FEMA, 2015b, *Rapid Visual Screening of Buildings for Potential Seismic Hazards: Supporting Documentation, Third Edition*, FEMA P-155, prepared by the Applied Technology Council for the Federal Emergency Management Agency, Washington, D.C.
- FEMA, 2018a, *Assessing Seismic Performance of Buildings with Configuration Irregularities, Calibrating Current Standards and Practices*, FEMA P-2012, prepared by the Applied Technology Council for the Federal Emergency Management Agency, Washington, D.C.

FEMA, 2018b, *Seismic Performance Assessment of Buildings, Methodology and Implementation*, FEMA P-58 Series, prepared by the Applied Technology Council for the Federal Emergency Management Agency, Washington, D.C.

FEMA, 2020a, *Short-Period Building Collapse Performance and Recommendations for Improving Seismic Design, Volume 1 – Overarching Findings, Conclusions, and Recommendations*, FEMA P-2139-1, prepared by the Applied Technology Council for the Federal Emergency Management Agency, Washington, D.C.

FEMA, 2020b, *Short-Period Building Collapse Performance and Recommendations for Improving Seismic Design, Volume 3 – Study of One-to-Four Story Special Reinforced Masonry Shear Wall Buildings*, FEMA P-2139-3, prepared by the Applied Technology Council for the Federal Emergency Management Agency, Washington, D.C.

FEMA, 2020c, *Short-Period Building Collapse Performance and Recommendations for Improving Seismic Design, Volume 4 – Study of One-to-Four Story Steel Special Concentrically Braced Frame Buildings*, FEMA P-2139-4, prepared by the Applied Technology Council for the Federal Emergency Management Agency, Washington, D.C.

Filiatrault, A., Christovasilis, I.P., Wanitkorkul A., and van de Lindt, J.W., 2010, “Experimental seismic response of a full-scale light-frame wood building,” *Journal of Structural Engineering*, American Society of Civil Engineers, Vol. 136, No. 3, pp. 246-254.

Fischer, D., Filiatrault, A., Folz, B., Uang, C.-M., and Seible, F., 2001, *Shake Table Tests of a Two-Story Woodframe House*, CUREE Publication No. W-06, Consortium of Universities for Research in Earthquake Engineering, Richmond, California.

Folz, B., and Filiatrault, A., 2001, “Cyclic analysis of wood shear walls,” *Journal of Structural Engineering*, Vol. 127, No. 4, pp. 433-441.

Folz, B., and Filiatrault, A., 2004, “Seismic analysis of woodframe structures. II: Model implementation and verification,” *Journal of Structural Engineering*, American Society of Civil Engineers, Vol. 130, No. 9, pp. 1361-1370.

- Gatto, K., and Uang, C-M., 2001, *Cyclic Response of Woodframe Shearwalls: Loading Protocol and Rate of Loading Effects*, Report No. SSRP-2001/06, Structural System Research Project, University of California, San Diego, La Jolla, California.
- Gazetas, G., and Roesset, J.M., 1976, "Forced vibrations of strip footings on layered soils," *Methods of Structural Analysis*, Vol. 1, pp. 115-131.
- Gazetas, G., and Roesset, J.M., 1979, "Vertical vibrations of machine foundations," *Journal of Geotechnical Engineering Division*, Vol. 105, pp. 1435-1454.
- HUD, 1994, *Assessment of Damage to Residential Buildings Caused by the Northridge Earthquake*, prepared by the National Association of Home Builders, for the U.S. Department of Housing and Urban Development, Office of Policy Development and Research, Washington, D.C.
- ICBO, 1988, *Uniform Building Code*, International Conference of Building Officials, Whittier, California.
- ICBO, 1994, *Uniform Building Code*, International Conference of Building Officials, Whittier, California.
- ICBO, 1997, *Uniform Building Code*, International Conference of Building Officials, Whittier, California.
- ICC, 2012a, *International Building Code*, International Code Council, Inc., Country Club Hills, Illinois.
- ICC, 2012b, *International Residential Code*, International Code Council, Inc., Country Club Hills, Illinois.
- ICC, 2015a, *International Building Code*, International Code Council, Inc., Country Club Hills, Illinois.
- ICC, 2015b, *International Residential Code*, International Code Council, Inc., Country Club Hills, Illinois.
- Isoda, I., Filiatrault, A., and Christovasilis, I.P., 2008, "Collapse Analysis of Japanese Wood Houses," *Proceedings of the 10th World Conference on Timber Engineering 2008*, Miyazaki, Japan, 7 p.
- Kircher, C.A., Seligson, H., Bouabid, J., and Morrow, G., 2006a, "When the big one strikes again – Estimated losses due to a repeat of the 1906 San Francisco earthquake," *Earthquake Spectra*, Vol. 22., Issue S2, pp. 297-339.

Kircher, C.A., Whitman, R.V., Holmes, W.T, 2006b, "HAZUS earthquake loss estimation methods," *Natural Hazards Review*, American Society of Civil Engineers, Vol. 7, No. 2, pp. 45-59.

Koliou, M., Filiatrault, A., and Kircher, C.A., 2017, "Assessing modeling complexities on the seismic performance of a short period instrumented hospital," *Journal of Performance of Constructed Facilities*, Vol. 31, No. 1.

Koliou, M., Filiatrault, A., Kelly, D.J., and Lawson, J., 2014, "Numerical framework for seismic collapse assessment of rigid wall-flexible diaphragm structures," *Proceedings of the 10th U.S. National Conference on Earthquake*, Anchorage, Alaska, Paper ID: 282.

Koliou, M., Filiatrault, A., Kelly, D.J., and Lawson, J., 2016, "Distributed yielding concept for improved seismic collapse performance of rigid wall-flexible diaphragm buildings," *Journal of Structural Engineering*, Vol. 142, No. 2, pp. 1-16.

Krawinkler, H., Parisi, F., Ibarra, L., Ayoub, A., and Medina, R., 2000. *Development of a Testing Protocol for Woodframe Structures*, CUREE Report No. W-02, Consortium of Universities for Research in Earthquake Engineering, Richmond, California.

Line, P., Hohbach, D., and Waltz, N., 2019, "In-Plane Racking Strength Tests of Wood-frame Wood Structural Panel Shear Walls with 2-inch Panel Edge Nail Spacing and Representative Multi-story Details," *Proceedings*, Structural Engineers Association of California Convention, Squaw Creek, California.

Line, P., Waltz, N., and Skaggs, T., 2008, "Seismic equivalence parameters for engineered wood frame wood structural panel shear walls," *Wood Design Focus*, Vol. 18, No. 2.

Line, P., Waltz, N., Skaggs, T., and Yeh, B., 2014, "Cyclic testing of unblocked wood-frame wood structural panel shear walls," *Wood Design Focus*, Vol 24. No. 2, pp. 3-9.

Miranda, E., and Bertero, V.V., 1994, "Evaluation of strength reduction factors for earthquake-resistant design," *Earthquake Spectra*, Vol. 10, No. 2, pp. 357-379.

Munich RE, 2015, *Loss Events Worldwide 1980-2014, 10 Costliest Events Ordered by Overall Losses*, Munchener Rückversicherungs-Gesellschaft, Geo Risks Research, NatCatService, Munich RE, Munich, Germany.

Newmark, N.M., and Hall, W.J., 1982, *Earthquake Spectra and Design*, Earthquake Engineering Research Institute, Oakland, California.

NIST, 2010, *Evaluation of the FEMA P-695 Methodology for Quantification of Building Seismic Performance Factors*, NIST GCR 10-917-8, prepared by the NEHRP Consultants Joint Venture, a partnership of the Applied Technology Council and the Consortium of Universities for Research in Earthquake Engineering, for the National Institute of Standards and Technology, Gaithersburg, Maryland.

NIST, 2011, *Selecting and Scaling Earthquake Ground Motions for Performing Response-History*, NIST GCR 11-917-15, prepared by the NEHRP Consultants Joint Venture, a partnership of the Applied Technology Council and the Consortium of Universities for Research in Earthquake Engineering, for the National Institute of Standards and Technology, Gaithersburg, Maryland.

NIST, 2012a, *Tentative Framework for Development of Advanced Seismic Design Criteria for New Buildings*, NIST GCR 12-917-20, prepared by the NEHRP Consultants Joint Venture, a partnership of the Applied Technology Council and the Consortium of Universities for Research in Earthquake Engineering, for the National Institute of Standards and Technology, Gaithersburg, Maryland.

NIST, 2012b, *Soil-Structure Interaction for Building Structures*, NIST GCR 12-917-21, prepared by the NEHRP Consultants Joint Venture, a partnership of the Applied Technology Council and the Consortium of Universities for Research in Earthquake Engineering, for the National Institute of Standards and Technology, Gaithersburg, Maryland.

NOAA, 1973, *San Fernando, California, Earthquake of February 9, 1971*, National Oceanic and Atmospheric Administration, U.S. Department of Commerce, Washington, D.C.

OES, 1995, *The Northridge Earthquake of January 17, 1994: Report of Data Collection and Analysis, Part A: Damage and Inventory Data*, The Governor's Office of Emergency Services of the State California, Sacramento, California.

OES, 1997, *The Northridge Earthquake of January 17, 1994: Report of Data Collection and Analysis, Part B: Analysis and Trends*, California Governor's Office of Emergency Services of the State California, Sacramento, California.

- Pang, W., Ziae, E., and Filiatrault, A., 2012, "A 3D model for collapse analysis of soft-story light-frame wood buildings," *Proceedings of the World Conference on Timber Engineering*, Auckland, New Zealand.
- Porter, K., Jones, L., Cox, D., Goltz, J., Hudnut, K., Milet, D., Perry, S., Ponti, D., Reichle, M., Rose, A.Z., Scawthorn, C.R., Seligson, H.A., Shoaf, K.I., Treiman, J., and Wein, A., 2011, "The ShakeOut Scenario: A Hypothetical M_w 7.8 Earthquake on the Southern San Andreas Fault," *Earthquake Spectra*, Vol. 27, No. 2, pp. 239-261.
- SAC, 1995, *Characterization of Ground Motions during the Northridge Earthquake of January 17, 1994*, SAC 95-03, prepared by the SAC Joint Venture, a partnership of the Structural Engineers Association of California (SEAOC), Applied Technology Council (ATC), and California Universities for Research in Earthquake Engineering (CUREe).
- Schierle, 2003, *Northridge Earthquake Field Investigations: Statistical Analysis of Woodframe Damage*, CUREE Publication No. W-09, Consortium of Universities for Research in Earthquake Engineering, Richmond, California.
- Seyhan, E., Stewart, J.P., Ancheta, T.D., Darragh, R.B., and Graves, R.W., 2014, "NGA-West 2 site database," *Earthquake Spectra*, Vol. 30, No. 3, pp. 1007-1024.
- Shirazi, S.M.H., and Pang, W., 2012, "Seismic performance variability of wood-frame shear walls designed in accordance to the National Design Specification (NDS)," *Proceedings, ASCE Structures Congress 2012*, Chicago, Illinois, pp. 1721-1732.
- SST, 2015, *Strong-Rod Systems*, F-L-SRS15, Simpson Strong-Tie Company, Pleasanton, California.
- Star, L.M., Givens, M.J., Nigbor, R.L., and Stewart, J.P., 2015, "Field testing of structure on shallow foundation to evaluate SSI effects," *Earthquake Spectra*, Vol. 31, No. 4, pp. 2511-2534.
- Sutoyo, D., and Hall, J., 2006, "Study of wood-frame building records from the Parkfield and San Simeon earthquakes," *SMIP06 Seminar Proceedings*, California Strong-Motion Instrumentation Program, California Geological Survey, Sacramento, California, pp. 81-100.

Thompson, E.M., Kayen, R.E., Carkin, B., and Tanaka, H., 2010, *Surface-Wave Site Characterization at 52 Strong-Motion Recording Stations Affected by the Parkfield, California, M6.0 Earthquake of 28 September 2004*, Open-File Report 2010-1168, U.S. Geological Survey, Menlo Park, California.

Tokas, C., and Lobo, R., 2012, "Hospital seismic safety program and strong motion instrumentation," *SMIP12 Seminar Proceedings*, California Strong-Motion Instrumentation Program, California Geological Survey, Sacramento, California, pp. 111-124.

van de Lindt, J., Symans, M.D., Pang, W., Shao, X., and Gershfeld, M., 2012, "Seismic risk reduction for soft-story woodframe building: the NEES-soft project," *Proceedings of the World Conference on Timber Engineering*, Auckland, New Zealand, pp. 237-243.

Veletsos, A.S., and Newmark, N.M., 1960, "Effect of inelastic behavior on the response of simple systems to earthquake motion," *Proceedings of the 2nd World Conference on Earthquake Engineering*, Tokyo, Japan, Vol. 2, pp. 895-912.

Veletsos, A.S., Newmark, N.M., and Chelapati, C.V., 1965, "Deformation spectra for elastic and elastoplastic systems subjected to ground shock and earthquake motions," *Proceedings of the 3rd World Conference on Earthquake Engineering*, New Zealand, Vol. II, pp. 663-682.

Wald, D.J., Quitoriano, V., Heaton, T.H., Kanamori, H., Scrivner, C.W., and Worden, C.B., 1999, "TriNet 'ShakeMaps': Rapid generation of instrumental ground motion and intensity maps for earthquakes in Southern California," *Earthquake Spectra*, Vol. 15, No. 3, pp. 537-555.

Wald, D.J., Worden, B.C., Quitoriano, V., and Pankow, K.L., 2005, *ShakeMap Manual: Technical Manual, User's Guide, and Software Guide*, U.S. Geological Survey, Menlo Park, California.

Yamaguchi, N., and Yamazaki, F., 2000, "Fragility curves for buildings in Japan based on damage surveys after the 1995 Kobe Earthquake," Paper No. 2451, *Proceedings of the 12th World Conference on Earthquake Engineering*, Auckland, New Zealand.

Yamazaki, F., and Murao, O., 2000, "Vulnerability functions for Japanese buildings based on damage data due to the 1995 Kobe Earthquake," *Implications of Recent Earthquakes on Seismic Risk*, Series on Innovation in Structures and Construction, Vol. 2., Imperial College Press, London, United Kingdom.

Project Participants

Federal Emergency Management Agency

Mai (Mike) Tong (Project Officer)
Federal Emergency Management Agency
500 C Street, SW, Room 416
Washington, D.C. 20472

Robert D. Hanson (Technical Advisor)
Federal Emergency Management Agency
5885 Dunabbey Loop
Dublin, Ohio 43017

Applied Technology Council

Jon A. Heintz (Project Executive)
Applied Technology Council
201 Redwood Shores Parkway, Suite 240
Redwood City, California 94065

Scott D. Schiff (Associate Project Manager)
Applied Technology Council
201 Redwood Shores Parkway, Suite 240
Redwood City, California 94065

Justin Moresco (Project Manager)
Applied Technology Council
201 Redwood Shores Parkway, Suite 240
Redwood City, California 94065

Project Technical Committee

Charles A. Kircher (Project Technical Director)
Kircher & Associates
1121 San Antonio Road, Suite D-202
Palo Alto, California 94303

Andre Filiatrault
University at Buffalo
Dept. of Civil, Structural and Environmental
Engineering
134 Ketter Hall
Buffalo, New York 14260

Jeffrey W. Berman
University of Washington
Dept. of Civil & Environmental Engineering
201 More Hall, Box 352700
Seattle, Washington 98195

James R. Harris
J. R. Harris & Company
1175 Sherman Street, Suite 2000
Denver, Colorado 80203

Kelly Cobeen
Wiss, Janney, Elstner Associates, Inc.
2000 Powell Street, Suite 1650
Emeryville, California 94608

Gregory Kingsley
KL&A, Inc.
1717 Washington Avenue, Suite 100
Golden, Colorado 80401

J. Daniel Dolan
Washington State University
Dept. of Civil and Environmental Engineering
P.O. Box 642910
Pullman, Washington 99164

Dawn Lehman
University of Washington
Dept. of Civil & Environmental Engineering
201 More Hall, Box 352700
Seattle, Washington 98195

Weichiang Pang
Clemson University
Glenn Department of Civil Engineering
312 Lowry Hall
Clemson, South Carolina 29634

P. Benson Shing
University of California, San Diego
Dept. of Structural Engineering
9500 Gilman Drive
La Jolla, California 92093

Project Review Panel

Anthony Court (ATC Board Contact)
A.B. Court & Associates
4340 Hawk Street
San Diego, California 92103

William T. Holmes
Structural Engineer
2600 La Cuesta Avenue
Oakland, California 94611

Onder Kustu
OAK Structural (retired)
P.O. Box 2074
Danville, California 94526

Phil Line
American Wood Council
222 Catoctin Circle SE, Suite 201
Leesburg, Virginia 20175

James O. Malley
Degenkolb Engineers
375 Beale Street, Suite 500
San Francisco, California 94105

Steve Pryor
Simpson Strong-Tie
5956 W. Las Positas Boulevard
Pleasanton, California 94588

Soil-Structure Interaction Working Group

Lisa Star
California State University, Long Beach
Dept. of Civil Engineering and Construction
Engineering Management
1250 Bellflower Boulevard
Long Beach, California 90840

Jonathan P. Stewart
University of California, Los Angeles
Dept. of Civil and Environmental Engineering
5731 Boelter Hall
Los Angeles, California 90095

Wood Working Group

D. Jared DeBock
California State University, Chico
Department of Civil Engineering
Chico, California 95929

Ershad Ziae
Youssef Hachem Consulting Engineering
99 NW 27th Avenue
Miami, Florida 33125

Maria Koliou
Texas A&M University
Dept. of Civil and Environmental Engineering
201 Dwight Look Engineering Building
College Station, Texas 77843

Wood Workshop Participants

Armin Bebamzadeh

University of British Columbia

6250 Applied Science Lane, CEME Room 2018

Vancouver, British Columbia V6T 1Z4 Canada

Colin Blaney

Buehler & Buehler Structural Engineers

951-A Industrial Boulevard

San Carlos, California 94070

Henry Burton

University of California, Los Angeles

5732E Boelter Hall

Los Angeles, California 90095

Mark Chang

City of Bellevue, Washington

450 110th Avenue NE

Bellevue, Washington 98056

Kelly Cobeen

Wiss, Janney, Elstner Associates, Inc.

2000 Powell Street, Suite 1650

Emeryville, California 94608

Richard Denio

California Division of the State Architect

1515 Clay Street, Suite 1201

Oakland, California 94612

Gregory Deierlein

Stanford University

Blume Earthquake Engineering Center

Stanford, California 94305

J. Daniel Dolan

Washington State University

P.O. Box 642910

Pullman, Washington 99164

Bradford Douglas

American Wood Council

222 Catoctin Circle SE, Suite 201

Leesburg, Virginia 20175

Gary Ehrlich

National Association of Home Builders

1201 15th Street NW

Washington, D.C. 20005

Andre Filiatral

University at Buffalo

134 Ketter Hall

Buffalo, New York 14260

Robert Hanson

Federal Emergency Management Agency

5885 Dunabney Loop

Dublin, Ohio 43017

James Harris

J.R. Harris & Company

1775 Sherman Street, Suite 1525

Denver, Colorado 80203

Jon Heintz

Applied Technology Council

201 Redwood Shores Parkway, Suite 240

Redwood City, California 94065

Richard Hemmen

DCI Engineers

818 Stewart Street, Suite 1000

Seattle, Washington 98101

Douglas Hohbach

Hohbach-Lewin, Inc.

260 Sheridan Avenue

Palo Alto, California 94306

William T. Holmes

Structural Engineer

2600 La Cuesta Avenue

Oakland, California 94611

John Hooper

Magnusson Klemencic Associates

1301 5th Avenue, Suite 3200

Seattle, Washington 98101

Edwin Huston

Smith & Huston, Inc.

8618 Roosevelt Way NE,

Seattle, Washington 98115

Erol Karacabeyli

FPInnovations

2665 East Mall,

Vancouver, British Columbia V6T 1Z4 Canada

Gregory Kingsley
KL&A, Inc.
1717 Washington Avenue, Suite 100
Golden, Colorado 80401

Charles Kircher
Kircher & Associates
1121 San Antonio Road, Suite D-202
Palo Alto, California 94303

Steven Kuan
FPI Innovations
2665 East Mall
Vancouver, British Columbia V6T 1Z4 Canada

Onder Kustu
OAK Structural (retired)
555 Bryant Street, Suite 884
Palo Alto, California 94301

Philip Line
American Wood Council
222 Catoctin Circle SE, Suite 201
Leesburg, Virginia 20175

Jeffrey Linville
Weyerhaeuser
P.O. Box 6049
Federal Way, Washington 98063

Bret Lizundia
Rutherford + Chekene
375 Beale Street, Suite 310
San Francisco, California 94105

Janiele Maffei
California Earthquake Authority
801 K Street, Suite 1000
Sacramento, California 95814

Stephen Mahin
University of California, Berkeley
777 Davis Hall, Mail Code 1710
Berkeley, California 94720

Bonnie Manley
American Iron and Steel Institute
25 Massachusetts Avenue NW, Suite 800
Washington, D.C. 20001

David McCormick
Simpson, Gumpertz & Heger Inc.
100 Pine Street, Suite 1600
San Francisco, California 94111

Cristopher Moen
NBM Technologies
1014 West 36th Street, 3rd Floor
Baltimore, Maryland 21211

John Osteraas
Exponent
149 Commonwealth Drive
Menlo Park, California 94025

Weichiang Pang
Clemson University
312 Lowry Hall
Clemson, South Carolina 29634

Steven Pryor
Simpson Strong-Tie
5956 West Las Positas Boulevard
Pleasanton, California 94588

Douglas Rammer
USDA Forest Products Laboratory
One Gifford Pinchot Drive
Madison, Wisconsin 53726

Badie Rowshandel
California Earthquake Authority
801 K Street, Suite 1000
Sacramento, California 95814

Scott Schiff
Applied Technology Council
1653 Duncan Drive NW
Atlanta, Georgia 30309

Jason Thompson
National Concrete Masonry Association
13750 Sunrise Valley Drive
Herndon, Virginia 20171

Mai (Mike) Tong
Federal Emergency Management Agency
500 C Street SW, Room 416
Washington, D.C. 20024

Tom VanDorpé
VanDorpé Chou Associates, Inc.
2200 West Orangewood Avenue, Suite 150
Orange, California 92868

Kevin Wong
National Institute of Standards and Technology
100 Bureau Drive
Gaithersburg, Maryland 20899



FEMA

FEMA P-2139-2